BREAKTHROUGH BCI APPLICATIONS IN MEDICINE

EDITED BY: Christoph Guger, Rossella Spataro, Adam Olding Hebb, Dean Krusienski and Vivek Prabhakaran

PUBLISHED IN: Frontiers in Neuroscience

frontiers Research Topics

frontiers

Frontiers eBook Copyright Statement

The copyright in the text of individual articles in this eBook is the property of their respective authors or their respective institutions or funders. The copyright in graphics and images within each article may be subject to copyright of other parties. In both cases this is subject to a license granted to Frontiers.

The compilation of articles constituting this eBook is the property of Frontiers.

Each article within this eBook, and the eBook itself, are published under the most recent version of the Creative Commons CC-BY licence. The version current at the date of publication of this eBook is CC-BY 4.0. If the CC-BY licence is updated, the licence granted by Frontiers is automatically updated to the new version.

When exercising any right under the CC-BY licence, Frontiers must be attributed as the original publisher of the article or eBook, as applicable.

Authors have the responsibility of ensuring that any graphics or other materials which are the property of others may be included in the CC-BY licence, but this should be checked before relying on the CC-BY licence to reproduce those materials. Any copyright notices relating to those materials must be complied with.

Copyright and source acknowledgement notices may not be removed and must be displayed in any copy, derivative work or partial copy which includes the elements in question.

All copyright, and all rights therein, are protected by national and international copyright laws. The above represents a summary only. For further information please read Frontiers' Conditions for Website Use and Copyright Statement, and the applicable CC-BY licence.

ISSN 1664-8714
ISBN 978-2-88966-450-4
DOI 10.3389/978-2-88966-450-4

About Frontiers

Frontiers is more than just an open-access publisher of scholarly articles: it is a pioneering approach to the world of academia, radically improving the way scholarly research is managed. The grand vision of Frontiers is a world where all people have an equal opportunity to seek, share and generate knowledge. Frontiers provides immediate and permanent online open access to all its publications, but this alone is not enough to realize our grand goals.

Frontiers Journal Series

The Frontiers Journal Series is a multi-tier and interdisciplinary set of open-access, online journals, promising a paradigm shift from the current review, selection and dissemination processes in academic publishing. All Frontiers journals are driven by researchers for researchers; therefore, they constitute a service to the scholarly community. At the same time, the Frontiers Journal Series operates on a revolutionary invention, the tiered publishing system, initially addressing specific communities of scholars, and gradually climbing up to broader public understanding, thus serving the interests of the lay society, too.

Dedication to Quality

Each Frontiers article is a landmark of the highest quality, thanks to genuinely collaborative interactions between authors and review editors, who include some of the world's best academicians. Research must be certified by peers before entering a stream of knowledge that may eventually reach the public - and shape society; therefore, Frontiers only applies the most rigorous and unbiased reviews.
Frontiers revolutionizes research publishing by freely delivering the most outstanding research, evaluated with no bias from both the academic and social point of view. By applying the most advanced information technologies, Frontiers is catapulting scholarly publishing into a new generation.

What are Frontiers Research Topics?

Frontiers Research Topics are very popular trademarks of the Frontiers Journals Series: they are collections of at least ten articles, all centered on a particular subject. With their unique mix of varied contributions from Original Research to Review Articles, Frontiers Research Topics unify the most influential researchers, the latest key findings and historical advances in a hot research area! Find out more on how to host your own Frontiers Research Topic or contribute to one as an author by contacting the Frontiers Editorial Office: frontiersin.org/about/contact

BREAKTHROUGH BCI APPLICATIONS IN MEDICINE

Topic Editors:
Christoph Guger, g.tec Medical Engineering GmbH, Austria
Rossella Spataro, University of Palermo, Italy
Adam Olding Hebb, Colorado Neurological Institute (CNI), United States
Dean Krusienski, Virginia Commonwealth University, United States
Vivek Prabhakaran, University of Wisconsin-Madison, United States

Citation: Guger, C., Spataro, R., Hebb, A. O., Krusienski, D., Prabhakaran, V., eds. (2021). Breakthrough BCI Applications in Medicine. Lausanne: Frontiers Media SA. doi: 10.3389/978-2-88966-450-4

Table of Contents

06 ***Editorial: Breakthrough BCI Applications in Medicine***
Christoph Guger, Vivek Prabhakaran, Rossella Spataro, Dean J. Krusienski and Adam O. Hebb

08 ***Characterization of Hand Clenching in Human Sensorimotor Cortex Using High-, and Ultra-High Frequency Band Modulations of Electrocorticogram***
Tianxiao Jiang, Su Liu, Giuseppe Pellizzer, Aydin Aydoseli, Sacit Karamursel, Pulat A. Sabanci, Altay Sencer, Candan Gurses and Nuri F. Ince

23 ***Dexterous Control of Seven Functional Hand Movements Using Cortically-Controlled Transcutaneous Muscle Stimulation in a Person With Tetraplegia***
Samuel C. Colachis, Marcie A. Bockbrader, Mingming Zhang, David A. Friedenberg, Nicholas V. Annetta, Michael A. Schwemmer, Nicholas D. Skomrock, Walter J. Mysiw, Ali R. Rezai, Herbert S. Bresler and Gaurav Sharma

37 ***A New Method to Generate Artificial Frames Using the Empirical Mode Decomposition for an EEG-Based Motor Imagery BCI***
Josep Dinarès-Ferran, Rupert Ortner, Christoph Guger and Jordi Solé-Casals

46 ***Machine Learning Classification to Identify the Stage of Brain-Computer Interface Therapy for Stroke Rehabilitation Using Functional Connectivity***
Rosaleena Mohanty, Anita M. Sinha, Alexander B. Remsik, Keith C. Dodd, Brittany M. Young, Tyler Jacobson, Matthew McMillan, Jaclyn Thoma, Hemali Advani, Veena A. Nair, Theresa J. Kang, Kristin Caldera, Dorothy F. Edwards, Justin C. Williams and Vivek Prabhakaran

60 ***BCI Performance and Brain Metabolism Profile in Severely Brain-Injured Patients Without Response to Command at Bedside***
Jitka Annen, Séverine Blandiaux, Nicolas Lejeune, Mohamed A. Bahri, Aurore Thibaut, Woosang Cho, Christoph Guger, Camille Chatelle and Steven Laureys

68 ***Decoding Inner Speech Using Electrocorticography: Progress and Challenges Toward a Speech Prosthesis***
Stephanie Martin, Iñaki Iturrate, José del R. Millán, Robert T. Knight and Brian N. Pasley

78 ***Evaluation of Switch and Continuous Navigation Paradigms to Command a Brain-Controlled Wheelchair***
Álvaro Fernández-Rodríguez, Francisco Velasco-Álvarez, Manon Bonnet-Save and Ricardo Ron-Angevin

93 ***Assessing Command-Following and Communication With Vibro-Tactile P300 Brain-Computer Interface Tools in Patients With Unresponsive Wakefulness Syndrome***
Christoph Guger, Rossella Spataro, Frederic Pellas, Brendan Z. Allison, Alexander Heilinger, Rupert Ortner, Woosang Cho, Ren Xu, Vincenzo La Bella, Günter Edlinger, Jitka Annen, Giorgio Mandalá, Camille Chatelle and Steven Laureys

102 ***Training in Use of Brain–Machine Interface-Controlled Robotic Hand Improves Accuracy Decoding Two Types of Hand Movements***
Ryohei Fukuma, Takufumi Yanagisawa, Hiroshi Yokoi, Masayuki Hirata, Toshiki Yoshimine, Youichi Saitoh, Yukiyasu Kamitani and Haruhiko Kishima

109 ***Comparison of the Efficacy of a Real-Time and Offline Associative Brain-Computer-Interface***
Natalie Mrachacz-Kersting and Susan Aliakbaryhosseinabadi

118 ***A Feasibility Clinical Trial to Improve Social Attention in Autistic Spectrum Disorder (ASD) Using a Brain Computer Interface***
Carlos Amaral, Susana Mouga, Marco Simões, Helena C. Pereira, Inês Bernardino, Hugo Quental, Rebecca Playle, Rachel McNamara, Guiomar Oliveira and Miguel Castelo-Branco

131 ***Effects of Sensorimotor Rhythm Modulation on the Human Flexor Carpi Radialis H-Reflex***
Aiko K. Thompson, Hannah Carruth, Rachel Haywood, N. Jeremy Hill, William A. Sarnacki, Lynn M. McCane, Jonathan R. Wolpaw and Dennis J. McFarland

137 ***Performance Differences Using a Vibro-Tactile P300 BCI in LIS-Patients Diagnosed With Stroke and ALS***
Alexander Heilinger, Rupert Ortner, Vincenzo La Bella, Zulay R. Lugo, Camille Chatelle, Steven Laureys, Rossella Spataro and Christoph Guger

147 ***Screening for Cognitive Function in Complete Immobility Using Brain–Machine Interfaces: A Proof of Principle Study***
Dorothée Lulé, Katharina Hörner, Cynthia Vazquez, Helena Aho-Özhan, Jürgen Keller, Martin Gorges, Ingo Uttner and Albert C. Ludolph

154 ***Early Findings on Functional Connectivity Correlates of Behavioral Outcomes of Brain-Computer Interface Stroke Rehabilitation Using Machine Learning***
Rosaleena Mohanty, Anita M. Sinha, Alexander B. Remsik, Keith C. Dodd, Brittany M. Young, Tyler Jacobson, Matthew McMillan, Jaclyn Thoma, Hemali Advani, Veena A. Nair, Theresa J. Kang, Kristin Caldera, Dorothy F. Edwards, Justin C. Williams and Vivek Prabhakaran

173 ***Improving Real-Time Lower Limb Motor Imagery Detection Using tDCS and an Exoskeleton***
Marisol Rodríguez-Ugarte, Eduardo Iáñez, Mario Ortiz and Jose M. Azorín

185 ***Behavioral Outcomes Following Brain–Computer Interface Intervention for Upper Extremity Rehabilitation in Stroke: A Randomized Controlled Trial***
Alexander B. Remsik, Keith Dodd, Leroy Williams Jr., Jaclyn Thoma, Tyler Jacobson, Janerra D. Allen, Hemali Advani, Rosaleena Mohanty, Matt McMillan, Shruti Rajan, Matt Walczak, Brittany M. Young, Zack Nigogosyan, Cameron A. Rivera, Mohsen Mazrooyisebdani, Neelima Tellapragada, Leo M. Walton, Klevest Gjini, Peter L.E. van Kan, Theresa J. Kang, Justin A. Sattin, Veena A. Nair, Dorothy Farrar Edwards, Justin C. Williams and Vivek Prabhakaran

201 ***Evaluation of Changes in the Motor Network Following BCI Therapy Based on Graph Theory Analysis***
Mohsen Mazrooyisebdani, Veena A. Nair, Po-Ling Loh, Alexander B. Remsik, Brittany M. Young, Brittany S. Moreno, Keith C. Dodd, Theresa J. Kang, Justin C. William and Vivek Prabhakaran

215 ***Ipsilesional Mu Rhythm Desynchronization and Changes in Motor Behavior Following Post Stroke BCI Intervention for Motor Rehabilitation***
Alexander B. Remsik, Leroy Williams Jr., Klevest Gjini, Keith Dodd, Jaclyn Thoma, Tyler Jacobson, Matt Walczak, Matthew McMillan, Shruti Rajan, Brittany M. Young, Zack Nigogosyan, Hemali Advani, Rosaleena Mohanty, Neelima Tellapragada, Janerra Allen, Mohsen Mazrooyisebdani, Leo M. Walton, Peter L. E. van Kan, Theresa J. Kang, Justin A. Sattin, Veena A. Nair, Dorothy Farrar Edwards, Justin C. Williams and Vivek Prabhakaran

233 ***Brain–Computer Interface (BCI) Applications in Mapping of Epileptic Brain Networks Based on Intracranial-EEG: An Update***
Rafeed Alkawadri

246 ***Median Nerve Stimulation Based BCI: A New Approach to Detect Intraoperative Awareness During General Anesthesia***
Sébastien Rimbert, Pierre Riff, Nathalie Gayraud, Denis Schmartz and Laurent Bougrain

frontiers in Neuroscience

EDITORIAL
published: 16 December 2020
doi: 10.3389/fnins.2020.598247

Editorial: Breakthrough BCI Applications in Medicine

Christoph Guger[1], Vivek Prabhakaran[2], Rossella Spataro[1,3], Dean J. Krusienski[4] and Adam O. Hebb[5]*

[1] g.tec medical engineering GmbH, Schiedlberg, Austria, [2] Radiology Department, University of Wisconsin-Madison, Madison, WI, United States, [3] University of Palermo, Palermo, Italy, [4] Biomedical Engineering, Virginia Commonwealth University, Richmond, VA, United States, [5] Knoebel Institute for Healthy Aging, University of Denver, Denver, CO, United States

Keywords: BCI, clinical applications, P300, motor imagery, EEG

Editorial on the Research Topic

Breakthrough BCI Applications in Medicine

SCOPE

A brain-computer interface (BCI) provides a direct connection between cortical activity and external devices. BCIs may use non-invasive methods such as the Electroencephalogram (EEG) or invasive methods such as the Electrocorticogram (ECoG) or neural spike recordings (Homer et al., 2013; Guger et al., 2015, 2018). In the last decades, many BCI approaches have been developed, based on slow waves, evoked potentials (EPs), steady-state evoked potentials (SSEPs), code-based EPs or motor imagery (MI) paradigms, with the aim of bringing medical applications that help people to the market. The first BCI systems were used to spell, control prosthetic devices, or move cursors on a computer screen (Guger et al., 2015; Allison et al., 2020). Early BCI work focused on locked-in or completely locked-in patients. Nowadays, many more clinical applications of BCIs technology are being developed.

RESEARCH HIGHLIGHTS

Several neurological disorders impair voluntary movements and communication, despite intact cognitive functioning. The spectrum of BCI usage for control is extremely wide and includes neural prostheses, wheelchairs (Fernández-Rodríguez et al.), home environments, humanoid robots, and much more (Fukuma et al.). Another exciting clinical application of BCIs focuses on facilitating the recovery of motor function after a stroke or spinal cord injury (Thompson et al.). BCIs for rehabilitation integrate BCIs with conventional methods and devices for rehabilitation like functional electrical stimulation (FES)-based neuroprostheses (Colachis et al.; Remsik et al.), transcranial direct current stimulation (tDCS) (Rodriguez-Ugarte et al.) etc. to enhance the brain's reorganization of corticospinal and cortico-muscular connections after acute, sub-acute, or chronic lesions.

Beside motor deficits, BCI-induced brain plasticity might contribute to the treatment of high-order cortical dysfunctions, such as improving social and emotional behaviors in autism spectrum disorder (Amaral et al.), training inhibitory control and working memory in ADHD, as well as contributing to the rehabilitation of cognitive deficits related to dementia. Moreover, BCI-based brain training can help preserve cognitive performance in healthy older adults, promoting successful aging and reducing the social burden of the population's increasing aging. BCIs are also used to establish closed-loop control of brain sensing and stimulation technology to

OPEN ACCESS

Edited and reviewed by:
Michele Giugliano, International School for Advanced Studies (SISSA), Italy

****Correspondence:***
Christoph Guger
guger@gtec.at

Specialty section:
This article was submitted to Neural Technology, a section of the journal Frontiers in Neuroscience

Received: *24 August 2020*
Accepted: *07 October 2020*
Published: *16 December 2020*

Citation:
Guger C, Prabhakaran V, Spataro R, Krusienski DJ and Hebb AO (2020) Editorial: Breakthrough BCI Applications in Medicine. Front. Neurosci. 14:598247. doi: 10.3389/fnins.2020.598247

improve, for example, tremor, or to provide sensation. Another new challenge described in this Research Topic refers to the inner speech detection, defined as the ability to generate internal speech representations, in the absence of any external speech stimulation or self-generated overt speech (Martin et al.).

Finally, BCIs may increase the diagnostic accuracy of brain disorders. For instance, BCIs could be used to detect neural signatures of cognitive processes in persons diagnosed with disorders of consciousness (DOC) (Annen et al.; Guger et al.; Heilinger et al.), provide real-time functional brain mapping for neurosurgery (Jiang et al.), improve visual function assessment in glaucoma, detect the intraoperative awareness during general anesthesia (Rimbert et al.), screening for cognitive function in complete immobility (Lulé et al.), etc.

SUMMARY

The articles here present different BCI approaches that could enter mainstream clinical practice, improving the assessment, rehabilitation, and management of several neurological diseases. All presented papers use elaborate, task-specific experiment setups with both invasive and non-invasive BCIs. Future research can build on these pioneering works and bring new standardized BCI applications in medicine.

AUTHOR CONTRIBUTIONS

CG wrote the editorial. All authors wrote the editorial.

REFERENCES

Allison, B. Z., Kübler, A., and Jin, J. (2020). 30+ years of P300 brain-computer interfaces. *Psychophysiology* 57:e13569. doi: 10.1111/psyp.13569

Guger, C., Kapeller, C., Ortner, R., and Kamada, K. (2015). "Motor imagery with brain-computer interface neurotechnology," in *Motor Imagery*, ed B. M. Garcia (Hauppauge, NY: Nova Science Publishers), 61–79.

Guger, C., Kapeller, C., Ogawa, H., Prückl, R., Grünwald, J., and Kamada, K. (2018). "Electrocorticogram based brain-computer interfaces," in *Smart Wheelchairs and Brain-Computer Interfaces*, ed P. Diez (Amsterdam: Elsevier), 197–227.

Homer, M. L., Nurmikko, A. V., Donoghue, J., and Hochberg, L. (2013). Sensors and decoding for intracortical brain computer interfaces. *Annu. Rev. Biomed. Eng.* 15, 383–405. doi: 10.1146/annurev-bioeng-071910-124640

Conflict of Interest: CG is CEO of g.tec.

The remaining authors declare that the research was conducted in the absence of any commercial or financial relationships that could be construed as a potential conflict of interest.

Copyright © 2020 Guger, Prabhakaran, Spataro, Krusienski and Hebb. This is an open-access article distributed under the terms of the Creative Commons Attribution License (CC BY). The use, distribution or reproduction in other forums is permitted, provided the original author(s) and the copyright owner(s) are credited and that the original publication in this journal is cited, in accordance with accepted academic practice. No use, distribution or reproduction is permitted which does not comply with these terms.

frontiers in Neuroscience

ORIGINAL RESEARCH
published: 27 February 2018
doi: 10.3389/fnins.2018.00110

Characterization of Hand Clenching in Human Sensorimotor Cortex Using High-, and Ultra-High Frequency Band Modulations of Electrocorticogram

*Tianxiao Jiang[1], Su Liu[1], Giuseppe Pellizzer[2], Aydin Aydoseli[3], Sacit Karamursel[4], Pulat A. Sabanci[3], Altay Sencer[3], Candan Gurses[5] and Nuri F. Ince[1]**

[1] Clinical Neural Engineering Lab, Department of Biomedical Engineering, University of Houston, Houston, TX, United States, [2] Research Service, Minneapolis VA Health Care System, Departments of Neurology and Neuroscience, University of Minnesota, Minnesota, MN, United States, [3] Department of Neurosurgery, Istanbul Faculty of Medicine, Istanbul University, Istanbul, Turkey, [4] Department of Physiology, Faculty of Medicine, Istinye University, Istanbul, Turkey, [5] Department of Neurology, Istanbul Faculty of Medicine, Istanbul University, Istanbul, Turkey

OPEN ACCESS

Edited by:
Dean Krusienski, Old Dominion University, United States

Reviewed by:
Martin Georg Bleichner, University of Oldenburg, Germany
Christian Herff, University of Bremen, Germany
Peter Brunner, Albany Medical College, United States

***Correspondence:**
Nuri F. Ince
nfince@uh.edu

Specialty section:
This article was submitted to Neural Technology, a section of the journal Frontiers in Neuroscience

Received: *25 September 2017*
Accepted: *13 February 2018*
Published: *27 February 2018*

Citation:
Jiang T, Liu S, Pellizzer G, Aydoseli A, Karamursel S, Sabanci PA, Sencer A, Gurses C and Ince NF (2018) Characterization of Hand Clenching in Human Sensorimotor Cortex Using High-, and Ultra-High Frequency Band Modulations of Electrocorticogram. Front. Neurosci. 12:110. doi: 10.3389/fnins.2018.00110

Functional mapping of eloquent cortex before the resection of a tumor is a critical procedure for optimizing survival and quality of life. In order to locate the hand area of the motor cortex in two patients with low-grade gliomas (LGG), we recorded electrocorticogram (ECoG) from a 113 channel hybrid high-density grid (64 large contacts with diameter of 2.7 mm and 49 small contacts with diameter of 1 mm) while they executed hand clenching movements. We investigated the spatio-spectral characteristics of the neural oscillatory activity and observed that, in both patients, the hand movements were consistently associated with a wide spread power decrease in the low frequency band (LFB: 8–32 Hz) and a more localized power increase in the high frequency band (HFB: 60–280 Hz) within the sensorimotor region. Importantly, we observed significant power increase in the ultra-high frequency band (UFB: 300–800 Hz) during hand movements of both patients within a restricted cortical region close to the central sulcus, and the motor cortical "hand knob." Among all frequency bands we studied, the UFB modulations were closest to the central sulcus and direct cortical stimulation (DCS) positive site. Both HFB and UFB modulations exhibited different timing characteristics at different locations. Power increase in HFB and UFB starting before movement onset was observed mostly at the anterior part of the activated cortical region. In addition, the spatial patterns in HFB and UFB indicated a probable postcentral shift of the hand motor function in one of the patients. We also compared the task related subband modulations captured by the small and large contacts in our hybrid grid. We did not find any significant difference in terms of band power changes. This study shows initial evidence that event-driven neural oscillatory activity recorded from ECoG can reach up to 800 Hz. The spatial distribution of UFB oscillations was found to be more focalized and closer to the central sulcus compared to LFB and HFB. More studies are needed to characterize further the functional significance of UFB relative to LFB and HFB.

Keywords: hybrid high-density grid, ECoG, ultra-high frequency band, hand movement, sensorimotor, postcentral shift

1. INTRODUCTION

Functional brain mapping is essential to improve the outcome of the neurosurgery by maximizing the excision while minimizing neurological deficits (Sanai and Berger, 2008; Chang et al., 2011). However, the mapping of the eloquent areas of the brain is a complex procedure due to the large variability of functional cortical organization between individuals (Brett et al., 2002; Farrell et al., 2007), as well as to the functional reorganization caused by brain injury, such as brain tumor (Dancause et al., 2005; Kong et al., 2016). As of today, direct cortical stimulation mapping (DCS) is still deemed as the gold standard in clinical practice. By directly injecting current to the cortical surface, DCS can either induce involuntary movement or suppress voluntary movement depending on the functional region (Brunner et al., 2009). However, some drawbacks of DCS are that it is time-consuming to adjust stimulation parameters, and test successively stimulation sites, and that it may induce spread of cortical activation that elicit seizures.

In the past decade, there has been a growing interest in the use of electrocorticogram (ECoG) to map functional areas without delivering electrical current to the cortex. By placing an electrode grid directly onto the cortex, it becomes possible to record oscillatory activity of the cortical circuits with unparalleled temporal and spatial resolution, as well as high signal quality. Previous work has shown that sensorimotor activity is associated with sub-band modulations of neural oscillations in the form of event-related desynchronization (ERD) in the alpha (7–13 Hz) and beta (13–32 Hz) bands and in the form of event-related synchronization (ERS) in the gamma band ranging from 40 to 200 Hz (Pfurtscheller and Lopes da Silva, 1999; Miller et al., 2007a). Recently it has been found that cognitive tasks related ECoG power modulations existed in an even broader band (60–500 Hz) (Gaona et al., 2011). High frequency band modulations are thought to be related to local neuronal processing while low frequency band changes are thought to reflect cortico-cortical, and cortico-subcortical interactions (Su and Ojemann, 2013). Although the exact physiological mechanisms underlying different subband modulations are yet to be elucidated, studies comparing ECoG functional mapping with DCS results generally showed that ERD in alpha and beta band were widespread and had low spatial specificity (Crone et al., 1998a; Leuthardt et al., 2007; Vansteensel et al., 2013). These clinical studies suggested that gamma band ERS correlated better with DCS in terms of specificity and sensitivity (Crone et al., 1998a). In recent years, ERS in gamma band has been proposed and successfully used for real-time functional mapping applications as well as brain machine interfaces (BMI) (Schalk et al., 2008; Miller et al., 2009, 2010; Hochberg et al., 2012; Branco et al., 2017).

Previous ECoG based functional brain mapping studies generally utilized regular clinical grid electrodes with large inter-electrode distance (1 cm) and small number of channels (<64) (Crone et al., 1998b; Aoki et al., 1999; Sinai et al., 2005; Leuthardt et al., 2007, 2012; Miller et al., 2007a,b, 2012; Schalk et al., 2008; Vansteensel et al., 2013). The frequency band of interest investigated in these studies were generally limited to 250 Hz. In this study, in order to map the hand function on the cortex, we recorded 113-channel high-density ECoG at 2.4 kHz from two patients with LGG while they performed voluntary hand clenching movements. There is ample evidence that these hand movements are controlled as a unit through motor synergies, rather than by individual control of fingers (Mason et al., 2001; Santello et al., 2013; Leo et al., 2016). We computed ECoG derived functional mapping in typical frequency bands of LFB and HFB. We also found that a small number of channels were associated with significant power modulations in an ultra-high frequency band ranging from 300 to 800 Hz. To the best of our knowledge, this is the first report showing that ECoG spectral modulations recorded from the hand area of the motor cortex can reach up to 800 Hz. These ultra high frequency modulations were found to be focally localized adjacent to the central sulcus, and close to the "hand knob" of the motor cortex (Yousry et al., 1997), and the DCS positive site. Moreover, in one of the patients, our ECoG based mapping results suggested that there had been a cortical reorganization of the hand motor function posterior to the central sulcus.

2. MATERIALS AND METHODS

2.1. Patients

Two right-handed male patients (P1 and P2) who were scheduled for resection of LGG requiring a craniotomy over the left motor and somatosensory brain areas were included in the study. Both patients gave informed consent before their participation to the study in accordance with the Declaration of Helsinki. The study protocol was reviewed and approved by the Institutional Review Boards (IRB) of Istanbul University, and of the University of Houston.

Functional mapping using intracranial electrodes were required to guide the resective surgeries since the tumor in both patients was in proximity to the motor cortex. A customized 113-channel hybrid electrode grid (INC electrode, CorTec GmbH) was used to map the border between the tumor and eloquent areas. The grid was positioned in a way to cover the border of the tumor and extend toward the "hand knob" of the primary motor area (M1). These hybrid ECoG grids have twice the density of typical clinical ECoG grids, which generally have 1 cm spacing between contacts, therefore providing higher spatial resolution. Specifically, the grid has 64 large contacts (MP35N nickel-cobalt alloy of 2.7 mm diameter, spaced every 1 cm) interlaced with 49 small contacts (platinum-iridium alloy of 1 mm diameter, spaced every 1 cm) and embedded in medical grade silicon rubber substrate (**Figure 3**). The spacing between adjacent small and large contacts is around 7 mm. The overall dimension of the electrode grid was $86 \times 80 \times 0.4$ mm.

The first patient (P1) was a 19 years old male who was initially diagnosed and operated for epilepsy at the age of 7. Histopathological investigations revealed a World Health Organization (WHO) grade II glioma (Louis et al., 2007). He received another operation 3 years prior to the current study. In this study, the patient was admitted to the clinic for a new onset of absence seizures which were resistant to antiepileptic drugs (oxcarbazepine 600 mg 3×1, levetiracetam 1,000 mg 3×1, topiramate 100 mg 3×1, lacosamide 100 mg 2 + 1 + 2). The preoperative and postoperative MRIs are provided in **Figure 1**. The head MRI indicated a recurrent left frontal tumor

adjacent to the motor cortex. The patient had no functional deficit postoperatively. However, although reduced, the patient was not seizure free at follow up of 1 year according to a routine neurological examination under his antiepileptic medical therapy.

The second patient (P2) was a 30 years old male who was admitted to the clinic due to right sided numbness affecting his hand for the previous 3 months. The head MRI (**Figure 2**) revealed a left posterior frontal cortico-subcortical tumor seated under the motor cortex. The determination of right hand weakness during surgery prompted its termination without further tumor resection (**Figure 2**). The patient had a postoperative right hand paresis that improved after 3 months. Pathological investigation revealed a WHO grade II glial tumor.

The clinical profiles of both patients and experiment information are shown in **Table 1**.

2.2. ECoG Recordings and Direct Cortical Stimulation

The ECoG recordings for patient P1 was carried out in the epilepsy monitoring unit (EMU) immediately after implantation of the ECoG grid for prolonged monitoring of seizure onset

TABLE 1 | Summary of subjects and experiments.

ID	Case	Sex	Age	HN[a]	LGG Site	Trials
P1	LGG, EP[b]	M[c]	19	Right	Left frontal	18
P2	LGG	M	30	Right	Left posterior frontal	30

[a] *Handedness.*
[b] *Epilepsy.*
[c] *Male.*

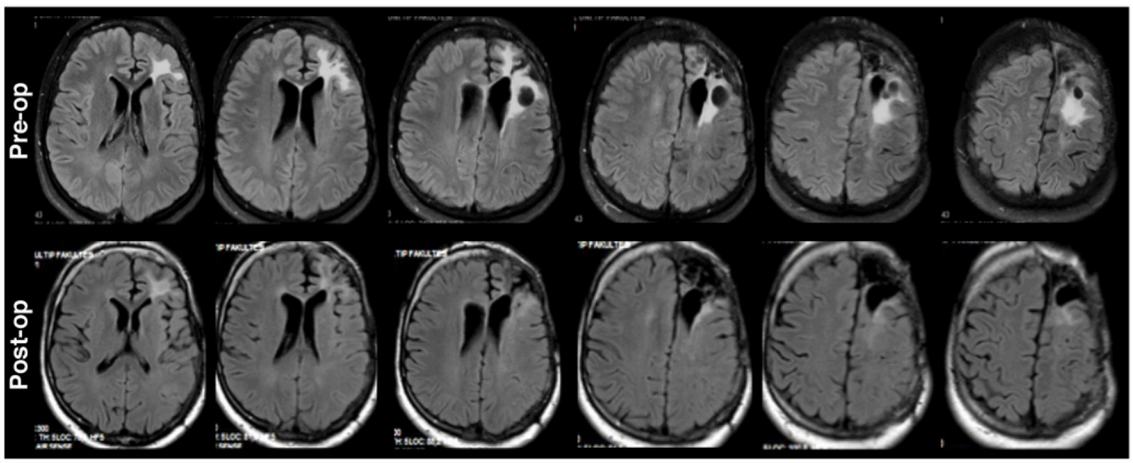

FIGURE 1 | Axial fluid-attenuated inversion recovery (FLAIR) brain MRI for P1 shown in radiological convention. Preoperative left frontal hyperdensities **(upper)** around the previous operation tumor space were reduced in size in postoperative MRI **(lower)**.

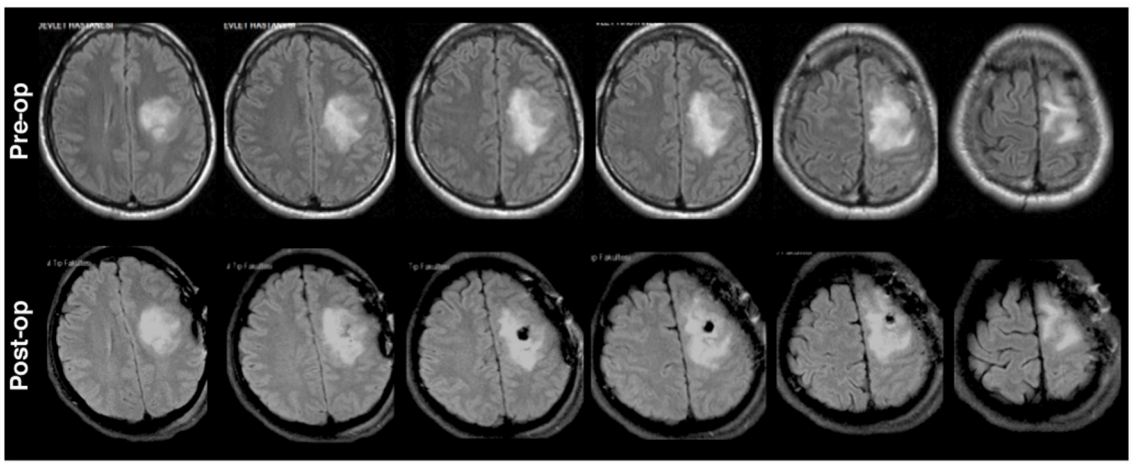

FIGURE 2 | Preoperative **(upper)** and postoperative **(lower)** axial MRI FLAIR sequences for P2. Surgery was terminated with incomplete resection due to determination of right hand weakness.

zone. For patient P2, ECoG recordings were performed in the operating room (OR) during awake-surgery to map and monitor the hand function throughout the resection. For both patients, ECoG data related to hand movements was obtained prior to DCS and surgical resection.

During the recordings, patients were asked to perform an alternate hand clenching and relax task. In each trial, subjects were instructed verbally to close the hand to a fist (i.e., hand clenching) and maintain this posture for around 2–3 s until instruction to relax. A resting period of at least 2 s was maintained between hand relaxation and the consecutive hand closing. ECoG, bipolar electrocardiogram (ECG), bipolar surface electromyogram (EMG) of the forearm flexor muscles, and hand movement data were recorded during the experiment with an in-house custom-made interface (Jiang et al., 2017b).

All biosignals including ECoG, bipolar ECG, and forearm EMG were recorded with a 256 channel bioamplifer gHIamp (g.tec medical engineering GmbH, Graz Austria) through an oversampling process at 2.4 kHz and 24 bit A/D resolution. To be more specific, the amplifier first digitized the signals at 614.4 kHz which is much higher than the required sampling frequency. Then, internally, the floating point digital signal processor (DSP) of the amplifier performed averaging of samples to increase the signal-to-noise ratio (SNR) and decimated the signal to the desired rate of 2.4 kHz.

The signal acquisition and real-time visualization was executed with a customized Simulink model (Matlab R2014a, Mathworks, Inc) and gHIsys real-time signal processing library (g.tec medical engineering GmbH, Graz Austria). The hand movements of both patients were recorded with a dataglove (DG5 VHand 3.0) and a high-definition webcam (Logitech HD C270). The finger positions and video frame-timestamp were recorded at 200 Hz with custom in-house software that we developed in C++ running under Windows 7 OS and transmitted over Ethernet via User Datagram Protocol (UDP) at 100 Mbits/s to the Simulink model (**Figure 3**). Video frame timestamps and finger position data were upsampled to 2.4 kHz for synchronization of neural data with behavioral data. Detailed system specifications can be found in our earlier publication (Jiang et al., 2017b).

Mapping of the hand area using DCS was performed on both patients after the ECoG recordings. Stimulation was conducted between pair of contacts with a current amplitude ranging from 1 to 15 mA, pulse width of 200–300 μs, and duration of 0.2 s, according to the patient;s individual tolerance. However, since both patients suffered from tumor related epilepsy, and DCS sometimes produced after discharges, the first site that elicited hand movements was labeled as DCS positive site. No additional stimulation was performed after that due to the risk of inducing seizures.

2.3. Electrode Localization and Relative Distance to Central Sulcus

Since the experiments were performed in the EMU for P1, postoperative CT after ECoG implantation and preoperative MRI were used to coregister the electrode positions. For P2, intraoperative photography and preoperative MRI were used instead for electrode localization as intraoperative CT was not available (Dalal et al., 2008; Gupta et al., 2014). For P1, CT+MRI coregistration and electrode segmentation were performed using Curry (version 7.0, Compumedics Neuroscan, Charlotte, NC, USA) by a trained neurologist. For P2, craniotomy photos were taken from the same position before and after the electrode placement. Each visible contact was manually segmented out and marked on the craniotomy picture taken before the electrode placement. Gray matter and white matter were automatically segmented out using SPM12 (Kiebel et al., 1997). The segmented volume was rendered in Matlab and visually compared with

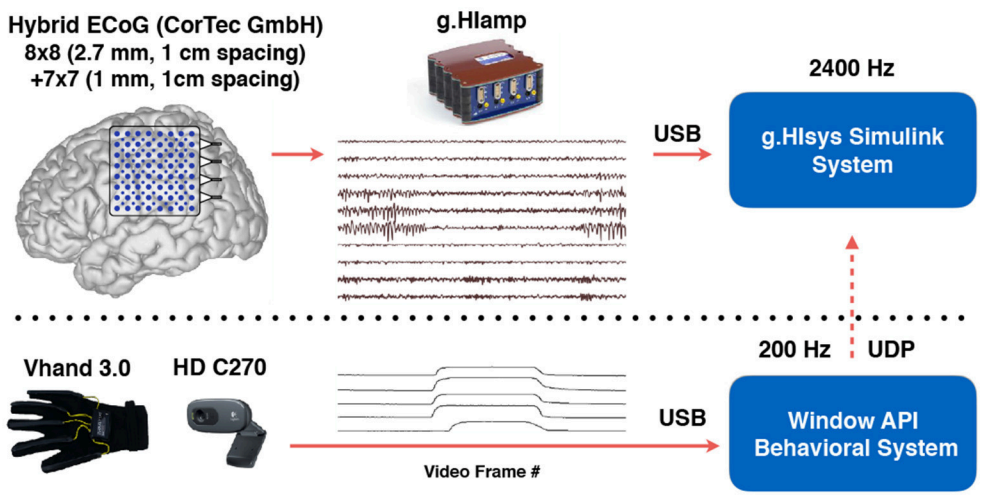

FIGURE 3 | Recording setup to collect ECoG and sensor data simultaneously. The layout of the custom hybrid ECoG grid with 113 channels was shown on a template brain surface. Video and hand position data were captured by the behavioral system and sent to g.HIsys Simulink system via UDP to synchronize with neural data (Jiang et al., 2017b).

the craniotomy picture. Landmarks such as blood vessels, sulci and gyri were used to co-register the electrodes from the photo and the rendered MRI volume. The positions of contacts that were not visually exposed were iteratively interpolated from the neighboring contacts (**Figure 4**). The photo based electrode localizations procedure was also performed for P1 and the result was compared with the CT+MRI based method for an estimate of concordance of the two methods.

To compute the relative distance between the electrodes and the central sulcus, the central sulcus outline was delineated on the individual MRI by a series of discrete points (**Figure 4I**). The continuous curve of the central sulcus was approximated by consecutive linear segments. The relative distance from each contact to the central sulcus was defined as the minimal Euclidean distance to all the linear segments.

2.4. Preprocessing

All data were scrutinized in Matlab, and corrupted channels were excluded from further analysis. Incomplete and noisy trials were also excluded by visually checking the neural and behavioral data with synchronized video recordings offline. Second-order Butterworth IIR notch filters with 2 Hz stop band were applied to eliminate the effect of 50 Hz power line noise and its harmonics. Movement onset from hand relaxed to clenched was determined using the minimum acceleration criterion with constraints (MACC) method (Botzer, 2009) on the dataglove data. The earliest movement onset detected among all five digits was used as the onset of hand clenching. We found that the output of the dataglove was more reliable than EMG to determine movement onset partly due to artifacts and occasional bursts of EMG that were not associated with hand movements, as could be verified from the video. An epoch of ECoG data, uncorrupted EMG, synchronized finger positions and movement onsets automatically determined using MACC is shown in **Figure 5A**. For selected trials with uncorrupted EMG, the onset of EMG signal was found to be 50 ms prior to the onset of the finger positions changes measured from the dataglove data (**Figure 5B**). To account for this delay, movement onset determined from the dataglove signal was shifted 50 ms earlier in the following analyses.

2.5. Time-Frequency and Power Spectral Density Analysis

For each channel, a time-frequency analysis was performed using short-time Fourier transform (STFT) on 3 s of ECoG data centered at each hand closing onset. Specifically, a 1,024-sample FFT was computed in each 1,024-sample Hanning window shifted with 90% overlap. Denoting movement onset as 0 s, each channel spectrogram (S_C) was computed by averaging across trials (S_A) and then normalized by the spectrum of the baseline period starting from −1.5 s and extending to −1 s (S_R). The normalized spectrogram (S_C) was transformed into dB scale:

$$S_C = 10 \times \log_{10} \frac{S_A}{S_R} \quad (1)$$

The normalized time-frequency maps (S_C) were visualized to investigate the ERD and ERS patterns in active channels of the electrode grid.

The power spectral densities of ECoG during baseline and hand close were estimated using Welch's method from 0.5 s of data segments. The baseline segment was the same as for the time-frequency analysis, while the hand movement segment was

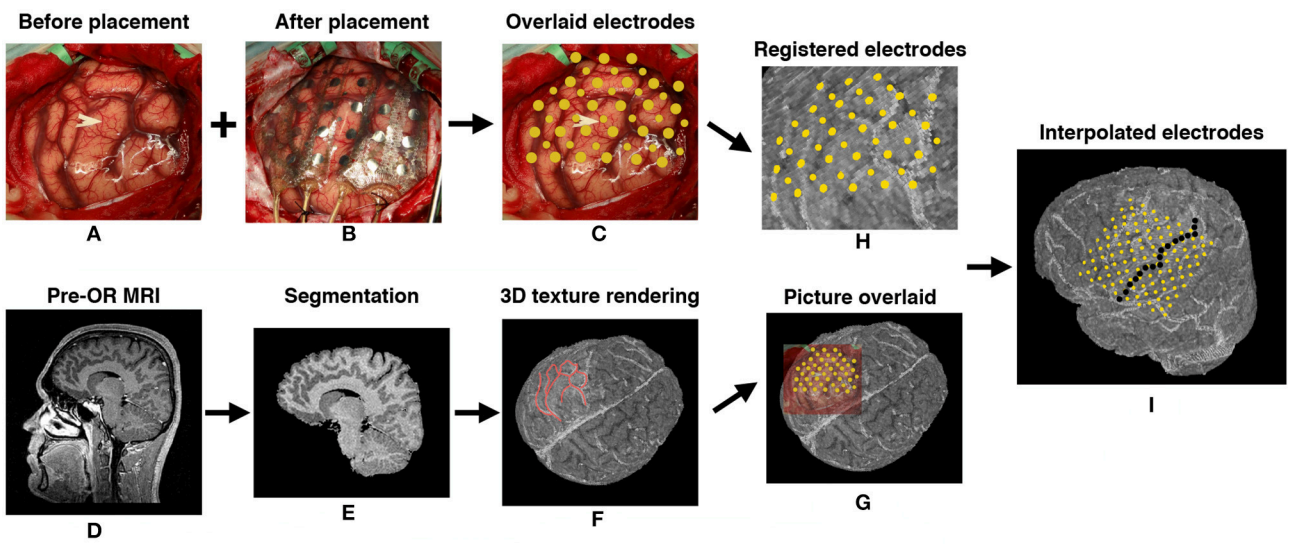

FIGURE 4 | Intraoperative photo based electrode registration procedure for P2. **(A)** Cortex photo before electrode placement. **(B)** Photo taken from the same position after electrode placement. **(C)** Electrodes (disks in gold) manually segmented out and overlaid on the cortex. **(D)** Patient's preoperative MRI. **(E)** Gray and white matter segmentation. **(F)** 3D texture rendering of gray and white matter. Blood vessels were accentuated by red lines as landmarks. **(G)** Picture overlaid on 3D rendering by comparing the landmarks. **(H)** Electrodes registered on 3D rendering of the brain. **(I)** The side view of the cortex with registered and interpolated electrodes, central sulcus was delineated by a series of discrete black points.

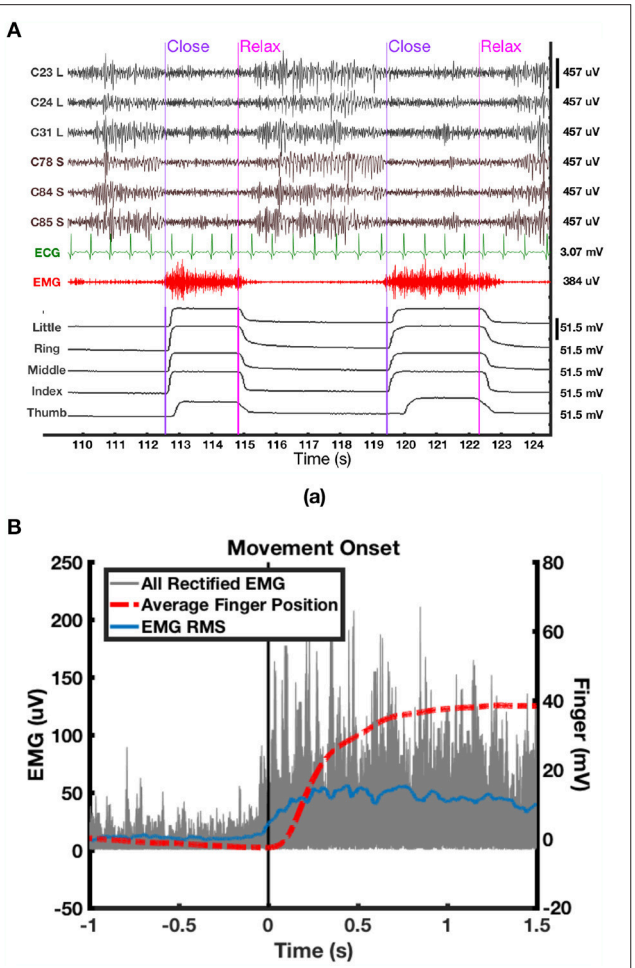

FIGURE 5 | (A) Synchronized epoch of data of ECoG, ECG, EMG, and finger positions data of P2. ECoG were high-pass filtered at 3 Hz, whereas EMG was high-pass filtered at 50 Hz for visualization. **(B)** Overlay of rectified EMG (gray) from uncorrupted trials, average of all five finger positions from the dataglove (red) and root mean square (RMS) average of rectified EMG (blue).

selected as −0.1 to +0.4 s to cover the movement initiation period. While the oversampling process executed by the amplifier provides exceptional SNR, the averaging step before decimation has a narrow band low-pass filtering effect where its passband response is not flat and has a droop. Consequently, the estimated power spectrum of ECoG does not have a visible flat noise floor and follows the magnitude response of the averaging filter which causes difficulties in the interpretation of the spectrum. In practice, in order to compensate the passband droop and obtain a flat passband response, an FIR filter is generally used after decimation (Lyons, 2004) with a magnitude response that is ideally an inverted version of the averaging filter passband response (Lyons, 2004). For this reason, we corrected the estimated spectrum with the inverted magnitude of the averaging filter in the passband.

Based on initial observations, the power spectral densities were estimated in two groups of channels for each patient: channels with ERS restricted in HFB and channels with ERS clearly extended to a higher frequency range.

Furthermore, we investigated three reactive frequency bands. The 8–32 Hz low frequency band (LFB); the 60–280 Hz high frequency band (HFB); and the 300–800 Hz ultra-high frequency band (UFB). The LFB was selected for its well-known movement-related ERD (Pfurtscheller and Lopes da Silva, 1999). The high frequency band (HFB) was selected to cover the high gamma activity where typically peri-movement ERS occurs (Miller et al., 2007a). In addition, we investigated an even higher frequency band at 300-800 Hz that manifested ERS during movements. We referred to this latter band as ultra-high frequency band (UFB) to distinguish it from the traditional high gamma range.

2.6. Spatial Patterns of LFB, HFB, and UFB and Relative Distance to DCS(+) Site

The movement-related spatial pattern of each frequency band from 0.1 s before movement onset (−0.1 s) to 0.4 s after it (+0.4 s) was obtained by computing the subband power ratio (R_p) between movement (P_m) and baseline (P_b) of individual channels and expressed in dB scale:

$$R_p = 10 \times \log_{10} \frac{P_m}{P_b} \tag{2}$$

The spatial matrices obtained from each channel's R_p in LFB, HFB, and UFB were interpolated by performing Delaunay triangulation (Lee and Schachter, 1980) on the registered electrode positions and visualized on the individual MRI rendering.

Channels were defined with significant ERD or ERS, when the change of power during hand clenching (R_p) was significantly >25% relative to baseline. The statistical significance of ERD in LFB, and ERS in HFB and UFB was tested using a one-tailed Student's t-test with a significance threshold p-value of 0.05 and corrected for multiple comparison by false discovery rate (FDR) method at the level of 0.05 (Genovese et al., 2002). For ERD, the alternative hypothesis (H_1) is $R_p < 0.75$ (−1.25 dB), while for ERS, H_1 is $R_p > 1.25$ (+0.97 dB). The sample population of the t-tests for each patient and channel was comprised of all hand clenching trials (P1: 18, P2: 30).

We also defined two metrics to compare DCS results and spatial patterns of different frequency bands. The distance between the peak activated electrode position of each subband and the DCS(+) site across the grid was defined as d_p. In addition, the distance between the activation map centroid for each subband and the DCS(+) site was defined as d_c. The map centroid was defined as the weighted summation of significant channel positions by the activation magnitude R_p of the subband. Both distance metrics were calculated on the 2D plane of the grid.

2.7. Early vs. Late ERS Onset

The temporal characteristics of the ERS across channels were studied by categorizing them into two groups, the early ERS group and the late ERS group. The early ERS group was determined by a significant power increase in HFB or UFB range using data segments from −0.5 to 0 s where 0 s represents

movement onset. While the late ERS group was determined by a significant power increase exclusively in the data segments from 0 to 0.5 s. In both cases, the baseline activity was selected from −1.5 to −1 s as before. The significances of HFB-ERS and UFB-ERS of each channel were tested using one-tailed Student's *t*-test ($p = 0.05$) with the null hypothesis that the power in each subband is equal to the baseline. To correct for multiple comparisons of channels, the Bonferroni correction was applied.

2.8. Small vs. Large Contact Groups

The power spectral densities for small and large contacts during baseline were estimated using Welch's method and averaged across each contact group. The ECoG noise floor of each channel was estimated using the band power within 800–1,000 Hz. The signal-to-noise ratio (SNR) in each band was computed from the ratio of the band power to the estimated noise floor. Channels with significant ERS in HFB were selected to compute the SNR in HFB and UFB between small and large contacts during both baseline and movement periods. In addition, the magnitude of ERD and ERS captured between small and large contacts were also compared within the selected HFB-ERS channels. A two-tailed Student's *t*-test with a *p*-value of 0.05 was used for significance test.

3. RESULTS

3.1. Power Spectral Density Estimation and Time-Frequency Analysis

The average power spectral density estimations and normalized time-frequency maps for channels with significant ERS in traditional high gamma band are shown in the first row of **Figure 6**. The compensated PSD clearly followed the 1/f nature of ECoG spectra and reached a noise floor after around 400 Hz in the baseline state. In the movement state, a visible noise floor was evident after 800 Hz. ERD covering a range including alpha and beta band (8–32 Hz) and ERS in traditional high gamma band (60–280 Hz) during hand movement can be clearly observed in the spectra and time-frequency maps of **Figure 6**. In addition, we observed that in a limited set of channels (i.e., 6 channels for P1 and 11 channels for P2), ERS presented itself in a broader frequency range (60–800 Hz) (second row of **Figure 6**). In order to differentiate the observed broad band ERS from traditional HFB-ERS, we further divided the broad band activity of 60–800 Hz into HFB and UFB. HFB was restricted within 60–280 Hz to be consistent with the high gamma frequency band modulations found in ours and others previous studies. UFB was selected to be above 300 Hz reaching up to 800 Hz. The lower bound of UFB

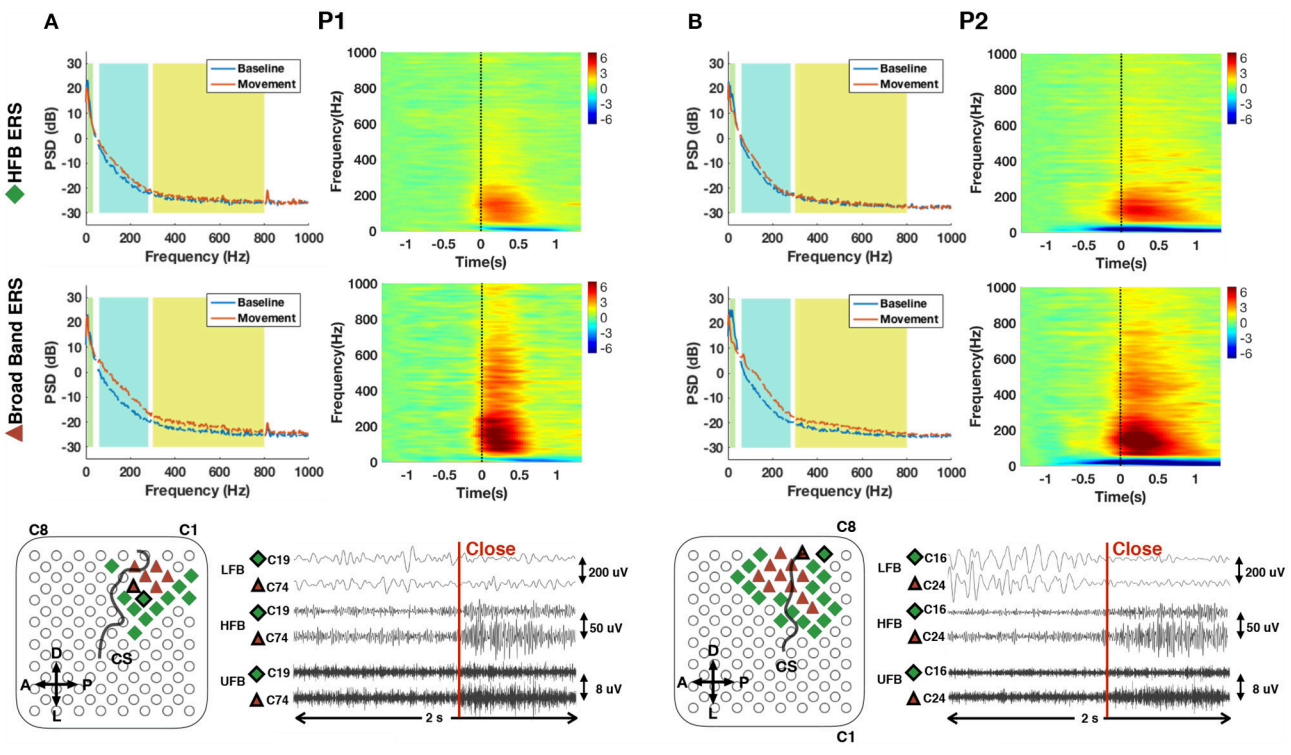

FIGURE 6 | Average power spectral density (PSD) and normalized time frequency maps of channels with exclusively significant HFB ERS (upper row) and broad band ERS (middle row) for P1 **(A)** and P2 **(B)**. LFB (8–32 Hz), HFB (60–280 Hz) and UFB (300–800 Hz) ranges are shaded in different background colors in the PSD plots. All time frequency maps were displayed from 6 to −6 dB. Channels with significant HFB ERS and broad band ERS are represented by green diamond and red triangle, respectively, on the grid of the bottom row. Central sulcus (CS) was marked by a black curve. Orientations were denoted by "A" (anterior), "P" (posterior), "D" (dorsal) and "L" (lateral). An epoch of 2 s of subband filtered signal around movement onset (close) from neighboring channels with different ERS characteristics is also shown at the bottom row for P1 (C19, C74) and P2 (C16, C24). The locations of the channel pairs are highlighted on the grid. The scale of each subband is provided on the right side of the data plot.

(i.e., 300 Hz) was at the "elbow" position in the power spectrum of hand movement (red). The channel positions associated with HFB-ERS (diamond) and UFB-ERS (triangle) are visualized in the bottom row of **Figure 6**.

According to the average time-frequency maps in **Figure 6**, it was observed that LFB-ERD in P1 initialized after movement onset, whereas LFB-ERD in P2 was observed at around 500 ms before movement onset. In addition, the absolute amplitude of LFB-ERD for P1 was smaller than ERS in HFB, whereas for P2 LFB-ERD was more prominent than HFB-ERS. It is also worthwhile to mention that although the hands of the patients were kept closed for 2–3 s during the task (**Figure 5**), the ERS in HFB or UFB generally vanished after 1.5 s following movement onset (**Figure 6**).

The bottom row of **Figure 6** shows raw subband filtered signals from two neighboring channels (C19, C74 for P1 and C16, C24 for P2) around hand movement onset. The corresponding channel positions were circled out in black on the grid. For P1, significant ERS in both HFB and UFB were observed in C74. However, there was only a significant ERS in HFB in the adjacent channel C19. Interestingly, for P1, ERD in LFB was weak despite clear ERS in HFB in some channels. For P2, both channels had clear ERD in LFB in addition to ERS in HFB. Similarly to P1, channel 24 had significant ERS in HFB and UFB, whereas the neighboring channel C16 had a significant ERS only in HFB. These results suggest that there was well delimited spatially localized activation in UFB.

3.2. Cortical Localization and Topographical Analysis of Subband Modulations

The ECoG grid localization was registered on the segmented 3D volume of the brain using a CT based method for P1 and a photo based method for P2 (**Figure 7**). For P1, intraoperative photo and postoperative CT based registration methods show concordant results on localizing the exposed electrodes relative to the central sulcus. ECoG spectral activity were mapped onto the individual brain surface using registered electrode locations. The ECoG grids were positioned to maximize the clinical requirements and partially covered the motor cortical "hand knob" for both patients.

The spatial distribution of significant modulation of ECoG subbands are visualized on the 3D cortical mesh in **Figure 7**. All spatial maps are displayed with power scale from −6 to +6 dB. The ECoG electrodes marked in white color in **Figure 7** represent channels with significant modulations in the respective subbands. The central sulcus is identified and accentuated by a black line on the figure. The DCS positive sites for hand function are also pointed out.

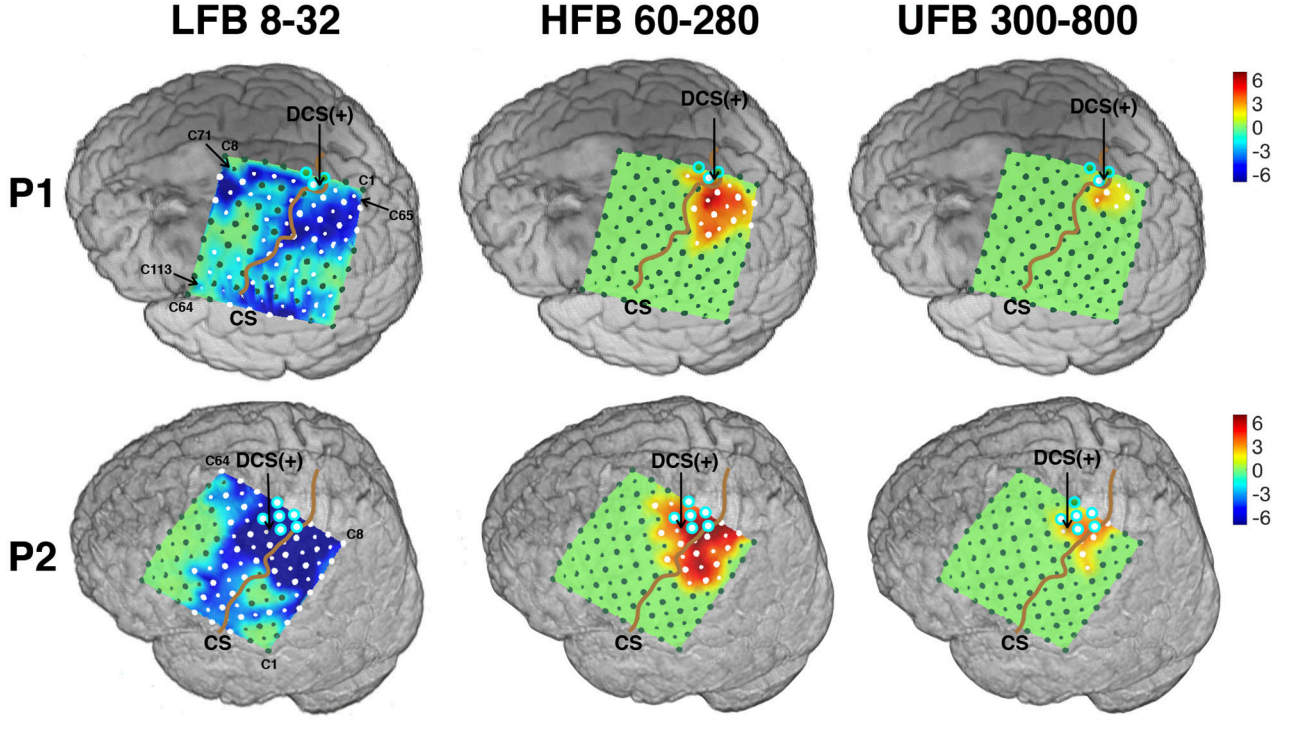

FIGURE 7 | Spatial spectral activities mapped onto subject's individual 3D MRI texture rendering. All maps were thresholded to reveal only channels with significant power changes of 25% or more (one tailed *t*-test, $p < 0.05$, $fdr < 0.05$). DCS (+) site for hand function was pointed out by an arrow for each subject. Contacts located on the "hand knob" were outlined in cyan. The central sulcus (CS) was accentuated by a brown curve. Significantly activated channels were marked as white. Peak activated channels (P) were also pointed out. The naming conventions of both large and small contacts are shown in the first map. All maps were displayed from −6 to 6 dB.

For each subband, the number of significantly activated channels anterior (N_a) and posterior (N_p) to the central sulcus are shown in **Table 2**. Compared to the traditional ERS in HFB, ERS in UFB was lower in magnitude (**Figure 6B**) and more focally localized in both subjects. For P1, 6 (5.3%) channels were associated with significant UFB-ERS, while there were 17 (15%) channels with significant HFB-ERS. More than half of channels (63) were associated with significant LFB-ERD. For P2, 11 (9.7%) channels were associated with significant UFB-ERS and 27 (23.9%) channels were associated with significant HFB-ERS. In addition, 66 (58.4%) channels exhibited significant LFB-ERD.

For P1, most of channels with significant ERS in HFB (15 over 17 in total) and UFB (5 over 6 in total) were posterior to the central sulcus which is presumed to be a somatosensory area. For P1 39 channels with LFB-ERD were distributed on the posterior side while 24 channels were on the anterior side. Significant modulations in all three subbands were found in one (C67) out of three contacts located on the "hand knob." The significant channel (C67) also appeared to be the closest to the DCS(+) site. Generally, the sensorimotor related activations in all three subbands for P1 were distributed posterior to the central sulcus, in contrast to the activations for P2.

The spatial organization of HFB and UFB ERS channels for P2 covered sensorimotor areas anterior and posterior to the central sulcus (**Figure 7**). Specifically, 13 out of 27 HFB-ERS channels and 6 out of 11 UFB-ERS channels were anterior to the central sulcus. For P2, 40 out of 66 channels associated with significant LFB-ERD were distributed on the anterior side. All six contacts covering the "hand knob" exhibited significant LFB-ERD and HFB-ERS while five of them exhibited significant UFB-ERS. The channel without significant UFB-ERS (C40) was at the anterior boundary of the precentral gyrus. The DCS(+) site was found slightly laterally to the anatomic "hand knob."

The left subplot of **Figure 8** illustrates the relative distance of significantly UFB-ERS contacts to the central sulcus on the MRI 3D rendering of P2. The distributions of average distances of ECoG mapping in LFB, HFB and UFB relative to the central sulcus (d_{cs}) are shown in the box plots on the right side of **Figure 8** and listed in detail in **Table 2**. The UFB modulated channels were consistently closer to the central sulcus compared to LFB and HFB modulated channels. Specifically, the average distance relative to central sulcus of significantly active UFB channels was 6 mm (±3.2 mm) for P1 and 5.7 mm (±4.1 mm) for P2. While the average distance of HFB modulated channels increased to 9.5 mm (±6.4 mm) and 8.6 mm (±6.1 mm) for P1 and P2, respectively. For both patients, the average distance of LFB modulated channels relative to central sulcus was greater than both HFB and UFB modulated channels.

The distance values of d_p and d_c of the spatial pattern of LFB, HFB, and UFB relative to DCS(+) sites are also given in **Table 2**. For P1, the channel with HFB-ERS peak was the same as for the UFB-ERS peak, which was recorded in C74. However, the distance between the centroid of the UFB map and the DCS(+) site (d_c) was smaller (9.0 mm) than the distance between the centroid of the HFB map and the DCS(+) site (14.4 mm). For P2, the peak of UFB-ERS was recorded in C31 while the peak of HFB-ERS was in C85. The latter was farther from the DCS(+) site compared to C31 (d_p: 3.5 vs. 12.7 mm). The centroid distance (d_c)

TABLE 2 | Distributions of spatial patterns relative to CS and DCS(+).

ID	LFB			HFB			UFB		
	N_a/N_p	d_{cs} (mm)	d_p/d_c (mm)	N_a/N_p	d_{cs} (mm)	d_p/d_c (mm)	N_a/N_p	d_{cs} (mm)	d_p/d_c (mm)
P1	24/39	17 ± 10.6	44.3/32.9	2/15	9.5 ± 6.4	12.7/14.4	1/5	6 ± 3.2	12.7/9.0
P2	40/26	14.5 ± 8.9	19.0/11.9	13/14	8.6 ± 6.1	10.6/8.9	6/5	5.7 ± 4.1	3.5/6.8

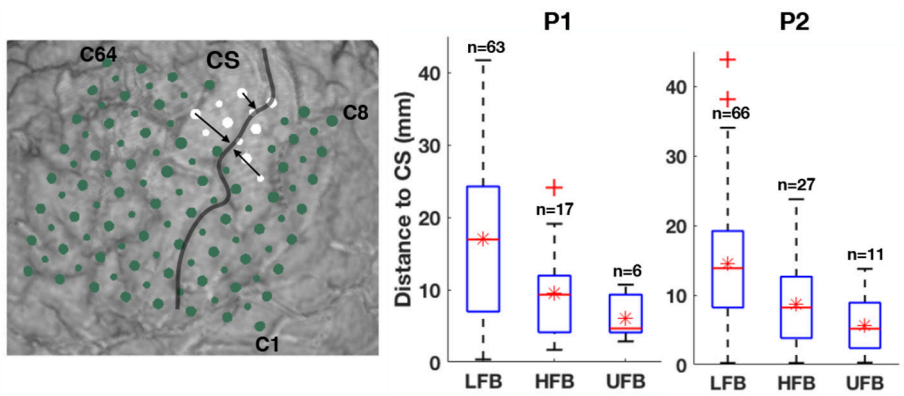

FIGURE 8 | The distances of significant UFB-ERS contacts relative to the central sulcus are partially denoted by black arrows on the MRI 3D rendering of P2 (left). Box and whisker diagram of relative distances to central sulcus (CS) in millimeter within significantly modulated channels in LFB, HFB, and UFB. Sample sizes are shown above the boxes. Red line denotes the median value. Red star denotes the mean value. Outliers of trials are marked as red crosses.

was also slightly smaller for UFB (9.5 mm) than for HFB (10.6 mm). For both patients, the LFB spatial pattern was even farther from the DCS(+) sites compared to HFB in terms of both d_p and d_c. In general, both peak distance and centroid distance revealed that UFB mapping was in closer proximity with the DCS(+) sites compared to HFB (**Table 2**).

3.3. Onset Timing Analysis of HFB and UFB ERS

Channels with early HFB-ERS (blue) and late HFB-ERS (red) are visualized on the first row of **Figure 9**. Time-frequency maps averaged in early and late HFB-ERS groups are also shown. Channels with significant ERS in UFB were excluded while averaging the time-frequency maps of HFB-ERS channels. For P1, five channels had an early HFB-ERS and were localized adjacent to the central sulcus on both anterior (C67, C68) and posterior (C88, C10, C11) sides. The channel (C67) located on the "hand knob" with significant modulations exhibited early HFB-ERS. For P2, 10 over 11 channels that exhibited early HFB-ERS were located on or anterior to the central sulcus. Four of the early HFB-ERS were located on the "hand knob." For both patients, most of the channels posterior to the central sulcus were associated with late HFB-ERS.

Channels with early UFB-ERS (blue) and late UFB-ERS (red) are visualized on the second row of **Figure 9**. Average time-frequency maps for the early and late UFB-ERS channels are shown on the right side. For P1, three channels exhibited early UFB-ERS. Specifically, C66 and C88 were posterior while C67 was anterior to the central sulcus and located on the "hand knob." In contrast, for P2, all five channels that exhibited early UFB-ERS were located anteriorly to the central sulcus, and four of those were located on the "hand knob." Most of the late UFB-ERS channels were posterior to the central sulcus. For both patients, early ERS in HFB and UFB generally appeared at the anterior channels of the activated region (**Figure 9**).

3.4. Small vs. Large Contact Groups

The average baseline PSD plots between small and large contacts for each patient are shown in **Figure 10**. For both subjects, the HFB band power was higher in small contacts (blue) compared to large contacts (red). The noise floor estimated from 800-1000 Hz of the spectrum for P1 was $1.86 \pm 0.16\ \mu V$ for small contacts (48 channels) and $1.83 \pm 0.15\ \mu V$ for large contacts (45 channels). For P2, the noise floor estimated was $1.62 \pm 0.25\ \mu V$ for small contacts (41 channels) and $1.53 \pm 0.23\ \mu V$ for large contacts (55 channels). For both subjects, although the statistical tests did not yield any significant difference between the noise floor of small and large contacts (P1: $p = 0.4$, P2: $p = 0.08$), the noise level tended to be higher in the smaller contacts.

The boxplot of SNR in HFB and UFB during baseline and movement between small and large contacts are shown in **Figure 11**. For P1, the average SNR was slightly higher in small contacts (9 channels) compared to large contacts (8 channels) in each band during both baseline (HFB: 17.4 > 16.8 dB, UFB: 1.33 > 1.25 dB) and movement (HFB: 18 > 15.7 dB, UFB: 1.86 > 1.34 dB). For P2, the average SNR was also higher in small contacts (11 channels) compared to large contacts (16 channels) during baseline (HFB: 14.9 > 12.8 dB, UFB: 1.05 > 0.65 dB) and movement (HFB: 18.5 > 17.2 dB, UFB 2.19 > 2.02 dB). However, the significance test did not yield any significant difference during both baseline (P1-HFB: $p = 0.15$, P1-UFB: $p = 0.2$, P2-HFB: $p = 0.39$, P2-UFB: $p = 0.69$) and movement (P1-HFB: $p = 0.2$, P1-UFB: $p = 0.31$, P2-HFB: $p = 0.69$, P2-UFB: $p = 0.58$).

The normalized time-frequency maps averaged between small and large contact groups with significant ERS in HFB are shown for both patients in **Figure 12**. All groups revealed ERS (red) in HFB and ERD (blue) in LFB. The results of ERD/ERS magnitude

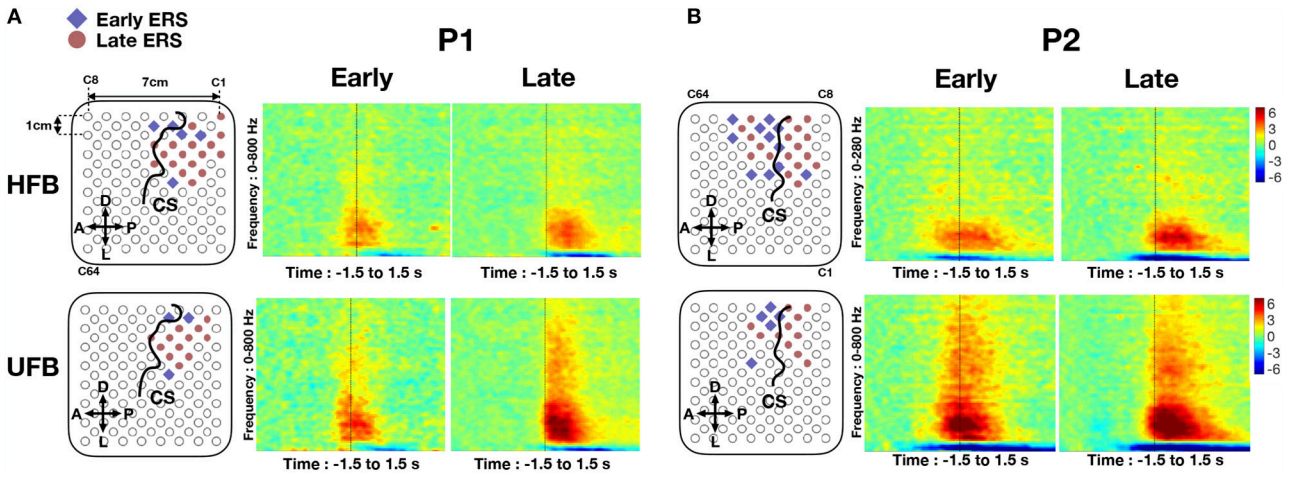

FIGURE 9 | (A) The early-ERS (blue diamond) and late-ERS (red circle) channel distributions on the grid and average time-frequency maps in HFB (top) and UFB (bottom) frequency range for P1. **(B)** Same analysis results for P2. Non significant channels were left as blank in the grid map. Central sulcus (CS) was denoted by a black curve. Orientations were denoted by "A" (anterior), "P" (posterior), "D" (dorsal) and "L" (lateral). The average time-frequency maps were visualized in a frequency range of 0–800 Hz and covered a period of −1.5 s to 1.5 s. All time-frequency maps were displayed in −6 to 6 dB.

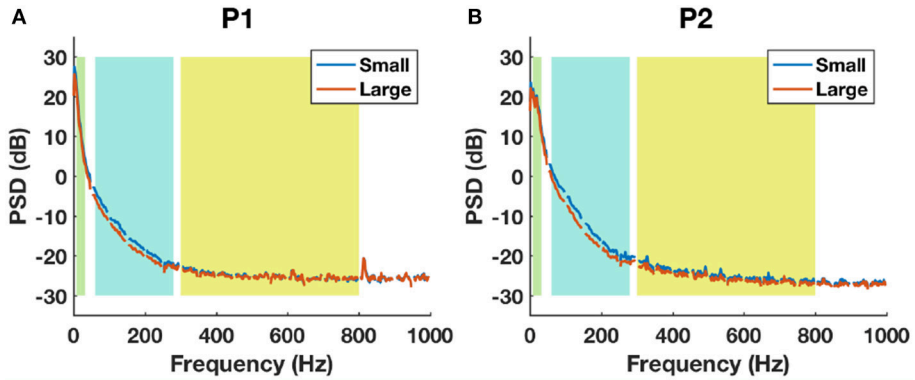

FIGURE 10 | The baseline power spectral density estimations between small (blue) and large (red) contact groups using all channels in P1 **(A)** and P2 **(B)**. Shaded backgrounds from left to right indicate respectively LFB, HFB, and UFB.

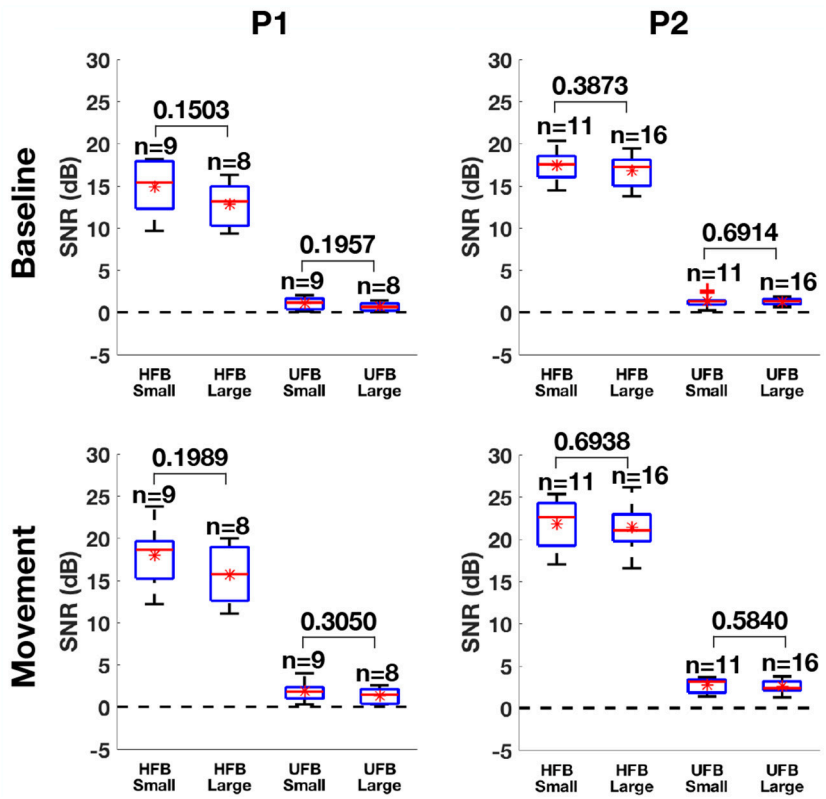

FIGURE 11 | The boxplots of SNR in HFB and UFB between small and large contacts for P1 **(left)** and P2 **(right)** computed from baseline (upper) and movement (bottom). The sample number of each group is displayed above the corresponding box. The *p*-value of two-tailed Student's *t*-test between small and large contacts is also shown. Red star denotes the mean value while the red band within the box denotes the median. The noise floor (0 dB) is represented by the horizontal dash line.

for each subband compared between small and large contact groups are provided in **Figure 12B**. The statistical tests did not yield any significant difference between small and large contacts in any of the frequency bands that we investigated [LFB (P1: $p = 0.17$, P2: $p = 0.67$); HFB (P1: $p = 0.88$, P2: $p = 0.57$); UFB (P1: $p = 0.44$, P2: $p = 0.92$)].

4. DISCUSSION

The frequency bands of interest in previous ECoG studies have generally been restricted at up to 250 Hz (Miller et al., 2007a,b; Leuthardt et al., 2012; Vansteensel et al., 2013). A recent study revealed that power modulations of up to 500 Hz were associated

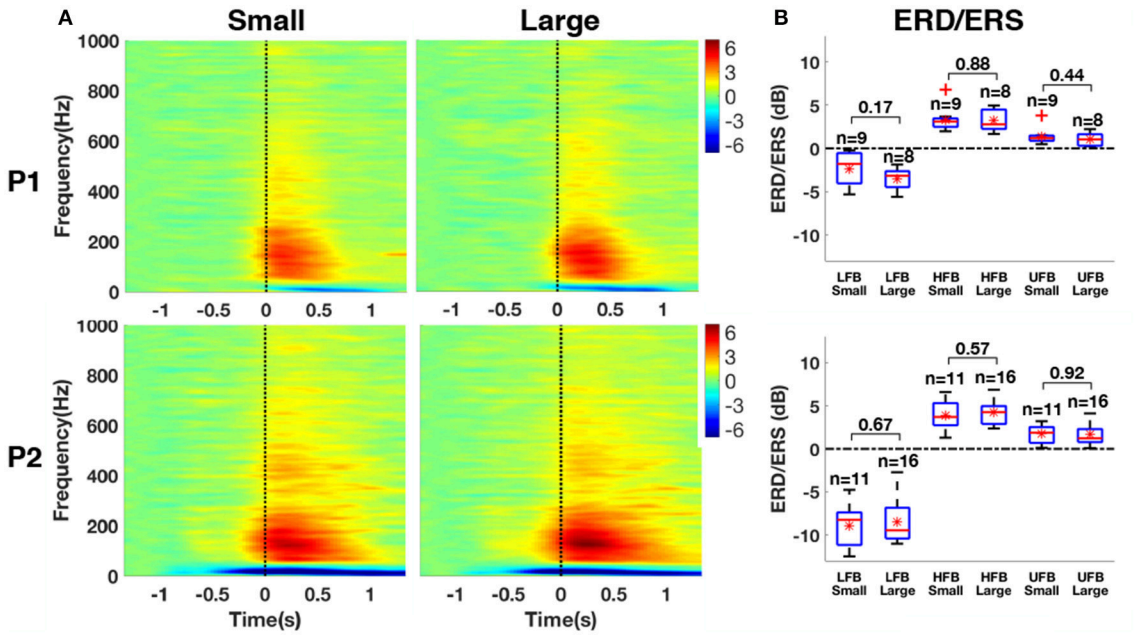

FIGURE 12 | (A) Average time-frequency maps between small and large contact groups with significant ERS in HFB. **(B)** Box-and-whisker plots of the magnitude of ERD in LFB, ERS in HFB, and ERS in UFB between small and large contact groups. Red asterisk denotes mean value, the red band within the box denotes the median and the outliers are represented by red plus signs.

with cognitive tasks (Gaona et al., 2011). In this study, ECoG was sampled at 2.4 kHz, which enabled us to study movement related spectral modulations of up to 1.2 kHz. The most important observation in this study is that in both patients ERS in ultra-high frequency of 300-800 Hz arose from a tightly localized cortical region close to the central sulcus. Although pathological high frequency oscillations (HFO) in epilepsy patients has been found to be reaching 800 Hz (de la Prida et al., 2015), the UFB found here was task-related and time-locked to movement onset. In addition, UFB oscillations lasted for several hundred milliseconds which is well beyond the typical duration of pathological fast ripples (<0.1 s) found in epileptogenic zones (Urrestarazu et al., 2007). Furthermore, no after-discharges were observed in the significant UFB-ERS channels for both patients during the ECoG recording phase. These points support the existence of non-pathological 300–800 Hz modulation of cortical activity related to hand movements. Due to the delimited spatially localized feature of UFB modulations, the typical clinical grids with large inter-electrode spacing might fail to capture them consistently.

The average time-frequency maps in **Figure 6** also revealed that both HFB and UFB modulations generally appeared at the beginning of the movement and gradually vanished after about 1.5 s even though the hand closure state was kept for 2–3 s. This correlation between ERS and the dynamic phase of movements has been observed in other ECoG studies of hand open/close movements (Jiang et al., 2017a), as well as of center-out reaching tasks (Ball et al., 2008). The spatial maps revealed that significant ERS in 300–800 Hz only occurred in a subset of electrodes with significant high gamma band ERS (60–280 Hz) (**Figure 7**). The distribution of UFB-ERS was closer to DCS(+) sites compared to HFB-ERS. However, since the DCS procedure was partially performed in this study due to after-discharges sometimes observed while stimulating the cortex, further studies with more comprehensive DCS procedures are required to test its correlation with UFB-ERS.

It is not yet conclusive as to which of these HFB- and UFB-ERS reflect motor activation or sensory feedback since they were localized on both sides of the central sulcus for both patients, and their modulation started either before or in coincidence with movement onset. Previous studies have shown that both primary motor cortex (M1) and somatosensory cortex (S1) were activated during attempted movements of individuals with spinal cord injury (SCI) (Cramer et al., 2005) or tetraplegia (Wang et al., 2013) as well as during motor imagery of able-bodied subjects (Porro et al., 1996; Lacourse et al., 2005). A recent ECoG BMI study also demonstrated that high decoding accuracy can be achieved on differentiating various hand gestures by using channels from S1 (Branco et al., 2017). For both patients in this study, most of the early-ERS channels were located at the anterior part of the activated region. However, the existence of early-ERS in HFB posterior to the central sulcus of P2 can be viewed as evidence of S1 activation in top-down movement preparation. There is still controversy as to whether pre-movement activations of S1 truthfully represent the top-down efference copy or merely reflect the somatosensory feedback of subtle muscle contractions before movement onset (Ryun et al., 2017).

Although the statistical test of SNR in HFB and UFB recorded by small and large contact groups during movement did not yield any significant difference, the small contacts were consistently associated with slightly higher average values in both subjects. This might indicate that small contacts has a slight advantage in detecting the high frequency rhythms compared to the large contacts. This could be due to the localized nature of high frequency rhythms of the cortical activity (Su and Ojemann, 2013). Statistical test of ERD/ERS in small and large contact groups did not yield any significance difference either. These results indicate that, in terms of ERD/ERS analysis, ECoG studies using a high-density grid with smaller contact size (Marathe and Taylor, 2013; Bleichner et al., 2014; Hotson et al., 2016; Wang et al., 2016; Jiang et al., 2017a) provide comparable information, in terms of time-frequency characteristics, as studies using standard larger clinical ECoG grids. It is also worthwhile to mention that UFB generally has much lower SNR than HFB during movements (**Figure 11**). This could lead to extra difficulty in detecting the UFB modulations. However, although small, the SNR of UFB oscillation in HFB-ERS channels (**Figure 7**) was still significantly higher than the noise level (0 dB) during both baseline and movement (one-tailed Student's t-test, $p < 0.05$). The oversampling process executed by the amplifier provides improved SNR in data acquisition which might have helped with the detection of ERS in UFB range. Nevertheless, besides the possibility of being generated by small cortical circuits, the localized spatial characteristic of UFB-ERS could also be due to its low SNR.

Motor functional reorganization has been extensively studied in stroke patients but less so in brain tumor patients. However, functional reorganization is more likely to occur in LGG patients than in stroke (Desmurget et al., 2007) and high-grade glioma (HGG) patients (Bryszewski et al., 2012) due to slowly growing tumor. In this study, the LFB-ERD, HFB-ERS, and UFB-ERS activation patterns for P1 were found mainly posteriorly to the central sulcus, in contrast to those for P2. Although, one channel (C67) on the "hand knob" of P1 remained active, the magnitude of its modulation was smaller compared to the posteriorly located channels. In addition, for P1 the majority of early HFB-ERS and early UFB-ERS were posterior to the central sulcus, again in contrast to those for P2. This posterior localization of motor-related activity for P1 probably results from a functional reorganization due to the combined factors of tumor progression and surgical resection (Seitz et al., 1995; Duffau, 2001; Bryszewski et al., 2012). This is consistent with other reports of postcentral shift of the hand motor function in LGG patients (Seitz et al., 1995). Consequently, we can surmise that the hand motor function area for P1 has reorganized posteriorly to the central sulcus through proliferation of novel, injury-induced corticocortical connections between the premotor and somatosensory cortex (Dancause et al., 2005). However, there was no obvious sign of functional reorganization under the brain area covered by the ECoG grid of P2. We assume that the history of previous tumor resection and of longer tumor progression for P1 since childhood elicited a greater brain functional reorganization than for P2.

Most functional reorganization studies so far were based on either fMRI (Bryszewski et al., 2012; Kurabe et al., 2016) or DCS (Duffau et al., 2002, 2003). Although deemed as the gold standard of functional mapping, DCS does not map functional motor behavior, and might induce seizures by injecting current to the cortex (Boulogne et al., 2016). On the other hand, fMRI is non-invasive and provides high spatial resolution. However, it indirectly estimates neuronal activity by measuring related hemodynamic changes and has poor temporal resolution (seconds). In comparison, ECoG can safely measure neuronal activity with high temporal resolution, whereas the spatial resolution is dependent on the density of the electrode grid. Unique spectral and temporal information related to functional activity can also be obtained from ECoG using dedicated signal processing techniques. As a result, ECoG functional mapping combined with robust electrode registration techniques could be a useful modality to complement existing techniques on both functional mapping and functional reorganizations studies. A better understanding of functional reorganization, especially in low-grade brain tumor patients, could improve the surgical outcome by maximizing the excision while preserving the reorganized functioning area.

5. CONCLUSIONS

In both patients, we were able to record movement-related ERD and ERS in multiple channels using a hybrid high-density ECoG grid. Consistently in both patients, ERS reached up to 800 Hz in a limited number of channels. To the best of our knowledge, this is the first time that ERS in an ultra-high frequency band up to 800 Hz of ECoG has been reported. In both patients, LFB-ERD was spatially broader compared to HFB- and UFB-ERS. We also explored the movement related patterns projected onto the individual MRI. We found that UFB-ERS observed around anatomic "hand knob" was more focally localized and resided closer to the central sulcus and DCS(+) sites than HFB-ERS. In addition, most of the sensorimotor-related cortical activation for P1 was found to be posterior to the central sulcus, in contrast to P2. This suggests a potential functional reorganization of the motor cortical functional area in P1. Finally, we did not find any significant difference between the task-related band power changes captured by the small and the large ECoG contacts.

This study has provided new understanding toward how the brain conveys information during functional hand motor tasks in terms of different frequency ranges of neural oscillatory activity. Also, we believe that the newly discovered UFB has great potential for increasing the precision of motor brain functional mapping. This unique wide band activity needs to be further explored in a larger population in our ongoing functional mapping and functional reorganization studies.

AUTHOR CONTRIBUTIONS

NI designed the study. NI, SL, AS, AA, SK, PS, and CG collected the data. TJ and NI conducted the analysis and TJ, NI, and GP wrote the manuscript and interpreted the results. AS, AA, SK, PS, and CG performed the surgeries, contributed to data collection,

imaging and DCS procedures and interpretation of the results. AS and CG performed the behavioral tests during surgery, evaluated the condition of subjects, and contributed to interpretation of the results. All authors reviewed the manuscript and approved the final version of the manuscript.

ACKNOWLEDGMENTS

We gratefully acknowledge Fatmanur Gunes for patient interactions, the assistance with the recordings and also the patients' cooperations in this study.

REFERENCES

Aoki, F., Fetz, E. E., Shupe, L., Lettich, E., and Ojemann, G. A. (1999). Increased gamma-range activity in human sensorimotor cortex during performance of visuomotor tasks. *Clin. Neurophysiol.* 110, 524–537. doi: 10.1016/S1388-2457(98)00064-9

Ball, T., Demandt, E., Mutschler, I., Neitzel, E., Mehring, C., Vogt, K., et al. (2008). Movement related activity in the high gamma range of the human EEG. *NeuroImage* 41, 302–310. doi: 10.1016/j.neuroimage.2008.02.032

Bleichner, M. G., Freudenburg, Z. V., Jansma, J. M., Aarnoutse, E. J., Vansteensel, M. J., and Ramsey, N. F. (2014). Give me a sign: decoding four complex hand gestures based on high-density ECoG. *Brain Struct. Funct.* 221, 203–216. doi: 10.1007/s00429-014-0902-x

Botzer, L. (2009). A simple and accurate onset detection method for a measured bell-shaped speed profile. *Front. Neurosci.* 3:61. doi: 10.3389/neuro.20.002.2009

Boulogne, S., Ryvlin, P., and Rheims, S. (2016). Single and paired-pulse electrical stimulation during invasive EEG recordings. *Revue Neurol.* 172, 174–181. doi: 10.1016/j.neurol.2016.02.004

Branco, M. P., Freudenburg, Z. V., Aarnoutse, E. J., Bleichner, M. G., Vansteensel, M. J., and Ramsey, N. F. (2017). Decoding hand gestures from primary somatosensory cortex using high-density ECoG. *NeuroImage* 147, 130–142. doi: 10.1016/j.neuroimage.2016.12.004

Brett, M., Johnsrude, I. S., and Owen, A. M. (2002). The problem of functional localization in the human brain. *Nat. Rev. Neurosci.* 3, 243–349. doi: 10.1038/nrn756

Brunner, P., Ritaccio, A. L., Lynch, T. M., Emrich, J. F., Wilson, J. A., Williams, J. C., et al. (2009). A practical procedure for real-time functional mapping of eloquent cortex using electrocorticographic signals in humans. *Epilepsy Behav.* 15, 278–286. doi: 10.1016/j.yebeh.2009.04.001

Bryszewski, B., Pfajfer, L., Antosik-Biernacka, A., Tybor, K., Śmigielski, J., Zawirski, M., et al. (2012). Functional rearrangement of the primary and secondary motor cortex in patients with primary tumors of the central nervous system located in the region of the central sulcus depending on the histopathological type and the size of tumor: examination by mean. *Polish J. Radiol.* 77, 12–20. doi: 10.12659/PJR.882576

Chang, E. F., Clark, A., Smith, J. S., Polley, M.-Y., Chang, S. M., Barbaro, N. M., et al. (2011). Functional mapping-guided resection of low-grade gliomas in eloquent areas of the brain: improvement of long-term survival. Clinical article. *J. Neurosurg.* 114, 566–573. doi: 10.3171/2010.6.JNS091246

Cramer, S. C., Lastra, L., Lacourse, M. G., and Cohen, M. J. (2005). Brain motor system function after chronic, complete spinal cord injury. *Brain* 128, 2941–2950. doi: 10.1093/brain/awh648

Crone, N. E., Miglioretti, D. L., Gordon, B., and Lesser, R. P. (1998a). Functional mapping of human sensorimotor cortex with electrocorticographic spectral analysis. II. Event-related synchronization in the gamma band. *Brain* 121(Pt 1), 2301–2315. doi: 10.1093/brain/121.12.2301

Crone, N. E., Miglioretti, D. L., Gordon, B., Sieracki, J. M., Wilson, M. T., Uematsu, S., et al. (1998b). Functional mapping of human sensorimotor cortex with electrocorticographic spectral analysis. I. Alpha and beta event-related desynchronization. *Brain* 121 (Pt 1), 2271–2299. doi: 10.1093/brain/121.12.2271

Dalal, S. S., Edwards, E., Kirsch, H. E., Barbaro, N. M., Knight, R. T., and Nagarajan, S. S. (2008). Localization of neurosurgically implanted electrodes via photograph-MRI-radiograph coregistration. *J. Neurosci. Methods* 174, 106–115. doi: 10.1016/j.jneumeth.2008.06.028

Dancause, N., Barbay, S., Frost, S. B., Plautz, E. J., Chen, D., Zoubina, E. V., et al. (2005). Extensive cortical rewiring after brain injury. *J. Neurosci.* 25, 10167–10179. doi: 10.1523/JNEUROSCI.3256-05.2005

de la Prida, L. M., Staba, R. J., and Dian, J. A. (2015). Conundrums of high-frequency oscillations (80-800 Hz) in the epileptic brain. *J. Clin. Neurophysiol.* 32, 207–219. doi: 10.1097/WNP.0000000000000150

Desmurget, M., Bonnetblanc, F., and Duffau, H. (2007). Contrasting acute and slow-growing lesions: a new door to brain plasticity. *Brain* 130(Pt 4), 898–914. doi: 10.1093/brain/awl300

Duffau, H. (2001). Acute functional reorganisation of the human motor cortex during resection of central lesions: a study using intraoperative brain mapping. *J. Neurol. Neurosurg. Psychiatry* 70, 506–513. doi: 10.1136/jnnp.70.4.506

Duffau, H., Capelle, L., Denvil, D., Sichez, N., Gatignol, P., Lopes, M., et al. (2003). Functional recovery after surgical resection of low grade gliomas in eloquent brain: hypothesis of brain compensation. *J. Neurol. Neurosurg. Psychiatry* 74, 901–907. doi: 10.1136/jnnp.74.7.901

Duffau, H., Denvil, D., and Capelle, L. (2002). Long term reshaping of language, sensory, and motor maps after glioma resection: a new parameter to integrate in the surgical strategy. *J. Neurol. Neurosurg. Psychiatry* 72, 511–516. doi: 10.1136/jnnp.72.4.511

Farrell, D. F., Burbank, N., Lettich, E., and Ojemann, G. A. (2007). Individual variation in human motor-sensory (rolandic) cortex. *J. Clin. Neurophysiol.* 24, 286–293. doi: 10.1097/WNP.0b013e31803bb59a

Gaona, C. M., Sharma, M., Freudenburg, Z. V., Breshears, J. D., Bundy, D. T., Roland, J., et al. (2011). Nonuniform high-gamma (60-500 Hz) power changes dissociate cognitive task and anatomy in human cortex. *J. Neurosci.* 31, 2091–2100. doi: 10.1523/JNEUROSCI.4722-10.2011

Genovese, C. R., Lazar, N. A., and Nichols, T. (2002). Thresholding of statistical maps in functional neuroimaging using the false discovery rate. *NeuroImage* 15, 870–878. doi: 10.1006/nimg.2001.1037

Gupta, D., Hill, N. J., Adamo, M. A., Ritaccio, A., and Schalk, G. (2014). Localizing ECoG electrodes on the cortical anatomy without post-implantation imaging. *NeuroImage Clin.* 6, 64–76. doi: 10.1016/j.nicl.2014.07.015

Hochberg, L. R., Bacher, D., Jarosiewicz, B., Masse, N. Y., Simeral, J. D., Vogel, J., et al. (2012). Reach and grasp by people with tetraplegia using a neurally controlled robotic arm. *Nature* 485, 372–375. doi: 10.1038/nature11076

Hotson, G., McMullen, D. P., Fifer, M. S., Johannes, M. S., Katyal, K. D., Para, M. P., et al. (2016). Individual finger control of a modular prosthetic limb using high-density electrocorticography in a human subject. *J. Neural Eng.* 13:026017. doi: 10.1088/1741-2560/13/2/026017

Jiang, T., Jiang, T., Wang, T., Mei, S., Liu, Q., Li, Y., et al. (2017a). Characterization and decoding the spatial patterns of hand extension/flexion using high-density ECoG. *IEEE Trans. Neural Syst. Rehabil. Eng.* 4320, 1–1. doi: 10.1109/TNSRE.2016.2647255

Jiang, T., Siddiqui, H., Ray, S., Asman, P., Ozturk, M., and Ince, Firat, N. (2017b). "A portable Platform to Collect and Review Behavioral Data Simultaneously with Neurophysiological Signals," in *Proceedings of 39th Annual International Conference of the IEEE Engineering in Medicine and Biology Society, EMBS* (Seogwipo), 1784–1787.

Kiebel, S. J., Ashburner, J., Poline, J. B., and Friston, K. J. (1997). MRI and PET coregistration–a cross validation of statistical parametric mapping and automated image registration. *NeuroImage* 5, 271–279. doi: 10.1006/nimg.1997.0265

Kong, N. W., Gibb, W. R., and Tate, M. C. (2016). Neuroplasticity: insights from patients harboring gliomas. *Neural Plasticity* 2016:2365063. doi: 10.1155/2016/2365063

Kurabe, S., Itoh, K., Nakada, T., and Fujii, Y. (2016). Evidence for cerebellar motor functional reorganization in brain tumor patients: an fMRI study. *Neurosci. Lett.* 622, 45–48. doi: 10.1016/j.neulet.2016.04.036

Lacourse, M. G., Orr, E. L. R., Cramer, S. C., and Cohen, M. J. (2005). Brain activation during execution and motor imagery of novel

and skilled sequential hand movements. *NeuroImage* 27, 505–519. doi: 10.1016/j.neuroimage.2005.04.025

Lee, D. T., and Schachter, B. J. (1980). Two algorithms for constructing a Delaunay triangulation. *Int. J. Comput. Inf. Sci.* 9, 219–242. doi: 10.1007/BF00977785

Leo, A., Handjaras, G., Bianchi, M., Marino, H., Gabiccini, M., Guidi, A., et al. (2016). A synergy-based hand control is encoded in human motor cortical areas. *eLife* 5:e13420. doi: 10.7554/eLife.13420

Leuthardt, E. C., Miller, K., Anderson, N. R., Schalk, G., Dowling, J., Miller, J., et al. (2007). Electrocorticographic frequency alteration mapping: a clinical technique for mapping the motor cortex. *Neurosurgery* 60, 260–270; discussion 270–271. doi: 10.1227/01.NEU.0000255413.70807.6E

Leuthardt, E. C., Pei, X.-M., Breshears, J., Gaona, C., Sharma, M., Freudenberg, Z., et al. (2012). Temporal evolution of gamma activity in human cortex during an overt and covert word repetition task. *Front. Human Neurosci.* 6:99. doi: 10.3389/fnhum.2012.00099

Louis, D. N., Ohgaki, H., Wiestler, O. D., Cavenee, W. K., Burger, P. C., Jouvet, A., et al. (2007). The 2007 WHO classification of tumours of the central nervous system. *Acta Neuropathol.* 114, 97–109. doi: 10.1007/s00401-007-0243-4

Lyons, R. G. (2004). *Understanding Digital Signal Processing*. 2 Edn., Upper Saddle River, NJ: Prentice Hall.

Marathe, A. R., and Taylor, D. M. (2013). Decoding continuous limb movements from high-density epidural electrode arrays using custom spatial filters. *J. Neural Eng.* 10:036015. doi: 10.1088/1741-2560/10/3/036015

Mason, C. R., Gomez, J. E., and Ebner, T. J. (2001). Hand synergies during reach-to-grasp. *J. Neurophysiol.* 86, 2896–2890. doi: 10.1152/jn.2001.86.6.2896

Miller, K. J., DenNijs, M., Shenoy, P., Miller, J. W., Rao, R. P. N., and Ojemann, J. G. (2007a). Real-time functional brain mapping using electrocorticography. *NeuroImage* 37, 504–507. doi: 10.1016/j.neuroimage.2007.05.029

Miller, K. J., Hermes, D., Honey, C. J., Hebb, A. O., Ramsey, N. F., Knight, R. T., et al. (2012). Human motor cortical activity is selectively phase-entrained on underlying rhythms. *PLoS Comput. Biol.* 8:e1002655. doi: 10.1371/journal.pcbi.1002655

Miller, K. J., Leuthardt, E. C., Schalk, G., Rao, R. P. N., Anderson, N. R., Moran, D. W., et al. (2007b). Spectral changes in cortical surface potentials during motor movement. *J. Neurosci.* 27, 2424–2432. doi: 10.1523/JNEUROSCI.3886-06.2007

Miller, K. J., Schalk, G., Fetz, E. E., den Nijs, M., Ojemann, J. G., and Rao, R. P. N. (2010). Cortical activity during motor execution, motor imagery, and imagery-based online feedback. *Proc. Natl. Acad. Sci. U.S.A.* 107, 4430–4435. doi: 10.1073/pnas.0913697107

Miller, K. J., Zanos, S., Fetz, E. E., den Nijs, M., and Ojemann, J. G. (2009). Decoupling the cortical power spectrum reveals real-time representation of individual finger movements in humans. *J. Neurosci.* 29, 3132–3137. doi: 10.1523/JNEUROSCI.5506-08.2009

Pfurtscheller, G., and Lopes da Silva, F. H. (1999). Event-related EEG/MEG synchronization and desynchronization: basic principles. *Clin. Neurophysiol.* 110, 1842–1857. doi: 10.1016/S1388-2457(99)00141-8

Porro, C. A., Francescato, M. P., Cettolo, V., Diamond, M. E., Baraldi, P., Zuiani, C., et al. (1996). Primary motor and sensory cortex activation during motor performance and motor imagery: a functional magnetic resonance imaging study. *J. Neurosci.* 16, 7688LP–7698LP.

Ryun, S., Kim, J. S., Jeon, E., and Chung, C. K. (2017). Movement-related sensorimotor high-gamma activity mainly represents somatosensory feedback. *Front. Neurosci.* 11:408. doi: 10.3389/fnins.2017.00408

Sanai, N., and Berger, M. S. (2008). Glioma extent of resection and its impact on patient outcome. *Neurosurgery* 62, 753–764; discussion 264–266. doi: 10.1227/01.neu.0000318159.21731.cf

Santello, M., Baud-Bovy, G., and Jörntell, H. (2013). Neural bases of hand synergies. *Fronti. Comput. Neurosci.* 7:23. doi: 10.3389/fncom.2013.00023

Schalk, G., Leuthardt, E. C., Brunner, P., Ojemann, J. G., Gerhardt, L. A., and Wolpaw, J. R. (2008). Real-time detection of event-related brain activity. *Neuroimage* 43, 245–249. doi: 10.1016/j.neuroimage.2008.07.037

Seitz, R. J., Huang, Y., Knorr, U., Tellmann, L., Herzog, H., and Freund, H. J. (1995). Large-scale plasticity of the human motor cortex. *Neuroreport* 6, 742–744. doi: 10.1097/00001756-199503270-00009

Sinai, A., Bowers, C. W., Crainiceanu, C. M., Boatman, D., Gordon, B., Lesser, R. P., et al. (2005). Electrocorticographic high gamma activity versus electrical cortical stimulation mapping of naming. *Brain* 128(Pt 7), 1556–1570. doi: 10.1093/brain/awh491

Su, D. K., and Ojemann, J. G. (2013). Electrocorticographic sensorimotor mapping. *Clin. Neurophysiol.* 124, 1044–1048. doi: 10.1016/j.clinph.2013.02.114

Urrestarazu, E., Chander, R., Dubeau, F., and Gotman, J. (2007). Interictal high-frequency oscillations (10-500 Hz) in the intracerebral EEG of epileptic patients. *Brain* 130, 2354–2366. doi: 10.1093/brain/awm149

Vansteensel, M. J., Bleichner, M. G., Dintzner, L. T., Aarnoutse, E. J., Leijten, F. S. S., Hermes, D., et al. (2013). Task-free electrocorticography frequency mapping of the motor cortex. *Clin. Neurophysiol.* 124, 1169–1174. doi: 10.1016/j.clinph.2012.08.048

Wang, P. T., King, C. E., McCrimmon, C. M., Lin, J. J., Sazgar, M., Hsu, F. P. K., et al. (2016). Comparison of decoding resolution of standard and high-density electrocorticogram electrodes. *J. Neural Eng.* 13:026016. doi: 10.1088/1741-2560/13/2/026016

Wang, W., Collinger, J. L., Degenhart, A. D., Tyler-Kabara, E. C., Schwartz, A. B., Moran, D. W., et al. (2013). An electrocorticographic brain interface in an individual with tetraplegia. *PLoS ONE* 8:e55344. doi: 10.1371/journal.pone.0055344

Yousry, T. A., Schmid, U. D., Alkadhi, H., Schmidt, D., Peraud, A., Buettner, A., et al. (1997). Localization of the motor hand area to a knob on the precentral gyrus. A new landmark. *Brain* 120, 141–157. doi: 10.1093/brain/120.1.141

Conflict of Interest Statement: The authors declare that the research was conducted in the absence of any commercial or financial relationships that could be construed as a potential conflict of interest.

Copyright © 2018 Jiang, Liu, Pellizzer, Aydoseli, Karamursel, Sabanci, Sencer, Gurses and Ince. This is an open-access article distributed under the terms of the Creative Commons Attribution License (CC BY). The use, distribution or reproduction in other forums is permitted, provided the original author(s) and the copyright owner are credited and that the original publication in this journal is cited, in accordance with accepted academic practice. No use, distribution or reproduction is permitted which does not comply with these terms.

frontiers in Neuroscience

ORIGINAL RESEARCH
published: 04 April 2018
doi: 10.3389/fnins.2018.00208

Dexterous Control of Seven Functional Hand Movements Using Cortically-Controlled Transcutaneous Muscle Stimulation in a Person With Tetraplegia

*Samuel C. Colachis IV[1,2,3], Marcie A. Bockbrader[2,3,4], Mingming Zhang[1], David A. Friedenberg[5], Nicholas V. Annetta[1], Michael A. Schwemmer[5], Nicholas D. Skomrock[5], Walter J. Mysiw[2,4], Ali R. Rezai[2], Herbert S. Bresler[1] and Gaurav Sharma[1]**

[1] Medical Devices and Neuromodulation Group, Battelle Memorial Institute, Columbus, OH, United States, [2] Neurological Institute, The Ohio State University, Columbus, OH, United States, [3] Department of Biomedical Engineering, The Ohio State University, Columbus, OH, United States, [4] Department of Physical Medicine and Rehabilitation, The Ohio State University, Columbus, OH, United States, [5] Advanced Analytics Group, Battelle Memorial Institute, Columbus, OH, United States

OPEN ACCESS

Edited by:
Christoph Guger,
Guger Technologies, Austria

Reviewed by:
An H. Do,
University of California, Irvine, United States
David Thomas Bundy,
Kansas University of Medical Center Research Institute, United States

***Correspondence:**
Gaurav Sharma
sharmag@battelle.org

Specialty section:
This article was submitted to Neural Technology, a section of the journal Frontiers in Neuroscience

Received: 25 September 2017
Accepted: 15 March 2018
Published: 04 April 2018

Citation:
Colachis SC IV, Bockbrader MA, Zhang M, Friedenberg DA, Annetta NV, Schwemmer MA, Skomrock ND, Mysiw WJ, Rezai AR, Bresler HS and Sharma G (2018) Dexterous Control of Seven Functional Hand Movements Using Cortically-Controlled Transcutaneous Muscle Stimulation in a Person With Tetraplegia. Front. Neurosci. 12:208. doi: 10.3389/fnins.2018.00208

Individuals with tetraplegia identify restoration of hand function as a critical, unmet need to regain their independence and improve quality of life. Brain-Computer Interface (BCI)-controlled Functional Electrical Stimulation (FES) technology addresses this need by reconnecting the brain with paralyzed limbs to restore function. In this study, we quantified performance of an intuitive, cortically-controlled, transcutaneous FES system on standardized object manipulation tasks from the Grasp and Release Test (GRT). We found that a tetraplegic individual could use the system to control up to seven functional hand movements, each with >95% individual accuracy. He was able to select one movement from the possible seven movements available to him and use it to appropriately manipulate all GRT objects in real-time using naturalistic grasps. With the use of the system, the participant not only improved his GRT performance over his baseline, demonstrating an increase in number of transfers for all objects except the *Block*, but also significantly improved transfer times for the heaviest objects (videocassette (*VHS*), *Can*). Analysis of underlying motor cortex neural representations associated with the hand grasp states revealed an overlap or non-separability in neural activation patterns for similarly shaped objects that affected BCI-FES performance. These results suggest that motor cortex neural representations for functional grips are likely more related to hand shape and force required to hold objects, rather than to the objects themselves. These results, demonstrating multiple, naturalistic functional hand movements with the BCI-FES, constitute a further step toward translating BCI-FES technologies from research devices to clinical neuroprosthetics.

Keywords: brain-computer interface, functional electrical stimulation, spinal cord injury, neuro-orthotics, functional hand grasping

INTRODUCTION

Approximately 130,000 people suffer a Spinal Cord Injury (SCI) worldwide every year. Nearly half of these SCI cases are at the C6 level or above, resulting in significant paralysis, impaired quality of life, and need for self-care assistance (ICCP, 2017). Moreover, patients with C6 or higher cervical level of SCI lack the critical ability to grasp objects that prevents them from living independently (Nas et al., 2015). Indeed, several studies on SCI patient priorities have consistently reported that upper limb strength and dexterity restoration is the most desirable function to regain (Anderson, 2004; Snoek et al., 2004; Simpson et al., 2012; Collinger et al., 2013; Blabe et al., 2015). In a survey of individuals with tetraplegia following SCI, more than 75% indicated that Functional Electrical Stimulation (FES) neuroprosthetics for hand grasp would be "very helpful" to restore function that would positively impact quality of life (Collinger et al., 2013). However, the FES systems that have been demonstrated to date are either limited to providing only a few hand functions or lack the ability to enable dynamic motor control for performing complex functional tasks that require synergistic integration of paralyzed and non-paralyzed muscles.

Advances in Brain Computer Interface (BCI)-controlled FES technology offers a potential new way to reconnect the brain directly to the paralyzed hand/arm, restoring functional hand use. FES devices with control mechanisms other than BCI (e.g., myoelectric, sip-and-puff, eye trackers) have been proposed, but are less desirable due to increased cognitive load and non-intuitive mapping between thought and action (Ajiboye et al., 2017). Thus, BCI approaches are preferred for their ability to provide a more intuitive and "high-fidelity" control signal that can allow for more complex and clinically-relevant functional limb movements (Chadwick et al., 2011; Ethier and Miller, 2015). Indeed, in recent surveys a majority of paralyzed patients showed interest in using a BCI technology that can help restore lost hand/arm function (Collinger et al., 2013; Blabe et al., 2015).

Several groups have investigated BCI-FES neuroprosthetics for restoring hand grasp function in paralyzed humans with varied success. Some groups have coupled an electroencephalogram (EEG)-BCI with FES systems and showed that the paralyzed participants were able to use the systems to enable up to two functional hand movements by imagining hand/arm movement (Müller-Putz et al., 2005) or by imagining a non-intuitive motion such as foot (Pfurtscheller et al., 2003) or cursor movement (Lauer et al., 1999). However, the low dimensional control signals of the EEG as well as non-intuitive mapping of thoughts-to-action makes it unlikely that these BCIs could provide naturalistic continuous control for complex hand functions. An alternative approach, utilizing electrocorticography (ECoG)-based signals, can provide better spatial resolution compared to EEG and thus a potential neuroprosthetic control mechanism based on high quality neural signals. Indeed, a paralyzed participant using an ECoG-BCI controlled transcutaneous FES system was successfully able to perform three movements (hand open, palmer, and lateral grasps) (Márquez-Chin et al., 2009). However, this demonstration was done in an offline mode where ECoG signals recorded from an able-bodied participant were used to control FES-evoked movements of the paralyzed participant. Therefore, the applicability of ECoG-BCI for real-time control of multiple hand movements via FES orthotics remains to be demonstrated. To overcome the limitations of EEG/ECoG control, researchers have implanted intracortical microelectrode arrays (MEAs) that can allow for higher information transfer rate (Baranauskas, 2014) and a more precise detection of movements for decoding and controlling hand/arm FES systems. In a prior study, we showed proof-of-concept that a person with C5-level paralysis could use a MEA-BCI to control a transcutaneous FES system to enable six independent finger, wrist, and hand movements (Bouton et al., 2016) We also demonstrated that the system could be used to perform a functional grasp-pour-and-stir task, providing the user with simultaneous, differential control of Hand Open, palmar grasp, and lateral key grip. A similar study showed proof-of-concept that a person with C4-level paralysis could use a MEA-BCI to control a hybrid exoskeleton and implanted FES system to evoke upper limb reaching, Hand Open, and lateral key grip (Ajiboye et al., 2017). The participant in this study used these movements to perform functional feeding tasks. However, no prior study has provided careful quantification and characterization of MEA-BCI enabled FES upper limb motor control to allow for study reproducibility and comparison with other neuroprosthetic devices.

In this study, we show a critical step in the clinic-to-home translational path of BCI-FES neuroprosthetics by demonstrating that a patient with tetraplegia can achieve volitional control of seven hand functions using an easy to train, cortically-controlled, non-invasive, FES orthotic. We used a MEA, implanted in the motor cortex of a 26-year old study participant with a C5-level SCI, to record neural signals. We then used machine learning algorithms to translate the neural activity to intended movement commands. These commands were then used to control the transcutaneous FES orthotic wrapped on the participant's forearm which stimulated the appropriate muscles to evoke the intended movement (**Figure 1**). With the system, the participant was able to use a trained decoder to volitionally select up to seven distinct functional hand states and use them to manipulate multiple objects of varying size, shape, and weight. The participant's functional gains were assessed using the Grasp and Release Test (GRT; Stroh-Wuolle et al., 1994), a standardized test developed for evaluating neuroprosthetic performance by patients with SCI. We found more efficient grasp and transfer of objects using the BCI-FES compared to the participant's baseline. Our results also revealed important insights into the neural representation of different hand movements. In particular, we observed that a robust mapping of multiple hand movements can form under the implanted MEA in a very small area of the motor cortex. We found overlap between representations for objects of similar size and weight and we report a strong correlation between the discriminability in the neural representations of hand movements and decoder performance.

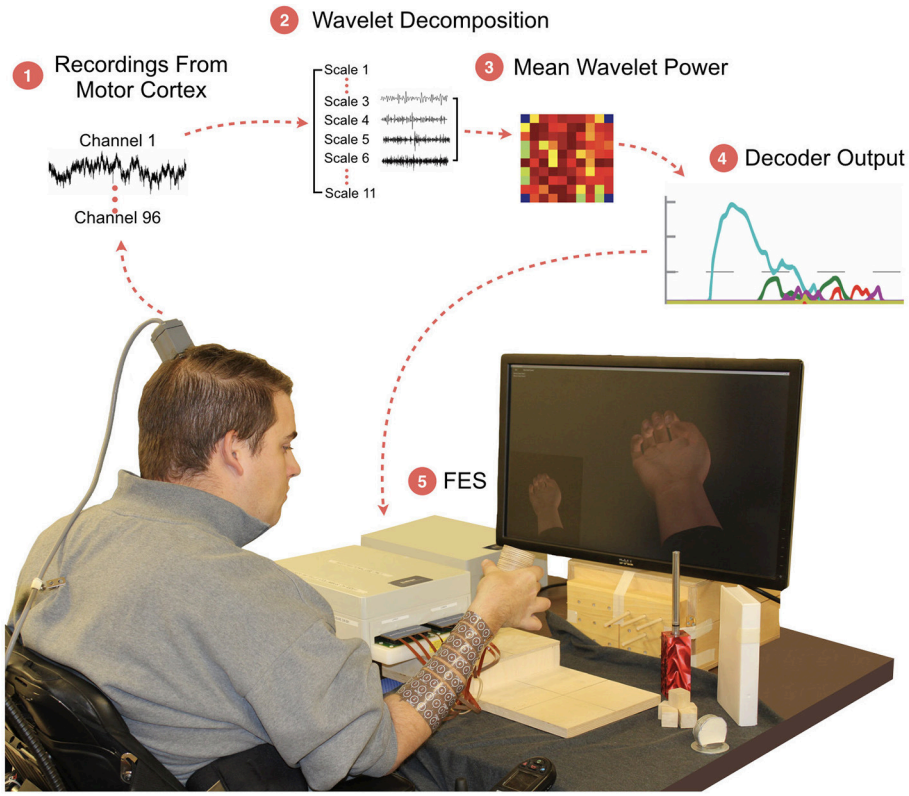

FIGURE 1 | The BCI-FES system and experimental setup. The participant sits on wheelchair in front of the monitor which shows him the cued hand movement. The participant is required to grasp and transfer the object to the raised platform. (1) Neural activity is recorded from a 96-channel MEA implanted in the motor cortex; (2) A wavelet decomposition is performed on the raw data to extract neural information related to motor intent; (3) Wavelet scales 3 through 6 are used to generate Mean Wavelet Power (MWP)-based neural features; (4) Machine-learning algorithms decode the MWP activity for each attempted hand movement; (5) Hand movement is evoked using targeted transcutaneous FES delivered through cuffs wrapped around the forearm.

MATERIALS AND METHODS

Study Design and Study Participant

The objective of this study was to characterize the level of upper limb motor control provided by a cortically controlled FES system in a patient with SCI. A secondary aim was to investigate the neural representations underlying grasps used for different objects. The study was approved by the US Food and Drug Administration (FDA) and The Ohio State University Wexner Medical Center Institution Review Board (Columbus, Ohio) and is registered on the ClinicalTrials.gov website (Identifier NCT01997125). The participant referenced in this work provided permission for photographs and videos and completed a written informed consent process prior to commencement of the study. The participant is a 26-year-old male with stable, non-spastic tetraparesis from a cervical SCI that he suffered at the age of 19. His use of the BCI-FES system was first reported in Bouton et al. (2016). The participant's International Standards for Neurological Classification of SCI neurologic level is C5 AIS A (motor complete) with zone of partial preservation to C6. He has full active range of motion in bilateral shoulders, full bilateral elbow flexion, a twitch of wrist extension (insufficient for tenodesis grip), and no motor function below the level of C6. His sensory level is C5 on the right (due to altered but present light touch on his thumb) and C6 on the left. He has intact proprioception in the right upper limb at the shoulder for internal rotation through external rotation, at the elbow for flexion through extension, at the forearm for pronation through supination, and at the wrist for flexion through extension. Proprioception for right digit flexion through extension at the metacarpal-phalangeal joints is impaired for all digits.

System Architecture

The system is comprised of three main components: (i) A Utah Microelectrode Array (MEA) implanted in the hand region (identified using preoperative fMRI activation maps) of the left-brain hemisphere motor cortex and a Neuroport neural data acquisition system (Blackrock Microsystem Inc., USA). **Figure 2A** shows the implant location in the motor cortex which was confirmed by co-registration of postoperative computed tomography (CT) imaging with preoperative fMRI. Full details of the fMRI and surgical procedures can be found in Bouton et al. (2016), (ii) a computer running data processing and machine learning algorithm to decode the user's intended movement from the neural activity, and (iii) A custom high-definition

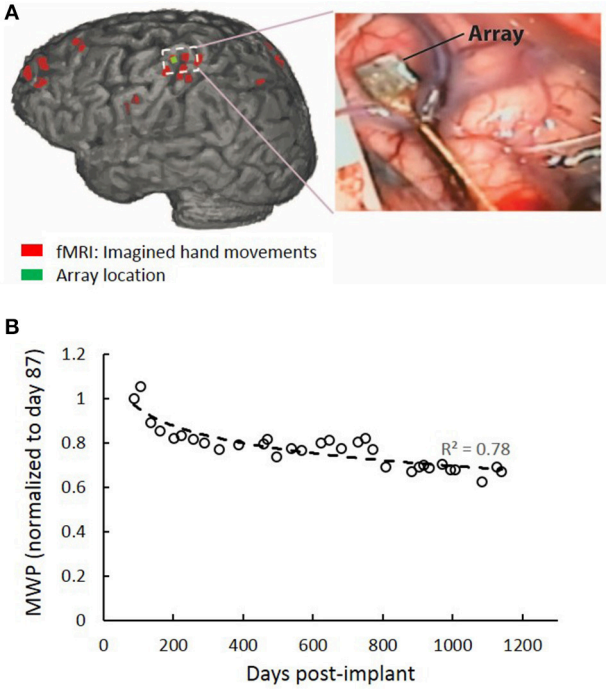

FIGURE 2 | MEA location and signal quality over time. **(A)** Red regions are brain areas active during imagined hand movements. The implanted MEA location from post-op CT is shown in green. **(B)** MWP data for all channels were collected over a 108 s period at the beginning of periodic test sessions where the participant was instructed to imagine cued hand movements. MWP features were calculated to approximate the power in the multiunit frequency bands a plotted as a function of post-implant days. A 33% decline in the signal quality was observed over time from the MWP data.

non-invasive FES system with 130 electrodes used to stimulate the hand/arm muscles to evoke desired hand movements. The stimulator was driven by custom MATLAB (ver 2014b, MathWorks Inc., USA) based code running on a PC.

Neural Data Acquisition and Signal Processing

The 96 MEA channels recorded the electrical activity in the cortex at a sampling rate of 30 kHz. The raw voltages were first filtered using a 0.3 Hz first-order high-pass filter and a 7.5 kHz third-order low-pass Butterworth analog hardware filter. Wavelet decomposition using the "db4" wavelet and 11 wavelets scales was applied to the neural data in 100 ms bins (Mallat, 1998). Wavelet scales 3–6 were used, corresponding to the multiunit activity (MUA) (234–3,750 Hz). The mean coefficients of scales 3–6 were standardized per channel, per scale, by subtracting the mean and dividing by the standard deviation of those scales and channels, respectively. The four scales were then combined by averaging the standardized coefficients for each channel, resulting in 96 values, one for each channel of the MEA, for every 100 ms of data. The resulting values were subsequently used as features, termed mean wavelet power (MWP), for input into the real-time decoders. Stimulation artifact in the data was removed by first applying a threshold at 500 μV that occurred simultaneously on at least 4 of 12 randomly selected channels. A 3.5 ms window of data encompassing each detected stimulation artifact was then removed and adjacent data segments were concatenated. To look at MWP signal quality over the study period, data for all channels were collected over a 108 s period at the beginning of periodic test sessions where the participant was instructed to imagine cued hand movements. MWP features were calculated to approximate the power in the multiunit frequency bands. We observed a 33% decline in the signal quality over time (**Figure 2B**).

Threshold crossings (TCs) were calculated by filtering the raw voltage recordings through a 250 Hz high pass filter, using the filtered data to determine the root-mean-square (RMS) value of the noise (defined by Blackrock Microsystems, Inc.), and then applying a threshold of −4.5 times the RMS of the noise to the voltage recording. The data was not spike sorted. Approximately 86 and 27 TC spikes could be detected on post-implant days 87 and 1,144, respectively, during the same 108 s test period as described above. Correlation between average MWP and TCs was calculated during the first 55 s of a representative training block. Average MWP was calculated by averaging MWP across channels. Global TCs were calculated by binning TCs for all channels in 100 ms bins.

Neural Decoding

A non-linear Support Vector Machine (SVM) decoder (Humber et al., 2010) was used to translate the MWP activity to intended hand movements. The decoder was trained in blocks consisting of multiple repetitions of all desired movements. Output classes were built for each movement and had scores that ranged from −1 to 1. Appropriate stimulation became activated when an output score of a given movement exceeded a threshold of zero. If multiple movement decoder output scores surpassed the threshold, the system enabled stimulation for the movement with the highest score. Individual movement accuracy was calculated from final training blocks as the percentage of 100 ms time points in which the decoder output for the given movement correctly matched the associated cue. Response probability for each cue (represented as a confusion matrix) was calculated from final training blocks as the percentage of activation for a single movement decoder class out of all active movement decoder classes within a cue. Individual movement accuracy scores and response probabilities were averaged across sessions of the same type. The final blocks of each training session were used for training the decoders. This was done to minimize the potential for muscle fatigue associated with repetitive FES of the same movements over a short period of time, which would have been required if we performed extra training blocks to measure decoder accuracy.

Stimulation

The FES system consists of a multi-channel stimulator and a flexible cuff with up to 130 electrodes that is wrapped around the participant's forearm. During use, hydrogel disks (Axelgaard, Fallbrook, CA) were placed between the electrodes and skin to act as a conduction enhancer. The electrodes are 12 mm in diameter and were spaced at 22 mm intervals along the longitudinal axis

of the forearm and 15 mm intervals in the transverse direction. Current-controlled, monophasic rectangular pulses (50 Hz pulse rate and 500 μs pulse width) were used to provide electrical stimulation. Pulse amplitudes ranged from 0 to 20 mA and were updated every 100 ms. Stimulator calibrations were performed for each movement using an anatomy-based trial-and-error method to determine appropriate electrode spatial patterns.

Experimental Design

The study sessions with the participant were typically conducted two or three times per week, lasting 3–4 h. Data used for this study were collected from eight sessions as follows: baseline GRT data on post-implant days 702 and 703; BCI-FES data on post-implant days 855, 857, 869, and 897; and imagined GRT data on post-implant days 1,042 and 1,043. The participant had prior experience using the BCI-FES system for other studies as reported in Bouton et al. (2016), Sharma et al. (2016), and Friedenberg et al. (2017). Sessions began with stimulation pattern calibrations for each hand movement. Stimulation patterns and intensity levels were saved in a database. In subsequent sessions with the participant, the previous calibrations were recalled and refined, if necessary. Calibrated movements included: (i) Index finger and thumb lateral key pinch for gripping a *Peg*, (ii) middle finger, index finger, and thumb tripod grip for gripping a *Block*, (iii) middle finger and thumb lateral key grip for gripping a *Paperweight*, (iv) ring finger and middle finger cylindrical power grip for gripping a depressible *Fork*, (v) tip-to-tip grip for gripping a videocassette (*VHS*), (vi) palmar power grip for gripping a *Can* (customized wooden cylinder), and (vii) finger and thumb extension (*Hand Open*) to open the hand. All objects used in this study conformed to specifications of the Grasp and Release Test (Stroh-Wuolle et al., 1994).

Neural Decoder Training

Training data for the decoder was obtained by prompting the participant to imagine performing specific hand movements using an animated virtual hand displayed on a computer monitor. During the cue duration, FES feedback allowed the participant to grasp the cued object in the starting area and transfer it to an elevated platform using the system. In the case of the *Fork* grip, the participant gripped the cylindrical handle of the *Fork* and applied downward pressure to displace a calibrated spring. Additionally, during cued *Hand Open*, the participant opened his hand by extending his digits. Each movement cue had a random duration between 3 and 4 s and was bounded by rest cues with random durations between 4 and 5 s. The ordering of the movement cues was randomly shuffled to eliminate cue anticipation. Each training block included 3 cues for each movement.

Grasp and Release Test (GRT) With FES

Functional grasps were assessed using the GRT (Stroh-Wuolle et al., 1994). The participant was presented with random, auditory cues for the different objects and was required to grasp the object in the starting area, lift and transfer the object to an elevated platform, and release the object in the target region as many times as possible in a 30 s test period. The participant was given a rest period of around 30 s between each 30 s test period. Dropping the object (or insufficient cylinder displacement for the *Fork*) was counted as a failure. The number of successful transfers, failed transfers, and incomplete transfers along with the associated transfer times for each object were recorded. For the *Fork*, successful "transfers" were counted if the spring-loaded piston was sufficiently displaced, indicated by a line on the piston. Two decoder classes were required for the *Can* transfer. The participant had to perform a *Hand Open* to position his hand in an optimal location around the *Can* and then initiate the *Can* grasp. During each cue, all movement decoder classes (seven possible) had equal potential to cross threshold and evoke FES stimulation. The GRT was performed 3 times per session for each object, with mean successful, failed and incomplete transfers reported per object and session. GRT testing was conducted over 4 sessions (for a total of 12 trials) for *Peg*, *Block*, *Paperweight*, *Fork*, and *VHS*. *Can* data was collected over 3 sessions (for a total of 9 trials). Test sessions were performed on post-implantation days 855, 857, 869, and 897.

GRT Without FES

To visualize the neural representation of hand movements in the motor cortex, MWP activity was examined during cued movements without any FES or movement feedback. Both movement and stimulation can create artifacts that can alter the MWP despite efforts to filter them. Thus, FES was turned off during the test blocks to remove the potential confounding effects of artifacts from the analysis. Three independent blocks of trials per object were conducted using decoders built as described in the Neural Decoder Training section in Methods, except that feedback was provided using only the animated hand and not FES. The subject was instructed to place his hand on the cued object and then imagine performing the grasp. This dataset was collected over 2 consecutive sessions (days 1,042, 1,043 post-implantation). The MWP spatial patterns were compared using a Principal Component Analysis (PCA) applied to the MWP on all 96 channels when the correct decoder outputs were above threshold and within the correct cue durations. Principal components 1 and 2 were used to determine clustering. Each cluster was fit with a Gaussian mixture distribution model for visualization purposes. For each movement, MWP was averaged across all blocks when the associated decoder was above threshold and within the correct cue duration. The average MWP at each channel was spatially mapped to the physical layout of the MEA and displayed as a heat map. Finally, to quantify the separation between MWP spatial patterns, Euclidian distances between each movement's vectorized spatial pattern were calculated. The MATLAB Pairwise Distance (pdist) function was used for this analysis. Euclidian distances for each movement compared to all others were summed to determine the amount of separation in neural representation.

Statistical Analysis

Paired comparisons between total number of transfers and object transfer times for the GRT were performed using a paired *t*-test. Correlations between MWP similarity and decoder performance was assessed using a linear regression model. Correlations

between TC and MWP were assessed using Pearson's correlation method. All statistical analyses were performed using MATLAB (ver 2014b) and $P < 0.05$ was considered statistically significant. Results are presented as Mean ± Standard Deviation (*SD*).

RESULTS

The cortically controlled FES system consisted of three main components: (1) an implanted 96-channel Utah MEA for recording neural signals, (2) a computer running data processing and a machine learning algorithm to decode the user's intended movement from the neural activity, and (3) a non-invasive FES cuff wrapped on the participant's forearm to stimulate the appropriate muscles to evoke the desired hand movement (**Figure 1**). Wavelet decomposition was used to process the raw cortical data into MWP neural features (see section Methods). These features were used as inputs to a SVM decoding algorithm that translated the neural activity to the user's intended movement, which was then used to control the electrical stimulation of the user's forearm (**Figure 1**). No device-related adverse events occurred during the duration of this study.

Performing Functional Hand Movements With High Accuracy

Using the BCI-FES system, the subject was trained to perform seven distinct functional hand movements that were specific to grasp, transfer, and release of standardized test objects. The objects conformed to specifications for the GRT (Stroh-Wuolle et al., 1994) and are described in **Figure 3**. The FES system was calibrated to evoke seven discrete, dynamic hand states which included a specific grasp for each of the six GRT objects and a *Hand Open* movement (see **Figure 3** for grasp schematics and **Figure S1** for stimulation parameters and targeted forearm muscles groups for enabling each hand movement).

During training, the participant received visual cues to initiate and terminate each hand movement interleaved with rest periods. **Figures 4A,B** shows a snapshot of the neural activity showing the MWP modulation and the corresponding threshold crossing (TC) neural activity raster plot. We observed a strong correlation between TC and MWP neural activity (correlation coefficient = 0.65, $p < 0.001$). The full set of MWP data was used as input for training and generating the neural decoder. **Figure 4C** shows representative decoder outputs during training as the participant attempted hand movements to manipulate the objects. When the decoder output for a particular movement crossed the zero threshold, the system initiated the FES to evoke the corresponding hand movement. The decoder was trained in 3-min blocks and it took 4–5 blocks of training (12–15 min of total training time) to generate a robust decoder set that could successfully classify seven hand movements for grasp, transfer, and release of different objects. **Movie S1** shows the participant manipulating the randomly cued objects during training. **Figure 4D** depicts the confusion matrix showing the probability of the decoder classifying each hand movement. The results indicate that, in general, the predicted hand movement was correctly classified as the cued hand movement. The grips for *Hand Open*, *Fork*, and *Can* were always predicted correctly with response probabilities of 1. However, the decoder had more difficulty discriminating between the *Peg*, *Paperweight*, and *Block* grips (response probabilities = 0.94, 0.91, and 0.90, respectively). Overall, across all trials, the individual accuracy for decoding each movement ranged from 96.3 ± 0.7% (*Paperweight*) to 99.0 ± 0.5% (*Hand Open*) demonstrating the system's ability to correctly classify the imagined movement from the eight possible hand states (seven hand movements and a rest) (**Table 1**).

Quantifying the Gains in Functional Performance Using the BCI-FES System

A board-certified physiatrist administered the GRT (see section Methods) to investigate the participant's ability to use the BCI-FES system to manipulate objects across a range of sizes, shapes, and weights. In addition to providing standardized test objects, the GRT also allowed us to compare the performance of our system with others' who have used this test to investigate their BCI-FES systems. **Figure 5A** shows representative snapshots of the participant transferring the *Can* object as part of the GRT. To complete one transfer, the participant used voluntary shoulder movements to align his hand above the *Can*, initiated a *Hand Open* movement to extend his fingers and position the *Can* in his palm, then initiated and maintained a palmar grasp while he transferred the *Can* laterally to a raised platform, and finally, terminated the grasp to release the object from his hand. **Movie S2** shows the participant manipulating the objects during one GRT block.

Figure 5B summarizes the participant's ability to manipulate GRT objects with and without use of the BCI-FES system. At baseline (Day 702–703 post-implant) and without the BCI-FES system, the participant could not efficiently manipulate (average number of successful transfers <1) the *Paperweight*, *Can*, *VHS,* and *Fork*. However, he was able to grasp and manipulate the *Block*, and *Peg* using adaptive grip strategies. With the BCI-FES system (days 855–897 post-implant), the participant was not only able to evoke the correct hand movement from the possible eight states available to him, but was also able to successfully grasp, transfer and release all objects and successfully depress the *Fork* multiple times in the 30 s test period. In general, with the use of the system, the number of successful (failed) transfers increased (decreased) over baseline (See **Figure S2** showing total number of failed transfer attempts with and without the use of the system). The *Block* was an exception, where the participant had fewer successes with the BCI-FES system than without, as the participant was able to use an adaptive grasp to transfer the *Block* on his own. In addition to being able to rapidly transfer the *Paperweight* (transfer time = 4.7 ± 1.2 s) and displace the *Fork* (displacement time = 5.1 ± 1.1 s) with the BCI-FES system, which he was otherwise not able to do on his own without the system, the participant also showed significant improvement in transfer times with the system for the other two heavier objects, i.e. the *VHS*, and *Can* (**Figure 5C**). However, it took the participant significantly longer to complete the *Block* transfer with the BCI-FES system (6.4 ±

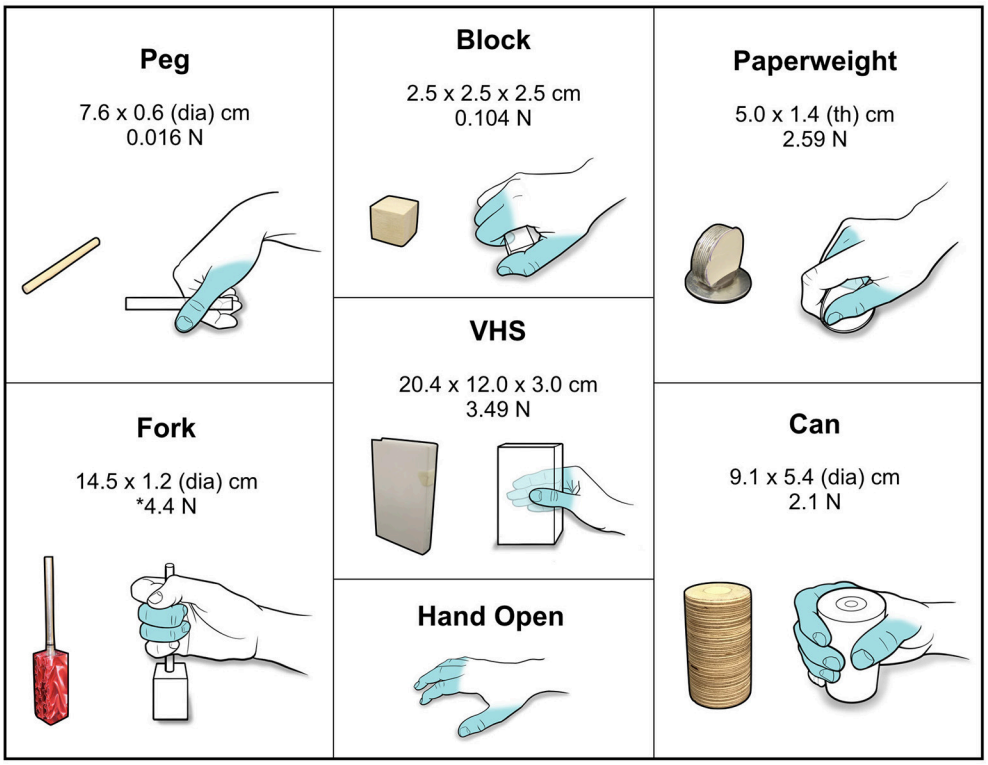

FIGURE 3 | Standardized GRT objects and functional grasps. Schematic showing the different GRT objects with associated dimensions and weights. Hand schematics illustrate the grasp/movement enabled by FES for the object. Fingers that were activated and used to perform the grasps/movements are highlighted in blue. *For the *Fork* object, a 4.4 N force is required to depress the cylinder.

3.0 s per *Block*) than without (2.8 ± 1.0 s per *Block*), while there was no significant change in the completion time for the *Peg* transfer.

Investigating the Correlation Between Neural Discriminability and Decoder Performance

As the participant performed the GRT, we observed a few instances of decoder misclassification. In particular, the decoder would sometimes trigger the *Paperweight* grip when the participant tried to release the *Block*. Similarly, the *VHS* grip was sometimes evoked during the *Can* release. **Figure 6** shows a representative decoder output plot from an entire GRT test block that provides examples of decoder misclassification. The participant was cued to transfer the *Block* beginning at 170 s. While the *Block* grip was correctly triggered for each of the transfers, the *Paperweight* grip was also incorrectly evoked 4 out of 5 times after the *Block* grip (see **Movie S2** which shows the *Block* transfers during this test period).

To further investigate these decoder misclassifications, we analyzed the neural modulation as the participant was asked to imagine the seven cued hand movements without FES (see section Methods). By not using the FES system, the neural modulation data we captured was free from stimulation and/or any movement induced artifacts. We applied a PCA to the MWP neural data to qualitatively illustrate clustering among different imagined hand movements (**Figure 7A**). We observed overlaps between the MWP clusters for the *Paperweight* and *Block* as well as the *VHS* and *Can*. **Figure 7B** shows the heat map of the average MWP for each imagined hand movement overlaid on the physical layout of the 96-channel cortical array showing the spatial distribution of MWP activity between different hand movements. To measure the discriminability of neural representations of different hand movements we computed the Euclidean distances between the MWP spatial distributions for all hand movements (**Figure 7C**). We found that the neural representation for the imagined *Paperweight* and *Block* grips as well as the *VHS* and *Can* grips were the most similar and might be one of the factors causing the decoder misclassifications observed during the GRT functional task. When compared to the results of the neural decoder training for the GRT task, we also observed a strong correlation ($R^2 = 0.74$, $p < 0.05$) between the individual decoder accuracy scores and the discriminability of neural representation of hand movements (**Figure 7D**). *Hand Open* movement had the most distinct neural representation and the highest individual movement accuracy while the *Paperweight* grasp had the least separated neural representation and the corresponding lowest movement accuracy.

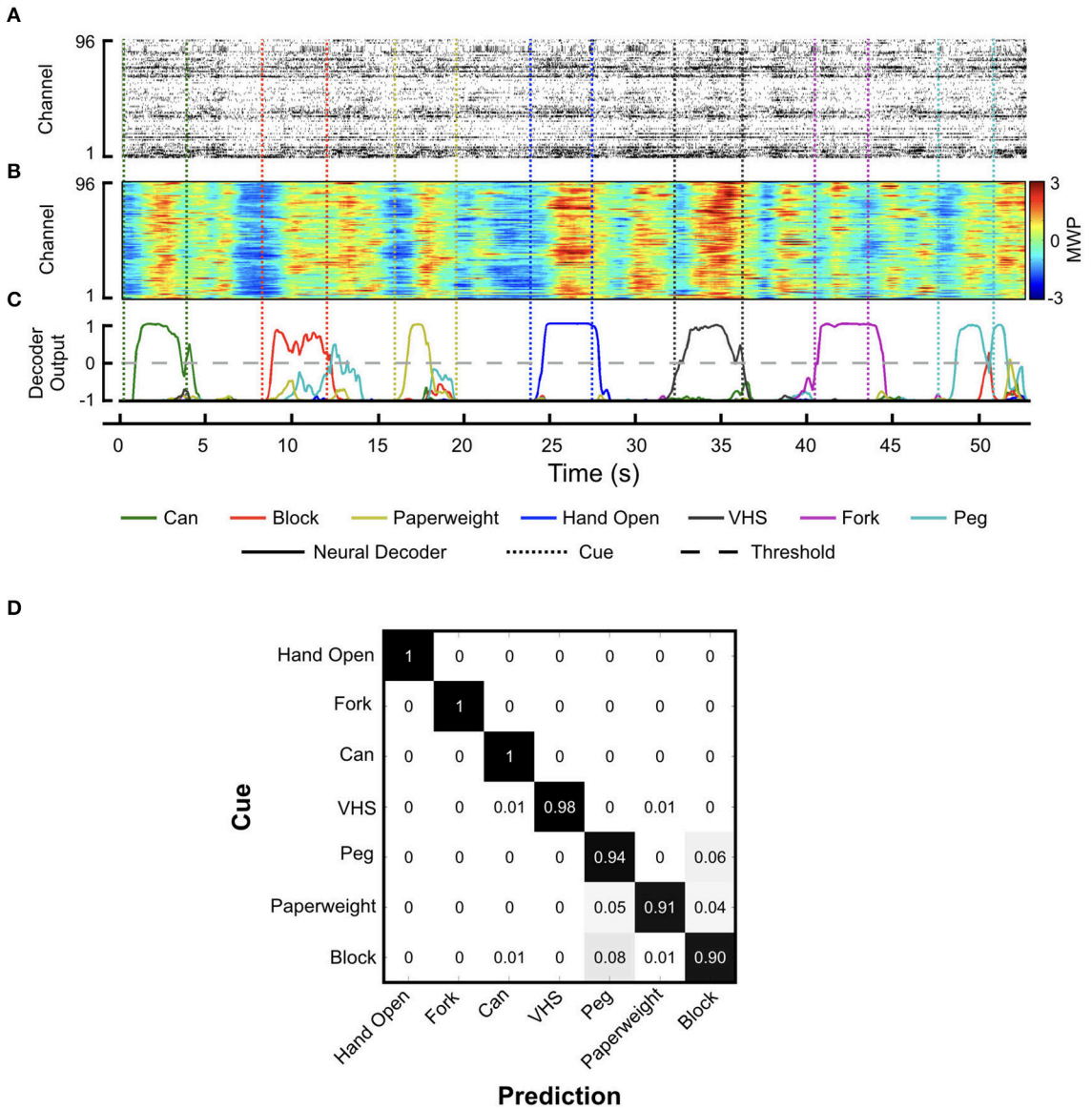

FIGURE 4 | Neural decoder training. Representative plots showing **(A)** threshold crossing raster plot, **(B)** the corresponding MWP activity across all channels of the MEA, and **(C)** neural decoder output as the participant attempts the seven cued hand movements. Solid lines indicate neural decoder output and dotted lines indicate the cue start and stop times. Of the seven possible hand movement states that can be predicted by the decoder, the output score from the one with the highest amplitude greater than zero was used to turn on/off the stimulation; **(D)** Confusion matrix showing the decoder response probability for each movement cue.

DISCUSSION

The ability to successfully manipulate multiple real-world objects encountered during activities of daily living remains a key challenge limiting the practical applicability of BCI-controlled FES devices for people living with tetraplegia. In our previous studies, we demonstrated proof-of-concept that implanted BCI-transcutaneous FES technology can achieve motor control of a paralyzed upper limb after SCI (Bouton et al., 2016). We focused on demonstrating that differential control of individual wrist, finger, and hand movements could be achieved, but did not attempt to quantify or characterize the behavioral or neural features of motor control. In this study, we advance prior knowledge by applying standardized tasks developed for neuroprosthetic studies (GRT object manipulation) to the evaluation of system performance. In this way, we not only allow for comparison between our BCI-FES technology and other neuroprosthetics but also develop a new understanding of the strengths and limitations of the BCI-FES system. We showed that the participant in our study could train to use the BCI-controlled FES system to perform functional tasks that required dynamic integration of FES-enabled paralyzed hand/arm muscles with non-paralyzed shoulder/elbow muscles. The system enabled the participant to select the desired hand movement, out of the seven

TABLE 1 | Individual decoder accuracy.

Hand movement	Individual decoder accuracy (%)
Hand open	99.0 ± 0.5
Can	96.9 ± 0.9
Block	97.4 ± 1.2
Peg	96.9 ± 0.6
Fork	98.4 ± 0.8
Paperweight	96.3 ± 0.7
VHS	98.1 ± 0.2

Individual decoder accuracies were calculated by determining the percentage of time points that the decoder output for a given movement correctly matched the associated cue during decoder training. Values presented as mean ± S.D.

possible trained movements as well as a rest state available to him, using motor intent. The BCI-FES also enabled the participant to manipulate objects of different sizes, shapes, and weights with skilled, forceful grasps. In addition, our study revealed insights into the neural representation of hand movements in the motor cortex. We showed that stable representations of different hand movements can form in a very small area of the motor cortex under the implanted MEA. Furthermore, we demonstrated that discriminability between these neural representations can affect decoder performance.

Because the test objects varied widely in size and shape, the FES system was calibrated for each object to evoke a unique hand shape/movement pattern that provided grip force and dexterity to enable palmar, lateral, and tip-to-tip type grasps. The FES system calibration for each grasp involved precise targeting of separate muscle groups in the forearm to evoke specific finger movements (see **Figure 3** and **Figure S1** showing the target muscle groups for each grasp). The use of MWP as neural features for decoding provided a high-fidelity spatiotemporal neural modulation signal that was strongly correlated with neuronal spiking activity, and could be used to discriminate between different hand movements in real-time without the need for thresholding or explicit spike sorting (**Figure 4**). During decoder training, the participant attempted to evoke the correct grasp for a particular object from seven movement states (plus rest) available to him. The results from decoder training show that the participant was able to use the decoder to control the system with high accuracy—the individual accuracy scores for each movement were all >96% (**Table 1**) during different neural decoder training sessions across 4 days. Several groups have observed that neuronal states associated with different imagined hand movements may be represented discriminably in the human brain (Klaes et al., 2015; Bleichner et al., 2016; Leo et al., 2016). Our finding that multiple hand movements can be decoded reliably from the motor cortex is further validation of these observations. The consistently high accuracy of the decoders in classifying individual hand grasps not only indicates the robustness of the neural representations in the motor cortex, but also suggests that this modulation can be reliably leveraged for precision control of a FES neuro-orthotic device that can restore multiple hand-grasp functions. The results also highlight that for our trained participant the decoder training time for the multiple object manipulation task was limited to 12–15 min. These results have implications as high accuracy and minimal training time are features that are desirable for potential users of neuroprosthetic devices (Collinger et al., 2013).

We used the standardized GRT to demonstrate the participant's ability to successfully use the trained decoder to manipulate multiple objects. The use of a standardized measure of functional outcomes not only helped us better assess the performance of our system but also provided standardized reportable scores that can facilitate objective comparison with other similar technologies, help identify areas of improvements, enhance reproducibility of research, and aid in decision making for clinicians and potential end-users. The results show that using the BCI-FES system, the participant was able to evoke the correct movement to manipulate each of the six test objects using naturalistic grips (**Figure 5** and **Movie S2**). It should be noted that the participant is able to transfer some of the objects on his own without using the BCI-FES system (see **Movie S2**, right panel showing the participant manipulating the objects on his own without FES). For example, the participant used adaptive strategies (such as biceps-mediated forearm supination with shoulder abduction/adduction) to easily grasp and release the *Peg* and *Block*. However, heavier objects that required a more forceful grip were difficult to transfer without the system (**Figure 5B**). Using the BCI-FES system, the participant was able to transfer the heavier objects (*VHS*, *Paperweight*, *Can, Fork*) and also showed significant improvement in transfer times (**Figure 5C**).

The transfer speed using the BCI-FES system during the GRT compares favorably to those reported for other BCI-FES systems. For example, our participant transferred the *Paperweight* at a rate of 4.7 ± 1.2 s per transfer compared to ∼36 s it took a participant to transfer the *Paperweight* using the EEG-Freehand system (Müller-Putz et al., 2005). It should be noted that the neurologic level of the participant in Muller-Putz et al. (C5 ASI A with residual shoulder and elbow movements) is functionally similar to the neurologic level of the participant in our study (C5 ASI A with residual shoulder and elbow movements). While the participant in our study had a twitch of wrist extension (yielding a zone of partial preservation to C6), he was not able to elicit the tenodesis grip of a person with a C6 neurologic level. The improved performance on the GRT with our BCI-FES system carries further significance as compared to the EEG-Freehand system where the participant only has a single grasp available, our participant had seven hand functions available to him and he can voluntarily choose the one which provides him the optimal grip for the target object. The transfer speed with our system also compares favorably with a BCI-controlled robotic arm used by paralyzed individuals—for example, a transfer rate of 6–10 transfers per minute for the *Block* vs. 0.1–1 transfers per minute reported for the BCI-robotic arm used to transfer similar sized blocks during the Box and Block (BBT) test (Wodlinger et al., 2015).

Analysis of the participant's neural modulation, as he imagined different hand movements, revealed interesting insights into the neural representations of hand grasps in the motor cortex. The PCA revealed overlaps in the MWP clusters of

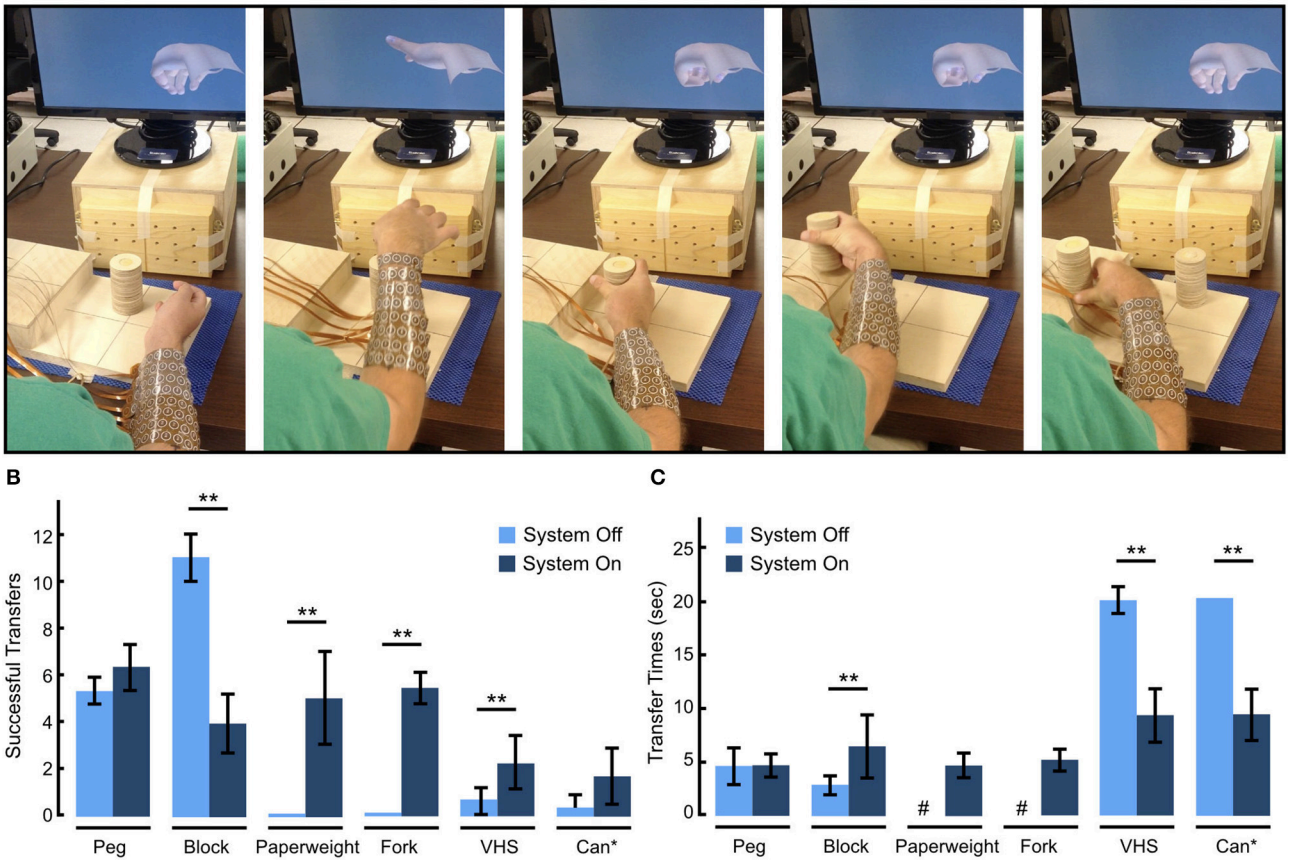

FIGURE 5 | Functional performance evaluation using the Grasp and Release Test (GRT). **(A)** Sequential snapshots of the participant manipulating the *Can* object as part of the GRT. The participant starts from a rest state, opens his hand and place it around the *Can*, grasps the *Can*, transfers it to the raised platform, and then releases the *Can*. A new object is then placed in front of the participant to attempt the next transfer. **(B)** GRT scores showing the mean number of successful transfers with and without the BCI-FES system. With the use of the system, the participant not only improved his GRT scores over his baseline, demonstrating an increase in number of transfers for all objects except the *Block*, but was also able to grip and transfer two objects (*Paperweight*, *Fork*) that he could not manipulate at baseline. **(C)** Mean transfer times for each object with and without the BCI-FES system. With the use of the system the participant's transfer speed increased for all objects except for the *Peg* and *Block* which he was able to transfer faster on his own using adaptive grips. #The participant was never able to transfer these objects without the system. *The *Can* transfer required two hand movements—*Hand Open* and *Can* grasp. $^{**}p < 0.05$ (paired *t*-test).

the grips for *Paperweight–Block* and the *Can–VHS* (**Figure 7A**). The similarities in neural representation for hand grasps were consistent with the spatial distribution of MWP on the cortical array where we observed a group of channels that appear to modulate similarly between these grasps (**Figure 7B**). The analysis of the differences in MWP modulation confirmed that the neural representation of the imagined *Block* and *Paperweight* as well as the *Can* and *VHS* grasps were, indeed, the most similar of all grasps (**Figure 7C**). This was consistent with hand morphology observed during performance of the grips, with *Block* and *Paperweight* grasp patterns being a synergy of lateral key and tip-to-tip precision grips and *Can* and *VHS* grasp patterns representing versions of a palmar power grip. This similarity in the neural representations for certain hand grasps may be one of the factors underlying the misclassification in decoding that we observed during the GRT test blocks. Other groups have made similar observations. For example, Leo et al. observed a clustering of neuronal representations based on postural differences in hand shapes (i.e., precision grasps and power grasps) which in turn affected the ability to correctly classify these hand shapes during decoding (Leo et al., 2016). Similarly, Bleichner et al. used an ECoG-based BCI to classify four different hand gestures and noted that the gestures that correlated strongest in neural representation were misclassified most often (Bleichner et al., 2016). The results not only expand on the total number of hand movements for which a stable representation could be observed in the motor cortex, but also show that it is possible to study and decode neural representations in a very small area under the implanted MEA. Regardless, our findings that there are overlaps between the MWP spatial patterns for some hand movements highlights that additional neural features (such as signal propagation or phase) and/or other decoding algorithms (such as deep learning algorithms) might need to be explored to expand the

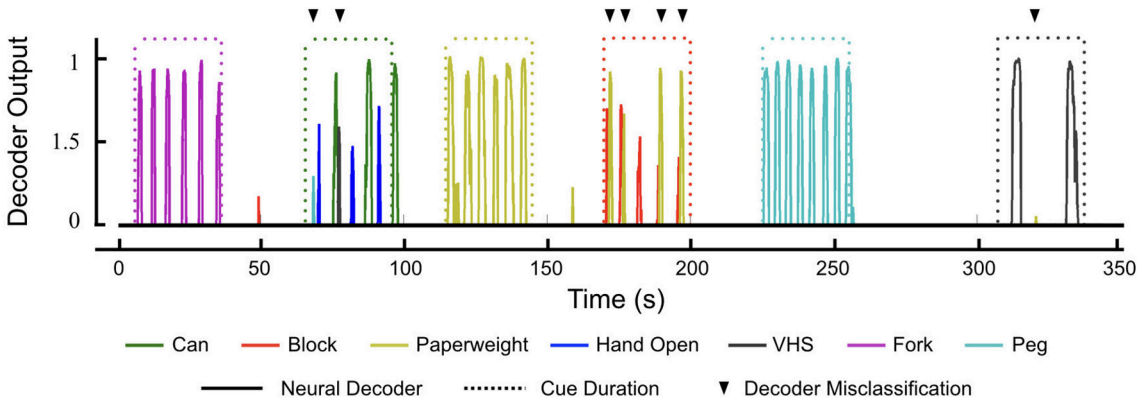

FIGURE 6 | Neural decoder outputs during the GRT. Representative decoder outputs during a GRT test block showing instances of decoder misclassification (black triangles). All seven hand movements are available to the participant as part of the decoder and he has to evoke the correct movement (solid lines) during the 30 s trial period (dotted lines) given to him to complete the GRT for that object. Only decoder outputs above the activation threshold of zero are shown for visual clarity. Successful transfer of *Can* required the participant to evoke two hand movements—*Hand Open* and *Can* grasp (70–100 s). During the *Can* transfer, the decoder had two misclassifications (one of each for the PEG and VHS grasps). However, the participant was able to evoke the correct hand movements to successfully complete two *Can* transfers during the trial period. Similarly, during the *Block* transfer (170–200 s), the participant incorrectly evoked the decoder for *Paperweight* on four occasions. This did not affect the GRT scores for the *Block*, however, as the decoder for *Paperweight* kicked in after the participant had completed the *Block* transfer.

repertoire of hand functions that can be reliably decoded using a single MEA.

Interestingly, the neural representation for *Hand Open* in our experiments was the most distinct from the six other hand grasps (**Figure 7C**). We hypothesize that this is due to the *Hand Open* posture being morphologically distinct from all other grasps. In addition, the FES pattern for *Hand Open* was primarily over wrist and hand extensors, while the FES pattern for grasps often included both flexor and extensor muscle compartments. Therefore, somatosensory and muscle stretch receptor feedback from stimulation of sensate areas could have propagated to the motor cortex and differentially influenced neural activation patterns in *Hand Open* vs. grasp states. Not surprisingly therefore, during neural decoder training we observed the highest accuracy when the participant attempted a *Hand Open* movement (**Table 1**). Overall, there was a strong correlation between the discriminability in neural representation of different hand states and the corresponding decoding accuracy (**Figure 7D**). It should be noted that, compared to GRT test blocks, we rarely observed this misclassification among hand movements during the decoder training. This may be due to the differences in how the training and GRT test blocks are performed. First, in contrast to training blocks, the participant does not receive visual cues to initiate, sustain, and terminate the grasp during the GRT test blocks. Second, the decoder training is more structured and motor imagery is more consistent and deliberate as the participant must grasp and transfer the cued object once during the cue period. The GRT test block, however, may be more challenging for the participant because he must quickly and repeatedly activate and deactivate decoders to transfer objects as many times as he can in a 30-s test window. We believe that it is the combination of the lack of reinforcing visual cues, and the rapid task switching during the "beat the clock" condition of the GRT that increases the misclassification probability of the decoder for grasps with most similar neural representations.

Enabling grasp and manipulation abilities using BCI-FES technology is challenging compared to, for example, a 3-D reaching task or individual finger/joint movement as it not only requires high fidelity control signals and strategies (Schaffelhofer et al., 2015), but may also require additional sensorimotor information related to the shape of the target object that may be needed to preshape the hand correctly (Leo et al., 2016). In addition, a reaching task in space involves coordinating only three degrees of freedom (DOF) whereas control of an anthropomorphic hand requires control of 23 DOF (Vargas-Irwin et al., 2010) thereby increasing the complexity of the problem. Not surprisingly therefore, there are only a few reports of successful demonstration of BCI-enabled hand grasp, most of which were limited by the number of functional hand movements that could be enabled (Bouton et al., 2016; Sharma et al., 2016; Ajiboye et al., 2017; Friedenberg et al., 2017). Not only are the number of hand functions regained by our tetraplegic participant to manipulate objects substantially more than achieved by any previous study of FES devices, but we also show that this improvement did not come at the cost of accuracy, speed, or training time. Our results also have implications beyond reanimation in tetraplegia. The enhanced understanding of the neural representation of hand gestures in the human brain and the ability to accurately decode these movements can provide a novel control signal for the development of other BCI tools; for instance, communication based on sign language (Bleichner et al., 2016). Another advantage of using an intuitive BCI paired with real-time FES is the potential to promote synaptic neuroplasticity in the cortico-spinal tract (McGie et al., 2015) or to promote neuroprosthetic "learning" in the motor cortex (Ganguly et al., 2011).

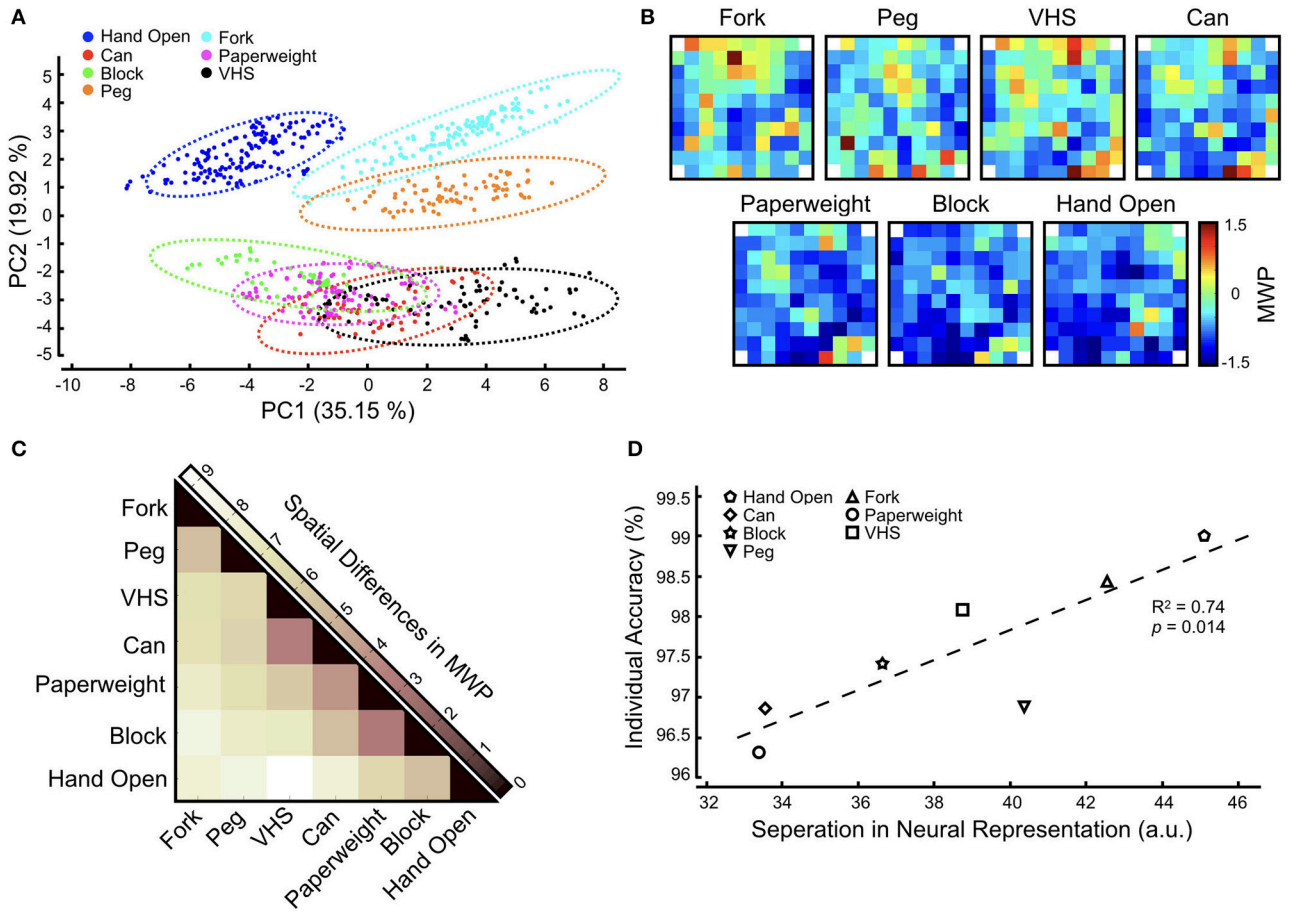

FIGURE 7 | Neural representation of functional hand movements in the motor cortex. The participant was asked to attempt the cued hand movement. No FES was provided during this task so that neural data can be captured without any stimulation artifact. **(A)** Principal component analysis (PCA) of MWP activity shows clustering of neural activity for each hand movement during decoder activation for each functional movement. Dotted lines indicate a Gaussian mixture distribution model fit. **(B)** Heat maps of averaged MWP activity during neural decoder activation overlaid on the physical layout of the electrode array for each attempted hand movement. Corner reference (non-active) electrodes in the electrode array are labeled with white squares. **(C)** Heat map showing the pairwise Euclidean distances between vectorized MWP spatial patterns and highlights the separability in neural representation between different hand movements. Darker colors indicate that the neural representations are similar while lighter colors indicate that the representations are dissimilar. **(D)** Correlation between individual decoder accuracy and separation in neural representation (aggregate Euclidean distance for each movement) shows that higher neural discriminability leads to higher decoder accuracy. The trend line indicates a linear fit.

It is important to note that this study is limited to one participant who had over two years of experience using the BCI to evoke hand and forearm states prior to performing GRT testing. Novice BCI users may take longer to achieve the same level of hand dexterity for object manipulation as described here. In addition, the transcutaneous FES cuff used in this study is designed to stimulate the paralyzed forearm muscles to control hand and wrist movements. It is therefore best suited to persons with C5 or lower levels of tetraparesis and who have some residual shoulder and biceps movements. Testing to assess whether the FES cuff can be used along with shoulder and triceps stimulation or a gravity assisting device in SCI patients with higher level of injury remains to be investigated. Our device was also limited by the lack of thenar (base of thumb) muscle stimulation, limiting the quality of hand grasps for small objects requiring precision grips (no objects of this type are represented in the GRT). The need for daily retraining of the decoders is another limitation of the current system that will need to be overcome in order to reduce setup time and facilitate translation of the device for daily use.

In summary, our BCI-FES neuro-orthotic device significantly improves upon the state-of-the-art for assistive devices capable of meeting tetraplegic individual's desired priorities of restoring multiple, voluntary, and naturalistic hand functions. We also demonstrate that our BCI-FES system can enable functional, skilled hand grasps that can generate adequate force to manipulate everyday objects with high-precision and practical speed. The fact that the participant could use the system to perform functional tasks ~900 days post-implantation further highlights the translational potential of our system. Future directions include addressing system limitations to make the next generation BCI-FES robust to daily neural

signal variability, portable, wearable, with more electrodes and sensors, and less obtrusive to further facilitate clinical translation.

AUTHOR CONTRIBUTIONS

GS conceptualized the study; GS, HB, SC, and MB designed the scientific experiments; SC, MZ, GS, and MB performed research; DF and MS developed the decoding algorithms; NA contributed to developing the stimulation hardware and software; AR performed the surgery; SC, MZ, NS, and GS analyzed data; WM and MB were involved in participant recruitment; GS and SC wrote the manuscript. All authors contributed to editing the manuscript.

FUNDING

Financial support for this study came from Battelle Memorial Institute and The Ohio State University Center for Neuromodulation.

ACKNOWLEDGMENTS

We thank the study participant and his family for their dedication and support. We thank Adam Jacobowitz for assistance with the clinical sessions, Patrick Ganzer for his helpful comments on the manuscript, Elly Nam and Krista Smith for their help with schematics. We thank Neil Austin for his time to fabricate the standardized test objects used in the study.

SUPPLEMENTARY MATERIAL

The Supplementary Material for this article can be found online at: https://www.frontiersin.org/articles/10.3389/fnins.2018.00208/full#supplementary-material

Figure S1 | FES parameters and target muscle groups for each hand movement. **(A)** Representative image showing spatial mapping of active electrodes on the lower and upper FES cuffs used to enable the *Can* grasp. Red and black electrodes indicate high-side and low-side electrodes, respectively. **(B)** Active electrodes, stimulation amplitude, and targeted muscle groups for each hand movement. L, Lower cuff; U, Upper cuff.

Figure S2 | Mean number of failed attempts on the GRT with and without the BCI-FES system. The participant had fewer failures with the use of the BCI-FES system. *The *Can* transfer required activation of two hand movements—*Hand Open* and *Can* grasp.

Movie S1 | Representative video of the participant manipulating the GRT objects during decoder training. Test objects were placed in front of the participant and he was cued to start and stop by the small virtual hand on the monitor in front of him.

Movie S2 | Representative video of the participant performing the GRT for all objects with and without the BCI-FES system. The participant was verbally cued to start and stop the 30 s GRT trial.

REFERENCES

Ajiboye, A. B., Willett, F. R., Young, D. R., Memberg, W. D., Murphy, B. A., Miller, J. P., et al. (2017). Restoration of reaching and grasping movements through brain-controlled muscle stimulation in a person with tetraplegia: a proof-of-concept demonstration. *Lancet* 389, 1821–1830. doi: 10.1016/S0140-6736(17)30601-3

Anderson, K. D. (2004). Targeting recovery: priorities of the spinal cord-injured population. *J. Neurotrauma* 21, 1371–1383. doi: 10.1089/neu.2004.21.1371

Baranauskas, G. (2014). What limits the performance of current invasive brain machine interfaces? *Front. Syst. Neurosci.* 8:68. doi: 10.3389/fnsys.2014.00068

Blabe, C. H., Gilja, V., Chestek, C. A., Shenoy, K. V., Anderson, K. D., and Henderson, J. M. (2015). Assessment of brain-machine interfaces from the perspective of people with paralysis. *J. Neural Eng.* 12:043002. doi: 10.1088/1741-2560/12/4/043002

Bleichner, M. G., Freudenburg, Z. V., Jansma, J. M., Aarnoutse, E. J., Vansteensel, M. J., and Ramsey, N. F. (2016). Give me a sign: decoding four complex hand gestures based on high-density ECoG. *Brain Struct. Funct.* 221, 203–216. doi: 10.1007/s00429-014-0902-x

Bouton, C. E., Shaikhouni, A., Annetta, N. V., Bockbrader, M. A., Friedenberg, D. A., Nielson, D. M., et al. (2016). Restoring cortical control of functional movement in a human with quadriplegia. *Nature* 533, 247–250. doi: 10.1038/nature17435

Chadwick, E. K., Blana, D., Simeral, J. D., Lambrecht, J., Kim, S. P., Cornwell, A. S., et al. (2011). Continuous neuronal ensemble control of simulated arm reaching by a human with tetraplegia. *J. Neural Eng.* 8:034003. doi: 10.1088/1741-2560/8/3/034003

Collinger, J. L., Boninger, M. L., Bruns, T. M., Curley, K., Wang, W., and Weber, D. J. (2013). Functional priorities, assistive technology, and brain-computer interfaces after spinal cord injury. *J. Rehabil. Res. Dev.* 50, 145–160. doi: 10.1682/JRRD.2011.11.0213

Ethier, C., and Miller, L. E. (2015). Brain-controlled muscle stimulation for the restoration of motor function. *Neurobiol. Dis.* 83, 180–190. doi: 10.1016/j.nbd.2014.10.014

Friedenberg, D., Schwemmer, M., Landgraf, A., Annetta, N., Bockbrader, M., Bouton, C., et al. (2017). Neuroprosthetic-enabled control of graded arm muscle contraction in a paralyzed human. *Sci. Rep.* 7:8386. doi: 10.1038/s41598-017-08120-9

Ganguly, K., Dimitrov, D. F., Wallis, J. D., and Carmena, J. M. (2011). Reversible large-scale modification of cortical networks during neuroprosthetic control. *Nat. Neurosci.* 14, 662–667. doi: 10.1038/nn.2797

Humber, C., Ito, K., and Bouton, C. (2010). Nonsmooth formulation of the support vector machine for a neural decoding problem. *arXiv:1012.0958*.

ICCP (2017). *International Campaign for Cures of Spinal Cord Injury Paralysis*.

Klaes, C., Kellis, S., Aflalo, T., Lee, B., Pejsa, K., Shanfield, K., et al. (2015). Hand shape representations in the human posterior parietal cortex. *J. Neurosci.* 35, 15466–15476. doi: 10.1523/JNEUROSCI.2747-15.2015

Lauer, R. T., Peckham, P. H., and Kilgore, K. L. (1999). EEG-based control of a hand grasp neuroprosthesis. *Neuroreport* 10, 1767–1771. doi: 10.1097/00001756-199906030-00026

Leo, A., Handjaras, G., Bianchi, M., Marino, H., Gabiccini, M., Guidi, A., et al. (2016). A synergy-based hand control is encoded in human motor cortical areas. *Elife* 5:e13420. doi: 10.7554/eLife.13420

Mallat, S. (1998). *A Wavelet Tour of Signal Processing*. Burlington, MA: Academic Press.

Márquez-Chin, C., Popovic, M. R., Cameron, T., Lozano, A. M., and Chen, R. (2009). Control of a neuroprosthesis for grasping using off-line classification of electrocorticographic signals: case study. *Spinal Cord* 47, 802–808. doi: 10.1038/sc.2009.41

McGie, S. C., Zariffa, J., Popovic, M. R., and Nagai, M. K. (2015). Short-term neuroplastic effects of brain-controlled and muscle-controlled electrical stimulation. *Neuromodulation* 18, 233–240. doi: 10.1111/ner.12185

Müller-Putz, G. R., Scherer, R., Pfurtscheller, G., and Rupp, R. (2005). EEG-based neuroprosthesis control: a step towards clinical practice. *Neurosci. Lett.* 382, 169–174. doi: 10.1016/j.neulet.2005.03.021

Nas, K., Yazmalar, L., Sah, V., Aydin, A., and Ones, K. (2015). Rehabilitation of spinal cord injuries. *World J. Orthop.* 6, 8–16. doi: 10.5312/wjo.v6.i1.8

Pfurtscheller, G., Muller, G. R., Pfurtscheller, J., Gerner, H. J., and Rupp, R. (2003). "Thought"–control of functional electrical stimulation to restore

hand grasp in a patient with tetraplegia. *Neurosci. Lett.* 351, 33–36. doi: 10.1016/S0304-3940(03)00947-9

Schaffelhofer, S., Agudelo-Toro, A., and Scherberger, H. (2015). Decoding a wide range of hand configurations from macaque motor, premotor, and parietal cortices. *J. Neurosci.* 35, 1068–1081. doi: 10.1523/JNEUROSCI.3594-14.2015

Sharma, G., Friedenberg, D. A., Annetta, N., Glenn, B., Bockbrader, M., Majstorovic, C., et al. (2016). Using an artificial neural bypass to restore cortical control of rhythmic movements in a human with quadriplegia. *Sci. Rep.* 6:33807. doi: 10.1038/srep33807

Simpson, L. A., Eng, J. J., Hsieh, J. T., and Wolfe, D. L. (2012). The health and life priorities of individuals with spinal cord injury: a systematic review. *J. Neurotrauma* 29, 1548–1555. doi: 10.1089/neu.2011.2226

Snoek, G. J., IJzerman, M. J., Hermens, H. J., Maxwell, D., and Biering-Sorensen, F. (2004). Survey of the needs of patients with spinal cord injury: impact and priority for improvement in hand function in tetraplegics. *Spinal Cord* 42, 526–532. doi: 10.1038/sj.sc.3101638

Stroh-Wuolle, K., Van Doren, C. L., Thrope, G. B., Keith, M. W., and Peckham, P. H. (1994). Development of a quantitative hand grasp and release test for patients with tetraplegia using a hand neuroprosthesis. *J. Hand Surg.* 19, 209–218. doi: 10.1016/0363-5023(94)90008-6

Vargas-Irwin, C. E., Shakhnarovich, G., Yadollahpour, P., Mislow, J. M., Black, M. J., and Donoghue, J. P. (2010). Decoding complete reach and grasp actions from local primary motor cortex populations. *J. Neurosci.* 30, 9659–9669. doi: 10.1523/JNEUROSCI.5443-09.2010

Wodlinger, B., Downey, J. E., Tyler-Kabara, E. C., Schwartz, A. B., Boninger, M. L., and Collinger, J. L. (2015). Ten-dimensional anthropomorphic arm control in a human brain-machine interface: difficulties, solutions, and limitations. *J. Neural Eng.* 12:016011. doi: 10.1088/1741-2560/12/1/016011

Conflict of Interest Statement: The authors declare that the research was conducted in the absence of any commercial or financial relationships that could be construed as a potential conflict of interest.

Copyright © 2018 Colachis, Bockbrader, Zhang, Friedenberg, Annetta, Schwemmer, Skomrock, Mysiw, Rezai, Bresler and Sharma. This is an open-access article distributed under the terms of the Creative Commons Attribution License (CC BY). The use, distribution or reproduction in other forums is permitted, provided the original author(s) and the copyright owner are credited and that the original publication in this journal is cited, in accordance with accepted academic practice. No use, distribution or reproduction is permitted which does not comply with these terms.

frontiers in Neuroscience

ORIGINAL RESEARCH
published: 11 May 2018
doi: 10.3389/fnins.2018.00308

A New Method to Generate Artificial Frames Using the Empirical Mode Decomposition for an EEG-Based Motor Imagery BCI

Josep Dinarès-Ferran[1,2], *Rupert Ortner*[2], *Christoph Guger*[2,3] *and Jordi Solé-Casals*[1*]

[1] Data and Signal Processing Research Group, Department of Engineering, University of Vic-Central University of Catalonia, Barcelona, Spain, [2] g.tec Medical Engineering Spain SL, Barcelona, Spain, [3] g.tec Medical Engineering GmbH, Schiedlberg, Austria

OPEN ACCESS

Edited by:
Ioan Opris,
University of Miami, United States

Reviewed by:
Dan Zhang,
Tsinghua University, China
Sun Zhe,
RIKEN, Japan

***Correspondence:**
Jordi Solé-Casals
jordi.sole@uvic.cat

Specialty section:
This article was submitted to Neural Technology, a section of the journal Frontiers in Neuroscience

Received: 05 February 2018
Accepted: 20 April 2018
Published: 11 May 2018

Citation:
Dinarès-Ferran J, Ortner R, Guger C and Solé-Casals J (2018) A New Method to Generate Artificial Frames Using the Empirical Mode Decomposition for an EEG-Based Motor Imagery BCI. Front. Neurosci. 12:308. doi: 10.3389/fnins.2018.00308

EEG-based Brain-Computer Interfaces (BCIs) are becoming a new tool for neurorehabilitation. BCIs are used to help stroke patients to improve the functional capability of the impaired limbs, and to communicate and assess the level of consciousness in Disorder of Consciousness (DoC) patients. BCIs based on a motor imagery paradigm typically require a training period to adapt the system to each user's brain, and the BCI then creates and uses a classifier created with the acquired EEG. The quality of this classifier relies on amount of data used for training. More data can improve the classifier, but also increases the training time, which can be especially problematic for some patients. Training time might be reduced by creating new artificial frames by applying Empirical Mode Decomposition (EMD) on the EEG frames and mixing their Intrinsic Mode Function (IMFs). The purpose of this study is to explore the use of artificial EEG frames as replacements for some real ones by comparing classifiers trained with some artificial frames to classifiers trained with only real data. Results showed that, in some subjects, it is possible to replace up to 50% of frames with artificial data, which reduces training time from 720 to 360 s. In the remaining subjects, at least 12.5% of the real EEG frames could be replaced, reducing the training time by 90 s. Moreover, the method can be used to replace EEG frames that contain artifact, which reduces the impact of rejecting data with artifact. The method was also tested on an out of sample scenario with the best subjects from a public database, who yielded very good results using a frame collection with 87.5% artificial frames. These initial results with healthy users need to be further explored with patients' data, along with research into alternative IMF mixing strategies and using other BCI paradigms.

Keywords: brain-computer interface, motor imagery, empirical mode decomposition, artificial frames, EEG

INTRODUCTION

Brain-Computer Interfaces (BCI) are systems capable of controlling external devices using direct measures of the brain signals (Wolpaw et al., 2002; Wolpaw and Wolpaw, 2012). A BCI has three main parts:

1. Brain signals acquisition system.
2. Processing system.
3. Device/feedback control.

The selection of the brain signal acquisition system relies on the intended BCI application (Wolpaw et al., 2002; Shih et al., 2012; Wolpaw and Wolpaw, 2012). EEG is a non-invasive approach with a high temporal resolution that is suited for real-time application (Shih et al., 2012). EEG signals are electrical potential differences from different areas of the scalp caused by the firing of different neurons, often in response to an external stimulus. The resulting synchronized activity across large groups of neurons leads to electrical changes over different brain regions that can be recorded and sent to the processing system.

In a BCI system (**Figure 1**), EEG signals are processed by a computer or processing unit (processing system). These signals are highly noisy, and the use of filtering and pattern recognition techniques are needed to acquire useful information from them (Wolpaw et al., 2002; Wolpaw and Wolpaw, 2012). Paradigms are instructions that the BCI user must follow to elicit known brain responses that the processing system can detect and use to control an external device. Many BCIs are designed to control monitors, but BCIs have been used with other external devices, such as functional electrical stimulator (FES) or orthosis as part of a BCI-based motor rehab system.

Recently, EEG-based BCIs have been extended to new tools for neurorehabilitation patients who have upper limb impairment due to a stroke (Ramos-Murguialday et al., 2013; Cho et al., 2016). They are also being used for patients with disorders of consciousness to assess their mental state and provide communication (Guger et al., 2013, 2017).

Different BCIs have used different paradigms (Farwell and Donchin, 1988; Pfurtscheller, 2001; Oehler et al., 2008), and one of the most widely used involves Motor Imagery or MI (Guger et al., 2015). In an MI BCI paradigm, the user is asked to imagine specific movements, such as left or right hand movements. This movement imagination activates areas of the motor cortex, much like the activation resulting from real movement. Thus, MI BCIs may determine whether a user is imaging left vs. right hand movement to provide a "yes" or "no" reply to a question or move a cursor horizontally.

In the MI paradigm, a trial is the time period which the user imagines movement, as well as any additional time needed for instructions, cues, or other delays. The BCI presents real-time feedback to the user that indicates how well the MI task is being performed and classified. This feedback might be visual information displayed on a screen, auditory feedback through headphones or proprioceptive or other feedback from other devices.

When using the MI BCI approach to help patients regain movement, the feedback often includes an avatar presented on a monitor that performs simulated hand/arm movements and FES electrodes placed over the affected limb. In conventional therapy, the patient is asked to imagine performing a movement such as wrist dorsiflexion while a therapist provides instructions and manages an FES device that triggers wrist dorsiflexion. By adding the MI BCI into the control loop, rewarding feedback such as avatar movement and FES activation is only possible when the patient performs the correct MI. This BCI-based feedback is much more tightly coupled to each patient's MI than conventional means, which should increase the functional improvement from therapy training (Remsik et al., 2016; Sabathiel et al., 2016).

BCIs, especially MI BCIs, usually require calibration for each user for at least two reasons. First, classifiers need time to learn the unique features of each new user's EEG activity, such as ERD/S used in MI BCIs. Second, these features may change within or across sessions or runs due to fatigue, medication, motivation, different cap placement, or other factors. Different cap placement from one session to another could be especially problematic if BCIs gain wider clinical adoption. Many therapists and other staff are not trained in precise cap positioning, and this process can require a few additional minutes. Calibration at the start of a session can lead to better classifier performance, but also requires additional time. Since MI BCIs typically require more calibration time than other BCIs, and patients with stroke may have limited time and motivation, new approaches to reduce calibration time with MI BCIs are needed.

In a typical BCI, a new EEG data frame is obtained from each trial. The quality of the classifier is directly proportional to the number of frames from each type of MI (such as left vs. right hand; Ramoser et al., 2000). This paper explores a new approach that creates artificial frames, which the classifier can use like real frames to reduce the need for calibration data. Because of the non-linear and non-stationary aspects of EEG signals, a new processing method based on the EMD decomposition (Huang et al., 1998) is proposed to generate those new artificial frames (Hawley et al., 2008; Huang et al., 2013; Riaz et al., 2015).

MATERIALS AND METHODS

Subjects

The experiment was performed on 7 healthy men aged 29.8 $\pm$ 5.76 years. All subjects reported no history of stroke or other cause of movement disability and signed an informed consent document prior to participating in the study.

Equipment

The paradigm was implemented using a closed-loop system that provides real-time feedback to the user and saves the data for later analysis. This system uses a 16 EEG channel cap (g.SCARABEO, g.tec medical engineering GmbH) with the electrodes placed over the sensorimotor cortex according to the 10/10 international system: FC5, FC1, FCz, FC2, FC6, C5 C3, C1, Cz, C2, C4, C6, CP5, CP1, CP2, CP6. The Fpz electrode is connected to the ground and a reference electrode is placed on the right earlobe. The EEG cap is connected to a biomedical amplifier (g.USBamp, g.tec medical engineering GmbH), which is connected to a

computer using a USB cable. The system provides two kinds of real-time feedback: a visual feedback through an avatar displayed on a screen, and proprioceptive feedback through FES electrodes placed on the extensor digitorum communis muscles of each subject's left and right arms.

Experimental Paradigm

At the beginning of each session, each subject was seated in a comfortable chair about 1 m in front of a monitor. The EEG cap was mounted and FES electrodes were affixed to both arms to stimulate wrist dorsiflexion. The experimenter visually inspected the subject's real-time EEG to check data quality and calibrated the FES parameters (pulse width and current) for each subject. Each subject was then asked to sit in front of the monitor and follow the instructions provided by the system.

Each subject completed one session with two runs. A short break was provided between these two runs, during which the subjects remained seated with the cap and FES electrodes in place. Each run presented 80 trials (40 for each side) to each subject. During the first 2 s of each trial, the subject rested, after which an acoustic signal (beep) indicated whether the subject should imagine left or right wrist dorsiflexion. The subject imagined the movement from seconds 3 to 8 while the system provided real-time feedback through the monitor and FES electrodes. After second 8, the trial ended and a new trial began (**Figure 2**). There were an equal number of cues to the left vs. right wrist during each run, and the order was chosen pseudorandomly. Data were stored for later offline analysis.

Empirical Mode Decomposition

Common analytical tools like FFT and wavelets would not be adequate to process EEG signals in this scenario because they are non-linear and non-stationary. The Empirical Mode Decomposition (EMD) method is based on an algorithm that allows users to conduct a data-driven analysis that is more fitting with non-stationary signals that have changes in the frequency structure within a short period of time.

The algorithm decomposes the original signal into a finite number of functions called IMFs (Intrinsic Mode Function) that each of which represents a non-linear oscillation of the signal (Huang et al., 1998). Theses intrinsic functions fulfill two conditions:

1. In the whole signal, the number of maxima is the same as the number of zero-crossing, or differs by at most one.
2. For any sample, the mean value between the envelope of the local maxima and the envelope of the local minima is zero.

The process to obtain the IMFs from a signal $x(t)$ is:

1. Set $s(t) = r_{i-1}(t)$. Initially, $i = 1$ and $r_0(t) = x(t)$.
2. Detect the local maxima and the local minima of $s(t)$.
3. Interpolate all local maxima to generate the upper envelope.
4. Interpolate all local minima to generate the lower envelope.

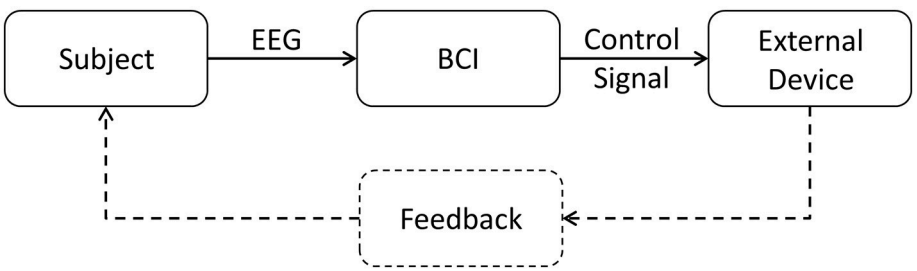

FIGURE 1 | Block diagram of a generic EEG-based BCI system. The BCI gets EEG data from the subject, processes it and generates the proper signals to control the external device and give feedback to the subject.

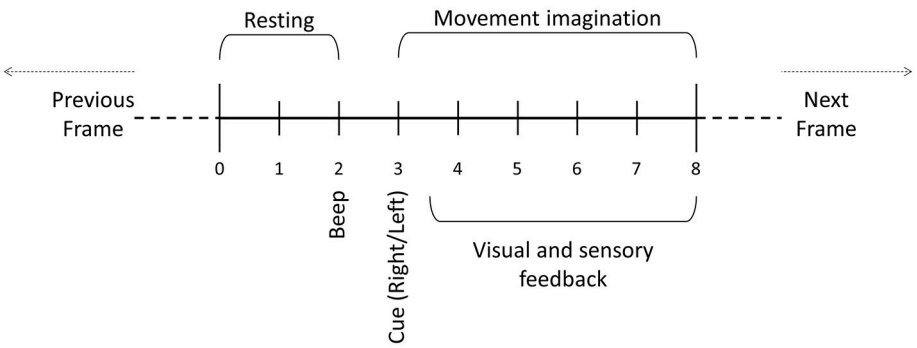

FIGURE 2 | Motor imagery paradigm trial. During the first 2 s, the user is asked to relax. After 2 s, a beep is played and then an auditory cue indicates whether the user should imagine left or right movement. One frame consists of the data resulting from one trial.

5. Obtain the local mean $m(t)$ by averaging the upper and lower envelopes.
6. Get a candidate for IMF by subtracting the local mean $m(t)$ from the signal: $h(t) = s(t) - m(t)$.
7. If $h(t)$ does not satisfy the IMF's conditions, begin a new loop from step 2, setting $s(t) = h(t)$.
8. Otherwise, $h(t)$ is defined as an IMF: $IMF_i(t) = h(t)$.
9. $r_i(t) = r_{i-1}(t) - IMF_i(t)$.
10. If $r_i(t)$ is a monotonic function or does not have enough extrema to calculate the upper and lower envelopes, then $IMF_i(t)$ is the last IMF function of $x(t)$ and the decomposition ends.
11. Otherwise, set $s(t) = r_i(t)$ and start a new loop from step 2 in order to obtain $IMF_{i+1}(t)$.

Once all the IMFs have been calculated, the signal can be recovered using its IMFs (1) and the final residue $r_n(t)$, where n is the number of extracted IMFs (**Figure 3**).

$$x(t) = \sum_{k=1}^{n} IMF_k(t) + r_n(t) \quad (1)$$

The number of IMFs depends on the structure of the EEG signal, and may vary among different EEG data samples. An EEG signal is completely restored by adding all its IMFs and the final residue. Likewise, if a single one of these IMFs is replaced with another IMF from other previously decomposed EEG signal, using the formula (1), then a different EEG signal is obtained.

New Artificial EEG Frames

Prior work has created EEG artificial frames using some stationary approaches that use Gaussian noise as a source into an FFT-based system(Paris et al., 2017), but this approach lacks the temporal features of the natural EEG signals. Otherwise, in some studies the artificial EEG is created by mixing different parts of different temporal EEG signals (Lotte, 2011). In this case, the method keeps the temporal features of the signal, but without control of its frequency features.

Using the EMD approach, the new artificial EEG signals can be created by combining some IMFs from different real EEG signals. Although those new EEG signals will be different from the real ones, they will exhibit similar features and the same underlying structure. Unlike the other approaches described above, the EMD analysis can keep the features within temporal and frequency domains, because each IMF is a representation in the temporal domain of a specific non-linear oscillation of the signal.

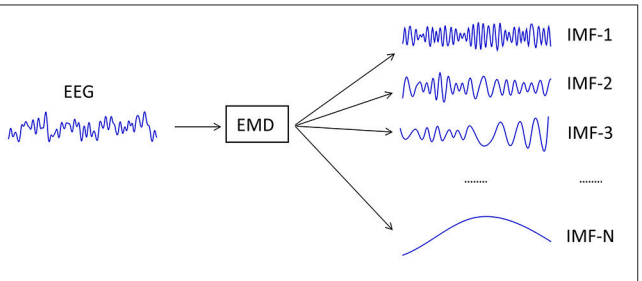

FIGURE 3 | Decomposition of an EEG signal into all of its IMFs.

In the paradigm used in this study, each MI frame is composed of 16 EEG signals, meaning that any new artificial frame needs 16 new artificial EEG signals.

Starting from a real frame collection, the new frame collection containing artificial frames is built following these steps:

1. Define the number of frames to be replaced. This requires replacing the same number of frames from each class (right-side and left-side) with a maximum of 40 frames.
2. Randomly select the frames to be replaced in the original frame collection. The rest of the frames contribute with their IMFs to build the new artificial frames.
3. The selected frames are split in two sets of frames according to their class (left vs. right).
4. To create an artificial frame of a specific class, a number of N frames are selected randomly from the set of frames belonging to the same class (**Figure 4**). The first selected frame contributes with all its first IMFs (16 IMFs, one per channel), the second one with its second IMFs, and successively until the nth frame, which contributes with its nth IMFs.
5. Add up all the IMFs corresponding to the same channel to build each new EEG channel of the new artificial frame.

Repeat step 4 for each new artificial frame necessary to complete the frame collection.

As explained in section Empirical Mode Decomposition, different EEG signals might have different numbers of IMFs, and it is necessary to establish beforehand the number of IMFs of the new artificial frames. In this study, we considered that an EEG signal to be completely represented using their first 15 IMFs, because none of the decomposed signals had more than 12 IMFs. Thus, in every real decomposed EEG signal with <15 IMFs, additional zero value IMFs were added, reaching 15 IMFs for every decomposed signal.

We used this procedure to create new frame collections for each subject's data. Each of these new frame collections contained a different number of artificial frames: 2 (2.5%), 4 (5%), 6 (7.5%), 8 (10%), 10 (12.5%), 20 (25%), 30 (37.5%), or 40 (50%). This process created 9 frame collections: the original data with 0 artificial frames, and eight collections with artificial frames. For each of those 9 frame collections, we constructed a classifier and determined the error rate.

Classifier Training and Implementation

The classifier is based on Linear Discriminant Analysis (LDA). Initially, the frame collection is divided in two groups of frames according to their class (right or left wrist movement). Next, every signal is bandpass filtered (8–30 Hz) and then artifact rejection is applied. With the non-rejected frames, a spatial CSP filter is calculated (Koles et al., 1990; Wang et al., 2005), keeping only the 2 first and 2 last result vectors as the spatial filter. Therefore, the 16 EEG signals of a frame are spatially filtered resulting in four signals. A 1.5 s window variance is calculated over each of these signals. Finally, these variances are normalized and scaled logarithmically, then used as features to build the LDA classifier (Cho et al., 2016).

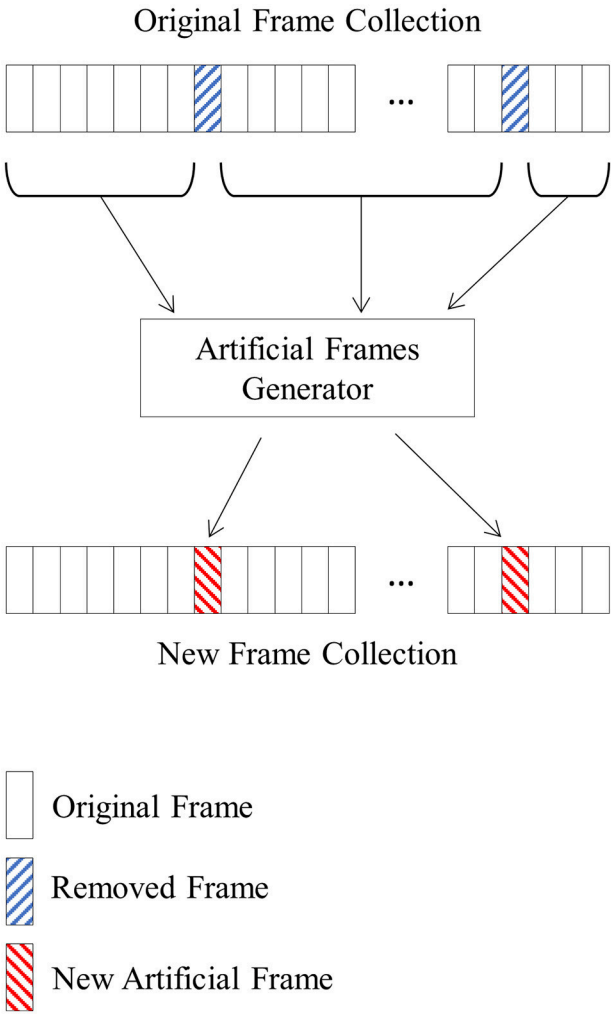

FIGURE 4 | A new frame collection containing artificial frames is created using an original frame collection and randomly selecting the removed frames. The IMFs of the non-selected frames are randomly mixed to create the artificial frames that will replace the removed ones.

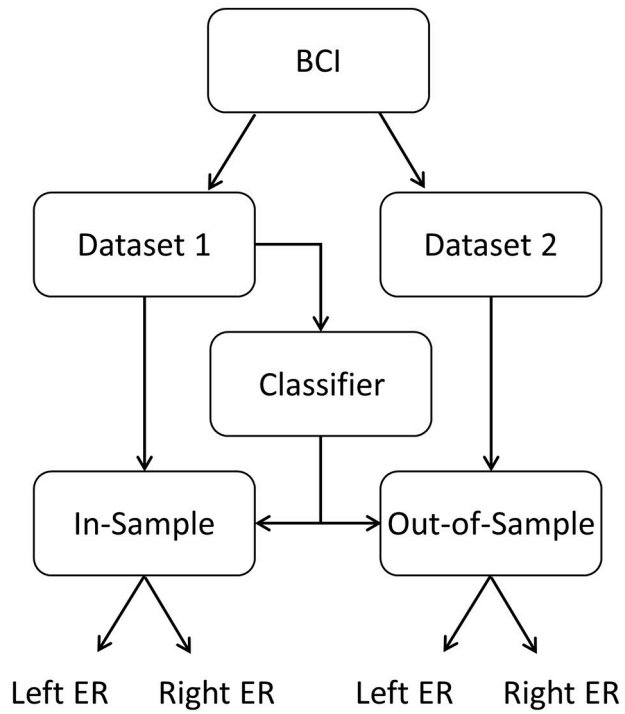

FIGURE 5 | The paradigm provided two datasets. The first dataset was used to build the classifier. Next, the classifier was assessed with both datasets: in-sample (dataset 1) and out-of-sample (dataset 2). Left-side and right-side error rate (ER) can then be determined to assess classifier performance.

A frame collection and classifier are needed to calculate the error rate. Each frame is passed through the classifier, which outputs a value indicating the estimation of that frame's class for each one of its 2,048 samples (256 samples a second). This result is then compared to the true class and marked as correct if they match, and incorrect otherwise. After determining the error of every single sample of a frame collection, a percentage of the incorrect samples is calculated over the feedback period of each trial (from second 3.5 to second 8), providing the global error rate for that classifier. The error rate is expressed as two different percentage values: right-side error rate and left-side error rate.

Data from each subject's first run were used to build all the classifiers, and data from the second run were used to assess the performance of these classifiers with out-of-sample data (**Figure 5**). The out-of-sample error rate of the classifiers without artificial frames were also calculated.

The new frame creation process relies on the random selection of the removed frames and the IMFs. Repeating the experiment with a different random seed leads to different frame collections and very likely to slightly different results. Hence, the frame creation procedure in section New Artificial EEG Frames and classification process described in this section were repeated 100 times for each subject.

Median Absolute Deviation

The MAD (Median Absolute Deviation) is a method to detect outliers from a statistical sample when the sample is small and has a non-normal distribution (Leys et al., 2013); instead of using the mean values to fix the boundaries it uses the median value. Usually, the upper boundary is defined as three times the MAD above the median, and the lower one as three times below (2). All samples outside those boundaries are considered as outliers, and all inside ones as inliers (3).

$$M - 3 \times MAD < x < M + 3 \times MAD \quad (2)$$

$$\left| \frac{x - M}{MAD} \right| < 3 \quad (3)$$

We used the MAD approach to validate the performance of each classifier with a specific number of artificial frames. We used the MAD and the sample's median to calculate a ratio (4), and two

values of this ratio were obtained using the error rates of the classifiers built without artificial frames.

$$R = \left| \frac{x - M}{MAD} \right| \quad (4)$$

For example, after 100 repetitions of the experiment for a specific subject, 100 classifiers with N artificial frames were created (using a frame collection with N artificial frames), and their right and left error rates were calculated. From this sample, the median and the MAD values were obtained. Then, the ratio R was calculated using the error rates of the classifier created with the frame collection without artificial frames.

This process sought to determine whether the original classifier could be considered as an inlier of the sample of the classifiers with N artificial frames. Thus, values of R below 3 meant that the original classifier was not an outlier and the replacement of the real frame collection with artificial ones is similar for this specific subject and with a maximum of N artificial frames.

RESULTS

In Sample Results

A classifier with a specific number of artificial frames is considered similar to its original if its right and left ratios are both below 3 (section Classifier Training and Implementation). Across all subjects and all classifiers, only one of the classifiers with 37.5% of artificial frames of subject S02 is considered as dissimilar (**Table 1**). From the same subject, the classifiers with 25.0 and 50.0% are just below 3. Using lower maximum ratios applied stricter conditions to test the classifiers. If we apply a ratio threshold of 2.6 instead of 3, these two outcomes from S02 would be considered an outlier. Further, subjects S03 and S06 also have high ratio values (above 2.6), but below 3. If a maximum ratio of 2 is applied, all the classifiers for all subjects were acceptable if the frames collection used at most 12.5% of artificial frames. All classifiers were statistically similar to their corresponding original classifiers for subjects S01, S04, S05, and S07.

Classifiers with more than 37.5% of artificial frames for subjects S01 and S06 showed a smaller ratio in the right-side class than the classifiers with fewer artificial frames. However, the left-side class of the same classifiers increased considerably.

Out of Sample Results

The previously created classifiers and the second recorded dataset were used to analyze performance with out-of-sample data. First, we calculated the error rate of the classifiers built without artificial frames. We only designated the classifiers with an error rate below of 33% in both sides as useful. Under these conditions, only subject S01 and S03 had valid error rates in both sides (**Table 2**).

Table 3 presents additional details from subjects S01 and S03. Subject S01 showed very good results, with very small and similar error rates between the original classifiers and the rest of his classifiers. Subject S03 showed higher error rates than subject S01, and the error rates increased slightly with the number of the artificial frames in the frame collection (**Table 3**). Nonetheless, the classifiers built with at most 37.5% of artificial frames had error rates in both sides below the 33% threshold. However, the right-side error rate of classifier with 50% of artificial frames is 34.06%, meaning that this classifier should not be considered as valid.

Considering that only 2 out of 7 subjects were considered valid to be analyzed in an out of sample scenario, and that an error rate below 33% can still lead to a valid classifier, we also used an external EEG MI dataset (Cho et al., 2017) to increase the number of subjects. We selected the four subjects with best accuracies and split their dataset in two different sets of data. The first dataset was used to create the classifier, and the second dataset was used to calculate the out of sample error rate. **Table 4** show the experimental results, which are very close to the results from the subjects recorded in the present study. Results are especially good for subjects E01 and E02. Subject E03 (only) showed a non-valid value in the classifier built with a density of 50%, meaning that all his other classifiers should be considered useful. On the other hand, subject E04 has no value below 33% and any classifier should be considered valid.

TABLE 1 | Ratio between the error rate for each side and its MAD (Median Absolute Deviation).

	S01		S02		S03		S04		S05		S06		S07	
AF[a]	R[b]	L[c]	R	L	R	L	R	L	R	L	R	L	R	L
2.5	0.12	0.67	0.22	0.64	0.58	1.27	0.32	0.31	0.32	0.27	0.33	0.64	0.34	0.69
5.0	0.05	1.03	0.82	0.56	1.11	1.02	0.46	0.45	0.18	0.35	0.47	0.83	0.01	0.63
7.5	0.29	0.88	1.03	0.07	1.06	1.51	0.51	0.51	0.00	0.02	1.17	1.49	0.46	0.62
10.0	0.37	1.13	0.99	0.11	1.19	1.75	0.80	0.46	0.38	0.08	1.04	1.66	0.49	0.84
12.5	0.24	0.94	1.42	0.04	1.89	1.86	1.00	0.44	0.46	0.27	0.87	1.52	0.40	0.85
25.0	0.09	1.44	2.79	0.44	2.13	1.94	1.28	0.61	0.96	0.78	0.71	2.09	0.51	1.28
37.5	0.11	1.55	3.12	0.41	1.97	2.01	1.20	0.69	1.07	1.18	0.57	2.66	0.73	1.92
50.0	0.15	1.45	2.86	1.00	2.18	2.68	1.27	1.06	1.42	1.23	0.62	2.76	0.73	1.86

[a] *AF, % of artificial frames in the classifier.*
[b] *R, right-side ratio.*
[c] *L, left-side ratio.*

TABLE 2 | Error rate of the classifier built with the frame collection without artificial frames.

S01		S02		S03		S04		S05		S06		S07	
R[a]	L[b]	R	L	R	L	R	L	R	L	R	L	R	L
5.50	6.68	11.20	66.67	29.83	20.39	42.67	32.96	36.24	35.79	27.27	39.60	58.34	22.74

[a]*R, right-side error rate.*
[b]*L, left-side error rate.*

TABLE 3 | Error rate of classifiers built with frame collections with artificial frames.

	S01		S03	
AF[a]	R[b]	L[c]	R	L
0.0	5.50	6.68	29.83	20.39
2.5	4.02	7.52	22.20	18.64
5.0	4.06	7.46	22.21	19.20
7.5	3.80	7.66	21.94	20.79
10.0	3.79	7.63	24.52	21.52
12.5	3.76	7.77	24.92	19.96
25.0	3.47	8.05	28.15	24.75
37.5	3.86	8.70	31.59	25.79
50.0	3.79	8.84	34.06	31.39

[a]*AF, % of artificial frames in the classifier.*
[b]*R, right-side error rate.*
[c]*L, left-side error rate.*

Additional Out of Sample Results

In the previous experiments we used a maximum density of artificial frames of 50%. Here we present new experiments increasing this density above 50% in order to determine the subject-specific maximum density possible that can still yield valid classifiers (both mean error rates below 33%). The experiment was repeated for densities of 62.5, 75, and 87.5%. As shown in **Table 5**, subjects S01, E01, and E02 had error rates below 33% with a frame collection composed of 87.5% of artificial frames and below. Subject E04 has no valid classifier, and the other two subjects (S03 and E03) showed error rates above 33% with densities above 50%. However, data from subject E04 had not yielded any valid classifier in the latter results with densities up to 50%.

DISCUSSION

This paper introduced a new method to create EEG artificial data frames to reduce the calibration time required for a MI BCI paradigm. The results suggest that the maximum number of artificial frames that are advisable in a frame collection varies substantially across different people. This could occur because the subject's MI varies within and across each trial, meaning that the mixing of different IMFs might produce a less helpful artificial frame. Longer training should help subjects learn to generate more consistent and distinct MI activity, and shorter trials and improved feedback could also be helpful.

The in-sample results demonstrate that the method is useful when creating similar classifiers for four out of seven subjects when the frame collection has at most 50% of artificial frames, which allows halving the training time for these subjects. This could reduce fatigue, stress and discouragement associated with the training, when feedback is often inaccurate. Additional research might identify methods to identify priori which subjects could tolerate frame collections with 50% or even more artificial frames.

While in-sample results are used to assess the capability of the neurorehabilitation patient or other users to control the BCI, out-of-sample processing is used to send the feedback to the patient. Typically, the BCI uses a classifier created from the preceding session from the patient. Reducing the error rate in out-of-sample data results in more accurate feedback, which should improve the closed-loop synergy between the user and the BCI. Out-of-sample results showed that subjects whose classifiers based on real data yielded acceptable error rates (below 33%) also had acceptable error rates when using the classifiers with artificial frames. However, only 2 out of the 7 subjects had original classifier error rates below 33%, which is insufficient to thoroughly validate this method on an out-of-sample environment.

Our study also included four subjects with good MI accuracy from an external database. Their out-of-sample error rates were very close to the ones achieved with the subjects of our study. Seeing these good out-of-sample results, we extend the experiment with densities beyond 50%. In 3 of these 6 subjects, the results showed that classifiers built with 87.5% of artificial frames still led to error rates below 33%. Additional research will be needed to explore whether the slight increase in error rate resulting from the increase of artificial frames in the frame collection is worth the reduced training time. Further research could also enlarge the density of artificial frames, which may help increase the generalization of the classifiers and thereby decrease their out of sample error rates.

The study showed a similar in-sample behavior in all subjects' classifiers created with a maximum of 12.5% of artificial frames in their frame collections and a strict ratio threshold of 2. Using 12.5% artificial frames would improve a motor imagery BCI system in two ways. First, it would reduce the training time from 720 to 630 s. Second, the method could be used to replace an artifacted frames with artificial ones. In the CSP calculation, the number of frames for each side must be exactly the same, and if there are some artifacted frames in one class, the number of frames in the other class must be reduced accordingly. This can reduce classifier accuracy and may necessitate additional training runs. Instead, up to 12.5% of artifacted frames could simply be replaced.

This study used an LDA classifier due to its widespread use in MI BCI paradigms. Further studies could explore test the artificial frame creation method using different classifiers. Another interesting direction is the mixing strategy of the IMF

TABLE 4 | External datasets.

	E01		E02		E03		E04	
AF[a]	R[b]	L[c]	R	L	R	L	R	L
0.0	12.82	11.43	2.99	18.08	14.56	21.08	4.65	31.51
2.5	12.68	10.85	3.12	17.87	14.04	21.50	4.04	33.49
5.0	12.88	10.65	2.98	18.30	15.37	22.93	4.34	33.66
7.5	13.21	10.48	3.36	17.90	15.13	21.83	4.42	36.77
10.0	13.36	10.80	3.50	17.36	14.65	22.69	4.91	35.91
12.5	13.19	10.64	3.47	17.70	15.54	24.98	4.85	38.27
25.0	14.74	11.10	3.66	17.00	19.47	27.18	7.11	37.38
37.5	15.45	11.72	4.73	16.40	20.90	32.44	7.46	39.52
50.0	15.80	13.34	6.24	17.06	31.04	34.32	9.87	38.20

Out of sample error rates of classifiers built with artificial frames.
[a]*AF, % of artificial frames in the classifier.*
[b]*R, right-side error rate.*
[c]*L, left-side error rate.*

TABLE 5 | Additional results.

	S01		S03		E01		E02		E03		E04	
AF[a]	R[b]	L[c]	R	L	R	L	R	L	R	L	R	L
0.0	5.50	6.68	29.83	20.39	12.82	11.43	2.99	18.08	14.56	21.08	4.65	31.51
25.0	3.47	8.05	28.15	24.75	14.74	11.10	3.66	17.00	19.47	27.18	7.11	37.38
50.0	3.79	8.84	34.06	31.39	15.80	13.34	6.24	17.06	31.04	34.32	9.87	38.20
67.5	10.11	10.76	36.04	46.75	16.15	16.63	7.30	19.28	31.85	41.76	13.15	39.34
75.0	17.98	12.86	39.07	47.67	19.05	18.93	10.87	20.54	34.32	47.03	15.67	44.33
87.5	17.67	28.27	45.30	45.36	23.54	32.25	17.25	26.99	36.56	51.06	26.26	46.39

Out of sample error rate of classifiers built with artificial frames.
[a]*AF, % of artificial frames in the classifier.*
[b]*R, right-side error rate.*
[c]*L, left-side error rate.*

to obtain the artificial frames. The described method mixes 15 IMF from different 15 randomly chosen real frame to build a new artificial frame. Mixing only the most significant IMFs (instead of fifteen), or even reducing the number of real frames to three or four, might both be worth exploring.

This approach might also be extended to other types of BCIs. For example, some passive approaches for evaluating alertness or fatigue might benefit. BCIs based on the P300 complex, steady-state evoked potentials, and similar BCI paradigms that require focused attention typically require much less training than MI and most other BCIs. However, this approach could still be useful for countering artifact or to improve classifier accuracy in some users, such as patients using a vibrotactile P300 system.

Most importantly, this new BCI method needs additional research with more subjects, especially to validate the out-of-sample behavior. These subjects should include target patients, including persons with stroke and other persons seeking rehabilitation. New paradigms could provide training of other types of rehabilitation, such as lower-limb training. Patients with locked-in syndrome (LIS) may also benefit from this approach for communication or other goals.

ETHICS STATEMENT

This study was carried out in accordance with the recommendations of the Ethics Committee of the Kepler Universitätsklinikum (Kepler University Hospital), Austria. The protocol was approved by the Ethikkommission des Landes OberÖsterreich (Ethics Committee of the Province of Upper Austria). All subjects gave written informed consent in accordance with the Declaration of Helsinki.

AUTHOR CONTRIBUTIONS

JS-C conceived and organized the artificial frame generation protocol and its application; JD-F collected the experimental data, implemented the protocol and the classification algorithm, and performed the statistical data analysis; RO contributed to the signal processing section; JS-C and CG had theoretical contributions on the analysis of the results; JD-F wrote the first draft of the paper. All authors reviewed the draft of the paper and approved the final manuscript.

ACKNOWLEDGMENTS

We thank Brendan Z. Allison for the critical comments and suggestions on the draft of the paper. We also thank the Ministry of Business and Knowledge of the Government of Catalonia that partially supported this study (ACCIO RD15-1-0020 project and the Industrial Doctorates Plan), and the SME Phase II Instrument recoveriX (No. 693928).

REFERENCES

Cho, H., Ahn, M., Ahn, S., Kwon, M., and Jun, S. C. (2017). EEG datasets for motor imagery brain-computer interface. *Gigascience* 6, 1–8. doi: 10.1093/gigascience/gix034

Cho, W., Sabathiel, N., Ortner, R., Lechner, A., Irimia, D. C., Guger, C., et al. (2016). Paired associative stimulation using brain-computer interfaces for stroke rehabilitation: a pilot study. *Eur. J. Transl. Myol.* 26:6132. doi: 10.4081/ejtm.2016.6132

Farwell, L. A., and Donchin, E. (1988). Talking off the top of your head: toward a mental prosthesis utilizing event-related brain potentials. *Electroencephalogr. Clin. Neurophysiol.* 70, 510–523. doi: 10.1016/0013-4694(88)90149-6

Guger, C., Kapeller, C., Ortner, R., and Kamada, K. (2015). *Motor Imagery with Brain- Computer Interface Neurotechnology*. New York, NY: Nova Science Publisher, Inc.

Guger, C., Sorger, B., Noirhomme, Q., Naci, L., Monti, M. M., Real, R., et al. (2013). "Brain-computer interfaces for assessment and communication in disorders of consciousness," in *Emerging Theory and Practice in Neuroprosthetics*, eds G. Naik and Y. Guo (Hershey, PA: IGI Global), 181–214. doi: 10.4018/978-1-4666-6094-6.ch010

Guger, C., Spataro, R., Allison, B., Heilinger, A., Ortner, R., Cho, W., et al. (2017). Complete locked-in and locked-in patients: command following assessment and communication with vibro-tactile P300 and motor imagery brain-computer interface tools. *Front. Neurosci.* 11:251. doi: 10.3389/FNINS.2017.00251

Hawley, S. D., Atlas, L. E., and Chizeck, H. J. (2008). "Some properties of an empirical mode type signal decomposition algorithm," in *2008 IEEE International Conference on Acoustics, Speech and Signal Processing* Vol. 3 (Las Vegas: IEEE), 3625–3628.

Huang, J. R., Fan, S. Z., Abbod, M. F., Jen, K. K., Wu, J. F., and Shieh, J. S. (2013). Application of multivariate empirical mode decomposition and sample entropy in EEG signals via artificial neural networks for interpreting depth of anesthesia. *Entropy* 15, 3325–3339. doi: 10.3390/e15093325

Huang, N. E., Shen, Z., Long, S. R., Wu, M. C., Shih, H. H., Liu, H. H., et al. (1998). The empirical mode decomposition and the hilbert spectrum for nonlinear and non-stationary time series analysis. *Proc. R. Soc. A Mathem. Phys. Eng. Sci.* 454, 903. doi: 10.1098/rspa.1998.0193

Koles, Z. J., Lazar, M. S., and Zhou, S. Z. (1990). Spatial patterns underlying population differences in the background EEG. *Brain Topogr.* 2, 275–284. doi: 10.1007/BF01129656

Leys, C., Ley, C., Klein, O., Bernard, P., and Licata, L. (2013). Detecting outliers: Do not use standard deviation around the mean, use absolute deviation around the median. *J. Exp. Soc. Psychol.* 49, 764–766. doi: 10.1016/j.jesp.2013.03.013

Lotte, F. (2011). "Generating artificial EEG signals to reduce BCI calibration time," in *5th International Brain-Computer Interface Workshop* (Graz), 176–179.

Oehler, M., Neumann, P., Becker, M., Curio, G., and Schilling, M. (2008). "Extraction of SSVEP signals of a capacitive EEG helmet for human machine interface," in *Conference Proceedings :... Annual International Conference of the IEEE Engineering in Medicine and Biology Society. IEEE Engineering in Medicine and Biology Society. Conference 2008* (Vancouver), 4495–4498.

Paris, A., Atia, G. K., Vosoughi, A., and Berman, S. A. (2017). A new statistical model of electroencephalogram noise spectra for real-time brain-computer interfaces. *IEEE Trans. Biomed. Eng.* 64, 1688–1700. doi: 10.1109/TBME.2016.2606595

Pfurtscheller, G. (2001). Functional brain imaging based on ERD/ERS. *Vision Res.* 41, 1257–1260. doi: 10.1016/S0042-6989(00)00235-2

Ramoser, H., Muller-Gerking, J., and Pfurtscheller, G. (2000). Optimal spatial filtering of single trial EEG during imagined hand movement. *IEEE Trans. Rehabil. Eng.* 8, 441–446. doi: 10.1109/86.895946

Ramos-Murguialday, A., Broetz, D., Rea, M., Läer, L., Yilmaz, O. L., and Brasil, F., et al. (2013). Brain-machine interface in chronic stroke rehabilitation: a controlled study. *Ann. Neurol.* 74, 100–108. doi: 10.1002/ana.23879

Remsik, A., Young, B., Vermilyea, R., Kiekhoefer, L., Abrams, J., Elmore, S., et al. (2016). A review of the progression and future implications of brain-computer interface therapies for restoration of distal upper extremity motor function after stroke. *Expert Rev. Med. Devices* 13, 445–454. doi: 10.1080/17434440.2016.1174572

Riaz, F., Hassan, A., Rehman, S., Niazi, I. K., and Dremstrup, K. (2015). EMD based temporal and spectral features for the classification of EEG signals using supervised learning. *IEEE Trans. Neural Syst. Rehabil. Eng.* 24, 28–35. doi: 10.1109/TNSRE.2015.2441835

Sabathiel, N., Irimia, D. C., Allison, B. Z., Guger, C., and Edlinger, G. (2016). "Paired associative stimulation with brain-computer interfaces: a new paradigm for stroke rehabilitation," in *Lecture Notes in Computer Science (Including Subseries Lecture Notes in Artificial Intelligence and Lecture Notes in Bioinformatics)* Vol. 9743 (Cham: Springer), 261–272.

Shih, J. J., Krusienski, D. J., and Wolpaw, J., R. (2012). Brain-computer Interfaces In MedicINE. *Mayo Clinic Proc.* 87, 268–279. doi: 10.1016/j.mayocp.2011.12.008

Wang, Y., Gao, S., and Gao, X. (2005). "Common spatial pattern method for channel selelction in motor imagery based brain-computer interface," in *2005 IEEE Engineering in Medicine and Biology Society 27th Annual Conference* (Shanghai), 5392–5395. doi: 10.1109/IEMBS.2005.1615701

Wolpaw, J. R., Birbaumer, N., McFarland, D. J., Pfurtscheller, G., and Vaughan, T. M. (2002). Brain computer interfaces for communication and control. *Front. Neurosci.* 4, 767–791. doi: 10.3389/conf.fnins.2010.05.00007

Wolpaw, J., and Wolpaw, E. W. (2012). *Brain–Computer Interfaces Principles and Practice*. New York, NY: Oxford University Press.

Conflict of Interest Statement: CG is the co-CEO of g.tec Medical Engineering. JD-F and RO are all employed by g.tec Medical Engineering. JS-C declares that the research was conducted in the absence of any commercial or financial relationships that could be construed as a potential conflict of interest.

Copyright © 2018 Dinarès-Ferran, Ortner, Guger and Solé-Casals. This is an open-access article distributed under the terms of the Creative Commons Attribution License (CC BY). The use, distribution or reproduction in other forums is permitted, provided the original author(s) and the copyright owner are credited and that the original publication in this journal is cited, in accordance with accepted academic practice. No use, distribution or reproduction is permitted which does not comply with these terms.

frontiers in Neuroscience

ORIGINAL RESEARCH
published: 29 May 2018
doi: 10.3389/fnins.2018.00353

Machine Learning Classification to Identify the Stage of Brain-Computer Interface Therapy for Stroke Rehabilitation Using Functional Connectivity

Rosaleena Mohanty[1,2], Anita M. Sinha[1,3], Alexander B. Remsik[1,4], Keith C. Dodd[1,3], Brittany M. Young[5,6], Tyler Jacobson[1,7], Matthew McMillan[1,3], Jaclyn Thoma[1,6], Hemali Advani[1], Veena A. Nair[1], Theresa J. Kang[1], Kristin Caldera[8], Dorothy F. Edwards[4], Justin C. Williams[3] and Vivek Prabhakaran[1,5,6,9]*

[1] Department of Radiology, University of Wisconsin-Madison, Madison, WI, United States, [2] Department of Electrical Engineering, University of Wisconsin-Madison, Madison, WI, United States, [3] Department of Biomedical Engineering, University of Wisconsin-Madison, Madison, WI, United States, [4] Department of Kinesiology, University of Wisconsin-Madison, Madison, WI, United States, [5] Medical Scientist Training Program, University of Wisconsin-Madison, Madison, WI, United States, [6] Neuroscience Training Program, University of Wisconsin-Madison, Madison, WI, United States, [7] Deparment of Psychology, University of Wisconsin-Madison, Madison, WI, United States, [8] Department of Orthopedics and Rehabilitation, University of Wisconsin-Madison, Madison, WI, United States, [9] Department of Medical Physics, University of Wisconsin-Madison, Madison, WI, United States

OPEN ACCESS

Edited by:
Mikhail Lebedev, Duke University, United States

Reviewed by:
Bruce C. Wheeler, University of Florida, United States
Zhong Yin, University of Shanghai for Science and Technology, China

***Correspondence:**
Rosaleena Mohanty
rmohanty@wisc.edu

Specialty section:
This article was submitted to Neural Technology, a section of the journal Frontiers in Neuroscience

Received: *02 February 2018*
Accepted: *07 May 2018*
Published: *29 May 2018*

Citation:
Mohanty R, Sinha AM, Remsik AB, Dodd KC, Young BM, Jacobson T, McMillan M, Thoma J, Advani H, Nair VA, Kang TJ, Caldera K, Edwards DF, Williams JC and Prabhakaran V (2018) Machine Learning Classification to Identify the Stage of Brain-Computer Interface Therapy for Stroke Rehabilitation Using Functional Connectivity. Front. Neurosci. 12:353. doi: 10.3389/fnins.2018.00353

Interventional therapy using brain-computer interface (BCI) technology has shown promise in facilitating motor recovery in stroke survivors; however, the impact of this form of intervention on functional networks outside of the motor network specifically is not well-understood. Here, we investigated resting-state functional connectivity (rs-FC) in stroke participants undergoing BCI therapy across stages, namely pre- and post-intervention, to identify discriminative functional changes using a machine learning classifier with the goal of categorizing participants into one of the two therapy stages. Twenty chronic stroke participants with persistent upper-extremity motor impairment received neuromodulatory training using a closed-loop neurofeedback BCI device, and rs-functional MRI (rs-fMRI) scans were collected at four time points: pre-, mid-, post-, and 1 month post-therapy. To evaluate the peak effects of this intervention, rs-FC was analyzed from two specific stages, namely pre- and post-therapy. In total, 236 seeds spanning both motor and non-motor regions of the brain were computed at each stage. A univariate feature selection was applied to reduce the number of features followed by a principal component-based data transformation used by a linear binary support vector machine (SVM) classifier to classify each participant into a therapy stage. The SVM classifier achieved a cross-validation accuracy of 92.5% using a leave-one-out method. Outside of the motor network, seeds from the fronto-parietal task control, default mode, subcortical, and visual networks emerged as important contributors to the classification. Furthermore, a higher number of functional changes were observed to be strengthening from the pre- to post-therapy stage than the ones weakening, both of which involved motor and non-motor regions of the brain. These findings may provide new evidence to support the potential clinical utility

of BCI therapy as a form of stroke rehabilitation that not only benefits motor recovery but also facilitates recovery in other brain networks. Moreover, delineation of stronger and weaker changes may inform more optimal designs of BCI interventional therapy so as to facilitate strengthened and suppress weakened changes in the recovery process.

Keywords: BCI therapy, stroke recovery, functional MRI, functional connectivity, motor network, non-motor networks, machine learning, support vector machine

INTRODUCTION

Recent advancements in neurotechnology have led to the emergence of the brain-computer interface (BCI), which records neural signals and translates them into signals that can control assistive devices, such as computers or prostheses. To date, BCI-based approaches are being investigated as therapeutic strategies to facilitate recovery for several neurological diseases, including stroke, epilepsy, and Parkinson's Disease. For stroke, the long-term objective of the rehabilitation is to improve impaired brain functions so as to restore autonomy in daily activities for stroke survivors. While conventional approaches such as physical therapy and occupational therapy have proven to be successful in aiding stroke recovery in the acute and sub-acute stages (Bütefisch et al., 1995; Gordon et al., 2004) modern technologies involving robotics (Kwakkel et al., 2008), transcranial magnetic stimulation (Corti et al., 2012), and virtual reality (Lohse et al., 2014) have demonstrated promise in promoting additional motor and cognitive recovery to improve autonomy and overall quality of life for stroke survivors even in the chronic stages. The use of an electroencephalogram (EEG)-based brain-computer-interface (BCI) is an unconventional rehabilitation strategy that has emerged as a potentially effective therapeutic modality for promoting motor recovery in patients with stroke (Silvoni et al., 2011). An EEG-based BCI detects and uses a patient's neural signals as inputs to provide real-time feedback, effectively enabling users to modulate their brain activity (Felton et al., 2009). Additional feedback presented by means of functional electrical stimulation (FES; De Kroon et al., 2002) and tongue stimulation (TS) (Wilson et al., 2012) also provide users with multi-modal feedback as a form of reward for producing certain brain activity patterns while performing tasks. While BCI therapy is often explicitly targeted at restoring motor functions, simultaneous changes in non-motor-related functions in the brain may also result after intervention; to date, neural reorganization of cortical regions outside of the motor network is not well-characterized. Distinction between the overall brain state before and after the therapy could facilitate a more thorough understanding of the mechanisms underlying both the strengthening and/or weakening in motor and non-motor networks in participants. Access to this information could allow us to optimize the design and execution of this therapy for stroke rehabilitation.

While EEG allows for study of real-time brain activity during the BCI therapy with a high temporal resolution, neuroimaging methods have afforded us the ability to study both large-scale and small-scale reorganization of brain networks (Van Den Heuvel and Pol, 2010) at a relatively higher spatial resolution. Resting state functional magnetic resonance imaging (rs-fMRI), specifically, has been demonstrated as a powerful and attractive tool to study changes in brain functions as it is non-invasive, time-efficient, and task-free. Rs-fMRI allows us to measure the temporal correlation of the spontaneous, low-frequency (<0.1 Hz) blood-oxygen-level dependent (BOLD) signals across regions in the resting brain. Oscillations in the BOLD fMRI signals are indicative of cortical dynamic self-organization and have been associated with the neural reorganization underlying cognitive and motor function during stroke recovery (Lee et al., 2013; Bajaj et al., 2015). Previous studies have demonstrated that there are overlapping networks between the rs-fMRI-derived motor network and those observed during motor imagery and motor execution fMRI tasks (Grefkes et al., 2008; Nair et al., 2015). A growing number of studies have utilized neuroimaging methods to study the efficacy of BCI therapy in stroke recovery and found modulating changes in neuroplasticity and improvement in motor functions (Di Bono and Zorzi, 2008; Várkuti et al., 2013; Song et al., 2014; Young et al., 2014b; Nair et al., 2015; Soekadar et al., 2015). In the present study, we aim to use rs-fMRI to examine changes in neuroplasticity in whole-brain networks and to examine interactions between motor and non-motor cortical regions in chronic stroke participants following BCI therapy.

A whole-brain analysis resulting in high-dimensional data calls for the application of machine learning-based approaches which have become increasingly more integrated in neuroimaging analysis as they enable discovery of multivariate relationships beyond those identifiable by traditional univariate analysis. Several studies have underscored the utility of machine learning to not only differentiate among population groups (Dai et al., 2012; Meier et al., 2012; Rehme et al., 2014; Fergus et al., 2016; Khazaee et al., 2016; Ding et al., 2017) but also make predictions about behavioral outcomes using regression models (Dosenbach et al., 2010; Vergun et al., 2013; Mohanty et al., 2017), all of which have advanced our understanding of altered brain functionalities associated with several neurological diseases. In the context of BCI systems, linear and non-linear machine learning classification algorithms (Muller et al., 2003; Lotte et al., 2007) including support vector machines (SVMs; Rakotomamonjy and Guigue, 2008), nearest neighbors (Mason

Abbreviations: BCI, brain-computer interface; BOLD, blood-oxygen-level dependent; EEG, Electroencephalography; FES, functional electrical stimulation; LOOCV, leave-one-out cross-validation; MAD, median absolute deviation; MNI, Montreal Neurological Institute; NIHSS, National Institutes of Health Stroke Scale; PCA, principal component analysis; Rs-FC, resting state functional connectivity; rs-fMRI, resting state functional magnetic resonance imaging; SVM, support vector machine; TS, tongue stimulation.

and Birch, 2000), and neural networks (Cecotti and Graser, 2011) have mainly been limited to improvement and optimization of the BCI2000 system from a design perspective to make the system more adaptive and user-friendly (Selim et al., 2008; Danziger et al., 2009; Alomari et al., 2013). Relatively fewer studies have applied machine learning techniques to elucidate the therapeutic impact of BCI interventional therapy in stroke patients based on the dynamics of brain connectivity changes. Specifically, SVM-based classifiers have demonstrated the ability to not only draw a distinction between different classes but also provide insight into underlying features that lead to the separation between them (Dosenbach et al., 2010; Vergun et al., 2013). Given that we aim to extensively investigate whole-brain effects of BCI therapy, a similar classification approach is befitting due to its efficiency in handling high-dimensional rs-fMRI data. Recent developments have brought deep learning approaches into view with applications in the field of medical imaging such as tissue/lesion/tumor segmentation (Birenbaum and Greenspan, 2016; Kamnitsas et al., 2017), image reconstruction/enhancement (Benou et al., 2016; Hoffmann et al., 2016) and population-based classification (Brosch et al., 2013; Payan and Montana, 2015). The efficiency of deep learning algorithms, however, is highly dependent on samples available for training a reliable model. Thus, we adhere to supervised machine learning classifiers given the limited sample size.

With the above considerations in mind, the goal of this study was to identify the stage of therapy using whole brain rs-fMRI data in stroke participants undergoing EEG-based BCI intervention along with additional feedback provided by FES and TS. We analyzed changes in non-motor regions of the brain in addition to the well-studied motor regions following BCI therapy in chronic stroke participants. To this end, we modeled this as a classification problem of discriminating between pre-therapy and post-therapy stages of intervention. Specifically, we illustrated using rs-fMRI that connectivity at the pre-therapy stage can be differentiated from that at post-therapy with reasonable accuracy. A SVM-based machine learning classifier was employed to identify specific functional nodes and connections in the brain between the two stages. The significance of this study is 4-fold: this study suggests that (i) a 10-min task-free rs-fMRI scan could aid in identifying and tracking changes in functional connectivity in the brain over the course of BCI therapy; (ii) SVM-based classification can automate the process of categorizing participants into pre-therapy or post-therapy stages and identify features discriminating between the stages of therapy; (iii) BCI therapy, targeted toward upper-extremity motor restoration, can promote recovery effects related to brain connectivity in both motor and non-motor networks; (iv) identification of specific functional changes that strengthen and weaken between stages of BCI-therapy could inform more tailored designs of BCI systems that facilitate stronger changes and suppress weaker changes to maximize the efficacy of this interventional therapy and improve outcomes for stroke survivors.

METHODS

Study Design

A permuted-block design (Zelen, 1974) that accounted for participant characteristics such as gender, stroke chronicity, and severity of motor impairment was used to randomly assign participants to one of two groups: crossover control group and BCI therapy group. The study paradigm is schematized in **Figure 1**. Ten participants in the BCI therapy group received interventional rehabilitation therapy and were scanned for MRI and rs-fMRI at four time points: pre-therapy (T4), mid-therapy (T5), immediately post-therapy (T6), and 1 month after completing the last BCI therapy (T7) as per the figure. Ten participants in the crossover control group first received three functional assessments and MRI scans during the control phase in which no BCI therapy was administered (T1 through T3 in **Figure 1**), and their assessments were spaced at intervals similar to those given during the BCI therapy phase. Upon completion of the control phase of the study, the crossover control group "crossed over" into the BCI therapy phase of the study. For this study, participants from the crossover control group and the BCI therapy were combined ($N = 20$), treated as a single sample group and studied at the pre-therapy (T4) and post-therapy (T6) stages to provide additional power to the analysis. Even though imaging data were collected at four distinct time-points, changes between pre-therapy and post-therapy were examined as maximal changes would be expected to occur between these two time-points. Therefore, results from this study should be used to demonstrate proof-of-concept.

Participants

All participants were recruited as part of an ongoing stroke rehabilitation study to investigate the effects of interventional therapy using an EEG-based BCI device targeting upper

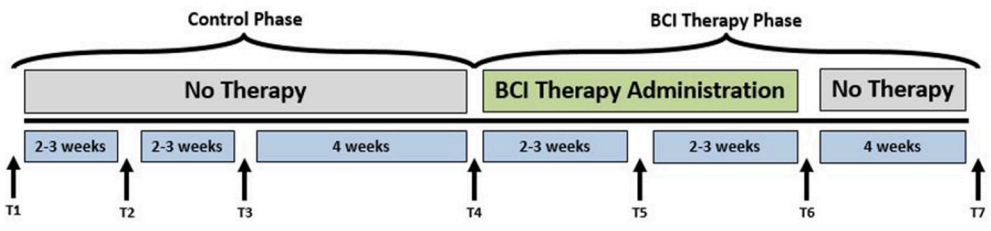

FIGURE 1 | Study paradigm. The time-points at which neuroimaging data were collected are represented by: T1: Control baseline 1, T2: Control baseline 2, T3: Control baseline 3, T4: Therapy baseline T5: Mid-therapy, T6: Post-therapy, and T7: 1-month post-therapy. While the crossover control group completed visits T1 through T7, the BCI therapy group completed visits T4 through T7 only.

extremity motor function. The inclusion criteria for participation were: (1) at least 18 years of age; (2) persistent upper extremity motor impairment resulting from an ischemic or hemorrhagic stroke; (3) ability to provide written informed consent. Exclusion criteria consisted of: (1) concomitant neurodegenerative or other neurological disorders; (2) psychiatric disorders or cognitive deficits that would preclude a participant's ability to provide informed consent; (3) pregnant or likely to become pregnant during the study; (4) allergies to electrode gel, metal and/or surgical tape, contraindications to MRI; (5) concurrent treatment for infectious disease. The study was approved by the University of Wisconsin-Madison Health Sciences Institutional Review Board. All participants provided written informed consent for participation prior to the start of their participation in the study. Participant age was reported corresponding to the first session of BCI therapy. This analysis was limited to chronic stroke participants only (time between stroke onset and the first session of BCI therapy >6 months) since participants in the acute or sub-acute stages often exhibit spontaneous post-stroke recovery that may prove difficult to distinguish from the effects of BCI therapy. While stroke severity was evaluated based on NIH Stroke Scale (NIHSS) score (Brott et al., 1989), the severity of motor impairment was assessed on the basis of standardized scores on the Action Research Arm Test (Carroll, 1965; Lang et al., 2006) and was dichotomized into severe and moderate. Group participant characteristics are summarized in **Table 1**.

BCI Therapy

The primary purpose of using BCI therapy in this work was to promote restorative function by providing neuromodulatory training with concurrent assistive stimulation that generated actual movement in the impaired upper limb. The BCI device was controlled by actual attempted movement of the user and not imagined movement. The attempted movement, in turn, generated neural activity, as recorded by EEG signals, which translated into computer-generated feedback in real time. Here we provide a concise summary of the procedure for the BCI intervention. The steps of intervention were consistent with those described in depth in prior studies (Wilson et al., 2009; Young et al., 2014a). Neural activity was recorded using a 16-channel EEG cap (g.GAMMA cap, Cortech Solutions) and amplifier (Guger Technologies) and processed using BCI2000 software (Schalk et al., 2004). Movements of the impaired upper extremity were facilitated with two forms of external stimulation: TS (TDU 01.30, Wicab Inc.) and FES (LG-7500, LGMedSupply; Arduino 1.0.4). Three main components were implemented: (i) open-loop attempted movement without any feedback for determination of channels and frequencies for subsequent steps; (ii) closed-loop attempted movement with visual feedback in the form of a cursor task that utilized EEG signals of the user in real time; and (iii) closed-loop attempted movement as in step (ii) with additional feedback in the form of TS and FES to the muscles of the impaired arm.

TABLE 1 | Study sample characteristics.

Characteristic	Value
Sample size	20
Age (mean age ± SD)	62.4 ± 14.3 years
Gender (male/female)	12/8
Lesion hemisphere (left/right)	8/12
Time since stroke (mean ± SD)	37.6 ± 40.8 months
Stroke severity (severe/moderate)	11/9

Data Acquisition: Neuroimaging Data

Structural MRI scans lasting about 5 min were acquired on 3T GE 750 scanners (GE Healthcare, Waukesha, WI) equipped with an eight-channel head coil. These were T1-weighted axial anatomical scans and were collected using FSPGR BRAVO sequence with the following specifications: $TR = 8.132$ ms, $TE = 3.18$ ms, $TI = 450$ ms over a 256×256 matrix and 156 slices, flip angle $= 12^{\circ}$, FOV $= 25.6$ cm, slice thickness $= 1$ mm. Ten-minute rs-fMRI were collected with participants lying in the scanner with their eyes closed. Participants were instructed to relax with their eyes closed while trying not to fall asleep during this scan. Rs-fMRI scans were obtained using single-shot echo-planar T2*-weighted imaging with the following parameters: $TR = 2.6$ s, 231 time-points, $TE = 22$ ms, FOV $= 22.4$ cm, flip angle $= 60^{\circ}$, voxel dimensions $3.5 \times 3.5 \times 3.5$ mm^3 and 40 slices.

Data Availability Statement

The raw data supporting the conclusions of this manuscript will be made available by the authors, without undue reservation, to any qualified researcher.

Individual Participant Analysis

Data Preprocessing

All scans were inspected visually to ensure they were free of any apparent artifacts. Rs-fMRI data were processed using Analysis of Functional NeuroImaging (AFNI) (Cox, 1996) software. Functional scans were despiked, slice time corrected, motion corrected, aligned with the anatomical scan, normalized to the standard MNI (Montreal Neurological Institute) space using the T1 scan, resampled to 3.5 mm^3, and spatially smoothed with a 4-mm full-width-half-maximum Gaussian kernel. Motion censoring (per TR motion >1 mm or 1°), regression of white matter and cerebrospinal fluid signals, and bandpass frequency filtering were performed simultaneously in one regression model. The bandpass filtering was focused to the typical low oscillation fluctuations within 0.01–0.1 Hz. Global signal regression was omitted due to ongoing controversy in the literature associated with its use (Murphy and Fox, 2016).

Seed-Based Functional Connectivity

Based on a previous study (Power et al., 2011), 236 seed regions of interest (ROI) spanning regions from 13 distinct networks were selected. This seed template provides full coverage of various motor and non-motor brain regions and has been utilized to study functional reorganization of the brain in healthy participants. The regions are depicted in **Figure 2,** as per the MNI coordinates, and the networks are encoded as per **Table 2**. Spherical seeds of 5 mm radius each were created for each

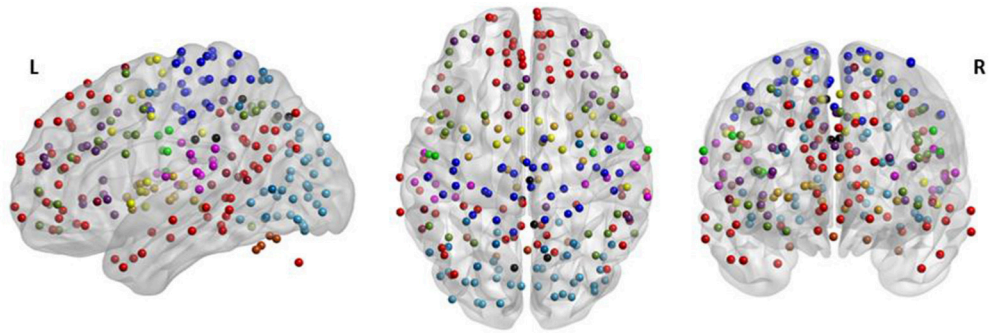

FIGURE 2 | The 236 seeds regions involving motor and non-motor regions include 13 major brain networks color coded according to **Table 2** and visualized using BrainNet Viewer (Xia et al., 2013). The seed regions falling outside the template of cerebrum were part of the cerebellum.

TABLE 2 | The seed template encompasses the whole brain comprising of 13 distinct brain networks coded by colors and specified number of regions.

Brain network	Seed color	Number of seeds
Sensory/somatomotor hand		30
Sensory/somatomotor mouth		5
Cingulo-opercular task control		14
Auditory		13
Default mode		58
Memory retrieval		5
Ventral attention		9
Visual		31
Fronto-parietal task control		25
Salience		18
Subcortical		13
Cerebellar		4
Dorsal attention		11

participant. This seed template was applied to the spatially normalized, smoothed, and filtered residuals of the resting data and BOLD time series was extracted at each of the 236 seed regions. A correlation matrix of size 236-by-236 was generated by temporally correlating time series from all pairs of seeds. Of the 55,696 correlation coefficients generated, 27,730 unique coefficients were retained for analysis and the duplicates were discarded. The unique correlation coefficients were computed from data at the pre- and post-therapy stages and used as input features for the discrimination between the stages. The methodology at single-participant level is outlined in **Figure 3.**

Group Level Analysis

Applications of classification using machine learning algorithms such as SVM on rs-fMRI have been demonstrated in multiple studies (Dosenbach et al., 2010; Vergun et al., 2013). For the purpose of this study, we adopted a similar strategy, i.e., we applied a binary linear-kernel SVM to rs-FC in order to classify between the two classes, namely pre-therapy and post-therapy. The rs-FC data for all participants were aggregated and the steps described as follows were implemented.

Outlier Removal

It is acknowledged that with a limited sample size, the data could be skewed due to the presence of outliers; therefore, possible outlier features were detected and removed from the data set. To this end, a median absolute deviation (MAD) (Leys et al., 2013) method detected any value that is more than three scaled MADs away from the median in a given feature which is deemed an outlier. This was repeated for each feature within the pre-therapy stage and post-therapy stage. The features containing these outliers were eliminated, saving only common features across pre- and post-therapy.

Feature Selection and Transformation

The rs-FC per participant consisted of 27,730 coefficients resulting in a high-dimensional dataset. Drawing useful conclusions based on a reasonable classifier is incumbent upon selecting meaningful and important features. One way to achieve this is by means of dimension reduction. Given that a large number of features with a small sample size can result in overfitting to noise, we adopted a feature selection step followed by a feature transformation step. The feature selection was a preprocessing step to select a subset of 27,730 features using a univariate paired t-test between the features of pre-therapy and post-therapy stages. Features were tested for normality using the Kolmogorov-Smirnov test (Massey, 1951) and a subset of normal features was selected on the basis of the p-value for each individual feature that indicated its effectiveness in the separation between the two aforementioned stages. However, the filtered features were still high-dimensional and could easily lead to overfitting. Therefore, the reduced data obtained from the previous step were transformed to a lower dimensional space using principal component analysis (PCA; Jolliffe, 1986; Jackson, 2005). A PCA-based feature transformation was suitably chosen as it assumes that data can consist of correlated variables (features) and the redundancy can be simplified by forming an uncorrelated basis composed of the principal components which is low-dimensional and

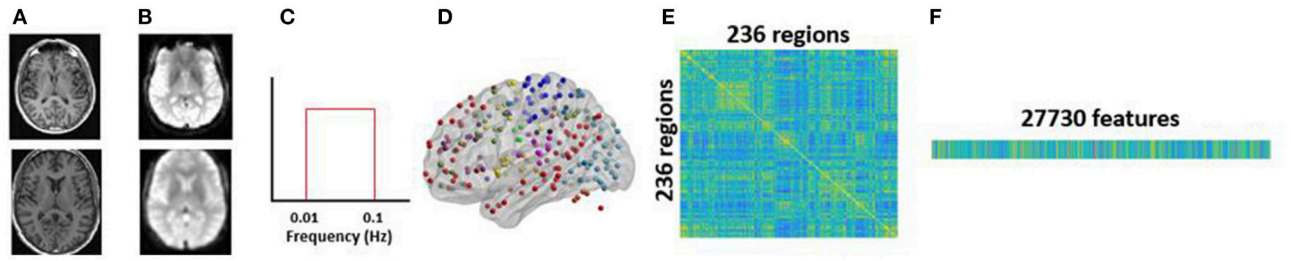

FIGURE 3 | Methodology for single-participant analysis: **(A)** raw structural T1 scan (top) was preprocessed and spatially normalized to MNI space (bottom); **(B)** raw functional scan (top) was preprocessed up to smoothing (bottom); **(C)** smoothed fMRI was temporally filtered to obtain the low frequency oscillations within the range of 0.01–0.1 Hz using a bandpass filter; **(D)** 236 seeds comprising of 13 major brain networks were used to extract BOLD time courses at each seed region; **(E)** 236 × 236 rs-FC matrix was computed using the BOLD time courses; **(F)** unique pairwise correlations contained in the lower triangle of the rs-FC matrix were extracted and vectorized into a 27,730-dimensional vector.

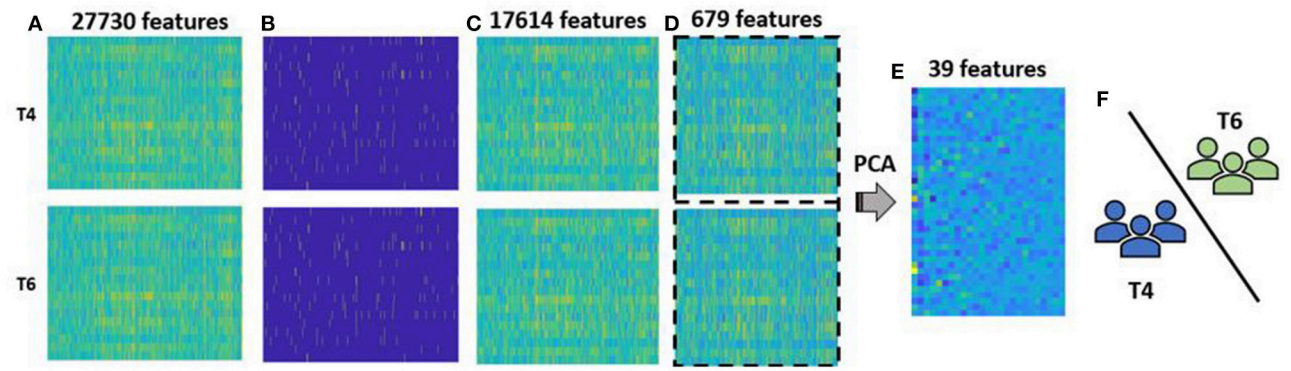

FIGURE 4 | Methodology for group-level analysis: **(A)** vectorized form of rs-FC matrix for each participant aggregated for T4, i.e., pre-therapy and T6, i.e., post-therapy time points. Each group had 20 participants with 27,730-dimesional features; **(B)** outliers (marked in yellow) at pre- and post-therapy were identified using MAD approach; **(C)** reduced rs-FC matrix after cumulative outliers were removed, i.e., each stage consisted of 20 participants and 17,614 features; **(D)** 679 features that were significantly different between pre- and post-therapy stages as identified by a paired *t*-test were retained and data across the two stages were combined together for a feature transformation step; **(E)** feature transformation using PCA was performed that resulted in data with 40 participants and 39 low-dimensional principal components features. Of them 25 features accounted for more than 85% variance and were used as final features for classification; **(F)** the selected features were fed to the binary SVM classifier that labels each test participant to either pre-therapy or post-therapy stage using LOOCV.

accounts for a large fraction of variance in the original data. Each principal component is simply a linear combination of the original rs-FC features. PCA is based upon computation of covariance matrix of the raw data. Only mean centering was applied to the raw data prior to application of PCA. Variance was not standardized as it can change the covariance matrix and lead to misleading principal components. The first few principal component scores were selected based on the amount of variance accounted for in the raw data and were used in the classification step.

Classification

Once the appropriate number of principal components was extracted in the feature selection and transformation step, classification between the pre-therapy and post-therapy stages was performed using the learned principal component-based features. The inputs to the classifier were no longer the raw rs-FC coefficients. Instead, the principal component scores, each of which corresponded to a linear combination of multiple rs-FC features, were fed into the classifier as features. Additionally, since SVM-based classifiers do not assume data to be normally distributed, the traditional Fisher z-transformation was not necessary. However, the principal component scores were scaled and standardized so that each component score had the same mean and variance to avoid some features from potentially dominating others due to large magnitude. This was realized by mean centering and scaling by the standard deviation of each component score. A binary classifier was trained on these features and cross-validated on an out-of-sample participant. To allow for more straightforward interpretation of results, a linear-kernel SVM was applied due to the advantage of ease of interpretation of results. Additionally, the choice of a linear-kernel classifier was supported by the linear separability in the data. As observed in three-dimensional space in **Figure 5**, the principal component features are almost linearly separable. Thus, there is a likelihood that the two classes are linearly separable in higher dimensions which are used for classification (Noble, 2006).

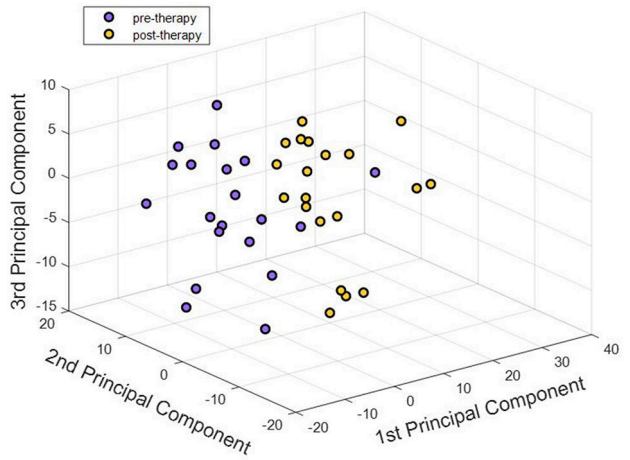

FIGURE 5 | First three principal components corresponding to pre-therapy rs-FC and post-therapy rs-FC for all participants were visualized. Each point in the 3-D plot corresponds to a participant. There appeared to be an almost clear separation between the two stages just with three principal components. Adding higher number of components better explained the variance in the data. Our analysis used 25 components that explained over 85% of the variance in the dataset.

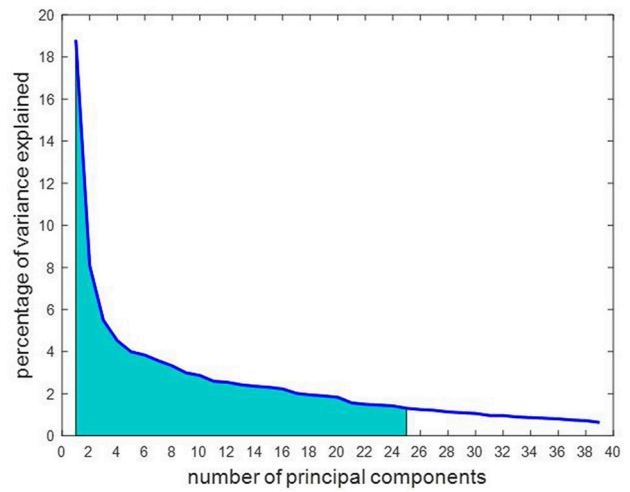

FIGURE 6 | The number of principal components are arranged in order of importance so that the first component accounts for the largest proportion of variance in the rs-FC data. Of the 39 principal components, 25 were chosen as marked in the graph as they cumulatively explained over 85% of the variance in the data, represented by the shaded area under the curve.

Cross-Validation

A leave-one-out cross-validation (LOOCV) method (Hastie et al., 2001) was adopted to estimate classifier performance as it provides an approximation of the test error with lower bias and is more suitable for a dataset with a small sample size such as here. Since our analysis followed a within-participant design, we performed a LOOCV by participant to avoid introducing possible "twinning" bias. This means that the data consisting of 40 observations (pre-FC and post-FC from 20 participants) were subdivided into 20-folds such that each fold comprised of pre-FC and post-FC data from a single participant. The classifier was trained using features from 19-folds (equivalent to 38 observations from pre- and post-stages of 19 participants) and tested on the left-out fold (2 observations from pre- and post-stages of 1 participant). This was repeated 20 times such that data from each participant was left out once while a model was generated using the rest of the data. The performance of the model was assessed by averaging the accuracies over all iterations.

TABLE 3 | The number of features derived from the rs-FC data utilized in various steps of the analysis.

Analysis step	Number of features	Feature space
Original features	27,730	rs-FC
After outlier removal	17,614	rs-FC
After univariate filtering	679	rs-FC
After principal component analysis	39	reduced
Chosen principal components for classification	25	reduced

The feature space indicates whether the corresponding features were measures of functional connectivity, i.e., rs-FC space or principal components comprised of linear combination of multiple rs-FC features, i.e., reduced space.

Model Parameter Optimization

To achieve high classification accuracy, the SVM classifier relies on both feature selection and learning optimized model parameters. Specifically, the misclassification cost and kernel scale parameters of the classifier were optimized with a Bayesian optimization (Snoek et al., 2012) approach. By minimizing the cross-validation error over a range of values for 30 iterations, the optimal parameter values were obtained that further improve the classification performance.

Feature Contribution

Once a model was learned with the optimal parameters, the use of a linear-kernel SVM allowed understanding of underlying discriminatory brain connections. The PCA feature transformation yielded linear coefficients that weigh features and the importance of each feature was dependent upon the magnitude of the associated coefficient.

Seed Contribution

Based upon the feature weights obtained for each of the discriminating functional connections, seed region weights were calculated for individual brain regions. This was achieved by halving the feature weight of each functional connection and assigning this value to the two seeds involved (Meier et al., 2012). A cumulative measure of weight corresponding to each seed was computed by averaging the half-weights across all discriminating connections.

Overview of Methodology

Overall, a classification model using rs-FC was learned and optimized, and the contributing rs-FC features and ROIs that provided the maximum discriminative power based on cross-validation performance were identified. All computations were carried out using the Statistics and Machine Learning Toolbox in

MATLAB R2017a (The MathWorks, Inc., Natick, Massachusetts, United States). The group-level analysis pipeline is illustrated in **Figure 4**.

RESULTS

Performance of Classifier

Outlier Removal

Each of the 27,730 features was tested for the presence of outliers within the pre- and post-therapy stages separately. Features were removed if they contained values that were more than three scaled deviations from the median. MAD was chosen as it is more robust in comparison to the standard deviation measure. Outliers constituted 21.99% of the features in the pre-therapy stage and 19.53% of the features in the post-therapy stage. After outliers across both time-points were removed, 17,614 features were retained in each class.

Feature Selection and Transformation

The 17,614 features remaining after outlier elimination were used as input to the feature selection step. Each feature was tested for normality and the univariate paired *t*-test resulted in 679 features that were significantly different between the two stages. During feature transformation using PCA, the number of principal components was determined to be the smaller of these two: number of samples-1 or number of input features. Thus, application of PCA resulted in 39 principal components in this case, each of which was uncorrelated to each other and was realized as a linear combination of the 679 input features. Of the 39 components, 25 components were able to account for over 85% of the variance in the data and were fed into the classifier. Due to lack of visualization tools in 25 dimensions, a simpler plot with the first three components was generated as displayed in **Figure 5**. The separation observed in the visualization suggests that PCA was able to build useful low-dimensional features that can help in differentiating between the two stages. For classification, the chosen number of components was based on the variance explained by them as shown in **Figure 6**. An account of number of features retained at each step of processing from original space (i.e., features are rs-FC coefficients) to reduced space (i.e., features are principal components) is provided in **Table 3**.

Cross-Validation

A binary SVM classifier was built using 25 principal component features. Classification performance was cross-validated using the LOOCV method and was used to assess and compare results as quantified in **Table 4**. The accuracy of LOOCV represents the percentage of individual samples that were correctly classified when left out. Since accuracy is a single-point statistic, the results were further broken down into a confusion matrix metric to understand the bias of the classifier toward each class, if any. In addition, multiple performance evaluation metrics were evaluated such as specificity, sensitivity, and area under the curve. The receiver operator curve (ROC) plotted in **Figure 7** indicated that the classifiers developed here have superior performance as compared to a random classifier.

Model Parameter Optimization

The optimal values of classifier parameters, i.e., the misclassification cost and scaling factor for the linear kernel were generated by the Bayesian approach for each classifier and are listed in **Table 4**. As observed, optimization of the model parameters improves the classifier performance further. This is also reflected in the ROC plot in **Figure 7**.

Strengthened and Weakened Functional Changes as Discriminating Features

From the evaluation of classification performance, it is possible to extract the features that were involved in classification, as well as the importance of each feature in making the distinction between classes. Our objective was to identify discriminating features between groups that strengthened from pre-therapy to post-therapy and those that weakened from pre-therapy to post-therapy. All changes in rs-FC were assessed in terms of group means. Considering the 679 features that went into the final classification model, the distribution of features is presented in **Table 5**. Stronger connections outnumbered weaker connections

TABLE 4 | Overall comparative results obtained from LOOCV of binary SVM classifier.

Metric	Performance without optimization			Performance with optimization		
LOOCV accuracy	90%			92.5%		
Confusion matrix		**Pre**	**Post**		**Pre**	**Post**
	Pre	18	2	Pre	18	2
	Post	2	18	Post	1	19
Specificity	0.90			0.95		
Sensitivity	0.90			0.90		
Area under the curve	0.9825			0.9850		
Misclassification cost	1 (default)			0.0010		
Kernel scale	1 (default)			0.0011		

The rows of confusion matrix represent the actual class while the columns show the predicted class.

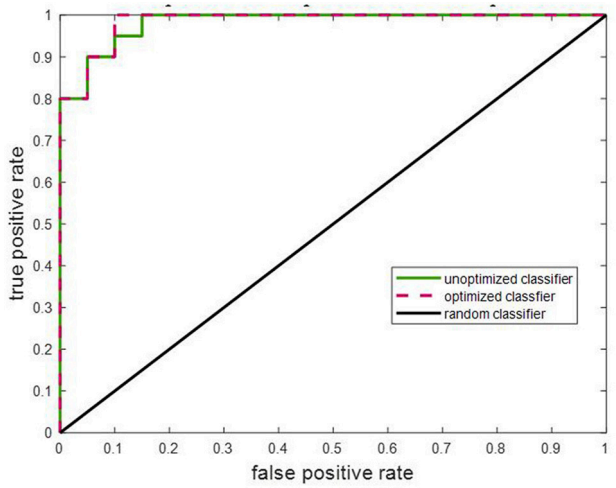

FIGURE 7 | The ROC for the learned SVM classifier was compared to that of a random classifier. The SVM classifier with optimized model parameters showed the best performance. The area under the curves for unoptimized and optimized SVM are specified in **Table 4**.

TABLE 5 | Breakdown of discriminating features into functional connections that strengthened and weakened from pre-therapy to post-therapy are shown for motor as well as non-motor regions.

	Motor	Non-motor	Total
Strengthened	105	336	441
Weakened	71	167	238
Overall	176	503	679

*The colors correspond to the edges in **Figure 8**. The specific stronger and weaker connections in terms of networks and anatomical locations are provided in Supplementary Tables 1, 2, respectively.*

in discriminating between the two stages of therapy both in the motor and non-motor networks. Individual functional changes that strengthened and weakened over time are listed in Supplementary Tables 1, 2, respectively in the order of their importance. These changes are also visualized in **Figure 8**.

Discriminating Seed Regions

Motor as well as non-motor regions were involved in differentiating between pre- and post-therapy. Among the 679 total input features, the distribution of frequency of involved seed regions by network is presented in **Figure 9**. As observed, seed regions from all major motor and non-motor networks showed involvement in the discriminating features. From **Figure 9A**, it appeared that the default mode network had the highest number of involved regions; however, the distribution of number of seeds across the networks was not equal as listed in **Table 2**. The number of discriminating features was normalized by the number of seeds available within each network and plotted in **Figure 9B**. In particular, networks that exhibited greater normalized involvement included regions from visual, subcortical, fronto-parietal task control, cingulo-opercular task control, default mode, and hand-mouth motor networks.

In addition to assessing the frequency of involvement, the seeds were also assigned weights to study the importance of each seed region based on the coefficients of the principle components. The coefficient corresponding to each feature or connection was halved and assigned to the involved seed regions as per prior work by Vergun et al. (2013). This was repeated across all 25 principal components, and the average of those weights determined the final weight of the seed regions. The weighted seed regions are shown in **Figure 10**. The complete list of weighted seeds, anatomical locations, and corresponding networks can be found in the Supplementary Table 3. The highly-weighted regions identified are known to be part of the fronto-parietal task control, hand motor, subcortical, visual, and default mode networks.

DISCUSSION

Rs-fMRI as a Tool to Track Stroke Recovery

Results from this study highlight the utility of rs-fMRI as a tool to track changes in the brain during stroke recovery through rehabilitative therapy. Rs-fMRI is particularly attractive because it only requires about 10 min for acquisition and is task-free. Our analysis suggests that a similar analysis might be extendable to incorporate more than one time-point to gain deeper insight into the recovery process.

Large-Scale Impact of BCI Stroke Rehabilitation

The majority of BCI-aided therapy programs are targeted at the recovery of a particular impairment, such as motor functions, as was the case for participants studied in this cohort. Our findings showed that such a therapy can impact not only motor but also non-motor networks in the brain. We demonstrate a greater number of functional connections growing stronger than ones growing weaker over time over the course of this therapy. These results can better guide the design and implementation of BCI systems to facilitate greater changes that strengthened in patients with stroke.

Machine Learning as a Tool to Identify Stage of Therapy and Relevant Functional Differences

As evident from the confusion matrix in **Table 4**, we were able to differentiate between the two stages of BCI therapy with high cross-validation accuracy. High-dimensional rs-FC extracted from whole brain analysis was downscaled by PCA-based feature transformation that helped elucidate differences across stages of therapy regarding underlying brain connections involved. In comparison to a random classifier that is 50% accurate, our machine learning classifier developed using low-dimensional features derived from rs-FC performed much better with over 90% accuracy. These results indicate that with a large sample size, a SVM classifier could be trained on rs-FC data to categorize a new participant into either the pre-therapy or post-therapy stage of the recovery process by identifying the most discriminative rs-FC features.

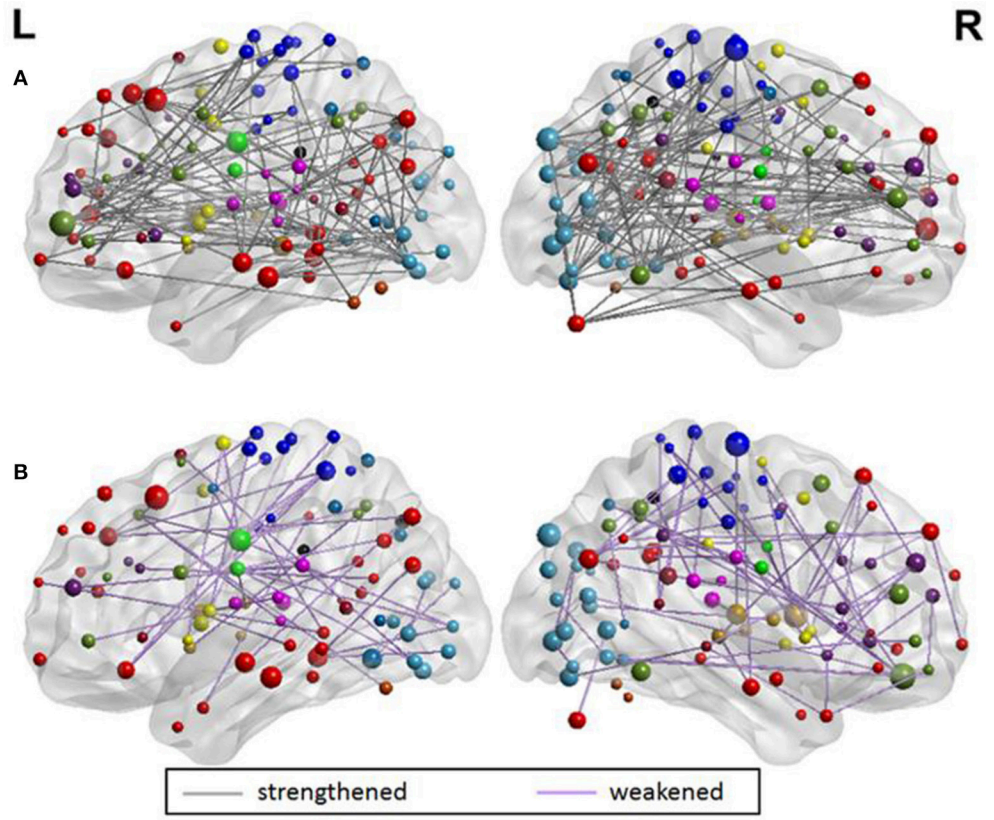

FIGURE 8 | Visualization of **(A)** 441 strengthening functional connections and **(B)** 238 weakening functional connections. The overall number of connections involved in the motor and non-motor networks can be found in **Table 5**. A detailed list of individual connections can be found in the Supplementary Tables 1, 2, respectively. All brain visualizations were performed using BrainNet Viewer Toolbox (Xia et al., 2013).

The Bigger Picture

The current study is presented from a neuroimaging perspective of the changes occurring after BCI therapy. However, other than the neuroimaging methods, EEG and behavioral data are the core components of this interventional study. Since this therapy is based on acquisition of simultaneous EEG, it would be important to understand the spectral data to support the effects of the therapy. Group-level EEG analyses were conducted on the associated cohort ($N = 21$) and the results are currently reported under separate covers to the same issue (Remsik et al., submitted, currently submitted for review to Frontiers in Neuroscience, section Neural Technology). The analysis studied the levels of desynchronization and coherence over the motor cortex and performance with respect to functional outcomes across all time-points. Similarly, rs-FC in the motor cortex before and after the therapy associated with subjective and objective behavioral outcomes have been quantified in another manuscript submitted to the same journal (Mohanty et al., submitted, currently submitted for review to Frontiers in Neuroscience, section Neural Technology).

The most common rehabilitative clinical applications of BCI systems (Bamdad et al., 2015) include speech (Brumberg et al., 2010; Mugler et al., 2013) and motor (Birbaumer, 2006; Neshige et al., 2007; Sun et al., 2011) rehabilitation. Fewer studies have adopted the BCI paradigm for cognitive rehabilitation (Gomez-Pilar et al., 2014). Most of these deal with improving a specific function and study changes occurring in the associated limited brain regions. As per Supplementary Table 3, the motor regions that contributed the most to classification were found over the bilateral precentral gyrus which forms the core of the primary motor cortex. This is in alignment with findings that focus specifically on post-stroke changes in the motor network (Lotze et al., 1999; Young et al., 2014b; Nair et al., 2015). In addition, our study expands the knowledge further by identifying brain changes that occurred in the non-motor areas involving fronto-parietal task control, default mode, and visual networks even though the BCI therapy was primarily targeted at the recovery of motor function. This demonstrates the importance of comprehending the gross impact of BCI therapy on a whole-brain level. Additionally, since the BCI system is adaptive in nature (Schalk et al., 2004), the knowledge about functional changes that are strengthening and/or weakening as a result of this therapy might point toward a better design of the intervention. Maladaptive changes caused by the compensatory activity of the unaffected side has been shown to prevent recovery on the affected side (Takeuchi and Izumi, 2012). One direction to harness this information could involve regulating the way EEG

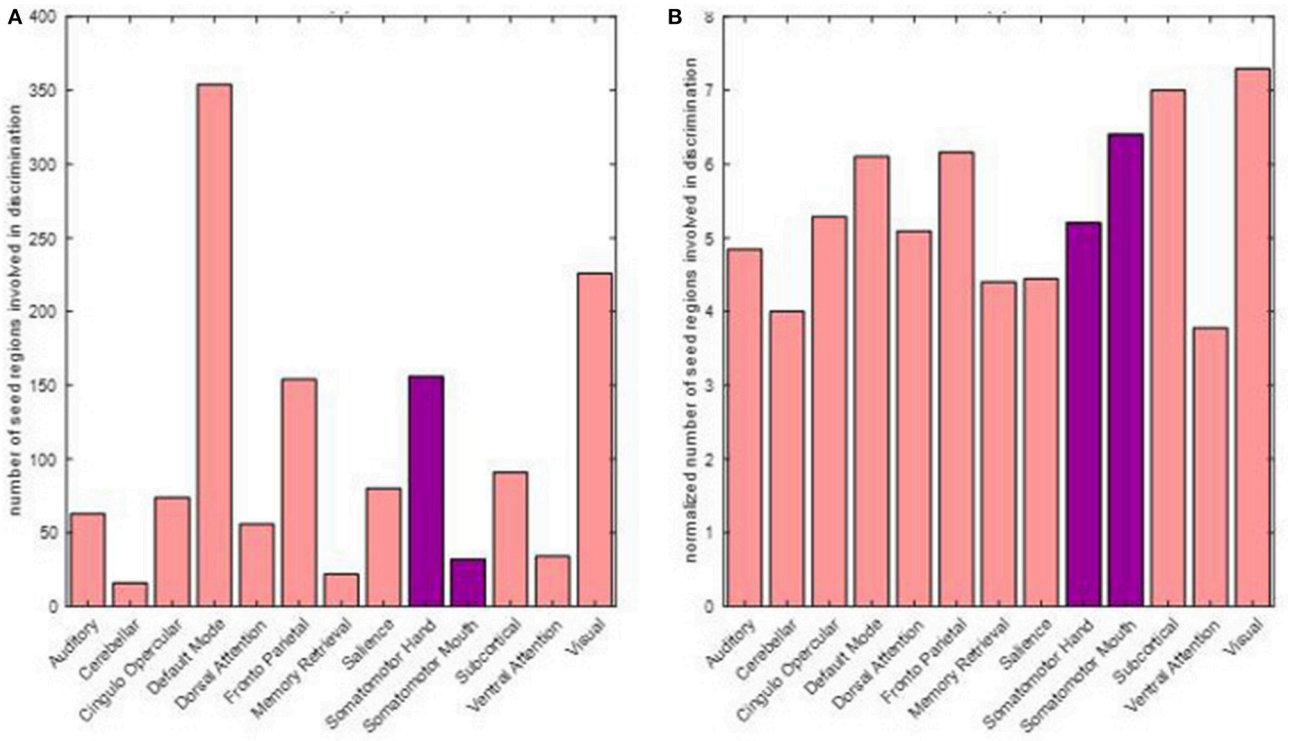

FIGURE 9 | Number of discriminating connections per network is plotted below: **(A)** shows the distribution of involvement of various networks in discriminating features; **(B)** shows the involvement of various networks when normalized with respect to the number of seeds found in each network. The two networks primarily associated with motor functions are highlighted.

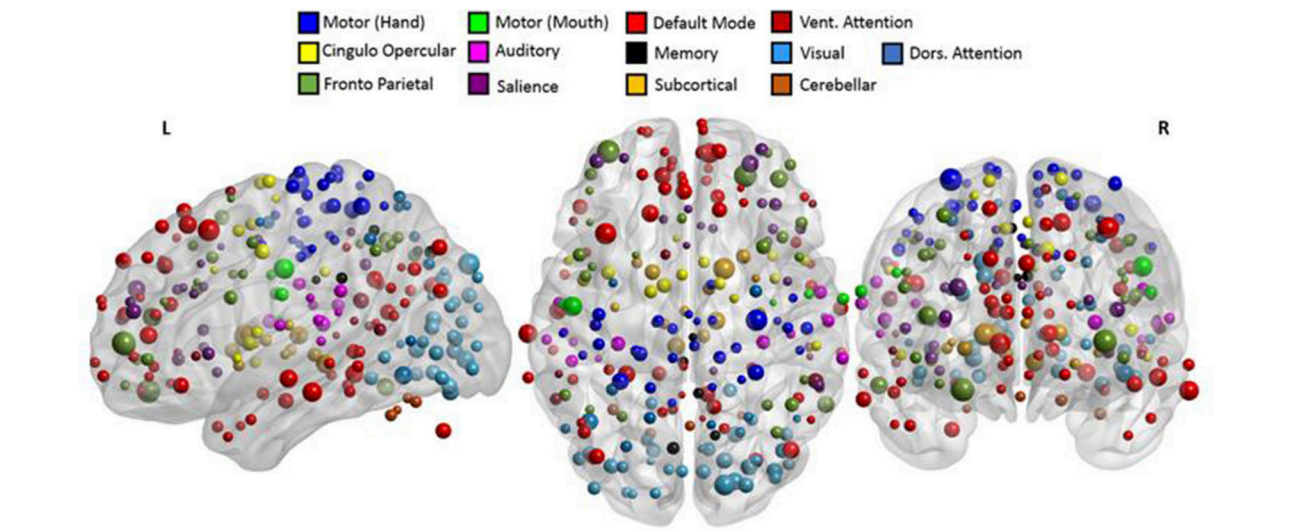

FIGURE 10 | Involved seed regions were weighted as per their contribution in classification. The size of each seed was directly proportional to assigned weight. The top weighted seeds belonged to fronto-parietal, hand motor, default mode, and visual networks. A detailed list of the networks and labels of ROIs ranked as per their weights are presented in Supplementary Table 3.

signals are processed within BCI device. The signal processing module of the BCI system that takes into account the signal generated at each output channel could be modulated so as to maximize the changes that grew stronger and minimize the changes that grew weaker, thus, tailoring the therapy for each user.

Limitations

Our results show that standard machine learning approach has the potential to track recovery through BCI therapy. However, the study was constrained in terms of the sample size since conventional machine learning analysis relies on training on a large dataset so as to have greater power of generalizability. Although we attempted to include a comparable number of participants of both genders, different lesion locations and volumes, and differing levels of stroke severity, heterogeneity in any of these factors might be relevant considerations for future analysis as they could potentially influence the results. In this analysis, the number of samples available for training impacted the number of principal components (rank of covariance matrix) evaluated in the feature transformation step using PCA. Higher number of samples would provide higher degree of freedom. With continuing recruitment, using a larger and more homogeneous participant cohort would allow for more generalizable conclusions. The definition of rs-FC was based upon Pearson's correlation, which is a classical approach and accounts for linear dynamics among the BOLD signals. Recent studies such as that conducted by Smith et al. (2011) provide alternate definitions of rs-FC such as mutual information, cosine similarity, and dynamic time warping; therefore, applying different definitions of seeds and rs-FC could impact the underlying discriminatory features in classification. Although several non-motor networks were identified as being recruited during recovery, we have not investigated the behavioral implications of this finding, i.e., whether strengthened connections in these networks correlate with behavioral gains in various brain functions. The notion of stronger and weaker changes in rs-FC in this study might not reflect adaptive and maladaptive changes in behavioral aspects even though we observed overall improvement at the group-level in measures such as the Action Research Arm Test (mean change $= 0.85$), and domains of the Stroke Impact Scale (mean change in hand function $= 0.75$; mean change in physical strength ≤ 0.13) from pre-therapy to post-therapy.

Future Scope

The ongoing recruitment for this study offers a broad future scope to incorporate more participants that can form a more homogenous cohort. Comparison between stroke participants undergoing rehabilitative therapy and healthy participants undergoing the same therapy will allow comprehension of recovery specifically associated with the event of a stroke. An analysis similar to our study could be extended to incorporate other time-points during the BCI therapy paradigm, such as the mid-therapy (T5) and 1-month post-therapy (T7) time points. Aside from rs-fMRI, alternative neuroimaging methods such as diffusion tensor imaging, task-fMRI, arterial spin labeling, and perfusion imaging capture complementary information and could be used to analyze and compare classification performance.

CONCLUSION

We utilized PCA-based feature transformation coupled with a SVM classifier to discriminate stroke participants by stage of BCI intervention (i.e., the pre-therapy stage to the post-therapy stage) on the basis of rs-FC in both motor and non-motor regions. The findings from this study can be summarized as follows: (i) data from a task-free rs-fMRI can help identify changes across stages of the BCI-aided stroke intervention and hence, has the potential to track stroke recovery; (ii) using a machine learning SVM classifier facilitates automation of discrimination between stages of therapy with a reasonably high accuracy and examination of discriminating connections; (iii) both motor and non-motor regions of the brain undergo reorganization during this intervention. Higher number of strengthening functional changes in comparison to the ones weakening between pre- and post-therapy suggests a greater overall positive impact of BCI intervention on stroke recovery at a whole-brain level; (iv) the capability of delineating such specific changes holds promise for better design of the BCI therapy that could incorporate the information by reinforcing stronger changes while suppressing weaker changes.

AUTHOR CONTRIBUTIONS

RM was involved in data collection, analysis, interpretation of results, and writing of the manuscript. AS was involved in data collection, preprocessing data, and writing the manuscript. BY was involved in subject recruitment, data collection, and editing of the manuscript. AR, KD, TJ, MM, JT, and HA were involved in data collection. VN contributed to data collection, manuscript editing, and intellectual content. TK was involved in the recruitment of study participants. KC was involved in subject recruitment. DE is the co-I and JW, VP are co-PIs, and were involved in study conception, design, manuscript editing, intellectual content, and supervised all aspects of the study.

FUNDING

This work was supported by NIH grants RC1MH090912-01, T32GM008692, UL1TR000427, K23NS086852, T32EB011434, R01EB000856-06, and R01EB009103-01 and by the DARPA RCI Program (MTO) N66001-12-C-4025 and HIST Program (MTO) N66001-11-1-4013. Additional funding was also provided through a Coulter Translational Research Award, the American Heart Association Grant 1T32EB011434-01A1, AHA Innovative Research Award-National (Marcus Foundation) 15IRG22760009, AHA Midwest Grant in Aid Award 15GRNT25780033, the Foundation of ASNR, UW Milwaukee-Madison Intercampus Grants, the UW Graduate School, and by Shapiro Foundation Grants.

ACKNOWLEDGMENTS

The authors would like to thank all the study participants and their families for participating in the study and all the MR technologists for their support in collection of data. The authors would also like to extend thanks to Dr. Justin Sattin for

referrals of stroke participants and clinical documentation and Dr. Klevest Gjini for his feedback during the review process. The authors would like to acknowledge that parts of this manuscript were presented at the Radiological Society of Northern America conference 2017, Chicago, IL.

SUPPLEMENTARY MATERIAL

The Supplementary Material for this article can be found online at: https://www.frontiersin.org/articles/10.3389/fnins.2018.00353/full#supplementary-material

REFERENCES

Alomari, M. H., Samaha, A., and AlKamha, K. (2013). Automated classification of L/R hand movement EEG signals using advanced feature extraction and machine learning. *arXiv:13122877*.

Bajaj, S., Butler, A. J., Drake, D., and Dhamala, M. (2015). Functional organization and restoration of the brain motor-execution network af ter stroke and rehabilitation. *Front. Hum. Neurosci.* 9:173. doi: 10.3389/fnhum.2015.00173

Bamdad, M., Zarshenas, H., and Auais, M. A. (2015). Application of BCI systems in neurorehabilitation: a scoping review. *Disabil. Rehabil. Assist. Technol.* 10, 355–364. doi: 10.3109/17483107.2014.961569

Benou, A., Veksler, R., Friedman, A., and Raviv, T. R. (2016). "De-noising of contrast-enhanced MRI sequences by an ensemble of expert deep neural networks," in *Deep Learning and Data Labeling for Medical Applications*, eds G. Carneiro, D. Mateus, P. Loïc, A. Bradley, J. M. R. S. Tavares, V. Belagiannis, J. P. Papa, J. C. Nascimento, M. Loog, Z. Lu, J. S. Cardoso, and J. Cornebise (Athens: Springer), 95–110.

Birbaumer, N. (2006). Breaking the silence: brain–computer interfaces, (BCI) for communication and motor control. *Psychophysiology* 43, 517–532. doi: 10.1111/j.1469-8986.2006.00456.x

Birenbaum, A., and Greenspan, H. (2016). "Longitudinal multiple sclerosis lesion segmentation using multi-view convolutional neural networks," in Deep Learning and Data Labeling for Medical Applications, eds G. Carneiro, D. Mateus, P. Loïc, A. Bradley, J. M. R. S. Tavares, V. Belagiannis, J. P. Papa, J. C. Nascimento, M. Loog, Z. Lu, J. S. Cardoso, and J. Cornebise (Athens: Springer), 58–67.

Brosch, T., Tam, R., ADN Initiative. (2013). "Manifold learning of brain MRIs by deep learning," in *International Conference on Medical Image Computing and Computer-Assisted, Intervention* (Berlin; Heidelberg: Springer), 633–640.

Brott, T., Adams, H. P., Olinger, C. P., Marler, J. R., Barsan, W. G., Biller, J., et al. (1989). Measurements of acute cerebral infarction: a clinical examination scale. *Stroke* 20, 864–870. doi: 10.1161/01.STR.20.7.864

Brumberg, J. S., Nieto-Castanon, A., Kennedy, P. R., and Guenther, F. H. (2010). Brain–computer interfaces for speech communication. *Speech Commun.* 52, 367–379. doi: 10.1016/j.specom.2010.01.001

Bütefisch, C., Hummelsheim, H., Denzler, P., and Mauritz, K.-H. (1995). Repetitive training of isolated movements improves the outcome of motor rehabilitation of the centrally paretic hand. *J. Neurol. Sci.* 130, 59–68. doi: 10.1016/0022-510X(95)00003-K

Carroll, D. (1965). A quantitative test of upper extremity function. *J. Chronic Dis.* 18, 479–491. doi: 10.1016/0021-9681(65)90030-5

Cecotti, H., and Graser, A. (2011). Convolutional neural networks for P300 detection with application to brain-computer interfaces. *IEEE Trans. Pattern Anal. Mach. Intell.* 33, 433–445. doi: 10.1109/TPAMI.2010.125

Corti, M., Patten, C., and Triggs, W. (2012). Repetitive transcranial magnetic stimulation of motor cortex after stroke: a focused review. *Am. J. Phys. Med. Rehabil.* 91, 254–270. doi: 10.1097/PHM.0b013e318228bf0c

Cox, R. W. (1996). AFNI: software for analysis and visualization of functional magnetic resonance neuroimages. *Comput. Biomed. Res.* 29, 162–173. doi: 10.1006/cbmr.1996.0014

Dai, Z., Yan, C., Wang, Z., Wang, J., Xia, M., Li, K., et al. (2012). Discriminative analysis of early Alzheimer's disease using multi-modal imaging and multi-level characterization with multi-classifier, (M3). *Neuroimage* 59, 2187–2195. doi: 10.1016/j.neuroimage.2011.10.003

Danziger, Z., Fishbach, A., and Mussa-Ivaldi, F. A. (2009). Learning algorithms for human–machine interfaces. *IEEE Trans. Biomed. Eng.* 56, 1502–1511. doi: 10.1109/TBME.2009.2013822

De Kroon, J., Van der Lee, J., IJzerman, M., and Lankhorst, G. (2002). Therapeutic electrical stimulation to improve motor control and functional abilities of the upper extremity after stroke: a systematic review. *Clin. Rehabil.* 16, 350–360. doi: 10.1191/0269215502cr504oa

Di Bono, M. G., and Zorzi, M. (2008). Decoding cognitive states from fMRI data using support vector regression. *Psychnol. J.* 6, 189–201.

Ding, X., Yang, Y., Stein, E. A., and Ross, T. J. (2017). Combining multiple resting-state fMRI features during classification: optimized frameworks and their application to nicotine addiction. *Front. Hum. Neurosci.* 11:362. doi: 10.3389/fnhum.2017.00362

Dosenbach, N. U., Nardos, B., Cohen, A. L., Fair, D. A., Power, J. D., Church, J. A., et al. (2010). Prediction of individual brain maturity using fMRI. *Science* 329, 1358–1361. doi: 10.1126/science.1194144

Felton, E., Radwin, R., Wilson, J., and Williams, J. (2009). Evaluation of a modified Fitts law brain–computer interface target acquisition task in able and motor disabled individuals. *J. Neural Eng.* 6:056002. doi: 10.1088/1741-2560/6/5/056002

Fergus, P., Hussain, A., Hignett, D., Al-Jumeily, D., Abdel-Aziz, K., and Hamdan, H. (2016). A machine learning system for automated whole-brain seizure detection. *Appl. Comput. Inform.* 12, 70–89. doi: 10.1016/j.aci.2015.01.001

Gomez-Pilar, J., Corralejo, R., Nicolas-Alonso, L., Álvarez, D., and Hornero, R. (2014). "Assessment of neurofeedback training by means of motor imagery based-bci for cognitive rehabilitation, Engineering in Medicine and Biology Society (EMBC)," in *36th Annual International Conference of the IEEE*, 2014 (Chicago, IL: IEEE), 3630–3633.

Gordon, N. F., Gulanick, M., Costa, F., Fletcher, G., Franklin, B. A., Roth, E. J., et al. (2004). Physical activity and exercise recommendations for stroke survivors. *Stroke* 35, 1230–1240. doi: 10.1161/01.STR.0000127303.19261.19

Grefkes, C., Eickhoff, S. B., Nowak, D. A., Dafotakis, M., and Fink, G. R. (2008). Dynamic intra-and interhemispheric interactions during unilateral and bilateral hand movements assessed with fMRI and DCM. *Neuroimage* 41, 1382–1394. doi: 10.1016/j.neuroimage.2008.03.048

Hastie, T., Tibshirani, R., and Friedman, J. (2001). *The Elements of Statistical Learning*. New York, NY: Springer.

Hoffmann, N., Koch, E., Steiner, G., Petersohn, U., and Kirsch, M. (2016). "Learning thermal process representations for intraoperative analysis of cortical perfusion during ischemic strokes," in *Deep Learning and Data Labeling for Medical Applications* (Athens: Springer), 152–160.

Jackson, J. E. (2005). *A User's Guide to Principal Components*. New York, NY: John Wiley and Sons.

Jolliffe, I. T. (1986) *Principal Component Analysis*. New York, NY: Springer-Verlag.

Kamnitsas, K., Ledig, C., Newcombe, V. F., Simpson, J. P., Kane, A. D., Menon, D. K., et al. (2017). Efficient multi-scale 3D CNN with fully connected CRF for accurate brain lesion segmentation. *Med. Image Anal.* 36, 61–78. doi: 10.1016/j.media.2016.10.004

Khazaee, A., Ebrahimzadeh, A., and Babajani-Feremi, A. (2016). Application of advanced machine learning methods on resting-state fMRI network for identification of mild cognitive impairment and Alzheimer's disease. *Brain Imaging Behav.* 10, 799–817. doi: 10.1007/s11682-015-9448-7

Kwakkel, G., Kollen, B. J., and Krebs, H. I. (2008). Effects of robot-assisted therapy on upper limb recovery after stroke: a systematic review. *Neurorehabil. Neural Repair* 22, 111–121. doi: 10.1177/1545968307305457

Lang, C. E., Wagner, J. M., Dromerick, A. W., and Edwards, D. F. (2006). Measurement of upper-extremity function early after stroke: properties of the action research arm test. *Arch. Phys. Med. Rehabil.* 87, 1605–1610. doi: 10.1016/j.apmr.2006.09.003

Lee, M. H., Smyser, C. D., and Shimony, J. S. (2013). Resting-state fMRI: a review of methods and clinical applications. *Am. J. Neuroradiol.* 34, 1866–1872. doi: 10.3174/ajnr.A3263

Leys, C., Ley, C., Klein, O., Bernard, P., and Licata, L. (2013). Detecting outliers: do not use standard deviation around the mean, use absolute deviation around the median. *J. Exp. Soc. Psychol.* 49, 764–766. doi: 10.1016/j.jesp.2013.03.013

Lohse, K. R., Hilderman, C. G., Cheung, K. L., Tatla, S., and Van der Loos, H. M. (2014). Virtual reality therapy for adults post-stroke: a systematic review

and meta-analysis exploring virtual environments and commercial games in therapy. *PLoS ONE* 9:e93318. doi: 10.1371/journal.pone.0093318

Lotte, F., Congedo, M., Lécuyer, A., Lamarche, F., and Arnaldi, B. (2007). A review of classification algorithms for EEG-based brain–computer interfaces. *J. Neural Eng.* 4:R1. doi: 10.1088/1741-2560/4/2/R01

Lotze, M., Montoya, P., Erb, M., Hülsmann, E., Flor, H., Klose, U., et al. (1999). Activation of cortical and cerebellar motor areas during executed and imagined hand movements: an fMRI study. *J. Cogn. Neurosci.* 11, 491–501. doi: 10.1162/089892999563553

Mason, S. G., and Birch, G. E. (2000). A brain-controlled switch for asynchronous control applications. *IEEE Trans. Biomed. Eng.* 47, 1297–1307. doi: 10.1109/10.871402

Massey, F. J. Jr. (1951). The Kolmogorov-Smirnov test for goodness of fit. *J. Am. Stat. Assoc.* 46, 68–78. doi: 10.1080/01621459.1951.10500769

Meier, T. B., Desphande, A. S., Vergun, S., Nair, V. A., Song, J., Biswal, B. B., et al. (2012). Support vector machine classification and characterization of age-related reorganization of functional brain networks. *Neuroimage* 60, 601–613. doi: 10.1016/j.neuroimage.2011.12.052

Mohanty, R., Sinha, A., Remsik, A., Allen, J., Nair, V., Caldera, K., et al. (2017). "Machine learning-based prediction of changes in behavioral outcomes using functional connectivity and clinical measures in brain-computer interface stroke, rehabilitation," in *International Conference on Augmented Cognition* (Vancoucer, BC: Springer), 543–557.

Mugler, E., Flint, R., Wright, Z., Schuele, S., Rosenow, J., and Patton, J. (2013). "Decoding articulatory properties of overt speech from electrocorticography," in *Proceeding Fifth International Brain-Computer Interface Meet 2013* (Pacific Grove, CA), 4–5.

Muller, K.-R., Anderson, C. W., and Birch, G. E. (2003). Linear and nonlinear methods for brain-computer interfaces. *IEEE Trans. Neural Syst. Rehabil. Eng.* 11, 165–169. doi: 10.1109/TNSRE.2003.814484

Murphy, K., and Fox, M. D. (2016). Towards a consensus regarding global signal regression for resting state functional connectivity MRI. *Neuroimage* 154, 169–173. doi: 10.1016/j.neuroimage.2016.11.052

Nair, V. A., Young, B. M., Nigogosyan, Z., Remsick, A., Weber, S., Diffee, K., et al. (2015). "Resting-state functional connectivity changes after stroke rehabilitation using closed loop neurofeedback," *International Stroke Conference* (Nashville, TN: American Heart Association).

Neshige, R., Murayama, N., Igasaki, T., Tanoue, K., Kurokawa, H., and Asayama, S. (2007). Communication aid device utilizing event-related potentials for patients with severe motor impairment. *Brain Res.* 1141, 218–227. doi: 10.1016/j.brainres.2006.12.003

Noble, W. S. (2006). What is a support vector machine? *Nat. Biotechnol.* 24, 1565–1567. doi: 10.1038/nbt1206-1565

Payan, A., and Montana, G. (2015). Predicting Alzheimer's disease: a neuroimaging study with 3D convolutional neural networks. *arXiv:150202506.*

Power, J. D., Cohen, A. L., Nelson, S. M., Wig, G. S., Barnes, K. A., Church, J. A., et al. (2011). Functional network organization of the human brain. *Neuron* 72, 665–678. doi: 10.1016/j.neuron.2011.09.006

Rakotomamonjy, A., and Guigue, V. (2008). BCI competition III: dataset II-ensemble of SVMs for BCI P300 speller. *IEEE Trans. Biomed. Eng.* 55, 1147–1154. doi: 10.1109/TBME.2008.915728

Rehme, A. K., Volz, L. J., Feis, D.-L., Bomilcar-Focke, I., Liebig, T., Eickhoff, S. B., et al. (2014). Identifying neuroimaging markers of motor disability in acute stroke by machine learning techniques. *Cereb. cortex* 25, 3046–3056. doi: 10.1093/cercor/bhu100

Schalk, G., McFarland, D. J., Hinterberger, T., Birbaumer, N., and Wolpaw, J. R. (2004). BCI2000: a general-purpose brain-computer interface (BCI) system. *IEEE Trans. Biomed. Eng.* 51, 1034–1043. doi: 10.1109/TBME.2004.827072

Selim, A., Wahed, M. A., and Kadah, Y. (2008). "Machine learning methodologies in brain-computer interface systems,"in *Biomedical Engineering Conference* 2008 (Cairo: Cairo International; IEEE), 1–5.

Silvoni, S., Ramos-Murguialday, A., Cavinato, M., Volpato, C., Cisotto, G., Turolla, A., et al. (2011). Brain-computer interface in stroke: a review of progress. *Clin. EEG Neurosci.* 42, 245–252. doi: 10.1177/155005941104200410

Smith, S. M., Miller, K. L., Salimi-Khorshidi, G., Webster, M., Beckmann, C. F., Nichols, T. E., et al. (2011). Network modelling methods for FMRI. *Neuroimage* 54, 875–891. doi: 10.1016/j.neuroimage.2010.08.063

Snoek, J., Larochelle, H., and Adams, R. P. (2012). "Practical bayesian optimization of machine learning algorithms," in *Advances in Neural Information Processing Systems* (Lake Tahoe), 2012, 2951–2959.

Soekadar, S. R., Birbaumer, N., Slutzky, M. W., and Cohen, L. G. (2015). Brain–machine interfaces in neurorehabilitation of stroke. *Neurobiol. Dis.* 83, 172–179. doi: 10.1016/j.nbd.2014.11.025

Song, J., Young, B. M., Nigogosyan, Z., Walton, L. M., Nair, V. A., Grogan, S. W., et al. (2014). Characterizing relationships of DTI, fMRI, and motor recovery in stroke rehabilitation utilizing brain-computer interface technology. *Front. Neuroeng.* 7:31. doi: 10.3389/fneng.2014.00031

Sun, H. Y., Xiang, Y. , and Yang, M. D. (2011). Neurological rehabilitation of stroke patients via motor imaginary-based braincomputer interface technology. *Neural Regen. Res.* 6, 2198–2202.

Takeuchi, N., and Izumi, S.-I. (2012). Maladaptive plasticity for motor recovery after stroke: mechanisms and approaches. *Neural Plast.* 2012:359728. doi: 10.1155/2012/359728

Van Den Heuvel, M. P., and Pol, H. E. H. (2010). Exploring the brain network: a review on resting-state fMRI functional connectivity. *Eur. Neuropsychopharmacol.* 20, 519–534. doi: 10.1016/j.euroneuro.2010.03.008

Várkuti, B., Guan, C., Pan, Y., Phua, K. S., Ang, K. K., Kuah, C. W. K., et al. (2013). Resting state changes in functional connectivity correlate with movement recovery for BCI and robot-assisted upper-extremity training after stroke. *Neurorehabil. Neural Repair* 27, 53–62. doi: 10.1177/1545968312445910

Vergun, S., Deshpande, A. S., Meier, T. B., Song, J., Tudorascu, D. L., Nair, V. A., et al. (2013). Characterizing functional connectivity differences in aging adults using machine learning on resting state fMRI data. *Front. Comput. Neurosci.* 7:38. doi: 10.3389/fncom.2013.00038

Wilson, J. A., Schalk, G., Walton, L. M., and Williams, J. C. (2009). Using an EEG-based brain-computer interface for virtual cursor movement with BCI2000. *J. Vis. Exp.* 2009:e1319. doi: 10.3791/1319

Wilson, J. A., Walton, L. M., Tyler, M., and Williams, J. (2012). Lingual electrotactile stimulation as an alternative sensory feedback pathway for brain–computer interface applications. *J. Neural Eng.* 9:045007. doi: 10.1088/1741-2560/9/4/045007

Xia, M., Wang, J., and He, Y. (2013). BrainNet viewer: a network visualization tool for human brain connectomics. *PLoS ONE* 8:e68910. doi: 10.1371/journal.pone.0068910

Young, B. M., Nigogosyan, Z., Nair, V. A., Walton, L. M., Song, J., Tyler, M. E., et al. (2014a). Case report: post-stroke interventional BCI rehabilitation in an individual with preexisting sensorineural disability. *Front. Neuroeng.* 7:18. doi: 10.3389/fneng.2014.00018

Young, B. M., Nigogosyan, Z., Walton, L. M., Song, J., Nair, V. A., Grogan, S. W., et al. (2014b). Changes in functional brain organization and behavioral correlations after rehabilitative therapy using a brain-computer interface. *Front. Neuroeng.*7:26. doi: 10.3389/fneng.2014.00026

Zelen, M. (1974). The randomization and stratification of patients to clinical trials. *J. Chronic Dis.* 27, 365–375. doi: 10.1016/0021-9681(74)90015-0

Conflict of Interest Statement: The authors declare that the research was conducted in the absence of any commercial or financial relationships that could be construed as a potential conflict of interest.

Copyright © 2018 Mohanty, Sinha, Remsik, Dodd, Young, Jacobson, McMillan, Thoma, Advani, Nair, Kang, Caldera, Edwards, Williams and Prabhakaran. This is an open-access article distributed under the terms of the Creative Commons Attribution License (CC BY). The use, distribution or reproduction in other forums is permitted, provided the original author(s) and the copyright owner are credited and that the original publication in this journal is cited, in accordance with accepted academic practice. No use, distribution or reproduction is permitted which does not comply with these terms.

frontiers in Neuroscience

ORIGINAL RESEARCH
published: 01 June 2018
doi: 10.3389/fnins.2018.00370

BCI Performance and Brain Metabolism Profile in Severely Brain-Injured Patients Without Response to Command at Bedside

Jitka Annen[1], Séverine Blandiaux[1], Nicolas Lejeune[1,2,3], Mohamed A. Bahri[4], Aurore Thibaut[1], Woosang Cho[5], Christoph Guger[5,6], Camille Chatelle[1,7†] and Steven Laureys[1*†]*

[1] GIGA Consciousness, Coma Science Group, University and University Hospital of Liège, Liège, Belgium, [2] Disorders of Consciousness Care Unit, Centre Hospitalier Neurologique William Lennox, Université Catholique de Louvain, Ottignies-Louvain-la-Neuve, Belgium, [3] Institute of Neuroscience, Université Catholique de Louvain, Brussels, Belgium, [4] GIGA-Cyclotron Research Centre in vivo Imaging, University of Liège, Liège, Belgium, [5] g.tec Medical Engineering GmbH, Schiedlberg, Austria, [6] Guger Technologies OG, Graz, Austria, [7] Laboratory for NeuroImaging of Coma and Consciousness, Department of Neurology, Massachusetts General Hospital, Harvard Medical School, Boston, MA, United States

OPEN ACCESS

Edited by:
Ioan Opris,
University of Miami, United States

Reviewed by:
Xiaoli Li,
Beijing Normal University, China
Veena A. Nair,
University of Wisconsin-Madison, United States

***Correspondence:**
Camille Chatelle
camille.chatelle@uliege.be
Steven Laureys
steven.laureys@uliege.be

† These authors have contributed equally to this work.

Specialty section:
This article was submitted to Neural Technology, a section of the journal Frontiers in Neuroscience

Received: *15 February 2018*
Accepted: *14 May 2018*
Published: *01 June 2018*

Citation:
Annen J, Blandiaux S, Lejeune N, Bahri MA, Thibaut A, Cho W, Guger C, Chatelle C and Laureys S (2018) BCI Performance and Brain Metabolism Profile in Severely Brain-Injured Patients Without Response to Command at Bedside. Front. Neurosci. 12:370. doi: 10.3389/fnins.2018.00370

Detection and interpretation of signs of "covert command following" in patients with disorders of consciousness (DOC) remains a challenge for clinicians. In this study, we used a tactile P3-based BCI in 12 patients without behavioral command following, attempting to establish "covert command following." These results were then confronted to cerebral metabolism preservation as measured with glucose PET (FDG-PET). One patient showed "covert command following" (i.e., above-threshold BCI performance) during the active tactile paradigm. This patient also showed a higher cerebral glucose metabolism within the language network (presumably required for command following) when compared with the other patients without "covert command-following" but having a cerebral glucose metabolism indicative of minimally conscious state. Our results suggest that the P3-based BCI might probe "covert command following" in patients without behavioral response to command and therefore could be a valuable addition in the clinical assessment of patients with DOC.

Keywords: covert command following, P3, FDG-PET, disorders of consciousness, consciousness, brain computer interface

INTRODUCTION

Severely brain-injured patients with disorders of consciousness (DOC) can be distinguished by their ability to show either only reflexive and thus unconscious behavior (unresponsive wakefulness syndrome, UWS) (Laureys et al., 2010), or more purposeful reactions to the environment without (minimally consciousness state minus, MCS–) or with signs of language preservation such as response to command (minimally consciousness state plus, MCS+) (Giacino et al., 2002; Bruno et al., 2012). A clinical challenge presents itself when diagnosing patients correctly, yet, accurate diagnosis is key for treatment and prognosis. Indeed, patients with residual consciousness have increased chances of recovery and respond better to various treatments such as tDCS (Thibaut et al., 2014), possibly modulating cortical excitability in DOC patients (Bai et al., 2017a), and amantadine (Maythaler et al., 2002).

Structured behavioral assessment, such as the Coma Recovery Scale-Revised (CSR-R), led to an important reduction of the misdiagnosis rate (Schnakers et al., 2009), especially when the behavioral assessment is repeated at least five times (Wannez et al., 2018). In addition, passive neuroimaging techniques can quantify structural and functional brain damage, and could ultimately be used as supplemental tools for diagnosis (Rosanova et al., 2012; King et al., 2013; Demertzi et al., 2015; Chennu et al., 2017). Among them, 18F-fluorodeoxyglucose positron emission tomography (FDG-PET) has been used to indicate that the absence of overt signs of consciousness does not necessarily indicate that the patient is unconscious (Stender et al., 2014). Resting state EEG can be used to passively assess DOC patients' consciousness level, for which spectral measures and functional connectivity are most successful and widely employed (for review see Bai et al., 2017b).

Active ways of assessing covert consciousness and command following are more challenging as it necessitates cognitive integrity for command following (e.g., language comprehension, memory) (Andrews et al., 1996). However, it brings additional key information as patients showing early signs of (covert) command following have a better chance of good outcome (Whyte et al., 2001). Furthermore, command following can potentially be used to establish functional communication which could dramatically increase the patient's quality of life.

About one decade ago, the first evidence for "covert command following" in absence of overt command following was reported using functional MRI (Owen et al., 2006), further used a couple of years later to enable an MCS– patient to functionally communicate (Monti et al., 2010; Bardin et al., 2011). However, fMRI is expensive and hardly accessible for repeated assessments. For this reason, other techniques that can measure voluntary responses not observable at bedside have been used to assess "covert command following." EEG-based detection of motor imagery showed their potential to establish command following in about 20% of the patients with DOC (Cruse et al., 2011, 2012). The P3 event related potential (ERP), which is observed about 300–500 ms after the presentation of a deviant sensory stimulus in a train of standard stimuli, reflects the novelty of the stimulus. The P3 can be present in varying contexts and levels of consciousness, for example in response to the subjects' own name (Perrin et al., 2006; Li et al., 2015), and it is less sensitive than spectral and connectivity measures in discriminating between UWS and MCS patients (Sitt et al., 2014). Nevertheless, it is also known that attention (which requires consciousness, by definition) can modify the amplitude of the P3 (for review Chennu and Bekinschtein, 2012). Other systems, that do not depend on brain activity directly, used subliminal limb movements (i.e., electromyogram; Habbal et al., 2014; Lesenfants et al., 2016), modulation of breathing (Charland-Verville et al., 2014) or of pH saliva (Wilhelm et al., 2006), pupil dilation during mental effort (Stoll et al., 2013) for detecting command following and communication in DOC or locked in syndrome patients (i.e., fully paralyzed but conscious). However, all these techniques are relying on experts for data acquisition and offline data analysis, and tools that can be directly implemented in clinical setting for non-experts are needed.

In this prospective study, we used a commercially available P3-based BCI system with direct feedback about the patient's performance in clinically well-characterized patients with DOC. Our aim was to identify patients with signs of "covert command following," and compare those results to cerebral glucose metabolism preservation as measured with FDG-PET (Stender et al., 2014). A secondary aim was to investigate whether there is a relationship between the BCI performance and the level of consciousness (as defined by the CRS-R and the FDG-PET) at the group level.

METHODS

Subjects

The study was conducted from November 2015 till July 2016 and included a convenience sample of 12 adult patients. Inclusion criteria were patients with DOC without response to command (i.e., UWS or MCS–) after a period of coma and the availability of FDG-PET within 1 week of the BCI assessment. Exclusion criteria were being less than 16 years old, history of developmental, neurologic, or major psychiatric disorder resulting in functional disability before the insult, and being in a (sub-)acute stage after injury (<3 months). All patients were hospitalized for 1 week in the University Hospital of Liège for a thorough clinical assessment of their medical and cognitive status. This assessment included FDG-PET, MRI, EEG and repeated behavioral assessments with the CRS-R. Diagnosis of UWS or MCS– was based on the best out of a minimum of five CRS-R assessments during this 1-week hospitalization. The ethics committee of the Faculty of Medicine of the University of Liège approved the study, and written informed consent was obtained from the patient's legal representative in accordance with the Declaration of Helsinki.

BCI Assessment and Data Processing

Hard- and software were developed by g.tec (mindBEAGLE g.tec Guger Technologies OG, Graz, Austria). Data were recorded from 8 active gel electrodes (Fz, Cz, C3, C4, CPz, CP1, CP2, Pz) sampled at 256 Hz, referenced to the mastoids, and filtered between 0.1 and 30 Hz using a Butterworth 4th order filter. The BCI analyzed the P3 ERP for the assessment of "covert command following" and potentially communication.

The employed oddball paradigms administered mechanical vibrations with a frequency of 225 Hz, which lasted for 30 ms, with an inter-stimulus interval of 270 ms. A total of 480 stimuli were presented, resulting in a paradigm duration of 2.4 min. In the first paradigm, the vibrotactile with two stimuli (VT2), stimuli were presented on the left (probability of 7/8) and right (probability of 1/8) wrist. Before the start of the session, the patient was aroused if needed (i.e., the patient presented multiple episodes of eye closure during the CRS-R before the BCI assessment) and instructed to mentally count the stimuli presented on the right wrist. If the patient showed eye closure lasting longer than 10 s, the paradigm was paused, the patient was aroused (using the CRS-R arousal facilitation protocol) and the instructions were repeated before continuation of the paradigm. In case of a BCI performance above 70% during the VT2

paradigm (without artifacts from the mechanical vibrations), the result was considered above chance level and the test was extended with a third stimulator (VT3). The threshold of 70% was chosen because it is suggested to be the minimal required performance allowing effective communication using a BCI (Noirhomme et al., 2015). The VT3 paradigm includes a stimulator on the right foot which then acts as standard stimulus (probability of 6/8), and the stimulators on the left and right wrists deliver deviant stimulations each with a probability of 1/8. The subject was instructed through headphones which hand to attend for every block, and mentally count the number of deviant stimulations. Four blocks of 15 target deviant (and 15 non-target deviant plus 90 standard) trials randomly assigned to the left and right wrist, were presented. After this initial training phase, 6 autobiographical questions were asked to the patient. In order to answer, the patient was instructed to concentrate on the left hand for answering "yes," and on the right hand for answering "no" during a 30-s period.

Data for ERP's was extracted from −100 to 600 around stimulus onset. Trials with an amplitude exceeding 100 μV were rejected from the further analysis. Baseline correction was done using the 100 ms before stimulus onset. The 600 ms after stimulus onset was down sampled to 7 samples. The data processing classified deviant trials using a linear discriminant analysis with 56 features (7 time-points of the down-sampled ERP, for 8 channels). The BCI performance (i.e., the percentage of detected deviant trials), ranging from 0 to 100%, was calculated using a 10-fold cross-validation. For more detailed information on the stimulus presentation and analysis, please refer to previous studies (Ortner et al., 2014; Guger et al., 2017).

FDG-PET Acquisition and Processing

Resting 18F-FDG-PET acquisition was performed about 30 min after intravenous injection of approximately 150 MBq radioactive labeled glucose (Gemini TF PET-CT scanner, Philips Medical Systems) in order to quantify cerebral glucose uptake. A low dose CT was acquired prior the 12-min emission scan and used for attenuation correction. PET images were reconstructed using the iterative LOR RAMLA algorithm and correction for dead-time, random events and scatter were applied.

Preprocessing and statistical analysis were done in the Statistical Parametric Mapping toolbox (SPM12, www.fil.ion.ucl.ac.uk/spm) implemented in MATLAB (R2017a). Preprocessing was done as described previously (Stender et al., 2014). Briefly, images were manually reoriented according to the SPM12 FDG-PET template, spatially normalized (using a template for patients and controls) and smoothed (with a 14 mm FWHM Gaussian kernel).

Statistics

We identified regions that showed preserved cerebral glucose metabolism in patients who showed "covert command following" as compared with patients with a FDG-PET typical for MCS (Stender et al., 2014) who did not show signs of "covert command following." This was done using a factorial design with four design matrices. Clusters with preserved metabolism were considered significant at FWE $p < 0.05$. The mean glucose uptake (in MBq/cc) of the largest significant cluster was extracted for these six subjects using Marsbar (version 0.44, http://marsbar.sourceforge.net/).

Additionally, for every subject, we identified regions with relative preserved metabolism compared to 34 healthy subjects to obtain a FDG-PET-based diagnosis, as described in more details elsewhere (Stender et al., 2014). A Wilcoxon rank-sum test and chi-square test were used to assess the difference in age and gender between patients and healthy subjects (the latter solely used for the FDG-PET analysis). The CRS-R and FDG-PET based diagnosis were confronted to the VT2 BCI performance at the group level using a Wilcoxon rank-sum tests.

RESULTS

Twelve patients were included in the study, of which four MCS- patients (age median = 47.5, IQR = 20 years; disease duration median = 7.5, IQR = 7.75 months; 3 males; 3 TBI, 1 anoxia), and eight UWS patients (age median = 43.5, IQR = 25.5 years; disease duration median = 50, IQR = 30.5 months; 4 males; 2 TBI, 5 anoxia, 1 hemorrhage). The VT3 was performed in only one patient (MCS1), for whom the BCI performance during the VT2 and VT3 reached 100 and 70% respectively. The BCI decoded an answer for one out of six questions, but the BCI did not decode replies during further attempts. This patient showed a preserved metabolism within the left hemisphere (i.e., language network) as compared to the other patients with a FDG-PET indicative of MCS (**Figure 1**). This preservation was confirmed when compared with healthy subjects (**Figure 2**).

All patients behaviorally diagnosed as MCS showed cortical metabolism preservation in accordance with a diagnosis of MCS. Six out of eight patients diagnosed as UWS had a FDG-PET in agreement with the CSR-R based diagnosis, while the other two patients showed preserved cortical glucose metabolism suggestive of MCS. The patients and healthy subjects used for the FDG-PET-based diagnosis did not differ in age ($Z = 0.32$, $p = 0.75$) or gender [$\chi^2_{(1)} = 1.98$, $p = 0.16$]. Patients' demographics, BCI performance, and FDG-PET diagnoses are reported in **Table 1**. BCI responses and preserved metabolism as compared to healthy subjects are presented in **Figure 2** for three patients (i.e., one UWS patient, one MCS– patient, and the patient with "covert command following").

At the group level, the BCI performance during the VT2 paradigm was lower for UWS than for MCS patients (UWS median = 10, IQR = 30; MCS median = 22.5, IQR = 47.5; $Z = 2.10$, $p = 0.04$). When comparing the BCI performance with the FDG-PET diagnosis, the performance during the VT2 paradigm was also lower for UWS than for MCS patients (UWS median = 10, IQR = 40; MCS median = 20, IQR = 15; $Z = 2.09$, $p = 0.04$).

DISCUSSION

In this prospective study, we used a commercially available P3-based BCI system in a convenience sample of 12 clinically well-characterized patients with DOC. We identified a patient with signs of "covert command following," and compared those findings to cerebral glucose metabolism preservation of patients without signs of "covert command following."

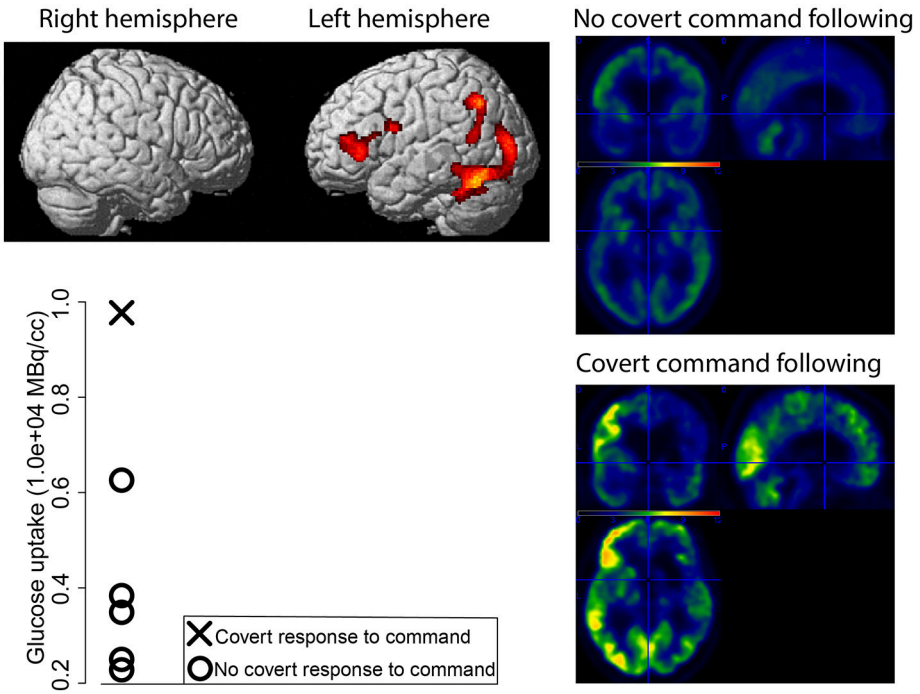

FIGURE 1 | Preserved glucose metabolism (in red-yellow) as measured with FDG-PET for the MCS– patient with signs of "covert command following" compared to patients with a FDG-PET indicative of MCS without signs of "covert command following" (top left). Mean glucose uptake of the more significant cluster (in MBq/cc) for every patient (bottom left, patients with a MCS FDG-PET in absence of "covert command following" represented with circles, the MCS– patient who did show signs of "covert command following" represented with a cross). Average standardized uptake value for the patients without "covert command following" (right top), and the standardized uptake value for the patient with "covert command following" (bottom right).

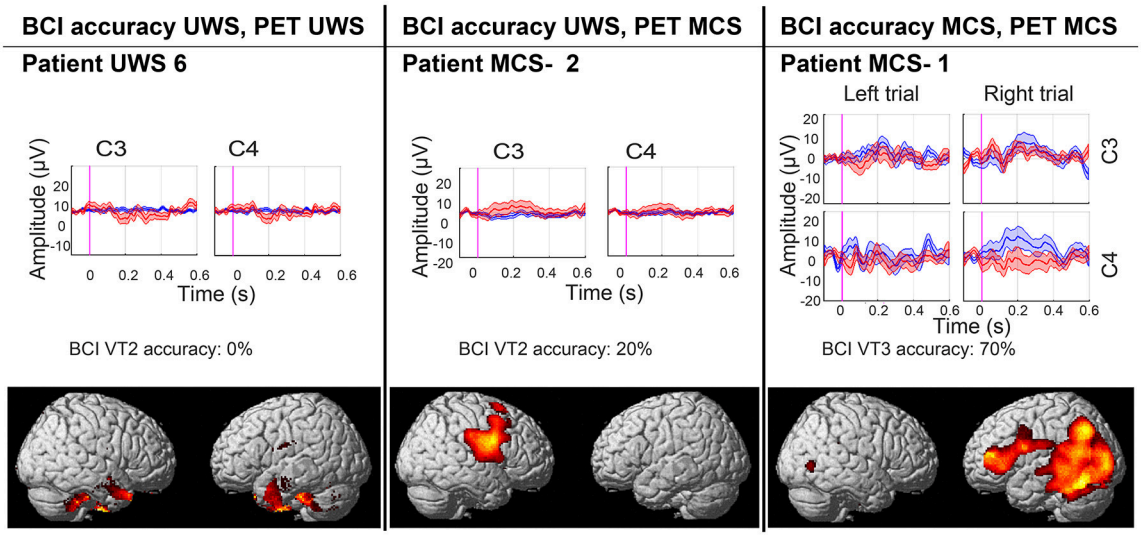

FIGURE 2 | BCI performance and areas of preserved (in red-yellow) cerebral glucose metabolism compared to healthy subjects (significant at <0.001 uncorrected). Results are presented for a representative UWS (left) and MCS (middle) patient without covert response to command, and for the patient with covert response to command (right). In the ERP plot blue lines represent the P3 for the attended hand, and red line represent the P3 for the unattended hand.

We have found that one behaviorally MCS- patient (i.e., showing visual pursuit but no response to command at the bedside) was able to show "covert command following" using the VT3 paradigm (i.e., attended toward the left or the right stimulated hand, as requested). This patient, who showed "covert response to command," had an FDG-PET in agreement with the diagnosis of MCS (Stender et al., 2014). This patient had already been assessed by our group about 1.5 years before the

TABLE 1 | Demographic, BCI and FDG-PET information per patient.

ID	Age range	Disease duration	Etiology	Handedness	Diagnosis stability	VT2 [%] (# rejected trials)	VT3 [%] (# rejected trials)	FDG-PET diagnosis
MCS– 1	40–45	60 m	TBI	Right	4/6	100 (3)	70 (1)	MCS
MCS– 2	20–25	40 m	TBI	Left	6/6	20 (1)	–	MCS
MCS– 3	55–60	8 m	Anoxia	Right	1/6	25 (42)	–	MCS
MCS– 4	55–60	70 m	TBI	?	4/6	10 (257)	–	MCS
UWS 1	65–70	3 m	Hemorrhage	Right	4/4	0 (3)	–	MCS
UWS 2	30–35	9 m	TBI	Left	5/5	20 (3)	–	MCS
UWS 3	55–60	6 m	Anoxia	?	5/5	75^{+} (0)	–	UWS
UWS 4	20–25	15 m	Anoxia	?	6/6	10 (51)	–	UWS
UWS 5	45–50	6 m	Anoxia	Right	6/6	0 (23)	–	UWS
UWS 6	65–70	5 m	Anoxia	Left	7/7	0 (21)	–	UWS
UWS 7	40–45	26 m	Anoxia	Right	6/6	40 (480*)	–	UWS
UWS 8	30–35	13 m	TBI	Right	6/6	10 (0)	–	UWS

*The clinical diagnosis of the patients is based on the best CRS-R of at least five assessments that were performed within the week of the BCI assessment. Fluctuations in the clinical diagnosis are presented as the proportion of best diagnosis out of the total number of assessments. Median BCI performance for the two (VT2 and VT3) paradigms and between brackets the number of rejected trials are presented together with the FDG-PET based diagnosis. Patient MCS- 1 showed signs of response to command when assessed with the BCI. * Very high amplitude response. $^{+}$ artifacted by mechanical artifact.*

BCI assessment and had been diagnosed in a clinical state of MCS–. The week of the BCI assessment, MRI examination showed a gray matter atrophy most severe in subcortical areas and in the middle and posterior cingulum, but relatively limited in other cortical areas, suggesting a higher level of consciousness (Annen et al., 2018). The clinical EEG showed a 5 Hz rhythm, which has been associated to a higher chance of being MCS+ (as compared to MCS–; Chennu et al., 2017). The FDG-PET also showed an increase in cerebral metabolism (as compared with previous assessment), mostly pronounced in the regions of the right dorsolateral prefrontal cortex, the inferior parietal junction and the inferior temporal gyrus. These regions, suggested before to be key regions differentiating MCS– (absence of language understanding) and MCS+ (presence of language understanding) patients (Bruno et al., 2012), were also more preserved in the patient with signs of "covert command following" than in the other patients with cerebral metabolism suggestive of MCS. However, the outcome at 1 year after the BCI assessment still suggested a diagnosis of MCS–. The relatively good results of the paraclinical assessment together with the limited motor response during clinical assessment (i.e., 1/6 assessment an automatic motor reaction and 5/6 (abnormal) flexion to noxious stimulation) and severe spasticity (i.e., Modified Ashworth Scale score of 3/4 for the upper limbs and 4/4 for the lower limbs) could therefore suggest that this patient's behavior was mainly limited by her physical rather than cognitive impairments.

Previous literature have reported that about 20% of the DOC patients show covert response to command if tested using active EEG-based paradigms (Cruse et al., 2011, 2012). However, one of the main challenges in this field is the heterogeneity in data analyses and statistical assumptions used. These choices can influence the results and lead to false positives or negatives (Cruse et al., 2013; Goldfine et al., 2013), even in locked in syndrome patients assessed with the same and a different system as employed in the current manuscript (Spüler, in review). It is key to keep this in mind when interpreting such data, especially in the context of DOC patients, where such false negative or positive results might have harmful effects in the short and long term, triggering end-of-life decisions or inversely nurturing false hopes (Jox et al., 2012). One way to avoid false negatives or positives is to confront the results obtained through different techniques and/or modalities as presented here. Multimodal approaches, even if they necessitate more time and resources, may help reduce the underestimation of the patient's levels of consciousness (Stender et al., 2014; Annen et al., 2018). In the present study, the FDG-PET data ensure the validity of the presented BCI results.

The fact that only one out of twelve patients showed signs of "covert command following" [i.e., 8%, vs. 19% (Cruse et al., 2011) or vs. 30% (Spataro et al., 2018)] as previously reported in UWS patients using BCI approaches) in our small sample could be explained by the high proportion of patients with anoxic brain damage in the included sample, which previously have been reported to show "covert command following" less often than patients with a traumatic etiology (Cruse et al., 2012). When considering TBI patients only, 20% of the patients show signs of covert command following (i.e., 1 of 5 in the current study, and 2 of 10 in Cruse et al., 2011). Additionally, we included solely chronic (i.e., > 3 months after injury) DOC patients as compared to the study including acute DOC patients which suggested that 30% of the patients show "covert command following" (Spataro et al., 2018). Even if recovery of consciousness in the chronic phase of the disease can happen (Estraneo et al., 2010), recovery is more common to start in the acute phase

after the injury (Whyte et al., 2013). Hence discordant results suggestive of covert command-following are expected to be more frequent in the acute phase, during which the P3 response is predictive for a good outcome (Tzovara et al., 2016). Still, the current small and heterogeneous convenience sample could limit the generalizability of the results. Especially since the provided data does not include offline analysis allowing for a tailored single-subject significance threshold for each session, the interpretation of these results remains limited. Furthermore, vigilance fluctuation (Piarulli et al., 2016) could also have an impact on the number of negative results. For behavioral assessment, it is advised to repeat the assessment at least five times, in order to avoid false negatives (Wannez et al., 2018). In this study, every patient was assessed only once with the P3 system. Moreover, the VT3 paradigm was only tested when the results for the VT2 paradigm were promising, here in one patient only. In the future, the BCI measurements should be repeated regularly to reduce false negatives as a result of arousal fluctuations, and to monitor the patient's recovery. This could aid diagnosis in the acute phase of the injury, as well as improve the quality of life of patients in the chronic phase of the disease by providing assistive technologies and communication tools (Whyte et al., 2013).

On the other hand, we would like to highlight several strong points of the current study. Both the VT2 and VT3 paradigm take only 2.4 min per session, which is much shorter than a motor imagery paradigm that usually takes about 10 min (Cruse et al., 2011, 2012), or fNIRS session which takes 9 min (Chaudhary et al., 2017). Secondly, the employed system has the potential to analyze (albeit imperfect) the data directly, and provides feedback about the patient's performance promptly. Last, the BCI results have been confronted to FDG-PET data on the single-subject level, and we have shown that neuroimaging and neurophysiological markers of consciousness and "covert command following" were in accordance with each other.

At the group level, the results for the VT2 paradigm showed higher BCI performance in MCS based on the CRS-R and/or FDG-PET than in UWS. Previous literature during various states of (un)consciousness such as sleep, anesthesia, and DOC (for review see Chennu and Bekinschtein, 2012) has shown evidence for the absence of a link between the P3 and consciousness. However, in the acute phase of the disease, outcome prediction using auditory irregularities has been successful in more than 90% of the cases (Tzovara et al., 2016). In a recent pilot study including a small sample of 12 patients, the accuracy of the vibrotactile paradigm, as employed here, was proposed to be higher in patients with an increased CRS-R score after 6 months (Spataro et al., 2018).

Together, this study highlights the interest of using a multimodal approach when interpreting results obtained through different techniques and points toward a potential added value of the VTP3 paradigm in the clinical assessment of DOC patients at the single-subject level.

AUTHOR CONTRIBUTIONS

JA designed the work, did the acquisition, analysis, and interpretation of data for the work and drafted the work. SB and NL did a significant part of the data acquisition and revised the manuscript critically for important intellectual content. CC, MB, AT, WC, CG were involved in data analysis and revised the manuscript. SL designed the work and revised it critically for important intellectual content. All authors gave their final approval of the version to be published and agree to be accountable for all aspects of the work in ensuring that questions related to the accuracy or integrity of any part of the work are appropriately investigated and resolved.

FUNDING

The study was supported by the University and University Hospital of Liège, the French Speaking Community Concerted Research Action (ARC 12-17/01), the Belgian National Funds for Scientific Research (FRS-FNRS), Human Brain Project (EU-H2020-fetflagship-hbp-sga1-ga720270), Luminous project (EU-H2020-fetopen-ga686764), the James McDonnell Foundation, Mind Science Foundation, IAP research network P7/06 of the Belgian Government (Belgian Science Policy), the European Commission, the Public Utility Foundation Université Européenne du Travail, Fondazione Europea di Ricerca Biomedica, the Bial Foundation, Belgian National *Plan Cancer* (139), ECH2020 project ComaWare. CC is a Marie Sklodowska-Curie fellow (H2020-MSCA-IF-2016-ADOC-752686).

ACKNOWLEDGMENTS

The authors would like to thank the patients and their caregivers for participation in the study and the Neurology department of the University Hospital of Liège for their dedication toward the patients.

REFERENCES

Andrews, K., Murphy, L., Munday, R., and Littlewood, C. (1996). Misdiagnosis of the vegetative state: retrospective study in a rehabilitation unit. *Br. Med. J.* 313, 13–16. doi: 10.1136/bmj.313.7048.13

Annen, J., Frasso, G., Crone, J. S., Heine, L., Di Perri, C., Martial, C., et al. (2018). Regional brain volumetry and brain function in severely brain-injured patients. *Ann. Neurol.* 83, 842–853. doi: 10.1002/ana.25214

Bai, Y., Xia, X., Kang, J., Yang, Y., He, J., and Li, X. (2017a). TDCS modulates cortical excitability in patients with disorders of consciousness. *Neuroimage Clin.* 15, 702–709. doi: 10.1016/j.nicl.2017.01.025

Bai, Y., Xia, X., and Li, X. (2017b). A review of resting-state electroencephalography analysis in disorders of consciousness. *Front. Neurol.* 8:471. doi: 10.3389/fneur.2017.00471

Bardin, J. C., Fins, J. J., Katz, D. I., Hersh, J., Heier, L. A., Tabelow, K., et al. (2011). Dissociations between behavioural and functional magnetic resonance imaging-based evaluations of cognitive function after brain injury. *Brain.* 134, 769–782. doi: 10.1093/brain/awr005

Bruno, M. A., Majerus, S., Boly, M., Vanhaudenhuyse, A., Schnakers, C., Gosseries, O., et al. (2012). Functional neuroanatomy underlying the clinical subcategorization of minimally conscious state patients. *J. Neurol.* 259, 1087–1098. doi: 10.1007/s00415-011-6303-7

Charland-Verville, V., Lesenfants, D., Sela, L., Noirhomme, Q., Ziegler, E., Chatelle, C., et al. (2014). Detection of response to command using voluntary control of breathing in disorders of consciousness. *Front. Hum. Neurosci.* 8:1020. doi: 10.3389/fnhum.2014.01020

Chaudhary, U., Xia, B., Silvoni, S., Cohen, L. G., and Birbaumer, N. (2017). Brain-computer interface-based communication in the completely locked-in state. *PLoS Biol.* 15:e1002593. doi: 10.1371/journal.pbio.1002593

Chennu, S., Annen, J., Wannez, S., Thibaut, A., Chatelle, C., Cassol, H., et al. (2017). Brain networks predict metabolism, diagnosis and prognosis at the bedside in disorders of consciousness. *Brain* 140, 2120–2132. doi: 10.1093/brain/awx163

Chennu, S., and Bekinschtein, T. A. (2012). Arousal modulates auditory attention and awareness: insights from sleep, sedation, and disorders of consciousness. *Front. Psychol.* 3:65. doi: 10.3389/fpsyg.2012.00065

Cruse, D., Chennu, S., Chatelle, C., Bekinschtein, T. A., Fernández-Espejo, D., Pickard, J. D., et al. (2011). Bedside detection of awareness in the vegetative state: a cohort study. *Lancet*. 378, 2088–2094. doi: 10.1016/S0140-6736(11)61224-5

Cruse, D., Chennu, S., Chatelle, C., Fernández-Espejo, D., Bekinschtein, T. A., Pickard, J. D., et al. (2012). Relationship between etiology and covert cognition in the minimally conscious state. *Neurology* 78, 816–822. doi: 10.1212/WNL.0b013e318249f764

Cruse, D., Chennu, S., Chatelle, C., Bekinschtein, T. A., Fernández-Espejo, D., Pickard, J. D., et al. (2013). Reanalysis of "Bedside detection of awareness in the vegetative state: a cohort study" - Authors' reply. *Lancet* 381, 291–292. doi: 10.1016/S0140-6736(13)60126-9

Demertzi, A., Antonopoulos, G., Heine, L., Voss, H. U., Crone, J. S., de Los Angeles, C., et al. (2015). Intrinsic functional connectivity differentiates minimally conscious from unresponsive patients. *Brain* 138, 2619–2631. doi: 10.1093/brain/awv169

Estraneo, A., Moretta, P., Loreto, V., Lanzillo, B., Santoro, L., and Trojano, L. (2010). Late recovery after traumatic, anoxic, or hemorrhagic long-lasting vegetative state. *Neurology* 75, 239–245. doi: 10.1212/WNL.0b013e3181e8e8cc

Giacino, J. T., Ashwal, S., Childs, N., Cranford, R., Jennett, B., Katz, D. I., et al. (2002). The minimally conscious state: definition and diagnostic criteria. *Neurology* 58, 349–353. doi: 10.1212/WNL.58.3.349

Goldfine, A. M., Bardin, J. C., Noirhomme, Q., Fins, J. J., Schiff, N. D., and Victor, J. D. (2013). Reanalysis of "Bedside detection of awareness in the vegetative state: a cohort study." *Lancet* 381, 289–291. doi: 10.1016/S0140-6736(13)60125-7

Guger, C., Spataro, R., Allison, B. Z., Heilinger, A., Ortner, R., Cho, W., et al. (2017). Complete locked-in and locked-in patients: command following assessment and communication with vibro-tactile P300 and motor imagery brain-computer interface tools. *Front. Neurosci.* 11:251. doi: 10.3389/fnins.2017.00251

Habbal, D., Gosseries, O., Noirhomme, Q., Renaux, J., Lesenfants, D., Bekinschtein, T. A., et al. (2014). Volitional electromyographic responses in disorders of consciousness. *Brain Inj.* 28, 1171–1179. doi: 10.3109/02699052.2014.920519

Jox, R. J., Bernat, J. L., Laureys, S., and Racine, E. (2012). Disorders of consciousness: responding to requests for novel diagnostic and therapeutic interventions. *Lancet Neurol.* 11, 732–738. doi: 10.1016/S1474-4422(12)70154-0

King, J. R., Faugeras, F., Gramfort, A., Schurger, A., El Karoui, I., Sitt, J. D., et al. (2013). Single-trial decoding of auditory novelty responses facilitates the detection of residual consciousness. *Neuroimage* 83, 726–738. doi: 10.1016/j.neuroimage.2013.07.013

Laureys, S., Celesia, G. G., Cohadon, F., Lavrijsen, J., León-Carrión, J., Sannita, W. G., et al. (2010). Unresponsive wakefulness syndrome: a new name for the vegetative state or apallic syndrome. *BMC Med.* 8:68. doi: 10.1186/1741-7015-8-68

Lesenfants, D., Habbal, D., Chatelle, C., Schnakers, C., Laureys, S., and Noirhomme, Q. (2016). Electromyographic decoding of response to command in disorders of consciousness. *Neurology* 87, 2099–2107. doi: 10.1212/WNL.0000000000003333

Li, R., Song, W. Q., Du, J. B., Huo, S., and Shan, G. X. (2015). Connecting the P300 to the diagnosis and prognosis of unconscious patients. *Neural Regen. Res.* 10, 473–480. doi: 10.4103/1673-5374.153699

Maythaler, J. M., Brunner, R. C., Johnson, A., Thomas, N. (2002). Amantadine to improve neurorecovery in traumatic brain injury – associated diffuse axonal injury: a pilot double-blind randomized trial. *J. Head Trauma Rehabil.* 17, 300–313. doi: 10.1097/00001199-200208000-00004

Monti, M. M., Vanhaudenhuyse, A., Coleman, M. R., Boly, M., Pickard, J. D., Tshibanda, L., et al. (2010). Willful modulation of brain activity in disorders of consciousness. *N. Engl. J. Med.* 362, 579–589. doi: 10.1056/NEJMoa0905370

Noirhomme, Q., Brecheisen, R., Lesenfants, D., Antonopoulos, G., and Laureys, S. (2015). "Look at my classifier's result": disentangling unresponsive from (minimally) conscious patients. *Neuroimage* 145, 288–303. doi: 10.1016/j.neuroimage.2015.12.006

Ortner, R., Espinosa, A., Rodriguez, J., Laureys, S., Lugo, Z.R., Guger, C., et al. (2014). A BCI-based tool for detection of awareness and for communication with non-responsive patients. *Lect. Notes Comput. Sci.* 8513, 527–535. doi: 10.1007/978-3-319-07437-5_50

Owen, A. M., Coleman, M. R., Boly, M., Davis, M.H., Laureys, S., and Pickard, J. D. (2006). Detecting awareness in the vegetative state. *Science* 313: 1402. doi: 10.1126/science.1130197

Perrin, F., Schnakers, C., Schabus, M., Degueldre, C., Goldman, S., Brédart, S., et al. (2006). Brain response to one's own name in vegetative state, minimally conscious state, and locked-in syndrome. *Arch Neurol.* 63, 562–569. doi: 10.1001/archneur.63.4.562

Piarulli, A., Bergamasco, M., Thibaut, A., Cologan, V., Gosseries, O., and Laureys, S. (2016). EEG ultradian rhythmicity differences in disorders of consciousness during wakefulness. *J. Neurol.* 263, 1746–1760. doi: 10.1007/s00415-016-8196-y

Rosanova, M., Gosseries, O., Casarotto, S., Boly, M., Casali, A. G., Bruno, M. A., et al. (2012). Recovery of cortical effective connectivity and recovery of consciousness in vegetative patients. *Brain* 135, 1–13. doi: 10.1093/brain/awr340

Schnakers, C., Vanhaudenhuyse, A., Giacino, J., Ventura, M., Boly, M., Majerus, S., et al. (2009). Diagnostic accuracy of the vegetative and minimally conscious state: clinical consensus versus standardized neurobehavioral assessment. *BMC Neurol.* 9:35. doi: 10.1186/1471-2377-9-35

Sitt, J. D., King, J.-R., El Karoui, I., Rohaut, B., Faugeras, F., Gramfort, A., et al. (2014). Large scale screening of neural signatures of consciousness in patients in a vegetative or minimally conscious state. *Brain* 137(Pt 8),2258–2270. doi: 10.1093/brain/awu141

Spataro, R., Heilinger, A., Allison, B., De Cicco, D., Marchese, S., Gregoretti, C., et al. (2018). Preserved somatosensory discrimination predicts consciousness recovery in unresponsive wakefulness syndrome. *Clin. Neurophysiol.* 129, 1130–1136. doi: 10.1016/j.clinph.2018.02.131

Stender, J., Gosseries, O., Bruno, M.-A., Charland-Verville, V., Vanhaudenhuyse, A., Demertzi, A., et al. (2014). Diagnostic precision of PET imaging and functional MRI in disorders of consciousness: a clinical validation study. *Lancet* 6736, 8–16. doi: 10.1016/S0140-6736(14)60042-8

Stoll, J., Chatelle, C., Carter, O., Koch, C., Laureys, S., and Einhäuser, W. (2013). Pupil responses allow communication in locked-in syndrome patients. *Curr. Biol.* 23, R647–R648. doi: 10.1016/j.cub.2013.06.011

Thibaut, A., Bruno, M.-A., Ledoux, D., Demertzi A, and Laureys S. (2014). tDCS in patients with disorders of consciousness. *Neurology* 82, 1–7. doi: 10.1212/WNL.0000000000000260

Tzovara, A., Rossetti, A. O., Juan, E., Suys, T., Viceic, D., Rusca, M., et al. (2016). Prediction of awakening from hypothermic postanoxic coma based on auditory discrimination. *Ann. Neurol.* 79, 748–757. doi: 10.1002/ana.24622

Wannez, S., Heine, L., Thonnard, M., Gosseries, O., Laureys, S., Coma Science Group Collaborators. (2018). The repetition of behavioral assessments

in diagnosis of disorders of consciousness. *Ann. Neurol.* 81, 883–889. doi: 10.1002/ana.24962

Whyte, J., Cifu, D., Dikmen, S., and Temkin, N. (2001). Prediction of functional outcomes after traumatic brain injury: a comparison of 2 measures of duration of unconsciousness. *Arch. Phys. Med. Rehabil.* 82, 1355–1359. doi: 10.1053/apmr.2001.26091

Whyte, J., Nakase-Richardson, R., Hammond, F. M., McNamee, S., Giacino, J. T., Kalmar, K., et al. (2013). Functional outcomes in traumatic disorders of consciousness: 5-year outcomes from the National Institute on Disability and Rehabilitation Research traumatic brain injury model systems. *Arch. Phys. Med. Rehabil.* 94, 1855–1860. doi: 10.1016/j.apmr.2012.10.041

Wilhelm, B., Jordan, M., and Birbaumer, N. (2006). Communication in locked-in syndrome: effects of imagery on salivary pH. *Neurology* 67, 534–535. doi: 10.1212/01.wnl.0000228226.86382.5f

Conflict of Interest Statement: The authors declare that the hard- and software was made available by Gtec. WC is employed by g.tec Medical Engineering GmbH, CG is the CEO of g.tec Medical Engineering GmbH and g.tec Guger technologies OG. SL is on the scientific advisory board of Gtec Medical Engineering.

The other authors declare that the research was conducted in the absence of any commercial or financial relationships that could be construed as a potential conflict of interest.

Copyright © 2018 Annen, Blandiaux, Lejeune, Bahri, Thibaut, Cho, Guger, Chatelle and Laureys. This is an open-access article distributed under the terms of the Creative Commons Attribution License (CC BY). The use, distribution or reproduction in other forums is permitted, provided the original author(s) and the copyright owner are credited and that the original publication in this journal is cited, in accordance with accepted academic practice. No use, distribution or reproduction is permitted which does not comply with these terms.

frontiers in Neuroscience

REVIEW
published: 21 June 2018
doi: 10.3389/fnins.2018.00422

Decoding Inner Speech Using Electrocorticography: Progress and Challenges Toward a Speech Prosthesis

Stephanie Martin[1,2]*, *Iñaki Iturrate*[1], *José del R. Millán*[1], *Robert T. Knight*[2,3] and *Brian N. Pasley*[2]

[1] Defitech Chair in Brain Machine Interface, Center for Neuroprosthetics, Ecole Polytechnique Fédérale de Lausanne, Lausanne, Switzerland, [2] Helen Wills Neuroscience Institute, University of California, Berkeley, Berkeley, CA, United States, [3] Department of Psychology, University of California, Berkeley, Berkeley, CA, United States

Certain brain disorders resulting from brainstem infarcts, traumatic brain injury, cerebral palsy, stroke, and amyotrophic lateral sclerosis, limit verbal communication despite the patient being fully aware. People that cannot communicate due to neurological disorders would benefit from a system that can infer internal speech directly from brain signals. In this review article, we describe the state of the art in decoding inner speech, ranging from early acoustic sound features, to higher order speech units. We focused on intracranial recordings, as this technique allows monitoring brain activity with high spatial, temporal, and spectral resolution, and therefore is a good candidate to investigate inner speech. Despite intense efforts, investigating how the human cortex encodes inner speech remains an elusive challenge, due to the lack of behavioral and observable measures. We emphasize various challenges commonly encountered when investigating inner speech decoding, and propose potential solutions in order to get closer to a natural speech assistive device.

Keywords: inner speech, electrocorticography, decoding, neuroprosthetics, brain-computer interface

OPEN ACCESS

Edited by:
Christoph Guger,
Guger Technologies, Austria

Reviewed by:
Christian Herff,
University of Bremen, Germany
Jonas Obleser,
Universität zu Lübeck, Germany

***Correspondence:**
Stephanie Martin
martin.stephanie.b@gmail.com

Specialty section:
This article was submitted to Neural Technology, a section of the journal Frontiers in Neuroscience

Received: *28 February 2018*
Accepted: *04 June 2018*
Published: *21 June 2018*

Citation:
Martin S, Iturrate I, Millán JdR, Knight RT and Pasley BN (2018) Decoding Inner Speech Using Electrocorticography: Progress and Challenges Toward a Speech Prosthesis. Front. Neurosci. 12:422. doi: 10.3389/fnins.2018.00422

INTRODUCTION

Neural engineering research has made tremendous advances in decoding motor (Ajiboye et al., 2017) or visual neural signals (Lewis et al., 2015) for assisting and restoring lost functions in patients with disabling neurological conditions. An important extension of these approaches is the development of assistive devices that restore natural communication in patients with intact language systems but limited verbal communication due to neurological disorder. Several brain-computer interfaces have allowed relevant communication applications, such as moving a cursor on the screen (Wolpaw et al., 1991) and spelling letters (Farwell and Donchin, 1988; Gilja et al., 2015; Jarosiewicz et al., 2015; Vansteensel et al., 2016; Pandarinath et al., 2017). Although this type of interface has proven to be useful, patients had to learn to modulate their brain activity in an unnatural and unintuitive way—i.e., performing mental tasks like a rotating cube, mental calculus, movement attempts to operate an interface (Millán et al., 2009), or detecting rapidly presented letters on a screen, such as in the P300-speller (see Fazel-Rezai et al., 2012 for a review) and steady-state visual evoked potentials paradigm(Srinivasan et al., 2006; Nijboer et al., 2008).

As an alternative, people with speech deficits would benefit from a communication system that can directly infer inner speech from brain signals—allowing them to interact more naturally with the world. Inner speech (also called imagined speech, internal speech, covert speech, silent speech, speech imagery, or verbal thoughts) is defined here as the ability to generate internal speech representations, in the absence of any external speech stimulation or self-generated overt speech. While much has been learnt about actual speech perception and production (see Price, 2000; Démonet et al., 2005; Hickok and Poeppel, 2007, for reviews), investigating inner speech has remained a challenging task due to the lack of behavioral output. Indeed, it remains difficult to study this internal neural process due to the difficulty to time-lock precise events (acoustic features, phonemes, words) to neural activity during inner speech. Therefore, substantial efforts have aimed to develop new strategies for analyzing these brain signals.

Investigating the underlying neural representations associated with these different speech features during inner speech is central for engineering speech neuroprosthetic devices. For instance, speech processing includes various processing steps—such as acoustic processing in the early auditory cortex, phonetic, and categorical encoding in posterior areas of the temporal lobe and semantic and higher level of linguistic processes in later stages (Hickok and Poeppel, 2007). One can ask what are the appropriate speech stimulus-neural response mappings to target for efficient decoding and designing optimal communication technologies. For example, a decoding model can target continuous auditory spectrotemporal features predicted from the brain activity. Alternatively, decoding discrete phonemes allows building words and sentences directly.

In this review article, we describe recent research findings on understanding and decoding the neural correlates associated with inner speech, for targeting communication assistive technologies. We focused on studies that have used electrocorticographic (ECoG) recordings in the human cortex, as this promising technique allows monitoring brain activity with high spatial, temporal, and spectral resolution, as compared to electroencephalographic recordings, and the electrodes cover broader brain areas compared to intracortical recordings (Ritaccio et al., 2015). We discuss different decoding and experimental strategies to deal with common challenges that are encountered when tackling inner speech decoding. We consider new avenues and future directions to meet the key scientific and technical challenges in development of a realistic, natural speech decoding device.

In the next section, we first briefly present the properties of electrocorticography, together with its advantages for investigating the neural representation of human speech. We next describe several neuro-computational modeling approaches to neural decoding of speech features.

Electrocorticographic Recordings

Electrocorticography (ECoG), also called intracranial recording or intracranial electroencephalography (iEEG), is used in patients with intractable epilepsy to localize the seizure onset zone, prior to brain tissue ablation. In this procedure, electrode grids, strips or depth electrodes are temporarily implanted onto the cortical surface, either above (epidural) or below (subdural) the dura mater (**Figure 1**). Because of its invasiveness, only in rare cases, patients are implanted with such electrodes, and it remains exclusively for clinical purposes; nevertheless, the implantation time provides a unique opportunity to investigate human brain functions, with high spatial (millimeters), temporal (milliseconds), and spectral resolution (0–500 Hz). In addition, it covers broad brain areas (typically frontal, temporal, and parietal cortex), which is beneficial given the complex and widely distributed network associated with speech. Finally, electrocorticography is suitable for neuroprosthetic and brain-computer interface applications (Leuthardt et al., 2004, 2006; Felton et al., 2007; Schalk et al., 2007; Blakely et al., 2009; Wang et al., 2013; Kapeller et al., 2014; Moses et al., 2018). Therefore, this technique is an ideal recording candidate for investigating speech functions and for targeting speech neuroprosthetic devices.

ECoG activity contains different signal components (Marshall et al., 2006; Miller et al., 2007; Buzsáki and Wang, 2012; Giraud and Poeppel, 2012) that may relate to different underlying physiological mechanisms, and therefore different mappings between speech stimulus and neural response. For example, the neural representation of speech has been mainly studied using both high frequency (∼70–500 Hz) and low frequency (∼4–8 Hz).

High frequency activity (HFA; ∼70–500 Hz) has been correlated with multiunit spike rate and asynchronous post-synaptic current of the underlying neuronal population (Manning et al., 2009; Whittingstall and Logothetis, 2009; Buzsáki et al., 2012; Lachaux et al., 2012; Rich and Wallis, 2017). In particular, HFA has been shown to robustly encode various speech representations, such as early spectrotemporal acoustic features of speech in the superior temporal gyrus (Pasley et al., 2012; Kubanek et al., 2013)—a region commonly associated with speech perception. In addition, the superior temporal gyrus plays an important role in transforming these acoustic cues into categorical speech units (Chang et al., 2010; Pasley et al., 2011; Mesgarani et al., 2014). HFA in the ventral sensorimotor cortex has been shown to encode acoustic (Pasley and Knight, 2013; Martin et al., 2014; Cheung et al., 2016) and phonetic representations during speech perception, and somatotopically arranged articulator representations (lips, tongue, larynx, and jaw) during speech production (Bouchard et al., 2013; Cheung et al., 2016; Conant et al., 2018).

Low frequencies, such as theta band, have been shown to track the acoustic envelope of speech, to correlate with syllabic rate, and to discriminate spoken sentences (Luo and Poeppel, 2007; Ding and Simon, 2012; Giraud and Poeppel, 2012; Zion Golumbic et al., 2013). In addition, theta rhythms showed significant power changes in Broca's area and temporal language areas during a verb generation task, and showed interactions with high frequency band, through amplitude-amplitude and phase-amplitude coupling (Hermes et al., 2014).

The next section briefly introduces neural decoding models, which have been widely used in the field of speech.

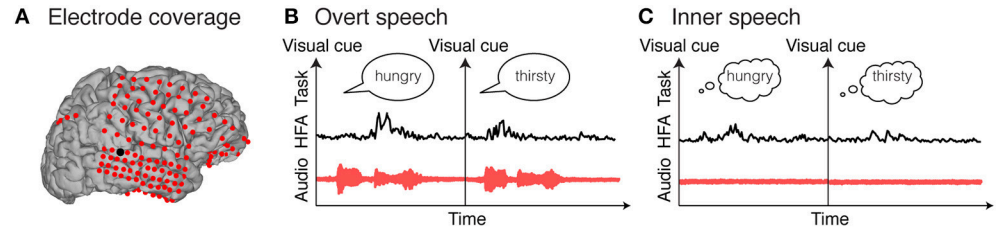

FIGURE 1 | Electrocorticographic recordings. Example of electrocorticographic grid locations overlaid on cortical surface reconstructions of a subject's MRI scan **(A)**. Examples of single trial high frequency activity (HFA) for an electrode highlighted in black in **(A)**. Single trials represent examples of overt speech word repetition **(B)** and inner speech word repetition **(C)**.

Decoding Models—General Framework

Traditionally, cognitive functions have been investigated using a set of stimuli that typically vary along a single dimension of interest (e.g., attended versus not attended target). Brain activity evoked by different stimuli are then averaged and compared in order to provide new insights about the neural mechanisms under study. Conversely, decoding these cognitive functions in real-time for targeting brain-machine interfaces requires more sophisticated predictive modeling. Decoding models allow researchers to apply multivariate neural features to rich, complex and naturalistic stimuli or behavioral conditions (Kay et al., 2008; Kay and Gallant, 2009; Naselaris et al., 2011).

A commonly used modeling approach uses a regression framework to link brain activity and a stimulus or mental state representation. For instance, the stimulus features at a given time can be modeled as a weighted sum of the neural activity, as follows:

$$Y(t) = \sum_{p} w(p) \bullet X(t,p)$$

where $Y(t)$ is the stimulus feature at time t, $X(t,p)$ is the neural activity at time t and feature p, $w(p)$ is the weight for a given feature p. Classification is a type of decoding model in which the neural activity is identified as belonging to a discrete event type from a finite set of choices. Both types of models can use various machine learning algorithms, ranging from simple regression techniques, to more complex non-linear approaches, such as hidden Markov models, support-vector algorithms and neural networks. Holdgraf et al. (2017) provide a review article that illustrates best-practices in conducting these analyses, and included a small sample dataset, along with several scripts in the form of *jupyter* notebooks. The general framework is common to all methods (**Figure 2**) and consists of the following steps:

1. Feature extraction: input and output features are extracted from the neural activity and from the stimulus features, respectively. Examples of speech representations typically used in decoding models are the auditory frequencies, the modulation rates, or phonemes for natural speech. For neural representations, firing rate from single unit spiking activity, or amplitudes in specific frequency bands are typically extracted from the recorded electrophysiological signal (for example, the high gamma band).
2. Model estimation: models are estimated by mapping input features to output features. The weights are calculated by minimizing a metric of error between the predicted and actual output on a training set. For example, in a linear regression model, the output is a weighted sum of input features.
3. Validation: Once a model is fit, it is then validated on new unseen data not used for training, in order to avoid overfitting and aid generalization to new data. To evaluate the accuracy, the predicted output is compared directly to the original representation.

In the next section, we review ECoG studies that have employed decoding models to understand and decode cognitive states associated with various inner speech representations.

DECODING INNER SPEECH USING ELECTROCORTICOGRAPHY

A key challenge to understanding the neural representation of inner speech is to quantify the relationship between neural response and the imagined stimulus, from low-level auditory to higher-level speech representations. Several studies have exploited the advantageous properties of intracranial recordings to characterize inner speech representations. For instance, a recent study described the spatiotemporal evolution of high frequency activity during an overt and covert word repetition using trial averaging (Pei et al., 2011b; Leuthardt et al., 2012). In particular, they revealed high frequency changes in the superior temporal lobe and the supramarginal gyrus during covert speech repetition. During a covert verb generation task, high frequency activity (65–95 Hz) showed significant brain activity in Broca's area, in the middle temporal gyrus, and temporal parietal junction, and interacted with theta frequency activity (4–8 Hz) through cross-frequency coupling (Hermes et al., 2014). Finally, a recent study compared the electrocorticographic activity related to overt vs. covert conditions, and revealed a common network of brain regions (Brumberg et al., 2016).

To directly quantify the relationship between inner speech and neural response, the decoding model framework can be applied. Recently, we used a decoding model approach to reconstruct continuous auditory features from high gamma neural activity (70–150 Hz) recorded during inner speech (Martin et al., 2014). Due to the lack of any measurable behavioral output, standard

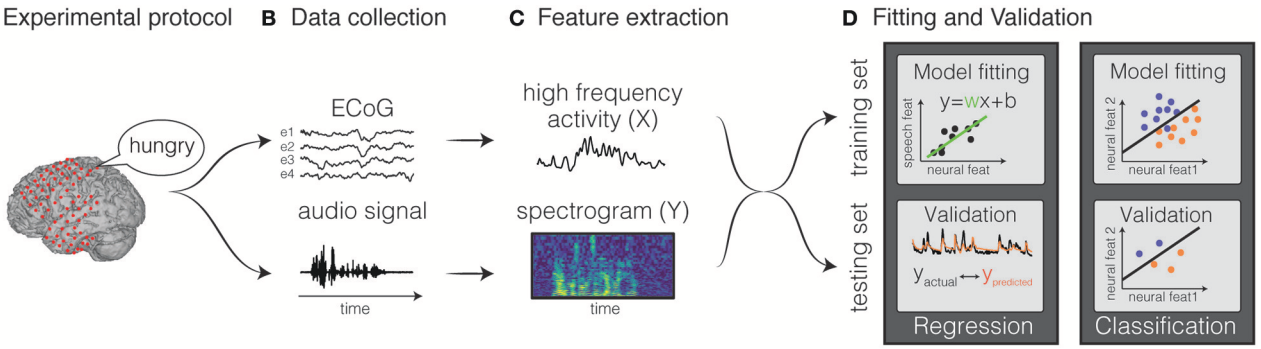

FIGURE 2 | Decoding framework. The general framework for fitting a decoding model is depicted. The first step consists in designing a protocol **(A)** and recording the data **(B)**. Then, input and output features are extracted **(C)**, and the data are split in training and testing set. The training set is used to fit the weights of the model and the testing set is used to validated the model **(D)**. Figures adapted from Holdgraf et al. (2017) with permissions.

decoding models (e.g., linear regression) that assume temporal alignment of input and output data are not immediately applicable. One simple approach is to take advantage of prior research demonstrating that speech perception and imagery, to some extent, share common neural mechanisms (Hinke et al., 1993; Yetkin et al., 1995; McGuire et al., 1996; Rosen et al., 2000; Palmer et al., 2001; Aleman, 2004; Aziz-Zadeh et al., 2005; Hubbard, 2010; Geva and Warburton, 2011; Perrone-Bertolotti et al., 2014). Under the assumption that perception and imagery share overlapping neural representations, we built a decoding model from an overt speech condition, and applied this decoder to neural data generated during inner speech. To evaluate performance, the reconstruction in the inner speech condition was compared to the representation of the corresponding original sound spoken out loud—using dynamic time warping (Ellis, 2003)—a temporal realignment algorithm. Results showed that spectrotemporal features of inner speech were decoded with significant predictive accuracy from models built from overt speech data in seven patients (**Figure 3A**). These findings provided further support that overt and inner speech share underlying neural mechanisms. However, this approach assumes that imagery neural data are generated from a similar neural process as perception. The predictive power of this "cross-condition" model is negatively impacted by discrepancies between perception and imagery neural mechanisms, and is therefore expected to be less optimal compared to directly modeling imagery data in train and test phases.

Beyond relatively low-level acoustic representation, invariant phonetic information is extracted from a highly variable continuous acoustic signal at a mid-level neural representation (Chang et al., 2010). During inner speech, behavioral studies have provided evidence that phoneme substitution errors occurred between phonemes sharing similar features (phonemic similarity effect; Corley et al., 2011), and a similar behavior occurs during overt speech. In addition, brain imaging studies have revealed anatomical brain regions involved in silent articulation, such as the sensorimotor cortex, the inferior frontal gyrus, and temporo-parietal brain areas (Pulvermuller et al., 2006). Recently, electrophysiological studies have shown that the neural activity of a listener that perceives a specific phoneme that has been acoustically degraded, replaced or masked by noise is grounded into acoustic neural representations (Holdgraf et al., 2016; Leonard et al., 2016). This phenomenon, called the phonetic masking effect shows that even in the absence of a given speech sound, the neural patterns correlate with those that would have been elicited by the actual speech sound. These findings suggest that phonemes are represented during inner speech in the human cortex. From a decoding perspective, several studies have succeeded in classifying individual inner speech units into different categories, such as covertly articulated vowels (Ikeda et al., 2014), vowels and consonants during covert word production (Pei et al., 2011a), and intended phonemes (Brumberg et al., 2011). These studies represent a proof of concept for basic decoding of individual speech units, but further research is required to define the ability to decode phonemes during continuous, conversational speech.

While several studies have demonstrated phoneme classification during inner speech (Brumberg et al., 2011; Pei et al., 2011a; Tankus et al., 2012; Ikeda et al., 2014), fewer results are available for word-level classification. Words have been decoded during overt speech from neural signals in the inferior frontal gyrus, superior temporal gyrus, and motor areas (Kellis et al., 2010; Pasley et al., 2012; Martin et al., 2014). In recent work, we classified individual words from high frequency activity recorded during an inner speech word repetition task (Martin et al., 2016). To this end, we took advantage of the high temporal resolution offered by ECoG, and classified neural features in the time domain using a support-vector machine model. In order to account for temporal irregularities across trials, we introduced a non-linear time alignment into the classification framework. Pairwise classification results showed that the classification accuracy was significant across five patients. An example of classification accuracy is depicted in **Figure 3B** (left panel), where the classification accuracy across the 15 pairs of word were above chance level (average across

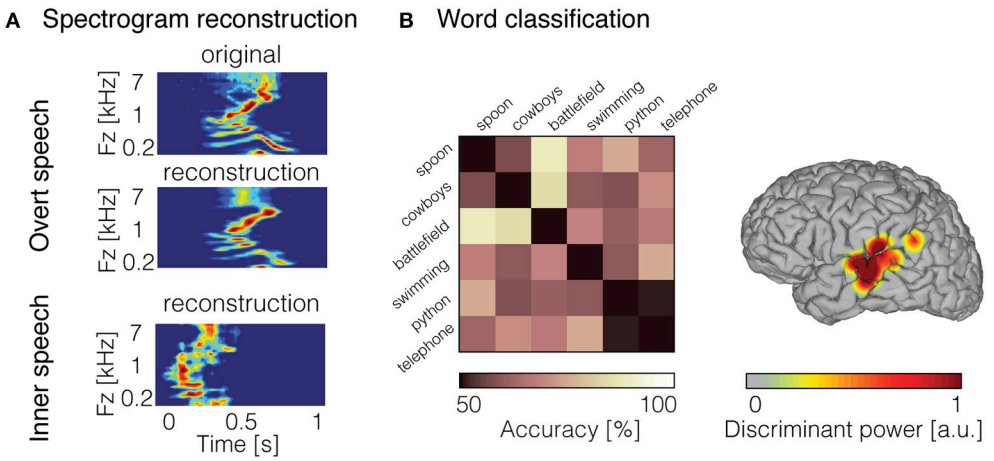

FIGURE 3 | Decoded inner speech representation. **(A)** Examples of overt speech and inner speech spectrogram reconstruction using linear regression models. Original spectrogram of the recorded overt speech sound is displayed (top panel). Reconstruction of the spectrogram for the overt speech condition (middle panel) and inner speech condition (bottom panel). **(B)** Examples of word pair classification during inner speech (left panel). Chance level was 50% (diagonal elements), whereas pairwise classification accuracy (off-diagonal elements) reached 88% and was significantly above chancel level across the 15 pairs of word (mean = 69%). Discriminant information displayed on the surface reconstruction of the participant's brain (right panel) for the classification accuracy shown in the left panel. Figures adapted from Martin et al. (2014, 2016) with permissions.

all pairs = 69%; chance level = 50%). Most of the discriminant information came from the posterior temporal gyrus (**Figure 3B**; right panel). This study represents a proof of concept for basic decoding of speech imagery, and highlights the potential for targeting a speech prosthesis that allows to communicate a few words that are clinically relevant (e.g., hungry, pain, etc.).

Finally, an alternative study that shows further evidence of acoustic processing during imagery comes from a music imagery study. In this study, we investigated the neural encoding of auditory features during imagery using a novel experimental paradigm that allowed direct modeling of auditory imagery data (as opposed to cross-condition) (Martin et al., 2017). This study is not directly related to speech representations, yet it helps understanding the neural representation of inner subjective experiences, such as general auditory imagery. In addition, evidence has shown that music and speech share common brain networks (Callan et al., 2006; Schön et al., 2010). This study relied on a rare clinical case in which a patient undergoing neurosurgery for epilepsy treatment was also an adept piano player. While previous brain imaging studies have identified anatomical regions active during auditory imagery (Zatorre et al., 1996; Griffiths, 1999; Halpern and Zatorre, 1999; Rauschecker, 2001; Halpern et al., 2004; Kraemer et al., 2005), underlying neural tuning to auditory frequencies in imagined sounds was uncharacterized. ECoG activity was recorded during a task that allowed direct alignment of neural response and the spectrotemporal content of the intended music imagery. The patient played two piano pieces with and without auditory feedback of the sound produced by the electronic piano. The audio signal from the keyboard was recorded in synchrony with the ECoG signal, which allowed synchronizing the audio output with neural activity in both conditions. In this task design, it is assumed that the patient's auditory imagery closely matches the output of the keyboard in both timing and spectral content. This study therefore provided a unique opportunity to apply direct (as opposed to cross-condition) receptive field modeling techniques (Aertsen et al., 1981; Clopton and Backoff, 1991; Theunissen et al., 2000; Chi et al., 2005; Pasley et al., 2012), which describe neural response properties, for example auditory frequency tuning. We found robust similarities between perception and imagery neural representations in both frequency and temporal tuning properties in auditory areas. Furthermore, these findings also demonstrated that decoding models, typically applied in neuroprosthetics for motor and visual restoration, are applicable to auditory imagery, representing an important step toward development of algorithms that could be used in neural interfaces for communication based on auditory or speech imagery.

CHALLENGES AND SOLUTIONS

An important but challenging step in future research is to describe the extent to which speech representations, such as acoustic processing, phonetic encoding and higher level of linguistic functions apply to inner speech. The lack of behavioral output during imagery and inability to monitor the spectrotemporal structure of inner speech represent a major challenge. Critically, inner speech cannot be directly observed by an experimenter. As a consequence, it is complicated to time-lock brain activity to a measurable stimulus or behavioral state, which precludes the use of standard models that assume synchronized input-output data. In addition, natural speech expression is not just operated under conscious control, but is affected by various factors, including gender, emotional state, tempo, pronunciation, and dialect, resulting in temporal irregularities (stretching/compressing, onset/offset delays) across repetitions.

As a result, this leads to problems in exploiting the temporal resolution of electrocorticography to investigate inner speech. In this section, we highlight several additional challenges that are encountered when investigating inner speech, as well as new avenues to improve the decoding outcome.

Improving Task Design

The lack of behavioral output and temporal irregularities may be alleviated by designing tasks that maximize the accuracy when labeling the content of inner speech, such as cueing the participants in a rhythmical manner. Despite this, results may still show inconsistencies between the actual cue and the intended speech onset/offset. Alternatively, a verb generation task (Hermes et al., 2014) or picture naming task (Riès et al., 2015) might improve the signal-to-noise ratio, as the cognitive load is more demanding than during a simple word repetition task.

Training Participants

In order to improve accuracy, patients should be familiarized with the tasks before entering in the epilepsy monitoring unit. Indeed, studies have shown that participants with musical training exhibited better pitch and temporal acuity in auditory imagery and enlarged tonotopic maps located in the STG than did participants with little or no musical training (Pantev et al., 1998; Janata and Paroo, 2006; Herholz et al., 2008). As such, we argue it would be beneficial to train subjects on speech imagery, in order to have an increased signal-to-noise ratio and for them to be more consistent in the way of performing the mental imagery. This will improve the performances of any pattern recognition algorithm.

Finding Behavioral Markers

Finding a behavioral or neural metric that allows marking more precisely the inner speech time course would reduce temporal variability during inner speech. This will be increasingly important when moving toward asynchronous protocols, i.e., when patients spontaneously produce inner speech, as opposed to experimental protocols that generally employ timing cues. For instance, behavioral and psychology studies rely on indirect measures to infer the existence and properties of the intended inner experience (Hubbard, 2010). For example, participants were instructed to image the pitch of a sine wave tone for a given instrument, and they had to subsequently judge if the timber of a second presented tone matched the timber of the first one (Crowder, 1989). Response times were faster, when the timbre of the second tone matched the timbre of the first one they had to imagine (see Hubbard, 2010 for a complete review). Therefore, objective monitoring of performance and vividness through external markers may allow certain sources of variability during inner speech to be estimated and accounted for in the modeling process.

Incorporating Speech Recognition Models

Recently, electrophysiological studies on speech decoding have shown promising results by integrating knowledge from the field of speech recognition (Herff et al., 2015; Moses et al., 2016, 2018). Speech recognition has been concerned with the statistical modeling of natural language for many decades, and has faced many problems that are similar to decoding neural pattern associated with speech. As such, we argue that integrating those tools into the field of neuroscience is a necessary element to succeed in the ultimate goal of a clinically reliable speech prosthesis. For instance, speech recognition has developed methodologies that enable the recognition and translation of spoken language into text. This was achieved by incorporating extensive knowledge about how speech is produced and perceived at various phonetic levels (acoustic, auditory, articulatory features), and from advances in computer resources and big data management to build now common applications, such as spellcheck tools, text-to-speech synthesizers, and machine translation programs. Similarly, advanced machine learning models might be more adapted in order to deal with problems associated with speech production temporal irregularities compared to approach like dynamic time warping, which is less robust for noisy data.

Increasing the Amount of Data

More complex models with increasing number of parameters can be used, but require more data to train and evaluate the models. When using electrocorticographic recordings, available data are limited. Experimental paradigms usually do not last long to avoid overloading the patients. As an alternative to traditional protocols, researchers are slowly moving toward continuous brain monitoring during the electrode implantation time. This allows increasing the amount of recorded data and is less constraining to the participant as he or she is recorded in the existing hospital environment, e.g., watching television, interacting with relatives and clinicians, reading, etc. Continuous monitoring of speech perception and production may provide sufficient data to develop more complex and robust decoding models.

Using Unsupervised Learning

The major problem with recording continuous data is how to label precisely the recordings. Indeed, while it is currently possible to monitor conversations with a microphone, the continuous labeling of categories or events during a movie or a dialogue is a tedious process, and often requires human intervention. In addition, as mentioned earlier, monitoring and labeling internal mental states, such as mood, emotions, internal speech, is problematical. We suggest that unsupervised learning methods might be adapted in this context, and alleviate issues associated with speech segmentation. Unsupervised learning is a type of machine learning algorithms that allows drawing inferences from unlabeled responses, i.e., the labels of the observations are not available. This approach has been used in the field of computer vision, such as to learn the features in order to recognize objects (e.g., a car or a motorcycle).

Improving the Electrode Design

Although electrocorticography provides the opportunity to investigate speech neural representation, the configuration, location and duration of implantation are not optimized for experiments, but rather solely for clinical purposes. The design

of the intracranial recording electrodes has been shown to be an important factor in motor decoding performance. Namely, the spatial resolution of a cortical surface electrode array depends on the size and spacing of the electrodes, as well as the volume of tissue to which each electrode is sensitive (Wodlinger et al., 2011). Many researchers have attempted to define what the optimal electrode spacing and size could be (Slutzky et al., 2010), but this is still an open area of research. Emerging evidence showed that decoding performance was improved when neural activity was derived from very high-density grids (Blakely et al., 2008; Rouse et al., 2013). However, although a smaller inter-electrode spacing increases the spatial resolution, it poses additional technical issues related to the electrode grid design. Higher density grids placed at specific speech locations would provide higher spatial resolution and potentially enhance the signal's discriminability. Ongoing work in many labs is aimed at increasing the number of recording contacts (Khodagholy et al., 2014) and using biocompatible materials and wireless telemetry for transmission of recordings from multiple electrode implants (Brumberg et al., 2011; Khodagholy et al., 2014). Finally, long-term implantation capability in humans is lacking, as compared to non-human primate studies that showed stable neural decoding for extended periods of time (weeks to months; Ashmore et al., 2012). Reasons for these technical difficulties are the increased impedance leading to loss of signal and increase in the foreign body response to electrodes (Groothuis et al., 2014). Indeed, device material and electrode-architecture influences the tissue reaction. Softer neural implants with shape and elasticity of dura mater increase electrode conductivity and improve the implant-tissue integration (Minev et al., 2015).

OPPORTUNITIES

Neural decoding models provide a promising research tool to derive data driven conclusions underlying complex speech representations, and for uncovering the link between inner speech representations and neural responses. Quantitative, model-based characterizations have showed that brain activity is tuned to various levels of speech representation.

The various types of language deficits exemplify the challenge in building a specific speech prosthesis that addresses individual needs. In this regard, the first step is to identify injured neural circuits and brain functions. Once damaged and healthy brain functions are identified, decoding models can be used for the design of effective speech prostheses. In particular, the feasibility to decode various speech representations during inner speech—i.e., acoustic features, phonetic representations, and individual words—suggests that various strategies and designs could be employed and combined for building a natural communication device depending on specific, residual speech functions. Every speech representation has pros and cons for targeting speech devices. For instance, decoding acoustic features opens the door to brain-based speech synthesis, in which audible speech is synthetized directly from decoded neural patterns. This approach has already been demonstrated, where predicted speech was synthesized, and acoustically fed back to the user (Guenther et al., 2009; Brumberg et al., 2010) from intracortical brain activity recorded from the motor cortex. Yet the understandability of the produced speech sounds and the best speech parameters to model remain to be demonstrated. Alternatively, decoding units of speech, such as phonemes or words provides greater naturalness, but the optimal speech unit size to be analyzed, is still a matter of debate—i.e., the longer the unit, the larger the database needed to cover the required domain, while smaller units offer more degrees of freedom, and can build a larger set of complex utterances, as shown in Herff et al. (2015) and Moses et al. (2016). A tradeoff is the decoding of a limited vocabulary of words (Martin et al., 2016), which carry specific semantic information, and would be relevant in a basic clinical setting ("hungry," "thirsty," "yes," "no," etc.).

An alternative to a speech-interface based solely on brain decoding is to build a system, which acquires sensor data from multiple elements of the human speech production system, and combine the different signals to optimize speech synthesis (see Brumberg et al., 2010, for a review). For instance, recording sensors allow characterizing the vocal tract by measuring its configuration directly or by sounding it acoustically using electromagnetic articulography, ultra-sound, or optical imaging of the tongue and lip. Alternatively, electrical measurements can infer articulation from actuator muscle signals [i.e., using surface electromyography (EMG)] or signals obtained directly from the brain (mainly EEG and ECoG). Using different sensors and different speech representations allow exploiting an individual's residual speech functions to operate the speech synthesis.

Unique opportunities for targeting communication assistive technologies are offered by combining different research fields. Neuroscience reveals which anatomical locations and brain signals should be modeled. Linguistic fields support development of decoding models that incorporate linguistic and contextual specifications—including segmental elements and supra-segmental elements. Combining insights from these research fields with machine learning and speech recognition algorithms is a key element to improve prediction accuracy. Finally, the success of speech neuroprostheses depends on the continuous technological improvements to enhance signal quality and resolution, and allow developing more portable and biocompatible invasive recording devices. Merging various fields together will allow tackling the challenges central to decoding inner speech.

CONCLUSION

To conclude, we described the potential of using decoding models to unravel neural mechanisms associated with complex speech functions. Speech representations during inner speech, such as acoustic features, phonetic features and individual words could be decoded from high frequency neural signals. Although, these results reveal a promising avenue for direct decoding of natural speech, they also emphasize that performance is currently insufficient to build a realistic brain-based device. Accordingly, we highlighted numerous challenges that likely precluded better performances, such as the low signal-to-noise-ratio, and the difficulty in monitoring precisely inner speech.

As such challenges are solved, decoding speech directly from neural activity opens the door to new communication interfaces that may allow for more natural speech-like communication in patients with severe communication deficits.

AUTHOR CONTRIBUTIONS

All authors listed have made a substantial, direct and intellectual contribution to the work, and approved it for publication.

FUNDING

This research was supported by NINDS Grant R3721135, DARPA D16PC00053.

ACKNOWLEDGMENTS

This article is adapted from the following doctorate thesis: Understanding and decoding imagined speech using intracranial recordings in the human brain (Martin, 2017).

REFERENCES

Aertsen, A. M. H. J., Olders, J. H. J., and Johannesma, P. I. M. (1981). Spectro-temporal receptive fields of auditory neurons in the grassfrog: III. analysis of the stimulus-event relation for natural stimuli. *Biol. Cybern.* 39, 195–209. doi: 10.1007/BF00342772

Ajiboye, A. B., Willett, F. R., Young, D. R., Memberg, W. D., Murphy, B. A., Miller, J. P., et al. (2017). Restoration of reaching and grasping movements through brain-controlled muscle stimulation in a person with tetraplegia: a proof-of-concept demonstration. *Lancet* 389, 1821–1830. doi: 10.1016/S0140-6736(17)30601-3

Aleman, A. (2004). The functional neuroanatomy of metrical stress evaluation of perceived and imagined spoken words. *Cereb. Cortex* 15, 221–228. doi: 10.1093/cercor/bhh124

Ashmore, R. C., Endler, B. M., Smalianchuk, I., Degenhart, A. D., Hatsopoulos, N. G., Tyler-Kabara, E. C., et al. (2012). Stable online control of an electrocorticographic brain-computer interface using a static decoder. *Conf. Proc. IEEE Eng. Med. Biol. Soc.* 2012, 1740–1744. doi: 10.1109/EMBC.2012.6346285

Aziz-Zadeh, L., Cattaneo, L., Rochat, M., and Rizzolatti, G. (2005). Covert speech arrest induced by rTMS over both motor and nonmotor left hemisphere frontal sites. *J. Cogn. Neurosci.* 17, 928–938. doi: 10.1162/0898929054021157

Blakely, T., Miller, K. J., Rao, R. P. N., Holmes, M. D., and Ojemann, J. G. (2008). Localization and classification of phonemes using high spatial resolution electrocorticography (ECoG) grids. *IEEE Eng. Med. Biol. Soc. Conf.* 2008, 4964–4967. doi: 10.1109/IEMBS.2008.4650328

Blakely, T., Miller, K. J., Zanos, S. P., Rao, R. P. N., and Ojemann, J. G. (2009). Robust, long-term control of an electrocorticographic brain-computer interface with fixed parameters. *Neurosurg. Focus* 27:E13. doi: 10.3171/2009.4.FOCUS0977

Bouchard, K. E., Mesgarani, N., Johnson, K., and Chang, E. F. (2013). Functional organization of human sensorimotor cortex for speech articulation. *Nature* 495, 327–332. doi: 10.1038/nature11911

Brumberg, J. S., Krusienski, D. J., Chakrabarti, S., Gunduz, A., Brunner, P., Ritaccio, A. L., et al. (2016). Spatio-temporal progression of cortical activity related to continuous overt and covert speech production in a reading task. *PLoS ONE* 11:e0166872. doi: 10.1371/journal.pone.0166872

Brumberg, J. S., Nieto-Castanon, A., Kennedy, P. R., and Guenther, F. H. (2010). Brain–computer interfaces for speech communication. *Speech Commun.* 52, 367–379. doi: 10.1016/j.specom.2010.01.001

Brumberg, J. S., Wright, E. J., Andreasen, D. S., Guenther, F. H., Kennedy, P. R. (2011). Classification of intended phoneme production from chronic intracortical microelectrode recordings in speech-motor cortex. *Front. Neurosci.* 5:65. doi: 10.3389/fnins.2011.00065

Buzsáki, G., Anastassiou, C. A., and Koch, C. (2012). The origin of extracellular fields and currents — EEG, ECoG, LFP and spikes. *Nat. Rev. Neurosci.* 13, 407–420. doi: 10.1038/nrn3241

Buzsáki, G., and Wang, X.-J. (2012). Mechanisms of gamma oscillations. *Annu. Rev. Neurosci.* 35, 203–225. doi: 10.1146/annurev-neuro-062111-150444

Callan, D. E., Tsytsarev, V., Hanakawa, T., Callan, A. M., Katsuhara, M., Fukuyama, H., et al. (2006). Song and speech: brain regions involved with perception and covert production. *Neuroimage* 31, 1327–1342. doi: 10.1016/j.neuroimage.2006.01.036

Chang, R. J. W., Johnson, K., Berger, M. S., Barbaro, N. M., and Knight, R. T. (2010). Categorical speech representation in human superior temporal gyrus. *Nat. Neurosci.* 13, 1428–1432. doi: 10.1038/nn.2641

Cheung, C., Hamiton, L. S., Johnson, K., and Chang, E. F. (2016). The auditory representation of speech sounds in human motor cortex. *eLife* 5:12577. doi: 10.7554/eLife.12577

Chi, T., Ru, P., and Shamma, S. A. (2005). Multiresolution spectrotemporal analysis of complex sounds. *J. Acoust. Soc. Am.* 118:887. doi: 10.1121/1.1945807

Clopton, B. M., and Backoff, P. M. (1991). Spectrotemporal receptive fields of neurons in cochlear nucleus of guinea pig. *Hear. Res.* 52, 329–344.

Conant, D. F., Bouchard, K. E., Leonard, M. K., and Chang, E. F. (2018). Human sensorimotor cortex control of directly measured vocal tract movements during vowel production. *J. Neurosci.* 38, 2955–2966. doi: 10.1523/JNEUROSCI.2382-17.2018

Corley, M., Brocklehurst, P. H., and Moat, H. S. (2011). Error biases in inner and overt speech: evidence from tongue twisters. *J. Exp. Psychol. Learn. Mem. Cogn.* 37, 162–175. doi: 10.1037/a0021321

Crowder, R. G. (1989). Imagery for musical timbre. *J. Exp. Psychol. Hum. Percept. Perform.* 15, 472–478. doi: 10.1037/0096-1523.15.3.472

Démonet, J.-F., Thierry, G., and Cardebat, D. (2005). Renewal of the neurophysiology of language: functional neuroimaging. *Physiol. Rev.* 85, 49–95. doi: 10.1152/physrev.00049.2003

Ding, N., and Simon, J. Z. (2012). Emergence of neural encoding of auditory objects while listening to competing speakers. *Proc. Natl. Acad. Sci. U.S.A.* 109, 11854–11859. doi: 10.1073/pnas.1205381109

Ellis, D. (2003). *Dynamic Time Warping (DTW) in Matlab*. Available online at: http://www.ee.columbia.edu/~dpwe/resources/matlab/dtw/ (Accessed November 21, 2014).

Farwell, L. A., and Donchin, E. (1988). Talking off the top of your head: toward a mental prosthesis utilizing event-related brain potentials. *Electroencephalogr. Clin. Neurophysiol.* 70, 510–523.

Fazel-Rezai, R., Allison, B. Z., Guger, C., Sellers, E. W., Kleih, S. C., and Kübler, A. (2012). P300 brain computer interface: current challenges and emerging trends. *Front. Neuroeng.* 5:14. doi: 10.3389/fneng.2012.00014

Felton, E. A., Wilson, J. A., Williams, J. C., and Garell, P. C. (2007). Electrocorticographically controlled brain-computer interfaces using motor and sensory imagery in patients with temporary subdural electrode implants. Report of four cases. *J. Neurosurg.* 106, 495–500. doi: 10.3171/jns.2007.106.3.495

Geva, S., Correia, M., and Warburton, E. A. (2011). Diffusion tensor imaging in the study of language and aphasia. *Aphasiology* 25, 543–558. doi: 10.1080/02687038.2010.534803

Gilja, V., Pandarinath, C., Blabe, C. H., Nuyujukian, P., Simeral, J. D., Sarma, A. A., et al. (2015). Clinical translation of a high-performance neural prosthesis. *Nat. Med.* 21, 1142–1145. doi: 10.1038/nm.3953

Giraud, A.-L., and Poeppel, D. (2012). Cortical oscillations and speech processing: emerging computational principles and operations. *Nat. Neurosci.* 15, 511–517. doi: 10.1038/nn.3063

Griffiths, T. D. (1999). Human complex sound analysis. *Clin. Sci. Lond. Engl.* 1979, 231–234.

Groothuis, J., Ramsey, N. F., Ramakers, G. M. J., and van der Plasse, G. (2014). Physiological challenges for intracortical electrodes. *Brain Stimulat.* 7, 1–6. doi: 10.1016/j.brs.2013.07.001

Guenther, F. H., Brumberg, J. S., Wright, E. J., Nieto-Castanon, A., Tourville, J. A., Panko, M., et al. (2009). A wireless brain-machine interface for real-time speech synthesis. *PLoS ONE* 4:e8218. doi: 10.1371/journal.pone.0008218

Halpern, A. R., and Zatorre, R. J. (1999). When that tune runs through your head: a PET investigation of auditory imagery for familiar melodies. *Cereb. Cortex* 9, 697–704. doi: 10.1093/cercor/9.7.697

Halpern, A. R., Zatorre, R. J., Bouffard, M., and Johnson, J. A. (2004). Behavioral and neural correlates of perceived and imagined musical timbre. *Neuropsychologia* 42, 1281–1292. doi: 10.1016/j.neuropsychologia.2003.12.017

Herff, C., Heger, D., de Pesters, A., Telaar, D., Brunner, P., Schalk, G., et al. (2015). Brain-to-text: decoding spoken phrases from phone representations in the brain. *Front. Neurosci.* 9:217. doi: 10.3389/fnins.2015.00217

Herholz, S. C., Lappe, C., Knief, A., and Pantev, C. (2008). Neural basis of music imagery and the effect of musical expertise. *Eur. J. Neurosci.* 28, 2352–2360. doi: 10.1111/j.1460-9568.2008.06515.x

Hermes, D., Miller, K. J., Vansteensel, M. J., Edwards, E., Ferrier, C. H., Bleichner, M. G., et al. (2014). Cortical theta wanes for language. *Neuroimage* 85, 738–748. doi: 10.1016/j.neuroimage.2013.07.029

Hickok, G., and Poeppel, D. (2007). The cortical organization of speech processing. *Nat. Rev. Neurosci.* 8, 393–402. doi: 10.1038/nrn2113

Hinke, R. M., Hu, X., Stillman, A. E., Kim, S. G., Merkle, H., Salmi, R., et al. (1993). Functional magnetic resonance imaging of Broca's area during internal speech. *Neuroreport* 4, 675–678.

Holdgraf, C. R., de Heer, W., Pasley, B., Rieger, J., Crone, N., Lin, J. J., et al. (2016). Rapid tuning shifts in human auditory cortex enhance speech intelligibility. *Nat. Commun.* 7:13654. doi: 10.1038/ncomms13654

Holdgraf, C. R., Rieger, J. W., Micheli, C., Martin, S., Knight, R. T., and Theunissen, F. E. (2017). Encoding and decoding models in cognitive electrophysiology. *Front. Syst. Neurosci.* 11:61. doi: 10.3389/fnsys.2017.00061

Hubbard, T. L. (2010). Auditory imagery: Empirical findings. *Psychol. Bull.* 136, 302–329. doi: 10.1037/a0018436

Ikeda, S., Shibata, T., Nakano, N., Okada, R., Tsuyuguchi, N., Ikeda, K., et al. (2014). Neural decoding of single vowels during covert articulation using electrocorticography. *Front. Hum. Neurosci.* 8:125. doi: 10.3389/fnhum.2014.00125

Janata, P., and Paroo, K. (2006). Acuity of auditory images in pitch and time. *Percept. Psychophys.* 68, 829–844. doi: 10.3758/BF03193705

Jarosiewicz, B., Sarma, A. A., Bacher, D., Masse, N. Y., Simeral, J. D., Sorice, B., et al. (2015). Virtual typing by people with tetraplegia using a self-calibrating intracortical brain-computer interface. *Sci. Transl. Med.* 7:313ra179. doi: 10.1126/scitranslmed.aac7328

Kapeller, C., Kamada, K., Ogawa, H., Prueckl, R., Scharinger, J., and Guger, C. (2014). An electrocorticographic BCI using code-based VEP for control in video applications: a single-subject study. *Front. Syst. Neurosci.* 8:139. doi: 10.3389/fnsys.2014.00139

Kay, K. N., and Gallant, J. L. (2009). I can see what you see. *Nat. Neurosci.* 12:245. doi: 10.1038/nn0309-245

Kay, K. N., Naselaris, T., Prenger, R. J., and Gallant, J. L. (2008). Identifying natural images from human brain activity. *Nature* 452, 352–355. doi: 10.1038/nature06713

Kellis, S., Miller, K., Thomson, K., Brown, R., House, P., and Greger, B. (2010). Decoding spoken words using local field potentials recorded from the cortical surface. *J. Neural Eng.* 7:056007. doi: 10.1088/1741-2560/7/5/056007

Khodagholy, D., Gelinas, J. N., Thesen, T., Doyle, W., Devinsky, O., Malliaras, G. G., et al. (2014). NeuroGrid: recording action potentials from the surface of the brain. *Nat. Neurosci.* 18, 310–315. doi: 10.1038/nn.3905

Kraemer, D. J. M., Macrae, C. N., Green, A. E., and Kelley, W. M. (2005). Musical imagery: Sound of silence activates auditory cortex. *Nature* 434:158. doi: 10.1038/434158a

Kubanek, J., Brunner, P., Gunduz, A., Poeppel, D., and Schalk, G. (2013). The tracking of speech envelope in the human cortex. *PLoS ONE* 8:e53398. doi: 10.1371/journal.pone.0053398

Lachaux, J.-P., Axmacher, N., Mormann, F., Halgren, E., and Crone, N. E. (2012). High-frequency neural activity and human cognition: past, present and possible future of intracranial EEG research. *Prog. Neurobiol.* 98, 279–301. doi: 10.1016/j.pneurobio.2012.06.008

Leonard, M. K., Baud, M. O., Sjerps, M. J., and Chang, E. F. (2016). Perceptual restoration of masked speech in human cortex. *Nat. Commun.* 7:13619. doi: 10.1038/ncomms13619

Luo, H., and Poeppel, D. (2007). Phase patterns of neuronal responses reliably discriminate speech in human auditory cortex. *Neuron* 54, 1001–1010. doi: 10.1016/j.neuron.2007.06.004

Leuthardt, E. C., Miller, K. J., Schalk, G., Rao, R. P. N., and Ojemann, J. G. (2006). Electrocorticography-based brain computer interface–the Seattle experience. *IEEE Eng. Med. Biol. Soc.* 14, 194–198. doi: 10.1109/TNSRE.2006.875536

Leuthardt, E. C., Pei, X.-M., Breshears, J., Gaona, C., Sharma, M., Freudenberg, Z., et al. (2012). Temporal evolution of gamma activity in human cortex during an overt and covert word repetition task. *Front. Hum. Neurosci.* 6:99. doi: 10.3389/fnhum.2012.00099

Leuthardt, S. G., Wolpaw, J. R., Ojemann, J. G., and Moran, D. W. (2004). A brain–computer interface using electrocorticographic signals in humans. *J. Neural Eng.* 1, 63–71. doi: 10.1088/1741-2560/1/2/001

Lewis, P. M., Ackland, H. M., Lowery, A. J., and Rosenfeld, J. V. (2015). Restoration of vision in blind individuals using bionic devices: a review with a focus on cortical visual prostheses. *Brain Res.* 1595, 51–73. doi: 10.1016/j.brainres.2014.11.020

Manning, J. R., Jacobs, J., Fried, I., and Kahana, M. J. (2009). Broadband shifts in local field potential power spectra are correlated with single-neuron spiking in humans. *J. Neurosci.* 29, 13613–13620. doi: 10.1523/JNEUROSCI.2041-09.2009

Marshall, L., Helgadóttir, H., Mölle, M., and Born, J. (2006). Boosting slow oscillations during sleep potentiates memory. *Nature* 444, 610–613. doi: 10.1038/nature05278

Martin, S. (2017). *Understanding and Decoding Imagined Speech using Electrocorticographic Recordings in Humans.* Ecole Polytechnique Fédérale de Lausanne.

Martin, S., Brunner, P., Holdgraf, C., Heinze, H.-J., Crone, N. E., Rieger, J., et al. (2014). Decoding spectrotemporal features of overt and covert speech from the human cortex. *Front. Neuroengineering* 7:14. doi: 10.3389/fneng.2014.00014

Martin, S., Brunner, P., Iturrate, I., del Millán, J. R., Schalk, G., Knight, R. T., et al. (2016). Word pair classification during imagined speech using direct brain recordings. *Sci. Rep.* 6:25803. doi: 10.1038/srep25803

Martin, S., Mikutta, C., Leonard, M. K., Hungate, D., Koelsch, S., Shamma, S., et al. (2017). Neural encoding of auditory features during music perception and imagery. *Cereb. Cortex* 27, 1–12. doi: 10.1093/cercor/bhx277

McGuire, P. K., Silbersweig, D. A., Murray, R. M., David, A. S., Frackowiak, R. S., and Frith, C. D. (1996). Functional anatomy of inner speech and auditory verbal imagery. *Psychol. Med.* 26, 29–38.

Mesgarani, N., Cheung, C., Johnson, K., and Chang, E. F. (2014). Phonetic feature encoding in human superior temporal gyrus. *Science* 343, 1006–1010. doi: 10.1126/science.1245994

Millán, G. F., Vanhooydonck, D., Lew, E., Philips, J., and Nuttin, M. (2009). Asynchronous non-invasive brain-actuated control of an intelligent wheelchair. *IEEE Eng. Med. Biol. Soc. Conf.* 2009, 3361–3364. doi: 10.1109/IEMBS.2009.5332828

Miller, K. J., Leuthardt, E. C., Schalk, G., Rao, R. P. N., Anderson, N. R., Moran, D. W., et al. (2007). Spectral changes in cortical surface potentials during motor movement. *J. Neurosci.* 27, 2424–2432. doi: 10.1523/JNEUROSCI.3886-06.2007

Minev, I. R., Musienko, P., Hirsch, A., Barraud, Q., Wenger, N., Moraud, E. M., et al. (2015). Electronic dura mater for long-term multimodal neural interfaces. *Science* 347, 159–163. doi: 10.1126/science.1260318

Moses, D. A., Leonard, M. K., and Chang, E. F. (2018). Real-time classification of auditory sentences using evoked cortical activity in humans. *J. Neural Eng.* 15:036005. doi: 10.1088/1741-2552/aaab6f

Moses, D. A., Mesgarani, N., Leonard, M. K., and Chang, E. F. (2016). Neural speech recognition: continuous phoneme decoding using spatiotemporal representations of human cortical activity. *J. Neural Eng.* 13:056004. doi: 10.1088/1741-2560/13/5/056004

Naselaris, T., Kay, K. N., Nishimoto, S., and Gallant, J. L. (2011). Encoding and decoding in fMRI. *NeuroImage* 56, 400–410. doi: 10.1016/j.neuroimage.2010.07.073

Nijboer, F., Sellers, E. W., Mellinger, J., Jordan, M. A., Matuz, T., Furdea, A., et al. (2008). A P300-based brain-computer interface for people

with amyotrophic lateral sclerosis. *Clin. Neurophysiol.* 119, 1909–1916. doi: 10.1016/j.clinph.2008.03.034

Palmer, E. D., Rosen, H. J., Ojemann, J. G., Buckner, R. L., Kelley, W. M., and Petersen, S. E. (2001). An event-related fMRI study of overt and covert word stem completion. *Neuroimage* 14, 182–193. doi: 10.1006/nimg.2001.0779

Pandarinath, C., Nuyujukian, P., Blabe, C. H., Sorice, B. L., Saab, J., Willett, F. R., et al. (2017). High performance communication by people with paralysis using an intracortical brain-computer interface. *eLife* 6:e18554. doi: 10.7554/eLife.18554

Pantev, C., Oostenveld, R., Engelien, A., Ross, B., Roberts, L. E., and Hoke, M. (1998). Increased auditory cortical representation in musicians. *Nature* 392, 811–814. doi: 10.1038/33918

Pasley, B., Crone, N., Knight, R., and Chang, E. (2011). Phonetic encoding by intracranial signals in human auditory cortex. *Front. Hum. Neurosci.* 5:287. doi: 10.3389/conf.fnhum.2011.207.00287

Pasley, B. N., David, S. V., Mesgarani, N., Flinker, A., Shamma, S. A., Crone, N. E., et al. (2012). Reconstructing speech from human auditory cortex. *PLoS Biol.* 10:e1001251. doi: 10.1371/journal.pbio.1001251

Pasley, B. N., and Knight, R. T. (2013). "Decoding speech for understanding and treating aphasia," in *Progress in Brain Research* (Elsevier), 435–456. Available online at: http://linkinghub.elsevier.com/retrieve/pii/B9780444633279000187 (Accessed May 3, 2015).

Pei, B. D. L., Leuthardt, E. C., and Schalk, G. (2011a). Decoding vowels and consonants in spoken and imagined words using electrocorticographic signals in humans. *J. Neural Eng.* doi: 10.1088/1741-2560/8/4/046028

Pei, X., Leuthardt, E. C., Gaona, C. M., Brunner, P., Wolpaw, J. R., and Schalk, G. (2011b). Spatiotemporal dynamics of electrocorticographic high gamma activity during overt and covert word repetition. *Neuroimage* 54, 2960–2972. doi: 10.1016/j.neuroimage.2010.10.029

Perrone-Bertolotti, M., Rapin, L., Lachaux, J.-P., Baciu, M., and Lœvenbruck, H. (2014). What is that little voice inside my head? Inner speech phenomenology, its role in cognitive performance, and its relation to self-monitoring. *Behav. Brain Res.* 261, 220–239. doi: 10.1016/j.bbr.2013.12.034

Price, C. J., (2000). The anatomy of language: contributions from functional neuroimaging. *J. Anat.* 197, 335–359. doi: 10.1046/j.1469-7580.2000.19730335.x

Pulvermuller, F., Huss, M., Kherif, F., Moscoso del Prado Martin, F., Hauk, O., and Shtyrov, Y. (2006). Motor cortex maps articulatory features of speech sounds. *Proc. Natl. Acad. Sci. U.S.A.* 103, 7865–7870. doi: 10.1073/pnas.0509989103

Rauschecker, J. P. (2001). Cortical plasticity and music. *Ann. N. Y. Acad. Sci.* 930, 330–336. doi: 10.1111/j.1749-6632.2001.tb05742.x

Rich, E. L., and Wallis, J. D. (2017). Spatiotemporal dynamics of information encoding revealed in orbitofrontal high-gamma. *Nat. Commun.* 8:1139. doi: 10.1038/s41467-017-01253-5

Riès, S. K., Karzmark, C. R., Navarrete, E., Knight, R. T., and Dronkers, N. F. (2015). Specifying the role of the left prefrontal cortex in word selection. *Brain Lang.* 149, 135–147. doi: 10.1016/j.bandl.2015.07.007

Ritaccio, A., Matsumoto, R., Morrell, M., Kamada, K., Koubeissi, M., Poeppel, D., et al. (2015). Proceedings of the seventh international workshop on advances in electrocorticography. *Epilepsy Behav.* 51, 312–320. doi: 10.1016/j.yebeh.2015.08.002

Rosen, H. J., Ojemann, J. G., Ollinger, J. M., and Petersen, S. E. (2000). Comparison of brain activation during word retrieval done silently and aloud using fMRI. *Brain Cogn.* 42, 201–217. doi: 10.1006/brcg.1999.1100

Rouse, A. G., Williams, J. J., Wheeler, J. J., and Moran, D. W. (2013). Cortical adaptation to a chronic micro-electrocorticographic brain computer interface. *J. Neurosci.* 33, 1326–1330. doi: 10.1523/JNEUROSCI.0271-12.2013

Schalk, G., Kubánek, J., Miller, K. J., Anderson, N. R., Leuthardt, E. C., Ojemann, J. G., et al. (2007). Decoding two-dimensional movement trajectories using electrocorticographic signals in humans. *J. Neural Eng.* 4, 264–275. doi: 10.1088/1741-2560/4/3/012

Schön, D., Gordon, R., Campagne, A., Magne, C., Astésano, C., Anton, J.-L., et al. (2010). Similar cerebral networks in language, music and song perception. *Neuroimage* 51, 450–461. doi: 10.1016/j.neuroimage.2010.02.023

Slutzky, M. W., Jordan, L. R., Krieg, T., Chen, M., Mogul, D. J., and Miller, L. E. (2010). Optimal spacing of surface electrode arrays for brain–machine interface applications. *J. Neural Eng.* 7:026004. doi: 10.1088/1741-2560/7/2/026004

Srinivasan, R., Bibi, F. A., and Nunez, P. L. (2006). Steady-state visual evoked potentials: distributed local sources and wave-like dynamics are sensitive to flicker frequency. *Brain Topogr.* 18, 167–187. doi: 10.1007/s10548-006-0267-4

Tankus, A., Fried, I., and Shoham, S. (2012). Structured neuronal encoding and decoding of human speech features. *Nat. Commun.* 3:1015. doi: 10.1038/ncomms1995

Theunissen, F. E., Sen, K., and Doupe, A. J. (2000). Spectral-temporal receptive fields of nonlinear auditory neurons obtained using natural sounds. *J. Neurosci.* 20, 2315–2331. doi: 10.1523/JNEUROSCI.20-06-02315.2000

Vansteensel, M. J., Pels, E. G. M., Bleichner, M. G., Branco, M. P., Denison, T., Freudenburg, Z. V., et al. (2016). Fully implanted brain–computer interface in a locked-in patient with ALS. *N. Engl. J. Med.* 375, 2060–2066. doi: 10.1056/NEJMoa1608085

Wang, W., Collinger, J. L., Degenhart, A. D., Tyler-Kabara, E. C., Schwartz, A. B., Moran, D. W., et al. (2013). An electrocorticographic brain interface in an individual with tetraplegia. *PLoS ONE* 8:e55344. doi: 10.1371/journal.pone.0055344

Whittingstall, K., and Logothetis, N. K. (2009). Frequency-band coupling in surface EEG reflects spiking activity in monkey visual cortex. *Neuron* 64, 281–289. doi: 10.1016/j.neuron.2009.08.016

Wodlinger, B., Degenhart, A. D., Collinger, J. L., Tyler-Kabara, E. C., and Wei, W. (2011). The impact of electrode characteristics on electrocorticography (ECoG). *Conf Proc IEEE Eng Med Biol Soc*. 2011, 3083–3086. doi: 10.1109/IEMBS.2011.6090842

Wolpaw, J. R., McFarland, D. J., Neat, G. W., and Forneris, C. A. (1991). An EEG-based brain-computer interface for cursor control. *Electroencephalogr. Clin. Neurophysiol.* 78, 252–259.

Yetkin, F. Z., Hammeke, T. A., Swanson, S. J., Morris, G. L., Mueller, W. M., McAuliffe, T. L., et al. (1995). A comparison of functional MR activation patterns during silent and audible language tasks. *AJNR Am. J. Neuroradiol.* 16, 1087–1092.

Zatorre, R. J., Halpern, A. R., Perry, D. W., Meyer, E., and Evans, A. C. (1996). Hearing in the mind's ear: a PET investigation of musical imagery and perception. *J. Cogn. Neurosci.* 8, 29–46. doi: 10.1162/jocn.1996.8.1.29

Zion Golumbic, E. M., Ding, N., Bickel, S., Lakatos, P., Schevon, C. A., McKhann, G. M., et al. (2013). Mechanisms underlying selective neuronal tracking of attended speech at a "cocktail party." *Neuron* 77, 980–991. doi: 10.1016/j.neuron.2012.12.037

Conflict of Interest Statement: The authors declare that the research was conducted in the absence of any commercial or financial relationships that could be construed as a potential conflict of interest.

Copyright © 2018 Martin, Iturrate, Millán, Knight and Pasley. This is an open-access article distributed under the terms of the Creative Commons Attribution License (CC BY). The use, distribution or reproduction in other forums is permitted, provided the original author(s) and the copyright owner are credited and that the original publication in this journal is cited, in accordance with accepted academic practice. No use, distribution or reproduction is permitted which does not comply with these terms.

frontiers in Neuroscience

ORIGINAL RESEARCH
published: 28 June 2018
doi: 10.3389/fnins.2018.00438

Evaluation of Switch and Continuous Navigation Paradigms to Command a Brain-Controlled Wheelchair

*Álvaro Fernández-Rodríguez[1], Francisco Velasco-Álvarez[1], Manon Bonnet-Save[2] and Ricardo Ron-Angevin[1]**

[1] Departmento de Tecnología Electrónica, Universidad de Málaga, Malaga, Spain, [2] IMS UMR Centre National de la Recherche Scientifique 5218, Cognitique et Ingénierie Humaine, Bordeaux INP-ENSC, Bordeaux, France

A brain-computer interface (BCI) is a technology allowing patients with severe motor dysfunctions to use their electroencephalographic signals to create a communication channel to control devices. The objective of this paper is to study the feasibility of continuous and switch control modes for a brain-controlled wheelchair (BCW) using sensorimotor rhythms (SMR) modulated through a right-hand motor imagery task. Previous studies, which used a continuous navigation control with SMR, have reported the difficulty of maintaining the motor imagery task for a long time, especially for the forward command. The switch control has been presented as a proposal that may help to solve this issue since this task is only used temporary for either disabling or enabling the movement. Regarding the methodology, 10 of 15 able-bodied users, who had overcome the criterion of 30% error rate in the calibration phase, controlled the BCW using both paradigms. The navigation tasks consisted of a straight path divided in five sections: in three of them the users had to move forward, and in the other two the users had to maintain their position. To assess user performance in the device management, a usability approach was adopted, measuring the factors of effectiveness, efficiency, and satisfaction. Then, variables related to the time employed and commands selected by the user or parameters related to the confusion matrix were applied. In addition, the scores in NASA-TLX and two *ad hoc* questionnaires were considered to discuss the user experience controlling the wheelchair. Despite the results showed that the best system for a specific user relies on his/her abilities and preferences, the switch control mode obtained better accuracy (0.59 ± 0.17 for continuous and 0.72 ± 0.05 for switch). Furthermore, the switch paradigm can be recommended for the advance sections as with it users could complete the advance sections in less time (42.2 ± 28.7 s for continuous and 15.47 ± 3.43 s for switch), while the continuous mode seems to be better at keeping the wheelchair stopped (42.45 ± 16.01 s for continuous and 24.35 ± 10.94 s for switch).

Keywords: brain-computer interface (BCI), wheelchair, navigation control, switch, continuous, usability

OPEN ACCESS

Edited by:
Christoph Guger,
Guger Technologies (Austria), Austria

Reviewed by:
Hasan Ayaz,
Drexel University, United States
Rifai Chai,
University of Technology Sydney, Australia

***Correspondence:**
Ricardo Ron-Angevin
rron@uma.es

Specialty section:
This article was submitted to Neural Technology, a section of the journal Frontiers in Neuroscience

Received: *02 November 2017*
Accepted: *11 June 2018*
Published: *28 June 2018*

Citation:
Fernández-Rodríguez Á, Velasco-Álvarez F, Bonnet-Save M and Ron-Angevin R (2018) Evaluation of Switch and Continuous Navigation Paradigms to Command a Brain-Controlled Wheelchair. Front. Neurosci. 12:438. doi: 10.3389/fnins.2018.00438

INTRODUCTION

Diseases such as amyotrophic lateral sclerosis (ALS) or brainstem lesions may result in a deterioration of the motor functions of affected patients, who could need to use assistive technology to facilitate tasks in their daily lives. However, some patients could not be benefitted from conventional systems, such as joystick or eye-tracker systems, due to the severe reduction of their motor functions. Therefore, the solution could be systems that do not require the motor capacity of the users to control them. Brain-computer interface (BCI) fullfils this requirement since it is a technology that allows the use of electroencephalographic (EEG) signals to create a communication channel between users and the device that they want to control. These systems have been implemented in devices such as a speller matrix (Farwell and Donchin, 1988), a home automation system (Corralejo et al., 2011) or a wheelchair (Millán et al., 2009). The study of the control of a wheelchair through EEG, i.e., a brain-controlled wheelchair (BCW) is the objective of the present work. Since the first BCW-related publication in 2005 by Tanaka et al. (2005), numerous proposals can be classified considering different aspects of the system. The main taxonomies divide these wheelchairs depending on the EEG signals registered or the navigation system implemented (Fernández-Rodríguez et al., 2016).

Firstly, the EEG signal most used for the control of a BCW in real environments has been the sensorimotor rhythms (SMRs) (e.g., Millán et al., 2009). This endogenous signal is based on the event-related (de)synchronization (ERD/ERS) phenomenon: mu (7–13 Hz) and beta (13–35 Hz) bands amplitude variations in the sensorimotor cortex area while performing a motor imagery (MI) task. Therefore, the SMR can be freely modulated by users and applied as a control command in a BCW without needing external visual, tactile or auditory stimuli (Pfurtscheller et al., 2006). As a result, a SMR-based BCW could allow sensorial channels to be dedicated to the maintenance of attention to the environment, an important factor when controlling a wheelchair. This is an advantage vs. other BCW based on an exogenous signal, such as the P300 (e.g., Iturrate et al., 2009 or Zhang et al., 2016) or steady-state evoked potentials (e.g., Ng et al., 2015 or Kim and Lee, 2017, who used visual and somatosensory signal, respectively), which usually require a graphic user interface (GUI) for its control.

Secondly, the main taxonomy of navigation systems distinguishes low and high level categories. On the one hand, in low-level navigation systems, wheelchair control is achieved through simple navigation commands such as "move forward" or "turn right." In this way, users can have a fine control and perform any path they want. On the other hand, high-level navigation lets users have a rough control of the BCW, selecting destination commands such as "take me to the kitchen" or "leave this room." Although the high-level navigation might induce a smaller workload, since the user simply selects the destinations, the present study is framed within the low-level systems because they could be more appropriate for uncontrolled environments. In particular, low-level navigation should allow the desired flexibility to avoid obstacles or adapt the trajectory of the wheelchair if new modifications occur in the environment. This navigation could help to maintain an adequate engagement and improve the user's experience, since he/she has a main role controlling the wheelchair and a strongest feeling of autonomy. Likewise, there are two main types of low-level systems for controlling a BCW: discrete and continuous control. In discrete control, the selection of a navigation command implies a prefixed action, e.g., a turn of 45° or a fixed advance distance of 1 m (e.g., Tsui et al., 2011 and Ron-Angevin et al., 2017). Otherwise, in the continuous control the user can control the extension of the movement after the selection of a navigation command, e.g., the turn amplitude or the advance distance (e.g., Millán et al., 2009 and Li J. et al., 2013). Usually, in this last control the movement continues as long as the user keeps the command active.

Another paradigm was proposed by Mason and Birch (2000), Müller-Putz et al. (2010), and Solis-Escalante et al. (2010): the brain switch. Usually, the aim of this paradigm applied in asynchronous BCWs has been to offer an on/off device control (Xu et al., 2012; Cao et al., 2014). However, the brain switch concept can be also applied directly on the control commands of a BCW. That is, not only to turn on/off the system but, for example, to activate/deactivate the wheelchair's forward command. Following this idea, a hybrid exogenous (SSVEP and P300) based BCW using a similar interpretation to the brain switch control applied in the control command was presented by Li Y. et al (2013).

Nevertheless, the application of the brain switch paradigm in the control commands of a MI based BCW could offer a remarkable improvement. Thanks to the brain switch the user could be able to maintain a state, e.g., the advance command, without using the MI task for a long time. The switch paradigm has been previously used in a MI based virtual wheelchair by Velasco-Álvarez et al. (2010) and Huang et al. (2012). Besides the paper of Velasco-Álvarez et al. (2010) the BCI group of the University of Malaga (UMA-BCI) has applied this paradigm on the management of a real mobile robot using SMR (Ron-Angevin et al., 2015).

The switch paradigm adapted by the UMA-BCI group to control a BCW is used for the selection of the forward navigation command without needing to maintain the MI task during the displacement. Specifically, if the user wants to select a forward (when he/she has stopped) or stop (when he/she is moving) command, he/she has to perform the MI task. Otherwise, in order to keep the current state of the wheelchair (i.e., to continue the advance or the stop), the user has to carry out an alternative task (e.g., arithmetic operation). Therefore, the main point of the switch handling is that the MI task is only used to change the movement state of the wheelchair, not to maintain it. Moreover, this management allows the user, as in continuous mode, to control the exact distance of displacement. In continuous mode, the user must maintain the desired task stably: on the one hand, a task to select an active command (i.e., move forward) and, on the other hand, a task to remain immobile. However, in switch mode, participants must have the ability to perform one task quickly (related to changing the present state of the wheelchair), but should have a stable control of the other (related to maintaining the present state of the wheelchair). Although in the present

work only one active command (besides the stop command) is used, the forward command, the obtained conclusions could be transferred to other paradigms with a larger number of commands. In addition, the simplicity of the design allows to isolate the object of study (i.e., the advance command in two control modes) and to establish a more reliable comparison. The detailed functioning of these paradigms will be presented in section Navigation Application.

Continuous concentration on a mental task for controlling BCI devices could be a tiring task that not all users can manage. This could be a considerable problem during the control of continuous navigation, for which at least two tasks must be stably controlled. Therefore, either because of the user's skills or the complexity of the task, sometimes it is difficult to find two tasks in which the user can maintain an acceptable performance over a long period of time. The switch mode could be a solution in which only one of these tasks should be maintained in a prolonged way: the task for keeping the current state. Due to the previously exposed, the switch navigation might improve the time needed to complete a path and the effort that the user has to employ carrying out the task.

In short, the brain switch paradigm could be a suitable option for controlling a real MI based BCW, especially for the forward command. Therefore, the present work will be focused on testing this hypothesis by comparing two navigation methods for a real wheelchair control: continuous and switch paradigms.

The approach used to study these paradigms will be based on the definition of usability given by the International Organization for Standardization (1998). According to them, this construct is divided into three factors: effectiveness, efficiency and satisfaction. For effectiveness, the user performance in controlling the BCW will be studied. The efficiency factor will take into account the resources used and costs to achieve the yield obtained. Finally, satisfaction will focus on measuring the user experience regarding comfort and subjective opinions about how they experienced controlling the wheelchair.

METHODS

Participants

Fifteen able-bodied participants took part in the study (mean age 23 ± 3.44 years; 7 men, 8 women), identified as P1–P15 here. Most of them were students from the University of Malaga and only P4 had previous experience in BCI systems, but none in a BCW control. They were mainly recruited through the use of social networks and word of mouth, having been offered an economic reward for their participation. The study was approved by the Experimental Ethics Committee of the University of Malaga and met the ethical standards of the Helsinki Declaration. Participants stated that they had no medical history of neurological or psychiatric disorders in the written informed consent, nor did they take any medication regularly. All these subjects participated in an initial calibration task consisting in a first test examining the ability of subjects to control their SMR signal (see section Calibration Task). This study needed users to have acceptable control of their SMRs, which would enable them to control the BCW in the navigation task (see section Navigation Task With the Brain-Controlled Wheelchair). For this reason, as a design criterion in the calibration task, a conventional limit of 30% in the classification error rate was considered to be the maximum that could allow efficient control of the paradigm; the same limit was used in Kübler et al. (2001) for efficient communication using a two-class BCI for spelling. In a similar way, this study needed users to have acceptable control of their SMRs, which would enable them to control the BCW in the navigation task (see section Navigation Task With the Brain-Controlled Wheelchair). In the case of a classification error rate over 30%, participants were rewarded (5 €) and the experiment ended; otherwise, they continued to the real BCW control (10 €, regardless of their performance controlling the wheelchair).

Data Acquisition and Signal Processing

EEG signals were recorded at a 200 Hz sampling rate using the following electrode positions: F3, F4, C3, C4, P3, P4, T7, T8, and Cz according to the 10/20 international system. Ground and reference were placed at AFz and Fz positions respectively. Signals were amplified by an actiCHamp amplifier (Brain Products GmbH, Munich, Germany). These electrode positions were combined to generate two large Laplacian channels (for extended details see McFarland et al., 1997) over C4 and C3 which correspond to the right and left sensorimotor areas, respectively. Neither online nor offline artifact detection techniques were employed.

As mentioned above, users participated in an initial training session for calibration purposes. This exercise consisted in performing two mental tasks (80 trials for each task) during which the EEG signals of the users were recorded. These data were used to obtain a reactive frequency band and the classification error rate for each subject (detailed below) by an automatic process. The selected subjects were those with a classification error rate under 30% and their calibration parameters were obtained to be used during the control navigation task. Data processing and feedback generation in the navigation exercise were based on the procedure detailed in Ron-Angevin and Díaz-Estrella (2009):

a. Although in some cases it is possible to find subjects whose reactive band belongs to the β band, the search for the optimal frequency band was limited to the μ band for simplicity. The reactive frequency band of each participant was automatically selected from all possible frequency intervals between 5 and 17 Hz (with a minimum bandwidth of 2 Hz). For each tested frequency interval, feature extraction, and classification were carried out, giving a frequency band-dependent error rate as a result. The band that led to the lowest classification error rate was regarded as the subject's reactive frequency band.
b. Feature extraction: the average power of the signal from the two EEG channels (right and left sensorimotor areas) was estimated in the specific frequency interval for each trial. This average was calculated by (i) digitally band-pass filtering the EEG using a fifth-order Butterworth filter, (ii) squaring each sample, and (iii) averaging over several consecutive past

samples. A total of 100 samples were averaged, giving an estimation of the band power for intervals of 500 ms.

c. Classification: the error rate time course of a linear discriminant analysis (LDA) classifier (Lange et al., 1997) was computed using features from both channels by means of a ten-times ten-fold cross-validation scheme. In this way, the estimated minimum error rate of the classifier from the given frequency band was obtained.
d. Feedback generation: the previously selected frequency band and the obtained parameters were used to set up LDA whose classification results determined the feedback "L," which was used in the next sessions. This feedback was computed online every 31.25 ms. All data processing was carried out in MATLAB.

Navigation Application

In the present work two control paradigms have been studied: continuous and switch mode. However, the criterion to detect the mental tasks remained similar. Two mental tasks were used: an active task which was a right-hand motor MI, and an alternative task used as a distractor to prevent thinking about the right hand task (detailed in section Calibration Task). Performing the MI task was used to control the extension of a bar—called "L," not visible to the user since the interface was only acoustic—as a result of the LDA classification. Specifically, if the classifier determined that the task performed was right-hand MI, the bar was extended; in other cases, its length remained at its minimum size. When the bar exceeded a selection threshold during a time larger than a "selection time" (around 1 s), a command selection was executed (the selected command depended on the paradigm handled). Besides, if the bar length was lower than the selection threshold for a period less than a "reset time," the accumulated "selection time" was not reset, but otherwise it was set to zero. Both control modes started in a rest state (not possible to manage the BCW) from which the users have to activate the availability of the two control commands to begin the movement with the wheelchair. To change from the rest state to the control state, after hearing the word "wait" in Spanish, the MI task needed to be executed. As the user executed this, the word "advance" was played to indicate the availability of the forward command and the possibility to start to move. At this point, the control mode used conditioned the next event.

In the continuous mode, the MI task was destined only to move the BCW, i.e., when the user performed this task, it extended the abovementioned bar ("L") and the device advanced continuously as long as the bar was over the selection time and threshold. Otherwise, to select the stop command, the user must perform the alternative task.

Regarding the switch mode, its control was similar to that employed for a light switch. If the user wanted to start an advance or to stop the wheelchair, i.e., to change the state of the wheelchair, he/she had to perform the MI task. On the contrary, if the user wanted to maintain the forward or stop command, he/she had to perform the alternative task.

An illustrative example of the movement of the bar and command selections is shown in **Figure 1**.

Robotic Wheelchair

The BCW used consisted of a customized Invacare Mistral3 electric wheelchair (**Figure 2**) equipped with a custom-built control board emulating its analog two-axis joystick in real time and receiving multiple sensor information through an I2C bus. This board was connected through a USB port to a control application written in C that ran on an external laptop. This application received, via a TCP connection, the commands (e.g., move forward) issued by the navigation application running in a MATLAB session, and then transformed them in real time into low-level commands that were fed back to the control board. Two AS5048 magnetic rotary encoders were attached to the wheelchair's driving wheels in order to carry out the odometry and thus compute the wheelchair's heading at every moment. This information was used by the application control to correct small drifts both online and just after having performed a displacement. The BCW took around 5–6 s to make a 1-meter advance.

Procedure

The study consisted in two sessions per participant (**Figure 3**) carried out in 1 day with a total duration of approximately 2 h: (i) a calibration session to know the initial skill of users to control their SMR and to obtain their parameters, and (ii) a navigation session with the BCW to assess the feasibility of the paradigms through their execution and three questionnaires (presented below). Both the calibration and the navigation were performed in a quiet and spacious room of the Higher Technical School of Telecommunication Engineering of the University of Malaga. Prior to their session, users were informed via email about the task and the proceedings of the experiment. However, the relevant details were re-explained at the beginning of the session before signing the consent. All this preparation process, including the EEG montage, had an approximate duration of 20–25 min.

Calibration Session

The present calibration session was based in the one previously used by Velasco-Álvarez et al. (2013) and consisted in a virtual environment guiding the user to perform two different mental tasks without any feedback. Hence, the aim of this phase was for the system to learn to recognize both user tasks when used as control commands. The user tasks were right hand MI and an alternative mental task (word chain or mental arithmetic) and were freely chosen by users who received some advice. Regarding the motor imagery task, they were advised to employ a fine MI-related fingers movement, using visual, and kinaesthetic imagery, while for the alternative mental tasks, on the one hand, the mental arithmetic should be difficult enough to maintain the user's focus but not to provoke frustration (e.g., to do a series of subtractions of 13 units starting from a random number between 90 and 300). On the other hand, the word chain task consisted of picking up some random word in Spanish and choosing another word whose first syllable was the same as the last syllable of the previous word (e.g., "*fies-ta,*" "*ta-pa,*" and "*pa-e-lla*"). If they were stuck with some word, they should pick another word, as the main objective of this task was just to remain concentrated on it. In addition,

they were instructed to always use the same two specific tasks, to continue to watch the screen, to avoid any muscular movement, to try to reduce blinks and to maintain a relaxed and motivated state.

The timing of the calibration virtual session ran as detailed below (**Figure 4**). Initially, a car was placed in the middle of the road and its engine started at the beginning of the trial. Then, after 2 s, the car started to move, resulting in the possible appearance of a water puddle on the left side of the screen, located next to the car from the instant 4.25 s until the end of the trial. If the water puddle was presented, the participant had to perform the right-hand MI task from the time he/she starts to see the puddle until the sound of the car's engine ceases. Otherwise, if the puddle did not appear, the user should concentrate on performing the alternative task along the trial, i.e., in the time interval from 2 to 8 s of the trial. The calibration was divided into four blocks of 40 trials −20 of MI and 20 of the alternative task randomly ordered—to prevent fatigue and let the users rest between blocks. Also, there was a short random variable rest of 0.5–3 s between trials so as to be able to perform any movement that should not be performed during the trials. This phase lasted for approximately half an hour, excluding the time

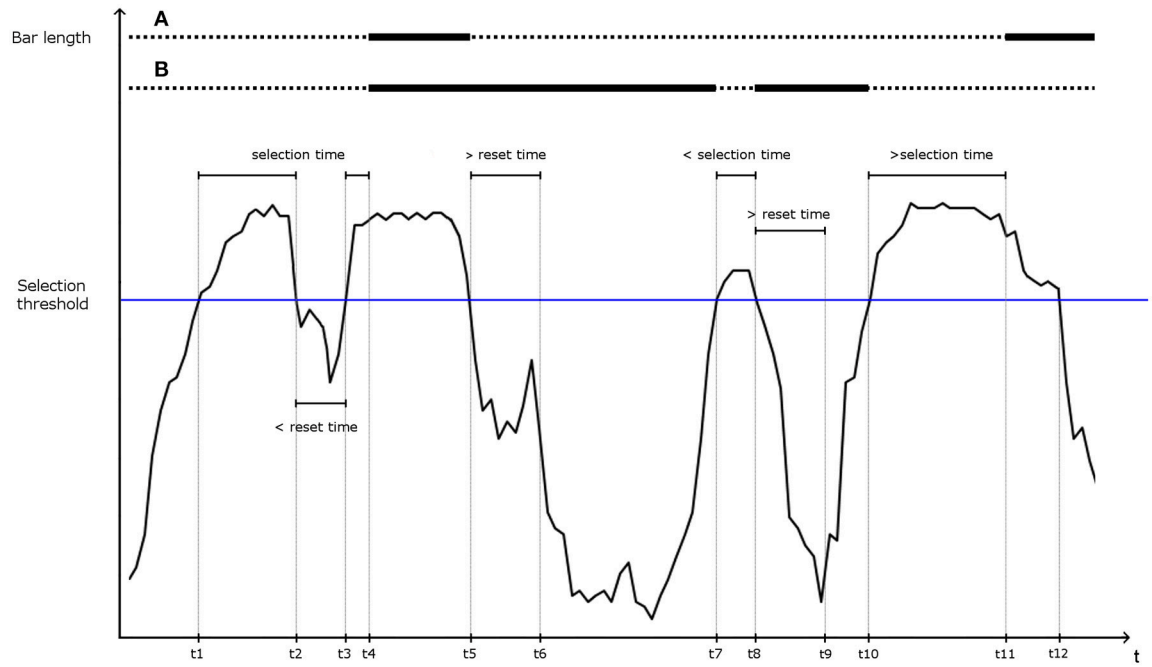

Time	Control	
	Continuous	Switch
t1	Selection time count starts	
t2	Selection time count is stopped and reset time count starts	
t3	The bar return is above the threshold in a lesser time than the reset time, so the previous accumulated selection time between t1 and t2 is not reset	
t4	Selection time is achieved, the command is selected and in both modes, the BCW starts to advance	
t5	Reset time count starts, the wheelchair stops	-
t6	Reset time is exceeded, so the accumulated time for command selecting is reset	-
t7	The bar exceeded the threshold, so the selection time count starts	The bar exceeded the threshold, so the selection time count starts, the BCW stops
t8	Accumulated time is stopped and reset time count starts, the BCW is still stopped	Accumulated time is stopped and reset time count starts, the BCW restarts to advance
t9	Reset time is exceeded, so the accumulated time is reset to zero	
t10	Selection time count starts	Selection time count starts, the BCW stops
t11	Selection time count is completed, the command is selected: the BCW advances	Selection time count is completed, the command is selected: the BCW remains stopped
t12	The bar is lower than the threshold, the reset time count starts, the BCW is stopped	-

FIGURE 1 | Operation of the interface through a detailed example. This example represents the bar length (axis *y*) over time (axis *x*) on the control of a brain-controlled wheelchair (BCW). At the beginning, the BCW is stopped. The horizontal lines *a* and *b* represent the executed command for the wheelchair for continuous and switch mode, respectively: a solid line for the forward command and a dashed line for the stop command. A detailed explanation of the events for continuous and switch control modes is offered at the bottom of the figure.

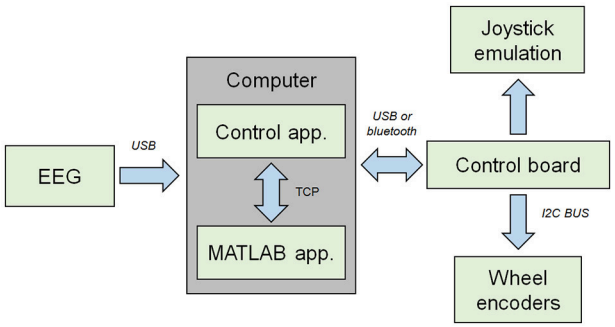

FIGURE 2 | Module structure of the developed brain-controlled wheelchair.

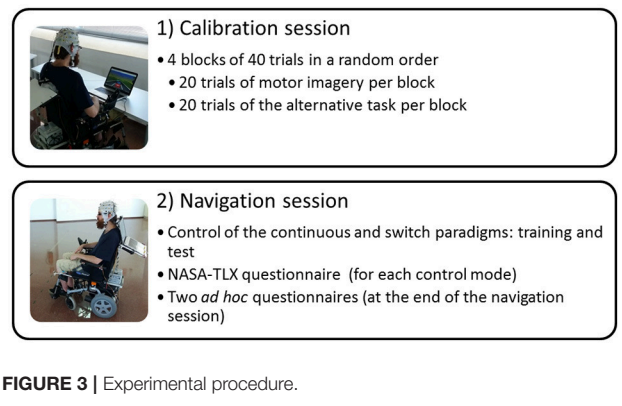

FIGURE 3 | Experimental procedure.

needed to set up the EEG recording equipment. Data from this phase were processed by the aforementioned algorithm to obtain the participant's reactive frequency band and optimal parameters of the LDA classifier. At this point, those participants whose EEG data could not be classified with an error rate lower than 30% were excluded. The virtual car environment was developed with VRML 2.0 and presented to users on a 15.6-inch laptop screen.

Navigation Session With the Brain-Controlled Wheelchair

The path to complete consisted in an 8.4 m straight section in which the user had to get through three forward and two stop sections (**Figure 5**). The participants' objective was to complete the advance sections in the shortest time possible while in the stop sections the BCW should be stopped for up to 60 s, it not being necessary to perform this stop time in a single stop. Acoustic cues were used to inform the subject about sections changes and the time reached. Specifically, 40 cm before the stop zone, the word "arriving" was used and once inside it "inside" could be heard. Once the goal time (60 s) was reached, the user received the "timeout, continue" command, indicating the stop task had been successfully completed. If this time had not been completed when the user went out of this area, "out, continue" could be heard, indicating he/she was no longer in the stop zone and should now focus on the forward section. All indications were given in Spanish language, known by all participants.

The path should be completed at least twice by participants, one time in each control mode, i.e., continuous and switch modes. The order presentation was counterbalanced to prevent fatigue or a learning effect. The total time of the navigation session was around 45 min, including both the training and the testing. The training consisted in a first contact with the BCW, controlling it at free will and understanding how it worked in practice. Instead, the testing phase involved the completion of the path described above. Users were invited to carry out the test a second time after each control mode and before trying out the next one. In the cases where the user decided to complete the second run for the current control paradigm, only the one with the highest performance (using the *performance factor*, see section Evaluation) was included in the results. Therefore, the comparison was made with the runs with the best performance for each control mode.

In addition, a NASA-TLX questionnaire (Hart and Staveland, 1988) was completed after ending each navigation paradigm. In the same way, at the end of the session, two *ad hoc* tests were completed in order to know the users' opinions and experience during the navigation session.

Evaluation

The evaluation was based on the definition of usability given by the International Organization for Standardization (1998), which considered three factors: effectiveness, efficiency and satisfaction.

Effectiveness

In order to analyse the performance controlling the BCW, we considered two basic parameters: (i) the number of command selections and (ii) measures related to the time employed in the advance and stop sections. From the number of command selections, we obtained statistical metrics based on the confusion matrix. Regarding the time measures, three *ad hoc* metrics were obtained that reflected the users' performance.

Confusion matrix metrics

Metrics related to the confusion matrix correspond to users' command selections (i.e., the bar exceeds the threshold for a longer time than a given "selection time") depending on their intent and what actually happened (Mason et al., 2006). In this matrix, selections and non-selections are denoted as "positive" and "negative" respectively and the output as "true" or "false" depending on whether these selections were desired or not. This desired-output relation classified each selection as one of four possible categories in the matrix: *true positive* (*TP*), *false positive* (*FP*), *true negative* (*TN*), *and false negative* (*FN*). In order to make the comparison among subjects' performance easier, we considered 1 s time slots when analyzing the results; i.e., if a command was held for 4 s, this was considered as four command selections. It is worth remembering that in the case of the continuous mode, the forward command is "positive" and the stop command is "negative." On the other hand, in the switch mode the "positive" selections are those changing the state of

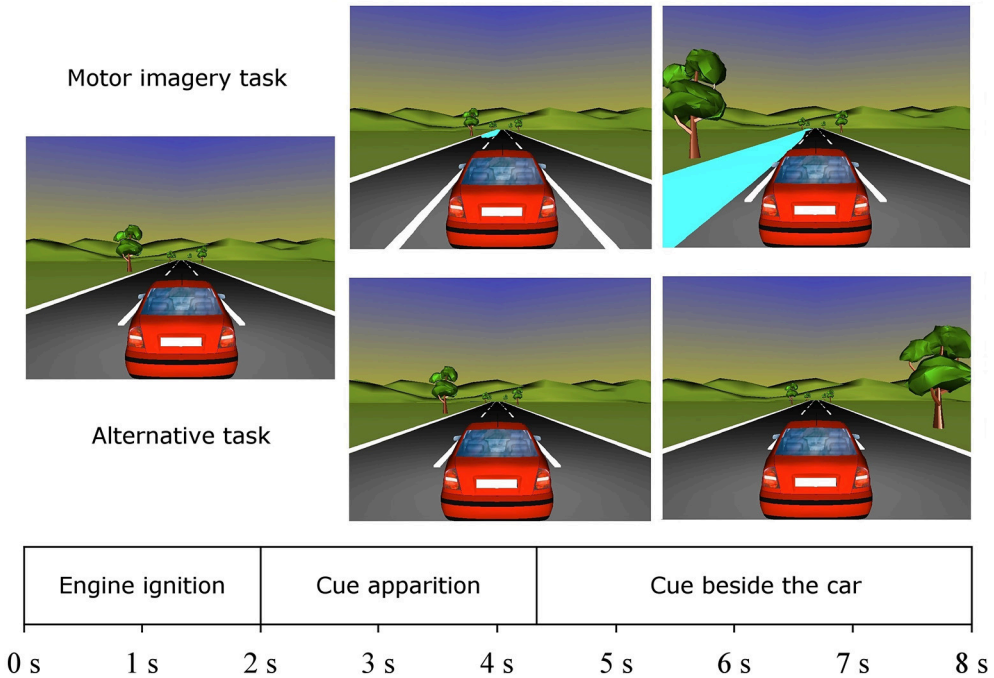

FIGURE 4 | Timing of calibration trials. Right-hand MI **(Top)** and alternative tasks **(Bottom)**.

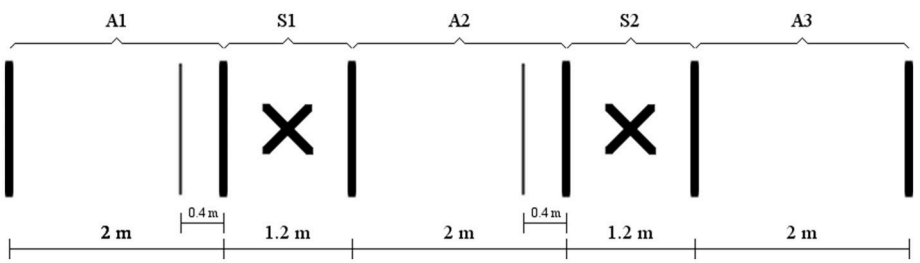

FIGURE 5 | Path to complete in the navigation task. Advances sections from first to third were denoted as A1, A2, and A3, respectively, while the two stop sections were denoted as S1 and S2.

the BCW, so the first selection of a command is considered a "positive," but keeping the same command active for several seconds is considered as "negative."

The following metrics were used:

(i) *True positive rate* (*TPR*; Equation 1) indicates the user's ability to select the desired command.

$$TPR = \frac{\sum TP}{\sum (TP + FN)} \quad (1)$$

(ii) *True negative rate* (*TNR*; Equation 2) indicates the user's ability to avoid unwanted commands.

$$TNR = \frac{\sum TN}{\sum (TN + FP)} \quad (2)$$

(iii) *Positive predictive value* (*PPV*; Equation 3) indicates which of the user's selections are correct.

$$PPV = \frac{\sum TP}{\sum (TP + FP)} \quad (3)$$

(iv) *Negative predictive value* (*NPV*; Equation 4) indicates which of the user's non-selections are correct.

$$NPV = \frac{\sum TN}{\sum (TN + FN)} \quad (4)$$

(v) *Accuracy* (*ACC*; Equation 5) shows the level of overall performance.

$$ACC = \frac{\sum TP + TN}{\sum (TP + TN + FP + FN)} \quad (5)$$

An illustrative example of a classification sequence into the four possibilities of the confusion matrix (i.e., *TP*, *FP*, *TN,* and *FN*) is shown in **Table 1**. As said above, the classification was updated one time per second, so as the example has 10 s, there will be 10 different classifications. The objective of the table is to show how the classification will depend on the paradigm handled.

Time-related metrics

Besides the confusion matrix metrics, we considered that new metrics related to each specific command (forward and stop) could be appropriate in order to better evaluate the performance of each control mode in the different commands. These metrics are related with the time employed in the advance and stop sections in relation to the minimum and maximum time required in each section, respectively. Two ratios are defined:

$$Advance\ performance\ ratio\ (APR) = \frac{At_{\min}}{At_o} \tag{6}$$

where At_{min} is the minimum time necessary to complete advance sections, 11 s, while At_o will be the observed time, i.e., the time executed by the user.

$$Stop\ performance\ ratio\ (SPR) = \frac{St_o}{St_{\max}} \tag{7}$$

where St_{max} is the maximum time required to complete the stop section task, 60 s, and St_o is the observed time, i.e., the time executed by the user. If the user stayed in the stop section for 60 s, the time needed to leave it was not included in any metric, neither for the *SPR* nor *APR*.

These equations induce the idea that a good performance will show a lower time to complete the advance sections (never under 11 s, which is the minimum time necessary to complete 2 m by the wheelchair) and a longer stop time (never exceeding 60 s, the time subjects were asked to remain stopped). In this way, Equation 6 will show the user performance in the advance sections, while Equation 7 will do it in the stop sections. The results of both equations will range between 0 and 1, where 1 indicates the best performance.

Furthermore, to obtain a general measure of the users' performance, a factor considering these two ratios was defined:

$$Performance\ factor = APR \cdot SPR \tag{8}$$

The fact of multiplying both ratios means that this factor presents a high value only in the case that both ratios are high as well. This means that a good performance is considered when both tasks can be voluntarily controlled. For example, in continuous mode, a system with an excellent performance in advances but deficient in stops (i.e., an uncontrollable BCW that always advanced) would have a high *APR*, but low *SPR*. If the mean value between these factors had been calculated, it would have offered a value near to 0.5; however, this performance would have been useless to allow users adequate control in a real environment. For this reason, as mentioned in section Navigation Session With the Brain-Controlled Wheelchair, the *performance factor* was used to select the best run with the BCW, since only one for each control mode was evaluated in the results section.

TABLE 1 | Example of classification according to the confusion matrix.

Time (s)	Command		Classification	
	Desired	Observed	Continuous	Switch
0–1	Forward	Forward	TP	TP
1–2	Forward	Forward	TP	TN
2–3	Forward	Forward	TP	TN
3–4	Forward	Forward	TP	TN
4–5	Stop	Forward	FP	FN
5–6	Stop	Stop	TN	TP
6–7	Stop	Stop	TN	TN
7–8	Forward	Stop	FN	FN
8–9	Forward	Forward	TP	TP
9–10	Forward	Forward	TP	TN

True positive (TP), false positive (FP), true negative (TN), and false negative (FN).

Efficiency

This factor has been mainly measured with the NASA-TLX questionnaire (Hart and Staveland, 1988), whose aim is to measure the user's workload executing a specific task once he/she has ended it. It is composed of six subscales (*mental demand*, *physical demand*, *temporal demand*, *performance*, *effort,* and *frustration*) in a scale ranging from 1 to 10 by users. Then, the participants have to indicate the relative contribution of the factors to their workload through 15 paired comparisons (e.g., *mental demand* vs. *physical demand*). A weighting average technique was used to compute the contribution of each subscale to the total workload. The total workload ranges between 0 and 100, while the weighted subscales are from 0 to 33.3. This questionnaire was applied two times, one for each control mode in the navigation task.

In addition, an *ad hoc* questionnaire about the experience controlling the wheelchair relative to relaxation, tiredness and performance (*ease to stop*, *ease to move forward*, *presence of false positives,* and *presence of false negatives*) was filled out by each participant at the end of the session. The variables of these questionnaires were ranged from 1 to 10 and written so that users could easily understand them (i.e., avoiding technical language).

Satisfaction

Satisfaction was measured employing another *ad hoc* questionnaire, whose items ranged from 1 to 10, to determine the comfort and subjective opinions of the user. These metrics were: *understanding of paradigm*, *control sense*, *motion smoothness*, *suitability,* and *efficacy of the paradigm*. In addition, at the end of the test users were asked to choose their favorite paradigm and to explain their choice.

RESULTS

This section will be divided into two parts in reference to the calibration and navigation tasks. Likewise, the navigation

task part will be in sections for the usability factors mentioned above: effectiveness, efficiency and satisfaction. All the analysis performed was sample characteristics dependent, i.e., parametric or non-parametric, which means that mainly *t* Student and Wilcoxon tests were used for paired means comparison, respectively.

Calibration Session

The reactive band power features and minimum error rate obtained for each subject are presented in **Table 2**. On average, the minimum error rate was 23.70 ± 8.68%. Of the 15 subjects, five (P2, P9, P10, P13, and P15) had error rates above the cut-off point of 30% and did not continue with the study.

Navigation Session

Effectiveness

In **Table 3**, the values of the different confusion matrix parameters obtained during the navigation task for each subject are shown. Regarding these measures, significant differences between continuous and switch mode were obtained for each of them: *TPR* [$t_{(9)} = 3.583$; $p = 0.006$], *PPV* [$t_{(9)} = 11.983$; $p < 0.001$], *TNR* [$Z = 2.803$; $p = 0.005$], *NPV* [$t_{(9)} = -3.154$; $p = 0.012$] and *ACC* [$t_{(9)} = -2.517$; $p = 0.033$].

Table 4 shows the time spent by users executing each of the two BCW commands—move forward or idle state—as well as the number of move forward selections done in each section of the path. The users' average time to complete an advance section offered significant differences between both control modes: 42.2 ± 28.7 s and 15.47 ± 3.43 s for continuous and switch modes, respectively [$Z = -2.803$; $p = 0.005$]. Significant differences were obtained for stop sections too: 42.45 ± 16.01 s and 24.35 ± 10.94 s, for continuous and switch modes, respectively [$t_{(9)} = 2.756$; $p = 0.022$]. Regarding to the reaction time to stop the wheelchair when the user was advised that he/she was in the stop section, there was no significant differences between control modes: continuous (2.55 ± 1.5 s) and switch mode (3.55 ± 1.32 s).

The average number of forward commands required to complete the advance sections was significantly different between conditions: 4.33 ± 1.58 s and 1.23 ± 0.52 s for the continuous and switch modes, respectively [$Z = -2807$; $p = 0.005$]. For the stop sections, similar results were obtained as the average number of forward commands was 2.75 ± 1.53 and 1.25 ± 0.42 for continuous and switch mode, respectively [$Z = -2.439$; $p = 0.015$].

Likewise, from the data in **Table 4**, performance ratios for each section and user can be calculated (**Figure 6**). A repeated measures ANOVA was performed to study the presence of main and interaction effects, involving the factors control mode (continuous or switch) and section type (advance or stop). The dependent variables included in this ANOVA were *APR* and *SPR*. The results showed significant differences in the interaction effect between the control mode and performance ratio variables [$F_{(1,9)} = 23.777$; $p = 0.001$; $\eta_p^2 = 0.725$] (**Figure 6C**). These results showed that the control mode affects each of the variables differently, as we saw in the previous specific analysis relative to the time required to go over a section, offering a better performance ratio with the switch mode in advances [$t_{(9)} = -6.363$; $p < 0.001$] (**Figure 6A**) but better with continuous mode in stops [$t_{(9)} = 2.756$; $p = 0.022$] (**Figure 6B**). In addition, there are no significant differences between the *performance factor* related to the continuous mode (0.31 ± 0.18) and the switch mode (0.29 ± 0.12) (**Figure 6D**).

Efficiency

Workload

The average weighted factor results obtained with the NASA-TLX questionnaire are shown in **Table 5**, while the resulting *total workload* of each user is shown in **Figure 7**. No significant differences could be noticed between control modes.

Subjective questionnaire

The average answers given by participants at the end of the session in the usability questionnaire related to specific control mode features are shown in **Table 5**. Regarding these measures, only the scores of seven participants (P5, P6, P7, P8, P11, P12, and P14) are given as previous users were part of preliminary tests not using this questionnaire. No differences could be found in any factor of the two control modes with a Wilcoxon test.

Satisfaction

The different mean values obtained in another subjective questionnaire are shown in **Table 5**. As with efficiency, no significant differences were found between control modes in any factor of the subjective questionnaire (Wilcoxon test). In addition, 4 out of the 7 users who filled out the questionnaire preferred continuous mode vs. switch mode. A pattern can be observed in the explanation offered by three of the four users

TABLE 2 | Results of the calibration session.

User	Frequency band (Hz)	Minimum error (%)
P1	7–17	8.81
P2	13–16	31.31
P3	12–14	18.44
P4	12–17	17.94
P5	5–15	20.94
P6	11–15	22.38
P7	10–14	22.13
P8	10–16	23.06
P9	7–10	30.31
P10	11–16	35.19
P11	9–12	25.06
P12	7–12	15.81
P13	5–12	35.44
P14	10–14	11.63
P15	10–17	39.06
Mean	9.27 ± 2.52 to 15.47 ± 2.17	23.7 ± 8.68

TABLE 3 | Results of the confusion matrix's parameters for each user and control mode.

User	Classification matrix's measures									
	TPR		PPV		TNR		NPV		ACC	
	Continuous	Switch	Continuous	Switch	Continuous	Switch	Continuous	Switch	Continuous	Switch
P1	0.55	0.32	0.79	0.54	0.84	0.94	0.63	0.86	0.69	0.83
P3	0.58	0.22	0.82	0.57	0.93	0.94	0.81	0.76	0.82	0.74
P4	0.28	0.17	0.84	0.60	0.92	0.94	0.45	0.70	0.53	0.69
P5	0.55	0.15	0.72	0.60	0.83	0.94	0.71	0.66	0.71	0.65
P6	0.47	0.27	0.82	0.64	0.89	0.94	0.62	0.76	0.68	0.74
P7	0.30	0.22	0.68	0.56	0.64	0.93	0.25	0.74	0.39	0.72
P8	0.72	0.15	0.71	0.56	0.67	0.94	0.68	0.70	0.69	0.69
P11	0.44	0.23	0.77	0.55	0.57	0.91	0.24	0.72	0.47	0.70
P12	0.19	0.35	0.77	0.53	0.73	0.86	0.16	0.74	0.28	0.70
P14	0.59	0.35	0.70	0.53	0.70	0.87	0.59	0.76	0.64	0.72
Mean	0.47 ± 0.17	0.24 ± 0.08	0.76 ± 0.06	0.57 ± 0.04	0.77 ± 0.13	0.92 ± 0.03	0.51 ± 0.22	0.74 ± 0.06	0.59 ± 0.17	0.72 ± 0.05
Satatistical test value	3.583		11.983		2.803		3.154		2.517	
p-value	0.006		0.001		0.005		0.012		0.033	

True positive rate (TPR), positive predictive value (PPV), true negative rate (TNR), and negative predictive value (NPV). The two last row corresponds to the $t_{(9)}$ Student comparison between continuous and switch modes for TPR, PPV, NPV, and ACC. In the case of TNR comparison, the Z-test value was calculated instead t.

who preferred continuous mode (P5, P8 and P11; P7 did not explain their choice) according to the difficulty of changing mental tasks quickly and the requirement to maintain higher attentional levels in switch mode. Otherwise, two participants who preferred switch mode (P6 and P12; P14 did not explain his/her choice) declared that this mode implies a lower mental effort (P12) and that it was easier to control the BCW (P6).

DISCUSSION

This section will be divided into two subparts, one regarding the results obtained in this work, comparing the two control paradigms, and the other referring to previous works using the switch system or ERD/ERS signal based BCW.

Discussion of the Navigation Control Presented in This Paper

First, the results obtained for the two control paradigms presented in the study will be discussed and compared in detail.

Effectiveness

According to the measure related to the general performance time, the *performance factor*, significant differences between paradigms are not observed but in specific sections of the path. On the one hand, the switch paradigm could be more effective in advance sections since it was possible to complete the same sections with fewer commands and better time-related metrics (i.e., time and *APR*). However, the opposite conclusion was obtained in the stop sections, where the continuous paradigm seems more convenient since users managed to stand still longer; however, the number of commands was significantly bigger too. The number of executed commands needed to leave the stop sections requires a more careful interpretation. Although the continuous mode was related with a larger number of forward commands in the stop section, when users selected a non-desired forward command in switch mode, they might not be able to stop the chair as quickly as needed, thus it made the BCW leave the stop section earlier than expected.

In general, these results may be explained by the false activations, i.e., *FPs*, which had a higher cost in switch mode than in continuous, in which the user could make these false selections with the slight cost of advancing just a few centimeters. Otherwise, in switch mode, these false activations could involve a larger displacement of the wheelchair, since quickly changing the movement state of the device could be difficult for some users (they should wait until the bar was lower than the threshold, then, they had to raise the bar again above the threshold during the "selection time" at least).

Measures related to the confusion matrix offered significant differences in all the considered variables. A pattern could be observed according to which the continuous mode obtained a better performance in the variables related to the *TPs* (*TPR* and *PPV*), while the switch mode obtained a better performance in the variables related to the *TNs* (*TNR* and *NPV*). These results make sense considering the desired results for each paradigm: the priority in the continuous mode was to have an adequate selection of the *TPs* in such a way that the displacement of the wheelchair was as fluid as possible. However, in the switch mode the intention was that the users could keep the state of the device as long as they wanted since, as we saw earlier, this could lead to a better performance. Nevertheless, in the most general measure of the confusion matrix, i.e., the *ACC*, the switch mode offered a better performance.

Despite these general differences in performance between control modes, it should be admitted that some users presented a better performance using one paradigm vs. the other. Thus, these

TABLE 4 | Results of the user performance: times and forward command selections.

User	Control mode	Section of the path														
		Advance 1			Stop 1			Advance 2			Stop 2			Advance 3		
		A	B	C	A	B	C	A	B	C	A	B	C	A	B	C
P1	Continuous	16	5	5	4	56	3	11	4	2	7	1	1	13	21	5
	Switch	11	0	1	7	26	1	10	2	1	8	43	2	13	5	2
P3	Continuous	13	4	2	6	54	2	11	0	0	2	58	1	16	17	5
	Switch	11	0	1	8	14	1	10	0	0	7	2	1	12	2	1
P4	Continuous	13	0	1	6	54	2	14	13	1	4	56	1	23	100	9
	Switch	13	8	2	7	19	1	7	7	1	7	53	2	15	13	2
P5	Continuous	16	6	4	12	48	8	16	18	5	7	53	3	18	11	5
	Switch	11	0	1	8	2	1	11	0	0	7	0	0	12	4	1
P6	Continuous	12	0	1	5	55	3	22	28	6	8	50	2	18	21	7
	Switch	11	0	1	8	26	1	11	4	1	8	6	2	11	2	1
P7	Continuous	14	48	3	12	10	4	22	64	7	13	34	4	18	17	4
	Switch	14	0	1	9	6	1	13	0	0	11	9	2	15	2	1
P8	Continuous	14	8	3	9	33	2	14	2	2	8	1	1	13	6	2
	Switch	11	0	1	6	36	1	12	17	2	7	0	0	11	2	1
P11	Continuous	19	23	5	9	20	2	13	2	3	6	0	0	18	38	5
	Switch	13	0	1	8	7	1	11	0	0	9	31	2	14	7	2
P12	Continuous	18	16	7	10	1	3	27	105	10	9	51	4	19	156	7
	Switch	14	3	2	7	24	2	12	2	1	8	4	1	13	5	3
P14	Continuous	14	1	2	14	39	7	18	16	4	9	15	2	22	21	8
	Switch	15	3	3	9	6	1	14	1	1	10	14	2	14	2	2

While the letters "A" and "B" indicate the time (s) moving forward and keeping the position with the wheelchair, respectively; the letter "C" indicates the number of forward command selections. Thus, for example, the column relative to "Advance 2" and subcolumn "B," would make reference to the time with the wheelchair stopped (B) in the second advance section.

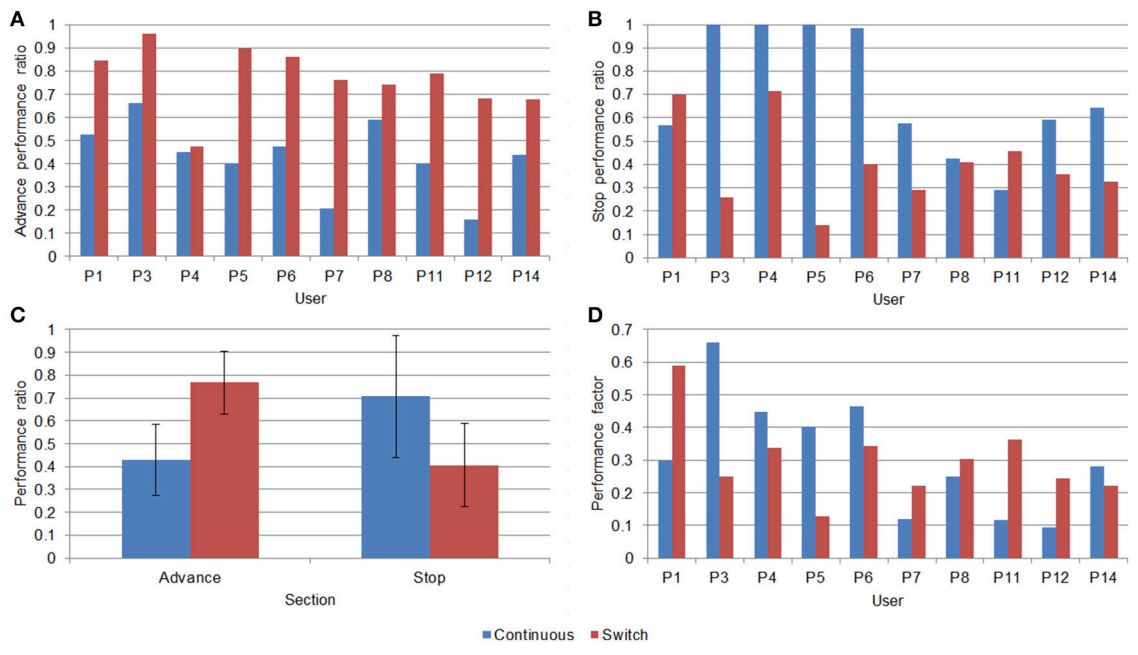

FIGURE 6 | Results of the user performance: time-related metrics. **(A)** *Advance performance ratio* (*APR*) for each user. **(B)** *Stop performance ratio* (*SPR*) for each user. **(C)** Average values, with the corresponding standard deviation, for the APR and SPR. **(D)** *Performance factor* for each user.

TABLE 5 | Average values and statistical result for the subjective measures reported by users.

Subjective measures	Control		Wilcoxon test	
	Continuous	Switch	*Z*	*p*
NASA-TLX				
Mental demand	22.03 ± 4.86	21.17 ± 6.95	−0.459	0.646
Physical demand	0.8 ± 2.2	0.17 ± 0.36	−0.816	0.414
Temporal demand	6.33 ± 4.01	7.53 ± 6.03	0.28	0.779
Performance	12.5 ± 5.24	8.87 ± 5.04	−1.955	0.051
Effort	14.97 ± 6.3	16.33 ± 8.49	0.561	0.575
Frustration	5.77 ± 7.06	5.87 ± 5.43	0.059	0.953
Total workload	62.4 ± 8.24	59.93 ± 17.95	−0.561	0.575
SUBJECTIVE QUESTIONNAIRE FOR EFFICIENCY				
Relaxed	8.29 ± 1.91	7.43 ± 2.44	−0.73	0.465
Tired	4.14 ± 2.03	4.86 ± 1.88	−0.73	0.465
Ease to stop	6.86 ± 2.17	5.43 ± 2.92	−1.084	0.279
Ease to move forward	5.57 ± 1.29	6.00 ± 1.85	−0.426	0.67
False positives presence	5.71 ± 1.67	6.29 ± 1.98	−0.687	0.492
False negatives presence	5.29 ± 1.75	5.43 ± 2.25	−0.69	0.49
SUBJECTIVE QUESTIONNAIRE FOR SATISFACTION				
Paradigm understanding	9.57 ± 0.49	9.14 ± 1.36	−1	0.317
Control sense	5.86 ± 1.73	4.86 ± 2.29	−0.681	0.496
Motion smoothness	5.43 ± 1.76	5.43 ± 1.76	−0.085	0.932
Suitability of the paradigm	7.29 ± 1.67	5.43 ± 2.44	−1.16	0.246
Efficacy of the paradigm	7.14 ± 1.73	6.86 ± 1.81	−0.632	0.527

results could support the idea that the paradigm should be chosen according the user preferences.

Efficiency

Regarding the usability questionnaires concerning efficiency, some points should be highlighted. At first, as expected, the most influential factor in the workload construct, measured with the NASA-TLX, was the *mental demand*, followed by *effort*, in both navigation paradigms. Most participants did not show appreciable differences in *total workload* between paradigms (**Figure 7**). However, for some participants one or the other paradigm noticeably involved more workload.

Regarding the subjective *ad hoc* questionnaire for efficiency, both paradigms shown similar values offering: (i) adequate results for relax state during the experiment, (ii) quite positive values for the metrics related to the ease to move or stop the wheelchair, although there were (iii) certain level of tiredness and (iv) quite negative values in reference at the presence of *FPs* and *FNs*.

Satisfaction

In reference to the subjective questionnaire for satisfaction: (i) all users adequately understood both paradigms, (ii) the control sense could be improved, especially for the switch mode, although there were no significant difference between them, (iii) both paradigms could be equally effective, (iv) the paradigm was not related to the motion smoothness as one might initially think, (v) the suitability of the paradigm offered acceptable scores, especially for the continuous mode despite there were no significant differences. The statements of those users who declared the continuous paradigm as their preference and explained their choice (P5, P8, and P11) agreed that the fast changes of mental tasks needed in the switch mode were difficult to perform.

Discussion of Previous Works

Several BCI groups had studied a switch paradigm to control a BCW. The cases where the user can achieve an appropriate control of the alternative task present a certain parallelism with

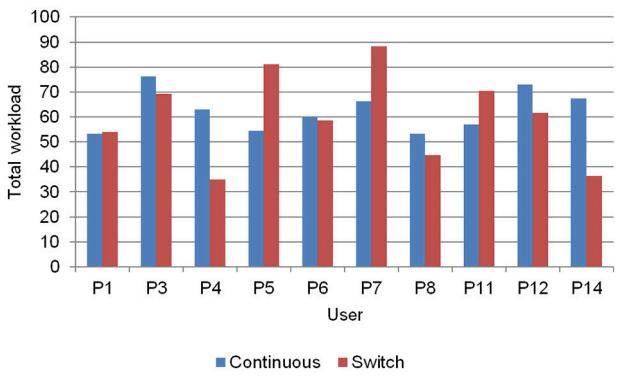

FIGURE 7 | *Total workload* measured by NASA-TLX.

TABLE 6 | Results of the brain switch proposals: confusion matrix's measures.

System	Control mode	TPR	PPV	TNR	NPV
Present proposal	Continuous	0.47	0.76	0.77	0.51
	Switch	0.24	0.57	0.92	0.74
Müller-Putz et al., 2010	Switch	0.79	0.84	–	–
Solis-Escalante et al., 2010	Switch	0.46	–	0.86	–
Ron-Angevin et al., 2017	Discrete	0.79	0.77	0.85	0.81

Brain-controlled wheelchair (BCW), event-related (des)synchronization (ERD/ERS), true positive rate (TPR), positive predictive value (PPV), true negative rate (TNR), and negative predictive value (NPV).

high level navigation paradigms (generally based on exogenous signal such as P300 or steady-state evoked potentials), since in these systems the user sends the order and he/she just has to wait while the command is executed. As it was shown in the introduction section, the brain switch control has been implemented in exogenous based BCWs with low level navigation to turn on/off the system, for example, in hybrid SSVEP based wheelchairs (Xu et al., 2012; Cao et al., 2014). The paper presented by Li Y. et al (2013) tested a hybrid (P300 and SSVEP) BCW where one the simultaneous detection of P300 and SSVEP stimulus was employed to change the advance state of the wheelchair (maintaining the advance or stop). Thus, this BCW applied the same concept used in the present paper with a MI based BCW. Furthermore, the SSVEP based BCWs are usually controlled through 4 or 5 control commands (Fernández-Rodríguez et al., 2016), so using the same stimulus to execute two allows that the number of commands can be incremented without the need of more stimuli.

Due to the specific experimental design to control the different devices and other factors such as the experience level of the participants, the comparison among switch systems will be limited to general aspects and to those which employed similar metrics. This problem has been declared in previous reviews about brain-controlled mobile devices (Bi et al., 2013; Fernández-Rodríguez et al., 2016) and BCI assessment (Thompson et al., 2013). As it is shown in **Table 6**, one of the main characteristics of the switch control presented here is the unbalance between the metrics related to the confusion matrix, especially between the *TPR* and *TNR*. This pattern was also obtained by Solis-Escalante et al. (2010). Regarding Müller-Putz et al. (2010), who calculated the *TPR* and the *PPV*, the presented switch proposal on the present paper shows more unbalanced *TPR* and *PPV* than them; however, the trend was the same: the *PPV* was higher than the *TPR*. Additionally, all switch control systems presented in **Table 6** show the *TNR* as the highest measurement, and the *TPR* as the lowest. These results could be convenient since the switch control mode must have the ability to maintain the current state during the desired time. However, this capability of true negative detection and this low occurrence of false selections can lead to a system that is activated with difficulty. This could cause many false non-selections and thus result in a low value in the *TPR*. This imbalance can be a problem especially when the user needs to stop the BCW urgently, so in future proposals it would be necessary to include intelligent systems that assist navigation. However, as Ron-Angevin et al. (2017) concluded in their proposal on discrete control for the control of a BCW, the optimal values of these parameters depend on the type of system used, so they should be studied in future assessments.

Regarding the workload, since there are no other studies using the NASA-TLX and controlling a BCW, it is difficult to discuss the observed values in the present study. In principle, it could only be compared with other studies that involve other tasks, such as the training to control the ERD/ERS signal (Felton et al., 2012), the handling of a complex P300 communication application (Riccio et al., 2011) or a simple P300 speller controlled by patients (Pasqualotto et al., 2015). Taking into account these previous works, whose *total workload* ranges between 30 and 67, approximately, it could be admitted that our values around 60 were adequate, especially if we keep in mind that the present work involve the control of a real wheelchair (i.e., the users move along with the BCW, they are not quietly seated in front of a computer).

CONCLUSIONS

The performance shown by users during the navigation was heterogeneous, as were the workload and the evaluations through subjective questionnaires. Moreover, the results suggest that each control paradigm had specific advantages and drawbacks that must be taken into account. Specifically, a tendency was observed for the switch mode to enable a better performance than continuous mode in the advance sections, since the user could travel a longer distance with a single command selection. Otherwise, this advantage is converted into a drawback in the stop sections since in some cases users went through the stop section and could not stop the BCW. Thus, in these sections continuous mode offered better results. Another aspect to emphasize is the variability found in the *performance factor* between both controls for the same user, pointing to the possibility that what matters is not only the suitability of the paradigm, but also the preference and users' ERD/ERS modulations skills.

In short, this work has offered a detailed evaluation of two paradigms controlling a BCW considering the usability approach. To this end, many metrics were employed: those related to the objective performance of the user (such as time, number of selected commands, metrics of confusion matrix and even *ad hoc* measures such as the *APR*, *SPR* and performance factor), in addition to the subjective questionnaires, from the widely used NASA-TLX to specific *ad hoc* questionnaires.

For future works, it would be convenient to re-examine the control over different types of paradigms with trained users during several sessions, since it should be taken into account that all users (except user P4) were inexperienced at controlling these interfaces through their EEG signals. In addition, it may be interesting to study the application of new navigation paradigms that could have advantages over these two modes of control, so that users' performance and, therefore, their experience during the management would be as convenient and comfortable as possible.

AUTHOR CONTRIBUTIONS

AF-R carried out the experimental sessions, collaborated in the experimental design, performed the statistical analysis and was a major contributor in writing the manuscript. FV-Á developed the BCW prototype, participated in the experimental sessions and was a major contributor in drafting the work. MB-S collaborated in the experimental design and carried out the experimental sessions. RR-A led the research, participated in the design of the BCW prototype, contributed in the experimental design and in the critical revision of the manuscript.

ACKNOWLEDGMENTS

This work was partially supported by the Spanish Ministry of Economy and Competitiveness through the projects LICOM (DPI2015-67064-R), by the European Regional Development Fund (ERDF) and by the University of Malaga. Moreover, the authors would like to thank all participants for their cooperation.

REFERENCES

Bi, L., Fan, X. A., and Liu, Y. (2013). EEG-based brain-controlled mobile robots: a survey. *IEEE Trans. Human-Machine Syst.* 43, 161–176. doi: 10.1109/TSMCC.2012.2219046

Cao, L., Li, J., Ji, H., and Jiang, C. (2014). A hybrid brain computer interface system based on the neurophysiological protocol and brain-actuated switch for wheelchair control. *J. Neurosci. Methods* 229, 33–43. doi: 10.1016/j.jneumeth.2014.03.011

Corralejo, R., Hornero, R., and Álvarez, D. (2011). "A domotic control system using Brain-Computer Interface (BCI)," in *Advances in Computational Intelligence. IWANN 2011. Lecture Notes in Computer Science, Vol. 6691*, eds J. Cabestany, I. Rojas, and G. Joya (Berlin; Heidelberg: Springer), 345–352.

Farwell, L. A., and Donchin, E. (1988). Talking off the top of your head: toward a mental prosthesis utilizing event-related brain potentials. *Electroencephalogr. Clin. Neurophysiol.* 70, 510–523. doi: 10.1016/0013-4694(88)90149-6

Felton, E. A., Williams, J. C., Vanderheiden, G. C., and Radwin, R. G. (2012). Mental workload during brain-computer interface training. *Ergonomics* 55, 526–537. doi: 10.1080/00140139.2012.662526

Fernández-Rodríguez, Á., Velasco-Álvarez, F., and Ron-Angevin, R. (2016). Review of real brain-controlled wheelchairs. *J. Neural Eng.* 13:61001. doi: 10.1088/1741-2560/13/6/061001

Hart, S. G., and Staveland, L. E. (1988). "Development of NASA-TLX (Task Load Index): results of empirical and theoretical research," in *Advances in Psychology*, eds P. A. Hancock and N. Meshkati (North Holland: Elsevier), 139–183. doi: 10.1016/S0166-4115(08)62386-9

Huang, D., Qian, K., Fei, D. Y., Jia, W., Chen, X., and Bai, O. (2012). Electroencephalography (EEG)-based brain-computer interface (BCI): A 2-D virtual wheelchair control based on event-related desynchronization/ synchronization and state control. *IEEE Trans. Neural Syst. Rehabil. Eng.* 20, 379–388. doi: 10.1109/TNSRE.2012.2190299

International Organization for Standardization (1998). *ISO 9241-11: Ergonomic Requirements for Office Work with Visual Display Terminals (VDTs) - Part 11: Guidance on Usability*.

Iturrate, I., Antelis, J. M., Kübler, A., and Minguez, J. (2009). A noninvasive brain-actuated wheelchair based on a P300 neurophysiological protocol and automated navigation. *IEEE Trans. Robot.* 25, 614–627. doi: 10.1109/TRO.2009.2020347

Kim, K. T., and Lee, S. W. (2017). "Towards an EEG-based intelligent wheelchair driving system with vibro-tactile stimuli," in *2016 IEEE International Conference on Systems, Man, and Cybernetics, SMC 2016 - Conference Proceedings* (Budapest), 2382–2385.

Kübler, A., Neumann, N., Kaiser, J., Kotchoubey, B., Hinterberger, T., and Birbaumer, N. P. (2001). Brain-computer communication: self-regulation of slow cortical potentials for verbal communication. *Arch. Phys. Med. Rehabil.* 82, 1533–1539. doi: 10.1053/apmr.2001.26621

Lange, N., Bishop, C. M., and Ripley, B. D. (1997). *Neural Networks for Pattern Recognition*. New York, NY: Oxford Univwersity Press.

Li, J., Liang, J., Zhao, Q., Li, J., Hong, K., and Zhang, L. (2013). Design of assistive wheelchair system directly steered by human thoughts. *Int. J. Neural Syst.* 23:1350013. doi: 10.1142/S0129065713500135

Li, Y., Pan, J., Wang, F., and Yu, Z. (2013). A hybrid BCI system combining P300 and SSVEP and its application to wheelchair control. *IEEE Trans. Biomed. Eng.* 60, 3156–3166. doi: 10.1109/TBME.2013.2270283

Mason, S. G., and Birch, G. E. (2000). A brain-controlled switch for asynchronous control applications. *IEEE Trans. Biomed. Eng.* 47, 1297–1307. doi: 10.1109/10.871402

Mason, S., Kronegg, J., Huggins, J., Fatourechi, M., and Schlögl, A. (2006). *Evaluating the Performance of Self-Paced Brain-Computer Interface Technology*. Tech Report. Available online at: http://ipl.ece.ubc.ca/bci_files/self_paced_tech_report-2006-05-19.pdf

McFarland, D. J., McCane, L. M., David, S. V., and Wolpaw, J. R. (1997). Spatial filter selection for EEG-based communication. *Electroencephalogr. Clin. Neurophysiol.* 103, 386–394. doi: 10.1016/S0013-4694(97)00022-2

Millán, J. D. R., Galán, F., Vanhooydonck, D., Lew, E., Philips, J., Nuttin, M., et al. (2009). "Asynchronous non-invasive brain-actuated control of an intelligent wheelchair," in *Proceedings of the 31st Annual International Conference of the IEEE Engineering in Medicine and Biology Society: Engineering the Future of Biomedicine, EMBC 2009* (Minneapolis), 3361–3364.

Müller-Putz, G. R., Kaiser, V., Solis-Escalante, T., and Pfurtscheller, G. (2010). Fast set-up asynchronous brain-switch based on detection of foot motor imagery in 1-channel EEG. *Med. Biol. Eng. Comput.* 48, 229–233. doi: 10.1007/s11517-009-0572-7

Ng, D. W. K., Soh, Y. W., and Goh, S. Y. (2015). "Development of an autonomous BCI wheelchair," in *IEEE SSCI 2014 - 2014 IEEE Symposium Series on Computational Intelligence - CIBCI 2014: 2014 IEEE Symposium on Computational Intelligence in Brain Computer Interfaces, Proceedings* (Orlando), 1–4.

Pasqualotto, E., Matuz, T., Federici, S., Ruf, C. A., Bartl, M., Olivetti Belardinelli, M., et al. (2015). Usability and workload of access technology for people with severe motor impairment. *Neurorehabil. Neural Repair* 29, 950–957. doi: 10.1177/1545968315575611

Pfurtscheller, G., Brunner, C., Schlögl, A., and Lopes da Silva, F. H. (2006). Mu rhythm (de)synchronization and EEG single-trial

classification of different motor imagery tasks. *Neuroimage* 31, 153–159. doi: 10.1016/j.neuroimage.2005.12.003

Riccio, A., Leotta, F., Bianchi, L., Aloise, F., Zickler, C., Hoogerwerf, E.-J., et al. (2011). Workload measurement in a communication application operated through a P300-based brain–computer interface. *J. Neural Eng.* 8:25028. doi: 10.1088/1741-2560/8/2/025028

Ron-Angevin, R., Aurélie, D., Yvan, M., Lespinet-Najib, V., and Andre Jean, M. (2015). Brain-computer interface: comparison of two control modes to drive a virtual robot. *Eur. Sci. J.* 7881, 177–189.

Ron-Angevin, R., and Díaz-Estrella, A. (2009). Brain-computer interface: changes in performance using virtual reality techniques. *Neurosci. Lett.* 449, 123–127. doi: 10.1016/j.neulet.2008.10.099

Ron-Angevin, R., Velasco-Álvarez, F., Fernández-Rodríguez, Á., Díaz-Estrella, A., Blanca-Mena, M. J., and Vizcaíno-Martín, F. J. (2017). Brain-Computer Interface application: auditory serial interface to control a two-class motor-imagery-based wheelchair. *J. Neuroeng. Rehabil.* 14, 49. doi: 10.1186/s12984-017-0261-y

Solis-Escalante, T., Müller-Putz, G., Brunner, C., Kaiser, V., and Pfurtscheller, G. (2010). Analysis of sensorimotor rhythms for the implementation of a brain switch for healthy subjects. *Biomed. Signal Process. Control* 5, 15–20. doi: 10.1016/j.bspc.2009.09.002

Tanaka, K., Matsunaga, K., and Wang, H. O. (2005). Electroencephalogram-based control of an electric wheelchair. *IEEE Trans. Robot.* 21, 762–766. doi: 10.1109/TRO.2004.842350

Thompson, D. E., Blain-Moraes, S., and Huggins, J. E. (2013). Performance assessment in brain-computer interface-based augmentative and alternative communication. *Biomed. Eng. Online* 12:43. doi: 10.1186/1475-925X-12-43

Tsui, C. S., Gan, J. Q., and Hu, H. (2011). A self-paced motor imagery based brain-computer interface for robotic wheelchair control. *Clin. EEG Neurosci.* 42, 225–229. doi: 10.1177/155005941104200407

Velasco-Álvarez, F., Ron-Angevin, R., Da Silva-Sauer, L., and Sancha-Ros, S. (2010). "Brain-computer interface: comparison of two paradigms to freely navigate in a virtual environment through one mental task," in *2010 5th International Conference on Broadband and Biomedical Communications, IB2Com 2010* (Malaga), 1–5.

Velasco-Álvarez, F., Ron-Angevin, R., da Silva-Sauer, L., and Sancha-Ros, S. (2013). Audio-cued motor imagery-based brain-computer interface: navigation through virtual and real environments. *Neurocomputing* 121, 89–98. doi: 10.1016/j.neucom.2012.11.038

Xu, Z., Li, J., Gu, R., and Xia, B. (2012). Steady-state visually evoked potential (SSVEP)-based brain-computer interface (BCI): a low-delayed asynchronous wheelchair control system. *Lect. Notes Comput. Sci.* 7663, 305–314. doi: 10.1007/978-3-642-34475-6_37

Zhang, R., Li, Y., Yan, Y., Zhang, H., Wu, S., Yu, T., et al. (2016). Control of a Wheelchair in an indoor environment based on a brain-computer interface and automated navigation. *IEEE Trans. Neural Syst. Rehabil. Eng.* 24, 128–139. doi: 10.1109/TNSRE.2015.2439298

Conflict of Interest Statement: The authors declare that the research was conducted in the absence of any commercial or financial relationships that could be construed as a potential conflict of interest.

Copyright © 2018 Fernández-Rodríguez, Velasco-Álvarez, Bonnet-Save and Ron-Angevin. This is an open-access article distributed under the terms of the Creative Commons Attribution License (CC BY). The use, distribution or reproduction in other forums is permitted, provided the original author(s) and the copyright owner are credited and that the original publication in this journal is cited, in accordance with accepted academic practice. No use, distribution or reproduction is permitted which does not comply with these terms.

frontiers in Neuroscience

ORIGINAL RESEARCH
published: 29 June 2018
doi: 10.3389/fnins.2018.00423

Assessing Command-Following and Communication With Vibro-Tactile P300 Brain-Computer Interface Tools in Patients With Unresponsive Wakefulness Syndrome

Christoph Guger[1,2], Rossella Spataro[3,4], Frederic Pellas[5], Brendan Z. Allison[6], Alexander Heilinger[1], Rupert Ortner[2], Woosang Cho[2], Ren Xu[1], Vincenzo La Bella[4], Günter Edlinger[1,2], Jitka Annen[7], Giorgio Mandalá[8], Camille Chatelle[7†] and Steven Laureys[7†]*

[1] Guger Technologies OG, Graz, Austria, [2] g.tec Medical Engineering GmbH, Schiedlberg, Austria, [3] IRCCS Centro Neurolesi Bonino Pulejo, Palermo, Italy, [4] ALS Clinical Research Center, BioNeC, University of Palermo, Palermo, Italy, [5] Post-ICU Neurorehabilitation Unit, University Hospital of Nîmes, Nîmes, France, [6] Department of Cognitive Science, University of California, San Diego, San Diego, CA, United States, [7] Coma Science Group, GIGA Consciousness, University of Liège, Liège, Belgium, [8] Rehabilitation Unit, Buccheri La Ferla Hospital, Palermo, Italy

OPEN ACCESS

Edited by:
Mikhail Lebedev, Duke University, United States

Reviewed by:
Ali Yadollahpour, Ahvaz Jundishapur University of Medical Sciences, Iran
Francesca Pistoia, University of L'Aquila, Italy
Sergio Bagnato, Fondazione Istituto G. Giglio di Cefalù, Italy

***Correspondence:**
Christoph Guger
guger@gtec.at

† Co-last authors.

Specialty section:
This article was submitted to Neural Technology, a section of the journal Frontiers in Neuroscience

Received: *12 March 2018*
Accepted: *04 June 2018*
Published: *29 June 2018*

Citation:
Guger C, Spataro R, Pellas F, Allison BZ, Heilinger A, Ortner R, Cho W, Xu R, La Bella V, Edlinger G, Annen J, Mandalá G, Chatelle C and Laureys S (2018) Assessing Command-Following and Communication With Vibro-Tactile P300 Brain-Computer Interface Tools in Patients With Unresponsive Wakefulness Syndrome. Front. Neurosci. 12:423. doi: 10.3389/fnins.2018.00423

Persons diagnosed with disorders of consciousness (DOC) typically suffer from motor disablities, and thus assessing their spared cognitive abilities can be difficult. Recent research from several groups has shown that non-invasive brain-computer interface (BCI) technology can provide assessments of these patients' cognitive function that can supplement information provided through conventional behavioral assessment methods. In rare cases, BCIs may provide a binary communication mechanism. Here, we present results from a vibrotactile BCI assessment aiming at detecting command-following and communication in 12 unresponsive wakefulness syndrome (UWS) patients. Two different paradigms were administered at least once for every patient: (i) VT2 with two vibro-tactile stimulators fixed on the patient's left and right wrists and (ii) VT3 with three vibro-tactile stimulators fixed on both wrists and on the back. The patients were instructed to mentally count either the stimuli on the left or right wrist, which may elicit a robust P300 for the target wrist only. The EEG data from −100 to +600 ms around each stimulus were extracted and sub-divided into 8 data segments. This data was classified with linear discriminant analysis (using a 10 × 10 cross validation) and used to calibrate a BCI to assess command following and YES/NO communication abilities. The grand average VT2 accuracy across all patients was 38.3%, and the VT3 accuracy was 26.3%. Two patients achieved VT3 accuracy ≥80% and went through communication testing. One of these patients answered 4 out of 5 questions correctly in session 1, whereas the other patient answered 6/10 and 7/10 questions correctly in sessions 2 and 4. In 6 other patients, the VT2 or VT3 accuracy was above the significance threshold of 23% for at least one run, while in 4 patients, the accuracy was always below this threshold. The

study highlights the importance of repeating EEG assessments to increase the chance of detecting command-following in patients with severe brain injury. Furthermore, the study shows that BCI technology can test command following in chronic UWS patients and can allow some of these patients to answer YES/NO questions.

Keywords: communication, unresponsive wakefulness syndrome, vegetative state, brain computer interface, evoked potentials, vibro-tactile P300

INTRODUCTION

Assessing consciousness and communication in persons with disorders of consciousness (DOC) is difficult. The current gold-standard is based on bedside observation of the patients' responses, but these patients may lack the ability to perform voluntary motor responses at the bedside. Standardized scales such as the Coma-Recovery-Scale-revised (CRS-R; Giacino et al., 2004) have been developed, but these tools are highly dependent on the patient's motor abilities. This dependence may prevent the detection of signs of consciousness or the possibility of communication in this population (Monti et al., 2010; Giacino et al., 2012; Risetti et al., 2013; Gibson et al., 2014; Ortner et al., 2017), and therefore also limit the diagnosis of some patients with locked in syndrome (LIS; i.e., paralyzed with remaining vertical eye movement control but conscious with preserved cognitive abilities; Patterson and Grabois, 1986).

Brain-computer interfaces (BCIs) were originally developed to establish a communication channel with LIS patients via brain activity alone, usually by measuring and analyzing the electroencephalographic (EEG) response for applications such as selecting letters (Wolpaw et al., 2002; Wolpaw and Wolpaw, 2012; Nam et al., 2018). Such BCIs have been validated with different types of EEG paradigms, including motor imagery (MI) (Guger et al., 2003; Acqualagna et al., 2016), steady-state visual evoked potentials (SSVEPs; Bin et al., 2009; Ahn et al., 2016) or P300 event-related potentials (ERPs; Guger et al., 2009, 2016; Lugo et al., 2014). The P300 may be elicited if an unlikely event occurs that is embedded in frequent events. P300 based-BCIs have been used widely due to several appealing features, including a short calibration time, robustness, and ease of use (Fazel-Rezai et al., 2012). Over the last decade, such BCIs have been developed using visual, auditory (Risetti et al., 2013; Rutkowski, 2016) or vibrotactile stimuli (Lugo et al., 2014; Gibson et al., 2016). A vibro-tactile P300 study with LIS patients showed that the BCI system can still extract information from the EEG, even if visual inspection of the averaged ERPs suggests this is impossible. This is because the EEG data from each single trial was analyzed using linear discriminate analysis (LDA), in contrast visual inspection of averaged ERPs (Lugo et al., 2014).

Vibro-tactile P300 testing has also been used with LIS/CLIS patients and healthy subjects, where the participant is asked to count a target (rare) tactile stimuli either on the right or left hand to answer YES/NO questions. Using this technique, healthy subjects without prior training achieved high accuracies and were able to communicate (Allison et al., 2017; Guger et al., 2017b). 12 LIS/CLIS patients achieved a mean accuracy of 76.6% in VT2 (vibro-tactile paradigm with 2 stimulators), 63.1% in VT3 (vibro-tactile paradigm with 3 stimulators), and 58.2% in MI modes after 1–2 training runs. 9 out of 12 LIS patients could communicate by using the vibro-tactile P300 paradigms (answering 8 out of 10 questions correctly on average) and 3 out of 12 could communicate with the MI paradigm (answering 4.7 out of 5 questions correctly on average). In previous work using vibrotactile P300 BCIs for LIS patients, 6 LIS patients attained a mean accuracy of 80% in a paradigm with 2 tactile stimulators (left and right hand) and 55.3% in a paradigm with 3 tactile stimulators (left and right hand, neck) (Lugo et al., 2014). In both paradigms, chance accuracy was 12.5%, and the results were statistically significant. Recently, a system using functional near infrared spectroscopy was used for communication with CLIS patients and patients entering CLIS in more than 40 sessions (Chaudhary et al., 2017).

BCIs are also of growing interest for the DOC population, as they may provide an online assessment of the patient's cognitive abilities when motor impairments prevent the patient from showing voluntary signs of consciousness at bedside (Guger et al., 2014, 2017a; Real et al., 2016; Chennu et al., 2017; Nam et al., 2018). This approach could be easily implemented in a clinical setting to supplement the behavioral diagnosis and decrease potential misdiagnosis, as shown in previous studies using active tasks (e.g., Monti et al., 2010; Cruse et al., 2011).

The current study uses vibro-tactile P300 tests with 2 (VT2) and 3 (VT3) tactors for the assessment of remaining brain response (classic oddball paradigm using 2 tactors) and command following with binary communication testing (active task using 3 tactors). The BCI classification accuracy and evoked potentials from the VT2 and VT3 paradigms are evaluated. We also aimed to assess the necessary classification accuracy for communication in unresponsive wakefulness syndrome (UWS) patients, and we investigated whether repeated assessments yield better results.

METHODS

Participants

Patients were recruited by the University of Palermo, Italy. Inclusion criteria were age >18 years and clinical diagnosis of UWS (awakening without any volitional response at the bedside examination), irrespective of delay from disease onset and etiology.

The clinical definition of UWS was based on the repetitive administration (at least five times) of the Italian version of the CRS-R scale (Lombardi et al., 2007). The patients had no history

of neurologic disorder prior to coma. The mechanical ventilation did not interfere with the EEG recordings because we used active EEG electrodes.

Ethical approval was available from the Ethical Committee Palermo from the University Hospital of Palermo. Written informed consent was obtained from a legal guardian. Measurements were performed by a medical doctor who was trained on the proper handling of the system.

A convenience sample of 12 patients enrolled in the study (12 UWS, 9 men; median age: 53.3 years, range: 19–91 years; time since injury: 1–28 months, median: 2 months) as shown in **Table 1**. The etiologies of the patients were: traumatic brain injury ($n = 4$), stroke ($n = 2$), hypoxia-ischemia brain injury ($n = 4$), subdural hematoma ($n = 1$), and meningoencephalitis ($n = 1$).

Materials

All data were acquired with the mindBEAGLE prototype (g.tec Guger Technologies OG, Austria). The system consists of active gel-based EEG electrodes connected to a biosignal amplifier (g.USBamp, g.tec) with 24 Bit resolution and a high oversampling rate to increase the signal to noise ratio of the data. The amplifier sends the EEG data via USB at 256 Hz to a computer system that runs the experimental paradigm in real-time. The system also presents the EEG data on a monitor for quality inspection, stores the data in floating point format for off-line processing, performs the real-time signal processing and manages all stimulus presentation.

The acquired EEG data are bandpass filtered between 0.1 and 30 Hz to remove baseline shifts and eliminate most EMG artifacts. The EEG electrodes used for the experiments were positioned at sites Fz, C3, Cz, C4, CP1, CPz, CP2, and Pz according to the extended International 10–20 System. The reference electrode was fixed on the right earlobe and the ground electrode was mounted on the forehead.

Behavioral Assessment

The CRS-R was administered after careful neurologic examination by trained neurologists (R.S., V.L.B.), about 30 min before the first BCI session. Patients were assessed when free of sedation for at least 24 h. **Table 1** presents the resulting scores.

BCI Assessment

Three paradigms were used: VT2 and VT3 assessment, and VT3 communication according the experimental procedure shown in **Figure 1**. VT2 uses two vibro-tactile stimulators that are fixed on the left and right wrists. Before each sequence of stimulations begins, the system verbally instructs the patient to silently count the stimuli on the target wrist. In the VT2 and VT3 assessment paradigms, the target wrist is selected pseudo-randomly, and each run has an equal number of left and right targets (15 each).

During stimulus presentation, the BCI system activates the vibro-tactile stimulation for 100 ms on the left or right wrist (also chosen pseudo-randomly), but the non-target wrist is stimulated more often (87.5%) than the target wrist to generate an oddball paradigm. The vibro-tactile stimulators are 3 cm long and 5 mm wide, and operate at 80 Hz. This paradigm is intended to generate a vibro-tactile P300 and other ERPs only when the target wrist is stimulated. In both VT3 modes, one additional stimulator is fixed on the back or shoulder as a distractor, which is active in 75% of stimulations. The other two stimulators are again fixed on the right and left wrist and each receive 12.5% of the stimuli. In all three modes, the BCI system instructs the subject to count the stimulations on either the left or right hand, which may elicit a P300 to the target hand. Each subject received 15 target stimulations and 7×15 non-target stimulations prior to a brief pause as an instruction to focus on the upcoming target wrist. During both the VT2 and VT3 assessment paradigms, each run lasted about 2.5 min. Each VT2 run contained 30 groups of eight stimuli (120 left, 120 right). Each VT3 run contains 30 groups of 8 stimuli (30 left, 30 right, 180 distractors).

TABLE 1 | Overview of patients participating in this study.

Clinical state and #	Age range (years)	Etiology	Disease duration at first session (months)	Mechanical ventilation	CRS-R score on day of first BCI assessment
UWS1	18-20	TBI	28	No	6
UWS2	18-20	TBI	9	No	6
UWS3	31-40	TBI	2	No	3
UWS4	31-40	HBI	9	No	6
UWS5	91-100	Stroke	1	No	6
UWS6	81-90	SDH	2	Yes	5
UWS7	61-70	ME	2	No	6
UWS8	51-60	HBI	1	Yes	4
UWS9	61-70	HBI	2	Yes	6
UWS10	71-80	HBI	1	Yes	5
UWS11	71-80	Stroke	1	No	6
UWS12	21-20	TBI	2	No	8

TBI, Traumatic Brain Injury; HBI, Hypoxia-Ischemia Brain Injury; SDH, Subdural Hematoma; ME, Meningoencefalitis; BT, Brain Trauma; UWS, Unresponsive Wakefulness Syndrome; The age is given as a range to avoid indirectly identifiable patient data.

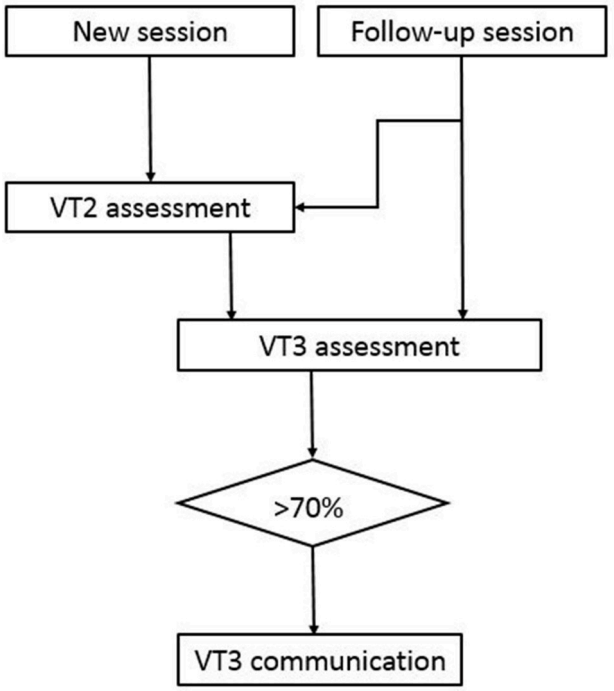

FIGURE 1 | Experimental procedure. The first session for a new patient always starts with a VT2 assessment followed by a VT3 assessment. If the accuracy is above 70%, then VT3 communication was tested. Some follow-up sessions also began with VT2 assessment, whereas the other follow-up sessions instead began with a VT3 assessment to assess communication quickly.

The VT2 paradigm is usually performed first as an assessment run to see if the patient responds to the paradigm. The system will create ERPs from the assessment run and will also calculate the classification accuracy to show how well the target ERPs can be separated from the non-target ERPs. Then, a VT3 assessment run is performed to assess whether the patient is following commands in a paradigm with a distractor stimulus, and ERPs and the classification accuracies are calculated. These data are also used to calibrate the system on the subject specific EEG data. When the clinical conditions (i.e., alertness, heart rate, need of suction etc.) allowed it, we repeated the VT3 assessment only, in order to avoid prolonged sessions. All patients were assessed once in a day, except UWS 1, who was available for 4 sessions in a period of 2 months. This calibration information is used in further communication runs that allow the patient to say either YES (by counting the stimuli on the right hand) or NO (by counting the stimuli on the left hand). To limit the total recording time, we decided to conduct a VT3 communication run if a patient's accuracy was >70% in an assessment run (well above the 95% confidence interval with a binomial test that yields about 23% accuracy).

In the VT3 communication paradigm, the operator asks the subject a question just before each run begins, and the subject can answer either YES or NO by counting the stimuli on either the left or right hand. Thus, unlike the other two paradigms, the subject chose which wrist was the target. Ten customized and standardized questions to which the answers are known were used to evaluate system accuracy (e.g., Is your name Maria?; Is your son named Ricardo?,…). In the VT3 communication paradigm, one question can be answered after 120 stimuli, which requires 38 s. The system only selects YES or NO if the result is significant, and provides an "undetermined" response otherwise. The examiner then verbally repeated the answer displayed on the monitor.

Data Analysis and Classification

Across all paradigms, we extracted data epochs of −100–600 ms around each stimulus and rejected trials in which the amplitude of the EEG signal exceeds ±100 μV. Each of these 700 ms data epochs was then sub-divided into 8 data segments of equal duration. We then created sub-averages for each of these data segments. Then, the data were classified using linear discriminant analysis (LDA), resulting in a classification accuracy ranging from 0 to 100% that describes how well the target vs. non-target data can be separated. The ratio of target to non-target stimuli is 1:7, resulting in a chance accuracy of 12.5%. (The classifier does not group the seven non-target stimuli together for classification purposes nor use a priori information about the target to improve accuracy.) In VT2 and VT3 mode, the data were randomly shuffled such that 50% of the data were used for training and 50% were used for testing to have independent training and testing data. This procedure was repeated 10 times.

A discriminable response was defined as a classification accuracy above 23% for VT2 and VT3 assessment (i.e., suggesting target vs. non-target ERPs could be discriminated). 23% is the 95% confidence interval tested with a binomial test. For VT3 communication testing, we defined communication as reliable if at least 70% of the questions were correctly answered.

In addition, we calculated the difference in ERPs between target and non-target stimuli during the VT2 and VT3 using a Kruskal-Wallis significance test using $p<.05$. Areas with significant differences between targets and non-targets are shaded green in **Figure 2**.

RESULTS

Behavioral Assessment

All the patients had at least 4 CRS-Rs within about 1 month (Median = 14.5 days, range = 7–34 days) before the first BCI study (8 patients had 5 CRS-Rs). The diagnosis was UWS before starting the study and remained the same for each BCI session.

Three patients could be assessed again a few weeks to a year post assessment. Two patients remained in a UWS after 1 year (UWS1 and UWS3), whereas one recovered signs of consciousness 15 days after the study (UWS12; visual fixation).

BCI Assessment

Eleven patients were seen for one or two runs in 1 day. The remaining patient (UWS1) was assessed for 2 runs per days on 4 different days (time between first and last day: 4 months).

The VT2/VT3 assessment and VT3 communication data are reported in **Table 2**. **Figure 2** presents the ERPs from all patients over three central electrode sites, as well as the BCI classification

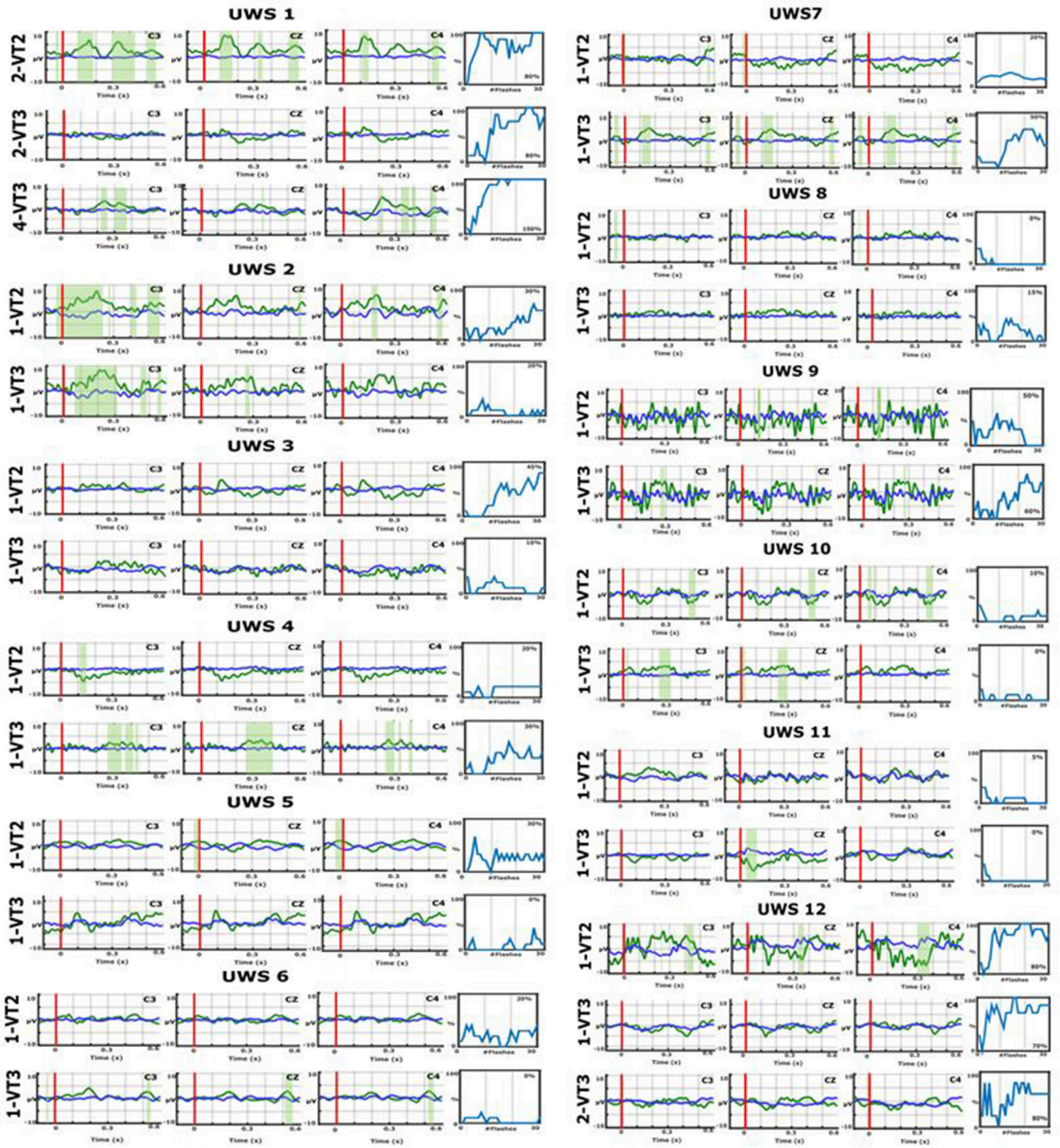

FIGURE 2 | Event-related potentials (ERPs) over electrode sites C3, Cz, and C4 and BCI accuracies for VT2 and VT3 runs from all participants. The x-axes of the ERP plots present the time relative to stimulus onset, and the vertical red lines show stimulus onset at 0 ms. The blue lines reflect non-target ERPs, the green lines show target ERPs, and the green shaded areas show significant differences between these two traces. For example, in UWS1, the green shaded areas are most pronounced in the VT2 task, particularly over C3.The accuracy plots to the right of these ERPs show the resulting BCI accuracy. In each plot, the y-axis shows the % accuracy and the x-axis shows the number of trial groups (groups of eight stimuli) that were used to derive that accuracy.

accuracies. In the first session, a VT2 run was always performed to check the patient's ERPs elicited by the oddball task, then the VT3 run was performed to confirm active command-following ability (i.e., counting the target). In subsequent sessions, the VT2 run was sometimes skipped to go directly to VT3 assessment and communication testing. Each of the 12 UWS patients performed

TABLE 2 | Median classification accuracies are shown for VT2 and VT3 assessment sessions for 12 UWS patients.

Patient	Session #	VT2 assessment accuracy 4 instructions [%]	VT3 assessment accuracy 4 instructions [%]	VT3 Communication
UWS1	1	100	0	-
		-	40	-
	2	25	20	-
		80	80	6/10 (4 wrong)
	3	60	0	-
		-	5	-
	4	-	100	7/10 (3 wrong)
UWS2	1	30	20	-
		-	0	-
UWS3	1	45	0	-
		-	10	-
UWS4	1	20	20	-
		-	30	-
UWS5	1	30	0	-
UWS6	1	20	0	-
UWS7	1	20	50	-
		-	0	-
UWS8	1	0	15	-
UWS9	1	50	30	-
		-	60	-
UWS10	1	10	0	-
UWS11	1	5	0	-
UWS12	1	80	70	-
		-	80	4/5 (1 undetermined)
Median		38.3	26.3	17/25 (7 wrong/1 undetermined)

VT3 communication accuracy is presented as the number of questions answered correctly out of either 5 or 10 questions. For example, 4/ 1 /5 means that 4 answers out of 5 questions were given correctly and 1 answer was either undetermined or wrong. Runs (recordings within a session) are shown in different rows for a session (recordings on one day). A "-" shows that the paradigm or communication was not performed. The VT2 and VT3 assessment runs each last 2.5 min (4 instructions with 15 targets each). In VT3 communication, it takes 38 s to answer 1 question. ERPs of segments shaded in gray are shown in ***Figure 2****.*

the VT2 and VT3 assessments at least once (between 1 and 4 runs for VT2, 1–7 runs for VT3).

Using VT2, target vs. nontarget ERPs could be discriminated effectively in seven out of the 12 patients. Using VT3, 5 out of the 12 patients showed ERP differences suggesting command following. All the patients who showed performance above chance during VT3 assessment had a discriminable response to VT2.

Two patients (UWS1 and UWS12) reached a VT3 assessment accuracy >70%, allowing for communication testing. UWS1 reached 80% in the second session, run 2, and was able to answer 6 out of 10 questions correctly (60%). In session 4, run 1, UWS1 achieved 100% assessment accuracy and answered 7 out of 10 questions correctly (70%; the remaining answers were incorrect). UWS12 reached a VT3 accuracy of 80% in run 2 and could answer 4 out of 5 questions correctly (80%; 1 question was undetermined).

When looking at the ERPs of the patients who communicated (UWS1 and UWS12), UWS1 showed significant ERP differences for VT2 with an assessment accuracy of 80% in session 2 (see **Figure 2**). In the same session, the VT3 ERPs did not show significant differences in visual inspection, but the assessment accuracy was also 80%. In session 4, the VT3 assessment accuracy reached 100%, and the ERP showed significant differences.

In UWS12, the VT2 assessment accuracy reached 80% and a significant difference in the ERP could be observed. In VT3 run 1, the assessment accuracy was 70% and there was no clear difference between target and non-target ERPs based on visual inspection. In run 2, the VT3 accuracy increases to 80% and the ERP showed a difference.

Some additional patients showed differences in the ERPs. UWS7 showed no clear target vs. non-target differences for VT2, but showed stronger differences for VT3. In VT2 run 1, the mean accuracy was only 20%, but was 50% for the first VT3 run. Therefore, the VT3 assessment run was repeated, but accuracy declined and therefore communication was not tested. UWS4 showed a P300 response for the VT3 paradigm and achieved 30% accuracy. All other patients did not reach the significance threshold of 23% during the VT3 testing. Patient UWS2 showed a significant ERP on channel C3 in VT2 and VT3 mode, but the classification accuracy was not high enough to test communication. The same was true for UWS10. The other patients did not show significant differences in the ERPs.

DISCUSSION

The current study employed vibrotactile paradigms designed to elicit the P300 and other ERPs to evaluate covert command following and communication in UWS patients.

We reported that 41% of our patients showed signs of covert command following using the VT3 paradigm. In addition, 2 (out of 12; 16%) of the patients could establish reliable communication with the VT3 paradigm.

In the case of UWS1, 2 sessions were necessary to achieve a VT3 classification accuracy >70% to test for communication. In session 3, the accuracy decreased, which might suggest fluctuation in the patient's ability to follow commands, although the time in between sessions (i.e., about 2 weeks after session 2) prevents us from making strong assumptions. Finally, in session 4, the patient achieved a classification accuracy of 100%, allowing him to answer 7 out of 10 questions correctly. Interestingly, 88 days elapsed between sessions 1 and 4, and the patient immediately reached 100% in the last session in VT3 and could communicate. This result further highlights that performance can vary across sessions, and thus it is important quickly calibrate the system, assess the patient and proceed directly to communication mode if possible.

In the case of UWS12, communication could be tested after only 2 VT3 runs within a single session, leading to 4/5 correctly answered questions.

Our data appear to contradict what have been reported in previous literature on covert consciousness in DOC. We observe a higher number of patient showing signs of covert command following (41 vs. 17–20%). This could be due to the fact that we repeated the assessment, allowing us to take into account, at least partially, fluctuations in vigilance (Piarulli et al., 2016; Wannez et al., 2017). However, the 2 patients who could communicate both had a traumatic brain injury, consistent with previous literature on the effect of the etiology in covert cognitive abilities in severely brain injured population (Cruse et al., 2012). Further research should explore the relationships between BCI accuracy fluctuations and etiology, as well as exact diagnosis, time since injury and other factors.

The high variability across runs (as well as sessions) in the results highlights a significant challenge associated with this patient group. Patient UWS1 reached 80% VT3 assessment accuracy and could successfully communicate. In the next run, the accuracy was only 0%. UWS1 achieved 100% VT2 accuracy in the first run, which showed that he was able to execute the task correctly at that time, but the accuracy dropped to 0% in the subsequent VT3 test. In a second assessment performed 2 weeks later, he repeatedly achieved accuracy scores > 80%. Since UWS patients in Italy are admitted to intensive rehabilitation, the detection of command following in this clinically unresponsive patient did not directly affect the care plan.

If this neurophysiological finding had suggested a different prognostic scenario for this patient, it would not have been not correlated with outcome at 1 year, as the patient was still in the UWS. We cannot determine whether changes in medication or other treatment might have led to a different outcome, which is an interesting question for further study.

However, UWS12, who could communicate on the second run, started showing signs of consciousness 15 days after the BCI session, suggestive of MCS minus (i.e., visual fixation). Therefore, our data not only highlight the importance of repeated assessments to increase our understanding about the patient's profile and abilities; the data also show the importance of more research on the prognostic value of such tools in the clinical setting.

Table 3 summarizes results for UWS patients from the current study and from a previously published study on LIS/CLIS and healthy subjects (Guger et al., 2017b). Healthy subjects attained VT2 accuracies of 94% and VT3 accuracies of 88% (both in assessment mode) and a VT3 communication accuracy of 80%. With LIS and CLIS patients, we showed that 9 out of 12 are able to establish communication with VT3. Two of 12 UWS patients were able to communicate and the mean VT3 accuracy was 43.9%. LIS patients had a higher VT2 and VT3 accuracy when they communicated, but lower accuracies than healthy subjects. The CLIS patients that communicated attained VT3 accuracy higher than UWS patients. Among patients that could not communicate, VT2 and VT3 results were worst for UWS patients.

With healthy subjects and LIS/CLIS patients, the VT3 assessment paradigm appeared to be more difficult to perform than the VT2 assessment paradigm. Therefore, we suggest starting with VT2 to familiarize the patient with the easier approach, and then moving to VT3 within the limited time available.

Limitations

This study would have benefited from additional patients. The study presents 12 patients with UWS resulting from different etiologies. The results showed that, regardless of the cause of the DOC, a considerable proportion of clinically unresponsive patients might show neurophysiological signs of command following. Due to the limited number of patients with each etiology, we cannot currently make strong claims about the relationship between etiology and command following. Further studies will explore this issue with more patients with different etiologies.

Similarly, we were only able to collect a limited amount of data from each patient. Communication was only tested if the accuracy was >70%, and communication was only tested in 1 or 2 sessions. In a previous study, the same VT2 and VT3 paradigms were used with 12 LIS/CLIS patients, and 9 of them could establish communication above an assessment accuracy threshold of 60% (Guger et al., 2017b). In addition, several patients were only assessed once. Hence, future work will assess the prospect of testing communication with lower assessment accuracies and collect data from more sessions. Training effects are also difficult to assess because UWS patients

TABLE 3 | VT2 and VT3 assessment accuracies, and VT3 communication accuracies, from healthy subjects and different patient groups (UWS, LIS, CLIS) from this study and a previous study (Guger et al., 2017a).

Patient group	# Subjects	VT2 Assess [%]	VT3 Assess [%]	VT3 Comm. [%]
Healthy	3	94	88	80
UWS	12	38.8	26.3	
UWS that communicated	2	69.0	43.9	75
UWS that did not communicate	10	23.0	15.7	-
LIS/CLIS	12	76.6	63.1	-
LIS that communicated	9	85.4	81.8	80
CLIS that communicated	2	60	85	80
LIS that did not communicate	3	56.7	24	-
CLIS that did not communicate	1	40	30	-

show fluctuations of awareness, and it is difficult to maintain a training schedule or study many sessions.

In UWS1, the first session was not promising, but sessions 2 and 4 showed that communication can be established. Furthermore, the communication testing could be improved by instructing the patient to say YES or NO to confirm that the patient understood the task correctly. In addition, more work should focus on defining the best threshold for assessing significance in such BCI systems. The CRS-R was done about 30 min before the VT2/VT3 testing and it lasts about 20 min, which might cause fatigue. Additional behavioral assessments in a shorter time-window, together with outcome data, may provide additional data to corroborate results from EEG assessments.

Another possible limitation is the lack of adequate somatosensory function. We did not test each patient's somatosensory capability, and thus cannot rule out the possibility that one or more patients would have exhibited better results with an auditory-based or motor imagery paradigm. The overall system used in this study can work with auditory evoked potentials and auditory-based motor imagery paradigms, but these were not tested here due to the very limited time available with each patient.

SUMMARY

Vibro-tactile P300 assessment using BCI technology provides a useful way to quickly test command following and establish YES/NO communication with some DOC patients. The paradigm provides a quick assessment that can be easily used to monitor fluctuations and to find the optimal times to communicate with these patients.

AUTHOR CONTRIBUTIONS

RS, GM, and VL recorded the data. CG, AH, RO, WC, RX, and GE contributed to software development and/or software-based data analysis. CG, RS, VL, BA, JA, CC, and SL contributed to study design, scientific protocols, and review/analysis of results. RS, BA, and CG were primarily responsible for writing, and all authors discussed the results and implications.

FUNDING

The research was funded by EC H2020 project ComAware, project number 696535.

REFERENCES

Acqualagna, L., Botrel, L., Vidaurre, C., Kübler, A., and Blankertz, B. (2016). Large-scale assessment of a fully automatic co-adaptive motor imagery-based brain computer interface. *PLoS ONE* 11:e0148886. doi: 10.1371/journal.pone.0148886

Ahn, S., Kim, K., and Jun, S. C. (2016). Steady-state somatosensory evoked potential for brain-computer interface-present and future. *Front. Hum. Neurosci.* 9:716. doi: 10.3389/fnhum.2015.00716

Allison, B. Z., Cho, W., Ortner, R., Heilinger, A., Edlinger, G., and Guger, C. (2017). "Validation of a brain-computer interface (BCI) system designed for patients with disorders of consciousness (DOC), regular and sham testing with healthy participants," in *International Conference on Augmented Cognition* (Cham: Springer), 253–265.

Bin, G., Gao, X., Yan, Z., Hong, B., and Gao, S. (2009). An online multi-channel SSVEP-based brain-computer interface using a canonical correlation analysis method. *J Neural Eng.* 6:046002. doi: 10.1088/1741-2560/6/4/046002

Chaudhary, U., Xia, B., Silvoni, S., Cohen, L. G., and Birbaumer, N. (2017). Brain-computer interface-based communication in the completely locked-in state. *PLoS Biol.* 15:e1002593. doi: 10.1371/journal.pbio.1002593

Chennu, S., Annen, J., Wannez, S., Thibaut, A., Chatelle, C., Cassol, H., et al. (2017). Brain networks predict metabolism, diagnosis and prognosis at the bedside in disorders of consciousness. *Brain* 140, 2120–2132. doi: 10.1093/brain/awx163

Cruse, D., Chennu, S., Chatelle, C., Bekinschtein, T. A., Fernández-Espejo, D., Pickard, J. D., et al. (2011). Bedside detection of awareness in the vegetative state, a cohort study. *Lancet* 378, 2088–2094. doi: 10.1016/S0140-6736(11)61224-5

Cruse, D., Chennu, S., Chatelle, C., Fernández-Espejo, D., Bekinschtein, T. A., Pickard, J. D., Laureys, S., et al. (2012). Relationship between etiology and covert cognition in the minimally conscious state. *Neurology* 78, 816–822. doi: 10.1212/WNL.0b013e31824 9f764

Fazel-Rezai, R., Allison, B. Z., Sellers, E., Guger, C., Kleih, S., and Kübler, A. (2012). P300 brain computer interfaces, Current challenges and future directions. *Front. Neuroeng.* 5:14. doi: 10.3389/fneng.2012.00014

Giacino, J. T., Fins, J. J., Laureys, S., and Schiff, N. D. (2012). Disorders of consciousness after acquired brain injury, the state of the science. *Nat. Rev.* 10, 99–114. doi: 10.1038/nrneurol.2013.279

Giacino, J. T., Kalmar, K., and Whyte, J. (2004). The JFK coma recovery scale-revised, measurement characteristics and diagnostic utility. *Arch. Phys. Med. Rehabil.* 85, 2020–2029. doi: 10.1016/j.apmr.2004. 02.033

Gibson, R. M., Chennu, S., Fernández-Espejo, D., Naci, L., Owen, A. M., and Cruse, D. (2016). Somatosensory attention identifies both overt and covert awareness in disorders of consciousness. *Ann. Neurol.* 80, 412–423. doi: 10.1002/ana.24726

Gibson, R. M., Fernández-Espejo, D., Gonzalez-Lara, L., Kwan, B. Y., Lee, D. H., Owen, A. M., et al. (2014). Multiple tasks and neuroimaging modalities increase the likelihood of detecting covert awareness in patients with disorders of consciousness. *Front. Hum. Neurosci.* 8:950, doi: 10.3389/fnhum. 2014.00950

Guger, C., Coyle, D., Mattia, D., De Lucia, M., Hochberg, L., Edlow, B., et al. (2017a). "Trends in BCI Research I, Brain-computer interfaces for assessment of patients with locked-in syndrome or disorders of consciousness," in Brain-Computer Interface Research, eds C. Guger, M. Lebedev, and B. Allison, A *State*-of-the-art *Summary* 6, (Cham: Springer), 105–125.

Guger, C., Daban, S., Sellers, E., Hollander, C., Krausz, G., Carabalona, R., et al. (2009). How many people are able to control a P300-based brain-computer interface (BCI)? *Neurosci. Lett.* 462, 94–98. doi: 10.1016/j.neulet. 2009.06.045

Guger, C., Edlinger, G., Harkam, W., Niedermayer, I., and Pfurtscheller, G. (2003). How many people are able to operate an EEG-based brain-computer interface (BCI)? *IEEE Trans. Neural Syst. Rehabil. Eng.* 11, 145–147. doi: 10.1109/TNSRE.2003.814481

Guger, C., Ortner, R., and Allison, B. Z. (2016). "A comparison of face speller approaches for P300 BCIs," in *IEEE SMC* (Budapest).

Guger, C., Sorger, B., Noirhomme, Q., Naci, L., Monti, M. M., Real, R., et al. (2014). "Brain-computer interfaces for assessment and communication in disorders of consciousness," in *Emerging Theory and Practice in Neuroprosthetics*, eds R. N. Ganesh, and Y. Gui (IGI Global), 181–214. doi: 10.4018/978-1-4666-6094-6.ch010

Guger, C., Spataro, R., Allison, B. Z., Heilinger, A., Ortner, R., Cho, W., et al. (2017b). Complete locked-in and locked-in patients: command following assessment and communication with vibro-tactile P300 and motor imagery brain-computer interface tools. *Front Neurosci.* 11:251. doi: 10.3389/fnins.2017.00251

Lombardi, F., Gatta, G., Sacco, S., Muratori, A., and Carolei, A. (2007). The Italian version of the Coma Recovery Scale-Revised (CRS-R). *Funct. Neurol.* 22, 47–61.

Lugo, Z. R., Rodriguez, J., Lechner, A., Ortner, R., Gantner, I. S., Kübler, A., et al. (2014). A vibrotactile P300-based BCI for consciousness detection and communication. *Clin. EEG Neurosci.* 45, 14–21. doi: 10.1177/1550059413505533

Monti, M. M., Vanhaudenhuyse, A., Coleman, M. R., Boly, M., Pickard, J. D., Tshibanda, L., et al. (2010). Willful modulation of brain activity in disorders of consciousness. *New Engl. J.* Med. 362, 579–589. doi: 10.1056/NEJMoa0905370

Nam, C. S., Nijholt, A., and Lotte, F. (2018). *Brain–Computer Interfaces Handbook, Technological and Theoretical Advances*. CRC Press.

Ortner, R., Allison, B. Z., Heilinger, A., Sabathiel, N., and Guger, C. (2017). Assessment of and communication for persons with disorders of consciousness. *J. Vis. Exp*. 126:53639. doi: 10.3791/53639

Patterson, J. R., and Grabois, M. (1986). Locked-in syndrome, a review of 139 cases. *Stroke*, 17, 758–764. doi: 10.1161/01.STR.17.4.758

Piarulli, A., Bergamasco, M., Thibaut, A., Cologan, V., Gosseries, O., and Laureys, S. (2016). EEG ultradian rhythmicity differences in disorders of consciousness during wakefulness. *J. Neurol*. 263, 1746–1760. doi: 10.1007/s00415-016-8196-y

Real, R. G. L., Veser, S., Erlbeck, H., Risetti, M., Vogel, D., Müller, F., et al. (2016). Information processing in patients in vegetative and minimally conscious states. *Clin. Neurophysiol.* 127, 1395–1402. doi: 10.1016/j.clinph.2015.07.020

Risetti, M., Formisano, R., Toppi, J., Quitadamo, L. R., Bianchi, L., Astolfi, L., et al. (2013). On ERPs detection in disorders of consciousness rehabilitation. *Front. Hum. Neurosci*. 7:775. doi: 10.3389/fnhum.2013.00775

Rutkowski, T. M. (2016). Robotic and virtual reality BCIs using spatial tactile and auditory oddball paradigms. *Front. Neurorobot*. 10:20. doi: 10.3389/fnbot.2016.00020

Wannez, S., Heine, L., Thonnard, M., Gosseries, O., and Laureys, S. (2017). The repetition of behavioral assessments in diagnosis of disorders of consciousness. *Ann. Neurol*. 81, 883–889, doi: 10.1002/ana.24962

Wolpaw, J. R., Birbaumer, N., McFarland, D. J., Pfurtscheller, G., and Vaughan, T. M. (2002). Brain-computer interfaces for communication and control. *Clin. Neurophysiol*. 113, 767–791. doi: 10.1016/S1388-2457(02)00057-3

Wolpaw, J., and Wolpaw, E. W. (2012). *Brain-Computer Interfaces, Principles and Practice*. Oxford, USA: Oxford University Publishing.

Conflict of Interest Statement: CG, AH, RX, and GE are employed by Guger Technologies OG, which is the company that built the mindBEAGLE system. CG, RO, WC, and GE are employed by g.tec medical engineering GmbH.

The remaining authors declare that the research was conducted in the absence of any commercial or financial relationships that could be construed as a potential conflict of interest.

The handling Editor declared a past co-authorship with the authors CG and BA.

Copyright © 2018 Guger, Spataro, Pellas, Allison, Heilinger, Ortner, Cho, Xu, La Bella, Edlinger, Annen, Mandalá, Chatelle and Laureys. This is an open-access article distributed under the terms of the Creative Commons Attribution License (CC BY). The use, distribution or reproduction in other forums is permitted, provided the original author(s) and the copyright owner(s) are credited and that the original publication in this journal is cited, in accordance with accepted academic practice. No use, distribution or reproduction is permitted which does not comply with these terms.

frontiers in Neuroscience

ORIGINAL RESEARCH
published: 11 July 2018
doi: 10.3389/fnins.2018.00478

Training in Use of Brain–Machine Interface-Controlled Robotic Hand Improves Accuracy Decoding Two Types of Hand Movements

Ryohei Fukuma[1,2†], Takufumi Yanagisawa[1,2,3,4,5†], Hiroshi Yokoi[6], Masayuki Hirata[1,3,5], Toshiki Yoshimine[1,5], Youichi Saitoh[1,7], Yukiyasu Kamitani[2,8] and Haruhiko Kishima[1]*

[1] Department of Neurosurgery, Graduate School of Medicine, Osaka University, Suita, Japan, [2] Department of Neuroinformatics, ATR Computational Neuroscience Laboratories, Seika-cho, Japan, [3] Center for Information and Neural Networks, National Institute of Information and Communications Technology, Suita, Japan, [4] Institute for Advanced Co-Creation Studies, Osaka University, Suita, Japan, [5] Endowed Research Department of Clinical Neuroengineering, Global Center for Medical Engineering and Informatics, Osaka University, Suita, Japan, [6] Department of Mechanical Engineering and Intelligent Systems, University of Electro-Communications, Chofu, Japan, [7] Department of Neuromodulation and Neurosurgery, Graduate School of Medicine, Osaka University, Suita, Japan, [8] Graduate School of Informatics, Kyoto University, Kyoto, Japan

OPEN ACCESS

Edited by:
Christoph Guger, Guger Technologies (Austria), Austria

Reviewed by:
Jose Luis Contreras-Vidal, University of Houston, United States
Ali Yadollahpour, Ahvaz Jundishapur University of Medical Sciences, Iran

***Correspondence:**
Takufumi Yanagisawa
tyanagisawa@nsurg.med.osaka-u.ac.jp

[†] These authors have contributed equally to this work.

Specialty section:
This article was submitted to Neural Technology, a section of the journal Frontiers in Neuroscience

Received: *26 January 2018*
Accepted: *25 June 2018*
Published: *11 July 2018*

Citation:
Fukuma R, Yanagisawa T, Yokoi H, Hirata M, Yoshimine T, Saitoh Y, Kamitani Y and Kishima H (2018) Training in Use of Brain–Machine Interface-Controlled Robotic Hand Improves Accuracy Decoding Two Types of Hand Movements. Front. Neurosci. 12:478. doi: 10.3389/fnins.2018.00478

Objective: Brain-machine interfaces (BMIs) are useful for inducing plastic changes in cortical representation. A BMI first decodes hand movements using cortical signals and then converts the decoded information into movements of a robotic hand. By using the BMI robotic hand, the cortical representation decoded by the BMI is modulated to improve decoding accuracy. We developed a BMI based on real-time magnetoencephalography (MEG) signals to control a robotic hand using decoded hand movements. Subjects were trained to use the BMI robotic hand freely for 10 min to evaluate plastic changes in the cortical representation due to the training.

Method: We trained nine young healthy subjects with normal motor function. In open-loop conditions, they were instructed to grasp or open their right hands during MEG recording. Time-averaged MEG signals were then used to train a real decoder to control the robotic arm in real time. Then, subjects were instructed to control the BMI-controlled robotic hand by moving their right hands for 10 min while watching the robot's movement. During this closed-loop session, subjects tried to improve their ability to control the robot. Finally, subjects performed the same offline task to compare cortical activities related to the hand movements. As a control, we used a random decoder trained by the MEG signals with shuffled movement labels. We performed the same experiments with the random decoder as a crossover trial. To evaluate the cortical representation, cortical currents were estimated using a source localization technique. Hand movements were also decoded by a support vector machine using the MEG signals during the offline task. The classification accuracy of the movements was compared among offline tasks.

Results: During the BMI training with the real decoder, the subjects succeeded in improving their accuracy in controlling the BMI robotic hand with correct rates of 0.28 ± 0.13 to 0.50 ± 0.11 ($p = 0.017$, $n = 8$, paired Student's t-test). Moreover, the classification accuracy of hand movements during the offline task was significantly increased after BMI training with the real decoder from 62.7 ± 6.5 to 70.0 ± 11.1%

($p = 0.022$, $n = 8$, $t_{(7)} = 2.93$, paired Student's *t*-test), whereas accuracy did not significantly change after BMI training with the random decoder from 63.0 ± 8.8 to 66.4 ± 9.0% ($p = 0.225$, $n = 8$, $t_{(7)} = 1.33$).

Conclusion: BMI training is a useful tool to train the cortical activity necessary for BMI control and to induce some plastic changes in the activity.

Keywords: brain-machine interface, robotic hand, magnetoencephalography, cortical plasticity, neurofeedback, closed-loop training, online decoding

INTRODUCTION

Brain–machine interfaces (BMIs) can reconstruct motor function in paralyzed subjects (Hochberg et al., 2006, 2012; Yanagisawa et al., 2012a; Collinger et al., 2013; Bouton et al., 2016) as well as induce functional alterations in cortical activity (Ganguly et al., 2011; Wander et al., 2013; Orsborn et al., 2014; Yanagisawa et al., 2016). A BMI works by first recording neural activity and then converting the recorded activity into control of some machine, such as a robotic hand or computer (Yanagisawa et al., 2009, 2011, 2012a,b; Nakanishi et al., 2013, 2014; Fukuma et al., 2015, 2016). Recent studies demonstrated that neurofeedback training using BMI induces plastic changes in neural activities in accordance with some functional alterations in the neural system. The neurofeedback of decoded information using functional magnetic resonance imaging (fMRI) demonstrated that the training induced alteration of cortical activities in accordance with alterations in cognition (Shibata et al., 2011, 2016; Amano et al., 2016; Ordikhani-Seyedlar et al., 2016). In addition, using a certain power spectrum of electroencephalographic signals, motor rehabilitation was improved in stroke patients (Shindo et al., 2011; Ramos-Murguialday et al., 2013). Moreover, we recently reported that BMI training to control a robotic hand induced plastic changes in the motor cortical representation of phantom limb pain patients and changed their pain in accordance with the plastic changes (Yanagisawa et al., 2016).

Such plastic changes are attributed to reinforcement learning with the BMI feedback (Watanabe et al., 2017). The closed-loop system with decoded information enables subjects to modulate the decoded information based on the feedback as a reward. Therefore, we expect that training to use a BMI based on the decoding information would improve the decoding accuracy better than training to use a BMI that is not based on the decoding information.

In this study, we demonstrate that BMIs based on magnetoencephalography (MEG) signals precisely decode hand movements in real time (Bradberry et al., 2009; Toda et al., 2011; Fukuma et al., 2015) and training to use the BMIs induces plastic changes in cortical activity of healthy subjects (Nishimura et al., 2013; Clancy et al., 2014; Luu et al., 2017), especially in the accuracy to decode hand movements.

SUBJECTS AND METHODS

Subjects

Nine young right-handed volunteers with normal neurological function (2 males and 7 females; mean age, 24.1 years; range, 21–30 years) participated in this study. The study adhered to the Declaration of Helsinki and was performed in accordance with protocols approved by the Ethics Committee of Osaka University Clinical Trial Center (no. 12107, UMIN000010180). All participants were informed of the purpose and possible consequences of this study, and written informed consent was obtained. We recruited subjects aged 20 years and older with normal neurological functioning. Inclusion criteria did not consider gender, race or any special experience.

MEG Recording

For the MEG recording, subjects were in the supine position with the head centered in the gantry. A projection screen in front of the face provided stimuli using a visual stimulus presentation system (Presentation; Neurobehavioral Systems, Albany, CA, USA) and a liquid crystal projector (LVP-HC6800; Mitsubishi Electric, Tokyo, Japan) (**Figure 1**). MEG signals were measured by a 160-channel whole-head MEG equipped with coaxial-type gradiometers (MEGvision NEO; Yokogawa Electric Corporation, Kanazawa, Japan) housed in a magnetically shielded room.

The MEG signals were sampled at 1,000 Hz with an online low-pass filter at 200 Hz and acquired online by FPGA DAQ boards (PXI-7854R; National Instruments, Austin, TX, USA) after passing through an optical isolation circuit. For the online control of the robotic hand, signals from 84 selected sensors (**Figure 1**) were used, except for one experiment in which 81 sensors were used for technical reasons. The same 84 sensors were used for offline analysis. Subjects were instructed to not move the head to avoid motion artifacts. A cushion was placed under the elbows to reduce motion artifacts.

Five head marker coils were attached to the subject's face before beginning the MEG recording, to provide the position and orientation of MEG sensors relative to the head (**Figure 1**). The positions of the five marker coils were measured to evaluate differences in the head position before and after each MEG recording. The maximum acceptable difference was 5 mm.

We also recorded electromyograms of the face and forearm to monitor muscle activities. Subjects were monitored by two video cameras to confirm their arousal.

Experimental Design

A crossover trial consisting of two experiments was performed with a washout period of more than 2 weeks. Each experiment consisted of three tasks, an offline task (pre-BMI), BMI training, and an offline task (post-BMI). For each training task, the participant controlled the robotic hand using two different

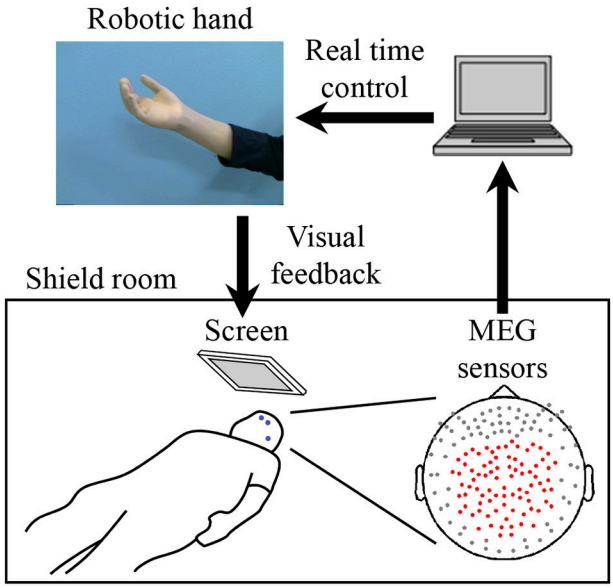

FIGURE 1 | System overview for training to use a robotic hand. MEG signals from 84 parietal sensors (shown with red dots) were acquired in real-time to decode performed movement. The robotic hand was controlled according to the results of the decoder. The participant received visual feedback of the robotic hand presented on the screen. Blue dots on the participant's face denote head marker coils used to determine position and orientation of MEG sensors relative to the head. Three marker coils (at the center of the forehead, above the left eyebrow, and on the left preauricular area) are shown.

decoders: a real decoder and a sham decoder. To balance which decoder type was selected first, the order for the real and sham decoders was randomized. Subjects were not informed about the order. Seven subjects participated in both experiments, one subject only participated in the experiment with the real decoder, and another only participated in the experiment with the sham decoder.

First, in the pre-BMI offline task, the subjects attempted to move their right hands (grasping and opening) at the presented times (Yanagisawa et al., 2012a) while MEG signals of the selected sensors were recorded (**Figure 1**). The subjects were visually instructed which movement to perform with the Japanese word for "grasp" or "open." After the instruction for movement type, four execution cues were given to the subject every 5.5 s. The execution cue was given both visually and aurally, and was presented 40 times for each movement type. The order of the requested movement type was randomized. We instructed the subjects to slightly move the hand once at the cued time, without moving other body parts.

The MEG signals from the selected sensors were recorded during the task (**Figure 1**) and then time-averaged using windows of 500 ms from −2,000 to 1,000 ms at 100-ms intervals, with respect to the time of the execution cues. The averaged signals were converted into *z*-scores using the mean and standard deviations estimated from the initial 50 s of the offline task. The acquired *z*-scores were used to construct the decoder to control the robotic hand (Fukuma et al., 2015).

During the BMI training task, the subjects were instructed to control the prosthetic hand in real time using the trained decoder. The screen fixed in front of the subject showed a picture of the robotic hand in real time as visual feedback (**Figure 1**). Subjects were instructed to control the robotic hand freely for 10 min to improve their ability to control it by moving their hands (see Supplementary Video 1). Just before starting the training, the experimenter changed the threshold for detecting movement onset, because the threshold estimated from the offline task was sometimes too low, resulting in the detection of movement onsets even during the resting state in the online task. The other parameters estimated from the offline task were not changed (Fukuma et al., 2016). The selected parameters were fixed for the 10 min of training. The post-BMI offline task was performed in the same way as the pre-BMI task, after the BMI training task.

The BMI training to control the robotic hand was performed as a randomized crossover trial consisting of two training sessions on different days. Each training session was performed with two different decoders to control the robotic hand: a real decoder and a sham decoder. Using the *z*-scored MEG sensor signals of the offline tasks to move the right hand, we constructed a decoder to infer hand movements at an arbitrary time, in order to control the robotic hand in real time (Fukuma et al., 2015). Each experiment was performed after more than 2 weeks had passed since the previous experiment. For the experiments with the real decoder and sham decoder, the order of the experiments was randomly assigned to the subjects. The experimenter was not blinded to the group allocation.

At the time of enrollment in this trial, we instructed the subjects to use their brain activity to control the robotic hand, but they were not informed of the decoder they used.

Decoder to Control the Prosthetic Hand

MATLAB R2013a (Mathworks, Natick, MA, USA) was used to calculate the decoding parameters and for online robotic hand control. First, MEG signals from the 84 selected sensors during the offline task were averaged in a 500-ms time window and converted to the *z*-score using the mean and standard deviations estimated from the initial 50 s of data during the offline task. The time-averaged MEG signals were calculated for the period from −2,000 to 1,000 ms at 100-ms intervals according to the execution cue.

The *z*-scored signals from the offline task were used to train the online decoder, which consisted of an onset detector and class decoder, to control the robotic hand online in the following BMI training task. The class decoder was trained at the peak classification accuracy of the offline task by the support vector machine (SVM). The onset detector was trained using the *z*-scored signals to differentiate time period of the hand movement from period of resting by SVM and Gaussian process regression (GPR). The details of the construction of the decoder are available in our previous reports (Fukuma et al., 2015; Yanagisawa et al., 2016).

Here, we constructed two types of online decoders depending on the data used to train the decoder. The real decoder was trained by the MEG signals of the offline task to move the

hand. The sham decoder was trained by the MEG signals of the same offline task with randomized types of movements (grasp or open).

Evaluation of Online BMI Control

The movements of subject's hand and robotic hand were evaluated from the video recording. We counted the subject's hand movements. Then, we evaluated the robotic hand movements within 1 s after each movement of the subject's hand. If the robotic hand moved into the same posture (grasp or open) as the subject's hand, we counted the movement as correctly controlled movement. The correct rate of BMI control was evaluated by the number of correctly controlled movements divided by the total number of hand movements. The correct rate was counted for 1 min at the beginning and at the end of the 10-min training.

Cortical Current Estimation by VBMEG

A polygonal model of the cortical surface was constructed based on structural MRI (T1-weighted; Signa HDxt Excite 3.0T; GE Healthcare UK Ltd., Buckinghamshire, UK) using the Freesurfer software (Martinos Center Software) (Dale et al., 1999). To align MEG data with individual MRI data, we scanned the three-dimensional facial surface and 50 points on the scalp of each participant (FastSCAN Cobra; Polhemus, Colchester, VT, USA). Three-dimensional facial surface data were superimposed on the anatomical facial surface provided by the MRI data. The positions of five marker coils before each recording were used to estimate cortical current with variational Bayesian multimodal encephalography (VBMEG) (Sato et al., 2004). VBMEG is free software for estimating cortical currents from MEG data (ATR Neural Information Analysis Laboratories, Kyoto, Japan; Cohen et al., 1991; Yoshioka et al., 2008). VBMEG estimated 4004 single current dipoles that were equidistantly distributed on and perpendicular to the cortical surface. An inverse filter was calculated to estimate the cortical current of each dipole from the selected 84 MEG sensor signals. The hyperparameters m0 and $\gamma 0$ were set to 100 and 10, respectively. The inverse filter was estimated by using MEG signals in all trials from 0 to 1000 ms in the offline task, with the baseline of the current variance estimated from the signals from −1,500 to −500 ms. The filter was then applied to sensor signals in each trial to calculate cortical currents.

Evaluation of Cortical Representation

We evaluated the cortical representation during the offline task using cortical current source estimation. First, VBMEG was used to estimate the cortical currents from the obtained MEG signals. Next, the estimated cortical currents were averaged using a 500-ms window starting from the execution cue and compared between two types of movements with a one-way analysis of variance (ANOVA) for each vertex. The F-value of the ANOVA was averaged for all subjects and color-coded on the normalized brain surface.

Evaluation of Classification Accuracy of Movement Types in the Offline Task

A nested cross-validation (Quian Quiroga and Panzeri, 2009) was performed with a linear support vector machine using the z-scores of the MEG signals from selected sensors (Fukuma et al., 2015) to evaluate the accuracy of classifying the performed movement types. The z-scores from 11 time windows (ranging from −500 to 500 ms at 100-ms intervals, with respect to the timing of the instruction to move) were concatenated to form a decoding feature. To calculate the classification accuracy, 10-fold cross-validation was applied. For each fold, the testing data set was classified with a decoder that was trained completely independently from the testing data set. To optimize hyperparameters of the decoder independently from the testing data set, another 10-fold cross-validation was applied to the training data set so that hyperparameters that achieved the highest classification accuracy within the training data set were selected. Finally, classification accuracies during the two offline tasks before and after the BMI training session were compared using a paired Student's t-test. Significance threshold for this t-test was set to 0.025, because this study employs two t-tests: one for training with a real decoder and another with a sham decoder (Bonferroni correction).

RESULTS

BMI Training With a Robotic Hand

During the 10-min BMI training, the accuracy in controlling the robotic hand was improved. The hand movements at an arbitrary timing were successfully detected and classified, with a correct rate of 0.28 ± 0.13 during the first 1 min of the BMI training with the real decoder. The correct rate increased significantly to 0.50 ± 0.11 for the final 1 min of the BMI training ($p = 0.017$, $n = 8$, paired Student's t-test). On the other hand, the correct rates during the BMI training with the random decoder were not significantly changed among the first 1 min and the last 1 min (0.51 ± 0.13 to 0.52 ± 0.10, $p = 0.92$, $n = 8$, paired Student's t-test). Notably, the increase of the correct rate during the BMI training with the real decoder was significantly larger than that during the BMI training with the random decoder (**Figure 2**). Also, it should be noted that correct rates during the first 1 min of the BMI training were not significantly different between the BMI trainings with the real decoder and the random decoder ($p = 0.11$, $n = 7$, paired Student's t-test).

BMI Training Changed the Cortical Representation of Hand Movements

After BMI training with the real decoder, the F-values increased in the contralateral sensorimotor cortex (**Figure 3A**), although the difference of the F-values (**Figure 3B**) between pre-BMI and post-BMI offline tasks was not statistically significant ($p > 0.05$, paired t-test, FDR corrected). After training with the random decoder, the F-value of the contralateral sensorimotor cortex did not increase (**Figures 3A,B**), although the subject was instructed in the same way as during the experiment with real decoder. These findings suggest that the BMI training with the real

decoder increased the discriminability of the cortical activity representing the hand movements.

BMI Training Altered Classification Accuracy of Hand Movements

We compared the accuracies for classifying the hand movements using the z-scored MEG signals at the selected sensors. **Figure 4** shows the classification accuracies of hand movements in the offline task before and after training task. The accuracy significantly increased after BMI training with the real decoder from 62.7 ± 6.5 to 70.0 ± 11.1% ($p = 0.022$, $n = 8$, $t_{(7)} = 2.93$, paired Student's t-test). In contrast, the BMI training with the random decoder did not increase the accuracy from 63.0 ± 8.8 to 66.4 ± 9.0% ($p = 0.225$, $n = 8$, $t_{(7)} = 1.33$). The BMI training with the real decoder significantly improved the cortical activity to decode the hand movements.

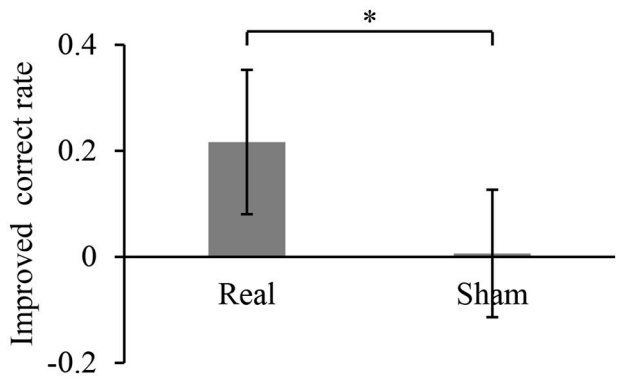

FIGURE 2 | Improved accuracy of controlling the robotic hand during online BMI training. The correct rate for robotic hand control was calculated for the first 1 min of the training and the last 1 min of the 10-min training. Each bar shows the averaged improvement of the correct rate for the training with real and sham decoder. Error bars are 95% confidence intervals of the improved correct rate. *$p < 0.05$ significant difference between two different decoders (unpaired Student's t-test).

DISCUSSION

Our findings demonstrated that MEG-based BMI training to control a robotic hand significantly improved the accuracy to control the robotic hand and induced significant changes of the cortical representation of hand movements in terms of classification accuracy. These results suggest that the BMI training will be useful for two important applications.

First, the non-invasive BMI training will be beneficial in training patients before applying invasive BMI. Previous studies demonstrated that the ability to control the BMI varies among patients (Yanagisawa et al., 2012a; Fukuma et al., 2016; Pandarinath et al., 2017). Before applying an invasive BMI for paralyzed patients, we need to evaluate their ability to control the BMI and to train them when the ability is poor. Our BMI training succeeded in improving the accuracy of controlling the BMI with improved cortical activities, which are also used for invasive BMI. Therefore, the proposed MEG-based BMI training will be beneficial for preoperative evaluation of the invasive BMI.

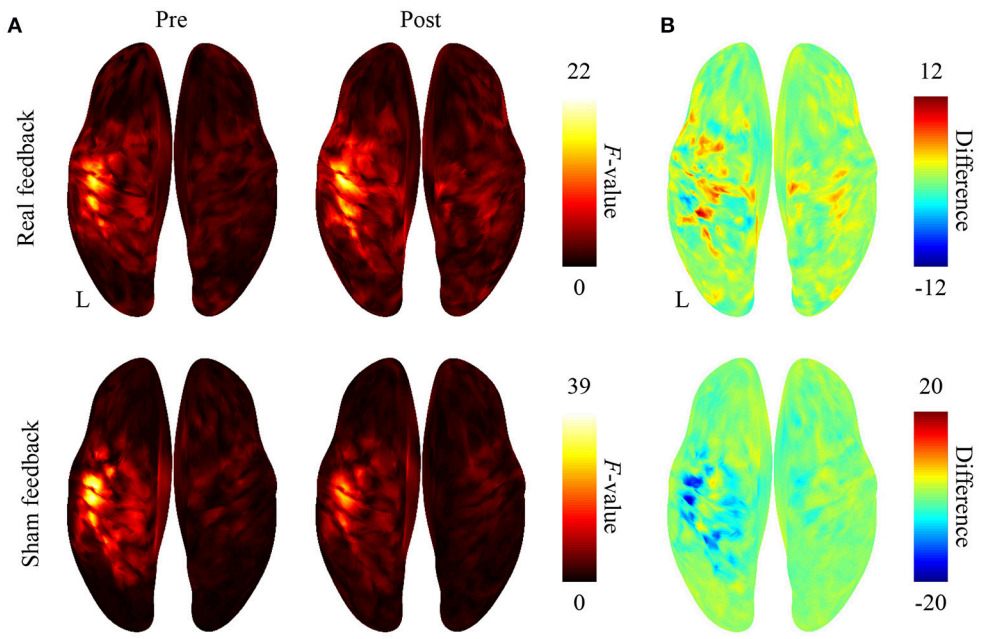

FIGURE 3 | Difference in cortical activation evoked by two types of movements during the offline task. **(A)** The averaged F-values of one-way ANOVA between 500-ms time-averaged cortical currents estimated during hand grasping or opening were color-coded and plotted on the normalized brain surface. **(B)** The differences of F-values shown in plot **(A)** were color-coded on the normalized brain surface.

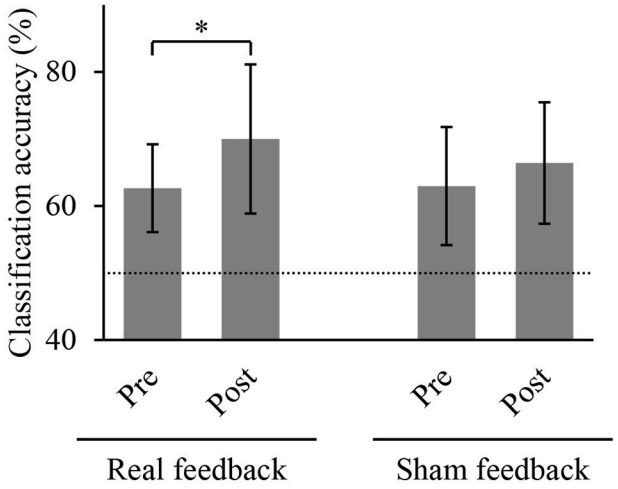

FIGURE 4 | Classification accuracy of hand movements before and after training. Each bar shows the averaged classification accuracy of hand movements during the offline task. Error bars are 95% confidence intervals of classification accuracy. Dotted line denotes chance level. *$p < 0.05$ significant difference between offline tasks before and after 10-min BMI training with feedback (paired Student's *t*-test with Bonferroni correction).

Second, the BMI training will be useful for inducing plastic changes in the cortical representation. Even for these subjects with normal motor function, the BMI training succeeded in improving the classification accuracy of the hand movements using the MEG signals. Our findings suggest that the BMI training did not induce the changes by normalizing the cortical activity but by modulating the activity depending on the decoder. The BMI training could be applied in clinical therapy to change maladapted cortical representation (Kuner and Flor, 2016).

Recent studies have revealed that BMI training in a closed-loop condition improves BMI performance. It has been demonstrated that closed-loop training improves the control of a neuroprosthetic device using multi-unit activities in accordance with some network plasticity and reorganization (Orsborn et al., 2014; Balasubramanian et al., 2017). Similarly, the performance of non-invasive BMI can be predicted by cortical activities and improved by closed-loop neurofeedback training (Hwang et al., 2009; Blankertz et al., 2010; Sugata et al., 2016; Wan et al., 2016). On the other hand, performance improvement depends on the properties of the cortical activities used by the BMI (Sadtler et al., 2014). Further studies are necessary to optimize the improvement of BMI performance for some clinical uses.

It should be noted that BMI training was effective to induce significant differences even with a limited number of subjects. Although the correct rate of robotic control varied among subjects, our BMI training induced a consistent effect on the correct rates. Indeed, our results successfully demonstrated that BMI training significantly improved classification accuracy during the offline task and the correct rates during the online BMI training even among a limited number of subjects.

In summary, neurofeedback training using MEG-based BMI provides a novel method to directly change the information content of motor representations by induced plasticity in the sensorimotor cortex.

DATA AVAILABILITY

The data that support the findings of this study are available on request from the corresponding author.

AUTHOR CONTRIBUTIONS

RF and TaY performed the research, wrote the manuscript, and prepared all the figures. TaY designed the study. HY, MH, ToY, YS, YK, and HK reviewed the manuscript.

FUNDING

This research was conducted under SRPBS by MEXT and AMED. This research was also supported in part by JST PRESTO; Grants-in-Aid for Scientific Research KAKENHI (JP24700419, JP26560467, JP22700435, JP17H06032 and JP15H05710); Brain/MINDS and SICP from AMED; ImPACT; Ministry of Health, Labor, and Welfare (18261201); the Japan Foundation of Aging and Health; the CANON Foundation; and the TERUMO Foundation for Life Sciences and Arts.

ACKNOWLEDGMENTS

We thank Ms. Yuki Kataoka and Ms. Miho Aoki of the Division of Functional Diagnostic Science, Osaka University Medical School for helping the MEG recordings in this study.

SUPPLEMENTARY MATERIAL

The Supplementary Material for this article can be found online at: https://www.frontiersin.org/articles/10.3389/fnins.2018.00478/full#supplementary-material

REFERENCES

Amano, K., Shibata, K., Kawato, M., Sasaki, Y., and Watanabe, T. (2016). Learning to associate orientation with color in early visual areas by associative decoded fMRI neurofeedback. *Curr. Biol.* 26, 1861–1866. doi: 10.1016/j.cub.2016.05.014

Balasubramanian, K., Vaidya, M., Southerland, J., Badreldin, I., Eleryan, A., Takahashi, K., et al. (2017). Changes in cortical network connectivity with long-term brain-machine interface exposure after chronic amputation. *Nat. Commun.* 8:1796. doi: 10.1038/s41467-017-01909-2

Blankertz, B., Sannelli, C., Halder, S., Hammer, E. M., Kubler, A., Muller, K. R., et al. (2010). Neurophysiological predictor of SMR-based BCI performance. *Neuroimage* 51, 1303–1309. doi: 10.1016/j.neuroimage.2010.03.022

Bouton, C. E., Shaikhouni, A., Annetta, N. V., Bockbrader, M. A., Friedenberg, D. A., Nielson, D. M., et al. (2016). Restoring cortical control of functional movement in a human with quadriplegia. *Nature* 533, 247–250. doi: 10.1038/nature17435

Bradberry, T. J., Rong, F., and Contreras-Vidal, J. L. (2009). Decoding center-out hand velocity from MEG signals during visuomotor

adaptation. *Neuroimage* 47, 1691–1700. doi: 10.1016/j.neuroimage.2009.06.023

Clancy, K. B., Koralek, A. C., Costa, R. M., Feldman, D. E., and Carmena, J. M. (2014). Volitional modulation of optically recorded calcium signals during neuroprosthetic learning. *Nat. Neurosci.* 17, 807–809. doi: 10.1038/nn.3712

Cohen, L. G., Bandinelli, S., Findley, T. W., and Hallett, M. (1991). Motor reorganization after upper limb amputation in man. a study with focal magnetic stimulation. *Brain* 114, 615–627. doi: 10.1093/brain/114.1.615

Collinger, J. L., Wodlinger, B., Downey, J. E., Wang, W., Tyler-Kabara, E. C., Weber, D. J., et al. (2013). High-performance neuroprosthetic control by an individual with tetraplegia. *Lancet* 381, 557–564. doi: 10.1016/S0140-6736(12)61816-9

Dale, A. M., Fischl, B., and Sereno, M. I. (1999). Cortical surface-based analysis. I. Segmentation and surface reconstruction. *NeuroImage* 9, 179–194. doi: 10.1006/nimg.1998.0395

Fukuma, R., Yanagisawa, T., Saitoh, Y., Hosomi, K., Kishima, H., Shimizu, T., et al. (2016). Real-Time control of a neuroprosthetic hand by magnetoencephalographic signals from paralysed patients. *Sci. Rep.* 6:21781. doi: 10.1038/srep21781

Fukuma, R., Yanagisawa, T., Yorifuji, S., Kato, R., Yokoi, H., Hirata, M., et al. (2015). Closed-Loop control of a neuroprosthetic hand by magnetoencephalographic signals. *PLoS ONE* 10:e0131547. doi: 10.1371/journal.pone.0131547

Ganguly, K., Dimitrov, D. F., Wallis, J. D., and Carmena, J. M. (2011). Reversible large-scale modification of cortical networks during neuroprosthetic control. *Nat. Neurosci.* 14, 662–667. doi: 10.1038/nn.2797

Hochberg, L. R., Bacher, D., Jarosiewicz, B., Masse, N. Y., Simeral, J. D., Vogel, J., et al. (2012). Reach and grasp by people with tetraplegia using a neurally controlled robotic arm. *Nature* 485, 372–375. doi: 10.1038/nature11076

Hochberg, L. R., Serruya, M. D., Friehs, G. M., Mukand, J. A., Saleh, M., Caplan, A. H., et al. (2006). Neuronal ensemble control of prosthetic devices by a human with tetraplegia. *Nature* 442, 164–171. doi: 10.1038/nature04970

Hwang, H. J., Kwon, K., and Im, C. H. (2009). Neurofeedback-based motor imagery training for brain-computer interface (BCI). *J. Neurosci. Methods* 179, 150–156. doi: 10.1016/j.jneumeth.2009.01.015

Kuner, R., and Flor, H. (2016). Structural plasticity and reorganisation in chronic pain. *Nat. Rev. Neurosci.* 18, 20–30. doi: 10.1038/nrn.2016.162

Luu, T. P., Nakagome, S., He, Y., and Contreras-Vidal, J. L. (2017). Real-time EEG-based brain-computer interface to a virtual avatar enhances cortical involvement in human treadmill walking. *Sci. Rep.* 7:8895. doi: 10.1038/s41598-017-09187-0

Nakanishi, Y., Yanagisawa, T., Shin, D., Chen, C., Kambara, H., Yoshimura, N., et al. (2014). Decoding fingertip trajectory from electrocorticographic signals in humans. *Neurosci. Res.* 85, 20–27. doi: 10.1016/j.neures.2014.05.005

Nakanishi, Y., Yanagisawa, T., Shin, D., Fukuma, R., Chen, C., Kambara, H., et al. (2013). Prediction of three-dimensional arm trajectories based on ECoG signals recorded from human sensorimotor cortex. *PLoS ONE* 8:e72085. doi: 10.1371/journal.pone.0072085

Nishimura, Y., Perlmutter, S. I., Eaton, R. W., and Fetz, E. E. (2013). Spike-timing-dependent plasticity in primate corticospinal connections induced during free behavior. *Neuron* 80, 1301–1309. doi: 10.1016/j.neuron.2013.08.028

Ordikhani-Seyedlar, M., Lebedev, M. A., Sorensen, H. B., and Puthusserypady, S. (2016). Neurofeedback therapy for enhancing visual attention: state-of-the-art and challenges. *Front. Neurosci.* 10:352. doi: 10.3389/fnins.2016.00352

Orsborn, A. L., Moorman, H. G., Overduin, S. A., Shanechi, M. M., Dimitrov, D. F., and Carmena, J. M. (2014). Closed-loop decoder adaptation shapes neural plasticity for skillful neuroprosthetic control. *Neuron* 82, 1380–1393. doi: 10.1016/j.neuron.2014.04.048

Pandarinath, C., Nuyujukian, P., Blabe, C. H., Sorice, B. L., Saab, J., Willett, F. R., et al. (2017). High performance communication by people with paralysis using an intracortical brain-computer interface. *Elife* 6:e18554. doi: 10.7554/eLife.18554

Quian Quiroga, R., and Panzeri, S. (2009). Extracting information from neuronal populations: information theory and decoding approaches. *Nat. Rev. Neurosci.* 10, 173–185. doi: 10.1038/nrn2578

Ramos-Murguialday, A., Broetz, D., Rea, M., Laer, L., Yilmaz, O., Brasil, F. L., et al. (2013). Brain-machine-interface in chronic stroke rehabilitation: a controlled study. *Ann. Neurol.* 74, 100–108. doi: 10.1002/ana.23879

Sadtler, P. T., Quick, K. M., Golub, M. D., Chase, S. M., Ryu, S.I., Tyler-Kabara, E. C., et al. (2014). Neural constraints on learning. *Nature* 512, 423–426. doi: 10.1038/nature13665

Sato, M. A., Yoshioka, T., Kajihara, S., Toyama, K., Goda, N., Doya, K., et al. (2004). Hierarchical Bayesian estimation for MEG inverse problem. *Neuroimage* 23, 806–826. doi: 10.1016/j.neuroimage.2004.06.037

Shibata, K., Watanabe, T., Kawato, M., and Sasaki, Y. (2016). Differential activation patterns in the same brain region led to opposite emotional states. *PLoS Biol.* 14:e1002546. doi: 10.1371/journal.pbio.1002546

Shibata, K., Watanabe, T., Sasaki, Y., and Kawato, M. (2011). Perceptual learning incepted by decoded fMRI neurofeedback without stimulus presentation. *Science* 334, 1413–1415. doi: 10.1126/science.1212003

Shindo, K., Kawashima, K., Ushiba, J., Ota, N., Ito, M., Ota, T., et al. (2011). Effects of neurofeedback training with an electroencephalogram-based brain-computer interface for hand paralysis in patients with chronic stroke: a preliminary case series study. *J. Rehabil. Med.* 43, 951–957. doi: 10.2340/16501977-0859

Sugata, H., Hirata, M., Yanagisawa, T., Matsushita, K., Yorifuji, S., and Yoshimine, T. (2016). Common neural correlates of real and imagined movements contributing to the performance of brain-machine interfaces. *Sci. Rep.* 6:24663. doi: 10.1038/srep24663

Toda, A., Imamizu, H., Kawato, M., and Sato, M. A. (2011). Reconstruction of two-dimensional movement trajectories from selected magnetoencephalography cortical currents by combined sparse bayesian methods. *Neuroimage* 54, 892–905. doi: 10.1016/j.neuroimage.2010.09.057

Wan, F., da Cruz, J. N., Nan, W., Wong, C. M., Vai, M. I., and Rosa, A. (2016). Alpha neurofeedback training improves SSVEP-based BCI performance. *J. Neural Eng.* 13:036019. doi: 10.1088/1741-2560/13/3/036019

Wander, J. D., Blakely, T., Miller, K. J., Weaver, K. E., Johnson, L. A., Olson, J. D., et al. (2013). Distributed cortical adaptation during learning of a brain-computer interface task. *Proc. Natl. Acad. Sci. U.S.A.* 110, 10818–10823. doi: 10.1073/pnas.1221127110

Watanabe, T., Sasaki, Y., Shibata, K., and Kawato, M. (2017). Advances in fMRI real-time neurofeedback. *Trends Cogn. Sci. (Regul. Ed).* 21, 997–1010. doi: 10.1016/j.tics.2017.09.010

Yanagisawa, T., Fukuma, R., Seymour, B., Hosomi, K., Kishima, H., Shimizu, T., et al. (2016). Induced sensorimotor brain plasticity controls pain in phantom limb patients. *Nat. Commun.* 7:13209. doi: 10.1038/ncomms13209

Yanagisawa, T., Hirata, M., Saitoh, Y., Goto, T., Kishima, H., Fukuma, R., et al. (2011). Real-time control of a prosthetic hand using human electrocorticography signals. *J. Neurosurg.* 114, 1715–1722. doi: 10.3171/2011.1.JNS101421

Yanagisawa, T., Hirata, M., Saitoh, Y., Kato, A., Shibuya, D., Kamitani, Y., et al. (2009). Neural decoding using gyral and intrasulcal electrocorticograms. *Neuroimage* 45, 1099–1106. doi: 10.1016/j.neuroimage.2008.12.069

Yanagisawa, T., Hirata, M., Saitoh, Y., Kishima, H., Matsushita, K., Goto, T., et al. (2012a). Electrocorticographic control of a prosthetic arm in paralyzed patients. *Ann. Neurol.* 71, 353–361. doi: 10.1002/ana.22613

Yanagisawa, T., Yamashita, O., Hirata, M., Kishima, H., Saitoh, Y., Goto, T., et al. (2012b). Regulation of motor representation by phase-amplitude coupling in the sensorimotor cortex. *J. Neurosci.* 32, 15467–15475. doi: 10.1523/JNEUROSCI.2929-12.2012

Yoshioka, T., Toyama, K., Kawato, M., Yamashita, O., Nishina, S., Yamagishi, N., et al. (2008). Evaluation of hierarchical Bayesian method through retinotopic brain activities reconstruction from fMRI and MEG signals. *Neuroimage* 42, 1397–1413. doi: 10.1016/j.neuroimage.2008.06.013

Conflict of Interest Statement: The authors declare that the research was conducted in the absence of any commercial or financial relationships that could be construed as a potential conflict of interest.

Copyright © 2018 Fukuma, Yanagisawa, Yokoi, Hirata, Yoshimine, Saitoh, Kamitani and Kishima. This is an open-access article distributed under the terms of the Creative Commons Attribution License (CC BY). The use, distribution or reproduction in other forums is permitted, provided the original author(s) and the copyright owner(s) are credited and that the original publication in this journal is cited, in accordance with accepted academic practice. No use, distribution or reproduction is permitted which does not comply with these terms.

frontiers in Neuroscience

ORIGINAL RESEARCH
published: 11 July 2018
doi: 10.3389/fnins.2018.00455

Comparison of the Efficacy of a Real-Time and Offline Associative Brain-Computer-Interface

Natalie Mrachacz-Kersting and Susan Aliakbaryhosseinabadi*

Center for Sensory-Motor Interaction, Department of Health Science and Technology, Faculty of Medicine, Aalborg University, Aalborg, Denmark

An associative brain-computer-interface (BCI) that correlates in time a peripherally generated afferent volley with the peak negativity (PN) of the movement related cortical potential (MRCP) induces plastic changes in the human motor cortex. However, in this associative BCI the movement timed to a cue is not detected in real time. Thus, possible changes in reaction time caused by factors such as attention shifts or fatigue will lead to a decreased accuracy, less pairings, and likely reduced plasticity. The aim of the current study was to compare the effectiveness of this associative BCI intervention on plasticity induction when the MRCP PN time is pre-determined from a training data set ($BCI_{offline}$), or detected online (BCI_{online}). Ten healthy participants completed both interventions in randomized order. The average detection accuracy for the BCI_{online} intervention was 71 ± 3% with 2.8 ± 0.7 min^{-1} false detections. For the BCI_{online} intervention the PN did not differ significantly between the training set and the actual intervention ($t_9 = 0.87$, $p = 0.41$). The peak-to-peak motor evoked potentials (MEPs) were quantified prior to, immediately following, and 30 min after the cessation of each intervention. MEP results revealed a significant main effect of time, $F_{(2,18)} = 4.46$, $p = 0.027$. The mean TA MEP amplitudes were significantly larger 30 min after (277 ± 72 μV) the BCI interventions compared to pre-intervention MEPs (233 ± 64 μV) regardless of intervention type and stimulation intensity ($p = 0.029$). These results provide further strong support for the associative nature of the associative BCI but also suggest that they likely differ to the associative long-term potentiation protocol they were modeled on in the exact sites of plasticity.

Keywords: human, plasticity, brain-computer-interface, offline, online, Hebbian plasticity, tibialis anterior

OPEN ACCESS

Edited by:
Christoph Guger,
Guger Technologies, Austria

Reviewed by:
Noman Naseer,
Air University, Pakistan
Jing Jin,
East China University of Science and Technology, China

****Correspondence:***
Natalie Mrachacz-Kersting
nm@hst.aau.dk

Specialty section:
This article was submitted to Neural Technology, a section of the journal Frontiers in Neuroscience

Received: *13 April 2018*
Accepted: *14 June 2018*
Published: *11 July 2018*

Citation:
Mrachacz-Kersting N and Aliakbaryhosseinabadi S (2018) Comparison of the Efficacy of a Real-Time and Offline Associative Brain-Computer-Interface. Front. Neurosci. 12:455. doi: 10.3389/fnins.2018.00455

INTRODUCTION

Since Daly et al. (2009) proposed the possibility of a Brain-Computer-Interface (BCI) designed for neuromodulation of stroke patients, the field has rapidly expanded with numerous novel BCIs being introduced and tested in the clinic (Ang et al., 2010; Broetz et al., 2010; Cincotti et al., 2012; Li et al., 2013; Ramos-Murguialday et al., 2013; Mukaino et al., 2014; Young et al., 2014; Pichiorri et al., 2015; Mrachacz-Kersting et al., 2016). To date the main focus has been on upper limb rehabilitation with relatively few targeting lower limb function (for a review see, Teo and Chew, 2014; Cervera et al., 2018). In addition, only one group has investigated patients in the sub-acute phases of stroke (Mrachacz-Kersting et al., 2017b), presumably due to the relatively stable condition that a chronic stroke patient presents. Effects from the use of a BCI are thus easier to control since patients in the acute and subacute phase are prone to spontaneous biological recovery (Krakauer and Marshall, 2015).

Typically, BCIs function by collecting the brain signals during a specific state such as performing a movement or motor imagery, extracting features of interest and then translating these into commands for external device control (Daly and Wolpaw, 2008). The available non-invasive BCIs for stroke patients have implemented both electroencephalography (EEG) or near-infrared spectroscopy (NIRS) to acquire the brain signals, extracted various spectral and temporal features [e.g., sensorimotor rhythm, movement related cortical potentials (MR)] and provided diverse types of afferent feedback to the patient such as those generated from using robotic devices, virtual reality or by driving direct nerve or muscular electrical stimulation (for review see, Cervera et al., 2018).

A vital component of any BCI designed for rehabilitation of lost motor function in stroke patients, is that the physiological theories behind learning and memory must be satisfied. One of the most influential theories was proposed in 1949 by Hebb (2005) from which we know that "*Cells that fire together, wire together*." Although Hebb proposed his theory on theoretical grounds, animal data later verified that if the pre-synaptic neuron is activated simultaneously with the post-synaptic cell, plasticity is induced, often referred to as long-term potentiation (for a review see, Cooke and Bliss, 2006). In 2000, a group from Rostock University were the first to demonstrate long-term potentiation like plasticity in the intact human brain (Stefan, 2000) with later applications to lower limb muscles (Mrachacz-Kersting et al., 2007). In this intervention [paired associative stimulation (PAS)], a peripheral nerve that innervates the target muscle is activated using a single electrical stimulus and once the generated afferent volley has arrived at the motor cortex, a single non-invasive transcranial magnetic stimulus (TMS) is provided to that area of the motor cortex that has a direct connection to the target muscle (for a review see, Suppa et al., 2017).

In a modified version of PAS, the TMS stimulus has been replaced by the movement related cortical potential (MRCP) (Mrachacz-Kersting et al., 2012). The MRCP, that can be readily measured using EEG, is a slow negative potential that arises approximately 1–2 s prior to movement execution or imagination and attains its peak negativity at the time of movement execution (Walter et al., 1964). This intervention, also termed an associative BCI, induces significant plasticity of the cortical projections to the target muscle and leads to significant functional improvements in chronic and subacute stroke patients (Mrachacz-Kersting et al., 2016, 2017b). In the first phase, patients are asked to attempt 30–50 movements (dorsiflexion of the foot), timed to a visual cue and they receive no sensory feedback. The time of the peak negativity (PN) of the resulting MRCP for every trial is extracted and an average calculated. During the second phase (the actual associative BCI intervention), this time is used to trigger the electrical stimulation of the target nerve such that the generated afferent volley arrives at the motor cortex at precisely peak negativity. Typically, 30–50 such pairings are performed over 3–12 sessions. Since the trigger of the electrical stimulator is not based on the online detection of the MRCP during the second phase, this intervention does not represent a BCI in the classical sense. In the current study the aim was to compare the effects of this associative BCI intervention on plasticity induction as quantified by the motor evoked potential (MEP) following TMS when the MRCP PN time is determined from the phase one trials ($BCI_{offline}$ modus) or detected during the second phase by using the phase one trials as a training data set (BCI_{online} modus).

MATERIALS AND METHODS

Participants

Ten participants (four females and six males, average age: 22.3 ± 1.2 years) without any known physical or neurological disorders all participants were classified as right side dominant with a mean laterality quotient of 0.97 (range: 0.59–1) according to the Edinburgh handedness inventory questionnaire (Oldfield, 1971). This study was carried out in accordance with the recommendations of the Scientific Ethics Committee of Northern Jutland guidelines. The protocol was approved by the Scientific Ethics Committee of Northern Jutland (Reference number: VN-20070015). All subjects gave written informed consent in accordance with the Declaration of Helsinki.

Apparatus and Instrumentation

Surface Electromyography

The electromyographic (EMG) activity of the target muscle, the tibialis anterior (TA) on the dominant side was quantified using disposable surface electrodes (Neuroline 720, Ambu, Ambu A/S, Denmark) that were placed according to the SENIAM guidelines[1]. For quantification of plasticity induction using non-invasive TMS, the EMG amplifier pod supplied by Rogue Research Inc. as part of the Brainsight™ system (Rogue Research, Inc.), was used to collect MEP data. During the BCI intervention, a single channel EMG was recorded to control for the participant's movement using the g.USBamps (g.tec GmbH, Austria) at a sampling frequency of 256 Hz.

Electroencephalography (EEG)

Monopolar EEG was obtained from 10 channels (FP1, Fz, FC1, FC2, C3, Cz, C4, CP1, CP2, and Pz according to the standard international 10–20 system) with the reference electrode on Fz and ground on the left earlobe. Channel Cz was the central channel based on the large Laplacian (McFarland et al., 1997). Signals were acquired using an active EEG electrode system (g.GAMMAcap[2], Austria) and g.USBamp amplifier (gTec, GmbH, Austria) at a sampling frequency of 1200 Hz (16 bits accuracy) and a hardware filter of 0 to 100 Hz.

Electrical Stimulation (ES)

The deep branch of the common peroneal nerve (dCPN) was stimulated using disposable surface electrodes (32 mm, PALS® Platinum, Patented Conductive Neurostimulation Electrodes, Axelgaard Manufacturing, Co., Ltd., United States) with the cathode proximal. A NoxiTest isolated peripheral stimulator (IES 230) supplied single pulses (1 ms width, 20–30 mA) every 3–5 s while a suitable stimulating position (where the TA M-wave attained the highest peak to peak amplitude and

[1] seniam.org

activity pf the synergistic peroneal muscles and the antagonist soleus was minimal) was determined. Next, the motor threshold was quantified as that stimulating intensity where an M-wave became visible in the TA EMG. This intensity was used in the subsequent BCI interventions (refer to see section "Associative BCI Interventions").

Transcranial Magnetic Stimulation (TMS)

To quantify the TA MEP, single TMS pulses with a posterior to anterior directed current were applied using a Magstim 200 (Magstim Company, Dyfed, United Kingdom) and a focal figure of eight coil (110 mm diameter).

Experimental Procedures

Participants attended two separated sessions spaced at least 48 h apart. Each session was comprised of pre-measures where TA MEP sizes were quantified, phase one and two of the associative BCI intervention, and post and 30 min post-measures of TA MEPs. During all parts, participants were seated in a comfortable chair with both feet resting on foot plates.

Following EMG electrode placements, the optimal placement of the TMS coil was determined using a stimulator output of 50%. Three stimuli were initially provided over the vertex and the peak to peak size of the TA MEP monitored online. This was repeated for 3–5 positions around the vertex and the site that resulted in the largest and most consistent TA MEPs deemed the hotspot. To ensure that the stimulation was always applied over the same area of the motor cortex the coil position was maintained by marking this spot using Brainsight^{TM} (Rogue Research, Inc.). Next the resting motor threshold (RMT) was established which was the highest stimulation intensity that produced TA MEPs with an amplitude of at least ∼50 μV while the muscle was at rest, in 5 out of 10 consecutive stimuli. Finally, 10 stimuli were provided randomly every 5–7 s at each intensity of 90, 100, 110, 120, 130, and 140% RMT (total of 60 stimuli).

Following the pre-measures, the participants were prepared for EEG recordings and once completed, were exposed to one of the associative BCI interventions as outlined in Section "Associative BCI Interventions." The EEG cap was then removed, and the post and 30 min post TA MEP measures taken (i.e., 10 stimuli provided randomly every 5–7 s at each intensity of 90, 100, 110, 120, 130, and 140% RMT (total of 60 stimuli)). **Figure 1** provides an overview of the intervention sessions.

Associative BCI Interventions

Phase One

Phase one of each session was the same for all participants regardless of the intervention. A cue provided on a computer screen placed at least 1.5 m in front of the participant indicated when to prepare, execute, and release a single ballistic dorsiflexion of the dominant foot. The cue consisted of five parts, (1) The word 'Focus' appeared (duration randomized between 2 and 3 s), (2) The drawing of a ramp appeared where the initial 2 s prior to the upwards turn served as the preparation time, (3) The upwards turning part of the ramp indicated when to execute the movement, (4) A holding phase of 2 s where the new position had to be held and 5. The word 'Rest' appeared (duration randomized between 4 and 5 s). A total of 30 such movements were performed.

Phase Two

This phase differed between the two sessions depending on whether the participant was exposed to the offline ($BCI_{offline}$) or online (BCI_{online}) modus of the associative BCI intervention as outlined below.

$BCI_{offline}$ Session

The onset of each movement was quantified from the TA EMG data and the continuous EEG data divided into epochs of 4 s (2 s prior to and 2 s following the onset of the movement). A band pass filter (0.05–10 Hz) and a Laplacian channel (McFarland et al., 1997) was used to enhance the MRCP in each epoch. Next, each epoch where the PN was not within a time window of −500 to 500 ms or contained electrooculographic (EOG) activity exceeding 70 mV were discarded. For the remaining epochs, the time of PN was extracted and averaged. This time was used during phase two to time the onset of the electric stimulator. More precisely, the timing was calculated as the mean PN-50 ms. The 50 ms represents the mean latency for the afferent inflow resulting from the peripheral stimulus to reach the somatosensory cortex plus a cortical processing delay and is based on previous work (Mrachacz-Kersting et al., 2007). Following the quantification of the PN, participants were asked to complete another 30 movements as for phase one, however this time imagined, and timed to the cue as for phase one. During each repetition they also received a single electrical stimulus as outlined in Section "Electrical Stimulation (ES)." In the offline modus, phase two thus contained 30 pairings of the MRCP and ES.

BCI_{online} Session

The EEG signals recorded in phase 1 were filtered [2nd order band-pass Butterworth filter (0.05–5 Hz)]. The EEG signals in the range of (−2 1) s with regards to movement onset were considered as 'signal intervals' while the remaining data were 'noise intervals.' Next, spectral and temporal analysis was performed on each trial of both signal and noise intervals to extract 25 spectral and 17 temporal features. This procedure was repeated for all recorded channels.

Twenty-five spectral features were computed from the power of the EEG trials in five main frequency ranges; Delta (0.05–3 Hz), Theta (4–8 Hz), Alpha (8–13 Hz), Beta (1331 Hz), and Gamma (32–100 Hz). These were extracted from five time intervals; [−2 0] s, [−2 −1] s, [−1 0] s, [−1 −0.5] s, and [−0.5 0] s with respect to the movement onset obtained from EMG signals. Seventeen temporal features were obtained from each trial by extracting the time and amplitude of the peak negativity of the MRCP. Pre-movement slopes were attained from linear regression in five time intervals; [−2 −1] s, [−2 0] s, [−1 0] s, [−1 −0.5] s, and [−0.5 0] s where 0 is the time of peak negativity. In addition, the variability of the MRCP defined as the standard deviation as well as the average MRCP across all trials were computed in the same five time ranges. **Figure 2** visualizes the time intervals implemented as well as the amplitude and time of peak negativity. Lastly, 27

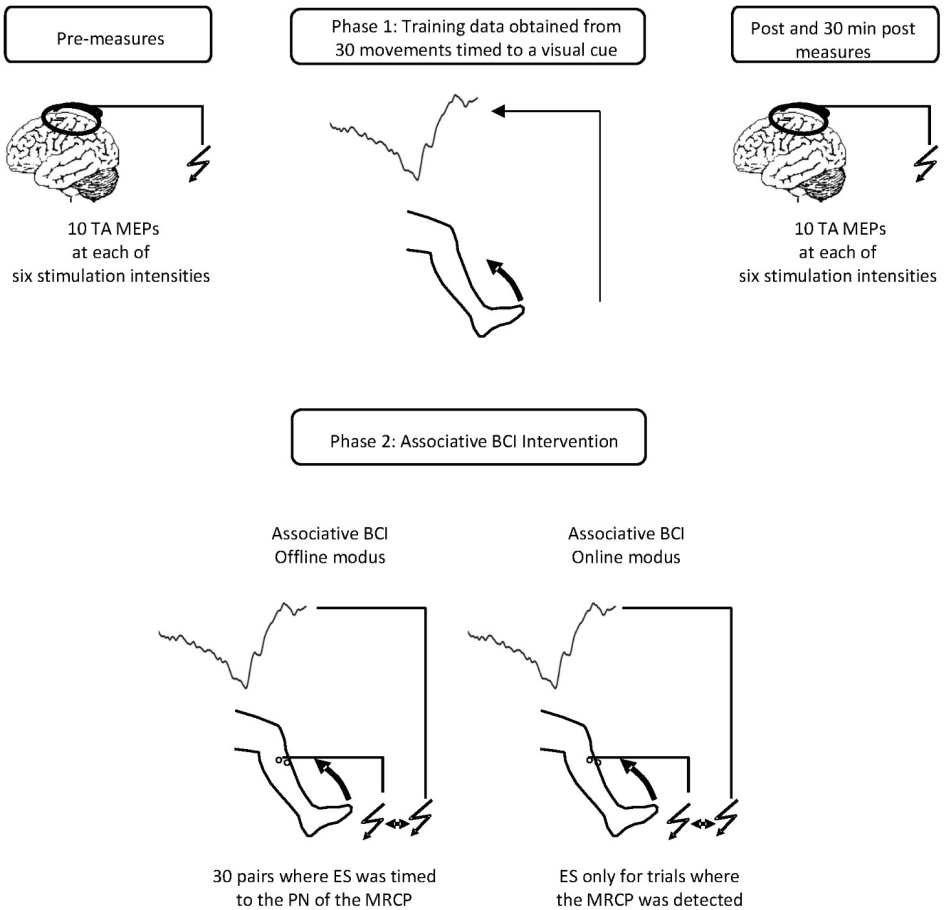

FIGURE 1 | Overview of the intervention sessions. Prior to the interventions 10 TMS stimuli were applied at each of six different intensities. The interventions (spaced at least 48 h apart) consisted of two phases. In phase one participants completed 30 dorsiflexion movements while EEG data were collected. In phase two, participants were exposed to concurrent motor imagination and peripheral nerve stimulation. In the associative $BCI_{offline}$ intervention, the stimulation was provided during each motor imagery trial and the timing set in relation to the peak negativity obtained from the EEG data of phase one. In the associative BCI_{online} intervention, the stimulation was only provided if an MRCP was detected. The detection algorithm was trained from the data obtained in phase one. For each modus participants completed 30 imagery trials. Immediately following and 30 min after the cessation of the interventions, another 10 TMS stimuli were applied at each of six different intensities.

tempo-spectral features were extracted by combining temporal and spectral features.

These features were subsequently used as the input for three types of classifiers, K-nearest neighbor (KNN, five neighbor points with Euclidean distance), Support vector machine (SVM, 2^{nd} order polynomial as the kernel function with automatic scale) and Decision Tree (the split criteria was Gini's diversity index). Data were classified to either signal or noise by applying fivefold cross validation divided into fivefold (4 for training and 1 for testing). The classification output for all channels was computed and the three channels with the highest accuracy and corresponding classifier and feature type was selected. In phase two of the intervention, the continuous incoming data of the selected channels (3 s long with 2.5 s overlapping) were classified by using the selected features and classifiers. The decision was made if more than one channel showed one of the two classes. True and false detections were recorded during phase two of the BCI_{online} session and used to calculate the true positive rate (TPR), false positive (FP), true negative rate (TNR), and false negative (FN) to assess BCI performance.

Statistical Analysis

To quantify the reliability of the PN time of the MRCP as well as the number of pairings of MRCP and ES for the $BCI_{offline}$ session, a Student's paired *t*-test was applied. To ensure that the pre-intervention MEP values were matched between sessions, a two-way repeated analysis of variance (rmANOVA) was conducted with the factors intervention ($BCI_{offline}$ and BCI_{online}) and TMS stimulation intensity (90, 100, 110, 120, 130, and 140% RMT). A three-way rmANOVA with the factors time (pre, post and 30 min post-intervention), intervention ($BCI_{offline}$ and BCI_{online}) and TMS stimulation intensity (90, 100, 110, 120, 130, and 140% RMT), tested the effectiveness of the two interventions in inducing alterations of the corticospinal tract excitability. Greenhouse–Geisser corrections were used in the

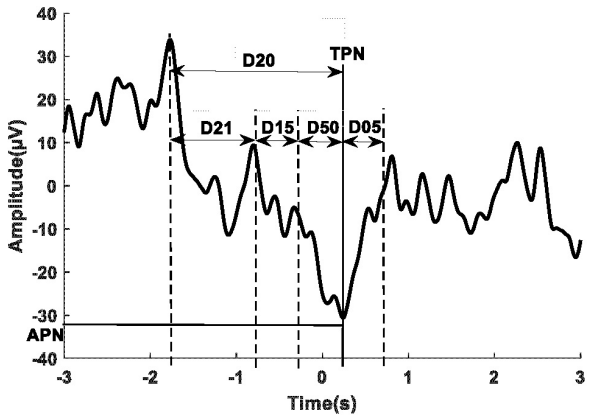

FIGURE 2 | A sample of a single trial of the MRCP with the time domains used for feature extraction. D21: [–2 –1] s, D15: [–1 –0.5] s, D50: [–.5 0] s, D20: [–2 0] s, and D05: [0.5] s where 0 represents the peak negativity obtained from the onset of the movement.

case of sphericity being violated. The significance level was set to $p < 0.05$.

RESULTS

MRCP Reliability

Figure 3 shows a sample of the MRCP of single trials (thin traces) and the average across all trials (thick trace) for one participant during phase one of the $BCI_{offline}$ (**Figure 3A**) and BCI_{online} (**Figure 3B**) experimental sessions respectively. The dashed vertical lines indicate the time of the cue to move. Across all participants the PN of the MRCP attained values of -10 ± 70 ms ($BCI_{offline}$ session) and -20 ± 60 ms (BCI_{online} session). A Student's paired *t*-test revealed no significant differences between sessions ($t_9 = 1.68$, $p = 0.13$).

BCI Performance During Phase Two of the Associative $BCI_{offline}$ and BCI_{online} Interventions

The time of PN of the MRCP during phase two of the $BCI_{offline}$ session was -10 ± 40 ms which was not significantly different to those values attained during phase one ($t_9 = 0.87$, $p = 0.41$). **Table 1** displays TPR, FP, TNR, and FN in phases 1 and 2 of the BCI_{online} session for single participants.

The performance of the BCI in the BCI_{online} session for all participants expressed as TPR, TNR, FP, and FN respectively, were 71 ± 3, $76 \pm 5\%$ and 2.8 ± 0.7, 3.1 ± 0.4 min^{-1}.

Changes in the Output Properties of the Motor Cortex Following the Associative $BCI_{offline}$ and BCI_{online} Interventions

Prior to the interventions, the amplitude of the TA MEPs induced at the highest stimulation intensity across all participants were 515 ± 186 and 464 ± 164 μV (mean ± SE) for the $BCI_{offline}$ and BCI_{online} training interventions, respectively. There was no significant interaction between intervention and stimulation intensity, $F_{(5,45)} = 0.47$, $p = 0.799$ for the pre-intervention measures. The experimental sessions started with a similar baseline excitability across all participants since the main effect of intervention was not significant, $F_{(1,9)} = 0.048$, $p = 0.83$, after pooling the interaction term.

Figures 4A,B show single TA MEP traces from one participant prior to, immediately following and 30 min after the cessation of the $BCI_{offline}$ and BCI_{online} training. **Figures 4C,D** contain the mean TA MEP amplitudes across all participants following and 30 min after the $BCI_{offline}$ and BCI_{online} training interventions for

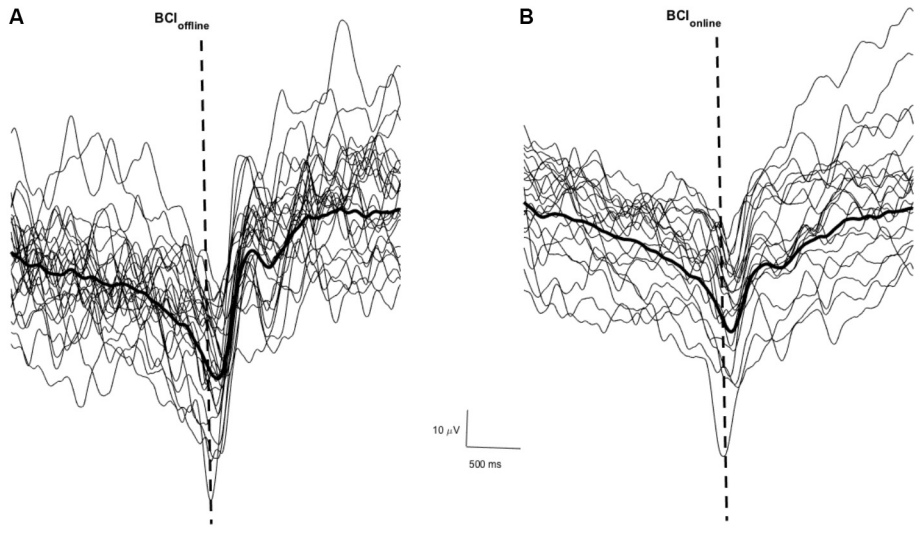

FIGURE 3 | Single trial MRCPs and the average MRCP for one participant for the $BCI_{offline}$ **(A)** and BCI_{online} **(B)** interventions respectively. The dashed vertical line indicates the time of the cue to perform the movement. Trials with EOG activity have been removed.

TABLE 1 | TPR, FP, TNR, and FN in phases 1 and 2 of the BCI_{online} session for single participants.

	Phase 1				Phase 2			
Participant	**TPR**	**FP**	**TNR**	**FN**	**TPR**	**FP**	**TNR**	**FN**
1	84	1.5	86	1.7	73	2.4	78	3.0
2	83	1.6	85	1.8	72	2.4	78	3.1
3	80	2.1	81	2.2	73	2.7	75	2.3
4	88	0.9	92	1.3	77	1.5	86	2.5
5	81	1.9	83	2.3	70	2.4	78	3.3
6	81	1.9	83	2.1	71	2.7	75	3.2
7	78	2.3	79	2.4	68	3.2	71	3.5
8	80	2.0	82	2.2	71	2.8	74	3.2
9	79	2.2	80	2.3	68	4.2	72	3.5
10	77	2.3	75	2.5	67	3.3	70	3.6
Average	81.1	1.9	82.6	2.1	71.0	2.8	75.7	3.1
SD	3.2	0.4	4.6	0.4	3.0	0.7	4.6	0.4

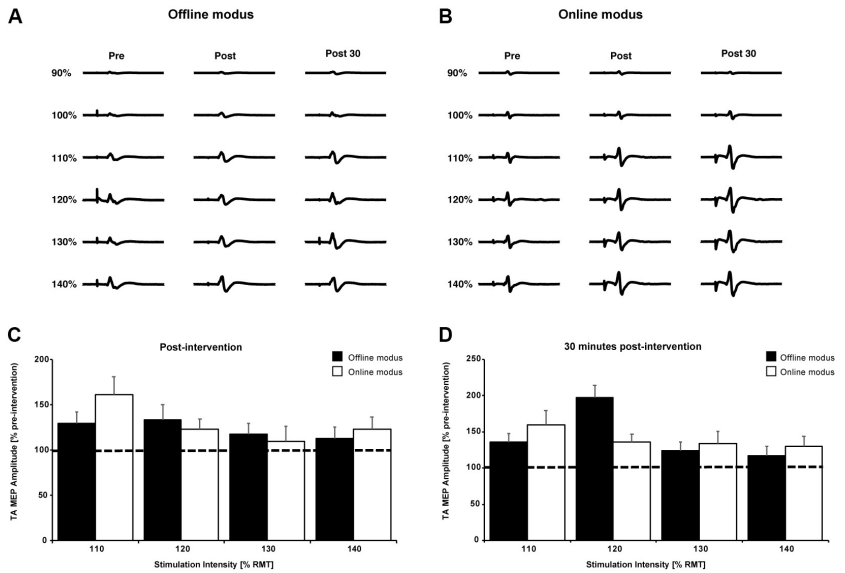

FIGURE 4 | Single TA MEP traces for 90–140% RMT prior to, following, and 30 min after the $BCI_{offline}$ **(A)** and BCI_{online} **(B)** interventions for one participant. **(C,D)** Mean TA MEP amplitudes for 110–140% RMT across all participants immediately following and 30 min after both interventions. Data are expressed as a percentage of pre-intervention values (black dashed line). Black bars represent the offline modus and the white bars represent the online modus. Error bars represent SEM.

all stimulation intensities, expressed as a percentage of the pre-intervention TA MEP amplitudes for all stimulation intensities.

The three-way interaction and all two-way interactions were not significant (all p's ≥ 0.26). After pooling the two- and three-way interaction terms, there was a significant main effect of time, $F_{(2,18)} = 4.46$, $p = 0.027$. The mean TA MEP amplitudes were significantly larger 30 min after (277 ± 72 μV) the BCI interventions compared to pre-intervention MEPs (233 ± 64 μV) with $p = 0.029$ (Bonferroni *post hoc* analysis). There was no significant difference between TA MEP amplitudes immediately following and pre-intervention ($p = 0.148$).

As expected, there was a significant main effect of stimulation intensity, $F_{(5,45)} = 5.323$, $p = 0.001$. The average TA MEP amplitudes were significantly larger at stimulation intensities of 140% RMT (463 ± 162 μV) compared to 130% (405 ± 135 μV), 120% (271 ± 61 μV), 110% (189 ± 27 μV), 100% (112 ± 13 μV), and 90% RMT (63 ± 10 μV) regardless of intervention type and stimulation time (all p's ≤ 0.037, Bonferroni *post hoc* analysis). TA MEP amplitudes were also significantly larger at stimulation intensities of: 130% RMT compared to 120, 110, 100, and 90% RMT (all p's ≤ 0.047); 120% RMT compared to 110, 100, and 90% RMT (all p's ≤ 0.02); 110% RMT compared to 100 and 90% RMT (both p's ≤ 0.02); and 100% compared to 90% RMT ($p < 0.026$).

MEP changes occurred independently of the type of BCI intervention used since there was no significant main effect of intervention, $F_{(1,9)} = 0.057$, $p = 0.816$. These analyses demonstrate the effectiveness of both BCI interventions in inducing significant neurophysiological changes. Both BCI

interventions resulted in a significant increase of the TA MEP amplitude that outlasted the intervention time by at least 30 min.

DISCUSSION

The aim of the current study was to compare the effects of an associative BCI intervention on plasticity induction when the MRCP PN time is pre-determined from a training data set ($BCI_{offline}$), or detected online (BCI_{online}). The results show that both interventions resulted in significant increases in the cortical projections to the target muscle.

BCI Performance During Phase Two of the Associative $BCI_{offline}$ and BCI_{online} Interventions

One of the advantages of asking participants to perform the BCI task to a cue is that it facilitates motor imagery or motor attempt (Heremans et al., 2009). Hence in our previous studies, we used the initial training data set to quantify the timing of the ES. Aside from the lower computation power required, this also ensures that patients do not become frustrated in the event that the detection rate is too low in the subsequent intervention. However, in a $BCI_{offline}$ modus a major concern is that since the movement is not detected in real time, possible changes in reaction time to the cue caused by factors such as attention shifts or fatigue will lead to a decreased accuracy in the timing between the peripherally generated afferent volley and the activation of the brain.

An important prerequisite in the associative BCI intervention we first introduced in 2012 in healthy participants (Mrachacz-Kersting et al., 2012) and later applied in a group of chronic stroke patients where it led to significant functional improvements (Mrachacz-Kersting et al., 2016), is thus that the PN of the MRCP is reliable across single trials. Typically, within a session, a training data set of 30–50 trials of attempted movements is performed and the extracted time of PN used in the subsequent intervention. The intervention is comprised of 30–50 pairings of an artificially generated afferent volley timed to arrive at PN. This timing is imperative as neither early nor late arrival results in plasticity induction (Mrachacz-Kersting et al., 2012). The average PN time in the initial training set was similar to what we have reported previously and did not differ significantly for the $BCI_{offline}$ and BCI_{online} sessions (Mrachacz-Kersting et al., 2012, 2017c). Since participants did not alter their reaction time to the visual cue within the $BCI_{offline}$ intervention set (the PN time was similar to the initial 30 trials), we may assume that indeed 30 pairs with the appropriate time were applied. However, for the BCI_{online} session, the TPR was only $71 \pm 3\%$ indicating that for almost 30% of the actual movements, no artificial volley was generated. In a self-paced BCI that follows the same principles of associativity the TPRs attained similar values of $67.15 \pm 7.87\%$ (Niazi et al., 2012) and $73.0 \pm 10.3\%$ (Xu et al., 2014).

In the previous self-paced associative BCI, participants were required to continue performing the task until at least 50 successful attempts were detected (Niazi et al., 2012; Xu et al., 2014). This number of pairings was based on previous studies of PAS targeting a hand muscle (Kujirai et al., 2006). As a result, the duration of the intervention session was between 8.9 and 22.1 min. In the current study, irrespective of the number of true detections, only 30 trials were completed with a total duration of approximately 5 min. In a BCI designed for neurorehabilitation of stroke patients it is imperative that each BCI session does not last longer than approximately 30 min. This includes all aspects such as preparation time, training and the intervention itself. This has several reasons, on the one hand, at least in Denmark, any therapy session for stroke patients takes maximally 30 min and maintaining the BCI session within this time frame will allow it to be scheduled alongside the classical therapy sessions. On the other hand, stroke patients fatigue at a faster rate compared to healthy controls with 30 min being the maximum time they are able to concentrate prior to necessitating a rest period.

Changes in the Output Properties of the Motor Cortex Following the Associative $BCI_{offline}$ and BCI_{online} Interventions

In the current study, participants were exposed to a significantly reduced number of pairings of the MRCP and the afferent inflow in the BCI_{online} intervention, compared to previous studies and the $BCI_{offline}$ intervention. However significant plasticity of the corticospinal tract to the TA muscle occurred. It is currently not established how many pairs of peripheral and central inputs are required for such changes to be induced. In previous studies both 50 pairings (Mrachacz-Kersting et al., 2012, 2016) and 30 pairings (Mrachacz-Kersting et al., 2017c) have resulted in significant changes. In the original PAS studies (see review by Suppa et al., 2017), 90 pairs were applied when targeting hand muscles (Stefan, 2000), and this could be further reduced to 50 when the muscle was pre-contracted (Kujirai et al., 2006). As a minimum, 360 pairs were required when targeting the lower limb muscle TA (Mrachacz-Kersting et al., 2007) and 200 for soleus (Kumpulainen et al., 2012, 2015). At least for PAS, other factors such as attention to the task, fatigue and history of muscle contraction have been shown to contribute to the changes in the excitability of the cortical projections to the target muscle (Suppa et al., 2017). Thus, any attention away from the main task as well as fatigue will lead to a decrease in the amount of plasticity induced (Stefan et al., 2004), while prior muscle activation will lead to an increase (Kujirai et al., 2006). Since the duration and the number of trials performed were exactly the same for the BCI_{online} and $BCI_{offline}$ intervention, it is likely that participants were able to attend to the task without experiencing attentional shifts or fatigue.

During the BCI_{online} intervention, a movement was falsely detected at a rate of $1.2 \pm 0.9\ min^{-1}$. Thus, on average six ES were not timed to the PN of the MRCP. Previously, afferent inflow that arrived either too early or too late resulted in no significant plasticity induction (Mrachacz-Kersting et al., 2012), while an ES timed randomly in relation to PN led to decreases of the excitability of the cortical projections to the TA in some chronic stroke patients while triggering no changes on average across all patients (Mrachacz-Kersting et al., 2016). These results taken together imply that although our associative

BCI intervention is modeled on PAS and associative LTP-like mechanisms, there are likely significant differences in the locus of effects (Suppa et al., 2017). Further studies are required to determine the exact sites of plasticity. Lastly, since participants performed the task in both the training and intervention sets, afferent inflow was generated naturally by the activation of the muscles, arriving at the motor cortex at the appropriate time. This afferent feedback is a combination of muscle, joint, and skin receptor activation. It may be speculated that in the event that the artificially generated afferent volley occurs at the wrong time in relation to the MRCP, it is simply filtered out by the nervous system. This is supported by our original findings that afferent feedback timed either too early or too late in relation to the PN of the MRCP leads to no plasticity induction. It is also substantiated by reports that the effects of afferent feedback to the brain and ongoing movement is modulated in a task dependent manner (Nielsen and Sinkjaer, 2002; Nielsen, 2004). Thus for example, during an active dorsiflexion movement, afferent information from antagonistic muscles is suppressed by disynaptic reciprocal inhibition (Crone and Nielsen, 1994; Geertsen et al., 2011). Indeed, afferent feedback from the activation of ankle plantarflexors of one leg will depress the activation of the homonymous muscle of the other leg through a short latency interlimb pathway (Stubbs and Mrachacz-Kersting, 2009) that includes the same interneuron responsible for disynaptic reciprocal inhibition (Mrachacz-Kersting et al., 2017a).

CONCLUSION

Here, we compared the effectiveness of an associative BCI_{online} and $BCI_{offline}$ intervention in inducing plasticity of the cortical projections to the TA. Regardless of whether the PN of the MRCP was determined offline from a training data set or detected online, similar changes in the excitability of the cortical projections to the TA were induced. These results provide further strong support for the associative nature of the interventions but also suggest that they likely differ to the PAS protocol they were modeled on in the exact sites of plasticity. Further studies are required to assess whether the associative BCI_{online} and $BCI_{offline}$ interventions have similar effects to PAS on the motor cortical network.

AUTHOR CONTRIBUTIONS

NM-K conceptualized and designed the study. NM-K and SA collected the data partly with a student group, analyzed the data, completed the statistical analysis and drafted the manuscript. All authors approved the final version.

FUNDING

This study was supported by the Lundbeck Foundation (R252-2017-1555), and Det Obelske Familiefond of Denmark.

ACKNOWLEDGMENTS

These go to all the subjects, student helpers and Mr. Jan Stavnshøj and Mr. Knud Larsen for their technical assistance as well as the funding agencies Lundbeck Foundation, and the Obel Family Foundation of Denmark.

REFERENCES

Ang, K. K., Guan, C., Chua, K. S., Ang, B. T., Kuah, C., Wang, C., et al. (2010). Clinical study of neurorehabilitation in stroke using EEG-based motor imagery brain-computer interface with robotic feedback. *Conf. Proc. IEEE Eng. Med. Biol. Soc.* 2010, 5549–5552. doi: 10.1109/IEMBS.2010.5626782

Broetz, D., Braun, C., Weber, C., Soekadar, S. R., Caria, A., and Birbaumer, N. (2010). Combination of brain-computer interface training and goal-directed physical therapy in chronic stroke: a case report. *Neurorehabil. Neural Repair* 24, 674–679. doi: 10.1177/1545968310368683

Cervera, M. A., Soekadar, S., Ushiba, J., Millan, J. D. R., Liu, M., Birbaumer, N., and et al. (2018). Bain-computer interfaces for post-stroke motor rehabilitation: a meta-analysis. *Ann. Clin. Trans. Neurol.* 5, 651–663. doi: 10.1002/acn3.544

Cincotti, F., Pichiorri, F., Aricò, P., Aloise, F., Leotta, F., de Vico Fallani, F., et al. (2012). EEG-based brain-computer interface to support post-stroke motor rehabilitation of the upper limb. *Conf. Proc. IEEE Eng. Med. Biol. Soc.* 2012, 4112–4115. doi: 10.1109/EMBC.2012.6346871

Cooke, S. F., and Bliss, T. V. (2006). Plasticity in the human central nervous system. *Brain* 129, 1659–1673. doi: 10.1093/brain/awl082

Crone, C., and Nielsen, J. (1994). Central control of disynaptic reciprocal inhibition in humans. *Acta Physiol. Scand.* 152, 351–363. doi: 10.1111/j.1748-1716.1994.tb09817.x

Daly, J. J., and Wolpaw, J. R. (2008). Brain-computer interfaces in neurological rehabilitation. *Lancet Neurol.* 7, 1032–1043. doi: 10.1016/S1474-4422(08)70223-70220

Daly, J. J., Cheng, R., Rogers, J., Litinas, K., Hrovat, K., and Dohring, M. (2009). Feasibility of a new application of noninvasive brain computer interface (BCI): a case study of training for recovery of volitional motor control after stroke. *J. Neurol. Phys. Ther.* 33, 203–211. doi: 10.1097/NPT.0b013e3181c1fc0b

Geertsen, S. S., Stecina, K., Meehan, C. F., Nielsen, J. B., and Hultborn, H. (2011). Reciprocal Ia inhibition contributes to motoneuronal hyperpolarisation during the inactive phase of locomotion and scratching in the cat. *J. Physiol.* 589, 119–134. doi: 10.1113/jphysiol.2010.199125

Hebb, D. O. (2005). *The Organization of Behavior*. London: Psychology Press.

Heremans, E., Helsen, W. F., De Poel, H. J., Alaerts, K., Meyns, P., and Feys, P. (2009). Facilitation of motor imagery through movement-related cueing. *Brain Res.* 1278, 50–58. doi: 10.1016/j.brainres.2009.04.041

Krakauer, J. W., and Marshall, R. S. (2015). The proportional recovery rule for stroke revisited. *Ann. Neurol.* 78, 845–847. doi: 10.1002/ana.24537

Kujirai, K., Kujirai, T., Sinkjaer, T., and Rothwell, J. C. (2006). Associative plasticity in human motor cortex during voluntary muscle contraction. *J. Neurophysiol.* 96, 1337–1346. doi: 10.1152/jn.01140.2005

Kumpulainen, S., Avela, J., Gruber, M., Bergmann, J., Voigt, M., Linnamo, V., et al. (2015). Differential modulation of motor cortex plasticity in skill- and endurance-trained athletes. *Eur. J. Appl. Physiol.* 115, 1107–1115. doi: 10.1007/s00421-014-3092-3096

Kumpulainen, S., Mrachacz-Kersting, N., Peltonen, J., Voigt, M., and Avela, J. (2012). The optimal interstimulus interval and repeatability of paired associative stimulation when the soleus muscle is targeted. *Exp. Brain Res.* 221, 241–249. doi: 10.1007/s00221-012-3165-x

Li, M., Liu, Y., Wu, Y., Liu, S., Jia, J., and Zhang, L. (2013). Neurophysiological substrates of stroke patients with motor imagery-based brain-computer interface training. *Int. J. Neurosci.* 124, 403–415. doi: 10.3109/00207454.2013.850082

McFarland, D. J., McCane, L. M., David, S. V., and Wolpaw, J. R. (1997). Spatial filter selection for EEG-based communication. *Electroencephalogr. Clin. Neurophysiol.* 103, 386–394. doi: 10.1016/S0013-4694(97)00022-22

Mrachacz-Kersting, N., Fong, M., Murphy, B. A., and Sinkjaer, T. (2007). Changes in excitability of the cortical projections to the human tibialis anterior after paired associative stimulation. *J. Neurophysiol.* 97, 1951–1958. doi: 10.1152/jn.01176.2006

Mrachacz-Kersting, N., Geertsen, S. S., Stevenson, A. J., and Nielsen, J. B. (2017a). Convergence of ipsi- and contralateral muscle afferents on common interneurons mediating reciprocal inhibition of ankle plantarflexors in humans. *Exp. Brain Res.* 235, 1555–1564. doi: 10.1007/s00221-016-4871-4876

Mrachacz-Kersting, N., Jiang, N., Stevenson, A. J., Niazi, I. K., Kostic, V., Pavlovic, A., et al. (2016). Efficient neuroplasticity induction in chronic stroke patients by an associative brain-computer interface. *J. Neurophysiol.* 115, 1410–1421. doi: 10.1152/jn.00918.2015

Mrachacz-Kersting, N., Kristensen, S. R., Niazi, I. K., and Farina, D. (2012). Precise temporal association between cortical potentials evoked by motor imagination and afference induces cortical plasticity. *J. Physiol.* 590, 1669–1682. doi: 10.1113/jphysiol.2011.222851

Mrachacz-Kersting, N., Stevenson, A. J. T., Aliakbaryhosseinabadi, S., Lundgaard, A. C., Jørgensen, H. R., Severinsen, K., et al. (2017b). "An associative brain-computer-interface for acute stroke patients," in *Converging Clinical and Engineering Research on Neurorehabilitation II Biosystems & Biorobotics*, eds J. Ibáñez, J. González-Vargas, J. M. Azorín, M. Akay, and J. L. Pons (Cham: Springer), 841–845. doi: 10.1007/978-3-319-46669-9-137

Mrachacz-Kersting, N., Voigt, M., Stevenson, A. J. T., Aliakbaryhosseinabadi, S., Jiang, N., Dremstrup, K., et al. (2017c). The effect of type of afferent feedback timed with motor imagery on the induction of cortical plasticity. *Brain Res.* 1674, 91–100. doi: 10.1016/j.brainres.2017.08.025

Mukaino, M., Ono, T., Shindo, K., Fujiwara, T., Ota, T., Kimura, A., et al. (2014). Efficacy of brain-computer interface-driven neuromuscular electrical stimulation for chronic paresis after stroke. *J. Rehabil. Med.* 46, 378–382. doi: 10.2340/16501977-16501785

Niazi, I. K., Mrachacz-Kersting, N., Jiang, N., Dremstrup, K., and Farina, D. (2012). Peripheral electrical stimulation triggered by self-paced detection of motor intention enhances motor evoked potentials. *IEEE Trans. Neural Syst. Rehabil. Eng.* 20, 595–604. doi: 10.1109/TNSRE.2012.2194309

Nielsen, J. B., and Sinkjaer, T. (2002). Afferent feedback in the control of human gait. *J. Electromyogr. Kinesiol.* 12, 213–217. doi: 10.1016/S1050-6411(02)00023-8

Nielsen, J. B. (2004). Sensorimotor integration at spinal level as a basis for muscle coordination during voluntary movement in humans. *J. Appl. Physiol.* 96, 1961–1967. doi: 10.1152/japplphysiol.01073.2003

Oldfield, R. C. (1971). The assessment and analysis of handedness: the edinburgh inventory. *Neuropsychologia* 9, 97–113. doi: 10.1016/0028-3932(71)90067-4

Pichiorri, F., Morone, G., Petti, M., Toppi, J., Pisotta, I., Molinari, M., et al. (2015). Brain-computer interface boosts motor imagery practice during stroke recovery. *Ann. Neurol.* 77, 851–865. doi: 10.1002/ana.24390

Ramos-Murguialday, A., Broetz, D., Rea, M., Läer, L., Yilmaz, Ö., Brasil, F. L., et al. (2013). Brain-machine interface in chronic stroke rehabilitation: a controlled study. *Ann. Neurol.* 74, 100–108. doi: 10.1002/ana.23879

Stefan, K. (2000). Induction of plasticity in the human motor cortex by paired associative stimulation. *Brain* 123, 572–584. doi: 10.1093/brain/123.3.572

Stefan, K., Wycislo, M., and Classen, J. (2004). Modulation of associative human motor cortical plasticity by attention. *J. Neurophysiol.* 92, 66–72. doi: 10.1152/jn.00383.2003

Stubbs, P. W., and Mrachacz-Kersting, N. (2009). Short-latency crossed inhibitory responses in the human soleus muscle. *J. Neurophysiol.* 102, 3596–3605. doi: 10.1152/jn.00667.2009

Suppa, A., Quartarone, A., Siebner, H., Chen, R., Di Lazzaro, V., Del Giudice, P., et al. (2017). The associative brain at work: evidence from paired associative stimulation studies in humans. *Clin. Neurophysiol.* 128, 2140–2164. doi: 10.1016/j.clinph.2017.08.003

Teo, W. P., and Chew, E. (2014). Is motor-imagery brain-computer interface feasible in stroke rehabilitation? *PM R* 6, 723–728. doi: 10.1016/j.pmrj.2014.01.006

Walter, W. G., Cooper, R., Aldridge, V. J., McCallum, W. C., and Winter, A. L. (1964). Contingent negative variation: an electric sign of sensorimotor association and expectancy in the human brain. *Nature* 203, 380–384. doi: 10.1038/203380a0

Xu, R., Jiang, N., Mrachacz-Kersting, N., Lin, C., Asín Prieto, G., Moreno, J. C., et al. (2014). A closed-loop brain-computer interface triggering an active ankle-foot orthosis for inducing cortical neural plasticity. *IEEE Trans. Biomed. Eng.* 61, 2092–2101. doi: 10.1109/TBME.2014.2313867

Young, B. M., Nigogosyan, Z., Walton, L. M., Song, J., Nair, V. A., Grogan, S. W., et al. (2014). Changes in functional brain organization and behavioral correlations after rehabilitative therapy using a brain-computer interface. *Front. Neuroeng.* 7:26. doi: 10.3389/fneng.2014.00026

Conflict of Interest Statement: The authors declare that the research was conducted in the absence of any commercial or financial relationships that could be construed as a potential conflict of interest.

Copyright © 2018 Mrachacz-Kersting and Aliakbaryhosseinabadi. This is an open-access article distributed under the terms of the Creative Commons Attribution License (CC BY). The use, distribution or reproduction in other forums is permitted, provided the original author(s) and the copyright owner(s) are credited and that the original publication in this journal is cited, in accordance with accepted academic practice. No use, distribution or reproduction is permitted which does not comply with these terms.

frontiers in Neuroscience

ORIGINAL RESEARCH
published: 13 July 2018
doi: 10.3389/fnins.2018.00477

A Feasibility Clinical Trial to Improve Social Attention in Autistic Spectrum Disorder (ASD) Using a Brain Computer Interface

Carlos Amaral[1], *Susana Mouga*[1,2], *Marco Simões*[1,3], *Helena C. Pereira*[1], *Inês Bernardino*[1], *Hugo Quental*[1], *Rebecca Playle*[4], *Rachel McNamara*[4], *Guiomar Oliveira*[2,5,6,7] *and Miguel Castelo-Branco*[7,8,9]*

[1] CNC.IBILI—Institute for Biomedical Imaging and Life Sciences, Faculty of Medicine, University of Coimbra, Coimbra, Portugal, [2] Unidade de Neurodesenvolvimento e Autismo do Serviço do Centro de Desenvolvimento da Criança, Pediatric Hospital, Centro Hospitalar e Universitário de Coimbra, Coimbra, Portugal, [3] Center for Informatics and Systems, University of Coimbra, Coimbra, Portugal, [4] Centre for Trials Research, Cardiff University, Cardiff, Wales, [5] University Clinic of Pediatrics, Faculty of Medicine, University of Coimbra, Coimbra, Portugal, [6] Centro de Investigação e Formação Clínica, Hospital Pediátrico, Centro Hospitalar e Universitário de Coimbra, Coimbra, Portugal, [7] Faculty of Medicine, University of Coimbra, Coimbra, Portugal, [8] CIBIT, Coimbra Institute for Biomedical Imaging and Translational Research, ICNAS - Institute of Nuclear Sciences Applied to Health, University of Coimbra, Coimbra, Portugal, [9] ICNAS—Produção Unipessoal, Coimbra, Portugal

OPEN ACCESS

Edited by:
Christoph Guger,
Guger Technologies, Austria

Reviewed by:
Chang-Hwan Im,
Hanyang University, South Korea
Ning Jiang,
University of Waterloo, Canada

***Correspondence:**
Miguel Castelo-Branco
mcbranco@fmed.uc.pt

Specialty section:
This article was submitted to Neural Technology, a section of the journal Frontiers in Neuroscience

Received: *31 January 2018*
Accepted: *25 June 2018*
Published: *13 July 2018*

Citation:
Amaral C, Mouga S, Simões M, Pereira HC, Bernardino I, Quental H, Playle R, McNamara R, Oliveira G and Castelo-Branco M (2018) A Feasibility Clinical Trial to Improve Social Attention in Autistic Spectrum Disorder (ASD) Using a Brain Computer Interface. Front. Neurosci. 12:477. doi: 10.3389/fnins.2018.00477

Deficits in the interpretation of others' intentions from gaze-direction or other social attention cues are well-recognized in ASD. Here we investigated whether an EEG brain computer interface (BCI) can be used to train social cognition skills in ASD patients. We performed a single-arm feasibility clinical trial and enrolled 15 participants (mean age 22y 2m) with high-functioning ASD (mean full-scale IQ 103). Participants were submitted to a BCI training paradigm using a virtual reality interface over seven sessions spread over 4 months. The first four sessions occurred weekly, and the remainder monthly. In each session, the subject was asked to identify objects of interest based on the gaze direction of an avatar. Attentional responses were extracted from the EEG P300 component. A final follow-up assessment was performed 6-months after the last session. To analyze responses to joint attention cues participants were assessed pre and post intervention and in the follow-up, using an ecologic "Joint-attention task." We used eye-tracking to identify the number of social attention items that a patient could accurately identify from an avatar's action cues (e.g., looking, pointing at). As secondary outcome measures we used the Autism Treatment Evaluation Checklist (ATEC) and the Vineland Adaptive Behavior Scale (VABS). Neuropsychological measures related to mood and depression were also assessed. In sum, we observed a decrease in total ATEC and rated autism symptoms (Sociability; Sensory/Cognitive Awareness; Health/Physical/Behavior); an evident improvement in Adapted Behavior Composite and in the DLS subarea from VABS; a decrease in Depression (from POMS) and in mood disturbance/depression (BDI). BCI online performance and tolerance were stable along the intervention. Average P300 amplitude and alpha power were also preserved across sessions. We have demonstrated

the feasibility of BCI in this kind of intervention in ASD. Participants engage successfully and consistently in the task. Although the primary outcome (rate of automatic responses to joint attention cues) did not show changes, most secondary neuropsychological outcome measures showed improvement, yielding promise for a future efficacy trial.

(clinical-trial ID: NCT02445625—clinicaltrials.gov).

Keywords: autism, clinical trial, brain-computer interface, EEG, virtual reality, social attention

INTRODUCTION

Autism spectrum disorder (ASD) is a set of pervasive and sustained neurodevelopmental conditions characterized by persistent deficits in social communication and social interaction, alongside restricted, repetitive patterns of behavior, interests, or activities (American Psychiatric Association, 2013). This condition has a significant economic and social impact due to its high prevalence [estimated at ∼1.5% in developed countries around the world (Baxter et al., 2015; Christensen et al., 2016; Lyall et al., 2017) and ∼10 per 10,000 children in Portugal (Oliveira et al., 2007)]. It is associated with high morbidity and impact on daily family life (Karst and Van Hecke, 2012; Boshoff et al., 2016; Harrop et al., 2016; Jones et al., 2016; Schlebusch et al., 2016).

Joint attention (JA) is an early-developing social communication skill defined by the non-verbal coordination of attention of two individuals toward a third object or event (Bakeman and Adamson, 1984). People with ASD show severe deficits in JA abilities (Baron-Cohen, 1989; Baron-Cohen et al., 1997; Swettenham et al., 1998; Leekam and Moore, 2001; Klin, 2002; Dawson et al., 2004) which plays a critical role in the development of their social and language capabilities (Charman, 1998, 2003).

Electroencephalography (EEG) based brain-computer interfaces (BCI), represent widely studied communication technologies (Farwell and Donchin, 1988; Kleih et al., 2011; Mak et al., 2011; Wolpaw and Wolpaw, 2012). Virtual reality (VR) has been increasingly used in neuro-rehabilitation, in particular of motor control and has shown promising results (Larson et al., 2011, 2014; Astrand et al., 2014; Tankus et al., 2014; Salisbury et al., 2016). However, concerning cognitive applications in the field of neuro-rehabilitation the use of combined VR and BCIs has only been used with children with attention deficit hyperactivity disorder (which includes the presence of frequent inattentive, impulsive, and hyperactive behaviors; American Psychiatric Association, 2013).

The review provided by Friedrich et al. (2014), grounded on a series of neurofeedback training studies, postulates that quantitative EEG-based neurofeedback training is viable as a personalized therapeutic approach in ASD. They also suggest the development of a game platform that includes social interactions and specific feedback based on behavior, neurophysiological, and/or peripheral physiological responses of the users. The ultimate goal is to reinforce significant behaviors, such as social interactions using neurobehavioral signals to promote behavioral, cognitive, and emotional improvement in ASD people. Along this line several studies do advocate (Wainer and Ingersoll, 2011; Bekele et al., 2014; Georgescu et al., 2014) that the use of ecological, realistic, and interactive virtual environments may be the solution for the well-known generalization problem of the rehabilitation of social skills in ASD subjects to real life settings. Golan and Baron-Cohen (2006) suggested that the use of computerized intervention in ASD individuals enables the development of skills in a highly standardized, predictable, and controlled environment, while simultaneously allowing an individual to work at his own pace and ability level.

Based on these suggestions, we propose a virtual reality P300-based BCI paradigm (which technical implementation is described in Amaral et al., 2017) that tries to couple the advantages of ecological, realistic and interactive virtual environments with the attention related nature of the P300 brain waveform to create a cognitive training tool for ASD. The P300-based paradigm that we present here consists on an immersive environment were the subject must follow a non-verbal social agent cue (head turn) and direct his/her attention to the target object. The attentional mental state of the subject is monitored through the detection of oddballs, which leads to a P300 signal which allows giving feedback about his/her attentional focus. The P300 signal is a well-known neural signature of attention processes for detection of rare items in a stimulus series—oddball paradigm—(for a review see Patel and Azzam, 2005; Polich, 2007; Duncan et al., 2009). We decided to couple the training of joint attention skills to the P300 signal because the latter is widely used in focused attention studies, and is related to integration of information with context and memory (Halgren et al., 1995). Moreover, with the automatic detection of P300 signals one can provide direct feedback about the participant's attentional focus. This provides information that the subject can use to self-monitor his/her performance about where to look and subsequently allow ASD subjects to adjust behavior. Given the repetitive nature of this type of oddball paradigm, and its operant learning properties, our motivation for the construction of this paradigm is based on the hypothesis that ASD subjects can assimilate joint attention skills by automating the response to the social cue that is given during the task we created. The current trial set out to assess the feasibility and potential clinical effects of the use of this type of technology in ASD and attempts to assess the use of neurophysiologic-based rehabilitation tools for improving social behavior in ASD.

APPARATUS AND METHODS

This was a single-arm clinical feasibility trial study conducted in Portugal.

Prior to subject recruitment, ethical approvals were obtained from the Ethics Commission of the Faculty of Medicine of the University of Coimbra (Comissão de Ética da Faculdade de Medicina da Universidade de Coimbra), the INFARMED-Autoridade Nacional do Medicamento e Produtos de Saúde, I.P. (Portuguese Authority of Medicines and Health Products) and CEIC—Comissão de Ética para a Investigação Clínica (Portuguese Ethics Committee for Clinical Research).

This study and all the procedures were approved and was conducted in accordance with the declaration of Helsinki. All subjects agreed and signed a written informed consent prior to screening procedures and recruitment (clinical-trial ID: NCT02445625-clinicaltrials.gov).

This study and all the procedures were approved and was conducted in accordance with the declaration of Helsinki.

All subjects agreed and signed a written informed consent prior to screening procedures and recruitment (clinical-trial ID: NCT02445625—clinicaltrials.gov).

Participants

Study included 15 adolescents and adults (mean age = 22 years and 2 months, ranging from 16 to 38 years old) with high-functioning ASD (Full-Scale Intelligent Quotient [FSIQ] (Wechsler, 2008): Mean = 102.53; SD = 11.64).

These participants met the inclusion criteria: positive diagnostic results for ASD assigned on the basis of the gold standard instruments: parental or caregiver interview—Autism Diagnostic Interview-Revised (Le Couteur et al., 2003); direct structured subject assessment—Autism Diagnostic Observation Schedule (Lord and Rutter, 1999); and/or the current diagnostic criteria for ASD according to the Diagnostic and Statistical Manual of Mental Disorders, Fifth Edition (DSM-5) (American Psychiatric Association, 2013).

All diagnostic and neuropsychological assessments were performed by a psychologist (SM or IB) under the supervision of a medical doctor—a neurodevelopmental pediatrician (GO) in a face to face standardized situation in our clinical research institute.

Participants were excluded if they had intellectual disability, with a FSIQ inferior to 80 (Wechsler, 2008) and associated medical conditions such as epilepsy, neurocutaneous, or other genetic known syndromes, or other usual comorbidity in ASD samples.

Intervention and Apparatus

The baseline visit was used to obtain consent and collect baseline data. Collected baseline data included demographics, medication, neuropsychological measures related to the ASD diagnosis [ADI-R (Le Couteur et al., 2003); ADOS (Lord and Rutter, 1999); and DSM-5 (American Psychiatric Association, 2013) criteria] and intellectual ability (IQ measured by WAIS-III; Wechsler, 2008) and the outcome measures detailed below.

The intervention comprised seven BCI sessions spread over 4 months. The first four sessions weekly and the remaining monthly. Adherence and compliance were evaluated using the following definitions: Adherence was defined as attending all seven BCI sessions. Compliance was assessed based on the

FIGURE 1 | Representation of the used scenarios. **(A)** Cafe scenario; **(B)** Classroom scenario; **(C)** Kiosk scenario; **(D)** Zebra crossing scenario.

percent of subjects who have performed the scheduled number of interventional sessions.

Participants outcome assessments were performed at baseline (session 0), post-training (session 7), and follow-up (6 months post-training).

The baseline visit was in the same day of the session 1. The 7 sessions included BCI intervention, before and after which the participants were asked to complete a questionnaire about how were they feeling in the moment—Profile of Mood States (POMS) (McNair et al., 1992; Faro Viana et al., 2012).

The Primary outcome measure was a customized ecologic "Joint-attention assessment task" (JAAT), assessing the detection of initiation of joint attention cues (from avatars—gazing or pointing cues). We recorded (using eye-tracking) the number of items of social attention that a patient could accurately identify from an avatar's action cues (e.g., looking at, pointing at).

JAAT consisted in four virtual scenarios. The scenarios were as follows:

Cafe: interior of a cafe with a maid (avatar) inside the balcony. The viewer's position is in front of the balcony. Several common objects in a cafe (packets of chips, several drinks, chewing gums, bottles, and a lamp) are distributed the around the avatar's position. (**Figure 1A**);
Classroom: standing in front of a table with a professor (avatar) and with a ruler, a book, a notebook, a protractor, a pencil, and an eraser on top of the table (**Figure 1B**). The scenario also has another tables and chairs;
Kiosk: standing in front of a street kiosk with the employee inside and several newspapers and magazines scattered on the kiosk, around the employee position (**Figure 1C**);
Zebra crossing: standing in one side of a street, waiting to cross the zebra crossing, with one person on the other side. The other side of the street has a traffic light, a traffic signal, a garbage can, and a map in a bus stop (**Figure 1D**).

Participants were sat in an adjustable rotary office chair wearing the Oculus Rift DK 2 headset. Eye movements were recorded with Eye Tracking HMD package from SMI embedded in the Oculus Rift itself, with sampling rate of 60 Hz, and accuracy of 0.5–1°. The scenes had a 360° perspective and a real-time fully immersive experience. JAAT started with the eye-tracker calibration and validation (5-point validation method built in-house). Next, the presentation of each scenario was done. The order by each scenario was presented was random. The task started with a 30 s free-viewing period followed by a series of avatar animations spaced by between 2 and 2.5 s. The animations were divided in joint attention animations and control animations. The joint attention animations comprise the head turning of the avatar or pointing to one object of interest in the scene.

The animations were repeated two times in a random order which gives a total of 18 joint attention animations in the café scenario, 10 in classroom scenario, 16 in kiosk, and 10 joint attention animations in zebra crossing scenario. The overall joint attention events were 54, and control (no joint attention) animations 32. Control animations included the avatar coughing, rolling the head, scratching the head and yawning. Participants were instructed to act naturally. They were not aware that their eye movements were being recorded.

The number of items of social attention that a patient could accurately identify from an avatar's action cues were obtained by defining areas of interest (AI) with 3D boxes. These AI overlap with objects in the scenes that were relevant in the context. For example, the drinks in the cafe, the notebook and the ruler in the classroom, the magazines in the kiosk and the traffic lights on the zebra crossing scenario. AI in each scenario are shown in **Figure 2**.

FIGURE 2 | Areas of interest in each scenario of JAAT.

The number of items of social attention were defined as eye fixations inside the AI after the start of the joint attention animation and until between 2 and 2.5 s. We assumed a fixation duration as a fixation with more than 300 ms (based on the range of mean fixation duration in scene perception presented in Rayner, 2009). Inside the JA responses we considered two types of responses:

JAAT_No face—Fixation on the target object of the joint attention animation after the animation starts.

JAAT_Face—Fixation on the target object of the joint attention animation after the animation beginning that is preceded by a fixation on the face of the avatar.

As secondary outcome measures we included the Autism Treatment Evaluation Checklist (ATEC) (Rimland and Edelson, 1999), specifically designed to measure treatment effectiveness, and Vineland Adaptive Behavior Scales (VABS), which focuses on adaptive functioning (Sparrow et al., 1984). Other neuropsychological measures related to mood, anxiety and depression were also assessed: Profile of Mood States (POMS) (McNair et al., 1992; Faro Viana et al., 2012); Hospital Anxiety & Depression Scale (HADS) (Zigmond and Snaith, 1983; Pais-Ribeiro et al., 2007) and Beck Depression Inventory (BDI) (Beck, 1961; Vaz-Serra and Abreu, 1973; Beck and Steer, 1990).

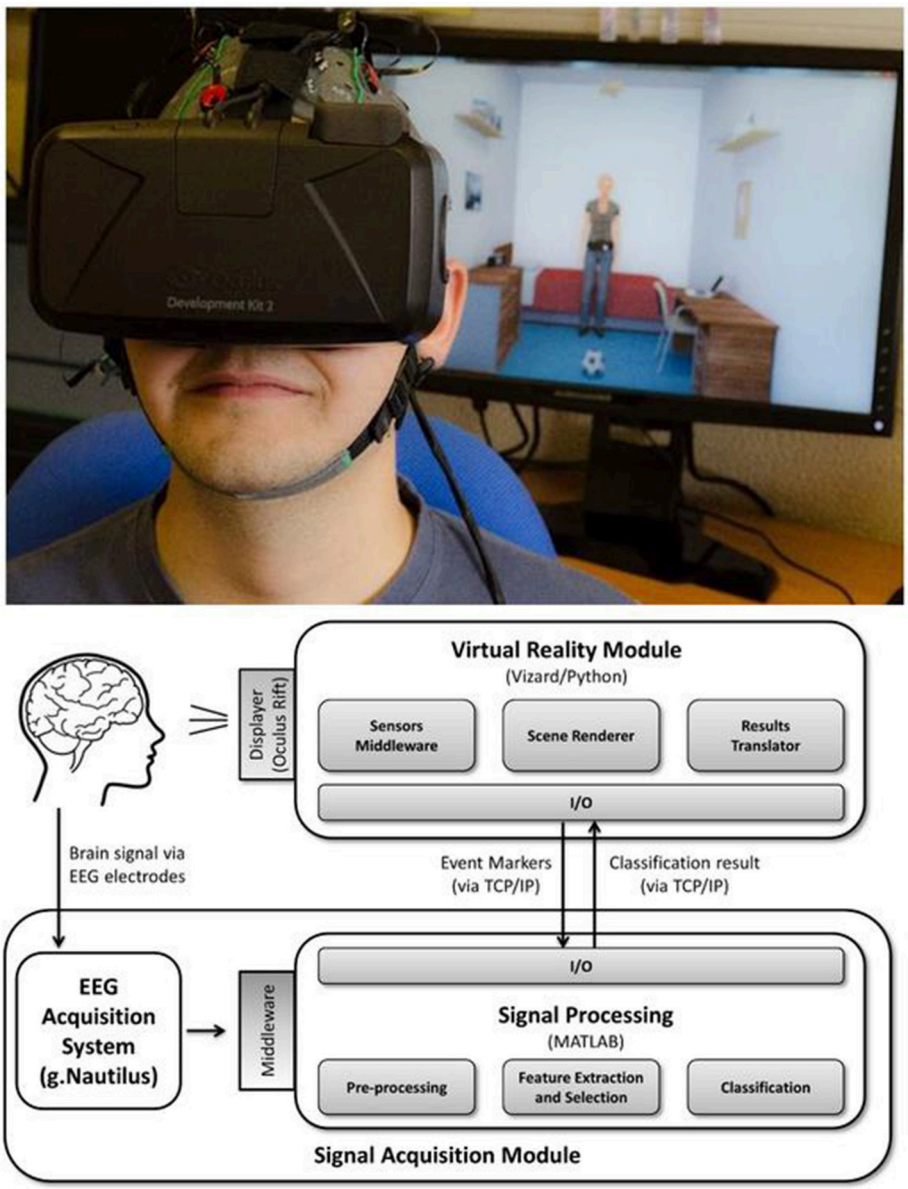

FIGURE 3 | BCI apparatus overview. **(Top)** Person wearing Oculus Rift and g.Nautilus EEG system (part of the virtual reality P300-based BCI) and the observer's viewing window on the screen. **(Bottom)** Block design of the system. Informed consent was obtained from the individual for the publication of this image.

The experimental apparatus used for the BCI interventions is shown in **Figure 3**.

BCI sessions were carried out in a spacious and quiet room with minimal electrical interference and participants were seated in an adjustable office chair in front of a table.

The virtual reality P300-based BCI paradigm used comprises an immersive virtual environment presented to the participants via the Oculus Rift Development Kit 2 headset (from Oculus VR) which participants wear in front of the eyes during the intervention sessions. An EEG cap was also placed in participants

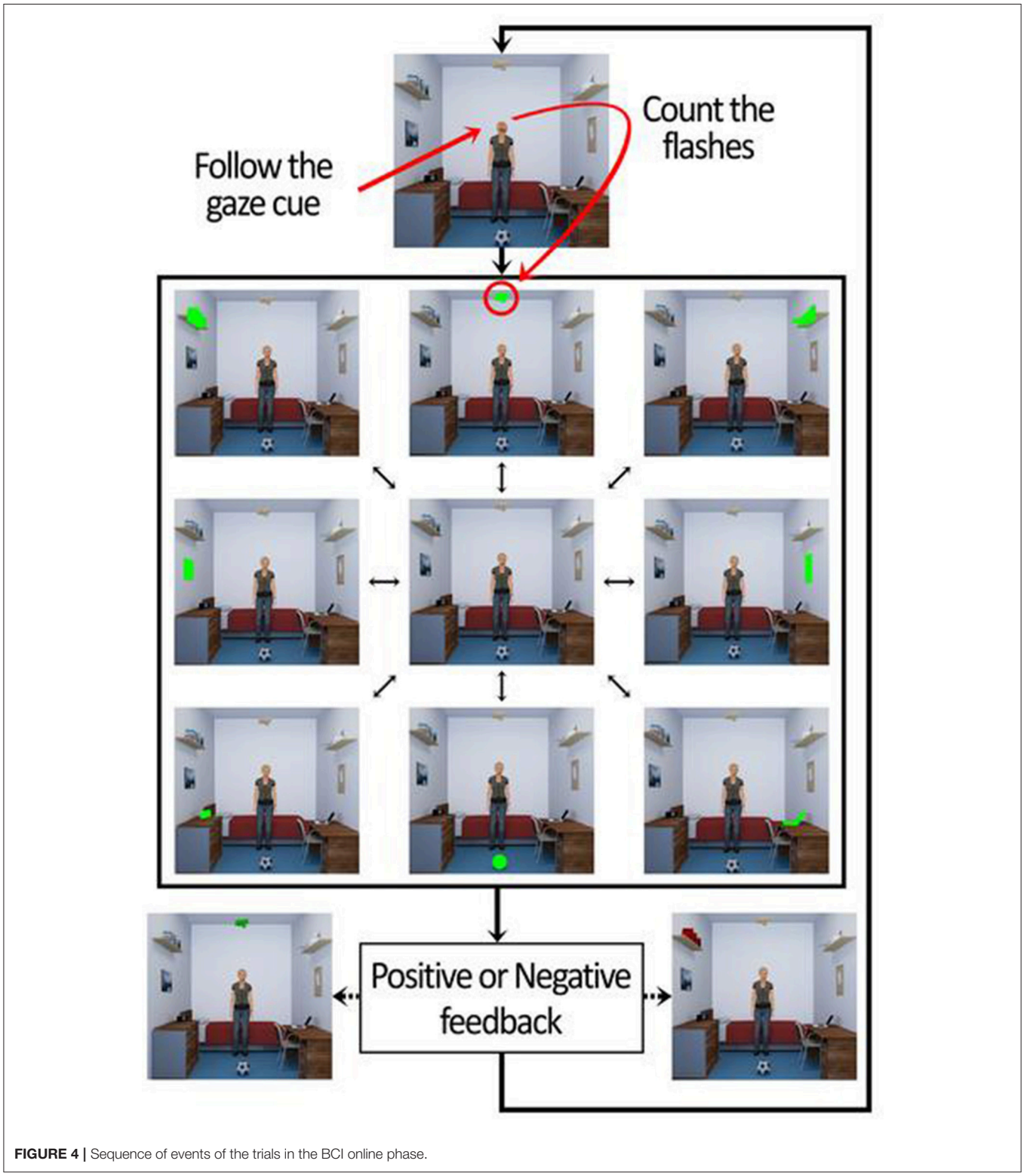

FIGURE 4 | Sequence of events of the trials in the BCI online phase.

head. The cap had 16 active electrodes that do not require abrasive skin treatment and with completely wireless signal transmission (g.Nautilus from gTEC, Austria). The EEG data were acquired from 8 electrodes positions (C3, Cz, C4, CPz, P3, Pz, P4, POz), the reference was placed at the right ear and the ground electrode was placed at AFz. Sampling rate was set at 250 Hz. EEG data were acquired notch filtered at 50 Hz and passband filtered between 2 and 30 Hz.

The virtual environment consists in a bedroom with common type of furniture (shelves, a bed, a table, a chair, and a dresser) and objects (frames, books, lights, a printer, a radio, a ball, a door, a window, and a laptop). The BCI task was divided in 3 phases. The first two were part of the calibration process of the BCI, and the last one the online phase. In the first phase the participants were directly and explicitly instructed to attend the target object in order to remove potential errors identifying the target object related with social attention deficits present in ASD. In the second phase the participants were asked about which object was chosen by the avatar (after avatar's animation) to guarantee the user learned to read the social joint attention cue of the avatar and use this information correctly. In the third phase the participants were asked to respond to the head cue of the avatar in the center of the scene, looking to the object of interest. In all the three phases of BCI, after the redirection of attention of participant in each trial, they were asked to mentally count the blinks of the object of interest. Each trial consisted in 10 sequential runs, and each such run consisted of flashing all the 8 objects in the scene (green flashes) in a randomized order: 1. a wooden plane hanging from the ceiling; 2. a printer on a shelf; 3. a corkboard on the wall; 4. a laptop on a table; 5. a ball on the ground; 6. a radio on top of a dresser; 7. a picture on the wall; 8. books on a shelf. The highlight (flash) of each object occurred with an inter-stimulus interval of 200 ms. Each flash had the duration of 100 ms. This gives a total of 80 flashes per trial. Participants performed a total of 70 trials (10 in the first phase, 10 in the second, and 50 in the online phase).

The data recorded from the first 20 calibration trials stores the P300 responses that occurs when the object of interest flashed, and statistical classifiers are used to identify this response. These classifiers are then used in the online phase to identify whether participants were counting the flashes of avatar's object of interest. If it was done properly by the participant the BCI gave a positive feedback (object of interest turns green at the end of the trial). If not, the object turned red. This mechanism is shown in **Figure 4**. The overall functioning of BCI is explained in detail in Amaral et al. (2017), where we tested the best setup to use in this BCI and also performed pilot tests in ASD participants.

TABLE 1 | Baseline demographic data.

	n	% or Mean (SD)
Age	15	22 years and 2 months (5 years and 6 months)
Gender	15	100% Male
Education	15	Junior Highschool (9 years) 6.67% Incomplete Highschool (11 years)13.33% Highschool (12 years) 66.67% Bachelor 6.67% Master 6.67%

TABLE 2 | Baseline outcome measures.

	n	Mean (SD)	Data completeness %
CORE OUTCOMES			
ADIR_Social interaction	14	16.14 (4.56)	93
ADIR_Communication	14	12.14 (5.39)	93
ADIR _Repetitive and restricted behavior	14	6.14 (2.41)	93
ADIR_Developmental delay	14	2.21 (1.89)	93
ADOS _Communication	15	3.20 (0.86)	100
ADOS_Social interaction	15	6.27 (1.34)	100
ADOS_Total	15	9.47 (1.92)	100
DSM_5 Criteria	15	5.73 (0.59)	100
WAIS-III (FSIQ)	15	102.53 (11.64)	100
WAIS-III (VIQ)	15	102.33 (16.63)	100
WAIS-III (PIQ)	15	102.47 (10.97)	100
HADS_Total	15	10.93 (5.78)	100
BDI_Total	15	9.13 (6.56)	100
POMS_Tension	15	6.40 (3.23)	100
POMS_Depression	15	7.53 (6.13)	100
POMS_Anger	15	4.00 (3.46)	100
POMS_Vigour	15	12.53 (6.80)	100
POMS_Fatigue	15	4.47 (3.96)	100
POMS_Confusion	15	6.80 (2.68)	100
POMS_Total	15	116.67 (18.54)	100
STUDY SPECIFIC OUTCOMES			
JAAT_NoFace	15	16.33 (9.36)	100
JAAT_Face	15	10.67 (9.35)	100
ATEC_SPEECH/LANGUAGE/ COMMUNICATION	15	4.07 (1.82)	100
ATEC_SOCIABILITY	15	12.64 (6.20)	100
ATEC_SENSORY/COGNITIVE AWARENESS	15	9.50 (5.13)	100
ATEC_HEALTH/PHYSICAL/BEHAVIOR	15	9.36 (6.25)	100
ATEC_Total	15	35.57 (12.53)	100
VABS_COM_S1	15	68.27 (21.53)	100
VABS_DLS_S1	15	77.53 (14.05)	100
VABS_SOC_S1	15	65.80 (16.79)	100
VABS_ABC_S1	15	65.73 (15.56)	100

TABLE 3 | Primary outcome—feasibility.

	% (n/n)
Recruitment/Consent	100
Retention (primary end point)	100
Retention (secondary end point)	100
Intervention uptake	100
Adherence/Completion	100
Compliance	100
Intervention delivery	100
Acceptability	100

Statistical Analysis

Our initial sample size was calculated using the G*Power tool (Faul et al., 2007). Based in other effects described in the literature, the effect size considered is 0.8 (the mean difference is 0.8 standard deviations). In these conditions, for power of 0.8 the estimated sample size is 15. Without the normality assumption of the distribution of the means differences, we would also need 15 subjects, considering a non-parametric test. However, these calculations were used only as a guide for sample size and in keeping with

TABLE 4 | Outcomes (for complete baseline and primary follow-up dataset).

	Baseline/Session 1		Primary follow-up time point (Session 7—post intervention)		Mean difference and 95% CI	
	n	Mean (SD)	*n*	Mean (SD)	Mean difference	95% CI
CORE OUTCOMES						
HADS_Total	15	10.93 (5.78)	15	9.13 (4.22)	1.80	(−0.40, 4.00)
BDI_Total	15	9.13 (6.56)	15	6.67 (5.25)	2.47	(0.38, 4.56)
POMS_Tension	15	6.40 (3.23)	15	5.20 (5.51)	1.20	(−2.06, 4.46)
POMS_Depression	15	7.53 (6.13)	15	3.80 (5.20)	3.73	(0.49, 6.97)
POMS_Anger	15	4.00 (3.46)	15	2.93 (6.12)	1.07	(−2.47, 4.60)
POMS_Vigour	15	12.53 (6.80)	15	12.87 (7.97)	−0.33	(−3.67, 3.00)
POMS_Fatigue	15	4.47 (3.96)	15	4.67 (5.92)	−0.20	(−3.20, 2.80)
POMS_Confusion	15	6.80 (2.68)	15	6.07 (3.60)	0.73	(−1.26, 2.72)
POMS_Total	15	116.67 (18.54)	15	109.80 (25.77)	6.87	(−7.20, 20.93)
STUDY SPECIFIC OUTCOMES						
JAAT_NoFace	15	16.33 (9.36)	15	13.73 (8.19)	2.60	(−2.20, 7.40)
JAAT_Face	15	10.67 (9.35)	15	7.80 (8.77)	2.87	(−0.07, 5.80)
ATEC_SPEECH/LANGUAGE/COMMUNICATION	15	4.07 (1.82)	15	2.93 (1.64)	1.07	(−0.23, 2.37)
ATEC_SOCIABILITY	15	12.64 (6.20)	15	8.50 (5.30)	4.33	(2.32, 6.35)
ATEC_SENSORY/COGNITIVE AWARENESS	15	9.50 (5.13)	15	6.14 (4.93)	3.47	(0.90, 6.03)
ATEC_HEALTH/PHYSICAL/BEHAVIOR	15	9.36 (6.25)	15	6.57 (5.39)	2.80	(0.65, 4.95)
ATEC_Total	15	35.57 (12.53)	15	24.29 (12.90)	11.53	(5.33, 17.74)
VABS_COM	15	68.27 (21.53)	15	71.33 (21.62)	−3.07	(−8.37, 2.24)
VABS_DLS	15	77.53 (14.05)	15	81.60 (14.46)	−4.07	(−6.40, −1.73)
VABS_SOC	15	65.80 (16.79)	15	67.67 (16.18)	−1.87	(−4.44, 0.70)
VABS_ABC	15	65.73 (15.56)	15	69.00 (15.20)	−3.27	(−5.48, −1.06)

TABLE 5 | Outcomes for complete baseline and secondary follow-up dataset.

	Baseline		Secondary follow-up time point (post intervention)		Mean difference and 95% CI	
	n	Mean (SD)	*n*	Mean (SD)	Mean difference	95% CI
STUDY SPECIFIC OUTCOMES						
JAAT_NoFace	15	16.33 (9.36)	15	15.00 (10.02)	1.33	(−4.47, 7.14)
JAAT_Face	15	10.67 (9.35)	15	7.53 (8.11)	3.13	(−2.00, 8.27)
ATEC_SPEECH/LANGUAGE/COMMUNICATION	15	4.07 (1.82)	14	1.79 (1.42)	2.29	(0.94, 3.63)
ATEC_SOCIABILITY	15	12.64 (6.20)	14	6.57 (5.14)	6.07	(3.23, 8.91)
ATEC_SENSORY/COGNITIVE AWARENESS	15	9.50 (5.13)	14	5.21 (4.28)	4.29	(1.31, 7.26)
ATEC_HEALTH/PHYSICAL/BEHAVIOR	15	9.36 (6.25)	14	4.86 (4.35)	4.50	(2.65, 6.35)
ATEC_Total	15	35.57 (12.53)	14	18.43 (11.77)	17.14	(10.38, 23.91)
VABS_COM	15	68.27 (21.53)	14	73.14 (17.29)	−7.36	(−12.53, −2.18)
VABS_DLS	15	77.53 (14.05)	14	86.29 (14.02)	−10.14	(−12.58, −7.71)
VABS_SOC	15	65.80 (16.79)	14	71.14 (16.11)	−6.79	(−10.13, −3.44)
VABS_ABC	15	65.73 (15.56)	14	72.00 (13.65)	−8.21	(−10.66, −5.77)

the feasibility design no explicit hypothesis testing was used.

The specific aim of the study was to assess the feasibility and effects of the use of virtual reality P300-based BCI paradigm in ASD. Based on this aforementioned aim, 95% confidence interval for differences in means are presented.

The assumptions of the statistical techniques used were validated. All statistical analysis was realized with the support of the version for Microsoft Windows® of the Statistical Package for Social Sciences, version 19 (SPSS®, Chicago, IL, USA).

Brain Computer Interface Evaluation of Signal Stability

We tested the stability across the seven sessions of three parameters: the BCI's balanced accuracy (see definition below) of target object detection, the average P300 maximum amplitude across trials and the mean alpha power variation in the band [8 12] Hz per trial. For the latter two, a cluster of the 8 channels was formed. For each subject, a linear regression was computed using the value of each parameter across sessions. The first order coefficient of the linear regressed model was extracted, and its distribution was tested against the hypothesis that its median value was equal to zero, using a Wilcoxon signed rank test. Graphical illustration of the stability of measures across sessions is provided. The tests were performed in Matlab 2014a.

RESULTS

Demographic data are provided in **Table 1**. Fifteen adolescents and adults (mean age = 22 years and 2 months, ranging from 16 to 38 years old) with high-functioning ASD (Full-Scale Intelligent Quotient [FSIQ] (Wechsler, 2008): Mean = 102.53; SD = 11.64) participated in the study between February 2016 and January 2017. Five patients were medicated (three with a neuroleptic, one with a psychostimulant and another with an antidepressant). We recruited 17 patients, because of two dropouts, which meets the target sample size. Dropouts were due to an eye abnormality in one patient, not reported during the recruitment, and a misdiagnosis of ASD in another patient.

Table 2 depicts the basic statistics related to core baseline and study specific outcome measures.

Concerning measures of feasibility, they are reported in **Table 3**.

Although an effect was not found for our primary measure of choice (JAAT), most secondary measures demonstrated a change (**Table 4**).

Table 4 shows the analysis of the clinical outcomes for complete baseline and primary follow-up. The analysis revealed no noticeable change in the total number of social attention items that a patient can accurately identify from avatar's action cues (JAAT_NoFace and JAAT_Face). On the other hand, there was variation in total ATEC scores, as well as in Sociability, Sensory/Cognitive Awareness, and Health/Physical/Behavior. Significant effects in Adapted Behavior Composite and in DLS (total and a subarea from VABS) were also observed. The depression subscale from POMS scores (POMS_Depression) showed a difference between the baseline and the primary follow-up time point. The mood disturbance/depression (BDI) scale also showed a change after the intervention.

In sum, we observed a 32% average decrease in total ATEC, rated autism symptoms (34% in Sociability; 37% in Sensory/Cognitive Awareness; 29% in Health/Physical/Behavior); 5% average improvement in Adapted Behavior Composite and 5% in DLS, subarea from VABS; 50% average decrease in Depression subscale from POMS and 27% average decrease in mood disturbance/depression (BDI).

Table 5 shows the analysis of the clinical outcomes for complete baseline and secondary follow-up. JAAT_NoFace and JAAT_Face scores also revealed

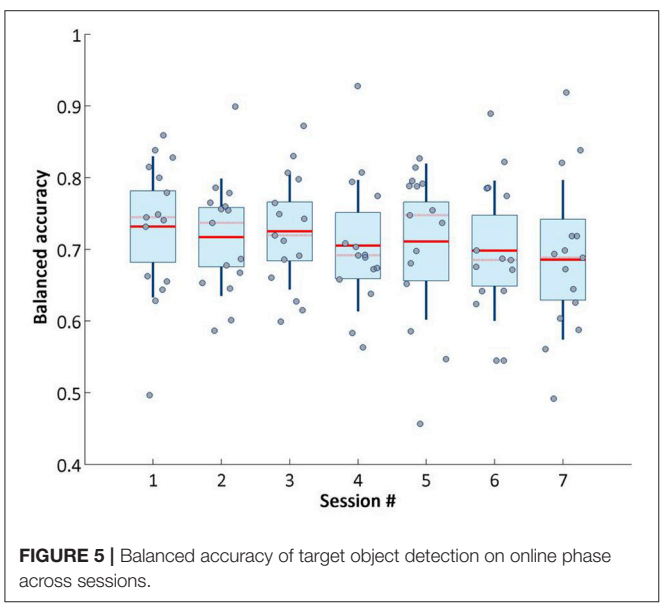

FIGURE 5 | Balanced accuracy of target object detection on online phase across sessions.

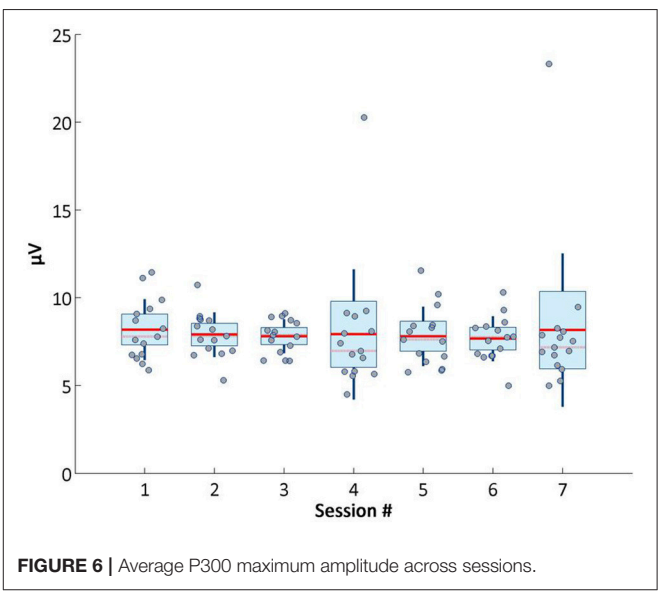

FIGURE 6 | Average P300 maximum amplitude across sessions.

no differences between baseline and the secondary follow-up time point. There were positive effects in all subscales (Speech/Language/Communication, Sociability, Sensory/Cognitive Awareness, and Health/Physical/Behavior) from ATEC and in ATEC total scores. There were also changes in Adapted Behavior Composite and in all subareas from VABS (COM, DLS, SOC).

No serious adverse events were reported.

Brain Computer Interface Evaluation of Signal Stability

We analyzed whether the signal quality and performance of our brain computer interface remained stable across intervention sessions. **Figure 5** shows across session balanced accuracy of our online classifier.

The unbalanced nature of the data set (the non-target objects flashes are 8 times more than the target ones, because of the different occurrence probability) makes the balanced accuracy the more reliable metric for assessing the classifier performance (Brodersen et al., 2010). Balanced accuracy is calculated following the formula: (*Specificity* + *Sensitivity*)/2. This value did not vary greatly across sessions. Although the overall trend decreased very slightly from session 1 to 7, our system retained stable performance across visits.

Concerning the P300 signal, which is pivotal for decoding attention related information, it also remained stable across sessions, as shown in **Figure 6**. Average P300 maximum amplitude was calculated averaging the maximum amplitude values (between 250 and 500 ms after the flashes onset) of the averaged event-related potentials of the target object flashes in the third phase of BCI (online).

In **Figure 7** it is possible to observe the P300 waveform across sessions.

Accordingly, P300 maximum amplitude did not vary and was statistical verified, demonstrating the presence of stable attention related signals across visits. Stability of neurophysiological patterns was further examined by investigating changes in alpha modulation (**Figure 8**), and remained around similar levels across sessions.

DISCUSSION

In this study we assessed a virtual reality P300-based BCI paradigm in ASD. Our device coupled an interactive virtual environment with the attention signature of the P300 brain waveform, featuring a cognitive training tool for ASD. Participants had to follow a non-verbal social agent cue. As a cautionary note, the fact that a P300 signal can be detected with

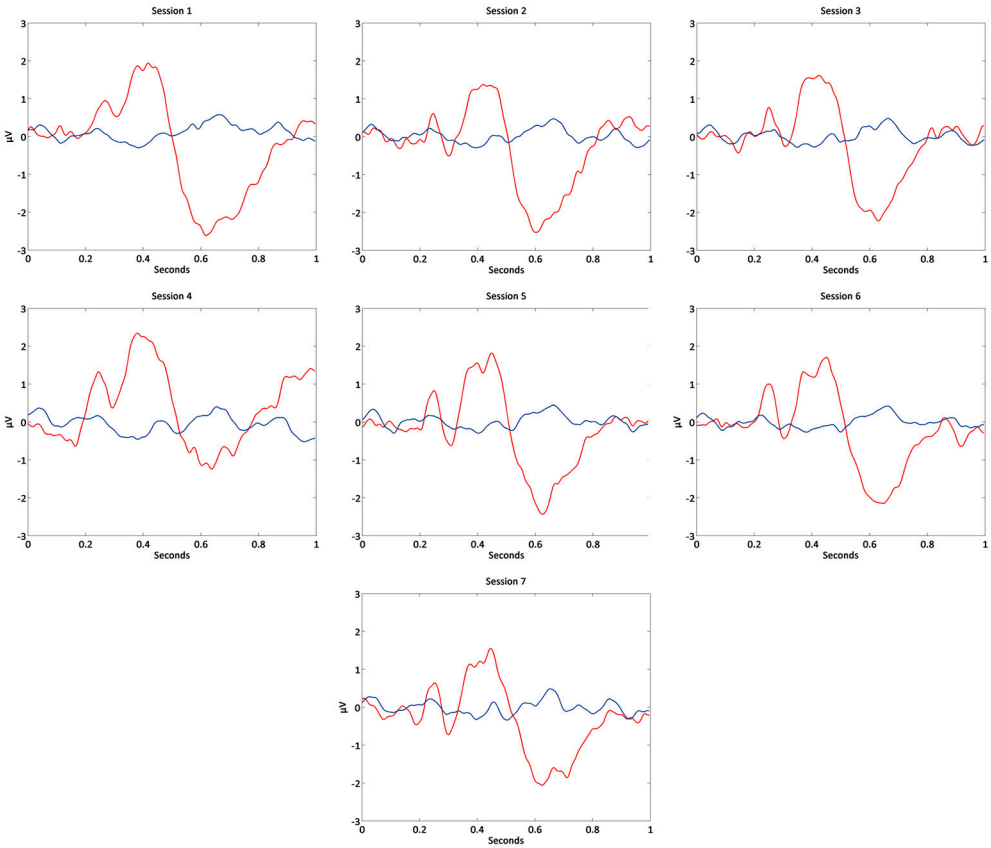

FIGURE 7 | Grand-average of event-related potentials in each BCI session of Cz channel.

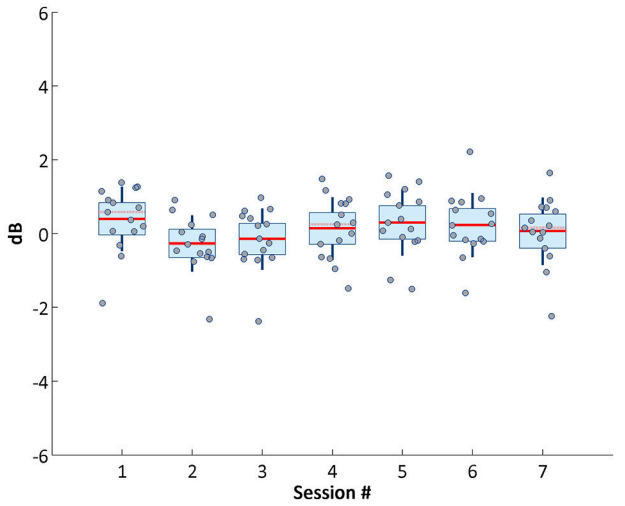

FIGURE 8 | Average alpha power across sessions.

high accuracy does not necessarily imply that the stimulus is suitable and well tolerated. Nevertheless, the current trial proved the feasibility and potentially useful clinical effects of the use of this type of technology in ASD.

Although the main goal of the study was not to test efficacy measures, some relevant effects were observed, even in spite of the fact that our eye-tracking based assessment tool did not show a change in the total number of social attention items that a patient can accurately identify from avatar's action cues (JAAT_NoFace and JAAT_Face, only a small non-significant trend is visible possibly due to familiarity).

However, in the primary follow-up time point, there was an effect on total ATEC scores, which translates to a decrease in the severity of autism symptoms (specifically the ones related to Sociability and Sensory/Cognitive Awareness) as wells as the ones reported as more general symptoms (Health/Physical/Behavior). Effects in Adapted Behavior Composite and in DLS (subareas from VABS) were observed. The daily living skills (DLS) are one of the most compromised areas in ASD and an improvement in this area translates in a better integration in the daily routines, and improved self-sufficiency.

In the secondary follow-up time point, analysis replicated the maintenance of positive changes observed at the in the primary follow-up time point, which is noteworthy, because a decay of effects did not occur, and significance was still present.

JAAT_NoFace and JAAT_Face scores did not alter between baseline and the secondary follow-up time point.

There were positive effects in all subscales from ATEC and in ATEC total scores. There were also changes in Adapted Behavior Composite and in all subareas from VABS.

Our study suggests a long term beneficial effect in patient's mood/mental state. This effect cannot at this stage be causally attributed to specific mechanisms related the intervention, but gives a good insight about the structure of the intervention, the compliance and reliability of the measures used, which show long term significant effects.

Strengths and Limitations

As strengths, we can list the high compliance, low/null dropout rates, and signal to noise stability and decoding accuracy of our BCI system across all seven sessions. Moreover, and in spite of the fact that our custom primary outcome measure failed to show improvement, most secondary clinical outcome measures (ATEC and VABS) suggested improvement. This improvement was maintained in the 6-months follow-up assessment, which reinforces the potential utility of these kind of interventions and the validity of this measures.

As limitations, we note the customized nature of our chosen primary outcome measure, which had no prior clinical validation, unlike the secondary measures. Moreover, in spite of the relatively realistic nature of our VR environment it can further be improved to train in a more effective way social attention skills.

Implications for Practice and Research

Given the very low rate of dropouts and the good classification accuracy over sessions, with stable neurophysiological signals, the system proves to be feasible as a tool in future efficacy trials. Given that several of the secondary clinical outcome measures showed improvement, we propose to use one of them (ATEC, VABS) or a combination of scores as the primary outcome measure in a future Phase 2 b clinical trial.

DATA AVAILABILITY STATEMENT

The raw data supporting the conclusions of this manuscript will be made available by the authors, without undue reservation, to any qualified researcher.

AUTHOR CONTRIBUTIONS

CA, SM, MS, RP, RM, GO, and MC-B conceived and designed the study. CA, SM, HP, and IB performed the study. CA and SM analyzed the data. CA, SM, HP, IB, HQ, and MC-B contributed with recruitment, data collection and tools. CA, SM, RP, and MC-B wrote the paper. All authors read and approved the final manuscript.

FUNDING

This work was supported by FTC—Portuguese national funding agency for science, research, and technology [Grants PAC—MEDPERSYST, POCI-01-0145-FEDER-016428, COMPETE 2020, POCI 030852, BIGDATIMAGE, CENTRO-01-0145-FEDER-000016 financed by Centro 2020 FEDER, COMPETE, FCT-UID/4539/2013—COMPETE, POCI-01-0145-FEDER-007440, and Fellowships SFRH/BD/78982/2011;SFRH/BD/77044/2011; SFRH/BD/102779/2014 and SFRH/BPD/101641/2014]; FLAD Life Sciences 2016, and the BRAINTRAIN Project—Taking imaging into the therapeutic domain: Self-regulation of brain systems for mental disorders [FP7-HEALTH-2013-INNOVATION-1–602186 20, 2013].

ACKNOWLEDGMENTS

We would like to acknowledge the Associação Portuguesa para as Perturbações do Desenvolvimento e Autismo (APPDA) from Coimbra and Viseu for their collaboration in the patient recruitment.

We would also like to acknowledge Professor Kerry Hood, Dr. Chao Huang, Gareth Watson, Sam Clarkstone, Vince Poile, and Liz Randell at the Centre for Trials Research at Cardiff University for their expertise and support in trial design, statistics, database development, and trial management throughout the research process.

REFERENCES

Amaral, C. P., Simões, M. A., Mouga, S., Andrade, J., and Castelo-Branco, M. (2017). A novel Brain Computer Interface for classification of social joint attention in autism and comparison of 3 experimental setups: a feasibility study. *J. Neurosci. Methods* 290, 105–115. doi: 10.1016/j.jneumeth.2017.07.029

American Psychiatric Association (2013). *Diagnostic and Statistical Manual of Mental Disorders, 5th Edn.* Arlington, VA: American Psychiatric Association.

Astrand, E., Wardak, C., and Ben Hamed, S. (2014). Selective visual attention to drive cognitive brain-machine interfaces: from concepts to neurofeedback and rehabilitation applications. *Front. Syst. Neurosci.* 8:144. doi: 10.3389/fnsys.2014.00144

Bakeman, R., and Adamson, L. B. (1984). Coordinating attention to people and objects in mother-infant and peer-infant interaction. *Child Dev*. 55, 1278–1289.

Baron-Cohen, S. (1989). Perceptual role taking and protodeclarative pointing in autism. *Br. J. Dev. Psychol.* 7, 113–127. doi: 10.1111/j.2044-835X.1989.tb00793.x

Baron-Cohen, S., Baldwin, D. A., and Crowson, M. (1997). Do children with autism use the speaker's direction of gaze strategy to crack the code of language? *Child Dev*. 68, 48–57.

Baxter, A. J., Brugha, T. S., Erskine, H. E., Scheurer, R. W., Vos, T., and Scott, J. G. (2015). The epidemiology and global burden of autism spectrum disorders. *Psychol. Med*. 45, 601–613. doi: 10.1017/S003329171400172X

Beck, A. T. (1961). Beck depression inventory. *Depression* 2006, 2–4.

Beck, A. T., and Steer, R. A. (1990). Manual for the beck anxiety inventory. *Behav. Res. Ther*. 37, 25–74.

Bekele, E., Crittendon, J., Zheng, Z., Swanson, A., Weitlauf, A., Warren, Z., et al. (2014). Assessing the utility of a virtual environment for enhancing facial affect recognition in adolescents with autism. *J. Autism Dev. Disord*. 44, 1641–1650. doi: 10.1007/s10803-014-2035-8

Boshoff, K., Gibbs, D., Phillips, R. L., Wiles, L., and Porter, L. (2016). Parents' voices: 'why and how we advocate'. A meta-synthesis of parents' experiences of advocating for their child with autism spectrum disorder. *Child Care Health Dev*. 42, 784–797. doi: 10.1111/cch.12383

Brodersen, K. H., Ong, C. S., Stephan, K. E., and Buhmann, J. M. (2010). "The balanced accuracy and its posterior distribution," in *20th International Conference on Pattern Recognition* (Istanbul), 3121–3124. doi: 10.1109/ICPR.2010.764

Charman, T. (1998). Specifying the nature and course of the joint attention impairment in autism in the preschool years. *Autism* 2, 61–79. doi: 10.1177/1362361398021006

Charman, T. (2003). Why is joint attention a pivotal skill in autism? *Philos. Trans. R. Soc. B Biol. Sci*. 358, 315–324. doi: 10.1098/rstb.2002.1199

Christensen, D. L., Baio, J., Braun, K. V. N., Bilder, D., Charles, J., Constantino, J. N., et al. (2016). Prevalence and characteristics of autism spectrum disorder among children aged 8 years - autism and developmental disabilities monitoring network, 11 sites, United States, 2012. *Morb. Mortal. Wkly. Rep. Surveill. Summ*. 65, 1–23. doi: 10.15585/mmwr.ss6503a1

Dawson, G., Toth, K., Abbott, R., Osterling, J., Munson, J., Estes, A., et al. (2004). Early social attention impairments in autism: social orienting, joint attention, and attention to distress. *Dev. Psychol*. 40, 271–283. doi: 10.1037/0012-1649.40.2.271

Duncan, C. C., Barry, R. J., Connolly, J. F., Fischer, C., Michie, P. T., Näätänen, R., et al. (2009). Event-related potentials in clinical research: guidelines for eliciting, recording, and quantifying mismatch negativity, P300, and N400. *Clin. Neurophysiol*. 120, 1883–1908. doi: 10.1016/j.clinph.2009.07.045

Faro Viana, M., Almeida, P., and Santos, R. C. (2012). Adaptação portuguesa da versão reduzida do Perfil de Estados de Humor – POMS. *Anál. Psicol.* 19, 77–92. doi: 10.14417/ap.345

Farwell, L. A., and Donchin, E. (1988). Talking off the top of your head: toward a mental prosthesis utilizing event-related brain potentials. *Electroencephalogr. Clin. Neurophysiol*. 70, 510–523. doi: 10.1016/0013-4694(88)90149-6

Faul, F., Erdfelder, E., Lang, A.-G., and Buchner, A. (2007). G*Power 3: a flexible statistical power analysis program for the social, behavioral, and biomedical sciences. *Behav. Res. Methods* 39, 175–191. doi: 10.3758/BF03193146

Friedrich, E. V., Suttie, N., Sivanathan, A., Lim, T., Louchart, S., and Pineda, J. A. (2014). Brain-computer interface game applications for combined neurofeedback and biofeedback treatment for children on the autism spectrum. *Front. Neuroeng*. 7:21. doi: 10.3389/fneng.2014.00021

Georgescu, A. L., Kuzmanovic, B., Roth, D., Bente, G., and Vogeley, K. (2014). The use of virtual characters to assess and train non-verbal communication in high-functioning autism. *Front. Hum. Neurosci*. 8:807. doi: 10.3389/fnhum.2014.00807

Golan, O., and Baron-Cohen, S. (2006). Systemizing empathy: teaching adults with Asperger syndrome or high-functioning autism to recognize complex emotions using interactive multimedia. *Dev. Psychopathol*. 18, 591–617. doi: 10.1017/S0954579406060305

Halgren, E., Baudena, P., Clarke, J. M., Heit, G., Marinkovic, K., Devaux, B., et al. (1995). Intracerebral potentials to rare target and distractor auditory and visual stimuli. II. Medial, lateral and posterior temporal lobe. *Electroencephalogr. Clin. Neurophysiol*. 94, 229–250. doi: 10.1016/0013-4694(95)98475-N

Harrop, C., McBee, M., and Boyd, B. A. (2016). How are child restricted and repetitive behaviors associated with caregiver stress over time? A parallel process multilevel growth model. *J. Autism Dev. Disord*. 46, 1773–1783. doi: 10.1007/s10803-016-2707-7

Jones, S., Bremer, E., and Lloyd, M. (2016). Autism spectrum disorder: family quality of life while waiting for intervention services. *Qual. Life Res*. 26, 331–342. doi: 10.1007/s11136-016-1382-7

Karst, J. S., and Van Hecke, A. V. (2012). Parent and family impact of autism spectrum disorders: a review and proposed model for intervention evaluation. *Clin. Child Fam. Psychol. Rev*. 15, 247–277. doi: 10.1007/s10567-012-0119-6

Kleih, S. C., Kaufmann, T., Zickler, C., Halder, S., Leotta, F., Cincotti, F., et al. (2011). Out of the frying pan into the fire-the P300-based BCI faces real-world challenges. *Prog. Brain Res*. 194, 27–46. doi: 10.1016/B978-0-444-53815-4.00019-4

Klin, A. (2002). Visual fixation patterns during viewing of naturalistic social situations as predictors of social competence in individuals with autism. *Arch. Gen. Psychiatry* 59, 809–816. doi: 10.1001/archpsyc.59.9.809

Larson, E. B., Feigon, M., Gagliardo, P., and Dvorkin, A. Y. (2014). Virtual reality and cognitive rehabilitation: a review of current outcome research. *NeuroRehabilitation* 34, 759–772. doi: 10.3233/NRE-141078

Larson, M. J., South, M., Krauskopf, E., Clawson, A., and Crowley, M. J. (2011). Feedback and reward processing in high-functioning autism. *Psychiatry Res*. 187, 198–203. doi: 10.1016/j.psychres.2010.11.006

Le Couteur, A., Lord, C., and Rutter, M. (2003). *The Autism Diagnostic Interview-Revised (ADI-R)*. (Los Angeles, CA: Western Psychological Services), 659–685.

Leekam, S. R., and Moore, C. (2001). "The development of attention and joint attention in children with autism," in *The Development of Autism: Perspectives from Theory and Research*, eds J. A. Burack, T. Charman, N. Yirmiya, and P. R. Zelazo (New Jersey, NJ: Lawrence Erlbaum), 105–129.

Lord, C., and Rutter, M. (1999). *Autism Diagnostic Observation Schedule-WPS (ADOS-WPS)*. Los Angeles, CA: Western Psychological and Counseling Services.

Lyall, K., Croen, L., Daniels, J., Fallin, M. D., Ladd-Acosta, C., Lee, B. K., et al. (2017). The changing epidemiology of autism spectrum disorders. *Annu. Rev. Public Health* 38, 81–102. doi: 10.1146/annurev-publhealth-031816-044318

Mak, J. N., Arbel, Y., Minett, J. W., McCane, L. M., Yuksel, B., Ryan, D., et al. (2011). Optimizing the P300-based brain-computer interface: current status, limitations and future directions. *J. Neural Eng.* 8:25003. doi: 10.1088/1741-2560/8/2/025003

McNair, D. M., Lorr, M., and Droppleman, L. F. (1992). *Profile of Mood States Manual*. San Diego, CA: Educational and Industrial Testing Service.

Oliveira, G., Ataíde, A., Marques, C., Miguel, T. S., Coutinho, A. M., Mota-Vieira, L., et al. (2007). Epidemiology of autism spectrum disorder in Portugal: prevalence, clinical characterization, and medical conditions. *Dev. Med. Child Neurol.* 49, 726–733. doi: 10.1111/j.1469-8749.2007.00726.x

Pais-Ribeiro, J., Silva, I., Ferreira, T., Martins, A., Meneses, R., and Baltar, M. (2007). Validation study of a Portuguese version of the hospital anxiety and depression scale. *Psychol. Health Med.* 12, 225–237. doi: 10.1080/13548500500524088

Patel, S. H., and Azzam, P. N. (2005). Characterization of N200 and P300: selected studies of the Event-Related Potential. *Int. J. Med. Sci.* 2, 147–154. doi: 10.7150/ijms.2.147

Polich, J. (2007). Updating P300: an integrative theory of P3a and P3b. *Clin. Neurophysiol.* 118, 2128–2148. doi: 10.1016/j.clinph.2007.04.019

Rayner, K. (2009). Eye movements and attention in reading, scene perception, and visual search. *Q. J. Exp. Psychol.* 62, 1457–1506. doi: 10.1080/17470210902816461

Rimland, B., and Edelson, M. (1999). *Autism Treatment Evaluation Checklist*. SanDiego, CA: Autism Research Institute.

Salisbury, D. B., Dahdah, M., Driver, S., Parsons, T. D., and Richter, K. M. (2016). Virtual reality and brain computer interface in neurorehabilitation. *Proc. (Bayl. Univ. Med. Cent).* 29, 124–127. Available online at: http://www.pubmedcentral.nih.gov/articlerender.fcgi?artid=PMC4790543

Schlebusch, L., Samuels, A. E., and Dada, S. (2016). South African families raising children with autism spectrum disorders: relationship between family routines, cognitive appraisal and family quality of life. *J. Intellect. Disabil. Res.* 60, 412–423. doi: 10.1111/jir.12292

Sparrow, S., Balla, D. A., and Cicchetti, D., V (1984). *Vineland Adaptative Behaviour Scales: Interview Edition, Survey Form*. Circle Pines, MN: American Guidance Service.

Swettenham, J., Baron-Cohen, S., Charman, T., Cox, A., Baird, G., Drew, A., et al. (1998). The frequency and distribution of spontaneous attention shifts between social and nonsocial stimuli in autistic, typically developing, and nonautistic developmentally delayed infants. *J. Child Psychol. Psychiatry* 39, 747–753. doi: 10.1017/S0021963098002595

Tankus, A., Fried, I., and Shoham, S. (2014). Cognitive-motor brain-machine interfaces. *J. Physiol. Paris* 108, 38–44. doi: 10.1016/j.jphysparis.2013.05.005

Vaz-Serra, A., and Abreu, J. (1973). Aferição dos quadros clínicos depressivos I: ensaio de aplicação do "Inventário Depressivo de Beck" a uma amostra portuguesa de doentes deprimidos. *Coimbra Med.* 20, 623–644.

Wainer, A. L., and Ingersoll, B. R. (2011). The use of innovative computer technology for teaching social communication to individuals with autism spectrum disorders. *Res. Autism Spectr. Disord.* 5, 96–107. doi: 10.1016/j.rasd.2010.08.002

Wechsler, D. (2008). *Escala de Inteligência de Wechsler Para Adultos -3.a edição: Manual [Wechsler Adult Intelligence Scale-3rd Edn. Manual]*. Lisbon: CEGOC-TEA.

Wolpaw, J., and Wolpaw, E. W. (2012). *Brain–Computer Interfaces. Principles and Practice*. Oxford University Press. doi: 10.1093/acprof:oso/9780195388855.001.0001

Zigmond, A. S., and Snaith, R. P. (1983). The hospital anxiety and depression scale. *Acta Psychiatr. Scand.* 67, 361–370. doi: 10.1111/j.1600-0447.1983.tb09716.x

Conflict of Interest Statement: The authors declare that the research was conducted in the absence of any commercial or financial relationships that could be construed as a potential conflict of interest.

Copyright © 2018 Amaral, Mouga, Simões, Pereira, Bernardino, Quental, Playle, McNamara, Oliveira and Castelo-Branco. This is an open-access article distributed under the terms of the Creative Commons Attribution License (CC BY). The use, distribution or reproduction in other forums is permitted, provided the original author(s) and the copyright owner(s) are credited and that the original publication in this journal is cited, in accordance with accepted academic practice. No use, distribution or reproduction is permitted which does not comply with these terms.

frontiers in Neuroscience

ORIGINAL RESEARCH
published: 25 July 2018
doi: 10.3389/fnins.2018.00505

Effects of Sensorimotor Rhythm Modulation on the Human Flexor Carpi Radialis H-Reflex

Aiko K. Thompson[1], Hannah Carruth[2], Rachel Haywood[2], N. Jeremy Hill[3,4], William A. Sarnacki[5], Lynn M. McCane[5], Jonathan R. Wolpaw[5,6] and Dennis J. McFarland[5]*

[1] Department of Health Sciences and Research, College of Health Professions, Medical University of South Carolina, Charleston, SC, United States, [2] Division Biomedical Engineering, School of Engineering, University of Glasgow, Glasgow, United Kingdom, [3] Burke Neurological Institute, White Plains, NY, United States, [4] Blythedale Children's Hospital, Valhalla, NY, United States, [5] National Center for Adaptive Neurotechnologies, Wadsworth Center, New York State Department of Health, Albany, NY, United States, [6] Albany Stratton VA Medical Center, Albany, NY, United States

People can learn over training sessions to increase or decrease sensorimotor rhythms (SMRs) in the electroencephalogram (EEG). Activity-dependent brain plasticity is thought to guide spinal plasticity during motor skill learning; thus, SMR training may affect spinal reflexes and thereby influence motor control. To test this hypothesis, we investigated the effects of learned mu (8–13 Hz) SMR modulation on the flexor carpi radialis (FCR) H-reflex in 6 subjects with no known neurological conditions and 2 subjects with chronic incomplete spinal cord injury (SCI). All subjects had learned and practiced over more than 10 <30-min training sessions to increase (SMR-up trials) and decrease (SMR-down trials) mu-rhythm amplitude over the hand/arm area of left sensorimotor cortex with ≥80% accuracy. Right FCR H-reflexes were elicited at random times during SMR-up and SMR-down trials, and in between trials. SMR modulation affected H-reflex size. In all the neurologically normal subjects, the H-reflex was significantly larger [116% ± 6 (mean ± SE)] during SMR-up trials than between trials, and significantly smaller (92% ± 1) during SMR-down trials than between trials ($p < 0.05$ for both, paired t-test). One subject with SCI showed similar H-reflex size dependence (high for SMR-up trials, low for SMR-down trials): the other subject with SCI showed no dependence. These results support the hypothesis that SMR modulation has predictable effects on spinal reflex excitability in people who are neurologically normal; they also suggest that it might be used to enhance therapies that seek to improve functional recovery in some individuals with SCI or other CNS disorders.

Keywords: EEG mu-rhythm, H-reflex, brain-computer interface (BCI), spinal cord injuries, task-dependent adaptation

OPEN ACCESS

Edited by:
Christoph Guger,
Guger Technologies (Austria), Austria

Reviewed by:
Damien Coyle,
Ulster University, United Kingdom
James W. Grau,
Texas A&M University, United States

****Correspondence:***
Aiko K. Thompson
thompsai@musc.edu

Specialty section:
This article was submitted to Neural Technology, a section of the journal Frontiers in Neuroscience

Received: *09 March 2018*
Accepted: *04 July 2018*
Published: *25 July 2018*

Citation:
Thompson AK, Carruth H, Haywood R, Hill NJ, Sarnacki WA, McCane LM, Wolpaw JR and McFarland DJ (2018) Effects of Sensorimotor Rhythm Modulation on the Human Flexor Carpi Radialis H-Reflex. Front. Neurosci. 12:505. doi: 10.3389/fnins.2018.00505

INTRODUCTION

The past several decades of non-invasive brain-computer interface (BCI) research show that people can learn through a series of brief training sessions to control mu (8–13 Hz) and/or beta (18–26 Hz) sensorimotor rhythms (SMR) recorded by electroencephalogram (EEG) over sensorimotor cortex (Wolpaw et al., 1991; Wolpaw and McFarland, 1994). Such BCI-based SMR training might help to improve motor function recovery in people with CNS disorders by guiding activity-dependent brain plasticity (Dobkin, 2007; Daly and Wolpaw, 2008). Boulay et al. (2011) showed that trained

SMR control affects reaction time, indicating that SMR modulation influences a simple motor performance. Furthermore, activity-dependent brain plasticity is thought to guide the spinal cord plasticity that contributes to motor skill learning (Wolpaw, 2010). To determine whether SMR modulation might be used to guide spinal cord plasticity so as to enhance functional recovery, the present study explored the impact of SMR amplitude on the size of the H-reflex (an electrical analog of spinal stretch reflex) in the forearm muscle flexor carpi radialis (FCR).

MATERIALS AND METHODS

Study Overview

The subjects were 6 people with no known neurological conditions (5 men and 1 woman; age 22–68 years) and two people with stable chronic incomplete spinal cord injury (SCI) [a 42-year-old man with a 2-yr-old incomplete SCI (AIS: American Spinal Injury Association Impairment Scale D) at C4 and a 33-year-old woman with a 10-yr-old incomplete SCI (AIS D) at C5-7]. Both people with SCI had been on stable doses of baclofen for >6 months prior to their study participation. Their inclusion was intended to provide some initial insight into the therapeutic potential of SMR training. The study was reviewed and approved by the Institutional Review Boards of Helen Hayes Hospital and the Wadsworth Center, New York State Department of Health. All subjects provided informed consent.

First, each subject learned and practiced over >10 training sessions (<30 min/session, 2–3 sessions/week) of a BCI cursor-control task (**Figure 1**, fully described in, Wolpaw and McFarland, 1994, 2004; McFarland et al., 2003) to increase (SMR-up trials) and decrease (SMR-down trials) mu-rhythm (8–13 Hz) amplitude over the hand/arm area of left sensorimotor cortex (electrode C3 or CP3, Jasper, 1958; Ebner et al., 1999; Nuwer et al., 1999; Jurcak et al., 2007) with ≥80% accuracy. The number of sessions before reaching ≥80% cursor control accuracy varied across subjects (from 2 to 8). Regardless of how soon the ≥80% accuracy was achieved, all subjects completed at least 10 training sessions. In these sessions, 32 channels of EEG were collected with active electrodes (g.tec Medical Engineering GMBH, Austria) and the general-purpose BCI software platform BCI2000 (Schalk et al., 2004). EEG was sampled at 256 Hz, referenced to the left earlobe (ground at the forehead electrode AFz) (Jasper, 1958; Ebner et al., 1999; Nuwer et al., 1999; Jurcak et al., 2007). EEG features (logarithms of the amplitudes in 3-Hz-wide frequency bands) were extracted by a surface-Laplacian spatial filter (McFarland et al., 1997) and autoregressive spectral estimation (model order 16) (Marple, 1987; McFarland and Wolpaw, 2008). Features in the mu-rhythm frequency range at C3 or CP3 controlled cursor movement. Every 100-ms, their values for the previous 200-ms segment were calculated and converted into vertical cursor movement by a linear equation. At the beginning of each cursor-movement trial, a target appeared randomly at the top right or the bottom right of the screen and the cursor appeared in the middle of the left edge of the screen. The cursor moved from left to right at a constant rate; the subject learned to control SMR amplitude to move the cursor up or down so that it hit the target when it reached the right edge. Each training session included 10 blocks of 16-18 trials each.

After >10 training sessions, (i.e., fully trained to hit the target at ≥80% accuracy), the subject began the H-reflex component of the study in which the right FCR H-reflex was elicited during SMRup and SMRdown trials and in between trials.

H-Reflex Recording

Surface EMG activity from FCR and its antagonist extensor carpi radialis (ECR) was amplified, band-pass filtered (10–1,000 Hz), and sampled at 3,200 Hz. To elicit the FCR H-reflex, the median nerve was stimulated in the cubital fossa, using surface Ag-AgCl electrodes (2.2 × 2.2 cm) and 0.5-ms square pulses. Stimulation was delivered when the subject had maintained 5–15% maximum voluntary contraction (MVC) level of FCR EMG activity with resting level ECR activity (typically <10 μV) for at least 2 s. For all H-reflex measurements, the subject's right arm was strapped to a custom-made arm support platform with the shoulder at ≈90° in the sagittal plane and ≈40° in the transverse plane, the elbow at full extension, and the hand in full supination.

To determine the stimulus intensity that elicited a submaximal H-reflex with a small M-wave, the FCR H-reflex/M-wave recruitment curve was obtained while the subject maintained the preset levels of FCR and ECR EMG activity (Zehr and Stein, 1999; Kido et al., 2004). This stimulus intensity was used to elicit the H-reflex during SMRup trials, SMRdown trials, and in between trials (see below). Then, the subject with right arm on the platform completed; a block of 16–18 SMRup or SMRdown trials with no voluntary EMG activation (i.e., similar to the SMR cursor task training sessions except for the arm and hand position); and a second block of 16–18 SMRup or SMRdown trials with the preset levels of FCR and ECR EMG activity without H-reflex elicitation. After these blocks confirmed that the subject was able to perform the SMR cursor task with ≥80% accuracy in this arm-hand position while maintaining the preset levels of FCR and ECR EMG activity, FCR H-reflex testing began.

While the subject performed cursor-movement trials [i.e., trials that required SMR increase (SMRup) or decrease (SMRdown)], median nerve stimulation occurred at random times during the trials and in between trials when FCR and ECR EMG activity met the preset requirements. About 30 H-reflexes were obtained from each subject in each of the three conditions (SMRup trials, SMRdown trials, in between trials).

Data Analysis

Rectified EMG activity in the 50-ms pre-stimulus period was averaged for each trial to measure the background activity level. The FCR H-reflex and the M-wave amplitudes were measured as peak-to-peak values in time windows determined for each subject. Typical time windows were 3-13 ms post-stimulus for the M-wave and 18–27 ms for the H-reflex. To ensure that the H-reflexes were measured with the same background EMG levels and the same stimulus intensity in all three SMR conditions, FCR and ECR background EMG and M-wave size were compared across the three conditions for each subject. Any trials that occurred with too large or small M-waves or background EMG levels were eliminated from the analysis. After removing these

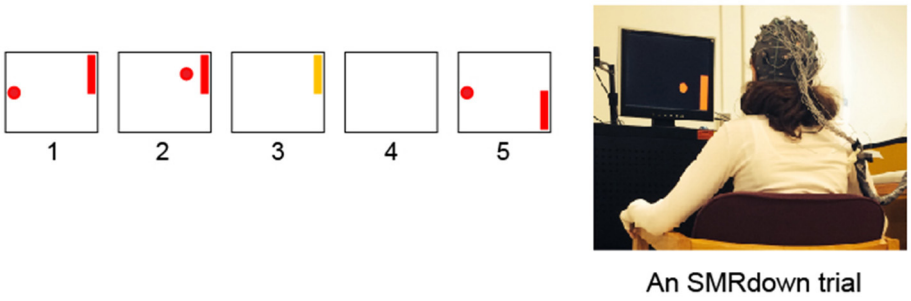

FIGURE 1 | Subjects learn over a series of training sessions to use SMR amplitudes in the μ (8–12 Hz) frequency band over left sensorimotor cortex (at/around the C3 or CP3 electrodes) to move a cursor vertically while it moves from left to right at a constant rate (Wolpaw et al., 1991; Wolpaw and McFarland, 1994; McFarland et al., 2003). (1) a target appears; (2) 1 s later the cursor appears and moves in two dimensions with vertical movement controlled by the subject's SMR amplitude; (3) the cursor reaches the target and the target flashes for 1 s; (4) the screen is blank for 1 s; and then (5) the next trial begins. (If the cursor misses the target, the flash does not occur, the screen simply goes blank for 2 s.) In each training session, the participant goes through 10 blocks of ≈18 SMR trials each, separated by ≥1-min rest periods.

trials, 15–30 trials were averaged for each condition of each subject.

RESULTS

Background EMG levels and M-wave size did not differ among SMRup, SMRdown, and in between conditions ($p > 0.12$ for FCR and ECR background EMG and the M-wave size by repeated measures ANOVA). Thus, the difference in H-reflex size among conditions can be confidently attributed to the SMR control.

In all 6 normal subjects, the FCR H-reflex was larger during SMRup trials and smaller during SMRdown trials, compared with in between trials. **Figure 2A** shows typical H-reflex responses during SMRup and SMRdown trials. A repeated-measures ANOVA and *t*-test with Bonferroni correction showed that H-reflex sizes in SMRup and SMRdown trials differed significantly from each other ($p = 0.02$ by ANOVA and $p = 0.0068$ by *t*-test). **Figure 2B** displays SMRup and SMRdown H-reflex sizes normalized to the between-trial H-reflex size in individual subjects. Group mean ± SE H-reflex size was 116 ± 6(SE)% for SMRup and 92 ± 1% for SMRdown trials.

In one of the subjects with SCI (Subject G), FCR H-reflex was modulated across the three SMR conditions (**Figure 2B**) as it was in normal subjects. In the other person with SCI (Subject H), H-reflex modulation across the conditions was not significant.

DISCUSSION

SMR activity in the μ and β rhythm frequency range decreases before and during active movement (Pfurtscheller, 1989; Pfurtscheller and Neuper, 1994; Pfurtscheller et al., 2006; Klimesch et al., 2007; Boulay et al., 2011; McFarland et al., 2015). Such SMR decrease, called event-related desynchronization (ERD), is also associated with motor imagery (McFarland et al., 2000). Indeed, in the initial stages of BCI-based SMR training, people often imagine moving (or not moving) to decrease (or increase) SMR amplitude (Wolpaw and McFarland, 2004). As they acquire SMR control, such imagery tends to drop away (Wolpaw and McFarland, 2004). Motor imagery increases corticospinal excitability (Kasai et al., 1997; Rossini et al., 1999; Stinear and Byblow, 2004; Stinear et al., 2006a,b; Bakker et al., 2008; Kang et al., 2011; Gündüz and Kiziltan, 2015; Kato et al., 2015; Im et al., 2016; Tatemoto et al., 2017) and resting motoneuron excitability (Gündüz and Kiziltan, 2015). Studies of the impact of motor imagery on the H-reflex are less consistent in their results (Oishi et al., 1994; Abbruzzese et al., 1996; Yahagi et al., 1996; Bonnet et al., 1997; Kasai et al., 1997; Hashimoto and Rothwell, 1999; Hale et al., 2003; Patuzzo et al., 2003; Cowley et al., 2008; Aoyama and Kaneko, 2011; Jarjees and Vuckovic, 2016). The discrepancies among studies probably reflect differences in the imagery (e.g., visual vs. kinesthetic, Neuper et al., 2005), as well as in H-reflex testing methods. Many studies measure the H-reflex when the muscle is inactive; they do not control for subthreshold changes in motoneuron excitability, which may markedly affect H-reflex size (Stein and Thompson, 2006).

In the present study, the FCR H-reflex was always measured in the presence of a given level of ongoing FCR EMG activity and M-wave size was kept stable; thus, motoneuron pool excitability and effective stimulus intensity were the same across the three SMR conditions (i.e., SMRup trials, SMRdown trials, and in between trials). The results were quite clear: the H-reflex was larger when SMR amplitude was high and smaller when SMR amplitude was low. Boulay et al. (2015) found a similar positive correlation between H-reflex size and SMR amplitude in rats.

In general, SMR amplitude in the mu-beta range is inversely correlated with cortical activation; high SMR [i.e., event-related synchronization (ERS)] reflects cortical inhibition, low SMR (ERD) reflects cortical activation (reviewed in Klimesch et al., 2007). SMR in the hand area of sensorimotor cortices decreases during movement planning or execution (Pfurtscheller, 1989; Pfurtscheller and Neuper, 1994; Pfurtscheller et al., 2006); and voluntary modulation of pre-movement SMR affects subsequent behavior (Boulay et al., 2011; McFarland et al., 2015). When SMR amplitude decreases, cortical drive to spinal motoneurons

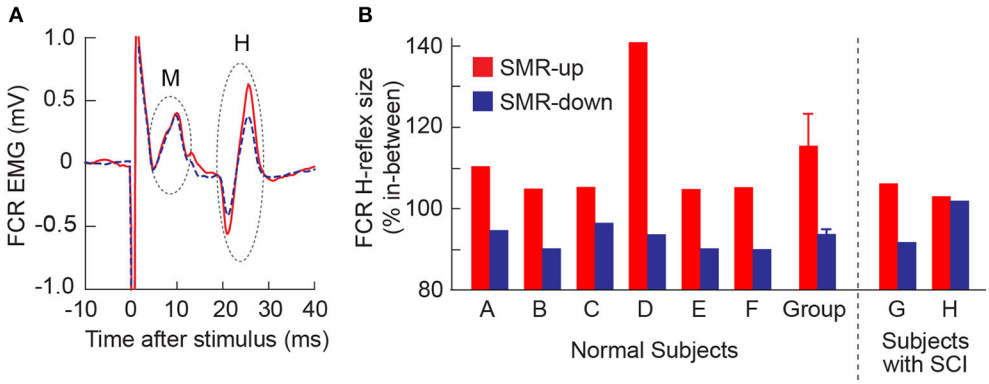

FIGURE 2 | Effects of learned SMR control on the FCR H-reflex. **(A)** FCR H-reflex during the SMRup (red, solid) and SMRdown (blue, dashed) trials in subject D. About 20 responses were averaged together for each sweep. **(B)** Average FCR H-reflex sizes during SMRup (red) and SMRdown (blue) trials in normal subjects (A–F) and subjects with SCI (G and H). Group data for normal subjects are also included: H-reflex size averages 116 ± 6 (mean ± SE)% for SMRup trials and 92 ± 1% for SMRdown trials.

increases (Rossini et al., 1991; Rau et al., 2003; Zarkowski et al., 2006; Sauseng et al., 2009; Takemi et al., 2013). When cortical drive to the motoneurons is increased by demanding motor tasks [e.g., beam-walking vs. treadmill-walking, (Llewellyn et al., 1990), greater postural complexity during standing (Yamashita and Moritani, 1989)], the H-reflex is smaller. This H-reflex suppression is thought to be mediated through corticospinal excitation of Ia inhibitory interneurons (Iles and Pisini, 1992; Nielsen et al., 1993) and/or interneurons affecting presynaptic inhibition of Ia afferents (Iles, 1996; Meunier and Pierrot-Deseilligny, 1998; see also Chen and Wolpaw, 2002; Chen et al., 2002).

Because learned SMR control can influence H-reflex size, it might serve as an aid in operant conditioning of the H-reflex, which can help to improve impaired locomotion after incomplete SCI (Manella et al., 2013; Thompson et al., 2013). As discussed by Thompson et al. (2009), an operant conditioning protocol can increase or decrease a targeted H-reflex. H-reflex change has two components: task-dependent adaptation that begins in several sessions and is thought to reflect plasticity in the brain; and subsequent long-term change that progresses gradually over sessions, is thought to reflect spinal plasticity, and persists after conditioning ends (Thompson et al., 2009). In this context, it is interesting to note that the magnitude of H-reflex change found in the present study (i.e., **Figure 2B**), is similar to the magnitude of task-dependent adaptation in the H-reflex produced by the H-reflex operant conditioning protocol (Thompson et al., 2009). This suggests that SMR training might be used to guide, and possibly even enhance, task-dependent adaptation in the H-reflex. It might thereby increase the conditioning success rate and augment the rapidity and magnitude of the long-term spinal plasticity that can trigger wider plasticity so as to improve complex motor functions (e.g., locomotion) after SCI or in other disorders (Thompson et al., 2013; Wolpaw, 2018). Such effects could increase the clinical efficacy and practicality of spinal reflex operant conditioning protocols.

AUTHOR CONTRIBUTIONS

AT, NH, and DM designed the study. AT, HC, RH, WS, LM, and DM collected the data. AT, HC, JW, and DM conducted the analysis. AT, HC, NH, JW, and DM interpreted the results and wrote the manuscript. HC and WS performed the majority of subject training sessions prior to the main experiments conducted in this study. All authors reviewed the manuscript and approved the final version of the manuscript.

FUNDING

This work was supported in part by the US National Institutes of Health [NS069551 (NINDS), GM104941 (NIGMS), 1P41EB018783 (NIBIB), HD30146 (NCMRR/NICHD), and EB00856 (NIBIB & NINDS)], and New York State Spinal Cord Injury Research Trust (C023685 and C029131).

REFERENCES

Abbruzzese, G., Trompetto, C., and Schieppati, M. (1996). The excitability of the human motor cortex increases during execution and mental imagination of sequential but not repetitive finger movements. *Exp. Brain Res.* 111, 465–472. doi: 10.1007/BF00228736

Aoyama, T., and Kaneko, F. (2011). The effect of motor imagery on gain modulation of the spinal reflex. *Brain Res.* 1372, 41–48. doi: 10.1016/j.brainres.2010.11.023

Bakker, M., Overeem, S., Snijders, A. H., Borm, G., van Elswijk, G., Toni, I., et al. (2008). Motor imagery of foot dorsiflexion and gait: effects on corticospinal excitability. *Clin. Neurophysiol.* 119, 2519–2527. doi: 10.1016/j.clinph.2008.07.282

Bonnet, M., Decety, J., Jeannerod, M., and Requin, J. (1997). Mental simulation of an action modulates the excitability of spinal reflex pathways in man. *Brain Res. Cogn. Brain Res.* 5, 221–228. doi: 10.1016/S0926-6410(96)00072-9

Boulay, C. B., Chen, X. Y., and Wolpaw, J. R. (2015). Electrocorticographic activity over sensorimotor cortex and motor function in awake behaving rats. *J. Neurophysiol.* 113, 2232–2241. doi: 10.1152/jn.00677.2014

Boulay, C. B., Sarnacki, W. A., Wolpaw, J. R., and McFarland, D. J. (2011). Trained modulation of sensorimotor rhythms can affect reaction time. *Clin. Neurophysiol.* 122, 1820–1826. doi: 10.1016/j.clinph.2011.02.016

Chen, X. Y., and Wolpaw, J. R. (2002). Probable corticospinal tract control of spinal cord plasticity in the rat. *J. Neurophysiol.* 87, 645–652. doi: 10.1152/jn.00391.2001

Chen, X. Y., Chen, L., Wolpaw, J. R., and Jakeman, L. B. (2002). Corticospinal tract transection reduces H-reflex circadian rhythm in rats. *Brain Res.* 942, 101–108. doi: 10.1016/S0006-8993(02)02702-6

Cowley, P. M., Clark, B. C., and Ploutz-Snyder, L. L. (2008). Kinesthetic motor imagery and spinal excitability: the effect of contraction intensity and spatial localization. *Clin. Neurophysiol.* 119, 1849–1856. doi: 10.1016/j.clinph.2008.04.004

Daly, J. J., and Wolpaw, J. R. (2008). Brain-computer interfaces in neurological rehabilitation. *Lancet Neurol.* 7, 1032–1043. doi: 10.1016/S1474-4422(08)70223-0

Dobkin, B. H. (2007). Brain-computer interface technology as a tool to augment plasticity and outcomes for neurological rehabilitation. *J. Physiol.* 579, 637–642. doi: 10.1113/jphysiol.2006.123067

Ebner, A., Sciarretta, G., Epstein, C. M., and Nuwer, M. (1999). EEG instrumentation. The International Federation of Clinical Neurophysiology. *Electroencephal. Clin. Neurophysiol. Suppl* 52, 7–10.

Gündüz, A., and Kiziltan, M. E. (2015). F-wave and motor-evoked potentials during motor imagery and observation in apraxia of Parkinson disease. *Muscle Nerve* 52, 1072–1077. doi: 10.1002/mus.24663

Hale, B. S., Raglin, J. S., and Koceja, D. M. (2003). Effect of mental imagery of a motor task on the Hoffmann reflex. *Behav. Brain Res.* 142, 81–87. doi: 10.1016/S0166-4328(02)00397-2

Hashimoto, R., and Rothwell, J. C. (1999). Dynamic changes in corticospinal excitability during motor imagery. *Exp. Brain Res.* 125, 75–81. doi: 10.1007/s002210050660

Iles, J. F. (1996). Evidence for cutaneous and corticospinal modulation of presynaptic inhibition of Ia afferents from the human lower limb. *J. Physiol.* 491(Pt 1), 197–207. doi: 10.1113/jphysiol.1996.sp021207

Iles, J. F., and Pisini, J. V. (1992). Cortical modulation of transmission in spinal reflex pathways of man. *J. Physiol.* 455, 425–446. doi: 10.1113/jphysiol.1992.sp019309

Im, H., Ku, J., Kim, H. J., and Kang, Y. J. (2016). Virtual reality-guided motor imagery increases corticomotor excitability in healthy volunteers and stroke patients. *Ann. Rehabil. Med.* 40, 420–431. doi: 10.5535/arm.2016.40.3.420

Jarjees, M., and Vucković, A. (2016). The effect of voluntary modulation of the sensory-motor rhythm during different mental tasks on H reflex. *Int. J. Psychophysiol.* 106, 65–76. doi: 10.1016/j.ijpsycho.2016.06.005

Jasper, H. H. (1958). Report of the committee on methods of clinical examination in electroencephalography: 1957. *Electroencephalogr. Clin. Neurophysiol.* 10, 370–375. doi: 10.1016/0013-4694(58)90053-1

Jurcak, V., Tsuzuki, D., and Dan, I. (2007). 10/20, 10/10, and 10/5 systems revisited: their validity as relative head-surface-based positioning systems. *Neuroimage* 34, 1600–1611. doi: 10.1016/j.neuroimage.2006.09.024

Kang, Y. J., Ku, J., Kim, H. J., and Park, H. K. (2011). Facilitation of corticospinal excitability according to motor imagery and mirror therapy in healthy subjects and stroke patients. *Ann. Rehabil. Med.* 35, 747–758. doi: 10.5535/arm.2011.35.6.747

Kasai, T., Kawai, S., Kawanishi, M., and Yahagi, S. (1997). Evidence for facilitation of motor evoked potentials (MEPs) induced by motor imagery. *Brain Res* 744, 147–150. doi: 10.1016/S0006-8993(96)01101-8

Kato, K., Watanabe, J., Muraoka, T., and Kanosue, K. (2015). Motor imagery of voluntary muscle relaxation induces temporal reduction of corticospinal excitability. *Neurosci. Res.* 92, 39–45. doi: 10.1016/j.neures.2014.10.013

Kido, A., Tanaka, N., and Stein, R. B. (2004). Spinal excitation and inhibition decrease as humans age. *Can. J. Physiol. Pharmacol.* 82, 238–248. doi: 10.1139/y04-017

Klimesch, W., Sauseng, P., and Hanslmayr, S. (2007). EEG alpha oscillations: the inhibition-timing hypothesis. *Brain Res. Rev.* 53, 63–88. doi: 10.1016/j.brainresrev.2006.06.003

Llewellyn, M., Yang, J. F., and Prochazka, A. (1990). Human H-reflexes are smaller in difficult beam walking than in normal treadmill walking. *Exp. Brain Res.* 83, 22–28. doi: 10.1007/BF00232189

Manella, K. J., Roach, K. E., and Field-Fote, E. C. (2013). Operant conditioning to increase ankle control or decrease reflex excitability improves reflex modulation and walking function in chronic spinal cord injury. *J. Neurophysiol.* 109, 2666–2679. doi: 10.1152/jn.01039.2011

Marple, S. (1987). *Digital Spectral Analysis with Applications*. Englewood Cliffs, NJ: Prentice-Hall.

McFarland, D. J., and Wolpaw, J. R. (2008). Sensorimotor rhythm-based brain-computer interface (BCI): model order selection for autoregressive spectral analysis. *J. Neural Eng.* 5, 155–162. doi: 10.1088/1741-2560/5/2/006

McFarland, D. J., McCane, L. M., David, S. V., and Wolpaw, J. R. (1997). Spatial filter selection for EEG-based communication. *Electroencephalogr. Clin. Neurophysiol.* 103, 386–394. doi: 10.1016/S0013-4694(97)00022-2

McFarland, D. J., Miner, L. A., Vaughan, T. M., and Wolpaw, J. R. (2000). Mu and beta rhythm topographies during motor imagery and actual movements. *Brain Topogr.* 12, 177–186. doi: 10.1023/A:1023437823106

McFarland, D. J., Sarnacki, W. A., and Wolpaw, J. R. (2003). Brain-computer interface (BCI) operation: optimizing information transfer rates. *Biol. Psychol.* 63, 237–251. doi: 10.1016/S0301-0511(03)00073-5

McFarland, D. J., Sarnacki, W. A., and Wolpaw, J. R. (2015). Effects of training pre-movement sensorimotor rhythms on behavioral performance. *J. Neural Eng.* 12:066021. doi: 10.1088/1741-2560/12/6/066021

Meunier, S., and Pierrot-Deseilligny, E. (1998). Cortical control of presynaptic inhibition of Ia afferents in humans. *Exper. Brain Res.* 119, 415–426. doi: 10.1007/s002210050357

Neuper, C., Scherer, R., Reiner, M., and Pfurtscheller, G. (2005). Imagery of motor actions: differential effects of kinesthetic and visual-motor mode of imagery in single-trial EEG. *Brain Res. Cogn. Brain Res.* 25, 668–677. doi: 10.1016/j.cogbrainres.2005.08.014

Nielsen, J., Petersen, N., Deuschl, G., and Ballegaard, M. (1993). Task-related changes in the effect of magnetic brain stimulation on spinal neurones in man. *J. Physiol.* 471, 223–243. doi: 10.1113/jphysiol.1993.sp019899

Nuwer, M. R., Comi, G., Emerson, R., Fuglsang-Frederiksen, A., Guérit, J. M., Hinrichs, H., et al. (1999). IFCN standards for digital recording of clinical EEG. The International Federation of Clinical Neurophysiology. *Electroencephalogr. Clin. Neurophysiol. Suppl.* 52, 11–14.

Oishi, K., Kimura, M., Yasukawa, M., Yoneda, T., and Maeshima, T. (1994). Amplitude reduction of H-reflex during mental movement simulation in elite athletes. *Behav. Brain. Res.* 62, 55–61. doi: 10.1016/0166-4328(94)90037-X

Patuzzo, S., Fiaschi, A., and Manganotti, P. (2003). Modulation of motor cortex excitability in the left hemisphere during action observation: a single- and paired-pulse transcranial magnetic stimulation study of self- and non-self-action observation. *Neuropsychologia* 41, 1272–1278. doi: 10.1016/S0028-3932(02)00293-2

Pfurtscheller, G. (1989). Functional topography during sensorimotor activation studied with event-related desynchronization mapping. *J. Clin. Neurophysiol.* 6, 75–84. doi: 10.1097/00004691-198901000-00003

Pfurtscheller, G., and Neuper, C. (1994). Event-related synchronization of mu rhythm in the EEG over the cortical hand area in man. *Neurosci. Lett.* 174, 93–96. doi: 10.1016/0304-3940(94)90127-9

Pfurtscheller, G., Brunner, C., Schlögl, A., and Lopes da Silva, F. H., (2006). Mu rhythm (de)synchronization and EEG single-trial classification of different motor imagery tasks. *Neuroimage* 31, 153–159. doi: 10.1016/j.neuroimage.2005.12.003

Rau, C., Plewnia, C., Hummel, F., and Gerloff, C. (2003). Event-related desynchronization and excitability of the ipsilateral motor cortex during simple self-paced finger movements. *Clin. Neurophysiol.* 114, 1819–1826. doi: 10.1016/S1388-2457(03)00174-3

Rossini, P. M., Desiato, M. T., Lavaroni, F., and Caramia, M. D. (1991). Brain excitability and electroencephalographic activation: non-invasive evaluation in healthy humans via transcranial magnetic stimulation. *Brain Res.* 567, 111–119. doi: 10.1016/0006-8993(91)91442-4

Rossini, P. M., Rossi, S., Pasqualetti, P., and Tecchio, F. (1999). Corticospinal excitability modulation to hand muscles during movement imagery. *Cereb. Cortex* 9, 161–167. doi: 10.1093/cercor/9.2.161

Sauseng, P., Klimesch, W., Gerloff, C., and Hummel, F. C. (2009). Spontaneous locally restricted EEG alpha activity determines cortical excitability in the motor cortex. *Neuropsychologia* 47, 284–288. doi: 10.1016/j.neuropsychologia.2008.07.021

Schalk, G., McFarland, D. J., Hinterberger, T., Birbaumer, N., and Wolpaw, J. R. (2004). BCI2000: a general-purpose brain-computer interface (BCI) system. *IEEE Trans. Biomed. Eng.* 51, 1034–1043. doi: 10.1109/TBME.2004.827072

Stein, R. B., and Thompson, A. K. (2006). Muscle reflexes in motion: how, what, and why? *Exerc. Sport Sci. Rev.* 34, 145–153. doi: 10.1249/01.jes.0000240024.37996.e5

Stinear, C. M., and Byblow, W. D. (2004). Modulation of corticospinal excitability and intracortical inhibition during motor imagery is task-dependent. *Exp. Brain Res.* 157, 351–358. doi: 10.1007/s00221-004-1851-z

Stinear, C. M., Byblow, W. D., Steyvers, M., Levin, O., and Swinnen, S. P. (2006a). Kinesthetic, but not visual, motor imagery modulates corticomotor excitability. *Exp. Brain Res.* 168, 157–164. doi: 10.1007/s00221-005-0078-y

Stinear, C. M., Fleming, M. K., and Byblow, W. D. (2006b). Lateralization of unimanual and bimanual motor imagery. *Brain Res.* 1095, 139–147. doi: 10.1016/j.brainres.2006.04.008

Takemi, M., Masakado, Y., Liu, M., and Ushiba, J. (2013). Event-related desynchronization reflects downregulation of intracortical inhibition in human primary motor cortex. *J. Neurophysiol.* 110, 1158–1166. doi: 10.1152/jn.01092.2012

Tatemoto, T., Tsuchiya, J., Numata, A., Osawa, R., Yamaguchi, T., Tanabe, S., et al. (2017). Real-time changes in corticospinal excitability related to motor imagery of a force control task. *Behav. Brain Res.* 335, 185–190. doi: 10.1016/j.bbr.2017.08.020

Thompson, A. K., Chen, X. Y., and Wolpaw, J. R. (2009). Acquisition of a simple motor skill: task-dependent adaptation plus long-term change in the human soleus H-reflex. *J. Neurosci.* 29, 5784–5792. doi: 10.1523/JNEUROSCI.4326-08.2009

Thompson, A. K., Pomerantz, F. R., and Wolpaw, J. R. (2013). Operant conditioning of a spinal reflex can improve locomotion after spinal cord injury in humans. *J. Neurosci.* 33, 2365–2375. doi: 10.1523/JNEUROSCI.3968-12.2013

Wolpaw, J. R. (2010). What can the spinal cord teach us about learning and memory? *Neuroscientist* 16, 532–549. doi: 10.1177/1073858410368314

Wolpaw, J. R. (2018). The negotiated equilibrium model of spinal cord functiontiated equilibrium model of spinal cord function. *J. Physiol.* doi: 10.1113/JP275532. [Epub ahead of print].

Wolpaw, J. R., and McFarland, D. J. (1994). Multichannel EEG-based brain-computer communication. *Electroencephalogr. Clin. Neurophysiol.* 90, 444–449. doi: 10.1016/0013-4694(94)90135-X

Wolpaw, J. R., and McFarland, D. J. (2004). Control of a two-dimensional movement signal by a noninvasive brain-computer interface in humans. *Proc. Natl. Acad. Sci. U.S.A.* 101, 17849–17854. doi: 10.1073/pnas.0403504101

Wolpaw, J. R., McFarland, D. J., Neat, G. W., and Forneris, C. A. (1991). An EEG-based brain-computer interface for cursor control. *Electroencephalogr. Clin. Neurophysiol* 78, 252–259. doi: 10.1016/0013-4694(91)90040-B

Yahagi, S., Shimura, K., and Kasai, T. (1996). An increase in cortical excitability with no change in spinal excitability during motor imagery. *Percept. Mot. Skills* 83, 288–290. doi: 10.2466/pms.1996.83.1.288

Yamashita, N., and Moritani, T. (1989). Anticipatory changes of soleus H-reflex amplitude during execution process for heel raise from standing position. *Brain Res.* 490, 148–151. doi: 10.1016/0006-8993(89)90441-1

Zarkowski, P., Shin, C. J., Dang, T., Russo, J., and Avery, D. (2006). EEG and the variance of motor evoked potential amplitude. *Clin. EEG Neurosci.* 37, 247–251. doi: 10.1177/155005940603700316

Zehr, E. P., and Stein, R. B. (1999). Interaction of the Jendrassik maneuver with segmental presynaptic inhibition. *Exp. Brain Res.* 124, 474–480. doi: 10.1007/s002210050643

Conflict of Interest Statement: The authors declare that the research was conducted in the absence of any commercial or financial relationships that could be construed as a potential conflict of interest.

Copyright © 2018 Thompson, Carruth, Haywood, Hill, Sarnacki, McCane, Wolpaw and McFarland. This is an open-access article distributed under the terms of the Creative Commons Attribution License (CC BY). The use, distribution or reproduction in other forums is permitted, provided the original author(s) and the copyright owner(s) are credited and that the original publication in this journal is cited, in accordance with accepted academic practice. No use, distribution or reproduction is permitted which does not comply with these terms.

frontiers in Neuroscience

ORIGINAL RESEARCH
published: 31 July 2018
doi: 10.3389/fnins.2018.00514

Performance Differences Using a Vibro-Tactile P300 BCI in LIS-Patients Diagnosed With Stroke and ALS

Alexander Heilinger[1], Rupert Ortner[2], Vincenzo La Bella[3], Zulay R. Lugo[4,5,6], Camille Chatelle[4], Steven Laureys[4], Rossella Spataro[3,7†] and Christoph Guger[1,8†]*

[1] g.tec medical engineering GmbH, Schiedlberg, Austria, [2] g.tec medical engineering Spain SL, Barcelona, Spain, [3] ALS Clinical Research Center, BioNeC, University of Palermo, Palermo, Italy, [4] GIGA Consciousness, Coma Science Group, University of Liège, Liège, Belgium, [5] French Association of Locked-in Syndrome (ALIS), Paris, France, [6] Research Department, Hospital Universitari Institut Pere Mata, Reus, Spain, [7] Centro Neurolesi Bonino Pulejo (IRCCS), Palermo, Italy, [8] Guger Technologies OG, Graz, Austria

OPEN ACCESS

Edited by:
Mikhail Lebedev, Duke University, United States

Reviewed by:
Ali Yadollahpour, Ahvaz Jundishapur University of Medical Sciences, Iran
Jing Jin, East China University of Science and Technology, China

***Correspondence:**
Alexander Heilinger
heilinger@gtec.at

† These authors have contributed equally to this work.

Specialty section:
This article was submitted to Neural Technology, a section of the journal Frontiers in Neuroscience

Received: *13 April 2018*
Accepted: *10 July 2018*
Published: *31 July 2018*

Citation:
Heilinger A, Ortner R, La Bella V, Lugo ZR, Chatelle C, Laureys S, Spataro R and Guger C (2018) Performance Differences Using a Vibro-Tactile P300 BCI in LIS-Patients Diagnosed With Stroke and ALS. Front. Neurosci. 12:514. doi: 10.3389/fnins.2018.00514

Patients with locked-in syndrome (LIS) are typically unable to move or communicate and can be misdiagnosed as patients with disorders of consciousness (DOC). Behavioral assessment scales are limited in their ability to detect signs of consciousness in this population. Recent research has shown that brain-computer interface (BCI) technology could supplement behavioral scales and allows to establish communication with these severely disabled patients. In this study, we compared the vibro-tactile P300 based BCI performance in two groups of patients with LIS of different etiologies: stroke (n = 6) and amyotrophic lateral sclerosis (ALS) (n = 9). Two vibro-tactile paradigms were administered to the patients to assess conscious function and command following. The first paradigm is called vibrotactile evoked potentials (EPs) with two tactors (VT2), where two stimulators were placed on the patient's left and right wrist, respectively. The patients were asked to count the rare stimuli presented to one wrist to elicit a P300 complex to target stimuli only. In the second paradigm, namely vibrotactile EPs with three tactors (VT3), two stimulators were placed on the wrists as done in VT2, and one additional stimulator was placed on his/her back. The task was to count the rare stimuli presented to one wrist, to elicit the event-related potentials (ERPs). The VT3 paradigm could also be used for communication. For this purpose, the patient had to count the stimuli presented to the left hand to answer "yes" and to count the stimuli presented to the right hand to answer "no." All patients except one performed above chance level in at least one run in the VT2 paradigm. In the VT3 paradigm, all 6 stroke patients and 8/9 ALS patients showed at least one run above chance. Overall, patients achieved higher accuracies in VT2 than VT3. LIS patients due to ALS exhibited higher accuracies that LIS patients due to stroke, in both the VT2 and VT3 paradigms. These initial data suggest that controlling this type of BCI requires specific cognitive abilities that may be impaired in certain sub-groups of severely motor-impaired patients. Future studies on a larger cohort of patients are needed to better identify and understand the underlying cortical mechanisms of these differences.

Keywords: locked-in syndrome, BCI performance, stroke, ALS, tactile stimulation, P300 event-related potential

INTRODUCTION

The term locked-in syndrome (LIS) was introduced to describe a clinical state of quadriplegia and anarthria due to a disruption of the corticospinal and corticobulbar tracts in the brainstem (Plum and Posner, 1983). The principal etiology of acute onset LIS is stroke (ischemic or hemorrhagic) affecting the ventral part of the pons (Patterson and Grabois, 1986). LIS can also result from the late stage of chronic degenerative neurological diseases such as amyotrophic lateral sclerosis (ALS), which affects the upper and lower motor neurons, leading to progressive paralysis of voluntary muscles and eventually to respiratory failure (Bäumer et al., 2014).

Based on the severity of motor deficits, three varieties of LIS have been described: classical LIS, in which the patient is unable to move – except for eye movements or blinking – or to speak; incomplete LIS, in which residual voluntary movements in addition to eye movements can be present; and total or complete LIS (CLIS), where patients show total immobility, including lack of voluntary eye movement (Bauer et al., 1979). Patients with CLIS/LIS can be mistaken with patients in coma or with other DOC such as the vegetative state/unresponsive wakefulness syndrome (VS/UWS), in which patients are eyes opened but do not show any sign of voluntary movement. Hence, reliable diagnostic tools for the differentiation of these clinical conditions are of utmost importance.

Despite the existence of well-defined clinical criteria for the diagnosis of DOC and LIS, differential diagnosis remains challenging and misdiagnosis still occurs. Standardized behavioral scales like the Glasgow Coma-Scale (GCS) (Teasdale and Jennett, 1974) and the Coma-Recovery-Scale revised (CRS-R) (Giacino et al., 2004) are widely used in clinical settings. However, such tools are limited when assessing patients with CLIS as they are highly dependent on motor abilities. For these patients, supplementary tools are needed.

Once the diagnosis of LIS has been established, another major challenge with this population is providing them with appropriate devices for communication and environmental management. These tools can increase quality of life and facilitate the assessment of cognitive impairments (e.g., fronto-temporal dementia), which has been described to be often associated with ALS (Phukan et al., 2007).

In this context, brain-computer interface (BCI) systems have been used for decades to establish communication with patients with LIS, usually via the electroencephalogram (EEG) (Wolpaw et al., 2002; Wolpaw and Wolpaw, 2012). Different EEG paradigms have been employed that use different stimuli or mental tasks, including motor imagery, steady-state visual evoked potentials (EPs) (Guger et al., 2003; Bin et al., 2009; Combaz et al., 2013; Ahn et al., 2015) and event-related potentials (ERPs), notably the P300 waveform (Fazel-Rezai et al., 2012; Blankertz et al., 2016). Most P300-BCIs rely on the visual modality, but auditory or vibro-tactile modalities have been explored for patients with visual/auditory impairments, which have been described to be present in an important percentage of patients with LIS (Lugo et al., 2015).

Kaufmann et al. (2013) compared different BCI modalities on a single LIS patient, reporting that the tactile modality was clearly superior compared to visual or auditory modalities. Prior work has shown that healthy subjects without prior training could achieve a mean classification accuracy of 93% with a vibro-tactile paradigm (Alison et al., 2017). Using the same method, 12 ALS patients (9 LIS/3 CLIS) achieved a median accuracy of 76.6% (min: 40/max: 100) using a vibro-tactile paradigm with two stimulators (VT2) (Guger et al., 2017). The same publication showed that 2/3 CLIS patients reached a classification of 100% using VT3. These two CLIS patients could also communicate correctly (9/10 and 8/10 questions answered correctly). In other work using vibrotactile P300 BCI for LIS patients, six patients achieved an average accuracy of 80% (min: 20%/max: 100%) in a paradigm with VT2 and 55.3% (min: 20%/max: 100%) in a paradigm with VT3 (Lugo et al., 2014).

Silvoni et al. (2016) investigated the neurophysiological correlates of vibrotactile stimulation processing in a group of 14 ALS patients and 10 healthy subjects, using a single vibro-stimulator placed on the left hand. They reported that responses to tactile stimuli were not altered in ALS, suggesting that this neurophysiological signal could be used in at least some ALS patients to control such a BCI.

In the current study, we investigated BCI performance in patients with LIS from different etiologies. We explored differences in classification accuracy and EPs using a vibro-tactile based BCI in two sub-groups of LIS due to ALS and stroke. Based on the literature suggesting preserved cognitive abilities in LIS patients from both etiologies (Phukan et al., 2011), we hypothesized that both groups would perform equally well using a vibro-tactile based BCI, even though the underlying pathological mechanisms differ between these two patient groups.

The results of this study could help to improve the assessment to detect the presence of consciousness in patients with stroke, ALS and other conditions. These findings may also help to shed light on the differences and clinical characteristics that should be considered with each patient group and underline the importance of a multimodal approach – using stimuli from different sensory modalities – to evaluate non-responsive patients.

MATERIALS AND METHODS

Population

This retrospective study included data acquired in LIS patients at the University of Palermo, Italy (PA) and by the French Association of Locked-In Syndrome (ALIS) in Paris, France, as part of other studies previously published (Lugo et al., 2014; Guger et al., 2017). For the ALS patients, the following inclusion criteria were used: patients had to be over 18 years old, diagnosed with definite ALS according to the El Escorial Diagnostic Criteria and LIS/CLIS state verified by experienced neurologists in motor neuron diseases, without evidence of cognitive and behavioral abnormalities along the disease's course. For stroke patients, the following inclusion criteria were used: the patients had to be over 18 years old and diagnosed

with stroke in the chronic (>1 year since diagnosis) LIS state.

Table 1 reports the patients' demographic data. We included a convenience sample of six stroke patients (three ischemic, three hemorrhagic; median age = 40, min: 21, max: 48) with a disease duration between 4 and 19 years (median = 10), and nine ALS patients (median age = 59, min: 37, max: 68) with a disease duration between 2, 3, and 12 years (median = 7). The difference between gender and age was tested using a Chi-Square-Test (significance = $p < 0.05$). There was no difference in age and gender between the two groups.

Brain-Computer Interface System

The mindBEAGLE system (g.tec Guger Technologies OG, Austria) was used for all data collection and real-time feedback. The system uses active gel-based EEG electrodes connected to a biosignal amplifier (g.USBamp, g.tec medical engineering GmbH). The amplifier has a 24-bit resolution and a high oversampling rate to increase the signal-to-noise ratio. The amplifier is connected to the computer via USB and sends the data in real-time at a sampling rate of 256 Hz. The EEG signal is presented on a monitor for quality inspection during the measurement, and the data are stored in floating point format for later data analysis.

The recorded EEG data were filtered between 48 and 50 Hz using a notch filter. Afterward the data were bandpass filtered between 0.1 and 30 Hz to remove baseline shifts and eliminate most of the EEG artifacts. Eight electrodes were used for the recording, placed on the Fz, C3, Cz, C4, CP1, CPz, CP2, and Pz position according to the extended international 10–20 electrode system. The reference electrode was fixed on the right earlobe and the ground electrode was mounted on the forehead.

Paradigm

Two P300 oddball paradigms were used: vibrotactile EPs with two tactors (VT2) and vibrotactile EPs with three tactors (VT3). Both paradigms presented 480 stimuli per run, with 60 groups of 8 stimuli. In both paradigms, the patient was instructed via earbuds to silently count vibrotactile pulses to either the left or right wrist. The left and right wrists had an equal chance of being chosen pseudo-randomly as the "target" wrist. All vibrotactile stimuli lasted 100 ms, with a 100 ms delay between stimuli. Both paradigms required about 2.5 min per run and were designed to elicit an oddball P300 to stimuli delivered to the target wrist only.

In the VT2 paradigm, the two tactors were placed on the left and right wrists. Each of the 60 groups of eight stimuli per run contained one target and seven non-target stimuli, presented in pseudorandom order. Thus, the target to non-target ratio was 1:7.

In the VT3 paradigm, an additional (third) tactor was placed on a third location on the patient's body. For the ALS patients, the third tactor was placed on the upper part of the back. For the stroke patients, the third tactor was placed on the neck. The position of the third tactor can be arbitrary, since it acts as a distractor. The other two tactors were fixed on the right and left wrists. In VT3, each sequence of eight stimuli included one stimulus to the left wrist, one stimulus to the right wrist, and six stimuli to the third tactor, in pseudorandom order. Thus, each sequence of eight stimuli also contained one target, like the VT2 paradigm, but six of the seven non-targets were meant as "distractor" stimuli that could never be designated as the target. The runtime for both VT modes was 2.5 min for one run.

In addition to these two paradigms to assess patients, we also explored communication using the VT3 paradigm. The experimenter asked yes/no questions and the patient was asked to answer by counting the stimuli on either the left or right wrist. One question can be answered after 120 stimuli, which requires 38 s. The system only selects YES or NO if the result is significant and presents no response otherwise. This result is presented to the experimenter via the monitor. Each patient was asked 10 questions. The communication was considered reliable if the patient could accurately answer at least 7/10 questions.

Each patient participated in one experimental session that included one VT3 communication run and at least one run (each) of VT2 and VT3 assessment. Some patients participated in additional VT2 and/or VT3 runs, as shown in **Table 1**. The total number of runs per session was limited to five per participant, to address concerns with possible fatigue or discomfort.

Data Analysis

For both paradigms, data segments of −100–600 ms around each stimulus were extracted. Each of these single trials was baseline corrected and averaged. Trials in which the EEG signal amplitude exceeded ±100 μV were rejected from the EP and classifier calculation. The EPs were visually inspected. For the classification, the data were classified using the linear discriminant analysis (LDA), which resulted in a classification accuracy between 0 and 100%. This result showed how well the data could be discriminated using the classifier. In one assessment run, 60 sequences of tactile stimuli were presented to the patient. Each sequence contained eight trials in randomized order, in which one trial was the target trial and seven were non-target trials. This resulted in 480 trials total (60 target trials/420 non-target trials). After removal of artifact trials, the ratio between non-target and target trials was set to 7:1 again. Trials in both pools were shuffled and split 50:50 into training and testing data. The training data were used to create an LDA classifier and tested on the testing data as follows: seven non-target trials and one target trial were randomly chosen and the LDA score was calculated for each of the trials. The trial with the highest LDA score was classified as target trial. If the classified target trial was the real target trial, the test classification was correct (100%), otherwise incorrect (0%). This step was repeated 1000 times, resulting in a classification plot.

Brain-computer interface performance was considered above chance when the classification accuracy was higher than 23% based on binomial distribution (Ortner et al., 2014). Non-parametric statistical method was chosen due to the small sample size. To compare the classification accuracies between the two groups, a Wilcoxon rank sum test was used. VT2 and VT3 paradigm results were compared separately. We considered significance at $p < 0.05$.

TABLE 1 | Overview of all patients including demographic information, classification accuracies, and communication mode results.

Patient	Sex	Age	Diagnosis	Disease duration (years)	Clinical syndrome	Paradigm	Accuracy [%]	Communication using VT3
S1	F	47	Stroke (ischemic)	4	LIS	VT2-1	79.9	4C/6U
						VT2-2	45.6	
						VT3-1	52.8	
						VT3-2	23.1	
S2	F	21	Stroke (ischemic)	4	LIS	VT2-1	42.2	10U
						VT2-2	16.5	
						VT3-1	28.3	
						VT3-2	13.4	
S3	M	46	Stroke (ischemic)	16	LIS	VT2-1	13.6	2C/8U
						VT2-2	10.1	
						VT3-1	35.5	
						VT3-2	7.9	
S4	M	33	Stroke (hemorrhagic)	12	LIS	VT2-1	44.4	6C/4U
						VT2-2	40.6	
						VT3-1	30.5	
						VT3-2	21.45	
S5	F	48	Stroke (hemorrhagic)	5	LIS	VT2-1	61.1	2C/8U
						VT2-2	9.0	
						VT3-1	14.2	
						VT3-2	14.2	
S6	F	46	Stroke (ischemic)	19	LIS	VT2-1	25.0	10U
						VT2-2	22.9	
						VT3-1	24.5	
						VT3-2	19.0	
A1	F	68	ALS	7.5	LIS	VT2	100.0	9C/1W
						VT3	99.6	
A2	F	65	ALS	7	LIS	VT2	21.6	10U
						VT3-1	12.4	
						VT3-2	1.6	
A3	F	65	ALS	7	LIS	VT2	100.0	7C/1W/2U
						VT3	90.0	
A4	F	76	ALS	12	LIS	VT2	100.0	8C/1U/1W
						VT3	87.5	
A5	F	46	ALS	11.3	LIS	VT2	98.2	7C/3U
						VT3-1	81.4	
						VT3-2	51.5	
A6	M	63	ALS	2.3	LIS	VT2	97.2	9C/1W
						VT3	91.0	
A7	M	68	ALS	4.3	LIS	VT2	94.2	8C/2W
						VT3	100.0	
A8	M	37	ALS	8.5	LIS	VT2	100.0	8C/2W
						VT3-1	52.4	
						VT3-2	95.1	
A9	F	47	ALS	2.5	LIS	VT2	21.2	7C/2U/1W
						VT3	99.7	

F, female; M, male; C, correct answers; U, undecided answers; W, wrong answers. Each participant completed one communication run with 10 questions.

RESULTS

Classification Accuracy

All patients performed the VT2 and VT3 paradigms, either once or multiple times. **Table 1** summarizes data obtained from all patients. All patients except one showed at least one run above chance in the VT2 paradigm. In the VT3 paradigm (i.e., active task), all 6 stroke patients and 8/9 ALS patients showed at least one run above chance. The ninth ALS patient (patient A2) attained at best 12.4% accuracy. Overall, patients achieved higher

accuracies in VT2 than VT3. The accuracy observed during VT2 was higher in ALS patients than in stroke patients, with a median accuracy of 98% (min: 22%, max: 100%) and 32.8% (min: 15%, max: 45%), respectively ($p < 0.05$). For VT3, ALS patients also achieved a higher accuracy than stroke patients, with a median classification accuracy of 82% (min: 42%; max: 97%) and 22% (min: 15%; max: 28%), respectively ($p < 0.01$). The results are reported in **Figure 1**.

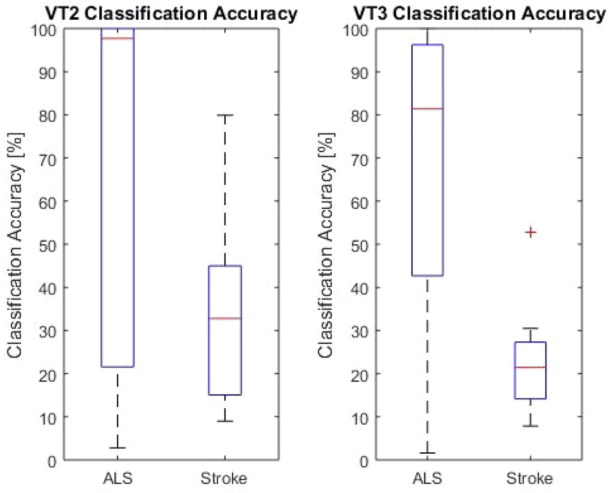

FIGURE 1 | VT2 and VT3 classification accuracies for both LIS groups. The red lines indicate the mean values for the group. The upper and lower end of the box represents the first quartile. The black lines are the end of the first and fourth quartile. The red cross marks an outlier.

Communication Mode

All patients participated in one communication run with 10 questions. None of the stroke patients could reliably communicate with the system. The classifier did not get any wrong answers for any of the stroke patients, but it did provide between 4 and 10 "undecided" answers.

For ALS patients, 8/10 patients could answer at least 7/10 questions accurately, while 2 were not able to reliably communicate with the system (the classifier provided "undecided" answers for all 10 questions).

Evoked Potentials

All EPs were visually inspected. With the VT2 paradigm, all patients showed a high P300 complex. **Figure 2** presents examples with classification accuracy and the EPs on the Cz electrode from patients A9 and S3.

With the VT3 paradigm, 4/10 ALS patients (A1, A7–A9) showed a high P300 or other components of the P300 complex, whereas none of the stroke patients did. These results can be seen in **Figures 3** and **4**.

DISCUSSION

The aim of this study was to compare performance with vibro-tactile BCI paradigms in patients with LIS resulting from ALS or stroke. Our hypothesis was that both groups would perform equally well using a vibro-tactile based BCI. Our results show higher performance in ALS than stroke patients, which might reflect the different pathological mechanisms underlying the LIS in each group.

The first explanation for the difference in both paradigms is the possible presence of reduced tactile sensitivity in patients with LIS due to stroke. Paterson and Grabois reported abnormalities of sensitivity in 34 of 62 patients (54%) (Patterson and Grabois, 1986) with LIS from various etiologies. This has also been reported in another study (Hawkes, 1974). Although it is not the main characteristic of the syndrome, the presence of such alterations is highly probable due to the possible lesion of the central lemniscus that runs just behind the pyramidal tracts.

We also observed lower accuracies in all patients during the consecutive runs except one in the ALS group. This could partly be explained by an increased fatiguability influenced by the lesion site of the stroke (Staub and Bogousslavsky, 2001). Even though the subject was asked to count the target, the responses to the VT2 paradigm could also be elicited without active participation of the person, which is not possible in VT3. This could also explain the decrease in performance. Additional research with more runs per patient, possibly across multiple sessions, could further elucidate the effects of consecutive runs.

Patient A9's performance improved considerably between the two VT3 runs (VT3-1 = 52.4%; VT3-2 = 95.1%), which could be a short-term learning effect. The results from all other patients may reflect fatigue or an absence of learning effects, since the VT3 task entails a more challenging discrimination task. Further studies could explore whether this accuracy reduction correlates with mental exhaustion or other factors and develop new paradigms that might be less tiring. **Figure 4** show that the classifier could attain high accuracy with fewer than 30 groups of eight trials for most ALS patients, which suggests that shorter runs may be feasible.

During visual inspection of the EPs, all patients showed a P300 complex during VT2, but four ALS patients elicited a high P300 or other signal during VT3, whereas when none of the stroke patients did. If the high classification accuracies observed in the four ALS patients correspond with the EPs observed, the BCI system also found some additional components in the signal to produce high classification accuracy in the other patients. As VT3 is an active task, and therefore more cognitively demanding, the data suggest that there are some underlying cortical activities in ALS contributing to a high classification accuracy even if the EPs did not exhibit robust differences based on visual inspection of averaged data.

While the approach used here is often called a P300 BCI in the literature, many of the participants produced target vs. non-target differences in other ERP components of the P300 complex, notably the N100 and P200. Other articles have also noted that so-called P300 BCIs often rely on non-P300 components within

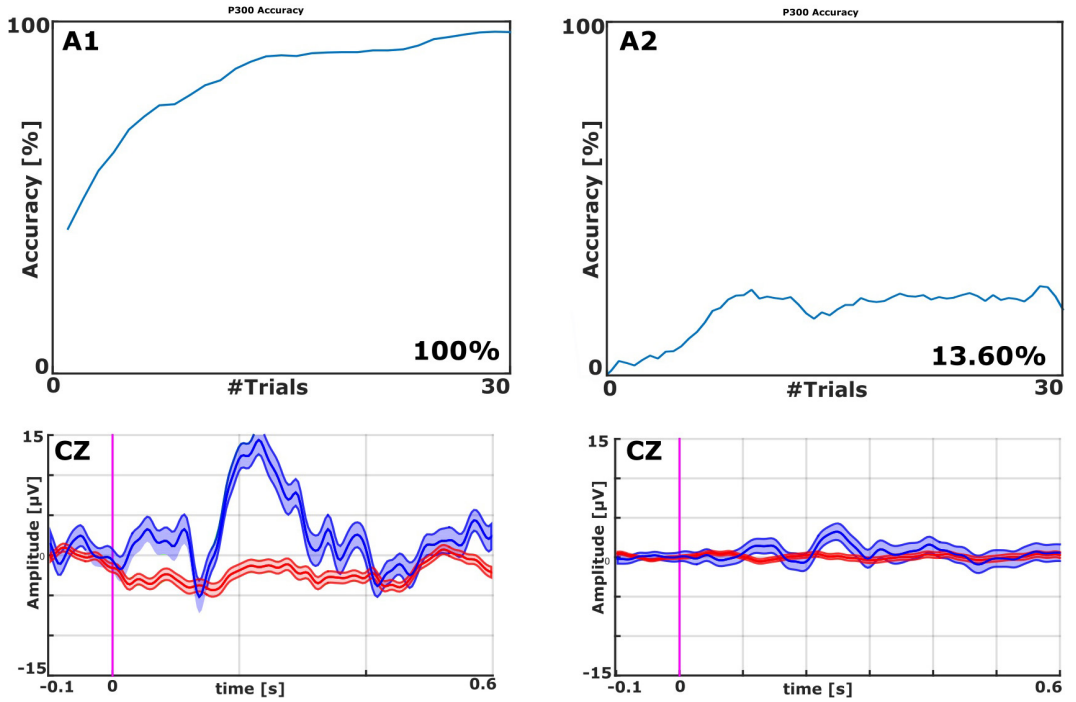

FIGURE 2 | Examples of EPs and Classification Accuracies from ALS patient A9 and stroke patient S3, both from the VT2 paradigm. The classification accuracy plot on the top left shows that one ALS patient achieved 100% accuracy (top left). The classifier could effectively discriminate target from non-target stimuli after about 10 trials with A9's data. Visual inspection of the averaged EPs (bottom left) shows a clear N1 followed by a robust P2 (Amplitude > 15 µV over site Cz) in patient A9 to target trials (blue lines). The non-target trials (red lines) did not exhibit these features. The top right panel shows that one stroke patient attained 13.6% accuracy. Concordantly, the ERPs in the bottom right do not exhibit robust differences between target and non-target ERPs.

the P300 complex (Fazel-Rezai et al., 2012; Allison et al., in review). Additional research is needed to further understand how these patients' ERPs are generated and resulting clinical impact.

In summary, ALS patients showed high P300 amplitudes or other often atypical complexes, which could both be classified with high accuracies by the BCI system. Prior work has shown that LIS patients diagnosed with ALS could control a P300-based BCI system, sometimes over months (Sellers and Donchin, 2006; Nijboer et al., 2008; Silvoni, 2009). Comparing the EPs of the ALS group with the results of the stroke group, the most likely explanation for these differences is an alteration in tactile sensitivity.

Classification accuracy could indicate whether the patient will successfully communicate. Prior work showed that communication could be successful at a classification accuracy >60% (Guger et al., 2017). Within the stroke patient group, all answers that were not "correct" were "undecided." As the stroke patients showed classification accuracies below 60% in the assessment runs, this could further suggest that the success of communication is dependent on classification accuracy. The ALS patient group showed a more heterogeneous response, with both "undecided" and "wrong" responses. This outcome could indicate that more stroke patients had concentration problems, fell asleep, forgot the instructions or were distracted. The possible presence of cognitive deficits in these patients must be also taken into account, since they have been described in previous studies of patients with LIS of vascular or traumatic etiology, especially with the presence of thalamic or hemispheric lesions (Schnakers et al., 2008; Rousseaux et al., 2009). In the case of patients with ALS, the A4 patient has associated a frontotemporal dementia, which may explain his poor performance and low response rate. The low classifier accuracy in the stroke patients and in ALS patients A2 and A4 might also accurately reflect that these patients are at least periodically unaware and/or unable to perform at least some of the mental tasks required for the paradigms used here.

This study used a montage with eight electrodes that were positioned to optimally record the P300. Previous work with a visual P300 BCI for spelling showed that a similar eight EEG electrode montage could yield a classification accuracy of 100% with 17 subjects (Guger et al., 2012). Additional electrodes did not substantially improve classifier accuracy (Guger et al., 2003). However, future work could explore expanded montages that could lead to better performance, especially with patient groups.

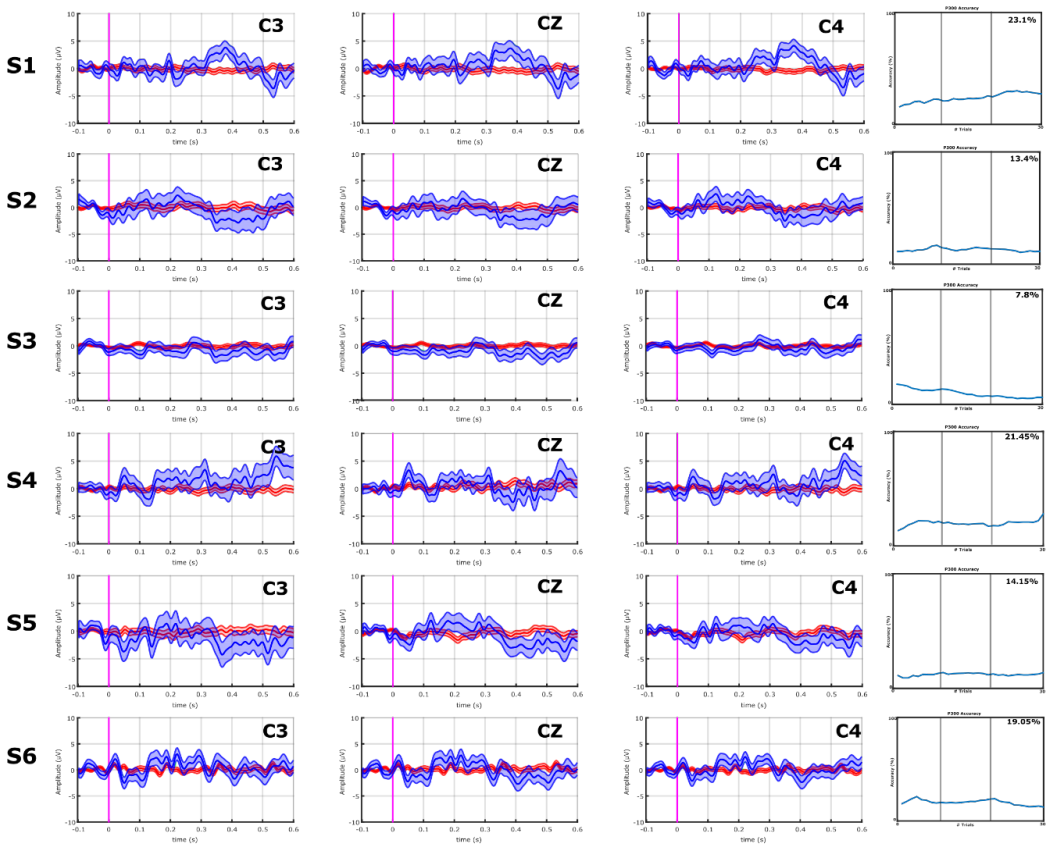

FIGURE 3 | EPs and classification accuracies of all stroke patients from the VT3 communication runs. All stroke patients produced a P300 $\leq$ 5 μV, and a classification accuracy of 23.1% (patient S1) or lower in the VT3 runs. Visual inspection of **Figures 3** and **4** shows that the differences in the target vs. non-target EPs in the stroke patient group appear small compared to the ALS group, and the classifier could not find consistent and robust differences.

Several limitations have to be considered for this study. First, a small convenience sample of 15 LIS patients was included. We acknowledge the limitations of using a small sample size but emphasize the difficulty of measuring this specific patient population. Second, the threshold chosen for defining above chance level performance and communication runs might not be adapted for single patient performance, as it would require additional offline analyses. Finally, it would be interesting to document more extensively the cognitive abilities and the severity of disease of the patients. As this was a retrospective study, no further information could be extracted regarding each patient's status, which also limits potential data analyses.

These results could contribute to improved mechanisms to assess the presence of consciousness in non-responsive patients, perhaps supplementing the CRS-R, GCS or other established clinical assessments. Our findings may also help to shed light on the differences and clinical characteristics that should be taken into account with each patient group and underline the importance of having a multimodal approach – using stimuli from different sensory modalities – to evaluate non-responsive patients to overcome sensory deficits and to adapt the means of communication to the remaining sensory capabilities.

The approach used here can objectively identify command following activity without any movement and could provide communication for some patients. All three parameters, i.e., classification accuracy, EPs and communication accuracy, might provide a more detailed and accurate information about each patient. However, results indicated that all three paradigms were more successfully used in ALS than stroke patients. As both the system and the paradigms used here are relatively new, substantial improvements are needed to answer these discrepancies.

SUMMARY

LIS Patients due to ALS attained better performance with the BCI paradigms employed in this study than LIS patients due to stroke. This could be explained by the lesion of the sensory pathways

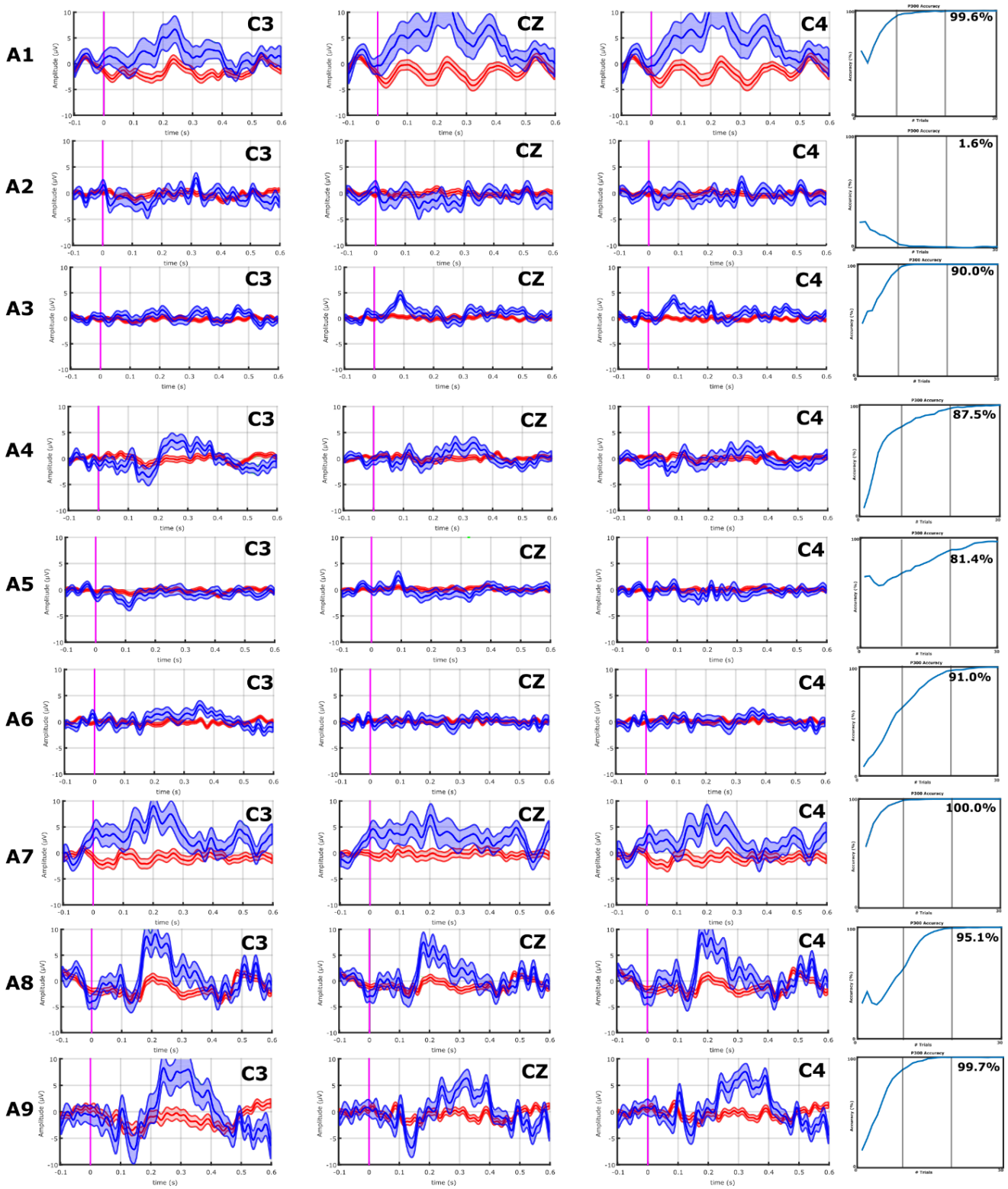

FIGURE 4 | EPs and classification accuracies of all ALS patients from the VT3 communication runs. ALS patients A1, A8, A9, and A10 had a P2 and/or P3 greater than 5 μV over C3, Cz, and C4. Consistently, these ALS patients all achieved an accuracy ≥95%. In ALS patients A2–A7, the P300 response is lower than 5 μV or non-existent, and only A7 exhibits modest target vs. non-target differences in visual inspection. Nonetheless, the classifier found some activity to facilitate accurate classification, resulting in mean accuracies of 81.4% (patient A6) or higher, excluding patients A2 (VT3 = 1.6%) and A4 (VT3 = 16.3%).

in patients with LIS due to brainstem stroke, and perhaps also a greater propensity toward fatigue in this group (such as due to brainstem damage). Future studies should elucidate these differences to design BCI paradigms that consider the underlying disease pathology, so as to best tailor BCIs accordingly for each patient.

AUTHOR CONTRIBUTIONS

ZL and RS were mainly responsible for data collection which occurred in collaboration with SL and VLB. AH was mainly responsible for data analysis and manuscript preparation. The remaining authors were responsible for study design and manuscript preparation.

FUNDING

This research was supported by the ALS Clinical Research Center, BioNeC, University of Palermo, the French Association of Locked in Syndrome (ALIS), the Belgian National Funds for Scientific Research (FNRS), the European Commission (European ICT Programme Project FP7-247919 DECODER), the University of Liège and the University Hospital of Liège, and the EC SME Phase 2 project ComaWare. CC is a Marie Sklodowska-Curie fellow (H2020-MSCA-IF-2016-ADOC-752686). This project has received funding from the European Union's Horizon 2020 research and innovation programme under the Marie Skłodowska-Curie grant agreement No 712949 (TECNIOspring PLUS).

REFERENCES

Ahn, S., Kim, K., and Jun, S. C. (2015). Steady-State somatosensory evoked potential for brain-computer interface—present and future. *Front. Hum. Neurosci.* 9:716. doi: 10.3389/fnhum.2015.00716

Alison, B. Z., Cho, W., Ortner, R., Heilinger, A., Edlinger, G., and Guger, C. (2017). "Validation of a brain-computer interface (BCI) system designed for patients with disorders of consciousness (DOC): regular and sham testing with healthy participants," in *Proceedings of the International Conference on Augmented Cognition*, Las Vegas, NV. doi: 10.1007/978-3-319-58625-0_18

Bauer, G., Gerstenbrand, F., and Rumpl, E. (1979). Varieties of the locked-in syndrome. *J. Neurosci.* 221, 77–91. doi: 10.1007/BF00313105

Bäumer, D., Talbot, K., and Turner, M. R. (2014). Advances in motor neurone disease. *J. R. Soc. Med.* 107, 14–21. doi: 10.1177/0141076813511451

Bin, G., Gao, X., Wang, Y., Hong, B., and Gao, S. (2009). VEP-based brain-computer interfaces: time, frequency, and code modulations [Research Frontier. *IEEE Comput. Intell. Mag.* 4, 22–26. doi: 10.1109/MCI.2009.934562

Blankertz, B., Acqualagna, L., Dähne, S., Haufe, S., Schultze-Kraft, M., Sturm, I., et al. (2016). The Berlin brain-computer interface: progress beyond communication and control. *Front. Neurosci.* 10:530. doi: 10.3389/fnins.2016.00530

Combaz, A., Chatelle, C., Robben, A., Vanhoof, G., Goeleven, A., Thijs, V., et al. (2013). A Comparison of two spelling brain-computer interfaces based on visual P3 and SSVEP in locked-in syndrome. *PLoS One* 8:e73691. doi: 10.1371/journal.pone.0073691

Fazel-Rezai, R., Allison, B. Z., Guger, C., Sellers, E. W., Kleih, S. C., and Kübler, A. (2012). P300 brain computer interface: current challenges and emerging trends. *Front. Neuroeng.* 5:14. doi: 10.3389/fneng.2012.00014

Giacino, J. T., Kalmar, K., and Whyte, J. (2004). The JFK coma recovery scale-revised: measurement characteristics and diagnostic utility11No commercial party having a direct financial interest in the results of the research supporting this article has or will confer a benefit upon the authors or upon any organization with which the authors are associated. *Arch. Phys. Med. Rehabil.* 85, 2020–2029. doi: 10.1016/j.apmr.2004.02.033

Guger, C., Allison, B. Z., Großwindhager, B., Prückl, R., Hintermüller, C., Kapeller, C., et al. (2012). How many people could use an SSVEP BCI. *Front. Neurosci.* 6:169. doi: 10.3389/fnins.2012.00169

Guger, C., Edlinger, G., Harkam, W., Niedermayer, I., and Pfurtscheller, G. (2003). How many people are able to operate an EEG-based brain-computer interface (BCI)? *Neural Syst. Rehabil. Eng. IEEE Trans.* 11, 145–147. doi: 10.1109/tnsre.2003.814481

Guger, C., Spataro, R., Allison, B. Z., Heilinger, A., Ortner, R., Cho, W., et al. (2017). Complete locked-in and locked-in patients: command following assessment and communication with vibro-tactile P300 and motor imagery brain-computer interface tools. *Front. Neurosci.* 11:251. doi: 10.3389/fnins.2017.00251

Hawkes, C. H. (1974). Locked-in. Syndrome: report of Seven Cases. *BMJ* 4, 379–382. doi: 10.1136/bmj.4.5941.379

Kaufmann, T., Holz, E. M., and Kübler, A. (2013). Comparison of tactile, auditory, and visual modality for brain-computer interface use: a case study with a patient in the locked-in state. *Front. Neurosci.* 7:129. doi: 10.3389/fnins.2013.00129

Lugo, Z. R., Bruno, M.-A., Gosseries, O., Demertzi, A., Heine, L., Thonnard, M., et al. (2015). Beyond the gaze: communicating in chronic locked-in syndrome. *Brain Inj.* 29, 1056–1061. doi: 10.3109/02699052.2015.1004750

Lugo, Z. R., Rodriguez, J., Lechner, A., Ortner, R., Gantner, I. S., Laureys, S., et al. (2014). A vibrotactile P300-based BCI for consciousness detection and communication. *Clin EEG Neurosci.* 45, 14–21. doi: 10.1177/1550059413505533

Nijboer, F., Sellers, E. W., Mellinger, J., Jordan, M. A., Matuz, T., Furdea, A., et al. (2008). A P300-based brain–computer interface for people with amyotrophic lateral sclerosis. *Clin. Neurophysiol.* 119, 1909–1916. doi: 10.1016/j.clinph.2008.03.034

Ortner, R., Espinosa, A., Rodriguez, J., Laureys, S., Lugo, Z. R., Guger, C., et al. (2014). "A BCI-Based tool for detection of awareness and for communication with non-responsive patients," in *Universal Access in Human-Computer Interaction. Design and Development Methods for Universal Access*, Vol. 8513, eds C. Stephanidis and M. Antona (Berlin: Springer), 527–535.

Patterson, J. R., and Grabois, M. (1986). Locked-in syndrome: a review of 139 cases. *Stroke* 17, 758–764. doi: 10.1161/01.STR.17.4.758

Phukan, J., Elamin, M., Bede, P., Jordan, N., Gallagher, L., Byrne, S., et al. (2011). The syndrome of cognitive impairment in amyotrophic lateral sclerosis: a population-based study. *Neurology* 80, 1590–1597. doi: 10.1136/jnnp-2011-300188

Phukan, J., Pender, N., and Hardiman, O. (2007). Cognitive impairment in amyotrophic lateral sclerosis. *Lancet Neurol.* 6, 994–1003. doi: 10.1016/S1474-4422(07)70265-X

Plum, F., and Posner, J. (1983). *The Diagnosis of Stupor and Coma*, 3rd Edn. Philadelphia, PA: Davis.

Rousseaux, M., Castelnot, E., Rigaux, P., Kozlowski, O., and Danze, F. (2009). Evidence of persisting cognitive impairment in a case series of patients with locked-in syndrome. *J. Neurol. Neurosurg. Psychiatry* 80, 166–170. doi: 10.1136/jnnp.2007.128686

Schnakers, C., Majerus, S., Goldman, S., Boly, M., Eeckhout, P., Gay, S., et al. (2008). Cognitive function in the locked-in syndrome. *J. Neurol.* 255, 323–330. doi: 10.1007/s00415-008-0544-0

Sellers, E. W., and Donchin, E. (2006). A P300-based brain–computer interface: initial tests by ALS patients. *Clin. Neurophysiol.* 117, 538–548. doi: 10.1016/j.clinph.2005.06.027

Silvoni, S. (2009). P300-based brain-computer interface communication: evaluation and follow-up in amyotrophic lateral sclerosis. *Front. Neurosci.* 3:60. doi: 10.3389/neuro.20.001.2009

Silvoni, S., Konicar, L., Prats-Sedano, M. A., Garcia-Cossio, E., Genna, C., Volpato, C., et al. (2016). Tactile event-related potentials in amyotrophic lateral sclerosis (ALS): implications for brain-computer interface. *Clin. Neurophysiol.* 127, 936–945. doi: 10.1016/j.clinph.2015.06.029

Staub, F., and Bogousslavsky, J. (2001). Fatigue after stroke: a major but neglected issue. *Cerebrovasc. Dis.* 12, 75–81. doi: 10.1159/000047685

Teasdale, G., and Jennett, B. (1974). Assessment of coma and impaired consciousness. A practical scale. *Lancet* 2, 81–84. doi: 10.1016/S0140-6736(74)91639-0

Wolpaw, J. R., Birbaumer, N., McFarland, D. J., Pfurtscheller, G., and Vaughan, T. M. (2002). Brain–computer interfaces for communication and control. *Clin. Neurophysiol.* 113, 767–791. doi: 10.1016/S1388-2457(02)00057-3

Wolpaw, J. R., and Wolpaw, E. W. (2012). *Brain-Computer Interfaces: Principles and Practice*, 1st Edn. New York, NY: Oxford University Press. doi: 10.1093/acprof:oso/9780195388855.001.0001

Conflict of Interest Statement: The authors declare that the hard- and software were made by g.tec medical engineering GmbH. Authors AH, RO, and CG are employed by g.tec. SL is on the scientific advisory board of g.tec.

The remaining authors declare that the research was conducted in the absence of any commercial or financial relationships that could be construed as a potential conflict of interest.

Copyright © 2018 Heilinger, Ortner, La Bella, Lugo, Chatelle, Laureys, Spataro and Guger. This is an open-access article distributed under the terms of the Creative Commons Attribution License (CC BY). The use, distribution or reproduction in other forums is permitted, provided the original author(s) or licensor are credited and that the original publication in this journal is cited, in accordance with accepted academic practice. No use, distribution or reproduction is permitted which does not comply with these terms.

frontiers in Neuroscience

ORIGINAL RESEARCH
published: 15 August 2018
doi: 10.3389/fnins.2018.00517

Screening for Cognitive Function in Complete Immobility Using Brain–Machine Interfaces: A Proof of Principle Study

Dorothée Lulé, Katharina Hörner, Cynthia Vazquez, Helena Aho-Özhan, Jürgen Keller, Martin Gorges, Ingo Uttner and Albert C. Ludolph*

Department of Neurology, University of Ulm, Ulm, Germany

Background: In many neurological conditions, there is a combination of decline in physical function and cognitive abilities. For far advanced stages of physical disability where speaking and hand motor abilities are severely impaired, there is a lack of standardized approach to screen for cognitive profile.

Methods: *N* = 40 healthy subjects were included in the study. For proof of principle, *N* = 6 ALS patients were additionally measured. For cognitive screening, we used the Edinburgh cognitive and behavioral ALS screen (ECAS) in the standard paper-and-pencil version. Additionally, we adapted the ECAS to a brain–machine interface (BMI) control module to screen for cognition in severely advanced patients.

Results: There was a high congruency between BMI version and the paper-and-pencil version of the ECAS. Sensitivity and specificity of the ECAS-BMI were mostly high whereas stress and weariness for the patient were low.

Discussion/Conclusion: We hereby present evidence that adaptation of a standardized neuropsychological test for BMI control is feasible. BMI driven neuropsychological test provides congruent results compared to standardized tests with a good specificity and sensitivity but low patient load.

Keywords: brain–machine interface, brain–computer interface, cognition, ECAS, neuropsychology, P300, oddball, amyotrophic lateral sclerosis

OPEN ACCESS

Edited by:
Rossella Spataro,
Università degli Studi di Palermo, Italy

Reviewed by:
Andrew Geronimo,
Penn State Milton S. Hershey Medical Center, United States
Mattia Siciliano,
Università degli Studi della Campania 'Luigi Vanvitelli' Naples, Italy

****Correspondence:***
Dorothée Lulé
dorothee.lule@rku.de;
dorothee.lule@uni-ulm.de

Specialty section:
This article was submitted to Neural Technology, a section of the journal Frontiers in Neuroscience

Received: *15 March 2018*
Accepted: *10 July 2018*
Published: *15 August 2018*

Citation:
Lulé D, Hörner K, Vazquez C, Aho-Özhan H, Keller J, Gorges M, Uttner I and Ludolph AC (2018) Screening for Cognitive Function in Complete Immobility Using Brain–Machine Interfaces: A Proof of Principle Study. Front. Neurosci. 12:517. doi: 10.3389/fnins.2018.00517

INTRODUCTION

In many neurological conditions such as amyotrophic lateral sclerosis (ALS), there is a combination of decline in physical function and cognitive abilities. About 50% of ALS patients present with cognitive deficits which are mostly mild and restricted to one cognitive domain; only 5–15% present with full blown fronto-temporal dementia (FTD; Phukan et al., 2012; Goldstein and Abrahams, 2013). In several studies on ALS, there has been evidence for specific impairments in fluency, language, executive function including social cognition, and verbal memory (Beeldman et al., 2016). It has been discussed controversially whether these impairments decline in the course of physical function loss. Whereas some find no evidence (Kasper et al., 2016; Xu et al., 2017), others report cognitive decline in the course of the disease (Elamin et al., 2013; Trojsi et al., 2016), but possibly only in a subsets of patients, e.g., with bulbar onset (Schreiber et al., 2005). Discrepancies between studies could either be explained by different subgroups or by a training effect in a

retest design. Most importantly, most studies so far did not use motor adapted neuropsychological tests which can be performed either written or verbally. The Edinburgh cognitive and behavioural ALS screen (ECAS) as a standardized test with parallel versions to be performed either written or verbally was a first approach to bridge this knowledge gap (Abrahams et al., 2014). Thus, for mildly advanced stages of physical impairments, standard neuropsychological tests are at hand. For moderately advanced stages of motor decline, eye-tracking controlled devices can be used for neuropsychological screening (Keller et al., 2015). However, for far advanced stages of physical disability where speaking and hand motor abilities are severely impaired, a state referred to as locked-in state, standardized approaches to measure cognitive function are lacking. Instead, in this state, there have been single case studies on cognitive profiles only, using near infrared spectroscopy (Fuchino et al., 2008), event-related potentials (ERPs; Kotchoubey et al., 2003; Ogawa et al., 2009) or visual recording of eye-blink responses (Lakerveld et al., 2008). Cohort studies have not been performed so far and there is lack of informative data on the cognitive abilities of the vast majority of these patients. Instead, many locked-in (LIS) patients including those with ALS are clinically regarded to have dementia despite no valid data on cognitive profile. Single case studies provide evidence for preserved cognitive function in LIS, e.g., Lakerveld et al. (2008) tested for memory and attentional abilities in LIS by asking the patient to respond via eye blink which was visually detected by the interviewer; they provided evidence for superior cognitive abilities in LIS. However, only recently have there been standardized approaches to screen for cognitive abilities in far advanced stages of motor impairments. First paradigms used state-of-the-art eye-tracking controlled setups in lab environment (Cipresso et al., 2012; Keller et al., 2015) and at bedside (Keller et al., 2017) to reliably detect cognitive impairment. LIS state Brain–machine interfaces (BMIs) have been widely used for patients with severe physical restriction for environment control (Mugler et al., 2010; Münßinger et al., 2010) and communication (Nijboer et al., 2008) and might provide additional information on state of alertness in complete LIS state (Chaudhary et al., 2016). BMIs might also be used to screen for cognitive function which has been tested in ALS for single cognitive domains already (Poletti et al., 2016). We hereby present a unique approach for the use of BMIs to conduct a standardized neuropsychological screening method on several cognitive functions in patients with ALS. We hereby use a commercially available EEG device which has been shown to be sufficient for BMI communication (Duvinage et al., 2013) and combine it with the widely used ECAS to enable clinicians and researchers to screen for disease specific cognitive functions to bridge the gap of knowledge with regard to cognitive profile in complete immobility.

MATERIALS AND METHODS

Subjects

In total, $N = 40$ healthy controls were included who were matched to ALS patients with regard to age, gender, and education according to previous studies (Keller et al., 2015). To test for feasibility in physically impaired patients, $N = 6$ ALS patients were included (**Table 1**). None of the participants had signs of any neurological or psychiatric illness (other than ALS) or dementia. They were all native German speakers. Patients were consecutively recruited from the clinics of the Department of Neurology at the Universitätsklinikum Ulm, Germany. The study was approved by the Ethics Committee of the University of Ulm (No. 19/12). All participants gave written informed consent to the study according to institutional guidelines.

Study Design

First, participants were screened for affective (ALS depression inventory 12 items, ADI-12; Kübler et al., 2005; Hammer et al., 2008), physical (ALS functional rating scale revised version, ALS-FRS-R; Cedarbaum et al., 1999), and cognitive function [German version of the Edinburgh cognitive and behavioral ALS screen (ECAS); Abrahams et al., 2014; Lulé et al., 2015; Loose et al., 2016] by a board certified neuropsychologist. In randomized order, half of the participants performed the ECAS in a standard paper-and-pencil version first (ECAS parallel version C) and then the adapted BMI ECAS version (ECAS original version A), whereas the other half performed both versions in reverse order. The procedure took about 2 h.

BMI Setup

For bedside BMI neuropsychological testing, the mobile BMI device Neuroheadset Emotiv Epoc+ was used (AF3, F7, F3, FC5, T7, P7, O1, O2, P8, T8, FC6, F4, F8, AF4, reference, for further information see www.emotiv.com). Electrode impedance was decreased by using saline liquid until the level required by the software was reached (in the 10–20 kOhm range) and was checked along the experiment.

Participants were positioned in front of a 8 × 5 speller matrix adapted according to Farwell and Donchin (1988) which was presented on a laptop screen (letters A–Z, German "Umlaute", ß, digits 0–9). Rows and columns of symbols were disguised for 62.5 ms by faces (a face of Albert Einstein)

TABLE 1 | m, male; f, female; ADI-12, ALS depression inventory 12 items; ALS-FRS-R, ALS-Functional Rating Scale – revised form ranging from 0 to 48, where 0 indicates complete immobility.

	Controls ($N = 40$)		ALS patients ($N = 6$)		p
	Mean *SD*	Range	Mean *SD*	Range	
Age	61.2 6.9	44–72	56.2 4.3	53–64	0.06
Gender (m/f)	15/25		4/2		0.36
Education years	15.7 2.7	8–20	12.8 1.3	12–15	0.01*
ADI-12	16.75 3.7	12–26	22.3 9.3	16.41	0.03*
Site of onset (Spinal/bulbar)			5/1		
Months since onset			13.7 8.9	6–27	
ALS-FRS-R			40§ 4.5	33–46	

§*indicates moderate physical impairment. Chi² test for gender and site of onset and Mann–Whitney U-test for all other comparisons were used. *p < 0.05.*

with a 125 ms interstimulus interval (Kaufmann et al., 2013; **Figure 1**). Participants were asked to fixate a target which was then highlighted twice (rare event eliciting a P300) in a row of 11 non-target highlight events. Selected stimulus according to P300 was presented above the speller matrix.

Each session was composed of one calibration set and one ECAS trial. Calibration of the Speller was performed by asking the participant to spell the sentence "Ulm is nice" ("Ulm ist schön") with the BMI. During this run, participants received no feedback (i.e., subjects did not see which character the system actually selected), since data were only collected for system calibration. The percentage of letters correctly selected by the system out of the phrase, considered as the measure of BMI calibration ('BMI calibration accuracy') was automatically calculated. Only when BMI calibration accuracy' was >85%, ECAS BMI was performed. In this study, all participants were above this accuracy threshold.

BMI Data Analysis

EEG data were recorded with the freeware BCI2000 (Schalk et al., 2004). Using an oddball paradigm, a P300 signal was measured. BCI200 classifier was used to determine P300 signal as a positive deflection in voltage (up to 5 μV) with a latency of 800 ms from the stimulus onset. The sampling rate was 128 Hz. The EEG signal was high-pass filtered at 1 Hz and analysed offline with a common average reference (CAR) spatial filter.

Correctness of the ECAS BMI Selection

Participants were asked to verbally indicate to the investigator when the selected item by the system was not the intended one. The percentage of correctly selected items by the system was recorded.

Stress and Weariness Rating

Following the BMI ECAS version, participants were asked to rate their emotional stress and weariness following the ECAS BMI use on a 5 point Likert scale.

Paper-and-Pencil Version of the ECAS

The ECAS is a widely used and well-validated ALS specific cognitive screening tool measuring five domains of ALS specific (executive function, language, and verbal fluency) and non-ALS specific cognitive functions (memory and visuospatial perception; Abrahams et al., 2014; Lulé et al., 2015; Loose et al., 2016[1]). In total, the ECAS encompasses 15 subtasks which are subsumed under the five domains. Maximum total ECAS score is 136 with decreasing score indicating lower cognitive performance.

BMI Version of the ECAS

For the BMI adaptation, specific subtasks of the original ECAS were selected such as language (naming and language comprehension), restricted phonematic fluency and executive functions (sentence completion and social cognition) for the ALS specific tasks. For the non-ALS specific tasks, memory (immediate recall and delayed recognition, key words of the ECAS instead of whole story) and visuospatial function (cube counting) was selected. For the patient BMI-ECAS version, the length of the test needed to be reduced by selecting the most discriminative items in the text according to previous research (Lulé et al., 2015). According to performance in healthy subjects, tables for verbal fluency scores and cut-off scores for cognitive

[1]www.ECAS.network

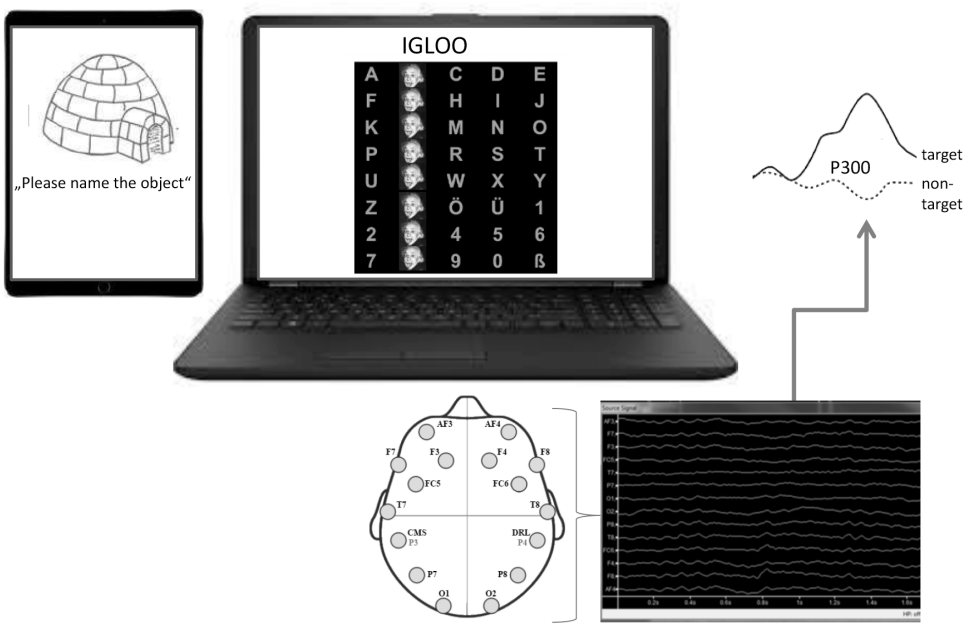

FIGURE 1 | BMI set-up. **Left:** Positions of the 14 electrodes of the Emotiv Epoc headset according to the 10–20 system. **Middle:** 8 × 5 speller matrix for the P300 speller. Rows and columns of symbols were disguised for 62.5 ms by faces (Albert Einstein) with a 200 ms interstimulus interval signal.

TABLE 2 | Congruency of Standard paper and pencil ECAS version and BMI adapted ECAS version.

	BMI naming	BMI comprehension	BMI fluency	BMI sentence completion	BMI social cognition	BMI immediate recall	BMI delayed recall	BMI cube counting
Standard naming	−0.076	–	0.081	−0.114	0.256	−0.135	−0.058	−0.065
Standard comprehension	–	–	–	–	–	–	–	–
Standard fluency	0.042	–	0.321*	0.248	−0.051	0.178	0.040	−0.010
Standard sentence completion	−0.069	–	0.206	0.329*	0.036	0.301	0.092	−0.105
Standard social cognition	0.364*	–	0.061	0.232	0.678**	0.382*	0.066	0.465**
Standard immediate recall	−0.103	–	0.144	0.028	0.299	0.300	−0.022	0.353*
Standard delayed recall	−0.018	–	−0.208	0.212	−0.088	0.152	0.160	0.076
Standard cube counting	0.060	–	0.032	0.300	0.344*	0.447*	0.171	0.355*

*Language comprehension is not possible to correlate as variance in values is too low; Spearman-Rho correlation with *$p < 0.05$, **$p < 0.01$.*

impairments were defined according to ECAS criteria (<2 SD from mean for cognitive impairments; Abrahams et al., 2014; **Table 2**).

Naming: scorpion and igloo had to be named (maximum 2 points; original ECAS 8 objects).

Language comprehension: 4 objects were presented numbered 1–4. Four sentences (original ECAS, 8 sentences) were acoustically presented of which one sentence described a property of one object each. Participants were asked to select the correct object for each consecutively presented sentence (maximum 4 points; original ECAS, 8 objects and 8 sentences).

Memory: 10 words (all words to be remembered from the original ECAS) were acoustically presented. Following, participants were asked to produce all words which they could remember (immediate recall). For delayed recognition, ten words were presented of which only 5 had actually been presented before. Subjects had to indicate "y" for yes or "n" for no according to whether this word had been presented before (maximum 10 points; original ECAS, a story is given but only the ten words of the BMI test are valid for scoring in the original ECAS).

Visuoconstruction: Two objects that were made of cubes were presented separately. Subjects had to determine the number of cubes of each object (maximum 2 points; original ECAS, 4 objects).

Sentence completion: three sentences with the last word missing were to be completed by the subject by providing a word which did not logically complete the sentence (maximum 3 points; original ECAS, 6 sentences).

Restricted phonematic fluency: subjects had to name 4 letter words with the given initial letter "G" within 8 min (maximum 12 points; same for original ECAS within 90 s time). Verbal fluency index was calculated according to healthy subjects' performance analogous to Abrahams et al. (2014).

Social cognition: subjects first had to indicate personal preference for one out of four numbered objects. Three sets of four objects were presented (original ECAS six sets of four objects). Subsequently, subjects had to indicate the preference of a face that was presented adjacent to the same sets of four objects (maximum 6 points).

All answers were spelled via the spelling matrix of the P300 speller (**Figure 1**).

According to performance in healthy subjects, tables for verbal fluency scores and cut-off scores for cognitive impairments were defined according to ECAS criteria (<2 SD from mean for cognitive impairments; Abrahams et al., 2014; **Table 2**).

Statistics

Data were managed in SPSS (SPSS version 21.0 IBM). Mann–Whitney *U*-test was used for group comparison with effect size *r*. For correlation analysis, Spearman–Rho test was used. All analyses were two-sided and significance level was set at $p = 0.05$.

RESULTS

General Cognitive Screening

When compared to healthy controls, patients scored significantly lower in the language function ($U = 65.00$, $z = -2.22$, $p = 0.027$, $r = -0.33$). Scores of the other domains (executive function, verbal fluency, memory, and visuospatial function) did not significantly differ between the groups (all $p > 0.05$).

Congruence of BMI and Paper–Pencil ECAS

To determine whether performance accuracy of the BMI ECAS could associate performance accuracy of the written paper–pencil version, a Spearman–Rho correlation analysis was performed, showing a significant correlation between the performance in both versions of healthy controls (Spearman–Rho $r = 0.64$, $p < 0.001$) and of both groups (Spearman–Rho $r = 0.51$, $p < 0.001$). For patients, congruency was also acceptable but did not reach significance due to the small sample size (Spearman–Rho $r = 0.40$, $p = 0.43$).

For different cognitive functions, there was a significant congruency for verbal fluency, sentence completion, social cognition, immediate recall, social cognition, and cube counting, for the other cognitive functions, congruency was low (**Figure 2** and **Table 3**).

TABLE 3 | Predictive validity of the ECAS BMI version.

	Max		Cut-off						Specificity [%]	Sensitivity [%]	PPV [%]
	BMI	Paper pencil	BMI	Paper pencil	a	b	c	d			
Language	6	28	5.6	25.8	0	4	1	35	90	0	0
Fluency	12	24	8.5	17.9	2	5	0	33	87	100	29
Executive	12	48	10.6	39.2	2	4	4	30	88	33	33
ALS specific	30	100	23.6	84.3	2	3	0	35	92	100	40
Memory	14	24	6.7	18.8	3	3	2	32	91	60	50
Visuospatial	2	12	1.7	10.9	1	2	3	34	94	25	33
Non-ALS specific	16	36	8.7	30.1	4	2	5	29	94	44	67
ECAS total	46	136	32.9	115.8	1	2	1	36	95	50	33

Cut-offs were defined according to performance in healthy subjects (<2 SD of mean score). BMI, brain–machine interface ECAS version; Paper Pencil, paper and pencil ECAS standard version; for a–d, cognitive impairment was defined as <cut-off for both BMI and paper and pencil version with a, correct positives; b, false positives; c, false negatives; d, correct negatives; PPV, positive predictive value.

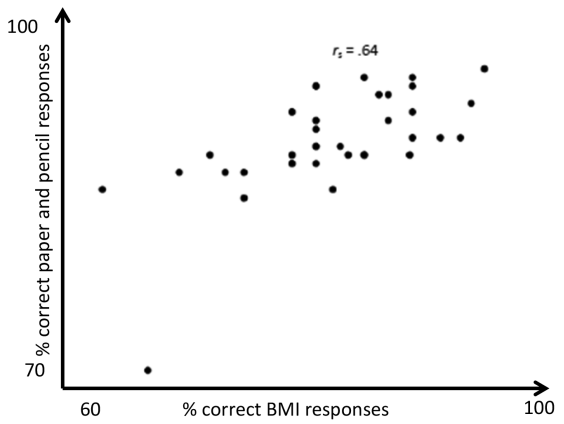

FIGURE 2 | Congruency of ECAS paper and pencil version and BMI version in healthy controls.

Validation of ECAS BMI Version in Healthy Controls

Cognitive impairments for the total score and the five domains were determined according to cut-off scores. Overall, one healthy subject performed 2 SD below the overall ECAS score and for the domain language, fluency, and executive function. Memory and visuospatial performance was impaired in three and four subjects, respectively.

Sensitivity and Specificity of the ECAS BMI Version

There was a high convergent validity of the BMI version of the ECAS, especially for fluency, sentence completion, social condition, and cube counting. Predictive validity of the ECAS BMI version was good. This was seen in a high sensitivity, specificity, and positive predictive values, especially for social cognition and verbal fluency (**Table 2**). The functions immediate recall and cube counting in addition to the domain executive function showed high specificity whereas sensitivity was in a medium range. Only language showed low sensitivity and positive predictive value. The overall specificity of the BMI version compared to the paper-and-pencil version was very high at 95%.

Correctness of the ECAS BMI Selection

The median of correct answers of the control group for the P 300 speller was 85% for healthy subjects and 86% for ALS patients.

Subjective Rating of the Test

Patients (88%) and healthy subjects (86%) mostly reported that they were not stressed by the ECAS BMI version and only a minority reported to be slightly stressed by the procedure (12 and 14%, respectively); 48% of healthy subjects and 18% of ALS patients regarded the BMI procedure to be wearisome.

DISCUSSION

So far, little is known about the cognitive state in complete immobility in the course of physical decline in ALS (Fuchino et al., 2008; Lakerveld et al., 2008). BMIs have been mainly used to communicate with the patients to unlock the patients mind. We hereby present a new BMI approach for neuropsychological assessment in physically severely handicapped patients. Using this approach, there is a standardized way to measure the cognitive profile in these subjects.

We used a mobile P 300-based BMI algorithm to drive an ALS specific neuropsychological test, the ECAS. Patients presented a reduced performance in the language function in the paper-and-pencil version compared to healthy controls. This is in line with the previous findings that language function is the most sensitive cognitive ability in the course of ALS (Keller et al., 2015; Lulé et al., 2015; Niven et al., 2015; Wei et al., 2015). For executive and visuospatial functions there was a trend but other cognitive functions were not significantly different between groups which was mainly attributed to small sample size. There was a high congruency (Schmidt-Atzert and Amelang, 2012) between the adapted ECAS BMI and the original version. Lack of congruency for some functions might be explained by the adaptations in the BMI versions, mainly the reduction of

items. The ECAS BMI version showed a high convergent and predictive validity. This was indicated by a high sensitivity, specificity, and positive predictive value, especially for social condition and verbal fluency. Functions of the domains memory and visual spatial abilities, and executive functions showed high specificity whereas sensitivity was in a medium range. Only language showed low sensitivity and low positive predictive value which was partly explained by the fact of low numbers of impaired controls in this domain. Interestingly, specificity of single functions was similarly high as for the domain itself. This implies that the measurement of one single function was sufficient to get an overall estimation of the cognitive domain. Future studies in larger samples are needed to verify this hypothesis.

The correctness of the P300 speller was 85% in healthy subjects and 86% in ALS patients, fulfilling the criterion of a minimum of 70% accuracy as a predictor for satisfactory communication (Choularton and Dale, 2004) and above the level of far advanced ALS patients in other studies (Marchetti and Priftis, 2014). Accordingly, patients were just as precise in spelling as the healthy subjects (McCane et al., 2015), despite that a commercial EEG device was used. For scientific P300 EEG analysis, there are more open source products available which might better suit these purposes than the hereby used Emotiv Epoc. However, for satisfying communication with BMI, an accuracy rate of 70% is required which was achieved by the hereby presented approach. Due to a high intrinsic motivation to learn BMI control for the future, the patients might have been especially concentrated during the task. Overall, the ECAS BMI seems to be a feasible way to easily and reliably detect cognitive deficits in ALS, especially since most subjects rated the BMI version to be valid and neither stressful nor explicitly strenuous.

The major limitation of the current study is the lack of validation in a large patient sample with severe physical impairments. We hereby present a first proof of principle design with promising results but future studies in patients with advanced physical impairments are warranted. Another limitation is that most tasks of the original ECAS were simplified and shortened and therefore not identical to the original version. Due to high congruency of both of versions, it can be assumed that both approaches measure similar cognitive constructs. However, in future trials similar ECAS versions need to be used for BMI and paper and pencil versions.

CONCLUSION

In this proof of principal study, we provide evidence that neuropsychological screening can be performed using BMI algorithms, even with off-the-shelf commercially available EEG systems. So far, the studies are incongruent whether there is cognitive decline in the course of physical function loss (Schreiber et al., 2005; Elamin et al., 2013; Trojsi et al., 2016) or not (Kasper et al., 2016; Xu et al., 2017). In which way cognitive function develop, especially in the final state of physical function decline, is so far mostly unknown. The main target of future trials will be to see whether BMI controlled cognitive screening methods are superior to previously introduced methods with eyetracking control for those patients with residual eye movement (Keller et al., 2016). For patients in complete locked-in state, BMI driven approaches are a cost-effective and simple means of neuropsychological examination of CLIS patients (Poletti et al., 2016). The hereby presented BMI version of a standard neuropsychological test is the next milestone to learn more about cognitive decline in the course of ALS (Cipresso et al., 2012; Poletti et al., 2016) but future studies are required to further develop this approach.

AUTHOR CONTRIBUTIONS

All the authors have participated and have made substantial contributions to the approval of the final version. DL contributed to the conception and design of the work. KH, CV, HA-Ö, and JK contributed to the acquisition and analysis of data. DL and KH contributed to the interpretation of data for the work. DL drafted the work and all authors revised it critically for important intellectual content.

FUNDING

This is an EU Joint Programme – Neurodegenerative Disease Research (JPND; 01ED1405) project. The project is supported through the following organizations under the aegis of JPND[2], e.g., Germany, Bundesministerium für Bildung und Forschung (BMBF, FKZ), Sweden, Vetenskapr å det Sverige, and Poland, Narodowe Centrum Bad á n i Rozwoju (NCBR). This work was supported by the Deutsche Forschungsgemeinschaft and the BMBF. Furthermore, this work was supported by the (BMBF #01GM1103A, MND-Net).

ACKNOWLEDGMENTS

We thank all patients and healthy subjects for participating in the project. Special thanks to Sharon Abrahams and Thomas Bak for developing and providing the original version of the ECAS and Andrea Kübler for providing us with the faces stimuli for the P300 paradigm.

[2] www.jpnd.eu

REFERENCES

Abrahams, S., Newton, J., Niven, E., Foley, J., and Bak, T. H. (2014). Screening for cognition and behaviour changes in ALS. *Amyotroph. Lateral Scler. Frontotemporal Degener.* 15, 9–14. doi: 10.3109/21678421.2013.805784

Beeldman, E., Raaphorst, J., Twennaar, M. K., de Visser, M., Schmand, B. A., and de Haan, R. J. (2016). The cognitive profile of ALS: a systematic review and meta-analysis up-date. *J. Neurol. Neurosurg. Psychiatry* 87, 611–619. doi: 10.1136/jnnp-2015-310734

Cedarbaum, J. M., Stambler, N., Malta, E., Fuller, C., Hilt, D., Thurmond, B., et al. (1999). The ALSFRS-R: a revised ALS functional rating scale that incorporates assessments of respiratory function. *J. Neurol. Sci.* 169, 13–21. doi: 10.1016/S0022-510X(99)00210-5

Chaudhary, U., Birbaumer, N., and Ramos-Murguialday, A. (2016). Brain-computer interfaces for communication and rehabilitation. *Nat. Rev. Neurol.* 12, 513–525. doi: 10.1038/nrneurol.2016.113

Choularton, S., and Dale, R. (2004). "User responses to speech recognition errors: consistency of behaviour across domains," in *Proceedings of the 10th Australian International Conference on Speech Science and Technology* Sydney, NSW.

Cipresso, P., Carelli, L., Solca, F., Meazzi, D., Meriggi, P., Poletti, B., et al. (2012). The use of P300-based BCIs in amyotrophic lateral sclerosis: from augmentative and alternative communication to cognitive assessment. *Brain Behav.* 2, 479–498. doi: 10.1002/brb3.57

Duvinage, M., Castermans, T., Petieau, M., Hoellinger, T., Cheron, G., and Dutoit, T. (2013). Performance of the Emotiv Epoc headset for P300-based applications. *Biomed. Eng. Online* 12:56. doi: 10.1186/1475-925X-12-56

Elamin, M., Bede, P., Byrne, S., Jordan, N., Gallagher, L., Wynne, B., et al. (2013). Cognitive changes predict functional decline in ALS: a population-based longitudinal study. *Neurology* 80, 1590–1597. doi: 10.1212/WNL.0b013e31828f18ac

Farwell, L. A., and Donchin, E. (1988). Talking off the top of your head: toward a mental pros-thesis utilizing event-related brain potentials. *Electroencephalogr. Clin. Neurophysiol.* 70, 510–523. doi: 10.1016/0013-4694(88)90149-6

Fuchino, Y., Nagao, M., Katura, T., Bando, M., Naito, M., Maki, A., et al. (2008). High cognitive function of an ALS patient in the totally locked-in state. *Neurosci. Lett.* 435, 85–89. doi: 10.1016/j.neulet.2008.01.046

Goldstein, L. H., and Abrahams, S. (2013). Changes in cognition and behaviour in amyotrophic lateral sclerosis: nature of impairment and implications for assessment. *Lancet Neurol.* 12, 368–380. doi: 10.1016/S1474-4422(13)70026-7

Hammer, E. M., Häcker, S., Hautzinger, M., Meyer, T. D., and Kübler, A. (2008). Validity of the ALS-Depression-Inventory (ADI-12)–a new screening instrument for depressive disorders in patients with amyotrophic lateral sclerosis. *J. Affect. Disord.* 109, 213–219. doi: 10.1016/j.jad.2007.11.012

Kasper, E., Zydatiss, K., Schuster, C., Machts, J., Bittner, D., Kaufmann, J., et al. (2016). No change in executive performance in ALS patients: a longitudinal neuro-psychological study. *Neurodegen. Dis.* 16, 184–191. doi: 10.1159/000440957

Kaufmann, T., Holz, E. M., and Kübler, A. (2013). Comparison of tactile, auditory, and visual modality for brain-computer interface use: a case study with a patient in the locked-in state. *Front. Neurosci.* 7:129. doi: 10.3389/fnins.2013.00129

Keller, J., Gorges, M., Horn, H. T., Aho-Özhan, H. E., Pinkhardt, E. H., Uttner, I., et al. (2015). Eye-tracking controlled cognitive function tests in patients with amyotrophic lateral sclerosis: a controlled proof-of-principle study. *J. Neurol.* 262, 1918–1926. doi: 10.1007/s00415-015-7795-3

Keller, J., Krimly, A., Bauer, L., Schulenburg, S., Böhm, S., Aho-Özhan, H. E. A., et al. (2017). A first approach to a neuropsychological screening tool using eye-tracking for bedside cognitive testing based on the Edinburgh Cognitive and Behavioural ALS Screen. *Amyotroph. Lateral Scler. Frontotemporal Degener.* 18, 443–450. doi: 10.1080/21678421.2017.1313869

Kotchoubey, B., Lang, S., Winter, S., and Birbaumer, N. (2003). Cognitive processing in completely paralyzed patients with amyotrophic lateral sclerosis. *Eur. J. Neurol.* 10, 551–558. doi: 10.1046/j.1468-1331.2003.00647.x

Kübler, A., Winter, S., Kaiser, J., Birbaumer, N., and Hautzinger, M. (2005). Das ALS-Depressionsinventar (ADI): Ein Fragebogen zur Messung von Depression bei dege-nerativen neurologischen Erkrankungen (amyotrophe Lateralsklerose). *Zeitschrift für Klinische Psychologie und Psychotherapie* 34, 19–26. doi: 10.1026/1616-3443.34.1.19

Lakerveld, J., Kotchoubey, B., and Kübler, A. (2008). Cognitive function in patients with late stage amyotrophic lateral sclerosis. *J. Neurol. Neurosurg. Psychiatry* 79, 25–29. doi: 10.1136/jnnp.2007.116178

Loose, M., Burkhardt, C., Aho-Özhan, H., Keller, J., Abdulla, S., Böhm, S., et al. (2016). Age and education-matched cut-off scores for the revised German/Swiss-German version of ECAS. *Amyotroph. Lateral Scler. Frontotemporal Degener.* 17, 374–376. doi: 10.3109/21678421.2016.1162814

Lulé, D., Burkhardt, C., Abdulla, S., Böhm, S., Kollewe, K., Uttner, I., et al. (2015). The Edinburgh cognitive and behavioural amyotrophic lateral sclerosis screen: a cross-sectional comparison of established screening tools in a German-Swiss population. *Amyotroph. Lateral Scler. Frontotemporal Degener.* 16, 16–23. doi: 10.3109/21678421.2014.959451

Marchetti, M., and Priftis, K. (2014). Effectiveness of the P3-speller in brain–computer interfaces for amyotrophic lateral sclerosis patients: a systematic review and meta-analysis. *Front. Neuroeng.* 7:12. doi: 10.3389/fneng.2014.00012

McCane, L. M., Heckman, S. M., McFarland, D. J., Townsend, G., Mak, J. N., Sellers, E. W., et al. (2015). P300-based brain-computer interface (BCI) event-related potentials (ERPs): people with amyotrophic lateral sclerosis (ALS) vs. *age-matched controls. Clin. Neurophysiol.* 126, 2124–2131. doi: 10.1016/j.clinph.2015.01.013

Mugler, E. M., Ruf, C. A., Halder, S., Bensch, M., and Kubler, A. (2010). Design and implementation of a P300-based brain–computer interface for controlling an internet browser. *IEEE Trans. Neural Syst. Rehabil. Eng.* 18, 599–609. doi: 10.1109/TNSRE.2010.2068059

Münßinger, J. I., Halder, S., Kleih, S. C., Furdea, A., Raco, V., Hösle, A., et al. (2010). Brain painting: first evaluation of a new brain–computer interface application with ALS-patients and healthy volunteers. *Front. Neurosci.* 4:182. doi: 10.3389/fnins.2010.00182

Nijboer, F., Sellers, E. W., Mellinger, J., Jordan, M. A., Matuz, T., Furdea, A., et al. (2008). A P300-based brain–computer interface for people with amyotrophic lateral sclerosis. *Clin. Neurophysiol.* 119, 1909–1916. doi: 10.1016/j.clinph.2008.03.034

Niven, E., Newton, J., Foley, J., Colville, S., Swingler, R., Chandran, S., et al. (2015). Validation of the Edinburgh Cognitive and Behavioural Amyotrophic Lateral Sclerosis Screen (ECAS): a cognitive tool for motor disorders. *Amyotroph. Lateral Scler. Frontotemporal Degener.* 16, 172–179. doi: 10.3109/21678421.2015.1030430

Ogawa, T., Tanaka, H., and Hirata, K. (2009). Cognitive deficits in amyotrophic lateral sclerosis evaluated by event-related potentials. *Clin. Neurophysiol.* 120, 659–664. doi: 10.1016/j.clinph.2009.01.013

Phukan, J., Elamin, M., Bede, P., Jordan, N., Gallagher, L., Byrne, S., et al. (2012). The syndrome of cognitive impairment in amyotrophic lateral sclerosis: a population-based study. *J. Neurol. Neurosurg. Psychiatry* 83, 102–108. doi: 10.1136/jnnp-2011-300188

Poletti, B., Carelli, L., Solca, F., Lafronza, A., Pedroli, E., Faini, A., et al. (2016). Cognitive assessment in amyotrophic lateral sclerosis by means of P300-brain com-puter interface: a preliminary study. *Amyotroph. Lateral Scler. Frontotemporal Degener.* 17, 473–481. doi: 10.1080/21678421.2016.1181182

Schalk, G., McFarland, D. J., Hinterberger, T., Birbaumer, N., and Wolpaw, J. R. (2004). BCI2000: a general-purpose brain-computer interface (BCI) system. *IEEE Trans. Biomed. Eng.* 51, 1034–1043. doi: 10.1109/TBME.2004.827072

Schmidt-Atzert, L., and Amelang, M. (2012). *Psychologische Diagnostik*, 5th Edn. Berlin: Springer. doi: 10.1007/978-3-642-17001-0

Schreiber, H., Gaigalat, T., Wiedemuth-Catrinescu, U., Graf, M., Uttner, I., Muche, R., et al. (2005). Cognitive function in bulbar- and spinal- onset amyotrophic lat-eral sclerosis: a longitudinal study in 52 patients. *J. Neurol.* 252, 772–781. doi: 10.1007/s00415-005-0739-6

Trojsi, F., Santangelo, G., Caiazzo, G., Siciliano, M., Ferrantino, T., Piccirillo, G., et al. (2016). Neuropsychological assessment in different King's clinical stages of amyotrophic lateral sclerosis. *Amyotroph. Lateral Scler. Frontotemporal Degener.* 17, 228–235. doi: 10.3109/21678421.2016.1143513

Wei, Q., Chen, X., Zheng, Z., Huang, R., Guo, X., Cao, B., et al. (2015). Screening for cognitive impairment in a Chinese ALS population. *Amyotroph. Lateral Scler. Frontotemporal Degener.* 16, 40–45. doi: 10.3109/21678421.2014.966311

Xu, Z., Alruwaili, A. R. S., Henderson, R. D., and McCombe, P. A. (2017). Screening for cognitive and behavioural impairment in amyotrophic lateral sclerosis: frequency of ab-normality and effect on survival. *J. Neurol. Sci.* 376, 16–23. doi: 10.1016/j.jns.2017.02.061

Conflict of Interest Statement: The authors declare that the research was conducted in the absence of any commercial or financial relationships that could be construed as a potential conflict of interest.

Copyright © 2018 Lulé, Hörner, Vazquez, Aho-Özhan, Keller, Gorges, Uttner and Ludolph. This is an open-access article distributed under the terms of the Creative Commons Attribution License (CC BY). The use, distribution or reproduction in other forums is permitted, provided the original author(s) and the copyright owner(s) are credited and that the original publication in this journal is cited, in accordance with accepted academic practice. No use, distribution or reproduction is permitted which does not comply with these terms.

frontiers in Neuroscience

ORIGINAL RESEARCH
published: 11 September 2018
doi: 10.3389/fnins.2018.00624

Early Findings on Functional Connectivity Correlates of Behavioral Outcomes of Brain-Computer Interface Stroke Rehabilitation Using Machine Learning

Rosaleena Mohanty[1,2]*, *Anita M. Sinha*[1,3], *Alexander B. Remsik*[1,4], *Keith C. Dodd*[1,3], *Brittany M. Young*[5,6], *Tyler Jacobson*[1,7], *Matthew McMillan*[1,3], *Jaclyn Thoma*[1,6], *Hemali Advani*[1], *Veena A. Nair*[1], *Theresa J. Kang*[1], *Kristin Caldera*[8], *Dorothy F. Edwards*[4], *Justin C. Williams*[3] and *Vivek Prabhakaran*[1,3,5,6,9]

[1] Department of Radiology, University of Wisconsin-Madison, Madison, WI, United States, [2] Department of Electrical Engineering, University of Wisconsin-Madison, Madison, WI, United States, [3] Department of Biomedical Engineering, University of Wisconsin-Madison, Madison, WI, United States, [4] Department of Kinesiology, University of Wisconsin-Madison, Madison, WI, United States, [5] Medical Scientist Training Program, University of Wisconsin–Madison, Madison, WI, United States, [6] Neuroscience Training Program, University of Wisconsin–Madison, Madison, WI, United States, [7] Department of Psychology, University of Wisconsin–Madison, Madison, WI, United States, [8] Department of Orthopedics and Rehabilitation, University of Wisconsin-Madison, Madison, WI, United States, [9] Department of Medical Physics, University of Wisconsin-Madison, Madison, WI, United States

OPEN ACCESS

Edited by:
Ioan Opris,
University of Miami, United States

Reviewed by:
Jose Luis Contreras-Vidal,
University of Houston, United States
Cuntai Guan,
Nanyang Technological University, Singapore
Ricardo Chavarriaga,
École Polytechnique Fédérale de Lausanne, Switzerland

***Correspondence:**
Rosaleena Mohanty
rmohanty@wisc.edu

Specialty section:
This article was submitted to Neural Technology, a section of the journal Frontiers in Neuroscience

Received: 02 February 2018
Accepted: 20 August 2018
Published: 11 September 2018

Citation:
Mohanty R, Sinha AM, Remsik AB, Dodd KC, Young BM, Jacobson T, McMillan M, Thoma J, Advani H, Nair VA, Kang TJ, Caldera K, Edwards DF, Williams JC and Prabhakaran V (2018) Early Findings on Functional Connectivity Correlates of Behavioral Outcomes of Brain-Computer Interface Stroke Rehabilitation Using Machine Learning. Front. Neurosci. 12:624. doi: 10.3389/fnins.2018.00624

The primary goal of this work was to apply data-driven machine learning regression to assess if resting state functional connectivity (rs-FC) could estimate measures of behavioral domains in stroke subjects who completed brain-computer interface (BCI) intervention for motor rehabilitation. The study cohort consisted of 20 chronic-stage stroke subjects exhibiting persistent upper-extremity motor deficits who received the intervention using a closed-loop neurofeedback BCI device. Over the course of this intervention, resting state functional MRI scans were collected at four distinct time points: namely, pre-intervention, mid-intervention, post-intervention and 1-month after completion of intervention. Behavioral assessments were administered outside the scanner at each time-point to collect objective measures such as the Action Research Arm Test, Nine-Hole Peg Test, and Barthel Index as well as subjective measures including the Stroke Impact Scale. The present analysis focused on neuroplasticity and behavioral outcomes measured across pre-intervention, post-intervention and 1-month post-intervention to study immediate and carry-over effects. Rs-FC, changes in rs-FC within the motor network and the behavioral measures at preceding stages were used as input features and behavioral measures and associated changes at succeeding stages were used as outcomes for machine-learning-based support vector regression (SVR) models. Potential clinical confounding factors such as age, gender, lesion hemisphere, and stroke severity were included as additional features in each of the regression models. Sequential forward feature selection procedure narrowed the search for important correlates. Behavioral outcomes at preceding time-points outperformed rs-FC-based correlates. Rs-FC and changes associated with bilateral primary motor

areas were found to be important correlates of across several behavioral outcomes and were stable upon inclusion of clinical variables as well. NIH Stroke Scale and motor impairment severity were the most influential clinical variables. Comparatively, linear SVR models aided in evaluation of contribution of individual correlates and seed regions while non-linear SVR models achieved higher performance in prediction of behavioral outcomes.

Keywords: brain-computer interface, stroke recovery, functional connectivity, motor impairment, machine learning, support vector regression

INTRODUCTION

Brain Computer Interface

Electroencephalogram (EEG)-based brain-computer interface (BCI) technology has emerged as a therapeutic modality for stroke rehabilitation that has been demonstrated to facilitate additional recovery that conventional therapies have not been able to accomplish thus far (Silvoni et al., 2011). EEG-based BCI detects and uses a patient's neural signals as inputs to provide real-time feedback, effectively enabling users to modulate their brain activity. This is a promising intervention for patients with motor impairment, as they can control external devices such as computers and robots during rehabilitative tasks without relying on residual muscle control (Felton et al., 2009) which could be tailored to individuals potentially yielding greater benefits from the system (Bhagat et al., 2016). Specifically, EEG-based BCI intervention using attempted movement with functional electrical stimulation (FES) (Biasiucci et al., 2018) and tongue stimulation (TS) enables us to detect intent-to-move brain signals and provide users with both visual and tactile sensory feedback as a form of reward for producing certain brain activity patterns while performing specific tasks. Thus far, several neuroimaging studies in the realm of stroke rehabilitation have shown potential functional benefits associated with the use of BCI technology including, but not limited to, modulating changes in neuroplasticity and restoring motor function (Várkuti et al., 2013; Young et al., 2014c; Nair et al., 2015; Soekadar et al., 2015).

Functional Magnetic Resonance Imaging

In recent years, neuroimaging has become integral in studying the progression in neurodegenerative processes and efficacy of rehabilitation procedures (Caria et al., 2011; Song et al., 2014; Young et al., 2014c; Nair et al., 2015). Task-free methods such as resting state functional magnetic resonance imaging (rs-fMRI) allow us to measure the temporal correlation of the spontaneous, low-frequency (<0.1 Hz) blood-oxygen-level-dependent (BOLD) signals across distinct brain regions at rest. Oscillations in these BOLD fMRI signals are believed to reflect cortical dynamic self-organization and have been associated with the neural reorganization underlying cognitive and motor function during stroke recovery (Lee et al., 2013; Bajaj et al., 2015). Additionally, recent neuroimaging studies have demonstrated overlap among networks identified during rs-fMRI, motor imagery fMRI tasks, and motor execution fMRI tasks (Grefkes et al., 2008; Nair et al., 2015). The motor network is a complex and highly dynamic system with a unique balance of excitatory and inhibitory mechanisms which has been postulated to be significantly disturbed after the event of stroke (Grefkes and Fink, 2011). This specific neuronal network commonly includes the primary motor area (M1), premotor cortex (PMC) and supplementary motor area (SMA), as it is established that activity in these cortical regions maintains a dynamic equilibrium at resting-state and is modulated during task performance (Debaere et al., 2001). Recently, we have demonstrated that changes in task-related brain connectivity can be used as a diagnostic tool to track cortical changes and behavioral outcomes following BCI intervention in patients with stroke (Young et al., 2014c). However, while there is evidence of overlap among resting-state and motor-related fMRI task (Grefkes et al., 2008), these resting state networks have yet to be completely characterized in the context of motor recovery facilitated by the use of a BCI device. Therefore, further investigation into changes in resting-state connectivity in relation to changes in associated behavioral function following BCI intervention is necessary.

Multivariate Data Analysis

The ability of data-driven machine learning techniques to model multivariate relationships can be attributed to their application in neuroimaging analysis. Several studies have shed light on the utility of machine learning to perform classification tasks (Dai et al., 2012; Meier et al., 2012; Rehme et al., 2014; Fergus et al., 2016; Khazaee et al., 2016; Ding et al., 2017; Mohanty et al., 2018). These advance our understanding of brain function by identifying brain patterns associated with specific neurological diseases and differentiating among patient groups. However, performing simple binary classification might not suffice to answer clinically relevant questions such as prediction of recovery associated with neuropathological disease and time until onset of specific disease-related symptoms. In comparison

Abbreviations: 9HPT, Nine Hole Peg Test; ARAT, Action Research Arm Test; BCI, brain-computer interface; BI, Barthel Index; BOLD, blood-oxygen-level dependent; EEG, Electroencephalogram; FES, functional electrical stimulation; fMRI, functional magnetic resonance imaging; LOOCV, leave-one-out cross validation; M1, primary motor area; MCA, middle cerebral artery; MNI, Montreal Neurological Institute; MSE, mean squared error; NIHSS, National Institute of Health Stroke Scale; PMC, premotor cortex; RMSE, root mean squared error; rs-FC, resting state functional connectivity; Δrs-FC, change in resting-state functional connectivity; SIS, Stroke Impact Scale; SMA, supplementary motor area; SVM, support vector regression; SVR, support vector regression; T1-T3, control period (no intervention); T4, pre-intervention; T6, post-intervention; T7, one-month post-intervention; TS, tongue stimulation; SF, Supplementary Figure; ST, Supplementary Table.

to classification-based studies, relatively fewer studies have examined neuroimaging data from the perspective of prediction of outcomes (Dosenbach et al., 2010; Vergun et al., 2013) using machine learning approaches. This underscores the need to use data modeling techniques that can predict outcomes on a more continuous scale while handling the high dimensionality of input data. Within machine learning, there exist a variety of algorithms to perform real-valued outcome prediction such as naïve Bayesian (Frank et al., 2000), k-nearest neighbors (Hastie and Tibshirani, 1996), Gaussian process (Marquand et al., 2010) regression models. Rapid developments in the field are utilizing neural networks (Pereira et al., 2016) in large datasets. However, in this work we focus on using the a support vector machine-based regression model which is proficient in modeling linear as well as non-linear relationships between variables with a modest sample size and present an extension of the work previously presented (Mohanty et al., 2017). In place of relying solely on non-linear models, we compared their performance to the linear case, which enabled us to pinpoint specific correlates of behavioral outcomes and improve interpretability for future clinical applications. Additionally, the relative contribution of individual seed regions was analyzed, and comparative analysis helped establish the trade-off involved in choosing one model over the other.

Overview of This Study

In the realm of stroke rehabilitation research, there have been concerted efforts focusing on evaluating the neurophysiological changes post-stroke (Rossini et al., 2003; Teasell et al., 2005; Kwakkel et al., 2008; Wang et al., 2010) and investigating novel therapeutic interventions to promote motor recovery and ultimately improve overall quality of life for patients (Levy et al., 2001; Kwakkel et al., 2008; Young et al., 2014d). While EEG-based BCI intervention has shown early promise as a form of rehabilitation post-stroke, neuroplastic changes in the form of functional connectivity and resulting therapeutic effects on behavioral outcomes following this intervention coupled with FES and TS remain to be elucidated. In this study, correlates of behavioral measures and associated changes following this EEG-based BCI intervention are investigated using brain connectivity as well as behavioral measures at preceding stages. Resting-state functional connectivity (rs-FC) was examined in previously identified (Grefkes et al., 2008) motor network comprised of eight seed regions that play a dominant role in motor initiation, specification, and execution. Immediate as well as carry-over effects were investigated by examining fMRI and behavioral measures at three stages: prior to the start of intervention, upon completion of intervention and 1-month post completion of intervention. To this end, a multivariate regression scheme, based on support vector machines, was employed to handle the multi-dimensional data and examine utility in estimating individual behavioral outcomes and associated changes. The purpose of this study was four-fold: (i) to identify neural correlates based on rs-FC within the motor network to estimate behavioral outcomes following BCI intervention; (ii) to identify neural correlates based on changes in rs-FC within the motor network to estimate changes in behavioral measures following the BCI intervention; (iii) to identify behavioral correlates at a preceding time-point to estimate behavioral measures at a succeeding time-point; and (iv) to study the impact of potential confounds relative to rs-FC and behavior as correlates of behavioral outcomes following the intervention.

MATERIALS AND METHODS

Study Design

This study followed a permuted-block design that accounted for gender, stroke chronicity, and severity of motor impairment in stroke subjects to randomly assign subjects to one of two groups: crossover control group or BCI therapy (intervention) group. The study paradigm is schematized in **Figure 1**. Subjects in the BCI therapy group received this intervention and were administered a battery of behavioral assessments and MRI scans at four time-points throughout the intervention: pre-intervention (T4), mid-intervention (T5), immediately post-intervention (T6), and 1-month after completing the last BCI intervention session (T7). Subjects in the crossover control group first received three functional assessments and MRI scans during the control phase in which no BCI intervention was administered (T1 through T3), and their assessments were spaced at intervals similar to those given during the BCI intervention phase. Upon completion of the control phase of the study, the crossover control group "crossed over" into the BCI therapy phase of the study. In this study, neuroimaging and behavioral data corresponding to pre-intervention, post-intervention and 1-month post-intervention time-points across the crossover control and the BCI intervention groups were combined and treated as a single sample group to provide additional power to the analysis.

Participants

Subjects for this analysis were recruited as part of an ongoing multi-arm stroke rehabilitation study intended to evaluate the effects of intervention using an EEG-based BCI device on the recovery of upper-extremity motor function. The inclusion criteria for participation in the study were: (1) at least 18 years of age; (2) persistent upper-extremity motor impairment resulting from an ischemic or hemorrhagic stroke; (3) ability to provide written informed consent. Exclusion criteria for the study consisted of: (1) concomitant neurodegenerative or other neurological disorders; (2) psychiatric disorders or cognitive deficits that would preclude a subject's ability to provide informed consent; (3) pregnant or likely to become pregnant during the study; (4) allergies to electrode gel, metal and/or surgical tape, contraindications to MRI; (5) concurrent treatment for infectious disease. The study was approved by the Health Sciences Institutional Review Board of University of Wisconsin-Madison. Written informed consent was obtained from all subjects prior to the start of their participation in the study. Twenty chronic stroke subjects (10 from crossover control group and 10 from BCI intervention group), who completed the BCI intervention, were included in this analysis. We limited the cohort for this study to chronic-stage (time since stroke onset $>$ 6 months) stroke subjects only. Excluding stroke subjects in

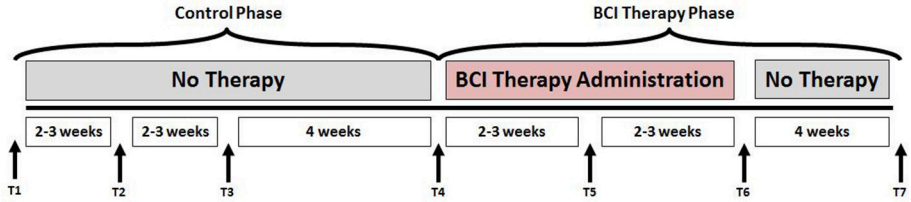

FIGURE 1 | Study paradigm. The time-points at which neuroimaging and behavioral data were collected are represented by - T1: Control baseline 1, T2: Control baseline 2, T3: Control baseline 3, T4: Intervention baseline T5: Mid-intervention, T6: Post-intervention, and T7: 1-month post-intervention.

TABLE 1 | Demographic and clinical characteristics of the study cohort.

Number of stroke subjects	20
Chronicity	Chronic (>6 months since stroke onset)
Age (mean ± std. dev in years)	62.4 ± 14.27
Gender	8 Females, 12 Males
Lesion hemisphere	8 Left, 12 Right
Stroke severity (mean NIHSS ± std. dev)	3.75 ± 3.5
Motor impairment severity	11 Severe, 9 Moderate
Time since stroke (mean ± std. dev in months)	37.65 ± 40.84
Post-stroke handedness	16 Right, 2 Left, 2 Ambidextrous

the acute (time since stroke onset $<$ 14 days) and sub-acute (time since stroke onset $<$ 6 months) stages was critical for this analysis to ensure that spontaneous recovery in these stages does not confound the effects of the BCI intervention. In other words, changes observed in both rs-FC and motor behavioral performance during the acute and sub-acute phases might result from spontaneous neuroplasticity processes rather than from the BCI intervention. Time since stroke was defined to be the period between stroke onset and baseline visit. In addition, subjects were excluded from this analysis if they exhibited bilateral brain lesions for the potential reason that they could be outliers and confound the results. All neuroimaging scans were inspected by a neuroradiologist for the purposes of lesion localization. The distribution of lesion site in the cohort was as follows: middle cerebral artery territory (MCA; $N = 10$), frontal lobe ($N = 3$), cerebellum ($N = 2$), putamen ($N = 2$), occipital lobe ($N = 1$), basal ganglia ($N = 1$), and internal carotid artery occlusion ($N = 1$). Stroke severity was determined by NIH Stroke Scale (NIHSS) (Brott et al., 1989) scores at baseline. Severity of motor impairment was assessed based on performance on Action Research Arm Test (Carroll, 1965; Lang et al., 2006) and visual inspection at the preliminary visit. Participants' handedness post-stroke was established before the start of intervention based on Edinburgh Handedness Inventory (Oldfield, 1971). Participant characteristics are summarized in **Table 1**.

BCI Intervention

All participants received at least 9 and up to 15 two-hour EEG-based BCI interventional sessions, with up to three sessions per week; the complete intervention lasted up to 6 weeks The BCI intervention was administered using BCI2000 software (Schalk et al., 2004) with modifications for administering TS (TDU 01.30, Wicab Inc.) and FES (LG-7500, LGMedSupply; Arduino 1.0.4). EEG signals, which served as the input for the BCI device, were detected and recorded from a 16-channel EEG cap and amplifier (Guger Technologies) during intervention.

A brief account of the three-step intervention is provided as follows. (i) Each intervention session began with an open-loop calibration screening task in which subjects were instructed to attempt movement of either their left or right hand with resting periods in-between by following randomly ordered visual cues on the screen, such as "Right," "Left," or "Rest," in 4-s blocks. During the initial screening session, participants did not receive any form of feedback. The EEG activity, recorded in the open-loop screening task, was used by the classifier for identifying activation patterns corresponding to volitional movement of the respective left and right hands in the closed-loop task. Both in the initial screening and closed-loop feedback conditions, attempted movement was utilized to simulate the training conditions of the neurofeedback task similar to the cognitive processes involved in real-world movement. (ii) Following the initial screening, subjects performed a closed-loop task, in which they received real-time visual feedback in the context of a cursor task game. The goal of the cursor task game was to move a cursor (ball) onto a target area, with target areas positioned on either the left or right side of the computer screen. Subjects were instructed to move their left or right hand to control the corresponding movement of the cursor in the direction of the target on the screen. A 70% accuracy was set as the criteria to establish control of a BCI system in this phase (Kübler et al., 2001, 2005). Real-time EEG signals were used to calculate and control lateral cursor movement, which served as the visual feedback for the remainder of the session. During each BCI intervention session, subjects completed 10 runs of this game, which included 8–12 trials per run, while receiving continuous visual feedback. (iii) After successful completion of 10 runs of the game with visual feedback, both TS and FES were simultaneously incorporated into the intervention session for the remaining trials (as many trials as possible within a 2-h session). FES, with a pulse rate of stimulation 60 Hz and varied up to 5 mA in increments of 0.5 mA as per the participant's comfort level, was administered to muscles of the subject's impaired forearm when their neural activity signals corresponding to impaired arm movement intent were detected during a trial in which subjects attempted to

move the cursor to a target on the screen corresponding to the side of the impaired arm. The stimulation thresholds for FES and TS were determined during the first intervention session and maintained at the same level in all the subsequent sessions for consistency. This EEG-based BCI system with FES and TS provides subjects with both visual and tactile sensory feedback. To keep subjects engaged throughout the task, the size of the target on the screen and speed of the cursor could be changed to modulate the difficulty of the task depending on their accuracy. Additional details of the procedure of the intervention can be found in prior studies such as those described by Wilson et al. (2009), and Young et al. (2014a,c).

Neuroimaging Data Acquisition

Neuroimaging data were acquired at the four aforementioned time points (T4 through T7). For the purposes of this work, we chose to use the data from three of these points, i.e., prior to starting the intervention or pre-intervention assessment (T4), immediately upon completion of intervention or post-intervention assessment (T6) and a month after completion of full intervention (T7) to study the potential peak and carry-over effects of the EEG-based BCI intervention. Rs-fMRI scans were acquired on GE 750 3T MRI scanners (GE Healthcare, Waukesha, WI) using an 8-channel head coil. Ten-minute resting state scans were acquired while participants' eyes were closed using single-shot echo-planar T2*-weighted imaging: TR = 2600 ms, 231 time-points, TE = 22 ms, FOV = 224 mm, 64 × 64 matrix size, flip angle = 60°, and 40 slices with voxel dimensions of 3.5 × 3.5 × 3.5 mm^3. Five-minute T1-weighted anatomical images were obtained at the start of each scan using a BRAVO FSPGR sequence with the following parameters: TR = 8.16 ms, TE = 3.18 ms and TI = 450, matrix size = 256 × 256, 156 slices, flip angle = 12°, FOV = 256 mm with slice thickness = 1 mm.

Behavioral Assessments

To assess the behavioral impact of the BCI intervention, a battery of objective and subjective measures was administered to participants at each time-point. Corresponding to the neuroimaging, we focused on behavioral measures at pre-intervention (T4), post-intervention (T6) and 1-month post-intervention (T7) in this study. To systematically quantify motor functional outcomes, the following standard behavioral measures were evaluated as summarized in **Table 2**: the Action Research Arm Test (ARAT) (Carroll, 1965; Lang et al., 2006), 9-Hole Peg Test (9HPT) (Chen et al., 2009), Barthel Index (BI) (Mahoney, 1965), and Stroke Impact Scale (SIS) (Duncan et al., 1999; Carod-Artal et al., 2008). The ARAT serves as a standardized and reliable functional measure for stroke rehabilitation that measures changes in specific upper limb function among individuals who sustained cortical damage resulting in hemiplegia. The 9HPT measure is used for quantifying hand dexterity. ARAT and 9HPT were observed for the affected [ARAT(A), 9HPT(A)] as well as unaffected [ARAT(U), 9HPT(U)] upper extremity. In this study, BI was administered in questionnaire form and not observed from functional performance as it was originally designed and validated. The BI score quantifies the ability of an individual to care for her/himself in their daily life. The SIS scores are self-reported outcomes that measure the health status of stroke subjects. SIS includes the following standard domains: Activities of Daily Living (ADL) for difficulty carrying out activities in a typical day, Hand Function (HF) for difficulty in using the hand most affected by stroke, Mobility (Mob) for difficulty in ability to be mobile at home and in community, and Physical Strength (PS) for overall strength in the upper and lower limbs of the affected side.

TABLE 2 | Summary of all the behavioral assessments used as outcomes.

Behavioral assessment	Category
ARAT(U): Action Research Arm Test for the upper extremity unaffected by stroke	Objective
ARAT(A): Action Research Arm Test for the upper extremity affected by stroke	Objective
9HPT(U): 9-Hole Peg Test for the upper extremity unaffected by stroke	Objective
9HPT(A): 9-Hole Peg Test for the upper extremity affected by stroke	Objective
BI: Barthel Index	Objective
SIS(ADL): Activities of daily life domain of Stroke Impact Scale	Subjective
SIS (HF): Hand function domain of Stroke Impact Scale	Subjective
SIS(Mob): Mobility domain of Stroke Impact Scale	Subjective
SIS(PS): Physical strength domain of Stroke Impact Scale	Subjective

Individual Level Analysis

The main steps involved in the processing of data on a single-subject level are outlined in **Figure 2** and described in detail in the following subsections.

Neuroimaging Preprocessing

Rs-fMRI scans of 20 subjects were visually inspected for artifacts and preprocessed in the following sequential manner: the first three volumes of each scan were removed, images were despiked, slice time corrected, aligned with the corresponding anatomical T1 scan, spatially smoothed with a 4-mm FWHM (full width at half maximum) Gaussian kernel, transformed into the standard MNI space (3.5 mm isotropic), motion censored (per TR motion > 1 mm or 1°), regressed for nuisance variables (regressed out the signal from locally averaged white matter and cerebrospinal fluid) and bandpass filtered (0.009–0.08 Hz). Given the controversial nature of global signal regression (Murphy and Fox, 2016), this processing step was not included in the analysis pipeline. All rs-fMRI data were preprocessed using Analysis of Functional NeuroImages (AFNI) (http://afni.nimh.nih.gov/afni) (Cox, 1996).

Rs-FC

A seed-based analysis was adopted based on prior work that investigated rs-FC within the motor network in stroke population (Grefkes et al., 2008; Nair et al., 2015). The seed regions were identified on the basis of a network of cortical and subcortical areas that exhibited activation during visually paced hand movements. The seed regions for this study included the primary motor cortex (M1), supplementary motor area (SMA),

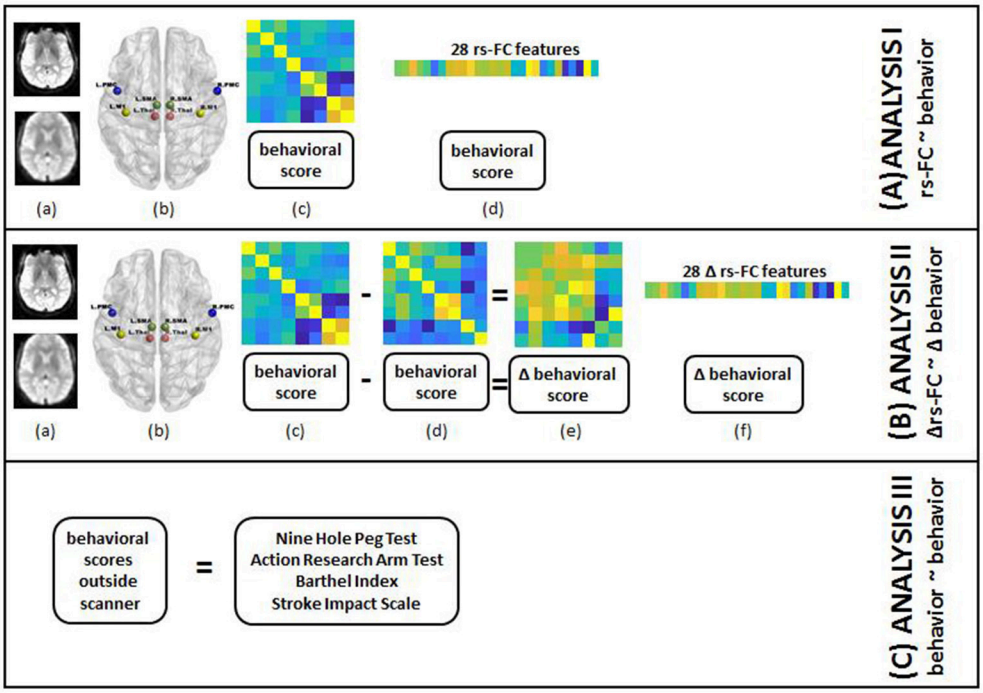

FIGURE 2 | Steps for individual subject analysis are shown below. **(A) rs-FC correlates of behavior:** (a) raw rs-fMRI (top) from pre-, post- and 1-month post-interventions were preprocessed (bottom); (b) 8 seed regions were chosen from the motor network to compute rs-FC at each time-point; (c) 8 × 8 rs-FC matrix was computed and corresponding behavioral scores were transformed as needed for each time-point; (d) rs-FC reflected in the lower triangle of 8 × 8 matrix was vectorized into 28 unique correlation coefficients per subject and 8 distinct behavioral measures were aggregated for group-level analysis. **(B) Δrs-FC correlates of Δbehavior:** (a) raw rs-fMRI (top) from pre-, post- and 1-month post-interventions were preprocessed (bottom); (b) 8 seed regions were chosen from the motor network to compute rs-FC at each time-point; (c) 8 × 8 rs-FC matrix was computed and corresponding behavioral scores were transformed as needed for a preceding time-point; (d) 8 × 8 rs-FC matrix was computed and corresponding behavioral scores were transformed as needed for a succeeding time-point; (e) change in rs-FC and behavioral scores were calculated between the two time-points; (f) change in rs-FC reflected in the lower triangle of 8 × 8 matrix was vectorized into 28 unique correlation coefficients per subject and change in 8 distinct behavioral measures were aggregated for group-level analysis. **(C) behavioral correlates at preceding time-point of behavior at succeeding time-point:** transformed scores for 8 behavioral measures at pre-, post- and 1-month post-interventions were aggregated for group-level analysis.

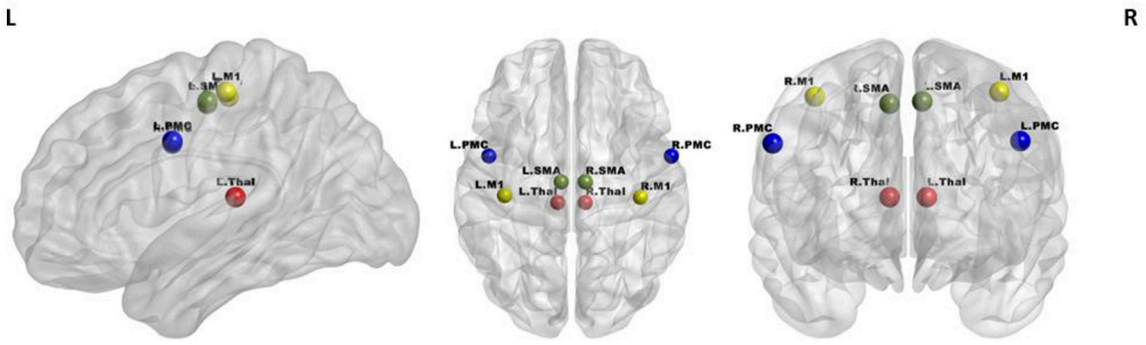

FIGURE 3 | Regions of interest in the motor network included four bilateral seeds: M1 (yellow), PMC (blue), SMA (green), and Thalamus (red).

thalamus, and lateral premotor cortex (PMC) in the right and left hemispheres, as illustrated in **Figure 3** using BrainNet Viewer (Xia et al., 2013) and abbreviated as per **Table 3**. The MNI coordinates, also specified in **Table 3**, for the eight regions were used to create 8-mm spherical seeds. For each subject, BOLD time series signal from each region was extracted from the spatially standardized residuals obtained in the preprocessing stage. The extracted time series for each region was used to compute an 8 × 8 ROI correlation matrix for each subject. From this symmetric matrix, 28 unique correlation coefficients were

TABLE 3 | Shorthand representation of the eight ROIs in the motor network used for the analysis is presented below.

ROI	Shorthand	X (MNI)	Y (MNI)	Z (MNI)
Left primary motor cortex	L.M1	−39	−22	57
Right primary motor cortex	R.M1	40	−23	55
Left premotor cortex	L.PMC	−48	1	36
Right premotor cortex	R.PMC	58	1	35
Left supplementary motor area	L.SMA	−6	−14	53
Right supplementary motor area	R.SMA	8	−14	52
Left thalamus	L.Thal	−8	−26	12
Right thalamus	R.Thal	8	−26	12

extracted to represent pairwise rs-FC within the motor network at each of the three stages of interest.

Potential Clinical Confounds

The study cohort was heterogeneous with respect to multiple clinical factors which could confound the contribution of rs-FC alone. Based on prior studies, we identified the following factors as potential confounds: age and stroke severity (Ferraro et al., 2003), severity of motor impairment, and time since stroke (Rehme et al., 2012), lesion hemisphere (Crinion et al., 2007), and gender (Kelly-Hayes et al., 2003). We included these clinical variables as features, built the regression model for each outcome, and compared the performances of models with and without the confounding variables. This strategy would help understand the impact of potential confounds on the performance of regression model as well as the contribution of confounds as correlates relative to rs-FC or behavioral features.

Group-Level Analysis

Applications of machine learning regression models such as SVR on rs-fMRI have been demonstrated in neuroimaging-based studies (Dosenbach et al., 2010; Vergun et al., 2013) as SVR-based methods can efficiently handle multi-dimensional data and model the linearity as well as non-linearity in a given dataset. For the purposes of this study, we adopt a strategy, similar to these studies. To understand the correlates of behavioral outcomes and changes, the following analyses were undertaken by applying SVR to correlate:

ANALYSIS I: rs-FC at preceding time-points with behavioral outcomes at succeeding time-points (T4 with T6; T4 with T7; T6 with T7).

ANALYSIS II: change (Δ) in rs-FC between pairs of time-points with corresponding change (Δ) in behavioral outcomes (T4 and T6; T4 and T7; T6, and T7).

ANALYSIS III: behavioral measures at preceding time-points with behavioral measures at succeeding time-points (T4 with T6; T4 with T7; T6 with T7).

In case of behavioral measures, total scores across comprising domains for BI and ARAT, average scores across two trials for 9HPT, and transformed scores to yield a percentage of possible points for the SIS domains of PS, Mob, HF, and ADL were considered.

To characterize changes among the three stages of interest (T4, T6 and T7), the following definitions were employed:

$$\Delta rs - FC = \frac{rs - FC_{succeeding\ stage} - rs - FC_{preceding\ stage}}{rs - FC_{preceding\ stage}} \quad (1)$$

where $rs - FC_{succeeding\ stage}$ and $rs - FC_{preceding\ stage}$ denote the values of $rs-FC$ correlation at succeeding (T6, T7) and preceding (T4, T6) stages respectively.

Unlike in case of $\Delta rs - FC$, the definition for changes in behavioral measures differed by case. For 9HPT(A), 9HPT(U), ARAT(U), BI, SIS (PS, Mob, and ADL) scales, the normalized change was gauged by:

$$\Delta behavior = \frac{behavior_{succeeding\ stage} - behavior_{preceding\ stage}}{behavior_{preceding\ stage}} \quad (2)$$

However, in case of ARAT(A) and SIS(HF), the possibility of $behavior_{preceding\ stage}$ being 0 invalidates the above normalization. Thus, for these two outcomes, a simple deviation was computed as follows:

$$\Delta behavior = behavior_{succeeding\ stage} - behavior_{preceding\ stage} \quad (3)$$

where $behavior_{succeeding\ stage}$ and $behavior_{preceding\ stage}$ correspond to the scores achieved by a participant in each behavioral task at succeeding (T6, T7) and preceding (T4, T6) stages respectively. Due to lack of variability across most time-points, the ARAT(U) was discarded as a behavioral outcome for all analyses.

Each of the three aforementioned analyses was examined by including the identified potential confounding variables as well. In each case, the input features for all subjects were aggregated and the steps described as follows were implemented.

Feature Selection

Each regression model was built using a subset of input features (28 rs-FC features, 28 Δ rs-FC features and 8 behavioral measures as described by ANALYSES I, II and III) through a feature selection procedure. A forward sequential feature selection (SFS) was helpful in reducing the dimensions of the original data for better interpretation of features involved (He et al., 2013; Lu et al., 2015). This method searches for a subset of features that optimally models a given outcome. The algorithm adds each candidate feature and checks the specified criteria by building a regression model based on selected features. The criteria specified for selection of a feature involved minimization of the mean squared error (MSE) arising from estimation error for SVR model. The SVR model is described in the following section. A nested leave-one out cross-validation approach allowed for testing of estimation error on the left-out sample, where the inner loop was used to choose the features during a training-validation phase. One advantage of methods such as SFS is that since it works in the raw feature space, it can be applied to both continuous and categorical features. During cross-validation, the features that were common across all the folds were reported as

the contributing features for each model. The weights assigned to these features were averaged across all folds and sorted to determine the rank or importance of individual features in the regression model.

Support Vector Regression (SVR)

Once a subset of features was selected by SFS, the SVR model was trained using the selected features for each behavioral outcome. SVR was chosen due to its ability to predict real valued behavioral outcomes based on multi-dimensional input features using the principle of supervised learning support vector machines (SVM) (Scholkopf and Smola, 2001). Typically used as a classifier, SVM can also be used for regression analysis (Vapnik, 2013). SVR forms a non-parametric method via the kernel trick. This method not only provides resilience to overfitting and good generalization performance, but also helps in interpreting the contribution of individual features in high-dimensional data with a linear kernel. The principle behind using the SVR analysis is described in **Supplementary Section 1**. In the case of linear regression, the mapping function lies in the input space, so it is possible to derive the weights corresponding to each input feature. However, in the case of non-linear regression, similar weights cannot be derived explicitly since the mapping function is no longer found in the input space but in the feature space in the kernel space. Both linear and non-linear kernel SVR models were employed for our analyses.

Cross-Validation

A leave-one-out cross-validation (LOOCV) approach (Hastie et al., 2001) was adopted to estimate the performance of the regression model in the outer loop of the nested cross-validation as it provides an approximation of the test error with a lower bias and is more suitable for a dataset with a limited number of samples such as that used in this analysis. We performed a LOOCV by subject in this validation-testing phase. This means that the data consisting of 20 observations were subdivided into 20 folds such that each fold comprised of data from a single subject. The regression model was trained using selected features from 19 folds and tested upon the left-out fold. This was repeated 20 times such that data from each subject was left out once while a model was trained using the rest of the data. The performance of the model was quantified in terms of the average root-mean-squared error (RMSE) for linear and non-linear SVR over all iterations of LOOCV given by:

$$RMSE = \sqrt{\frac{1}{l}\sum_{i=1}^{l}(y_{est_i} - y_i)^2} \quad (4)$$

where the $y_{est_i} - y_i$ term is the measure of error between the estimated outcome and the true outcome. Reasonable performance of SVR is characterized by values of RMSE closer to 0. In addition to RMSE, the linear SVR can also be assessed in terms of goodness of fit in terms of the coefficient of determination (R^2). However, it is not an appropriate measure for non-linear models as illustrated by simulations performed by Spiess and Neumeyer (2010). Thus, we quantified performance of linear SVR models by R^2 and RMSE but compared linear and non-linear models in terms of RMSE.

Model Parameter Optimization

The generalization performance is dependent upon both the selected features and model parameters C, ε (Burges, 1998; Smola and Schölkopf, 2004), and the kernel parameters. The parameter C is used to trade-off between the complexity of the model and the extent to which estimated deviations larger than ε are tolerated in formulation of the optimization. Parameter ε controls the width of the ε -insensitive zone, used to fit the training data. Both C, ε values have an impact on complexity of the model. The data points are scaled by the parameter depending upon the kernel used for regression. A randomized search method based on Bayesian optimization process attempts to minimize the MSE in the separate LOOCV by varying the parameters for 30 evaluations (Bull, 2011; Snoek et al., 2012; Gelbart et al., 2014) which corresponded to the inner loop of the training-validation phase, training on all samples but one with the best chosen parameters and testing on the left out sample.

Evaluation of Regression Model

In order to validate the results against chance levels, non-parametric permutation tests were performed. For each regression model, the outcome labels were randomly permuted 1,000 times and feature selection and LOOCV were repeated for each permuted dataset to create a null distribution. The performance of the regression model corresponding to the non-permuted data was considered significantly better than chance if the RMSE of the model was lower than at least 95% of those obtained from the null-hypothesis.

Overview of Methodology

Overall, we trained SVR models using selected rs-FC, Δrs-FC, or behavioral measures, optimized the model and identified the contributing input features that provided the minimum RMSE upon LOOCV. All computations were carried out using the Statistics and Machine Learning Toolbox in MATLAB R2017a (The MathWorks, Inc., Natick, Massachusetts, United States). The group-level pipeline of analysis is visualized in **Figure 4**.

RESULTS

We present the findings from the linear-kernel SVR here (results corresponding to the non-linear kernel models can be found in **Supplementary Materials ST1–3**).

Choice of Time-Points of Interest

The analyses, undertaken here, revolved around three time-points, namely T4, T6, and T7, i.e., pre-intervention, post-intervention and 1-month post-intervention. The objective was to study the immediate as well as potential residual impact of the intervention after a month. A comparison of group medians of behavioral outcomes at these three time-points, evident from **SF 1**, showed increased values at T7 relative to T4 or T6 for SIS(Mob), SIS(HF), ARAT(A) although not significant (based on a Mann Whitney U-test). The time-points from the control

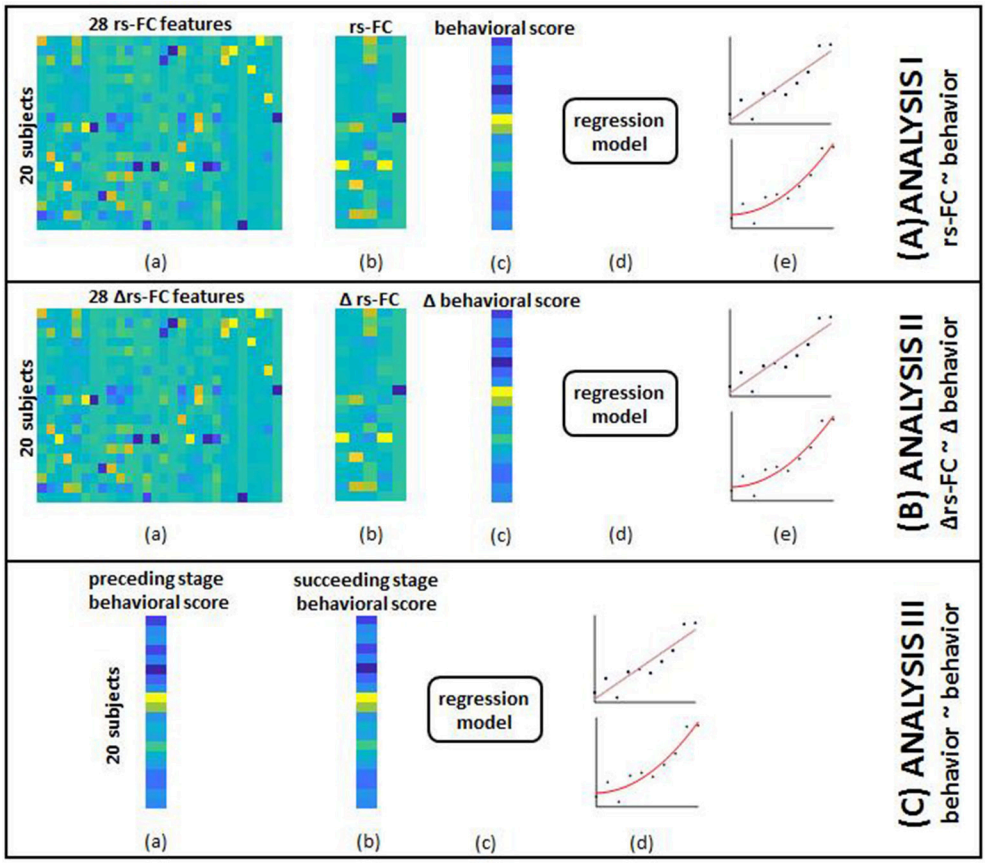

FIGURE 4 | The overview of group-level analysis is provided here. **(A) rs-FC correlates of behavior:** (a) aggregated data from single-subject analysis gave 28 rs-FC features for each of the 20 subjects; (b) SFS was used to select specific correlates corresponding to each behavioral outcome; (c) aggregated behavioral scores for 20 subjects served as outcomes in separate models; (d) data from (b) and (c) were fed into the SVR model; (e) linear (top) and non-linear (bottom) kernels were specified to perform regression. Steps (a through e) were repeated by adding identified clinical variables to rs-FC data as input features. **(B) Δrs-FC correlates of Δbehavior:** (a) aggregated data from single-subject analysis gave 28 change in rs-FC features for each of the 20 subjects between pairs of time-points; (b) SFS was used to select specific correlates corresponding to each behavioral outcome; (c) aggregated change in behavioral scores between corresponding pair of time-points for 20 subjects served as outcomes in separate models; (d) data from (b) and (c) were fed into the SVR model; (e) linear (top) and non-linear (bottom) kernels were specified to perform regression. Steps (a–e) were repeated by adding identified clinical variables to change in rs-FC data as input features. **(C) behavioral correlates at preceding time-point of behavior at succeeding time-point:** (a) aggregated behavioral scores from a preceding time point gave 8 distinct measures; (b) aggregated behavioral scores from a succeeding time-point gave the corresponding 8 measures; (c) data from steps (a) and (b) were fed to the SVR model; (d) linear (top) and non-linear (bottom) kernels were specified to perform regression.

period, i.e., T1 through T3 were not included in the regression analyses due to limited samples ($N = 10$). However, we did not find significant differences (using Mann Whitney U-test on each pair of time-points) when the group medians of the behavioral outcomes during the control period were compared with T4 as illustrated in **SF 2**. Thus, presumably, we could consider measures at T4 to serve as representative scores for the control period.

Performance of Correlates

Behavioral outcomes were estimated using rs-FC, Δrs-FC as well as behavioral measures at preceding time-points. In terms of R^2, better estimation of outcomes was observed using behavioral correlates, followed by rs-FC and Δrs-FC in order. This held true with and without the impact of clinical variables.

Rs-FC as Correlates of Behavioral Outcomes

The performances of SVR using rs-FC as correlates of behavioral outcomes are presented in **Table 4** (and **ST 1**). All the SVR models, developed here, performed better than chance-level based on permutation test ($p < 0.05$) as depicted in **SF3** of Supplementary Section 2. Individual predictors involved in estimating the different outcomes are listed in **Table 5** (and **ST 4**). Overall, rs-FC associated with L.M1, R.M1, and R.PMC were the main contributors toward estimation, both with and without clinical variables. Among the three time-points, better performances were found in cases of correlating rs-FC at T6 and behavioral measures at T7.

TABLE 4 | Linear-kernel SVR performances based on leave-one out cross-validation to correlate rs-FC at preceding time-point with behavioral measures at succeeding time-point are presented.

Outcome	T4 rs-FC∼T6 behavior			T4 rs-FC∼T7 behavior			T6 rs-FC∼T7 behavior		
	Features	RMSE	R^2	Features	RMSE	R^2	Features	RMSE	R^2
(A) WITHOUT CLINICAL VARIABLES									
9HPT(A)	9	110.93*	0.21	14	116.69*	0.14	6	109.25*	0.25
9HPT(U)	5	4.2*	0.27	3	4.05*	0.26	6	2.86*	0.63
ARAT(A)	2	20.58*	0.33	6	17.87*	0.49	4	15.48*	0.61
BI	3	8.01*	0.24	5	6.31*	0.31	11	6.39*	0.3
SIS(ADL)	4	10.93*	0.14	4	10.62*	0.51	5	109.25*	0.25
SIS(HF)	4	31.81*	0.37	6	26.84*	0.36	5	33.47*	0.64
SIS(Mob)	6	7.88*	0.19	8	13.17*	0.10	4	11.34*	0.34
SIS(PS)	10	18.44*	0.18	5	11.93*	0.47	4	11.7*	0.49
(B) WITH CLINICAL VARIABLES									
9HPT(A)	10	69.627*	0.69	14	71.349*	0.68	7	61.391*	0.76
9HPT(U)	4	4.187*	0.28	4	3.822*	0.34	9	1.508*	0.9
ARAT(A)	2	5.143*	0.96	4	5.723*	0.95	2	7.009*	0.92
BI	7	9.452*	0.43	7	13.378*	0.22	12	14.099*	0.13
SIS(ADL)	7	16.146*	0.78	2	23.484*	0.51	11	15.1018	0.8
SIS(HF)	5	9.766*	0.03	8	9.4*	0.54	5	10.514*	0.43
SIS(Mob)	1	16.361*	0.37	4	13.523*	0.32	6	12.528*	0.41
SIS(PS)	4	6.796*	0.41	7	4.591*	0.64	10	3.817*	0.75

*Specific correlates are listed in **Table 5**.*

(*) = significant against chance-level based on permutation-test ($p < 0.05$); T4 = pre-therapy; T6 = post-therapy; T7 = 1-month post-therapy.

Δrs-FC as Correlates of ΔBehavioral Outcomes

The performance of SVR using Δrs-FC as correlates of Δbehavioral outcomes are presented in **Table 6** (and **ST 2**). SVR models corresponding to ARAT(A) and SIS(HF) performed better than chance-level based on permutation test ($p < 0.05$) as depicted in **SF 4**. Individual predictors involved in estimating the different outcomes are listed in **Table 7** (and **ST 5)**. Overall, rs-FC associated with L.M1, R.M1, L.Thal and L.M1, R.M1, R.Thal were the main contributors toward estimation without and with clinical variables respectively. Among the three time-points, better performances were found in cases of correlating Δrs-FC between T6 and T7 and Δbehavioral measures between the same time-period.

Behavioral Correlates at Preceding Stages of Behavioral Outcomes at Succeeding Stages

The performance of SVR using behavioral measures at preceding time-points as correlates of behavioral outcomes at succeeding time-points are presented in **Table 8** (and **ST 3**). All the SVR models performed better than chance-level based on permutation test ($p < 0.05$) as depicted in **SF 5**. Individual predictors involved in estimating the different outcomes are listed in **Table 9** (and **ST 6)**. Overall, the behavioral measures from the preceding time-point were almost always the highest-ranked correlates, relative to the clinical variables. Among the three time-points, better overall performances were found in cases of correlating behavior at T4 with those at T6.

Impact of Clinical Variables

We tested each SVR model with and without the impact of the identified clinical variables to account for potential confounding effects they might have. In general, the SVR performance improved upon addition of clinical variables as input features. Contribution of individual clinical variables, relative to rs-FC, Δrs-FC and behavioral input features can be found in **ST 4-6** respectively. The most involved clinical features were: NIHSS, motor impairment severity for ANALYSIS I and III and NIHSS, motor impairment severity and lesion hemisphere for ANALYSIS II. In terms of ROI contribution, rs-FC associated with L.M1, R.M1 and R.PMC were the important contributors for ANALYSIS I even after adjusting for clinical confounds. For ANALYSIS II, the important contributors included L.M1, R.M1 and L.Thal without clinical variables and L.M1, R.M1, and R.Thal with clinical variables.

Linear vs. Non-linear Regression

The overall performances of the linear and non-linear SVR models were compared in terms of their RMSE values computed via LOOCV (**SF 6–8**). Comparing the RMSE values revealed that the linear and non-linear SVR models performed approximately similarly with the non-linear model being slightly more generalizable with lower error when rs-FC and Δrs-FC were used as input variables. When behavioral measures were used as input variables, linear SVR appeared to perform better.

TABLE 5 | List of rs-FC correlates of behavior between all pairs of time-points identified by using linear-kernel SVR are presented below.

Rank	9HPT(A)	9HPT(U)	ARAT(A)	SIS(ADL)	SIS(HF)	SIS(Mob)	SIS(PS)	BI
(A) WITHOUT CLINICAL VARIABLES								
Outcomes at T6 and Input rs-FC Features at T4								
1	L.SMA-R.M1	L.SMA-R.PMC	R.PMC-L.PMC	R.PMC-R.M1	L.SMA-L.PMC	R.PMC-R.M1	R.SMA-R.M1	L.SMA-R.M1
2	R.SMA-R.M1	R.PMC-R.M1	L.SMA-R.M1	L.Thal-L.M1	R.SMA-R.M1	R.SMA-L.SMA	L.Thal-R.SMA	R.PMC-L.PMC
3	R.M1-L.M1	R.SMA-R.PMC		R.SMA-L.M1	L.SMA-L.M1	L.Thal-R.PMC	R.SMA-L.M1	R.Thal-L.SMA
4	R.PMC-R.M1	L.PMC-R.M1		R.M1-L.M1	R.M1-L.M1	L.Thal-R.M1	L.SMA-L.PMC	
5	R.Thal-L.Thal	L.Thal-L.M1				R.Thal-R.PMC	L.Thal-L.M1	
6	R.Thal-L.M1					R.SMA-R.M1	L.PMC-L.M1	
7	R.SMA-R.PMC						R.M1-L.M1	
8	R.PMC-L.PMC						L.Thal-R.M1	
9	L.Thal-L.M1						R.PMC-L.PMC	
10							R.Thal-L.M1	
Outcomes at T7 and Input rs-FC Features at T4								
1	L.SMA-R.M1	L.Thal-L.SMA	R.SMA-R.PMC	R.Thal-L.M1	R.SMA-R.M1	R.PMC-R.M1	R.Thal-R.PMC	L.PMC-L.M1
2	R.SMA-R.M1	R.SMA-L.SMA	L.SMA-R.M1	R.PMC-R.M1	L.PMC-L.M1	L.SMA-L.M1	R.SMA-R.M1	R.SMA-R.M1
3	R.PMC-R.M1	R.Thal-L.PMC	R.SMA-R.M1	L.Thal-R.M1	R.M1-L.M1	R.SMA-L.SMA	R.Thal-L.Thal	R.Thal-L.SMA
4	R.Thal-L.SMA		R.PMC-R.M1	R.SMA-L.M1	L.SMA-L.M1	R.SMA-L.M1	L.Thal-R.M1	L.Thal-L.M1
5	R.M1-L.M1		R.PMC-L.PMC		L.Thal-R.PMC	L.Thal-R.PMC	R.M1-L.M1	R.Thal-L.M1
6	R.SMA-R.PMC		L.PMC-L.M1		R.SMA-L.SMA	L.SMA-L.PMC		
7	L.Thal-R.M1					R.Thal-L.SMA		
8	R.Thal-L.Thal					R.Thal-R.PMC		
9	R.Thal-R.SMA							
10	R.Thal-R.M1							
11	R.PMC-L.PMC							
12	R.Thal-L.M1							
13	L.SMA-R.PMC							
14	L.Thal-L.M1							
Outcomes at T7 and Input rs-FC Features at T6								
1	R.PMC-R.M1	L.Thal-R.PMC	R.PMC-R.M1	L.SMA-R.M1	R.PMC-L.M1	R.PMC-R.M1	R.Thal-L.SMA	L.Thal-R.M1
2	R.PMC-L.PMC	L.SMA-R.PMC	R.Thal-R.PMC	R.PMC-L.M1	R.Thal-L.PMC	R.Thal-L.PMC	R.Thal-L.PMC	L.Thal-L.SMA
3	R.Thal-R.PMC	R.SMA-L.M1	L.SMA-R.PMC	R.SMA-R.PMC	L.SMA-R.M1	R.SMA-L.PMC	R.Thal-L.M1	L.SMA-R.PMC
4	R.M1-L.M1	R.Thal-L.M1	R.M1-L.M1	L.SMA-R.PMC	R.Thal-R.M1	R.SMA-L.SMA	R.PMC-L.M1	R.SMA-R.M1
5	L.SMA-R.PMC	R.Thal-R.M1		R.Thal-R.PMC	L.Thal-L.SMA			R.Thal-R.PMC
6	R.SMA-L.PMC	R.PMC-L.M1						L.PMC-L.M1
7								R.SMA-R.PMC
8								R.PMC-R.M1
9								R.M1-L.M1
10								L.Thal-L.M1
11								R.Thal-L.PMC
(B) WITH CLINICAL VARIABLES								
Outcomes at T6 and Input rs-FC and Clinical Features at T4								
1	Motor Imp.	L.PMC-R.M1	Motor Imp.	TSS	Motor Imp.	L.Thal-R.PMC	NIHSS	Motor Imp.
2	NIHSS	Age	NIHSS	R.SMA-R.PMC	L.SMA-R.PMC		Lesion Hemi	R.Thal-L.SMA
3	Lesion Hemi	L.SMA-L.M1		R.Thal-R.PMC	R.M1-L.M1		R.SMA-R.M1	NIHSS
4	R.M1-L.M1	NIHSS		Motor Imp.	R.PMC-R.M1		L.Thal-R.PMC	Age
5	R.SMA-R.PMC			Lesion Hemi	R.Thal-R.M1			L.SMA-R.M1
6	L.SMA-R.M1			R.Thal-L.M1				R.Thal-L.PMC
7	TSS			R.PMC-R.M1				L.PMC-L.M1
8	R.Thal-L.Thal							
9	R.SMA-R.M1							
10	R.PMC-R.M1							

(Continued)

TABLE 5 | Continued

Rank	9HPT(A)	9HPT(U)	ARAT(A)	SIS(ADL)	SIS(HF)	SIS(Mob)	SIS(PS)	BI
Outcomes at T7 and Input rs-FC and Clinical Features at T4								
1	Motor Imp.	R.SMA-L.SMA	Motor Imp.	R.SMA-L.M1	R.PMC-L.M1	R.PMC-R.M1	Motor Imp.	TSS
2	NIHSS	R.SMA-L.M1	NIHSS	R.Thal-L.M1	Motor Imp.	L.SMA-L.M1	R.Thal-L.Thal	Motor Imp.
3	Lesion Hemi	R.PMC-R.M1	L.Thal-R.PMC		R.SMA-R.M1	R.SMA-L.M1	L.Thal-R.SMA	Age
4	TSS	NIHSS	R.Thal-R.PMC		R.PMC-L.PMC	L.SMA-L.PMC	L.Thal-R.PMC	R.PMC-R.M1
5	R.SMA-R.M1				R.SMA-L.M1		L.Thal-R.M1	R.PMC-L.PMC
6	R.M1-L.M1				L.PMC-L.M1		R.Thal-L.PMC	R.M1-L.M1
7	L.PMC-L.M1				TSS		NIHSS	R.SMA-R.M1
8	L.SMA-R.M1				NIHSS			
9	L.Thal-L.M1							
10	R.Thal-L.SMA							
11	R.Thal-L.PMC							
12	R.Thal-R.SMA							
13	R.SMA-L.M1							
14	R.PMC-R.M1							
Outcomes at T7 and Input rs-FC and Clinical Features at T6								
1	Motor Imp.	L.Thal-L.M1	Motor Imp.	R.PMC-L.M1	Motor Imp.	R.Thal-L.PMC	L.SMA-L.PMC	Motor Imp.
2	NIHSS	L.Thal-R.SMA	NIHSS	R.SMA-R.PMC	L.SMA-L.PMC	R.Thal-L.SMA	R.SMA-L.SMA	R.Thal-L.PMC
3	Lesion Hemi	L.Thal-R.PMC		TSS	TSS	R.Thal-L.M1	Motor Imp.	R.PMC-L.PMC
4	R.SMA-L.PMC	R.Thal-L.M1		L.SMA-R.M1	R.Thal-L.PMC	R.PMC-L.PMC	L.Thal-R.M1	R.Thal-R.M1
5	R.PMC-L.PMC	R.SMA-L.M1		NIHSS	NIHSS	L.Thal-L.M1	R.SMA-R.M1	R.Thal-R.PMC
6	L.SMA-R.PMC	NIHSS		L.SMA-L.PMC		R.PMC-L.M1	R.PMC-L.M1	R.Thal-R.SMA
7	R.PMC-R.M1	Gender		R.Thal-R.M1			R.PMC-L.PMC	Age
8		L.Thal-L.SMA		L.PMC-L.M1			NIHSS	TSS
9		R.SMA-R.PMC		R.PMC-R.M1			L.Thal-R.SMA	R.PMC-R.M1
10				R.SMA-L.M1			R.Thal-R.PMC	R.M1-L.M1
11				R.Thal-L.PMC				NIHSS
12								R.SMA-R.M1

T4 = pre-therapy; T6 = post-therapy; T7 = 1-month post-therapy.

DISCUSSION

Impact of BCI Intervention Based on Identified Correlates

The objective of this study was to assess behavioral outcomes following the described BCI intervention. To do so, rs-FC, Δrs-FC, and behavioral measures were utilized. Evaluation of outcomes at the third time-point, namely the 1-month post-intervention, would be particularly important to understand the potential long-term impact of the intervention. As would be expected, behavioral measures at preceding time-points estimated the behavioral measures at succeeding time-points better than rs-FC or Δrs-FC. However, using behavioral measures alone does not provide the knowledge of possible neural reorganization in the brain. Neuroimaging-based rs-FC features can offer this complementary information and serve as an alternative means to assess outcomes. In comparison to pre-intervention measures, the post-intervention input (rs-FC, Δrs-FC, behavioral) measures were more indicative of outcomes at 1-month post-intervention. That could suggest neural reorganization occurring between pre- and post-intervention that is at least partially retained at 1-month post-therapy.

Rs-FC as a Tool for Predicting Behavioral Changes

FMRI has been shown as a useful biomarker in predicting the impact of several forms of rehabilitation on the recovery of function in the stroke population (Johansen-Berg et al., 2002; Ward et al., 2003a; Sharma et al., 2009; Várkuti et al., 2013; Young et al., 2014b). Rs-fMRI, in particular, is a useful non-invasive method used to study impaired subjects such as stroke survivors, as it is time-efficient and task-free, reducing the burden on study participants. In our study, the impact of BCI intervention was examined using rs-FC and associated changes corresponding to several objective and subjective behavioral outcomes. Rs-FC as correlates formed reliable SVR models across all outcomes. However, with Δrs-FC, models corresponding to ARAT(A) and SIS(HF) were only significant above chance-level. ARAT(A) and SIS(HF) are objective and subjective measures of impairment due to stroke and ability to use the impaired hand respectively. Improvement in these outcomes following the intervention demonstrates the impact of BCI-aided therapy. The models that were not significant against chance level could potentially be due to low variability in the normalized outcomes as well as limited sample size. Additionally, the main contributing regions

TABLE 6 | Linear-kernel SVR performances based on leave-one out cross-validation to correlate Δrs-FC between two time-points with Δ behavioral measures between corresponding time-points are presented.

Outcome	Δrs-FC$_{T6-T4}$~Δbehavior$_{T6-T4}$			Δrs-FC$_{T7-T4}$~Δbehavior$_{T7-T4}$			Δrs-FC$_{T7-T6}$~Δbehavior $_{T7-T6}$		
	Features	RMSE	R^2	Features	RMSE	R^2	Features	RMSE	R^2
(A) WITHOUT CLINICAL VARIABLES									
Δ9HPT(A)	3	110.93	0.22	1	116.69	0.14	4	109.25	0.25
Δ9HPT(U)	1	4.2	0.28	1	4.05	0.26	6	2.86	0.63
ΔARAT(A)	7	20.58*	0.33	4	17.87*	0.49	6	15.48*	0.61
ΔBI	5	8.01	0.18	5	0.05	0.53	6	6.39	0.3
ΔSIS(ADL)	2	10.93	0.24	5	10.62	0.51	8	0.08	0.73
ΔSIS(HF)	5	8.52*	0.26	4	26.84*	0.36	6	33.47*	0.42
ΔSIS(Mob)	4	7.88	0.37	2	13.17	0.1	3	11.34	0.34
ΔSIS(PS)	3	18.44	0.2	3	11.93	0.47	6	0.81	0.2
(B) WITH CLINICAL VARIABLES									
Δ9HPT(A)	5	69.63	0.69	3	71.35	0.68	3	61.39	0.76
Δ9HPT(U)	3	4.19	0.28	3	0.1	0.22	3	1.51	0.9
ΔARAT(A)	16	5.14*	0.96	8	5.72*	0.95	16	7.01*	0.92
ΔBI	3	0.05	0.1	7	4.59	0.64	8	3.82	0.75
ΔSIS(ADL)	4	9.45	0.43	5	13.38	0.22	4	14.1	0.13
ΔSIS(HF)	5	16.15*	0.78	5	23.48*	0.51	4	15.1*	0.8
ΔSIS(Mob)	4	9.77	0.03	7	9.4	0.54	5	10.51	0.43
ΔSIS(PS)	4	16.36	0.37	4	13.52	0.32	8	12.53*	0.41

*Specific correlates are listed in **Table 7**. (*) = significant against chance-level based on permutation-test ($p<0.05$); T4 = pre-therapy; T6 = post-therapy; T7 = 1-month post-therapy.*

remained focused on bilateral M1 areas with and without the influence of the clinical features. These findings illustrate that rs-FC serves as a stable imaging biomarker in understanding the functional correlates of the recovery process and could, thus, guide future rehabilitative studies in tracking changes over time.

Machine Learning as a Tool For Predictive Modeling

In the context of fMRI studies, fewer studies have used prediction of outcomes on a continuous scale (Ganesh et al., 2008; Dosenbach et al., 2010; Michel et al., 2011; Vergun et al., 2013), where SVR-based models have been adopted to address different parts of data analysis, the majority of which, are based on a simple linear-kernel SVR. Even fewer studies have explored the improved performance offered by non-linear kernels. For instance, non-linear SVR has been incorporated in the preprocessing pipeline of fMRI data to accurately detect activation by accounting for intrinsic spatio-temporal autocorrelations (Wang et al., 2003) and cognitive states of participants in a virtual reality environment have been predicted based on fMRI data using non-linear SVR (Di Bono and Zorzi, 2008). With inclusion of non-linear-kernel SVR, our work adds to the growing literature that provides insight on adopting the more generalizable non-linear approaches for regression based on fMRI data. This could indicate that while the underlying relationship between rs-FC and behavioral measures might not necessarily be linear, the relationship within a given behavioral measure could be better expressed linearly. While linear models were useful in interpreting the contributing features, non-linear models performed slightly better in explaining possible non-linear interactions with better generalizability. Our findings suggest promise in that, given fMRI data from a large cohort, machine learning-based regression models may be trained to predict behavioral change resulting from BCI intervention on a single-subject level. From the clinical perspective, such an application could serve as a supplementary prognostic tool for patients and their families in estimating the timeline and/or capacity of potential recovery through this intervention.

The Bigger Picture

Our work adds to the ongoing investigation of understanding the trajectory of motor recovery in the chronic stage of stroke as a result of BCI-aided rehabilitative intervention using a data-driven approach. These findings are in line with works that suggest that using rehabilitative therapies have enabled recovery even at the chronic stage of stroke (Fasoli et al., 2003; Caria et al., 2011). This means that even though motor recovery associated with the paretic side might have plateaued, there could still be potential for further recovery. This was evident from the predominant involvement of rs-FC and Δrs-FC associated with the bilateral M1, which is primarily known to be a center for voluntary motor behavior including but not limited to movement planning, movement initiation and motor learning. While the roles of neuroimaging methods such as task-fMRI (Young et al., 2014b) and diffusion images (Song et al., 2014) in relation to motor recovery facilitated by BCI in our cohort have been explored, the current study fills a gap by examining rs-fMRI as a potential biomarker for recovery. Since it is established that activations identified by task-fMRI have overlapping functional

TABLE 7 | List of Δrs-FC correlates of Δbehavior between all pairs of time-points identified by using linear-kernel SVR are presented below.

Rank	Δ9HPT(A)	Δ9HPT(U)	ΔSIS(ADL)	ΔSIS(Mob)	ΔSIS(PS)	ΔBI	ΔARAT(A)	ΔSIS(HF)
(A) WITHOUT CLINICAL VARIABLES								
Outcomes at T6 and Input Δrs-FC Features at T4								
1	R.Thal-R.SMA	L.SMA-L.PMC	L.SMA-R.PMC	R.PMC-R.M1	L.SMA-R.M1	R.Thal-L.PMC	L.Thal-L.M1	R.PMC-L.M1
2	R.Thal-R.M1		L.Thal-R.PMC	L.Thal-L.M1	R.SMA-L.SMA	L.SMA-L.PMC	L.Thal-L.PMC	R.SMA-R.M1
3	R.SMA-R.PMC			R.PMC-L.M1	R.PMC-L.M1		L.SMA-L.PMC	L.PMC-L.M1
4				L.Thal-R.PMC			L.SMA-R.M1	L.Thal-R.SMA
5							L.SMA-R.PMC	L.PMC-R.M1
6							R.M1-L.M1	
7							L.Thal-R.PMC	
Outcomes at T7 and Input Δrs-FC Features at T4								
1	R.Thal-L.SMA	L.Thal-R.PMC	R.Thal-R.M1	L.Thal-L.M1	R.Thal-L.PMC	L.Thal-R.PMC	R.Thal-R.SMA	R.Thal-L.M1
2			L.Thal-R.PMC	R.Thal-R.M1	R.SMA-L.M1	L.PMC-L.M1	L.Thal-L.PMC	L.PMC-L.M1
3			R.PMC-R.M1		R.SMA-R.M1	R.SMA-R.PMC	L.Thal-L.M1	R.Thal-R.PMC
4			R.PMC-L.PMC			R.SMA-R.M1	R.Thal-L.SMA	L.SMA-L.M1
5			L.SMA-L.M1			L.SMA-R.M1		
Outcomes at T7 and Input Δrs-FC Features at T6								
1	L.SMA-L.PMC	R.PMC-R.M1	R.Thal-R.SMA	R.SMA-R.M1	L.Thal-R.SMA	R.SMA-L.SMA	L.Thal-L.M1	L.SMA-L.M1
2	L.SMA-R.PMC	R.PMC-L.PMC	L.Thal-R.SMA	R.Thal-R.M1	L.Thal-R.M1	L.PMC-R.M1	L.Thal-L.SMA	L.Thal-L.M1
3	R.M1-L.M1	L.SMA-R.PMC	R.SMA-R.PMC	R.PMC-L.M1	R.Thal-R.PMC	R.SMA-R.M1	R.Thal-L.PMC	L.SMA-L.PMC
4	R.SMA-L.M1	R.SMA-L.PMC	R.SMA-R.M1		L.SMA-L.M1	R.Thal-L.PMC	L.Thal-R.PMC	L.Thal-R.PMC
5		L.Thal-L.M1	R.PMC-L.PMC		R.PMC-L.M1	R.SMA-R.PMC	R.Thal-R.SMA	L.Thal-L.SMA
6		L.Thal-L.SMA	L.SMA-L.PMC		L.Thal-L.M1	L.PMC-L.M1	R.PMC-R.M1	L.PMC-L.M1
7			L.Thal-L.PMC					
8			L.PMC-R.M1					
(B) WITH CLINICAL VARIABLES								
Outcome at T6 and Input Δrs-FC at T4 + Clinical Features								
1	R.Thal-R.SMA	NIHSS	L.SMA-R.PMC	R.Thal-L.M1	L.SMA-R.M1	R.PMC-L.M1	NIHSS	R.PMC-L.M1
2	Gender	R.Thal-L.PMC	L.Thal-R.PMC	L.Thal-R.M1	L.SMA-L.M1	R.Thal-L.PMC	Motor Imp.	R.Thal-L.SMA
3	R.SMA-L.M1	L.SMA-R.PMC	TSS	R.PMC-R.M1	R.SMA-L.SMA	R.SMA-L.M1	L.SMA-R.PMC	R.Thal-R.SMA
4	R.Thal-R.M1		R.M1-L.M1	L.SMA-R.M1	L.Thal-R.M1		R.Thal-L.PMC	L.Thal-R.M1
5	R.Thal-L.PMC						Lesion Hemi	R.SMA-L.PMC
6							R.Thal-L.SMA	
7							L.SMA-L.PMC	
8							L.SMA-L.M1	
9							R.Thal-R.SMA	
10							R.PMC-R.M1	
11							L.SMA-R.M1	
12							R.M1-L.M1	
13							R.SMA-R.M1	
14							L.Thal-L.M1	
15							R.PMC-L.M1	
16							TSS	
Outcome at T7 and Input Δrs-FC at T4 + Clinical Features								
1	R.Thal-L.SMA	R.SMA-R.PMC	Motor Imp.	R.Thal-R.M1	R.SMA-L.M1	L.PMC-L.M1	L.Thal-L.PMC	R.Thal-L.M1
2	NIHSS	R.Thal-R.M1	R.Thal-R.M1	Age	R.Thal-L.PMC	L.Thal-R.PMC	NIHSS	L.PMC-L.M1
3	R.Thal-R.PMC	Lesion Hemi	L.SMA-R.PMC	L.Thal-L.M1	R.PMC-L.M1	R.SMA-R.M1	R.SMA-L.M1	R.Thal-R.PMC
4			R.SMA-L.M1	R.Thal-L.SMA	Lesion Hemi	L.Thal-L.M1	R.Thal-R.SMA	L.Thal-R.PMC
5			R.SMA-R.PMC	L.Thal-L.PMC		R.M1-L.M1	R.Thal-L.M1	R.SMA-L.M1
6				Motor Imp.		R.Thal-L.PMC	L.Thal-R.PMC	
7				L.Thal-R.SMA		NIHSS	L.PMC-R.M1	
8							L.SMA-L.PMC	

(Continued)

TABLE 7 | Continued

Rank	Δ9HPT(A)	Δ9HPT(U)	ΔSIS(ADL)	ΔSIS(Mob)	ΔSIS(PS)	ΔBI	ΔARAT(A)	ΔSIS(HF)
Outcome at T7 and Input Δrs-FC at T6 + Clinical Features								
1	R.Thal-R.SMA	R.PMC-R.M1	L.SMA-L.PMC	R.SMA-R.M1	L.SMA-R.M1	R.SMA-L.SMA	L.Thal-L.SMA	L.SMA-L.M1
2	L.PMC-L.M1	L.SMA-R.PMC	R.SMA-R.M1	R.Thal-R.M1	Lesion Hemi	L.PMC-R.M1	L.Thal-L.PMC	L.Thal-L.M1
3	R.PMC-L.PMC	R.SMA-L.PMC	L.SMA-R.M1	Motor Imp.	R.SMA-L.PMC	L.Thal-L.PMC	L.Thal-L.M1	R.SMA-R.PMC
4			L.Thal-L.PMC	R.Thal-L.Thal	R.Thal-L.Thal	R.Thal-L.PMC	R.SMA-R.PMC	R.Thal-L.Thal
5				R.PMC-L.M1	L.Thal-R.PMC	R.SMA-L.M1	Age	
6					L.SMA-L.M1	R.Thal-L.SMA	TSS	
7					L.PMC-L.M1	R.Thal-R.PMC	L.PMC-R.M1	
8					NIHSS	L.Thal-R.M1	L.SMA-L.M1	
9							R.Thal-L.Thal	
10							R.M1-L.M1	
11							L.PMC-L.M1	
12							Gender	
13							L.Thal-R.SMA	
14							NIHSS	
15							L.Thal-R.PMC	
16							L.Thal-R.M1	

TABLE 8 | Linear-kernel SVR performances based on leave-one out cross-validation to correlate behavioral measures at preceding time-point and clinical variables with behavioral measures at succeeding time-point are presented.

Outcome	T4 behavior∼T6 behavior			T4 behavior∼T7 behavior			T6 behavior∼T7 behavior		
	Features	RMSE	R^2	Features	RMSE	R^2	Features	RMSE	R^2
9HPT(A)	2	2.52*	0.74	1	3.28*	0.52	3	3.25*	0.53
9HPT(U)	4	37.36*	0.91	5	23.4*	0.97	5	9.05*	0.99
ARAT(A)	3	2.73*	0.99	3	3.31*	0.98	3	3.13*	0.98
BI	1	5.48*	0.62	2	5.19*	0.54	3	4.83*	0.6
SIS(ADL)	3	8.56*	0.54	3	10.24*	0.54	3	11.42*	0.43
SIS(HF)	4	12.74*	0.86	4	13.03*	0.85	4	7.9*	0.94
SIS(Mob)	4	5.36*	0.71	2	11.8*	0.28	3	10.09*	0.47
SIS(PS)	2	14.7*	0.49	2	12.03*	0.46	3	8.85*	0.71

*Specific correlates are listed in **Table 9**. (*) = significant against chance-level based on permutation-test ($p < 0.05$); T4 = pre-therapy; T6 = post-therapy; T7 = 1-month post-therapy.*

areas with rs-fMRI within the motor network (Biswal et al., 1995), it allows us to draw parallels between our study and those based on task-fMRI. Additionally, thalamic Δrs-FC also emerged as a region with strong involvement in estimating changes in ARAT(A) and SIS(HF), which was demonstrated using task-fMRI activation associated with the same outcomes in our precedent study (Young et al., 2014b). Another task-fMRI-based study by Ward et al. (2003b) also reported thalamic correlations with motor recovery especially in stroke subjects (time since stroke onset > 3 months) with MCA lesions. It could be possible that our findings are similar as half of the subjects included in our study exhibited MCA lesions as well. From data modeling perspective, while traditional methods such as general linear models assume a certain distribution of data, SVR offers a non-parametric method that can model both linear and non-linear relationships in the data and adds to the growing body of studies using machine learning prediction models to analyze fMRI (Di Bono and Zorzi, 2008; Dosenbach et al., 2010; Vergun et al., 2013).

Limitations

This study highlights how machine learning holds potential to provide useful information by correlating neuroimaging changes to behavioral changes. However, the results can be limited by the sample size that can, in turn, affect the capability of drawing generalizable conclusions as machine learning models such as SVR are typically based on training on data from a much larger cohort. Involvement of NIHSS stroke severity as a feature across multiple outcomes could suggest that lesion size and/or volume might be an important consideration (Chen et al., 2000; Shelton and Reding, 2001) and should be included in future analysis. Feature selection, realized by SFS, was important in deciding the role of relevant correlates of each behavioral scale. However, SFS suffers from the drawback that it cannot remove features from

TABLE 9 | List of behavioral and clinical correlates at preceding time-points using linear-kernel SVR for estimation of measures at succeeding time-points are presented below.

Rank	9HPT(A)	9HPT(U)	ARAT(A)	SIS(ADL)	SIS(HF)	SIS(Mob)	SIS(PS)	BI
Outcome at T6 and Input Behavior at T4 + Clinical Variables								
1	9HPT(A)	9HPT(U)	Motor Imp.	SIS(ADL)	SIS(HF)	SIS(Mob)	SIS(PS)	BI
2	NIHSS	Motor Imp.	ARAT(A)	Lesion Hemi	NIHSS	NIHSS	NIHSS	
3		NIHSS	NIHSS	NIHSS	TSS	TSS		
4		Lesion Hemi			Motor Imp.	Lesion Hemi		
Outcome at T7 and Input Behavior at T4 + Clinical Variables								
1	9HPT(A)	9HPT(U)	ARAT(A)	SIS(ADL)	SIS(HF)	SIS(Mob)	SIS(PS)	BI
2		NIHSS	Motor Imp.	Motor Imp.	NIHSS	Motor Imp.	Motor Imp.	TSS
3		Motor Imp.	NIHSS	TSS	TSS			
4		Lesion Hemi			Motor Imp.			
5		TSS						
Outcomes at T7 and Input Behavior at T6 + Clinical Variables								
1	9HPT(A)	9HPT(U)	ARAT(A)	SIS(ADL)	SIS(HF)	SIS(Mob)	SIS(PS)	BI
2	TSS	Lesion Hemi	Motor Imp.	Motor Imp.	Motor Imp.	Motor Imp.	Age	TSS
3	Motor Imp	Motor Imp.	NIHSS	TSS	NIHSS	NIHSS	Motor Imp.	Motor Imp.
4		TSS			TSS			
5		NIHSS						

T4 = pre-therapy; T6 = post-therapy; T7 = 1-month post-therapy.

the model that become obsolete upon addition of new features. Recent work suggested that rs-FC can be quantified in several ways using metrics such as cosine similarity and dynamic time warping (Smith et al., 2011). Thus, the choice of metric used for rs-FC might affect the features selected for each outcome.

Future Scope

With ongoing recruitment, a larger and more generalizable prediction model could be developed by considering the following. The complete BCI-aided intervention involved both imaging as well as behavioral data at multiple distinct time points, of which only pre-, post- and 1-month post-intervention data have been used in the current analysis. With a larger sample size, the analysis, therefore, could be expanded further by considering the changes in rs-FC over other time-points and correlating them with corresponding behavioral outcomes and changes. Since recovery is a multi-faceted process, other imaging methods, such as diffusion tensor images, structural images, and perfusion images can provide complementary information about brain changes and could be incorporated as features to SVR. Potentially, multiple of these neuroimaging methods could be combined so as to assess the relative importance of each as a biomarker of stroke recovery through the BCI-intervention. Correlation and interaction among the different behavioral measures could be simultaneously accounted for by implementing a multiple-output SVR that uses a single model to predict multiple outcomes. Additionally, differences and similarities among predictors between stroke subjects and matched healthy subjects undergoing the BCI-intervention will help to further understand the impact of this intervention.

CONCLUSION

We showed that rs-FC, changes in rs-FC and early-stage behavior can estimate behavioral outcomes and changes in chronic-stage stroke subjects following this BCI-aided intervention for rehabilitation. Machine learning-based SVR models helped to identify specific correlates of for objective as well as subjective behavioral scales. Among the neural substrates identified, important regions contributing to the estimation involved the left and right primary motor areas. Linear and non-linear kernels for SVR indicated similar results with non-linear SVR being slightly more accurate in estimating the outcomes and forming more generalizable models. The results, however, were more interpretable using the linear-kernel models. For further research, the kernel for SVR must be chosen based on the trade-off between lower error rates and interpretability. Given the promise of this kind of BCI intervention in stroke rehabilitation, the coupling of machine learning with neuroimaging and behavioral measures can aid further identification of neuroplastic changes corresponding to behavioral outcomes to estimate and track stroke recovery, both in terms of neural reorganization and improvements to motor function.

DATA AVAILABILITY STATEMENT

The raw data supporting the conclusions of this manuscript will be made available by the authors, without undue reservation, to any qualified researcher.

AUTHOR CONTRIBUTIONS

RM was involved in data collection, analysis, interpretation of results and writing of the manuscript. AS was involved in

data collection, preprocessing data and writing the manuscript. BY was involved in subject recruitment, data collection and editing of the manuscript. AR, KD, TJ, MM, JT, and HA were involved in data collection. VN contributed to data collection, manuscript editing and intellectual content. TK was involved in the recruitment of study participants. KC was involved in subject recruitment. DE is the co-I and JW, VP are co-PIs and were involved in study conception, design, manuscript editing, intellectual content and supervised all aspects of the study.

FUNDING

This work was supported by NIH grants RC1MH090912-01, T32GM008692, UL1TR000427, K23NS086852, T32EB011434, R01EB000856-06, and R01EB009103-01 and by the DARPA RCI Program (MTO) N66001-12-C-4025 and HIST Program (MTO) N66001-11-1-4013. Additional funding was also provided through a Coulter Translational Research Award, the AHA Grant 1T32EB011434-01A1, AHA Innovative Research Award–National (Marcus Foundation) 15IRG22760009, AHA Midwest Grant in Aid Award 15GRNT25780033, the Foundation of ASNR, UW Milwaukee-Madison Intercampus Grants, the UW Graduate School, and by Shapiro Foundation Grants.

ACKNOWLEDGMENTS

The authors would like to thank all the study subjects and their families for participating in the study and all the MR technologists for their support in collection of data. The authors would also like to extend thanks to Dr. Justin Sattin for referrals of stroke subjects and clinical documentation. The authors would like to acknowledge that parts of this manuscript were presented in the form of a platform talk at the International Stroke Conference 2015 and as a poster at the International Stroke Conference 2018.

SUPPLEMENTARY MATERIAL

The Supplementary Material for this article can be found online at: https://www.frontiersin.org/articles/10.3389/fnins.2018.00624/full#supplementary-material

REFERENCES

Bajaj, S., Butler, A. J., Drake, D., and Dhamala, M. (2015). Functional organization and restoration of the brain motor-execution network after stroke and rehabilitation. *Front. Hum. Neurosci.* 9:173. doi: 10.3389/fnhum.2015.00173

Bhagat, N. A., Venkatakrishnan, A., Abibullaev, B., Artz, E. J., Yozbatiran, N., Blank, A. A., et al. (2016). Design and optimization of an EEG-based brain machine interface (BMI) to an upper-limb exoskeleton for stroke survivors. *Front. Neurosci.* 10:122. doi: 10.3389/fnins.2016.00122

Biasiucci, A., Leeb, R., Iturrate, I., Perdikis, S., Al-Khodairy, A., Corbet, T., et al. (2018). Brain-actuated functional electrical stimulation elicits lasting arm motor recovery after stroke. *Nat. Commun.* 9:2421. doi: 10.1038/s41467-018-04673-z

Biswal, B., Yetkin, Z. F., Haughton, V. M., and Hyde, J. S. (1995). Functional connectivity in the motor cortex of resting human brain using echo-planar mri. *Magn. Reson. Med.* 34, 537–541. doi: 10.1002/mrm.1910340409

Brott, T., Adams, H. P., Olinger, C. P., Marler, J. R., Barsan, W. G., Biller, J., et al. (1989). Measurements of acute cerebral infarction: a clinical examination scale. *Stroke* 20, 864–870. doi: 10.1161/01.STR.20.7.864

Bull, A. D. (2011). Convergence rates of efficient global optimization algorithms. *J. Machine Learn. Res.* 12, 2879–2904.

Burges, C. J. (1998). A tutorial on support vector machines for pattern recognition. *Data Mining Knowledge Disc.* 2, 121–167. doi: 10.1023/A:1009715923555

Caria, A., Weber, C., Brötz, D., Ramos, A., Ticini, L. F., Gharabaghi, A., et al. (2011). Chronic stroke recovery after combined BCI training and physiotherapy: a case report. *Psychophysiology* 48, 578–582. doi: 10.1111/j.1469-8986.2010.01117.x

Carod-Artal, F. J., Coral, L. F., Trizotto, D. S., and Moreira, C. M. (2008). The stroke impact scale 3.0. *Stroke* 39, 2477–2484. doi: 10.1161/STROKEAHA.107.513671

Carroll, D. (1965). A quantitative test of upper extremity function. *J. Chronic Dis.* 18, 479–491. doi: 10.1016/0021-9681(65)90030-5

Chen, C. L., and Tang, F. T., Chen, H. C., Chung, C. Y., Wong, M. K. (2000). Brain lesion size and location: effects on motor recovery and functional outcome in stroke patients. *Arch. Phys. Med. Rehabil.* 81, 447–452. doi: 10.1053/mr.2000.3837

Chen, H. M., Chen, C. C., Hsueh, I. P., Huang, S. L., and Hsieh, C. L. (2009). Test-retest reproducibility and smallest real difference of 5 hand function tests in patients with stroke. *Neurorehabil. Neural Repair* 23, 435–40. doi: 10.1177/1545968308331146

Cox, R. W. (1996). AFNI: software for analysis and visualization of functional magnetic resonance neuroimages. *Comput. Biomed. Res.* 29, 162–173. doi: 10.1006/cbmr.1996.0014

Crinion, J., Ashburner, J., Leff, A., Brett, M., Price, C., and Friston, K. (2007). Spatial normalization of lesioned brains: performance evaluation and impact on fMRI analyses. *Neuroimage* 37, 866–875. doi: 10.1016/j.neuroimage.2007.04.065

Dai, Z., Yan, C., Wang, Z., Wang, J., Xia, M., Li, K., et al. (2012). Discriminative analysis of early Alzheimer's disease using multi-modal imaging and multi-level characterization with multi-classifier (M3). *Neuroimage* 59, 2187–2195. doi: 10.1016/j.neuroimage.2011.10.003

Debaere, F., Swinnen, S. P., Béatse, E., Sunaert, S., Van Hecke, P., and Duysens, J. (2001). Brain areas involved in interlimb coordination: a distributed network. *Neuroimage* 14, 947–958. doi: 10.1006/nimg.2001.0892

Di Bono, M. G., and Zorzi, M. (2008). Decoding cognitive states from fMRI data using support vector regression. *PsychNol. J.* 6, 189–201.

Ding, X., Yang, Y., Stein, E. A., and Ross, T. J. (2017). Combining multiple resting-state fMRI features during classification: optimized frameworks and their application to nicotine addiction. *Front. Hum. Neurosci.* 11:362. doi: 10.3389/fnhum.2017.00362

Dosenbach, N. U., Nardos, B., Cohen, A. L., Fair, D. A., Power, J. D., Church, J. A., et al. (2010). Prediction of individual brain maturity using fMRI. *Science* 329, 1358–1361. doi: 10.1126/science.1194144

Duncan, P. W., Wallace, D., Lai, S. M., Johnson, D., Embretson, S., and Laster, L. J. (1999). The stroke impact scale version 2.0. *Stroke* 30, 2131–2140. doi: 10.1161/01.STR.30.10.2131

Fasoli, S. E., Krebs, H. I., Stein, J., Frontera, W. R., and Hogan, N. (2003). Effects of robotic therapy on motor impairment and recovery in chronic stroke. *Arch. Phys. Med. Rehabil.* 84, 477–482. doi: 10.1053/apmr.2003.50110

Felton, E. A., Radwin, R. G., Wilson, J. A., and Williams, J. C. (2009). Evaluation of a modified Fitts law brain–computer interface target acquisition task in able and motor disabled individuals. *J. Neural Eng.* 6:056002. doi: 10.1088/1741-2560/6/5/056002

Fergus, P., Hussain, A., Hignett, D., Al-Jumeily, D., Abdel-Aziz, K., and Hamdan, H. (2016). A machine learning system for automated whole-brain seizure detection. *Appl. Comput. Informatics* 12, 70–89. doi: 10.1016/j.aci.2015.01.001

Ferraro, M., Palazzolo, J. J., Krol, J., Krebs, H. I., Hogan, N., and Volpe, B. T. (2003). Robot-aided sensorimotor arm training improves outcome in patients with chronic stroke. *Neurology* 61, 1604–1607. doi: 10.1212/01.WNL.0000095963.00970.68

Frank, E., Trigg, L., Holmes, G., and Witten, I. H. (2000). Naive bayes for regression. *Machine Learn.* 41, 5–25. doi: 10.1023/A:1007670802811

Ganesh, G., Burdet, E., Haruno, M., and Kawato, M. (2008). Sparse linear regression for reconstructing muscle activity from human cortical fMRI. *Neuroimage* 42, 1463–1472. doi: 10.1016/j.neuroimage.2008.06.018

Gelbart, M. A., Snoek, J., and Adams, R. P. (2014). *Bayesian Optimization With Unknown Constraints*. arXiv *[preprint]:*1403.5607.

Grefkes, C., Eickhoff, S. B., Nowak, D. A., Dafotakis, M., and Fink, G. R. (2008). Dynamic intra-and interhemispheric interactions during unilateral and bilateral hand movements assessed with fMRI and DCM. *Neuroimage* 41, 1382–1394. doi: 10.1016/j.neuroimage.2008.03.048

Grefkes, C., and Fink, G. R. (2011). Reorganization of cerebral networks after stroke: new insights from neuroimaging with connectivity approaches. *Brain* 134, 1264–1276. doi: 10.1093/brain/awr033

Hastie, T., and Tibshirani, R. (1996). "Discriminant adaptive nearest neighbor classification and regression, in *Advances in Neural Information Processing Systems*, (Denver, CO), 409–415.

Hastie, T., Tibshirani, R., and Friedman, J. (2001).*The Elements of Statistical Learning*. New York, NY: Springer.

He, L., Hu, Y., Li, Y., and Li, D. (2013). Channel selection by Rayleigh coefficient maximization based genetic algorithm for classifying single-trial motor imagery EEG. *Neurocomputing* 121, 423–433. doi: 10.1016/j.neucom.2013.05.005

Johansen-Berg, H., Dawes, H., Guy, C., Smith, S. M., Wade, D. T., and Matthews, P. M. (2002). Correlation between motor improvements and altered fMRI activity after rehabilitative therapy. *Brain* 125, 2731–2742. doi: 10.1093/brain/awf282

Kelly-Hayes, M., Beiser, A., Kase, C. S., Scaramucci, A., D'Agostino, R. B., and Wolf, P. A. (2003). The influence of gender and age on disability following ischemic stroke: the Framingham study. *J. Stroke Cerebrovasc. Dis.* 12, 119–126. doi: 10.1016/S1052-3057(03)00042-9

Khazaee, A., Ebrahimzadeh, A., and Babajani-Feremi, A. (2016). Application of advanced machine learning methods on resting-state fMRI network for identification of mild cognitive impairment and Alzheimer's disease. *Brain Imag. Behav.* 10, 799–817. doi: 10.1007/s11682-015-9448-7

Kübler, A., Neumann, N., Kaiser, J., Kotchoubey, B., Hinterberger, T., and Birbaumer, N. P. (2001). Brain-computer communication: self-regulation of slow cortical potentials for verbal communication. *Arch. Phys. Med. Rehabil.* 82, 1533–1539. doi: 10.1053/apmr.2001.26621

Kübler, A., Nijboer, F., Mellinger, J., Vaughan, T. M., Pawelzik, H., Schalk, G., et al. (2005). Patients with ALS can use sensorimotor rhythms to operate a brain-computer interface. *Neurology* 64, 1775–1777. doi: 10.1212/01.WNL.0000158616.43002.6D

Kwakkel, G., Kollen, B. J., and Krebs, H. I. (2008). Effects of robot-assisted therapy on upper limb recovery after stroke: a systematic review. *Neurorehabil. Neural Rep.* 22, 111–121. doi: 10.1177/1545968307305457

Lang, C. E., Wagner, J. M., Dromerick, A. W., and Edwards, D. F. (2006). Measurement of upper-extremity function early after stroke: properties of the action research arm test. *Arch. Phys. Med. Rehabil.* 87, 1605–1610. doi: 10.1016/j.apmr.2006.09.003

Lee, M. H., Smyser, C. D., and Shimony, J. S. (2013). Resting-state fMRI: a review of methods and clinical applications. *Am. J. Neuroradiol.* 34, 1866–1872. doi: 10.3174/ajnr.A3263

Levy, C. E., Nichols, D. S., Schmalbrock, P. M., and Keller, Chakeres, D. W. (2001). Functional MRI evidence of cortical reorganization in upper-limb stroke hemiplegia treated with constraint-induced movement therapy. *Am. J. Phys. Med. Rehabil.* 80, 4–12. doi: 10.1097/00002060-200101000-00003

Lu, J., Mamun, K. A., and Chau, T. (2015). Pattern classification to optimize the performance of Transcranial Doppler Ultrasonography-based brain machine interface. *Pattern Recogn. Lett.* 66, 135–143. doi: 10.1016/j.patrec.2015.07.020

Mahoney, R. (1965). *Barthel Index (BI). Surya Shah, PhD, OTD, MEd, OTR, FAOTA, Professor Occupational Therapy and Neurology, Visiting Professor Neurorehabilitation. University of Tennessee Health Sciences Center* 930:1.

Marquand, A., Howard, M., Brammer, M., Chu, C., Coen, S., and Mourão-Miranda, J. (2010). Quantitative prediction of subjective pain intensity from whole-brain fMRI data using Gaussian processes. *Neuroimage* 49, 2178–2189. doi: 10.1016/j.neuroimage.2009.10.072

Meier, T. B., Desphande, A. S., Vergun, S., Nair, V. A., Song, J., Biswal, B. B., et al. (2012). Support vector machine classification and characterization of age-related reorganization of functional brain networks. *Neuroimage* 60, 601–613. doi: 10.1016/j.neuroimage.2011.12.052

Michel, V., Gramfort, A., Varoquaux, G., Eger, E., and Thirion, B. (2011). Total variation regularization for fMRI-based prediction of behavior. *IEEE Trans. Med. Imag.* 30, 1328–1340. doi: 10.1109/TMI.2011.2113378

Mohanty, R., Sinha, A., Remsik, A., Allen, J., Nair, V., Caldera, K., et al. (2017). "Machine learning-based prediction of changes in behavioral outcomes using functional connectivity and clinical measures in brain-computer interface stroke rehabilitation," in *International Conference on Augmented Cognition* (Vancouver, BC: Springer), 543–557.

Mohanty, R., Sinha, A. M., Remsik, A. B., Dodd, K. C., Young, B. M., Jacobson, T., et al. (2018). Machine learning classification to identify the stage of brain-computer interface therapy for stroke rehabilitation using functional connectivity. *Front. Neurosci.* 12:353. doi: 10.3389/fnins.2018.00353

Murphy, K., and Fox, M. D. (2016). Towards a consensus regarding global signal regression for resting state functional connectivity MRI. *Neuroimage* 154, 169–173. doi: 10.1016/j.neuroimage.2016.11.052

Nair, V. A., Young, B. M., Nigogosyan, Z., Remsick, A., Weber, S., Diffee, K., et al. (2015). "Resting-state functional connectivity changes after stroke rehabilitation using closed loop neurofeedback." in *International Stroke Conference from February 11 – 13, 2015*, Vol. 46 (Nashville, TN). doi: 10.1161/str.46.suppl_1.6

Oldfield, R. C. (1971). The assessment and analysis of handedness: the Edinburgh inventory. *Neuropsychologia* 9, 97–113. doi: 10.1016/0028-3932(71)90067-4

Pereira, S., Pinto, A., Alves, V., and Silva, C. A. (2016). Brain tumor segmentation using convolutional neural networks in MRI images. *IEEE Trans. Medical Imag.* 35, 1240–1251. doi: 10.1109/TMI.2016.2538465

Rehme, A. K., Eickhoff, S. B., Rottschy, C., Fink, G. R., and Grefkes, C. (2012). Activation likelihood estimation meta-analysis of motor-related neural activity after stroke. *Neuroimage* 59, 2771–2782. doi: 10.1016/j.neuroimage.2011.10.023

Rehme, A. K., Volz, L. J., Feis, D. L., Bomilcar-Focke, I., Liebig, T., Eickhoff, S. B., et al. (2014). Identifying neuroimaging markers of motor disability in acute stroke by machine learning techniques. *Cereb. Cortex* 25, 3046–3056. doi: 10.1093/cercor/bhu100

Rossini, P. M., Calautti, C., Pauri, F., and Baron, J. C. (2003). Post-stroke plastic reorganisation in the adult brain. *Lancet Neurol.* 2, 493–502. doi: 10.1016/S1474-4422(03)00485-X

Schalk, G., McFarland, D. J., Hinterberger, T., Birbaumer, N., and Wolpaw, J. R. (2004). BCI2000: a general-purpose brain-computer interface (BCI) system. *IEEE Trans. Biomed. Eng.* 51, 1034–1043. doi: 10.1109/TBME.2004.827072

Scholkopf, B., and Smola, A. J. (2001). *Learning With Kernels: Support Vector Machines, Regularization, Optimization, and Beyond.* Cambridge, MA: MIT press.

Sharma, N., Baron, J. C., and Rowe, J. B. (2009). Motor imagery after stroke: relating outcome to motor network connectivity. *Ann. Neurol.* 66, 604–616. doi: 10.1002/ana.21810

Shelton, F. N., and Reding, M. J. (2001). Effect of lesion location on upper limb motor recovery after stroke. *Stroke* 32, 107–112. doi: 10.1161/01.STR.32.1.107

Silvoni, S., Ramos-Murguialday, A., Cavinato, M., Volpato, C., Cisotto, G., Turolla, A., et al. (2011). Brain-computer interface in stroke: a review of progress. *Clin. EEG Neurosci.* 42, 245–252. doi: 10.1177/155005941104200410

Smith, S. M., Miller, K. L., Salimi-Khorshidi, G., Webster, M., Beckmann, C. F., Nichols, T. E., et al. (2011). Network modelling methods for FMRI. *Neuroimage* 54, 875–891. doi: 10.1016/j.neuroimage.2010.08.063

Smola, A. J., and Schölkopf, B. (2004). A tutorial on support vector regression. *Stat. Comput.* 14, 199–222. doi: 10.1023/B:STCO.0000035301.49549.88

Snoek, J., Larochelle, H., and Adams, R. P. (2012). "Practical bayesian optimization of machine learning algorithms," in *Advances in Neural Information Processing Systems*, (Lake Tahoe), 2951–2959.

Soekadar, S. R., Birbaumer, N., Slutzky, M. W., and Cohen, L. G. (2015). Brain–machine interfaces in neurorehabilitation of stroke. *Neurobiol. Dis.* 83, 172–179. doi: 10.1016/j.nbd.2014.11.025

Song, J., Young, B. M., Nigogosyan, Z., Walton, L. M., Nair, V. A., Grogan, S. W., et al. (2014). Characterizing relationships of DTI, fMRI, and motor recovery in stroke rehabilitation utilizing brain-computer interface technology. *Front. Neuroeng.* 7:31. doi: 10.3389/fneng.2014.00031

Spiess, A.-N., and Neumeyer, N. (2010). An evaluation of R 2 as an inadequate measure for nonlinear models in pharmacological and biochemical research: a Monte Carlo approach. *BMC Pharmacol.* 10:6. doi: 10.1186/1471-2210-10-6

Teasell, R., Bayona, N. A., and Bitensky, J. (2005). Plasticity and reorganization of the brain post stroke. *Topics Stroke Rehabil.* 12, 11–26. doi: 10.1310/6AUM-ETYW-Q8XV-8XAC

Vapnik, V. (2013). *The Nature of Statistical Learning Theory*. New York, NY: Springer-Verlag.

Várkuti, B., Guan, C., Pan, Y., Phua, K. S., Ang, K. K., Kuah, C. W. K., et al. (2013). state changes in functional connectivity correlate with movement recovery for BCI and robot-assisted upper-extremity training after stroke. *Neurorehabil. Neural Rep.* 27, 53–62. doi: 10.1177/1545968312445910

Vergun, S., Deshpande, A. S., Meier, T. B., Song, J., Tudorascu, D. L., Nair, V. A., et al. (2013). Characterizing functional connectivity differences in aging adults using machine learning on resting state fMRI data. *Front. Comput. Neurosci.* 7:38. doi: 10.3389/fncom.2013.00038

Wang, L., Yu, C., Chen, H., Qin, W., He, Y., Fan, F., et al. (2010). Dynamic functional reorganization of the motor execution network after stroke. *Brain* 133, 1224–1238. doi: 10.1093/brain/awq043

Wang, Y. M., Schultz, R. T., Constable, R. T., and Staib, L. H. (2003). "Nonlinear estimation and modeling of fMRI data using spatio-temporal support vector regression," in *Biennial International Conference on Information Processing in Medical Imaging* (Berlin, Heidelberg: Springer), 647–659.

Ward, N. S., Brown, M. M., Thompson, A. J., and Frackowiak, R. S. (2003a). Neural correlates of motor recovery after stroke: a longitudinal fMRI study. *Brain* 126, 2476–2496. doi: 10.1093/brain/awg245

Ward, N. S., Brown, M. M., Thompson, A. J., and Frackowiak, R. S. (2003b). Neural correlates of outcome after stroke: a cross-sectional fMRI study. *Brain* 126, 1430–1448. doi: 10.1093/brain/awg145

Wilson, J. A., Schalk, G., Walton, L. M., and Williams, J. C. (2009). Using an EEG-based brain-computer interface for virtual cursor movement with BCI2000. *J. Visual. Exp.* 29:1319. doi: 10.3791/1319

Xia, M., Wang, J., and He, Y. (2013). BrainNet Viewer: a network visualization tool for human brain connectomics. *PLoS ONE* 8:e68910. doi: 10.1371/journal.pone.0068910

Young, B. M., Nigogosyan, Z., Nair, V. A., Walton, L. M., Song, J., Tyler, M. E., et al. (2014a). Case report: post-stroke interventional BCI rehabilitation in an individual with preexisting sensorineural disability. *Front. Neuroeng.* 7:18. doi: 10.3389/fneng.2014.00018

Young, B. M., Nigogosyan, Z., Remsik, A., Walton, L. M., Song, J., Nair, V. A., et al. (2014b). Changes in functional connectivity correlate with behavioral gains in stroke patients after therapy using a brain-computer interface device. *Front. Neuroeng.* 7:25. doi: 10.3389/fneng.2014.00025

Young, B. M., Nigogosyan, Z., Walton, L. M., Song, J., Nair, V. A., Grogan, S. W., et al. (2014c). Changes in functional brain organization and behavioral correlations after rehabilitative therapy using a brain-computer interface. *Front. Neuroeng.* 7:26. doi: 10.3389/fneng.2014.00026

Young, B. M., Williams, J., and Prabhakaran, V. (2014d). BCI-FES: could a new rehabilitation device hold fresh promise for stroke patients? *Expert Rev. Med. Devices* 11, 537–539. doi: 10.1586/17434440.2014.941811

Conflict of Interest Statement: The authors declare that the research was conducted in the absence of any commercial or financial relationships that could be construed as a potential conflict of interest.

Copyright © 2018 Mohanty, Sinha, Remsik, Dodd, Young, Jacobson, McMillan, Thoma, Advani, Nair, Kang, Caldera, Edwards, Williams and Prabhakaran. This is an open-access article distributed under the terms of the Creative Commons Attribution License (CC BY). The use, distribution or reproduction in other forums is permitted, provided the original author(s) and the copyright owner(s) are credited and that the original publication in this journal is cited, in accordance with accepted academic practice. No use, distribution or reproduction is permitted which does not comply with these terms.

frontiers in Neuroscience

ORIGINAL RESEARCH
published: 23 October 2018
doi: 10.3389/fnins.2018.00757

Improving Real-Time Lower Limb Motor Imagery Detection Using tDCS and an Exoskeleton

Marisol Rodríguez-Ugarte, Eduardo Iáñez, Mario Ortiz and Jose M. Azorín*

Brain-Machine Interface Systems Lab, Systems Engineering and Automation Department, Miguel Hernández University of Elche, Elche, Spain

The aim of this work was to test if a novel transcranial direct current stimulation (tDCS) montage boosts the accuracy of lower limb motor imagery (MI) detection by using a real-time brain-machine interface (BMI) based on electroencephalographic (EEG) signals. The tDCS montage designed was composed of two anodes and one cathode: one anode over the right cerebrocerebellum, the other over the motor cortex in Cz, and the cathode over FC2 (using the International 10–10 system). The BMI was designed to detect two MI states: relax and gait MI; and was based on finding the power at the frequency which attained the maximum power difference between the two mental states at each selected EEG electrode. Two different single-blind experiments were conducted, E1 and a pilot test E2. E1 was based on visual cues and feedback and E2 was based on auditory cues and a lower limb exoskeleton as feedback. Twelve subjects participated in E1, while four did so in E2. For both experiments, subjects were separated into two equally-sized groups: sham and active tDCS. The active tDCS group achieved 12.6 and 8.2% higher detection accuracy than the sham group in E1 and E2, respectively, reaching 65 and 81.6% mean detection accuracy in each experiment. The limited results suggest that the exoskeleton (E2) enhanced the detection of the MI tasks with respect to the visual feedback (E1), increasing the accuracy obtained in 16.7 and 21.2% for the active tDCS and sham groups, respectively. Thus, the small pilot study E2 indicates that using an exoskeleton in real-time has the potential of improving the rehabilitation process of cerebrovascular accident (CVA) patients, but larger studies are needed in order to further confirm this claim.

Keywords: transcranial direct current stimulation (tDCS), real-time, brain-machine interface (BMI), lower limb, exoskeleton, motor imagery (MI)

OPEN ACCESS

Edited by:
Christoph Guger, g.tec Medical Engineering GmbH, Austria

Reviewed by:
Adam Olding Hebb, Colorado Neurological Institute (CNI), United States
Xiaoli Li, Beijing Normal University, China
Enrique Hortal, Maastricht University, Netherlands

****Correspondence:***
Eduardo Iáñez
eianez@umh.es

Specialty section:
This article was submitted to Neural Technology, a section of the journal Frontiers in Neuroscience

Received: *28 February 2018*
Accepted: *01 October 2018*
Published: *23 October 2018*

Citation:
Rodríguez-Ugarte M, Iáñez E, Ortiz M and Azorín JM (2018) Improving Real-Time Lower Limb Motor Imagery Detection Using tDCS and an Exoskeleton. Front. Neurosci. 12:757. doi: 10.3389/fnins.2018.00757

1. INTRODUCTION

Transcranial direct current stimulation (tDCS) is a non-invasive brain stimulation technique based on weak direct electrical current transferred between electrodes (from anode to cathode) over the scalp in order to modulate the neural membrane resting potential (Nelson et al., 2014; Rodríguez-Ugarte et al., 2016b; Lefaucheur et al., 2017). It modifies cortical excitability in a polarity-specific manner (Coffman et al., 2014). This means that neural excitability is generated under the area of the anode because the current flow goes into the brain, whereas in the underlying cortex where the cathode is, inhibition of neural activity is produced because the current flow goes

out from the brain (Filmer et al., 2014; Wiethoff et al., 2014). Furthermore, the use of this technique implies adjusting four parameters: current density, stimulation duration, electrode size and electrode position. The vast majority of the studies focus their tDCS experiments on improving the performance of the upper limbs, the speech, or the balance; where the areas stimulated are either the motor cortex, the frontal area or the cerebellum (Monti et al., 2013; Hortal et al., 2015; Foerster et al., 2017). In these studies, the range of current density used is typically between 0.04 and 0.06 mA/cm^2 with a duration of 15 or 20 min (Marquez et al., 2013) and electrode sizes of about 35 cm^2. However, there are just few studies that center their goals in meliorating lower limb performance and therefore, much remains to be investigated. In addition, stimulation with such big electrode surface areas gives only a vague idea of the areas of the brain that are important in producing the results.

Brain machine interfaces (BMIs) are a non-invasive technique that records and decodes electroencephalographic (EEG) signals to control an external device (Barrios et al., 2017). Two of the most common EEG-based BMIs are motor imagery (MI) and motor execution (ME). MI is defined as a mentally repetitive action without any overt motor movement (Park et al., 2013). Various functional magnetic resonance imaging (fMRI) studies have demonstrated that MI and ME activate common neural networks including the primary motor cortex (M1), supplementary motor area (SMA), premotor area (PM) and cerebellum (Allali et al., 2013; Hétu et al., 2013; Sharma and Baron, 2013; Zapparoli et al., 2013). Furthermore, MI is characterized by the decrease of power in the bands θ high (6–7 Hz), μ (8–12 Hz), and β (13–35 Hz) (Reynolds et al., 2015).

The purpose of this work is to test if a novel tDCS montage boosts the accuracy of lower limb MI detection using a real-time BMI. The tDCS montage is composed by three small electrodes that focus on the lower limbs: two anodes and one cathode. One anode is located over the right cerebrocerebellum, the other one over M1 in Cz, and the cathode over FC2 (using the International 10–10 system). Many studies have researched the stimulation just over the motor cortex or the cerebellum (Boehringer et al., 2013; Sehm et al., 2013; Clancy et al., 2014; Ferrucci and Priori, 2014), but never the two areas at the same time, like in this study. The effects of the stimulation over the cerebellum are still unclear, but recent studies showed an improvement of the task performed when the anode was over the cerebellum (Hardwick and Celnik, 2014; Bradnam et al., 2015). However, the anode over the cerebellum is also believed to cause neural inhibition over the motor cortex (Galea et al., 2009; Grimaldi et al., 2016). This is why a second anode was added over Cz. This anode supplied a slightly higher current than the one over the cerebellum to counteract this effect and to excite neural activity in M1.

Abbreviations: tDCS, transcranial direct current stimulation; MI, motor imagery; ME, motor execution; BMI, brain-machine interface; EEG, electroencephalographic; fMRI, functional magnetic resonance imaging; M1, primary motor cortex; SMA, supplementary motor area; PM, premotor area; CVA, cerebrovascular accident; SVM, support vector machine.

Two single-blind studies, E1 and E2, were conducted where subjects were randomly separated into two groups: sham and active tDCS. The sham group received a fake stimulation while the active tDCS group was given 0.3 mA over Cz and 0.2 mA over the right cerebrocerebellum. A BMI based on power difference in θ, μ and β bands was designed to detect two MI tasks: relax and gait MI. Both experiments had a duration of five consecutive days (for each subject). The first one, E1, was based on visual cues and feedback. The second one, E2, was a smaller pilot test which was based on auditory cues, where subjects wore a lower limb exoskeleton as feedback. It should be noted that the combination of a real-time BMI with a lower limb exoskeleton and tDCS is quite challenging and has the strong potential of improving (via tDCS) the quality of many clinical applications that involve the real-time control of these machines. Indeed, the intention of this second setup is the later use on real-time rehabilitation therapies of cerebrovascular accident (CVA) patients with lesions on the right leg. The main output to measure the effectiveness of the experiments was the MI detection accuracy, but given the experiments' duration, the development of brain plasticity over the course of the 5 days was also analyzed. Our hypothesis was that the active tDCS group would obtain better detection accuracy results than the sham group.

2. MATERIALS AND METHODS

This work studies a novel tDCS montage with two different experimental setups regarding cues and feedback. The first one, called in this paper E1, gives visual cues and visual feedback, while the second, named E2, gives auditory cues with the feedback coming from the movement/non-movement of an exoskeleton. E2 is a smaller pilot test to check if the feedback of the exoskeleton provides an improvement of the results, so that it can possibly be used later in the rehabilitation of CVA patients.

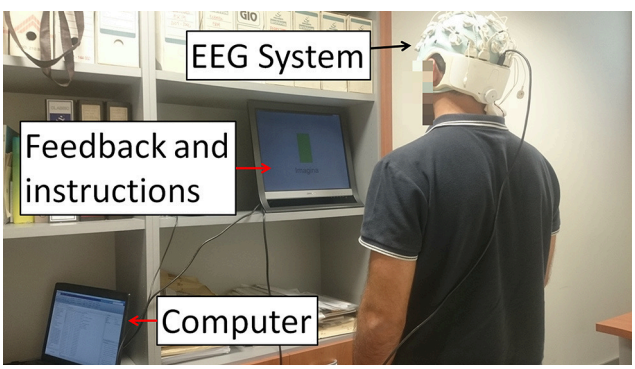

FIGURE 1 | E1 experimental setup. Subjects stood in front of a screen that supplied instructions while their EEG signals were recorded. The instructions given were: *Relax*, *Imagine* and + (transition). During *Relax*, subjects had to clear their mind as much as possible. During *Imagine*, they had to visualize they were walking. Tasks appeared at random but two tasks of the same type never appeared more than twice in a row. The + (transition) period represented a transition to separate the *Relax* and *Imagine* tasks. Written informed consent was given by the subject to publish the photo.

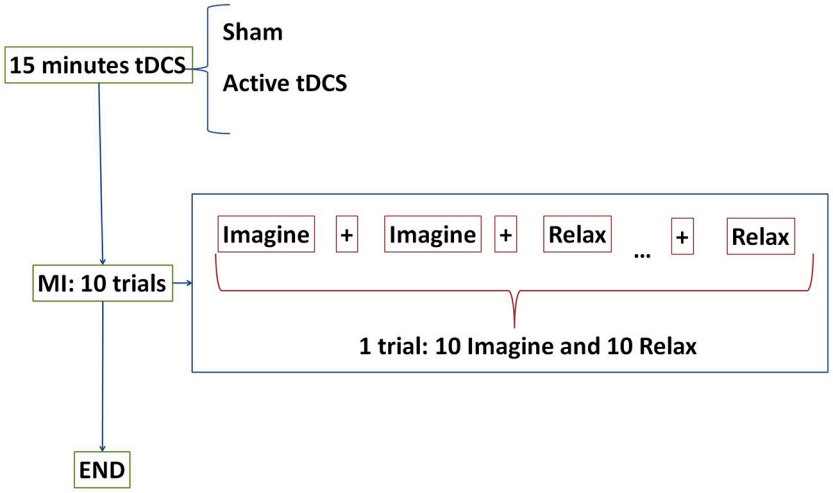

FIGURE 2 | E1 temporal sequence on each day. Subjects were randomly separated into two groups: sham or active tDCS. During 15 min participants received the corresponding stimulation according to their group. After that, subjects performed 10 trials of motor imagery (MI) tasks. The tasks were composed of *Relax* and *Imagine* tasks separated by transition periods represented by + displayed on the screen. One trial consisted of 10 *Relax* and 10 *Imagine* tasks.

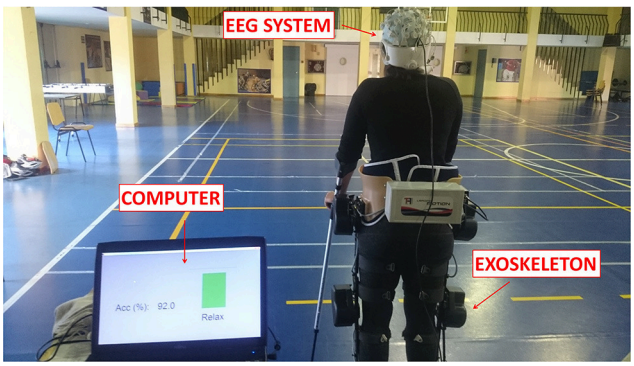

FIGURE 3 | E2 experimental setup. Subjects stood wearing an exoskeleton while their EEG signals were recorded. Once the experiment started, subjects had to relax, clearing their mind as much as possible. Then, a beep auditory signal indicated to the subject to start gait imagery until they heard a double beep auditory signal. After this second beep, subjects had to relax again until the experimental trial finished.Written informed consent was given by the subject to publish the photo.

2.1. Subjects

Twelve healthy subjects with a mean age of 26.9 ± 5.8 years old (age range 20–39) volunteered to perform E1 and four volunteers with a mean age of 25.8 ± 0.7 years old (age range 22–34) participated in E2. All of them received information prior to the experiment and gave written informed consent according to the Helsinki declaration. None of the subjects had a history of neurological and/or psychiatric diseases or was receiving medication during the experiment that could alter the central nervous system. The Ethics Committee of the Office for Project Evaluations (Oficina Evaluadora de Proyectos: OEP) of the Miguel Hernández University of Elche (Spain) approved the study.

2.2. Experimental Design

The aim of both single-blind experiments was to detect two different cognitive states: relax and gait MI, using a real-time BMI based on EEG signals. For both experiments, initially subjects were randomly separated into sham or active tDCS groups of the same size (six participants in each group of E1 and two participants in each group of E2). For five consecutive days (Monday to Friday), each participant was subjected to one experimental session, which initiated with a period of stimulation. The sham group received 15 min of fake stimulation, while the active tDCS group received 15 min of real stimulation (more details in section 2.3).

2.2.1. E1 Experiment

Participants performed one session each day for five consecutive days. One session was composed of the initial stimulation, followed by 10 MI trials. For each trial, subjects stood in front of a screen that provided instructions while their EEG signals were being recorded (**Figure 1**). Three types of instructions were supplied: *Relax*, *Imagine* and + (transition). During *Relax* periods, subjects had to clear their minds as much as possible; during *Imagine* periods, they had to imagine a gait movement. *Relax* and *Imagine* tasks appeared at random, but to avoid mind tiredness or getting bored, two tasks of the same type never appeared more than twice in a row. The transition periods, or + periods, separated different tasks of *Relax* or *Imagine*. *Relax* and *Imagine* lasted between 6 and 7.4 s, while the + (transition) periods lasted 3 s. Subjects were instructed to avoid blinking, swallowing, performing head movements or any other kind of artifact during the *Relax* and *Imagine* periods, postponing these actions to the + (transition) periods. Each trial consisted of 10 Relax and 10 Imagine periods. **Figure 2** represents the temporal sequence of this experiment.

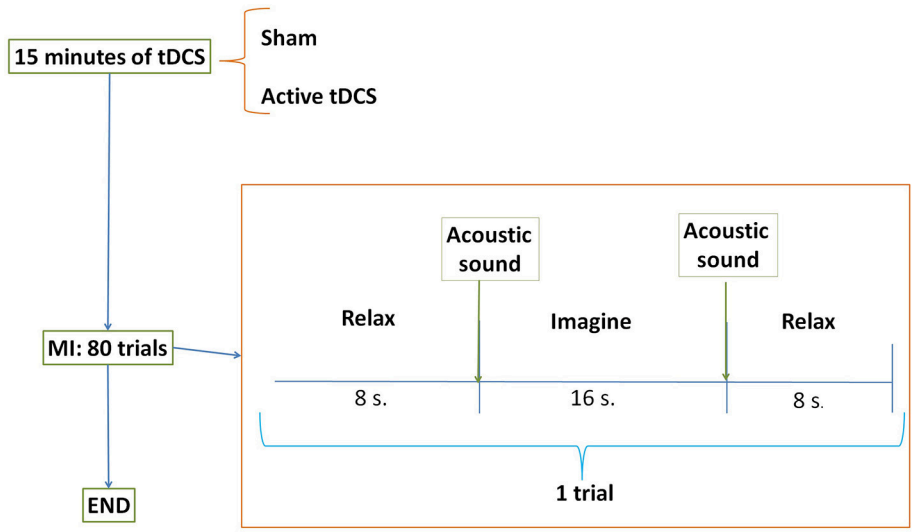

FIGURE 4 | E2 temporal sequence on each day. Subjects were randomly separated into two groups: sham or active tDCS. During 15 min participants received the corresponding stimulation according to their group. After that, subjects performed 80 trials of motor imagery (MI) tasks. The trial was composed of two relax periods separated by one task of gait imagination.

2.2.2. E2 Experiment

On the very first day, before any stimulation protocols, subjects were familiarized with the lower limb exoskeleton. They were mounted in the exoskeleton, and the exoskeleton was activated. Through verbal cues, the subjects were instructed to imagine gait until they felt comfortable that they were not trying to execute the motor task, but rather were imagining it. This pre-training phase was intended to remove any strong noise associated to the subjects trying to solely execute the movement later in the experiment.

Participants performed one session each day for five consecutive days. Throughout each session subjects stood wearing a lower limb exoskeleton while their EEG signals were recorded, as shown in **Figure 3**. One session was composed of the initial stimulation, followed by 80 MI trials. Each trial lasted around 35 s and was comprised of: an initial relax period where they had to clear their mind as much as possible; then, a beep auditory signal which indicated the subject to start the gait (walking) imagination until they heard a double beep auditory signal; after this, they had to relax again until the experiment finished. Therefore, there were two *Relax* periods which lasted 8 s each, separated by a longer *Imagine* period that lasted 16 s. A couple of seconds were needed to establish the connection between the BMI and the exoskeleton. **Figure 4** represents the temporal sequence of this experiment.

In this experiment, the first 40 trials were used to train the BMI and the rest to test it. During the training, the exoskeleton moved by itself during the gait imagery period in order to provide the subjects with a more realistic feeling. Then, during the remaining 40 trials, the exoskeleton was turned off during the *Relax* periods and was activated according to the subject's EEG signals (i.e., using the BMI output) during the *Imagine* periods. The subjects were supposed to imagine the motor task instead of trying to execute it. More details on the BMI can be found in section 2.5.

2.3. Supply of tDCS

As previously mentioned, the idea was to excite simultaneously the right cerebrocerebellum and the motor cortex because both areas are involved in motor imagery. To do that, one anode was located over the right cerebrocerebellum (two centimeters right and one centimeter down of the inion) and the other one over Cz on M1. The cathode was placed over FC2 (right hemisphere). **Figure 5** shows a scheme of the position and placement of the electrodes. The cathode produces neural inhibition, meaning that the left hemisphere is being favored. This is because, in the future, the idea is to focus on patients that have suffered a CVA over the left hemisphere, which in turn affects their right lower limb.

The intensity was established to 0.2 and 0.3 mA for the cerebrocerebellum and Cz anodes, respectively. These intensities were chosen because anodal tDCS over the right cerebrocerebellum produces inhibition over the brain motor area (Angulo-Sherman et al., 2017), so to counteract this effect and excite the motor area, the second anode was placed over Cz with a slightly higher current. Using this configuration resulted in a cathode current density of 0.16 mA/cm^2, which is higher than that used in most studies (about 0.06 mA/cm^2). Having said that, this current density is well within the range of neurological safety that avoids brain damage (Bikson et al., 2016).

In order to corroborate that the areas of interest in the brain (motor area, right cerebrocerebellum, thalamus, contralateral hemisphere, red nucleus) were involved during the stimulation, an electric field simulation was carried out first. SimNIBS free platform (Thielscher et al., 2015) was used for the simulation. The parameters of the electrodes were set according to the

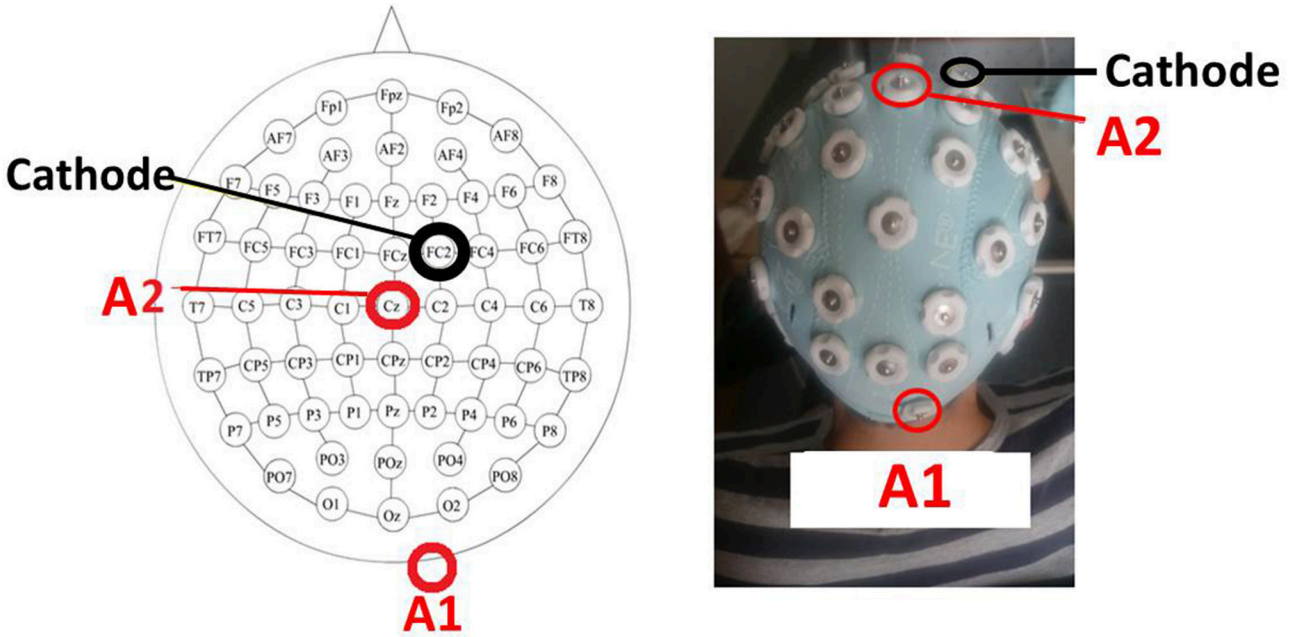

FIGURE 5 | The tDCS montage. Placement of tDCS electrodes as a scheme **(Left)** and experimentally **(Right)**. The first anode (A1) is over the right cerebrocerebellum (two centimeters right and one centimeter down of the inion), the second anode (A2) is over Cz, and the cathode is over FC2.

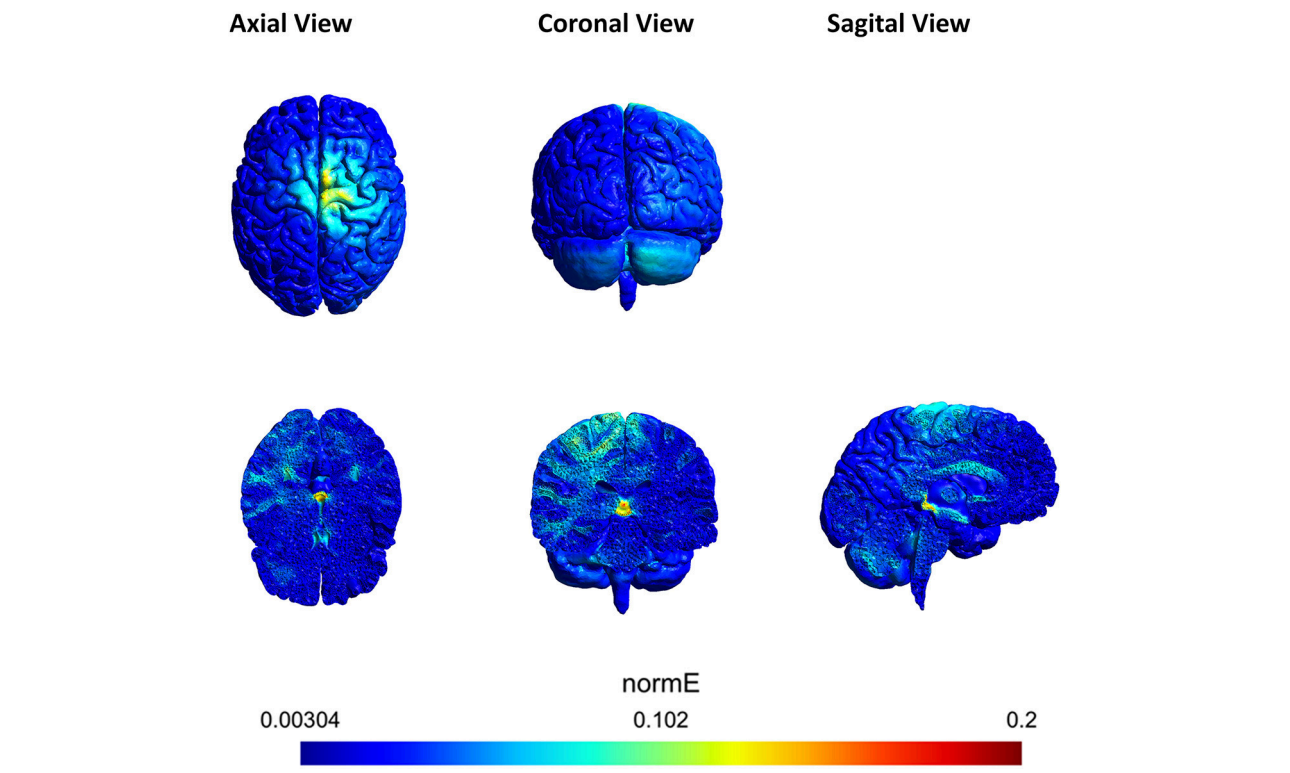

FIGURE 6 | Axial, coronal and sagittal view of the tDCS simulation using SimNIBS. The scale represents the magnitude of the electric field (V/m) induced by the anodes A1 and A2. A1 was located over the right cerebrocerebellum and A2 over Cz. The cathode was located over FC2. A1 supplied 0.2 mA and A2 0.3 mA. The most affected area (red) is close to the red nucleus.

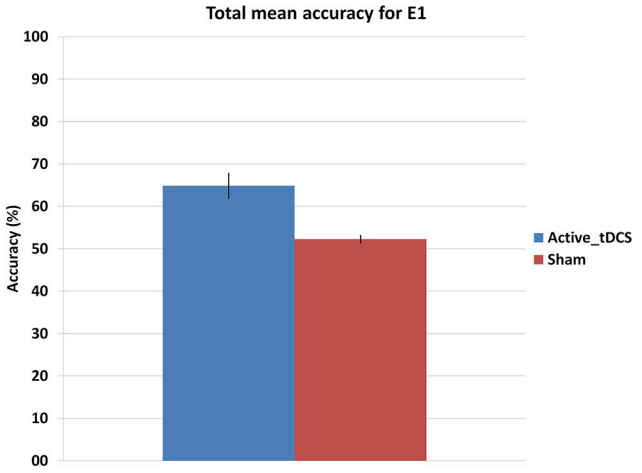

FIGURE 7 | Mean accuracy for each group in the E1 experiment. The error bars indicate a standard deviation from the mean.

TABLE 1 | Pairwise comparison of detection accuracy for each day between the tDCS and sham groups (E1).

Day	*p*-value
1	0.06
2	0.04*
3	0.04*
4	0*
5	0.02*

*The values statiscally significant were indicated with the * symbol.*

materials employed in the experiments. All the electrodes were 1 cm of radius (surface area of π cm^2), 3 mm of thickness and with 4 mm of space for the conductive gel. **Figure 6** shows the magnitude of the electric field generated by the two anodes and one cathode in axial, coronal and sagittal views. The electric field produced was analyzed and it was confirmed that the sign of the electric field was negative over the cathode (showing directionality). Furthermore, the most affected area (red) is close to the thalamus and the red nucleus. Both areas belong to the cerebellum ascending output pathways to M1 and PM (Llinas and Negrello, 2015).

At the beginning of each experimental session, the StarStim R32 (Neuroelectrics, Barcelona, Spain) supplied direct current stimulation to the subject's brain. The duration was taken to be 15 min (each of the 5 days of the experiment), since various studies which treat different diseases obtained satisfactory results applying tDCS for that duration during 5 consecutive days (Marangolo et al., 2011; Bolognini et al., 2015; Ferrucci et al., 2016). Subjects in the active tDCS group were subjected to 15 min of such stimulation, while those in the sham group received a fake stimulation to create a placebo effect. This consisted of a 3 s ramp up followed by a 3 s ramp down to zero; then, 15 min of zero current; and lastly, another repetition of 3 s ramp up and ramp down.

2.4. EEG Acquisition

The StarStim R32 (Neuroelectrics, Barcelona, Spain) was also used to acquire 30 EEG signals based on the International 10-10 system (P7, P4, CZ, PZ, P3, P8, O1, O2, C2, C4, F4, FP2, FZ, C3, F3, FP1, C1, OZ, PO4, FC6, FC2, AF4, CP6, CP2, CP1, CP5, FC1, FC5, AF3, PO3) with two reference electrodes (CMS and DRL) at a frequency of 500 Hz. The device was connected to the computer through a USB isolator.

2.5. Brain-Machine Interface (BMI)

Custom software in MATLAB (MathWorks Inc., Massachusetts, United States) was utilized for all data analysis. The first four trials of E1 and the first 40 trials of E2 were used to train a support vector machine (SVM) classifier with a radial basis function as kernel. This classifier was chosen because it was effective in previous studies and is one of the most robust classifiers (Rodríguez-Ugarte et al., 2016a). The SVM was in charge of categorizing data and determining if it belonged to relax or gait MI tasks. The remaining trials, six of E1 and 40 of E2, were utilized to test the BMI by measuring the detection accuracy, which was defined as the percentage of total correct classifications divided by the total number of classifications in each run.

Both training and test data in the two experiments were processed in very similar ways. The first 2 s of each task were discarded to assure the total concentration of the subject in the task and to get rid of the cue (visual or auditory) artifacts on the EEG. Data was processed in 1 s epochs each 0.2 s. For each epoch, the following process was carried out:

- a 4th order Butterworth high-pass filter with a cut-off frequency of 0.05 Hz was applied to remove the direct current;
- a Notch filter was used to eliminate the power line interference at 50 Hz;
- a 4th order Butterworth low-pass filter with cut-off frequency of 45 Hz was utilized;
- a Laplacian spacial filter was employed as in McFarland et al. (1997) to eliminate the influence of the other electrodes by means of weighting by their distance;
- nine electrodes from the M1, SMA and PM were selected: Cz, CP1, CP2, C1, C2, C3, C4, FC1, and FC2.

In both experiments, the training data was further analyzed. For each electrode, the power at each integer frequency from 6 to 35 Hz was calculated. This data was separated into relax and imagine groups for each frequency, and the frequency that attained the maximum power difference between relax and imagine was designated as the optimum frequency of that electrode. Finally, the power at the optimum frequency for each electrode was computed. Therefore, each epoch was associated with nine features (one for each electrode). Using the features, the SVM classifier was trained.

For the actual testing of the real-time BMI, the nine features of each epoch were computed using the power at the precomputed optimum frequencies from the training phase. Then the data was classified using the SVM classifier into relax or gait MI. As visual feedback, in E1 every correct classification resulted in the increase in size of a green bar shown in the screen. Meanwhile, in E2 the

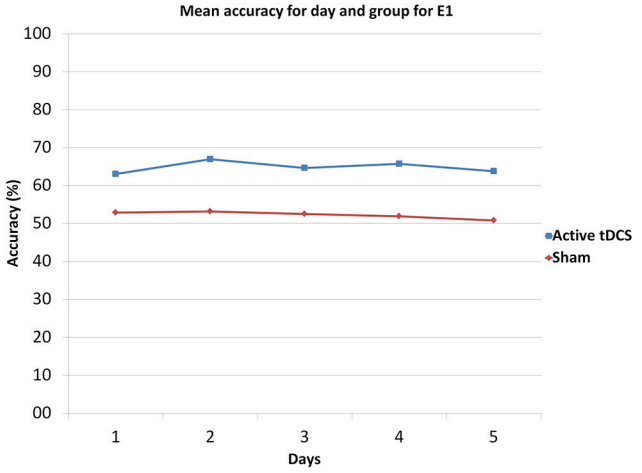

FIGURE 8 | Mean accuracy for each day and group in E1.

exoskeleton moved one step forward whenever three consecutive gait MI classifications were detected.

2.6. Exoskeleton

The lower limb robotic exoskeleton used was the H2 (Technaid, Madrid, Spain) designed by Bortole et al. (2015). The H2 has six degrees of freedom where hip, knee and ankle of each leg are powered joints. It was constructed for adults of heights between 1.5 m and 1.95 m and a maximum weight of 100 kg. The H2 has a lithium polymer battery of 22.5 VDC voltage and 12 Ah of capacity. It also has direct current (DC) motors to activate the joints actuators and sensors: potentiometers, Hall effect sensors, strain gauges and foot switches to determine the joint angles and human-orthosis interaction torques on the links.

The communication between the BMI and the H2 was through a bluetooth port. The connection was established in an Intel Core i7 laptop using MATLAB (MathWorks Inc., Massachusetts, United States) software. Each 0.5 s and during gait imagination periods, the BMI sent the user's output from the classifier to the exoskeleton.

2.7. Post-processing

2.7.1. Statistical Analysis

For the E1 experiment, data was analyzed via the Statistical Package Social Science (SPSS), version 22.0 (IBM Corporation, Armonk, NY, United States). The dependent variable was the classification accuracy and the independent variables were the group (sham or active tDCS) and the day of the experiment (from day 1 to day 5). Therefore, there were two types of studies: the difference between groups and the evolution of the performance of the subjects (here called plasticity) within groups. Hence, the appropriate statistical test to make was a mixed factorial ANOVA, but before doing so, the Kolmogorov-Smirnov (K-S) normality test was computed to check the existence of outliers. Then, for the study within groups, Mauchly's sphericity test was carried out to check the equality of the variances (Field, 2013). Lastly, the mixed factorial ANOVA analysis was completed. Furthermore, Bonferroni adjustments were applied for multiple pairwise comparisons between groups and within groups. A value of $p < 0.05$ was considered statistically significant.

For the E2 pilot experiment, the sample sizes were too small (two users per group) to rigorously justify the statistical analysis mentioned above. Therefore, the average accuracies were used directly to make the appropriate and relevant comparisons. Having said that, these results and their implications should come with a warning that this is only a preliminary study, and the sample sizes are small, so larger samples are needed to increase the accuracy of predictions.

2.7.2. Analysis of Optimal Frequencies

As mentioned in section 2.5, based on the training data, an optimal frequency (where the greatest differences between relax and gait imagery was observed) was assigned to each electrode of each subject on any given day. These frequencies form a fundamental part of the model used to construct the BMI. Having said that, analyzing these frequencies independently provides more useful information. Indeed, after removing any outliers, it is possible to make a histogram of the optimal frequencies associated to each group on each day (each relevant subject in the group will have 9 optimal frequencies, one for each electrode, on any given day) that discriminates between three distinct frequency bands: high theta and mu rhythm (6–12 Hz), low and mid-range beta rhythm (13–20 Hz) and high beta rhythm (21–30 Hz). With this histogram, one can then determine the preferred frequency bands for each group and their evolution throughout the experiment.

2.7.3. ERD/ERS Analysis

Event-related desynchronization and synchronization (ERD/ERS) are EEG fluctuations during cognitive or motor processes. They are highly frequency-band specific and while ERD represents an increase of excitability, ERS represents the opposite (Pfurtscheller, 2001). For an electrode e, and for a fixed frequency f, let

$$ERD_e(f) = \left(\frac{G(f) - R(f)}{R(f)}\right) \quad (1)$$

where $G(f)$ is the average of the power at the frequency f over all gait-imagery-epochs, and $R(f)$ is the same but averaged over all relax-imagery-epochs. Low values of G, resulting in negative values of ERD_e, represent ERD, while higher values of G, resulting in positive values of ERD_e, represent ERS. To obtain an average value of ERD_e over a frequency band, simply average over all integer frequencies, f, of interest (e.g., in the 6–12 Hz band, it would be the average of $ERD_e(f)$ for $f = 6, 7, 8, 9, 10, 11, 12$). A frequency-band ERD_e can be calculated for each electrode on each day of the experiment for each subject. This allows to produce a topographic map of the variable in the scalp, which one can then analyze to determine patterns of activation across the different areas of the brain.

TABLE 2 | E1 histogram of optimal frequencies for each day and group.

Group	Frequency range	Day 1 (%)	Day 2 (%)	Day 3 (%)	Day 4 (%)	Day 5 (%)
Active tDCS	(6–12) Hz	81.5	77.8	81.5	85.2	79.6
	(13–20) Hz	11.1	13.0	11.1	7.4	16.7
	(21–30) Hz	7.4	9.3	7.4	7.4	3.7
Sham	(6–12) Hz	75.6	57.8	68.9	64.4	64.4
	(13–20) Hz	4.4	17.8	4.4	28.9	20.0
	(21–30) Hz	20.0	24.4	26.7	6.7	17.8

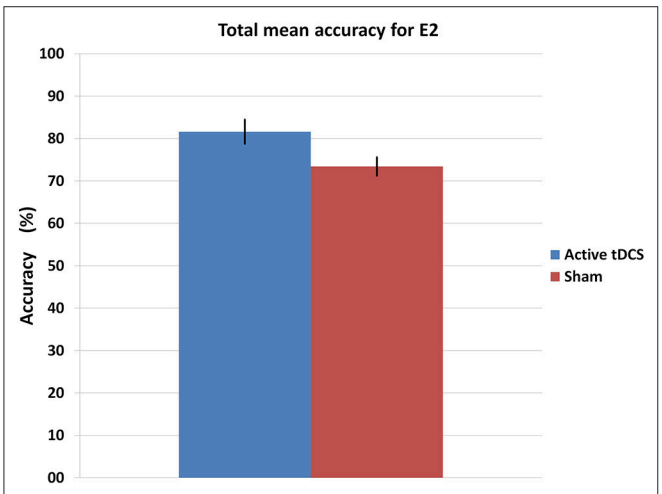

FIGURE 9 | Mean accuracy for each group in the E2 experiment. The error bars indicate a standard deviation from the mean.

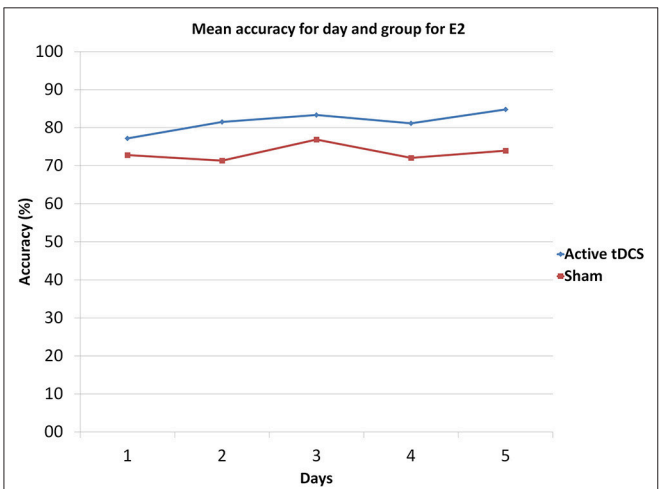

FIGURE 10 | Mean accuracy for each day and group in E2.

3. RESULTS

3.1. E1 Experiment

The normality test indicated that there was an outlier within the sham group. This subject was removed from the data.

3.1.1. Effects of tDCS in MI

This section studies if there exist any effects of tDCS on the subjects. Results from the mixed factorial ANOVA showed that subjects were significantly affected by the group they belonged, $F_{(1,9)} = 9.47$, $p < 0.05$. **Figure 7** shows the mean accuracy achieved by each group, with the tDCS and sham groups getting 65 and 52.4% of detection accuracy, respectively.

Moreover, the comparison was broken down on a day by day basis, by making pairwise comparisons. **Table 1** shows the p-values of those comparisons and **Figure 8** illustrates the mean accuracy achieved by each group on each day. The results show that there were significant differences ($p < 0.05$) between the sham and tDCS groups from the second day onwards.

3.1.2. MI Plasticity

This section analyzes the interaction effects between the days within groups. The results of Mauchly's test of sphericity show that the condition of sphericity was met, $\chi^2(9) = 17.52, p > 0.05$, so it was not necessary to apply a correction factor.

The mixed factorial ANOVA showed no significant interaction between the days and the group, $F_{(4,\ 36)} = 0.27$, $r = 0.1$, $p > 0.05$, meaning that there does not seem to be any major plasticity development throughout the 5 days of the experiment.

3.1.3. Optimal Frequencies and ERD/ERS Results

A histogram showing the percentage of electrode optimal frequencies lying in the relevant frequency bands (high theta and mu rhythm, low and mid-range beta rhythm, and high beta rhythm) for each group and day of the E1 experiment is shown in **Table 2**. Clearly, the preferred frequency band is the high theta and mu rhythm (6-12 Hz).

Since the high theta and mu rhythm (6–12 Hz) was the preferred frequency band, on each day of the E1 experiment and for each electrode, e, the variable ERD_e was averaged over all subjects common to a group (excluding outliers) and over the relevant frequency band (6–12 Hz). The resulting topographic map for the active tDCS and the sham groups is shown in **Figure 11** (top).

3.2. E2 Experiment

3.2.1. Effects of tDCS in MI

Figure 9 shows the mean accuracy achieved by each group, with the tDCS and sham groups getting 81.6 and 73.4% of detection accuracy, respectively. Furthermore, **Figure 10** illustrates the

TABLE 3 | E2 histogram of optimal frequencies histogram for each day and group.

Group	Frequency range	Day 1 (%)	Day 2 (%)	Day 3 (%)	Day 4 (%)	Day 5 (%)
Active tDCS	(6–12) Hz	100.0	100.0	100.0	100.0	94.4
	(13–20) Hz	0.0	0.0	0.0	0.0	0.0
	(21–30) Hz	0.0	0.0	0.0	0.0	5.6
Sham	(6–12) Hz	66.7	66.7	50.0	50.0	50.0
	(13–20) Hz	0.0	0.0	0.0	0.0	0.0
	(21–30) Hz	33.3	33.3	50.0	50.0	50.0

mean accuracy achieved by each group on each day, and there does not seem to be any significant changes in the accuracy as the days progress for either group (i.e., no plasticity is evident). Having said this, due to the preliminary nature of the E2 pilot study, these results have limitations as they involve very small sample sizes (two subjects per group), and larger data sets are necessary to be able to produce more robust results from the statistical standpoint.

3.2.2. Optimal Frequencies and ERD/ERS Results

As in section 3.1.3, the associated histogram for E2 is shown in **Table 3**. The preferred frequency band was once again the high theta and mu rhythm (6–12 Hz).

Meanwhile, the analogous topographic map for E2 for the preferred frequency band (6–12 Hz) is shown in **Figure 11** (bottom).

4. DISCUSSION

The results of E1 and the preliminary results of the pilot test in E2, seem to support the hypothesis that this novel tDCS montage improves the real-time classification of lower limb MI tasks. Before discussing the specific results further, a deeper neurological explanation for why the tDCS montage seems to have successfully worked is merited. The aim of the setup was to enhance the brain's learning abilities while stimulating the motor cortex which is responsible for lower limb movement (and imagination). With this in mind, an anode was placed over the cerebellum, since this improves the brain's learning abilities according to several studies (Mandolesi et al., 2003; Ferrucci et al., 2013; Shah et al., 2013; Hardwick and Celnik, 2014). However, placing this anode over the cerebellum also has other consequences. Namely, it produces the activation of Purkinje cells which inhibit the dentate nucleus and provoke disfacilitation of the motor cortex (Grimaldi et al., 2014; Cengiz and Boran, 2016; Lefaucheur et al., 2017), which is the opposite of what is desired regarding the activation of the motor cortex. For this reason, to counteract the effect of the first anode and excite the neural activity of the motor cortex, a second anode was placed directly in Cz over the motor cortex, and with a slightly higher current. Indeed, the currents used were 0.2 mA for the first anode and 0.3 mA for the second anode. The tDCS electrodes were not in direct contact with the skin, but rather with the hair. This reduced the probability of skin burns (Wang et al., 2015), which were not observed during the experiments (participants were encouraged to report any discomfort, but none was reported in association with the tDCS).

The active tDCS group achieved average detection accuracies of 65 and 81.6% for E1 and E2, respectively. When compared to the sham group, the active tDCS group obtained 12.6 and 8.2% higher accuracy performance in E1 and E2, respectively (**Figures 7**, **9**). In addition, the active tDCS group of E1 was at least 10% better than the sham group at each given day (see **Figure 8**), while in E2, it was at least 4% better on each day (see **Figure 10**). Lastly, this data and the *p*-values from **Table 1** indicate that from the second day onwards, the active tDCS group obtained significantly different and better results than the sham group in E1.

These conclusions are further supported with the results of analyzing the optimal frequencies and the ERD/ERS patterns in the brain. Regarding the optimal frequencies, **Table 2** and the preliminary results of **Table 3** show the stability of the frequency band trained, which in both cases corresponded to the high theta and mu rhythms (6–12 Hz). In E1 (**Table 2**) the preferred frequency band for the active tDCS group represented at least 78% of the optimal frequencies on any given day, while for the sham group it varied between 57 and 76%. The results of E2 show an even starker difference, with at least 94% of optimal frequencies lying in the preferred frequency band for the active tDCS group, while they ranged between 50 and 66% for the sham group. This seems to indicate that the tDCS favors a specific frequency band to train the new task.

Moreover, the ERD/ERS analysis shows that overall for both E1 and E2, there seems to be more desynchronization (ERD) on the mu rhythms of the tDCS group than in the sham group (see **Figure 11**). Furthermore, this mu wave desynchronization is occurring mostly in the sensorimotor area, as is reported widely in the literature when there is either motor execution or motor imagery (Pfurtscheller and Da Silva, 1999; Matsumoto et al., 2010). This desynchronization seems to be more evident in the preliminary study E2 than in E1, but in both cases it is observed. Thus, the active tDCS group for both experiments appears to enhance the modulation of the mu rhythm and the BMI control.

As observed from **Figures 8**, **10**, for both experiments, the changes in accuracy for each group as the days progressed seems to have been minimal. Thus, one can say that there was little plasticity developed in the brain during the 5 days of the experiment. This is probably due to the simplicity of the task and the fact that the brain could have quickly adapted to this task early on in the training phase of the experiment of the first day.

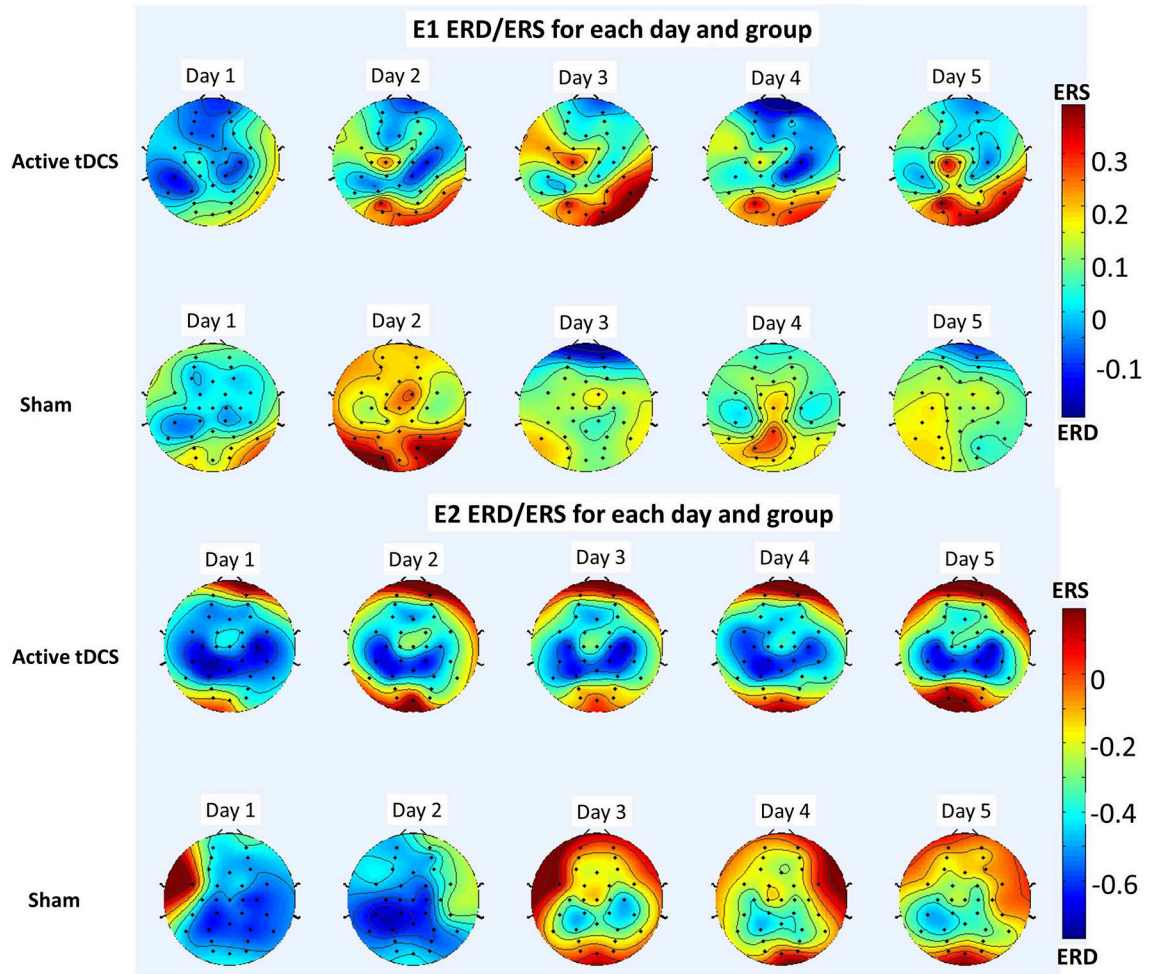

FIGURE 11 | Topographic maps showing ERD (red) and ERS (blue) for the 6–12 Hz frequency band averaged over all participants for each day and group of each experiment. The results of E1 are shown in the top and those of E2 are shown in the bottom.

Comparing the differences between E1 and E2 is very interesting but one must be careful in rushing to any conclusions, as the experimental protocols were different, and more importantly, the results of E2 are only preliminary at the time. Overall, E2 produced better accuracy results than E1: the active tDCS and sham groups of E2 were 16.7 and 21.2% more accurate than the respective groups of E1. Some differences in the protocol that could have led to these results, are that the duration of *Relax* and *Imagine* periods between the two experiments was different; and more notably, that the nature of the cues and feedback was different as well. Indeed, it should be mentioned that all subjects in E1 reported frustration about the visual feedback (a green bar that increased with each real-time correct detection), saying that they became anxious when the green bar did not move. Naturally, this could have affected the results. Meanwhile, in E2 the feedback was much more natural as it involved movement of the body. In fact, no such frustration was reported by the users in E2.

Comparing the results of E1 and the preliminary results of E2 through the ERD/ERS analysis is also of interest (see **Figure 11**). Indeed, the desynchronization is observed to be stronger and more consistent in E2 than in E1. This seems to be consistent with some results in the literature involving upper limb exoskeletons (Gomez-Rodriguez et al., 2011), which found the discriminative power of the sensorimotor area to be higher when using an exoskeleton, thus providing a benefit in terms of the resulting BMI designed.

It should be noted that the pilot test E2 was a challenging experiment as it involved combining tDCS with a real-time BMI connected to an exoskeleton. Exoskeletons are often simply pre-programmed or controlled directly through third party interfaces (joysticks, cellphone applications, etc.), but only until relatively recently have they begun to be controlled via BMIs. Designing a real-time BMI is also not trivial in itself (it is sometimes preceded by the design of offline BMIs). Thus, the study of real-time BMI control of exoskeletons is only starting and has many potential clinical applications, especially in the rehabilitation of patients. Thus, combining this concept with tDCS, which is aimed to improve and accelerate cognitive ability, enriches and increases those applications even more. Indeed, the intention is to use this

setup in the future to enhance the recovery of CVA patients with an affected lower right limb. Having said that, the study carried out here was only a preliminary pilot study involving only a few subjects. To confirm the results, a larger sample of subjects or even patients is necessary, but the limited results obtained for now look promising.

Some final comments are warranted regarding the real-time functioning of the exoskeleton in E2. To have a realistic usability of the BMI with the exoskeleton, the analysis of the false detections during relax periods is important, and reducing it is an essential objective. The rate of such detections is referred to as the false positive rate, or FPR (which is the complement of the accuracy when restricted to only relax periods). When averaging both groups in E2, the FPR was 11.7% (equivalently, an accuracy of 88.3% during relax), with an FPR of 11.3% for the tDCS group and of 12.1% for the sham group. The values for both groups were very similar, which shows that the overall increase in accuracy resulting from the stimulation of the tDCS group, was due to an increase in accuracy during the imagination periods (indeed, the accuracy on those periods was 92.7% for the tDCS group and of 80.4% for the sham group). In any case, overall, these values of FPR seem reasonable for this preliminary experiment, but reducing them further should be a future design goal.

5. CONCLUSION

A novel tDCS configuration was successfully designed to improve the detection of two MI tasks (relax and gait MI) using a real-time BMI. Two anodes and one cathode were used: one anode was located over the right cerebrocerebellum and supplied 0.2 mA, the other anode was over Cz and supplied 0.3 mA, and the cathode was located over FC2. Two single-blind experiments, E1 and E2, were carried out, where subjects were randomly separated into two groups of the same size: sham and active tDCS. The sham group received a fake stimulation while the active tDCS group was truly stimulated. E1 involved twelve healthy subjects in total who received visual instructions and real-time feedback through a screen. Meanwhile, E2 was a pilot study involving only four healthy subjects who received auditory cues and wore a lower limb exoskeleton as feedback. E2 has potentially many clinical applications in the future. In particular, it can be used in the rehabilitation of patients that have suffered a cerebrovascular accident (CVA) affecting their right lower limb. The analysis indicated differences between the active tDCS and sham group in both experiments. The active tDCS group achieved 12.6 and 8.2% higher detection accuracy than the sham group in E1 and E2, respectively, reaching 65 and 81.6% mean accuracy in each experiment. Furthermore, the preliminary results indicate that the exoskeleton (in E2) enhanced the detection of the MI tasks with respect to the visual feedback (in E1), increasing the accuracy obtained in 16.7 and 21.2% for the active tDCS and sham groups, respectively. Having said that, more studies with larger samples of actual patients are needed to validate this observation.

AUTHOR CONTRIBUTIONS

MR-U is responsible for the design, implementation, acquisition and data analysis. In addition, EI and MO supervised the work and contributed with the revision process. JA actively contributed as director of the work.

FUNDING

This research was carried out in the framework of the project Associate titled: Decoding and stimulation of motor and sensory brain activity to support long term potentiation through Hebbian and paired associative stimulation during rehabilitation of gait (DPI2014-58431-C4-2-R), which is funded by the Spanish Ministry of Economy and Competitiveness and by the European Union through the European Regional Development Fund (ERDF), A way to build Europe.

ACKNOWLEDGMENTS

MR-U wishes to thank Federico Fuentes for useful discussions and the revision of the manuscript. Furthermore, Brain-Machine Interface Systems Lab wishes to thank the R & D Unit in Biomechanics and Technical Aid of the National Paraplegic Centre at Toledo for providing users and lending the exoskeleton.

REFERENCES

Allali, G., Van Der Meulen, M., Beauchet, O., Rieger, S. W., Vuilleumier, P., and Assal, F. (2013). The neural basis of age-related changes in motor imagery of gait: an fMRI study. *J. Gerontol. A* 69, 1389–1398. doi: 10.1093/gerona/glt207

Angulo-Sherman, I. N., Rodríguez-Ugarte, M., Sciacca, N., Iáñez, E., and Azorín, J. M. (2017). Effect of tdcs stimulation of motor cortex and cerebellum on EEG classification of motor imagery and sensorimotor band power. *J. Neuroeng. Rehabil.* 14:31. doi: 10.1186/s12984-017-0242-1

Barrios, L. J., Hornero, R., Perez-Turiel, J., Pons, J. L., Vidal, J., and Azorin, J. M. (2017). State of the art in neurotechnologies for assistance and rehabilitation in spain: fundamental technologies. *Rev. Iberoamer. Autom. Inform. Indust.* 14, 346–354. doi: 10.1016/j.riai.2017.06.003

Bikson, M., Grossman, P., Thomas, C., Zannou, A. L., Jiang, J., Adnan, T., et al. (2016). Safety of transcranial direct current stimulation: evidence based update 2016. *Brain Stimul.* 9, 641–661. doi: 10.1016/j.brs.2016.06.004

Boehringer, A., Macher, K., Dukart, J., Villringer, A., and Pleger, B. (2013). Cerebellar transcranial direct current stimulation modulates verbal working memory. *Brain Stimul.* 6, 649–653. doi: 10.1016/j.brs.2012.10.001

Bolognini, N., Spandri, V., Ferraro, F., Salmaggi, A., Molinari, A. C., Fregni, F., et al. (2015). Immediate and sustained effects of 5-day transcranial direct current stimulation of the motor cortex in phantom limb pain. *J. Pain* 16, 657–665. doi: 10.1016/j.jpain.2015.03.013

Bortole, M., Venkatakrishnan, A., Zhu, F., Moreno, J. C., Francisco, G. E., Pons, J. L., et al. (2015). The H2 robotic exoskeleton for gait rehabilitation after stroke: early findings from a clinical study. *J. Neuroeng. Rehabil.* 12:54. doi: 10.1186/s12984-015-0048-y

Bradnam, L. V., Graetz, L. J., McDonnell, M. N., and Ridding, M. C. (2015). Anodal transcranial direct current stimulation to the cerebellum improves handwriting and cyclic drawing kinematics in focal hand dystonia. *Front. Hum. Neurosci.* 9:286. doi: 10.3389/fnhum.2015.00286

Cengiz, B., and Boran, H. E. (2016). The role of the cerebellum in motor imagery. *Neurosci. Lett.* 617, 156–159. doi: 10.1016/j.neulet.2016.01.045

Clancy, J. A., Johnson, R., Raw, R., Deuchars, S. A., and Deuchars, J. (2014). Anodal transcranial direct current stimulation (tDCS) over the

motor cortex increases sympathetic nerve activity. *Brain Stimul.* 7, 97–104. doi: 10.1016/j.brs.2013.08.005

Coffman, B. A., Clark, V. P., and Parasuraman, R. (2014). Battery powered thought: enhancement of attention, learning, and memory in healthy adults using transcranial direct current stimulation. *Neuroimage* 85, 895–908. doi: 10.1016/j.neuroimage.2013.07.083

Ferrucci, R., Brunoni, A. R., Parazzini, M., Vergari, M., Rossi, E., Fumagalli, M., et al. (2013). Modulating human procedural learning by cerebellar transcranial direct current stimulation. *Cerebellum* 12, 485–492. doi: 10.1007/s12311-012-0436-9

Ferrucci, R., Mameli, F., Ruggiero, F., and Priori, A. (2016). Transcranial direct current stimulation as treatment for Parkinson's disease and other movement disorders. *Basal Ganglia* 6, 53–61. doi: 10.1016/j.baga.2015.12.002

Ferrucci, R., and Priori, A. (2014). Transcranial cerebellar direct current stimulation (tcDCS): motor control, cognition, learning and emotions. *Neuroimage* 85, 918–923. doi: 10.1016/j.neuroimage.2013.04.122

Field, A. (2013). *Discovering Statistics using IBM SPSS Statistics*. London: Sage.

Filmer, H. L., Dux, P. E., and Mattingley, J. B. (2014). Applications of transcranial direct current stimulation for understanding brain function. *Trends Neurosci.* 37, 742–753. doi: 10.1016/j.tins.2014.08.003

Foerster, Á., Melo, L., Mello, M., Castro, R., Shirahige, L., Rocha, S., et al. (2017). Cerebellar transcranial direct current stimulation (ctdcs) impairs balance control in healthy individuals. *Cerebellum* 16, 872–875. doi: 10.1007/s12311-017-0863-8

Galea, J. M., Jayaram, G., Ajagbe, L., and Celnik, P. (2009). Modulation of cerebellar excitability by polarity-specific noninvasive direct current stimulation. *J. Neurosci.* 29, 9115–9122. doi: 10.1523/JNEUROSCI.2184-09.2009

Gomez-Rodriguez, M., Peters, J., Hill, J., Schölkopf, B., Gharabaghi, A., and Grosse-Wentrup, M. (2011). Closing the sensorimotor loop: haptic feedback facilitates decoding of motor imagery. *J. Neural Eng.* 8:036005. doi: 10.1088/1741-2560/8/3/036005

Grimaldi, G., Argyropoulos, G., Boehringer, A., Celnik, P., Edwards, M., Ferrucci, R., et al. (2014). Non-invasive cerebellar stimulation–a consensus paper. *Cerebellum* 13, 121–138. doi: 10.1007/s12311-013-0514-7

Grimaldi, G., Argyropoulos, G. P., Bastian, A., Cortes, M., Davis, N. J., Edwards, D. J., et al. (2016). Cerebellar transcranial direct current stimulation (ctDCS) a novel approach to understanding cerebellar function in health and disease. *Neuroscientist* 22, 83–97. doi: 10.1177/1073858414559409

Hardwick, R. M., and Celnik, P. A. (2014). Cerebellar direct current stimulation enhances motor learning in older adults. *Neurobiol. Aging* 35, 2217–2221. doi: 10.1016/j.neurobiolaging.2014.03.030

Hétu, S., Grégoire, M., Saimpont, A., Coll, M.-P., Eugène, F., Michon, P.-E., et al. (2013). The neural network of motor imagery: an ALE meta-analysis. *Neurosci. Biobehav. Rev.* 37, 930–949. doi: 10.1016/j.neubiorev.2013.03.017

Hortal, E., Planelles, D., Resquin, F., Climent, J. M., Azorín, J. M., and Pons, J. L. (2015). Using a brain-machine interface to control a hybrid upper limb exoskeleton during rehabilitation of patients with neurological conditions. *J. Neuroeng. Rehabil.* 12:92. doi: 10.1186/s12984-015-0082-9

Lefaucheur, J.-P., Antal, A., Ayache, S. S., Benninger, D. H., Brunelin, J., Cogiamanian, F., et al. (2017). Evidence-based guidelines on the therapeutic use of transcranial direct current stimulation (tDCS). *Clin. Neurophysiol.* 128, 56–92. doi: 10.1016/j.clinph.2016.10.087

Llinas, R., and Negrello, M. N. (2015). Cerebellum. *Scholarpedia* 10:4606. doi: 10.4249/scholarpedia.4606

Mandolesi, L., Leggio, M., Spirito, F., and Petrosini, L. (2003). Cerebellar contribution to spatial event processing. *Eur. J. Neurosci.* 18, 2618–2626. doi: 10.1046/j.1460-9568.2003.02990.x

Marangolo, P., Marinelli, C., Bonifazi, S., Fiori, V., Ceravolo, M., Provinciali, L., et al. (2011). Electrical stimulation over the left inferior frontal gyrus (IFG) determines long-term effects in the recovery of speech apraxia in three chronic aphasics. *Behav. Brain Res.* 225, 498–504. doi: 10.1016/j.bbr.2011.08.008

Marquez, C. M. S., Zhang, X., Swinnen, S. P., Meesen, R., and Wenderoth, N. (2013). Task-specific effect of transcranial direct current stimulation on motor learning. *Front. Hum. Neurosci.* 7:333. doi: 10.3389/fnhum.2013.00333

Matsumoto, J., Fujiwara, T., Takahashi, O., Liu, M., Kimura, A., and Ushiba, J. (2010). Modulation of mu rhythm desynchronization during motor imagery by transcranial direct current stimulation. *J. Neuroeng. Rehabil.* 7:27. doi: 10.1186/1743-0003-7-27

McFarland, D. J., McCane, L. M., David, S. V., and Wolpaw, J. R. (1997). Spatial filter selection for EEG-based communication. *Electroencephalogr. Clin. Neurophysiol.* 103, 386–394. doi: 10.1016/S0013-4694(97)00022-2

Monti, A., Ferrucci, R., Fumagalli, M., Mameli, F., Cogiamanian, F., Ardolino, G., et al. (2013). Transcranial direct current stimulation (tdcs) and language. *J. Neurol. Neurosurg. Psychiatry* 84, 832–842. doi: 10.1136/jnnp-2012-302825

Nelson, J. T., McKinley, R. A., Golob, E. J., Warm, J. S., and Parasuraman, R. (2014). Enhancing vigilance in operators with prefrontal cortex transcranial direct current stimulation (tDCS). *Neuroimage* 85, 909–917. doi: 10.1016/j.neuroimage.2012.11.061

Park, C., Looney, D., ur Rehman, N., Ahrabian, A., and Mandic, D. P. (2013). Classification of motor imagery BCI using multivariate empirical mode decomposition. *IEEE Trans. Neural Syst. Rehabil. Eng.* 21, 10–22. doi: 10.1109/TNSRE.2012.2229296

Pfurtscheller, G. (2001). Functional brain imaging based on ERD/ERS. *Vis. Res.* 41, 1257–1260. doi: 10.1016/S0042-6989(00)00235-2

Pfurtscheller, G., and Da Silva, F. L. (1999). Event-related eeg/meg synchronization and desynchronization: basic principles. *Clin. Neurophysiol.* 110, 1842–1857. doi: 10.1016/S1388-2457(99)00141-8

Reynolds, C., Osuagwu, B. A., and Vuckovic, A. (2015). Influence of motor imagination on cortical activation during functional electrical stimulation. *Clin. Neurophysiol.* 126, 1360–1369. doi: 10.1016/j.clinph.2014.10.007

Rodríguez-Ugarte, M., Costa, Á., Iáñez, E., Úbeda, A., and Azorín, J. (2016a). "Pseudo-online detection of intention of pedaling start cycle through EEG signals," in *2016 38th Annual International Conference of the IEEE Engineering in Medicine and Biology Society (EMBC)* (Orlando, FL: Springer), 1496–1499. doi: 10.1109/EMBC.2016.7590993

Rodríguez-Ugarte, M., Sciacca, N., and Azorín, J. M. (2016b). "Transcranial direct current stimulatio (tDCS) and transcranial current alternating stimulation (tACS) review," in *Proceedings of the XXXVII Jornadas de Automática* (Madrid), 137–143.

Sehm, B., Kipping, J., Schäfer, A., Villringer, A., and Ragert, P. (2013). A comparison between uni-and bilateral tDCS effects on functional connectivity of the human motor cortex. *Front. Hum. Neurosci.* 7:183. doi: 10.3389/fnhum.2013.00183

Shah, B., Nguyen, T. T., and Madhavan, S. (2013). Polarity independent effects of cerebellar tDCS on short term ankle visuomotor learning. *Brain Stimulat.* 6, 966–968. doi: 10.1016/j.brs.2013.04.008

Sharma, N., and Baron, J.-C. (2013). Does motor imagery share neural networks with executed movement: a multivariate fMRI analysis. *Front. Hum. Neurosci.* 7:564. doi: 10.3389/fnhum.2013.00564

Thielscher, A., Antunes, A., and Saturnino, G. B. (2015). "Field modeling for transcranial magnetic stimulation: a useful tool to understand the physiological effects of TMS?," in *Engineering in Medicine and Biology Society (EMBC), 2015 37th Annual International Conference of the IEEE* (Milano: IEEE), 222–225.

Wang, J., Wei, Y., Wen, J., and Li, X. (2015). Skin burn after single session of transcranial direct current stimulation (tdcs). *Brain Stimulat.* 8, 165–166. doi: 10.1016/j.brs.2014.10.015

Wiethoff, S., Hamada, M., and Rothwell, J. C. (2014). Variability in response to transcranial direct current stimulation of the motor cortex. *Brain Stimulat.* 7, 468–475. doi: 10.1016/j.brs.2014.02.003

Zapparoli, L., Invernizzi, P., Gandola, M., Verardi, M., Berlingeri, M., Sberna, M., et al. (2013). Mental images across the adult lifespan: a behavioural and fMRI investigation of motor execution and motor imagery. *Exp. Brain Res.* 224, 519–540. doi: 10.1007/s00221-012-3331-1

Conflict of Interest Statement: The authors declare that the research was conducted in the absence of any commercial or financial relationships that could be construed as a potential conflict of interest.

Copyright © 2018 Rodríguez-Ugarte, Iáñez, Ortiz and Azorín. This is an open-access article distributed under the terms of the Creative Commons Attribution License (CC BY). The use, distribution or reproduction in other forums is permitted, provided the original author(s) and the copyright owner(s) are credited and that the original publication in this journal is cited, in accordance with accepted academic practice. No use, distribution or reproduction is permitted which does not comply with these terms.

frontiers in Neuroscience

ORIGINAL RESEARCH
published: 08 November 2018
doi: 10.3389/fnins.2018.00752

Behavioral Outcomes Following Brain–Computer Interface Intervention for Upper Extremity Rehabilitation in Stroke: A Randomized Controlled Trial

Alexander B. Remsik[1,2,3†], Keith Dodd[1,4†], Leroy Williams Jr.[1,5,6], Jaclyn Thoma[1,7], Tyler Jacobson[1,7], Janerra D. Allen[1,8], Hemali Advani[1], Rosaleena Mohanty[1,9], Matt McMillan[1,4], Shruti Rajan[1,10], Matt Walczak[1], Brittany M. Young[1,3,7,11,12], Zack Nigogosyan[1], Cameron A. Rivera[1], Mohsen Mazrooyisebdani[1], Neelima Tellapragada[1], Leo M. Walton[4,7], Klevest Gjini[1,13], Peter L.E. van Kan[2], Theresa J. Kang[1,13], Justin A. Sattin[7], Veena A. Nair[1], Dorothy Farrar Edwards[2], Justin C. Williams[2,14] and Vivek Prabhakaran[1,7,10,12,13,15]*

[1] Department of Radiology, University of Wisconsin – Madison, Madison, WI, United States, [2] Department of Kinesiology, University of Wisconsin – Madison, Madison, WI, United States, [3] Institute for Clinical and Translational Research, University of Wisconsin – Madison, Madison, WI, United States, [4] Department of Biomedical Engineering, University of Wisconsin – Madison, Madison, WI, United States, [5] Department of Educational Psychology, University of Wisconsin – Madison, Madison, WI, United States, [6] Center for Women's Health Research, University of Wisconsin – Madison, Madison, WI, United States, [7] Neuroscience Training Program, University of Wisconsin School of Medicine and Public Health, Madison, WI, United States, [8] Department of Materials Science and Engineering, University of Wisconsin – Madison, Madison, WI, United States, [9] Department of Electrical and Computer Engineering, University of Wisconsin – Madison, Madison, WI, United States, [10] Department of Psychology, University of Wisconsin – Madison, Madison, WI, United States, [11] Clinical Neuroengineering Training Program, University of Wisconsin – Madison, Madison, WI, United States, [12] Medical Scientist Training Program, University of Wisconsin School of Medicine and Public Health, Madison, WI, United States, [13] Department of Neurology, University of Wisconsin – Madison, Madison, WI, United States, [14] Department of Neurological Surgery, University of Wisconsin – Madison, Madison, WI, United States, [15] Department of Psychiatry, University of Wisconsin – Madison, Madison, WI, United States

OPEN ACCESS

Edited by:
Mikhail Lebedev, Duke University, United States

Reviewed by:
Waldemar Karwowski, University of Central Florida, United States
Yufeng Ke, Tianjin University, China

***Correspondence:**
Alexander B. Remsik
Aremsik@wisc.edu

[†]These authors have contributed equally to this work as co-first authors

Specialty section:
This article was submitted to Neural Technology, a section of the journal Frontiers in Neuroscience

Received: *15 March 2018*
Accepted: *28 September 2018*
Published: *08 November 2018*

Citation:
Remsik AB, Dodd K, Williams L Jr, Thoma J, Jacobson T, Allen JD, Advani H, Mohanty R, McMillan M, Rajan S, Walczak M, Young BM, Nigogosyan Z, Rivera CA, Mazrooyisebdani M, Tellapragada N, Walton LM, Gjini K, van Kan PLE, Kang TJ, Sattin JA, Nair VA, Edwards DF, Williams JC and Prabhakaran V (2018) Behavioral Outcomes Following Brain–Computer Interface Intervention for Upper Extremity Rehabilitation in Stroke: A Randomized Controlled Trial. Front. Neurosci. 12:752. doi: 10.3389/fnins.2018.00752

Stroke is a leading cause of persistent upper extremity (UE) motor disability in adults. Brain–computer interface (BCI) intervention has demonstrated potential as a motor rehabilitation strategy for stroke survivors. This sub-analysis of ongoing clinical trial (NCT02098265) examines rehabilitative efficacy of this BCI design and seeks to identify stroke participant characteristics associated with behavioral improvement. Stroke participants (n = 21) with UE impairment were assessed using Action Research Arm Test (ARAT) and measures of function. Nine participants completed three assessments during the experimental BCI intervention period and at 1-month follow-up. Twelve other participants first completed three assessments over a parallel time-matched control period and then crossed over into the BCI intervention condition 1-month later. Participants who realized positive change (≥1 point) in total ARAT performance of the stroke affected UE between the first and third assessments of the intervention period were dichotomized as "responders" (<1 = "non-responders") and similarly analyzed. Of the 14 participants with room for ARAT improvement, 64% (9/14) showed some positive change at completion and approximately 43% (6/14) of the participants had changes of minimal detectable change (MDC = 3 pts) or minimally clinical important difference (MCID = 5.7 points). Participants with room for improvement in the primary

outcome measure made significant mean gains in $ARAT_{total}$ score at completion ($\Delta ARAT_{total}$ = 2, p = 0.028) and 1-month follow-up ($\Delta ARAT_{total}$ = 3.4, p = 0.0010), controlling for severity, gender, chronicity, and concordance. Secondary outcome measures, $SIS_{mobility}$, SIS_{adl}, $SIS_{strength}$, and $9HPT_{affected}$, also showed significant improvement over time during intervention. Participants in intervention through follow-up showed a significantly increased improvement rate in $SIS_{strength}$ compared to controls (p = 0.0117), controlling for severity, chronicity, gender, as well as the individual effects of time and intervention type. Participants who best responded to BCI intervention, as evaluated by ARAT score improvement, showed significantly increased outcome values through completion and follow-up for $SIS_{mobility}$ (p = 0.0002, p = 0.002) and $SIS_{strength}$ (p = 0.04995, p = 0.0483). These findings may suggest possible secondary outcome measure patterns indicative of increased improvement resulting from this BCI intervention regimen as well as demonstrating primary efficacy of this BCI design for treatment of UE impairment in stroke survivors.

Clinical Trial Registration: ClinicalTrials.gov, NCT02098265.

Keywords: brain–computer interface (BCI), stroke, recovery, rehabilitation, motor function, hemiparesis, upper extremity

INTRODUCTION

Stroke

Each year there are approximately 800,000 new incidences of stroke in the United States (Benjamin et al., 2017), and in 2010 there were an estimated 16.9 million stroke events globally (Mozaffarian et al., 2015). Stroke occurs as a result of a blockage of blood flow in an area of the brain or by rupture of brain vasculature causing death or damage to local and distal brain tissue. In either etiology, survivors may experience some level of upper extremity (UE) physical impairment. Despite recent advances in acute care, an increasing number of stroke survivors face long-term motor deficits (Benjamin et al., 2017). Costs of care for long-term disability resulting from stroke are substantial with the direct medical costs of stroke estimated to $17.9 billion in 2013 (Benjamin et al., 2017). It is crucial that motor therapy for stroke enhances a survivor's capacity to autonomously participate in activities of daily living (ADLs), thereby decreasing dependency on caregivers as well as the cost and level of care necessary (Dombovy, 2009; Stinear, 2016). Efficacious motor therapy should be designed to improve the overall quality of life for the individual survivor based on their goals and needs (Remsik et al., 2016; Stinear, 2016).

Need for Treatment

Survivors in the chronic stage of stroke are the most desperate for rehabilitation. Existing pharmacological treatments and behavioral therapy methods primarily serve to treat symptoms associated with stroke (Benjamin et al., 2017) and may not bring about optimal changes in brain function or connectivity (Power et al., 2011; Nair et al., 2015). While a growing population of research suggests the greatest potential for recovery in the post-stroke brain occurs within the first months after insult (Stinear and Byblow, 2014), neuroplastic capacity has been demonstrated in both acute and chronic phases (Caria et al., 2011; Ang et al., 2015). Spontaneous biological recovery (SBR) (Beebe and Lang, 2009; Cramer and Nudo, 2010) in the initial days and weeks following stoke (acute phase) is thought to represent a critical period in the complex progression of motor recovery, which combines neurobiological processes and learning-related elements. After this window of SBR, it is posited a sensitive period of neurorecovery persists, plateauing around 6 months post-stroke (Wolf et al., 2006, 2010; Dromerick et al., 2009; Cramer and Nudo, 2010). Traditional rehabilitation therapies generally lose efficacy after such time and the course of standard of care treatment options is exhausted leaving chronically impaired persons with few options.

Potential for Treatment

Motor and cognitive recovery after these initial windows may no longer occur in the same spontaneous nature as is observed during SBR. However, innovative therapeutic techniques show some efficacy generating functional motor recovery beyond the traditional rehabilitation windows (Cramer and Nudo, 2010; Ang et al., 2015; Irimia et al., 2016). Brain–computer interfaces (BCIs), a novel rehabilitation tool, have shown proof of concept for rehabilitating volitional movements in stroke survivors (Muralidharan et al., 2011; Song et al., 2014, 2015; Young et al., 2014a,b,c,d, 2015; Irimia et al., 2016). In this growing area of research, developing technologies demonstrate promising potential for treating hemiparesis in a clinically viable and efficient manner and they may offer an avenue to increased autonomy for patients reducing their cost and burden of care.

Effectiveness of Current BCI Therapies

There is currently considerable variability in design and efficacy of BCI therapies as well as little consensus with respect to proper arrangement, administration, and dosing

(Muralidharan et al., 2011; Ang and Guan, 2013; Young et al., 2014a; Ang et al., 2015; Irimia et al., 2016; Remsik et al., 2016; Bundy et al., 2017; Dodd et al., 2017). Although acute stroke care has improved morbidity outcomes significantly, current treatments for persistent UE motor impairment resulting from stroke offer only limited restoration of UE motor function the further from stroke a survivor progresses (Wolf et al., 2006, 2010; Dromerick et al., 2009; Benjamin et al., 2017; Stinear et al., 2017). Evidence suggests both acute and chronic stroke patients respond to various neuro-rehabilitative BCI therapy strategies and can achieve clinically significant changes in measures of UE impairment (Young et al., 2014c; Irimia et al., 2016; Remsik et al., 2016). Furthermore, recent research also suggests that BCI therapy targeted at motor recovery may provide benefits in other brain regions outside of only the motor network (Mohanty et al., 2018).

Overview of This Study

This *post hoc* analysis of an ongoing clinical trial (NCT02098265) (Song et al., 2014, 2015; Young et al., 2014a,b,c,d, 2015) evaluates the effects of an interventional, non-invasive closed-loop electroencephalography (EEG)-based BCI intervention for the restoration of distal UE motor function in stroke survivors. Participants who showed measurable change in the primary outcome measure were grouped *post hoc*. This sub-analysis seeks to identify whether there are participant characteristics strongly associated with motor improvement as measured by primary and secondary outcome measures of UE function. These analyses are intended to inform future BCI research approaches and intervention designs as well as suggest and encourage appropriate participant selection.

MATERIALS AND METHODS

Ethics Statement

Participants were recruited as part of an ongoing prospective randomized, cross-over control design stroke rehabilitation study. This study was designed to investigate interventional BCI intervention targeting UE motor function in stroke survivors. This study was approved by the University of Wisconsin Health Sciences Institutional Review Board (Study ID 2015-0469); all subjects provided written informed consent upon enrollment. A CONSORT flow diagram is made available in the **Supplementary Material**.

Study Design and Subjects

Recruitment and Enrollment

This ongoing study, registered with ClinicalTrials.gov (study ID NCT02098265), utilizes an open call for participants with a wide range of (1) UE hemiparesis resulting from stroke, (2) time-since-stroke, (3) stroke type, (4) lesion location, (5) number of previous stokes, and (6) stroke severity. Subsequent to informed, written consent, stroke survivors were randomized, by permuted-block design accounting specifically for gender, stroke chronicity ($<$1 year, $\geq$1 year), and severity of motor impairment (mild, severe) as measured by the Action Research Arm Test (ARAT) (mild = $ARAT_{total}$ of $>$28, severe = $ARAT_{total} \leq 27$) [n = 21, mean age = 61.6 years $\pm$ 15 years, 10 female, 4 concordant lesions (stroke lesion impairs preferred dominant hand as assessed by the Edinburgh Inventory (Oldfield, 1971), mean chronicity = 1127 $\pm$ 1327 days, 12 participants presented with severe UE motor deficit, mean baseline ARAT score of impaired side = 26.6 $\pm$ 26.1, Delayed Therapy Group (DTG) n = 12, Immediate Therapy Group (ITG) n = 9]. Chronicity is measured as time since stroke, in days, to baseline measurement day. Participant characteristics are displayed in **Table 1**.

Inclusion–Exclusion Criteria

Potential participants met inclusion criteria if they were aged 18 years or older, had persistent UE motor impairment resulting from stroke, and no other known neurologic, psychiatric, or developmental disabilities. Exclusion criteria were: allergies to electrode gel, surgical tape, and/or metals, concurrent treatment for infectious disease, apparent lesions or inflammation of the oral cavity, pregnancy or intention to become pregnant during the study, and any contraindication for magnetic resonance imaging (MRI). Subjects were excluded from the presented analyses if they (1) failed to complete at least 9 of 15, 2-h BCI intervention sessions occurring at least twice each week, (2) failed to complete all four MRI and behavioral testing sessions occurring in the intervention phase (**Figure 1**; see **Supplementary CONSORT Flow Diagram**).

Randomization and Study Schema

Participants were randomly assigned to either receive BCI intervention immediately (ITG) following consent or to a DTG wherein participants were neither prohibited continuation of customary care, nor did they receive any BCI intervention. Participants, when receiving the BCI intervention condition, had at least 9 and up to 15 BCI intervention sessions (two-to-three sessions/week) wherein they received BCI intervention (**Figure 2**) lasting up to 2 h for a potential total dosing of 30 h of BCI intervention. Along with the BCI intervention sessions, subjects also received fMRI and behavioral testing at four-time points: prior to the first BCI intervention session (baseline, T4), after the first few weeks of intervention (midpoint, T5), immediately following the final intervention session (completion, T6), and again 1 month after the endpoint assessment (follow-up, T7) (**Figure 1**). Later in this publication, the authors will refer to time points 1–4 with the intention of describing time points 1–4 of the intervention phase (T4–7 from **Figure 1**). Because T1–4 in **Figure 1** refer to the control phase, the authors from here forward will refer to any data from these points by explicitly stating when the control phase is being considered.

Crossover Design

Following the final testing session, participants in the DTG cross over to the experimental or intervention phase and begin study visits for the BCI intervention condition as illustrated in **Figure 1**. For participants in the DTG, the crossover time point (T4) represents baseline as it is measured immediately prior to participation in BCI intervention sessions.

TABLE 1 | Participant demographics and baseline characteristics.

Participants	Age (years)	Chronicity days	Severity	Clinical cause lesion location	Baseline ARAT	Completion ARAT	Follow up ARAT	ARAT change	FMA-UE change
1	47–51	160	Severe	L-Lateral medulla	3	2	7	−1 (4**)	−2 (9***)
2	49–53	490	Severe	R-MCA stroke	3	4	8	1* (5**)	2* (11***)
3	76–80	658	Mild	Leg/periventricular white, MHR	57	57	57	0 (0)	0 (0)
4	67–51	2723	Severe	R-PLIC putamen	23	40	39	17*** (16***)	l3*** (12***)
5	81–85	580	Mild	Cerebellar vermis	47	52	52	5** (5**)	2* (2*)
6	73–77	197	Severe	R-prefrontal, midfrontal, temporal	0	0	3	0 (3**)	0 (7***)
7	62–66	101	Mild	R-white matter	56	57	57	1* (1*)	7*** (7***)
8	40–44	2645	Severe	R-frontal parietal	7	7	7	0 (0)	0 (0)
9	55–59	588	Severe	R-MCA	3	4	0	1* (−3)	2* (−7)
10	45–49	452	Severe	L-hemorrhagic stroke	0	2	0	2* (0)	4** (0)
11	30–34	494	Mild	L-ICA	57	57	57	0 (0)	0 (0)
12	60–64	44	Mild	L-PCA	57	57	57	0 (0)	0 (0)
13	57–61	849	Mild	L-MCA	57	57	57	0 (0)	0 (0)
14	44–48	3017	Severe	R-MCA/R-FI	3	4	5	1* (2*)	2* (4**)
15	69–73	790	Severe	R-MCA/R-TP	3	0	3	−3 (0)	−7 (0)
16	78–82	631	Mild	R-Occipital	57	57	57	0 (0)	0 (0)
17	75–79	5125	Severe	R-MCA/ACA	9	11	10	2* (1*)	4** (2*)
18	42–46	177	Mild	L-MCA	57	57	57	0 (0)	0 (0)
19	62–66	392	Severe	R-frontal hematoma R-VAOA	3	5	16	2* (13***)	4* (29***)
20	55–59	2767	Mild	Subarachnoid hemorrhage	57	57	57	0 (0)	0 (0)
21	69–73	783	Severe	R-MCA	0	0	0	0 (0)	0 (0)
Mean	61.6	1127			26.6	28.1	26.8	1.3 (2.2)	1.5 (3.6)
(A) Median	61.9	588			9	11	16	0 (0)	0 (0)
SD	15	1327			26.4	26.3	25.9	3.9 (4.5)	3.8 (7.4)
Mean	61.1	1289			11.4	13.4	14.8*	2 (3.4)	2.2 (5.4)
(B) Median	64	584			3	4	7	1 (1.5)	2.0 (3.0)
SD	13.5	1497			18	20.2	19.6	4.7 (5.2)	4.5 (8.5)

*ARAT indicates Action Research Arm Test; FMA-UE indicates fugl-meyer assessment of upper extremity; MCA indicates middle cerebral artery; ICA indicates internal carotid artery; PCA indicates posterior cerebral artery; FI indicates frontoparietal infarct; TP indicates temporalfrontal-parietal; ACA indicates anterior cerebral artery; MHR indicates motor hand region; VAOA indicates vertebral artery origin aneurysm; L, left; R, right. ARAT change: completion-baseline (follow up-baseline). (A) indicates descriptive statistics for all (n = 21) participants; (B) indicates descriptive statistics for (n = 14) participants able to achieve ARAT improvements (ceilings removed). FMA-UE is a predicted change that was used to approximate equivalent score that assesses the association between the categorical range of ARAT scores, * indicates responder (Δ_{ARAT} = 1); ** indicates minimal detectable change (MDC) (Δ_{ARAT} = 3); *** indicates minimal clinically important difference (MCID) (Δ_{ARAT} = 5.7).*

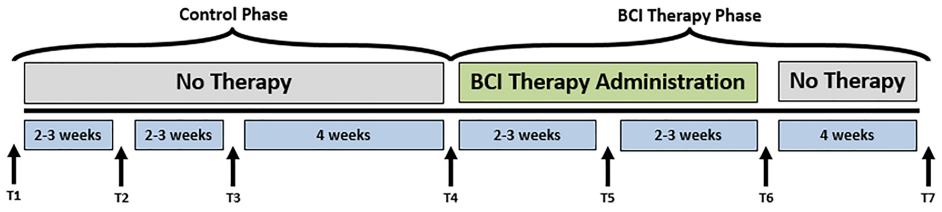

FIGURE 1 | Study design. The time-points at which neuroimaging data were collected are represented by Tl, control baseline 1; T2, control baseline 2; T3, control baseline 3; T4, therapy baseline; T5, mid-therapy; T6, post-therapy; and T7, one-month post-therapy. While the crossover control group (DTG) completed visits T1–T7, the immediate therapy group (ITG) completed visits T4–T7 only.

Outcomes

For these sub-analyses, and consistent with original study design, a primary objective outcome measure of UE function, the ARAT (Mathiowetz et al., 1985; Beebe and Lang, 2009; Malhotra et al., 2016), and secondary outcome measures of function (capacity and performance) including the self-report Stroke Impact Scale

(SIS) (Duncan et al., 1999; Lin et al., 2010), Hand Grip Strength (An et al., 1980; Malhotra et al., 2016), and the 9-Hole Peg Test (9HPT) (Mathiowetz et al., 1985) were assessed in the 21 participants who met the aforementioned criteria. The primary outcome measure, with registered minimal detectable change (MDC) and minimal clinically important difference (MCID) values (ARAT $MDC_{90} \geq 3$ point change, MCID ≥ 5.7 point change) (Lang et al., 2006; Simpson and Eng, 2013), was chosen to obtain clinically reliable measures of UE motor function change as a result of BCI intervention. 9HPT was included in this report as an additional objective (time) measure of motor function. The 9HPT is an assessment of fine motor control and speed of distal UE movement capacity and performance. The 9HPT requires finger dexterity and grip, and supplements the ARAT as they both assess gross UE capacity and function. This study analyzes ARAT scores, 9HPT performance by the affected UE ($9HPT_{affected}$), and SIS sub-scores of the impaired hand from the four time points, illustrated in **Figure 1**. The Fugl-Meyer Assessment of the Upper Extremity (FMA-UE) is another objective measure of function commonly used to assess UE capacity in several BCI studies. Although the FMA-UE was not intended as an assessment in this design, associations between categorical ranges of ARAT score and FMA-UE score, as presented in Hoonhorst et al. (2015), were used to approximate equivalent FMA-UE scores for the purpose of convenient comparison between the presented ARAT outcome scores and behavioral changes presented in previous publications. ARAT scores within the Upper-Limb category defined by baseline measures (Hoonhorst et al., 2015) were mapped to the FMA-UE score within the same category, rounded to the nearest whole integer, as FMA-UE measurements give scores in integer values.

Description of the Behavioral Outcome Measures

The primary outcome measure was the ARAT. The ARAT is a 57-point metric capable of assessing specific changes in upper limb function with sub-components for grasp, grip, pinch, and gross motor movement all of which sum to the total ARAT (Hsieh et al., 1998). The secondary outcome measures included the SIS, widely used to measure quality of life in stroke survivors, that consists of eight dimensions and a composite disability score (Vellone et al., 2015). The SIS is a 59-item patient-reported outcome measure, covering eight domains: strength (4 items), hand function (5 items), mobility (9 items), ADLs (10 items), memory (7 items), communication (7 items), emotion (9 items), and handicap (8 items). The domains are scored on a metric of 0–100, with higher scores indicating better self-reported health (Vellone et al., 2015). As it is possible the ARAT does not entirely capture the extent to which participants can functionally interact with their surroundings outside the laboratory, this subjective measure was chosen to support and record the participants' personal experience and opinion of their functional capacities relative to real-world application (Waddell et al., 2017). Self-report metrics are important for understanding the extent to which a participant is recovering UE motor activities subjectively in a real-world setting (outside the testing room setting) (Stinear et al., 2017). An additional secondary outcome measure was the 9HPT, which is a brief, standardized, quantitative test of UE function (Mathiowetz et al., 1985). The score for the 9HPT is an average of the two trials (Mathiowetz et al., 1985). Finally, a Smedley spring-type dynamometer tested the average grip strengths in pounds (lbs.) over three repeated trials per assessment to measure participant grip strength (An et al., 1980; Malhotra et al., 2016).

Analysis of Outcome Measures

Data analysis of outcome measures examined four central relationships: (1) Change in outcome measure scores over time (**Table 2**); (2) primary outcome measure improvement rate differences between intervention and control (**Table 3**); (3) improvement rate differences in outcome scores between subjects who realized an increase in primary outcome (responders) and non-responders (**Table 4**); and (4) differences in covariates and outcome measurements between responders and non-responders (**Table 4**) for the purpose of discerning characteristic trends of those participants who best respond to this BCI intervention. It is important to note that for all responder analyses, participants who scored a perfect 57 total score at baseline and completion were excluded from the sample ($n = 7$ excluded) due to an inability to show improvement in primary outcome leaving $n = 14$ subjects remaining for all the responder sub-analyses. Likelihood ratio tests of linear mixed effect (LME) models offered rigorous analysis for each research question while paired and independent samples *t*-tests provided analysis of more general trends that LME may miss. Testing excluding the follow-up time period (time periods 1–3 of intervention) allowed for examination of direct effects of the BCI intervention while parallel analyses including the follow-up time point (time periods 1–4) gave insight into potential lasting effects of the BCI intervention.

Outcome measures used in all analyses included ARAT, Hand Grip Strength, and the 9HPT as well as SIS measures of Hand Function, Mobility, ADLs, and Strength of the hemiparetic side. For each analysis, and for each outcome measure utilized, ceiling scores (participants who recorded a maximum outcome score at baseline and completion for ARAT) were removed given the impossibility for measured improvement. On the other hand, floor scores (participant data that demonstrated a minimum outcome score at the intervention baseline measure) remained in all analyses akin to an intent-to-treat standard. Given this selection, the sample size across all data remained at $n = 21$ and $n = 14$ for the responder sub-analyses for most outcome measures. The outcome measurements with sample size adjustments following the above criteria include ARAT ($n = 14$ for both analyses) and SIS_{hf} ($n = 20$). Additionally, the sample size of $9HPT_{affected}$ ($n = 9$ overall, $n = 2$ in the responder dichotomization) was greatly reduced from the original sample of 21 due to participants' inability to complete the task given the extent and severity of their UE impairment.

Independent samples *t*-tests utilized only DTG control data and ITG intervention data (neglecting the use of DTG intervention data) so as not to introduce an inter-subject dependence of the analyses. Meanwhile, the LME analyses used a random effect for subjects to account for the non-independence of the longitudinal data and used all subject time points. For each mixed model testing a specific outcome, relevant covariates to

TABLE 2 | Summary of outcome measures during assessment and including follow-up of BCI therapy.

Outcome measures	Improvement score Mean ± SD	LME Estimate ± SE	Covariates	*T*-test *p*-Value	Time LME *p*-Value
Stroke impact scale (SIS)					
$SIS_{Hand\ Function}$	5.7 ± 16.4	2.9 ± 1.9	Severity, gender	0.134	0.139
	(5.7 ± 13.9)	(2 ± 1.1)		(0.180)	(0.07)
$SIS_{mobility}$	8.7 ± 9.8	4.4 ± 0.9	Severity, age, chronicity,	0.001***	0.00001***
	(7.2 ± 11.2)	(2.6 ± 0.7)	gender	(0.010)**	(0.00009)***
SIS_{ADL}	5.9 ± 10.1	3.1 ± 0.2	Severity, concordance, age,	0.041*	0.0086**
	(4.9 ± 9.6)	(1.7± 0.8)	gender	(0.035)*	(0.054)*
$SIS_{Strength}$	7.4 ± 13.9	3.7 ± 1.6	Severity, chronicity, gender	0.024*	0.021*
	(11.3 ± 12./)	(1.7 ± 0.8)		(0.001)***	(0.00039)***
Grip strength	3.8 ± 8.1	1.9 ± 0.9	Severity, chronicity,	0.046*	0.037*
	(2.1 ± 7.7)	(1.0 ± 0.6)	concordance	(0.246)	(0.062)
9-HPT$_{Affect}$	−5.9 ± 8.9	−2.9 ± 1.2	Chronicity	0.0081**	0.0201*
	(−4.5 ± 5.3)	(−1.9 ± 0.7)		(0.046)*	(0.0118)**
Action research arm test (ARAT)					
$ARAT_{Total}$	1.3 ± 2.4	0.6 ± 0.3	Severity, gender, chronicity,	0.046*	0.275
	(3.3 ± 4.9)	(1.1 ± 0.3)	gender	(0.020)*	(0.001)***
$ARAT_{Grip}$	0.1 ± 0.5	0.03 ± 0.1	Severity, gender,	0.582	0.802
	(0.9 ± 1.4)	(0.3 ± 0.1)	concordance, chronicity, age	(0.025)*	(0.0059)**
$ARAT_{Grasp}$	0.8 ± 1.6	0.4 ± 0.3	Severity, gender,	0.106	0.129
	(1.5 ± 3.6)	(0.5 ± 0.2)	concordance, chronicity,	(0.163)	(0.03)*
$ARAT_{Pitch}$	0.4 ± 1.6	0.2 ± 0.2	age Seventy, gender,	0.289	0.215
	(0.6 ± 1.5)	(0.2 ± 0.1)	concordance	(0.106)	(0.039)*
$ARAT_{Gross}$	0 ± 1.6	0 ± 0.02	Severity, age, chronicity,	1.00	1.00
	(0.3 ± 1.4)	(0.1 ± 0.1)	concordance, gender	(0.453)	(0.437)

*Scores, Covariates, and p-values are reported for n = 21 participants during BCI intervention: Mean improvement scores between time points 1 and 3, (parentheses) indicate mean improvement scores between time points 1 and 4. The time LME p-value is a p-value for the likelihood test between two models differing only in the inclusion of time as a covariate. *p < 0.05, **p < 0.01, ***p < 0.00l.*

control for were chosen based on stepwise regression analysis. For each outcome measure with the selected covariates, two nearly identical mixed models were created that differed only in the inclusion of a single covariate of interest. When examining how subjects' outcome scores changed with time, the covariate of interest was the time period (1, 2, 3, or 4) of interventional assessment. For comparing the intervention to control, both LME models included the independent effects of time and therapy type (control or intervention) and stringently tested for improvement rate differences by inclusion of an interaction term between time and type as the covariate of interest. Similarly, both models in the responder sub-analyses included independent effects of time and response (responder or non-responder) and stringently tested for improvement rate changes through an interaction term between time and response. Meanwhile, response was used as the covariate of interest to test if responders showed general differences in secondary outcome measures compared to non-responders. Finally, a similarly run generalized linear model (GLM) analysis examined potential significant covariates that helped predict whether a subject would become a responder through this BCI intervention. The specific covariates tested included stroke severity, chronicity, and concordance, as well as age, gender, and baseline ARAT scores. All mixed modeling analyses were completed in RStudio (Version 0.99.903 –© 2009–2016 RStudio, Inc.). The *t*-tests were run using SPSS (Version 22). Thresholds for significance were set *a priori* at $p \leq 0.05$ for all statistical analyses.

Post Hoc Rational: Dichotomizing Responders

Two groups, deemed "responders" and "non-responders" (Snapinn and Jiang, 2007), were generated *post hoc* from this sample based on whether positive change in the primary objective measure of UE function was realized following BCI intervention (completion assessment score – baseline assessment score). The grouping of responders vs. non-responders is represented in **Tables 1** and **5**. **Table 1**, the main demographics table, denotes responders with asterisks in the completion ARAT score column. **Table 5** demonstrates relevant summary characteristic differences between the dichotomized groups.

The BCI System

BCI Software and EEG Hardware

The BCI system and intervention sequence were consistent with those previously described (Wilson et al., 2012; Song et al., 2014, 2015; Young et al., 2014a,b,c,d, 2015), using BCI

TABLE 3 | Summary of Outcome Measures During Assessment and Including Follow-Up of BCI Therapy for Intervention vs. Control

Outcome measures	Control Improvement score Mean ± SD	Intervention Improvement score Mean ± SD	LME Estimate ± SE	Covariates	*T*-test *p*-value	Interaction LME *p*-value
Stroke impact scale (SIS)						
$SIS_{Hand\ Function}$	0.4 ± 10.6	3.8 ± 10.8	2.6 ± 3.3	Severity, age, time, type	0.419	0.407
	(−0.9 ± 18.0)	(5.6 ± 7.3)	(2.1 ± 1.9)		(0.180)	(0.278)
$SIS_{mobility}$	5.1 ± 9.2	11.7 ± 12.0	1.8 ± 1.6	Seventy, chronicity, age,	0.197	0.237
	(2.7 ± 8.1)	(8.6 ± 13.1)	(1.5 ± 1.1)	gender, concordance, time, type	(0.085)	(0.148)
SIS_{ADL}	3.5 ± 12.5	9.2 ± 13.4	1.2 ± 2.1	Severity, concordance,	0.397	0.567
	(0.2 ± 12.4)	(5.0 ± 10.3)	(1.8 ± 1.3)	chronicity, gender, age, time, type	(0.156)	(0.175)
$SIS_{Strength}$	2.6 ± 17.1	12.5 ± 8.8	2.4 ± 2.8	Severity, chronicity, gender,	0.149	0.379
	(4.1 ± 18.3)	(14.6 ± 10.3)	(4.4 ± 1.7)	time, type	*(0.019)	**(0.012)
Grip strength	−0.3 ± 6.4	1.7 ± 5.0	2.1 ± 1.5	Severity, age, time, type	0.526	0.163
	(3.4 ± 11.0)	(1.3 ± 3.6)	(−0.3 ± 0.9)	(chronicity)	(0.749)	(0.792)
$9\text{-HPT}_{Affected}$	−7.7 ± 12.4	−2.6 ± 4.8	0.9 ± 2.8	Time, type (chronicity)	0.826	0.741
	(−2.5 ± 19.2)	(−3.8 ± 5.41)	(−0.8 ± 1.81)		(0.183)	(0.640)
Action research arm test (ARAT)						
$ARAT_{Total}$	3.1 ± 4.08	0.4 ± 2.1	−0.8 ± 0.6	Severity, gender, age,	0.228	0.154
	(1.8 ± 3.8)	(3.2 ± 5.5)	(0.5 ± 0.5)	chronicity, time, type, concordance	(0.699)	(0.256)
$ARAT_{Grip}$	0.3 ± 6.5	0.2 ± 0.4	−0.5 ± 0.3	Severity, gender, age,	0.514	0.075
	(3.4 ± 11.0)	(1.2 ± 1.6)	(0.1 ± 0.2)	concordance, chronicity, time, type	(0.195)	(0.458)
$ARAT_{Grasp}$	1.1 ± 2.1	1.2 ± 1.9	0.03 ± 0.4	Severity, gender, age,	0.579	0.949
	(0.1 ± 0.4)	(1.0 ± 3.5)	(0.5 ± 0.3)	concordance, chronicity, time, type	(1.00)	(0.146)
$ARAT_{Pitch}$	0.8 ± 2.1	−0.2 ± 0.4	−0.2 ± 0.3	Seventy, concordance,	0.391	0.508
	(0.3 ± 2.1)	(0.3 ± 0.8)	(0.2 ± 0.2)	time, age, gender, type (chronicity)	(0.704)	(0.501)
$AKAT_{Gross}$	0.3 ± 0.5	1.0 ± 1.9	−0.2 ± 0.3	Severity, age, concordance,	1.00	0.46
	(0.8 ± 1.2)	(0.2 ± 0.5)	(−0.2 ± 0.2)	chronicity, time, type (gender)	0.252	(0.303)

*Scores, covariates, and p-values are reported for n = 21 participants during BCI intervention: mean improvement scores between time points 1 and 3, (parentheses) indicates mean improvement scores between time points 1 and 4. Interaction LME p-value is a p-value for the likelihood ratio test between two LME models differing only in the inclusion of a time:type interaction term (where type is either intervention period or control) as a covariate. *p < 0.05, **p < 0.01, ***p < 0.001.*

2000 software (Schalk et al., 2004) version 2 with in-house modifications for input from a 16-channel EEG cap and amplifier (Guger Technologies) and integration with tongue stimulation (TDU) (TDU 01.30 Wicab Inc.) (Kaczmarek, 2011) and functional electrical stimulation (FES) of distal UE muscles (LG-7500, LGMedSupply; Arduino 1.0.4) associated with grasping behavior.

Functional Electrical Stimulation

Functional electrical stimulation of the UE was delivered using the LG-7500 Digital Muscle Stimulator (LGMedSupply, Cherry Hill, NJ, United States). Stimulus was conducted through a pair of 2" × 2" square electrodes placed securely on the affected forearm using highly conductive Electrolyte Spray. The electrodes were placed to facilitate either a grasping motion (finger flexion), or finger extension according to participant preference. Specific placement sites were superficial to digitorum superficialis to facilitate hand and finger flexion, or superficial to extensor digitorum communis to facilitate hand and finger extension. The natural absence of a flexor digitorum superficialis tendon to the fifth digit in some individuals was not considered by this study design. Stimulation was controlled through the PC using an Arduino Uno R3 (Adafruit Industries, New York, NY, United States) and a simple reed relay circuit, with the amplitude set to elicit observable muscle activation (e.g., finger grasping) without pain. The pulse rate of the stimulation was set to 60 Hz to produce tetanic contraction of the muscle; the pulse width was set to 150 μs. The input signal, initially set to zero, was adjusted by steps of 0.5 mA, unless the stimulation became uncomfortable for the subject. The device was never set to deliver an output greater than 5.0 mA.

Tongue Display Unit

In previous publications, the TDU has been described and its use in a BCI paradigm detailed (Schalk et al., 2004; Kaczmarek,

TABLE 4 | Summary of outcome measures during assessment and including follow-up for responders vs. non-responder.

Outcome Measures	Responder improvement score	Non-responder improvement score	LME			*T*-test	Interaction LME	Response LME
	Mean ± SD	Mean ± SD	Estimate ± SE		Covariates	*p*-value	*p*-value	*p*-value
Stroke impact scale (SIS)								
$SIS_{Hand\ Function}$	4.4 ± 21.4	10.0 ± 11.8	−2.8 ± 4.2	6 ± 5.9	Severity, *time, response*	0.901	0.498	0.26
	(7.7 ± 19.54)	(3.0 ± 4.5)	(0.4 ± 2.3)	(7 ± 5.6)	(chronicity)	(0.544)	(0.877)	(0.179)
$SIS_{mobility}$	9.2 ± 8.0	12.8 ± 13.4	−1.3 ± 2.3	19.6 ± 5.8	Seventy, age, chronicity,	0.382	0.564	0.000213***
	(8.0 ± 8.6)	(11.6 ± 18.9)	(−1.4 ± 1.8)	(18.6 ± 6.9)	concordance, gender, *time, response*	(0.487)	(0.405)	(0.00155)**
SIS_{ADL}	8.6 ± 11.0	10.0 ± 10.8	−0.7 ± 3.1	10 ± 6.8	Seventy, concordance,	0.295	0.819	0.0515
	(6.3 ± 9.8)	(9.5 ± 9.6)	(−2.0 ± 2.0)	(9.7 ± 7.4)	gender, age, *time*, *response*	(0.523)	(0.291)	(0.0795)
$SIS_{Strength}$	6.2 ± 13.6	2.5 ± 15.7	1.9 ± 4.4	15.4 ± 9.7	Severity, gender, *unit,*	0.255	0.661	0.049*
	(11.8 ± 11.0)	(10.0 ± 16.9)	(0.04 ± 2.8)	(14.8 ± 9.2)	*response*	(0.430)	(0.988)	(0.048)*
Grip Strength	3.0 ± 7.4	1.0 ± 2.2	1.0 ± 2.1	6.1 ± 3.7	Seventy, chronicity,	0.399	0.617	0.082
	(1.7 ± 11.0)	(1.3 ± 2.3)	(0.4 ± 1.2)	(5.5 ± 3.5)	concordance, *time, response*	(0.864)	(0.766)	(0.095)
9-HPT Affected	–	–	–	–	–	–	–	–
Action research arm test (ARAT)								
$ARAT_{Total}$	3.5 ± 5.2	−0.8 ± 1.3	1.6 ± 0.5	4.4 ± 4.8	Severity, gender, age,	0.242	0.0026**	0.239
	(4.4 ± 6.2)	(*l*.4 ± 1.9)	(1.2 ± 0.6)	(5.1 ± 5.3)	concordance, chronicity, *time*, *response*	(0.204)	(0.078)	(0.214)
$ARAT_{Grip}$	0.2 ± 0.4	−0.2 ± 0.4	0.2 ± 0.2	0.9 ± 1.1	Severity, gender, chronicity,	0.399	0.212	0.226
	(1.3 ± 1.4)	(0.4 ± 1.5)	(0.3 ± 0.2)	(1.2 ± 1)	concordance, *time, response*	(0.208)	(0.158)	(0.099)
$ARAT_{Grasp}$	1.6 ± 1.8	−0.2 ± 0.4	0.9 ± 0.5	1.9 ± 2	*Time*, *response* (age,	0.347	0.09	0.236
	(2.4 ± 4.6)	(0.4 ± 1.5)	(0.6 ± 0.4)	(2.4 ± 1.7)	chronicity)	(0.495)	(0.151)	(0.159)
$ARAT_{Pitch}$	0.7 ± 2.1	0 ± 0	0.04 ± 0.04	1.0 ± 1.1	Severity, chronicity, *time*,	1.0	0.322	0.296
	(1.1 ± 1.8)	(0.3 ± 2.1)	(0.4 ± 0.2)	(1.1 ± 1.1)	*response*	(0.907)	(0.067)	(0.236)
$AKAT_{Gross}$	0.2 ± 1.5	0.4 ± 1.8	0.3 ± 0.4	0.8 ± 1.3	Severity, age, concordance,	0.621	0.463	0.43
	(0.1 ± 1.6)	(0.6±0.9)	(−0.1 ± 0.3)	(0.4 ± 1.4)	gender, *time*, *response* (chronicity)	0.864	(0.727)	(0.509)

*Scores, covariates, and p-values are reported for n = 21 participants during BCI intervention: mean improvement scores between time points 1 and 3, (parentheses) indicate mean improvement scores between time points 1 and 4. Interaction LME p-value is a p-value for the likelihood ratio test between two LME models differing only in the inclusion of a time:response interaction term as a covariate. Response LME p-value is a p-value for the likelihood ratio test between two LME models differing only in the inclusion of a response term as a covariate with neither models including an interaction term. *p < 0.05, **p < 0.0l, and ***p < 0.001.*

TABLE 5 | Demographic distribution by ARAT score response.

Response	Participants	Age (years) mean ± SD	Females (males)	Acute (chronic)	Mild (severe)	Concordant (non-concordant)
Responder	9	62.6 ± 14.3	5 (4)	1 (8)	2 (7)	2 (7)
Non-responder	5	58.3 ± 12.9	3 (2)	2 (3)	0 (5)	0 (5)
Total	14	61.1 ± 13.5	8 (6)	3 (11)	2 (12)	2 (12)

Concordant strokes are classified as those predominantly affecting the preferred arm as assessed by the Edinburgh Handedness Inventory [30]. Individual responder and non-responder demographics are highlighted on ARAT outcome denoting the responders.

2011; Wilson et al., 2012). This BCI system uses the same TDU stimulation parameters as were previously reported (Wilson et al., 2012).

BCI Intervention Procedure

Familiarization With the BCI Device and Procedures

The first BCI session was focused on assisting the participant to comprehend and engage the BCI device and protocol. Stroke survivors often present with a myriad of cognitive, affective, and physical impairments (Nair et al., 2015; Stinear, 2016) and out of respect for individual participant needs and abilities, the researchers provide at outset an opportunity for a generous orientation rather than rigorous acquisition. During this preliminary session, the EEG cap, FES device, and TDU device were faithfully administered as described previously (Wilson et al., 2012). Participants were instructed before each session, and as needed, to aim for successful completion of BCI tasks and for each attempted movement to be performed to the participant's autonomously elected level of comfort, ability, and pleasure. The proposed design entails at least 10 runs for each closed-loop condition per session; however, enforcement discretion was encouraged until a participant demonstrated task comprehension.

Cursor Task and User Integration

In the closed-loop BCI intervention task, participants perform attempted actual hand movements in response to a left or right target cue displayed on a computer screen as a virtual *ball-and-target* (Young et al., 2015; **Figure 2**). To accommodate initial movement capacity and recovery goals, best possible attempts at repeated hand grasping (finger extension and flexion) were used. Participants learn to control horizontal movement of a virtual ball displayed on the monitor by modulating their sensorimotor rhythm (SMR) activity (SMR activity represents Mu and Beta rhythm changes over the motor cortex – this process is indicative of healthy normal brain electrophysiology of attempted movement) as they perform the task (Wilson et al., 2012). The SMR activity related to attempted left (or right) hand movements, as recorded by the EEG, is then translated into leftward (or rightward) ball movement via the BCI (Wilson et al., 2012). Mu and beta SMRs in human subjects (Muralidharan et al., 2011) are recorded exclusively over sensorimotor areas at frequencies of about 8–12 and 16–24 Hz (Pfurtscheller et al., 1997; Riehle and Vaadia, 2004; Birbaumer et al., 2006), with the source of human SMR in the sensorimotor regions following the homuncular organization of the motor and somatosensory cortical strip (Pfurtscheller et al., 1997; Riehle and Vaadia, 2004). At the start of each intervention trial, a virtual target randomly appears on the left or right side of the screen. After 1 s, a virtual ball appears in the center of the screen, and the subject is instructed to move the ball toward the target by eliciting SMR modulation using attempted hand movement. For a trial to be considered successful, the ball must hit the target within 5 s of its appearance. Trials are aborted and considered unsuccessful if, after 5 s, the ball has not reached the target. The inter-trial interval is 3 s regardless of aborted or successful trial (**Figure 2**).

Adjuvant Stimulus Schedule

Following completion of at least 10 runs of the visual only BCI task described above, adjuvant FES stimulation was applied to the muscles of the impaired hand, and electro-tactile feedback (visual replication and supplementation) was presented when available through the TDU for the duration of the trials possible in a 2-h session. In this way, subjects might utilize visual feedback, muscle stimulation, and electro-tactile feedback (or visual replacement or supplementation in the case of uncorrected visual impairment) to monitor their task performance. FES-driven stimulation, however, was only applied to the impaired limb and concordant with both ball movement toward the impaired side, and the virtual target presenting on the impaired side. In this way, externally facilitated muscle stimulation never occurred while the subject was attempting to move the ball toward their unimpaired side.

RESULTS

Primary Effect of BCI Intervention

Of the n = 21 participants, 14 participants had room for improvement in the ARAT of which 64% (9/14) realized improved scores in the primary outcome measure ($ARAT_{total}$) from baseline to completion of intervention, both at immediate completion and/or 1-month post-completion (**Table 1**). 43% (6/14) had changes in the ARAT that are considered to meet significant ARAT specific thresholds [four of these participants had MDC $\geq$ 3 (MDC_{90} = 3.0; Simpson and Eng, 2013) and two of these participants had MCID $\geq$ 5.7 both at immediate completion and/or 1-month post-completion]. The seven participants who had no room for improvement, or had a max score of 57 at

ARAT, stayed at the same max level in ARAT both at immediate completion and 1-month post-completion.

Effect of Intervention Time on Outcome Scores

A paired samples *t*-test found a significant effect of time on ARAT outcome improvement score ($p = 0.046$). Secondary outcome measures found to have significant effect over time included $SIS_{mobility}$ ($p = 0.001$), SIS_{adl} ($p = 0.041$), $SIS_{strength}$ ($p = 0.024$), as well as Hand Grip Strength ($p = 0.046$) and $9HPT_{affected}$ ($p = 0.0081$) (**Table 2**).

Likelihood ratio tests of LME models over time periods 1–3 controlling for severity, gender, chronicity, and concordance did demonstrate a significant effect of time on ARAT outcome score improvement ($p = 0.02754$) (**Table 2**). Specifically, the full LME model revealed an estimate improvement rate of ARAT score by 0.64 ± 0.28 ($\mu \pm$ SE) between time periods. In addition, the LME model found significance for the secondary outcome measures of $SIS_{mobility}$ ($p = 0.00001$), SIS_{adl} ($p = 0.008613$), $SIS_{strength}$ ($p = 0.0212$), Hand Grip Strength ($p = 0.0368$), and $9HPT_{affected}$ ($p = 0.0201$) while controlling for the most significant covariates as determined by forward stepwise regression (**Table 2**).

Including Follow-Up

A paired samples *t*-test evaluated between baseline and follow-up demonstrated a significant effect of ARAT improvement score ($p = 0.020$). Many secondary measurements at follow-up demonstrated similarly significant improvements including $SIS_{mobility}$ ($p = 0.010$), SIS_{adl} ($p = 0.035$), $SIS_{strength}$ ($p = 0.001$), and $9HPT_{affected}$ ($p = 0.046$) (**Table 2**).

The likelihood ratio tests of the LME models across follow-up also demonstrated significant improvement in ARAT, controlling for severity, gender, chronicity, and concordance ($p = 0.0010$) (**Table 2**). The estimated improvement rate of ARAT score was 1.06 ± 0.31 ($\mu \pm$ SE) between time periods. The likelihood ratio tests also revealed significance among $SIS_{mobility}$ ($p = 0.00009$), $SIS_{strength}$ ($p = 0.00039$), and $9HPT_{affected}$ ($p = 0.01178$) (**Table 2**).

ARAT Improvement Rate Between Control and Intervention (Therapy Type)

During Assessment Period

When testing between Control ($n = 12$) vs. Intervention ($n = 9$) therapy types, the independent samples *t*-tests did not find that subjects during intervention improved in ARAT outcome score at a significantly faster rate than controls. Additional measures via *t*-tests found no significant differences between control and intervention from time points 1–3 (**Table 3**).

A likelihood ratio test controlling for severity, gender, age, chronicity, concordance, and the independent effects of time and therapy type (control or intervention) also did not find a significant effect of the specific interaction term between time and therapy type for ARAT outcome score ($p = 0.1543$) (**Table 3**). Similarly, improvement rates for secondary measurement outcome scores between intervention and control from time points 1–3 were not significant while controlling with forward stepwise regression selected covariates and the independent effects of time and therapy type (**Table 3**).

Including Follow-Up

The *t*-test assessed at follow-up did not find a significant effect of ARAT outcome improvement score. However, there was a significant effect of $SIS_{strength}$ improvement score ($p = 0.019$) (**Table 3**). The likelihood ratio tests at follow-up for ARAT, controlling for severity, gender, age, chronicity, concordance, and the independent effects of time and type were not significant ($p = 0.256$) (**Table 3** and **Figure 3A**). Like the *t*-test, there was a significant effect between control and intervention for $SIS_{strength}$ ($p = 0.0117$) when controlling for severity, chronicity, gender, and the independent effects of time and therapy type (**Table 3** and **Figure 3B**).

ARAT Improvement Rate Between Responders and Non-responders (Response Type)

During Assessment Period

When testing between responders ($n = 9$) vs. non-responders ($n = 5$), neither *t*-tests nor likelihood ratio tests of generalized mixed effect models found the individual covariates of age, gender, chronicity, severity, concordance of strokes, or baseline ARAT scores to significantly predict a subject's ability to improve in ARAT outcome over the course of intervention. LME analyses demonstrated that, while controlling for severity, gender, chronicity, concordance, and the independent effects of time and response, responders improved significantly faster than non-responders by 1.62 ± 0.51 ($\mu \pm$ SE) points per time point through intervention (**Table 4**). LME analyses further revealed significant positive differences between responders and non-responders in $SIS_{mobility}$ by intervention completion ($p = 0.0002$) and $SIS_{strength}$ ($p = 0.04995$) (**Table 4** and **Figure 3C**). Specifically, responders demonstrated increased $SIS_{mobility}$ scores of 19.63 ± 5.75 ($\mu \pm$ SE) and increased $SIS_{strength}$ scores of 15.38 ± 9.67 through intervention.

Including Follow-Up

When testing between responders ($n = 9$) vs. non-responders ($n = 12$), neither *t*-tests nor likelihood ratio tests of generalized mixed effect models found the individual covariates of age, gender, chronicity, severity, concordance of strokes, or baseline ARAT scores to significantly predict a subject's ability to improve in ARAT outcome through follow-up. LME analyses did not demonstrate a significant difference in improvement rates in ARAT between responders and non-responders through follow-up while controlling for severity, gender, chronicity, concordance, and the independent effects of time and response ($p = 0.07821$) (**Table 4**). However, LME analyses did reveal significant positive differences between responders and non-responders in $SIS_{mobility}$ ($p = 0.00155$) and $SIS_{strength}$ ($p = 0.04828$) through follow-up while controlling for the forward-step selected covariates (**Table 4** and **Figure 3C**). Specifically, responders demonstrated increased $SIS_{mobility}$ and $SIS_{strength}$ scores of 18.59 ± 6.88 and 14.80 ± 9.23 ($\mu \pm$ SE), respectively, through follow-up while controlling for the selected covariates (**Table 4** and **Figure 3D**).

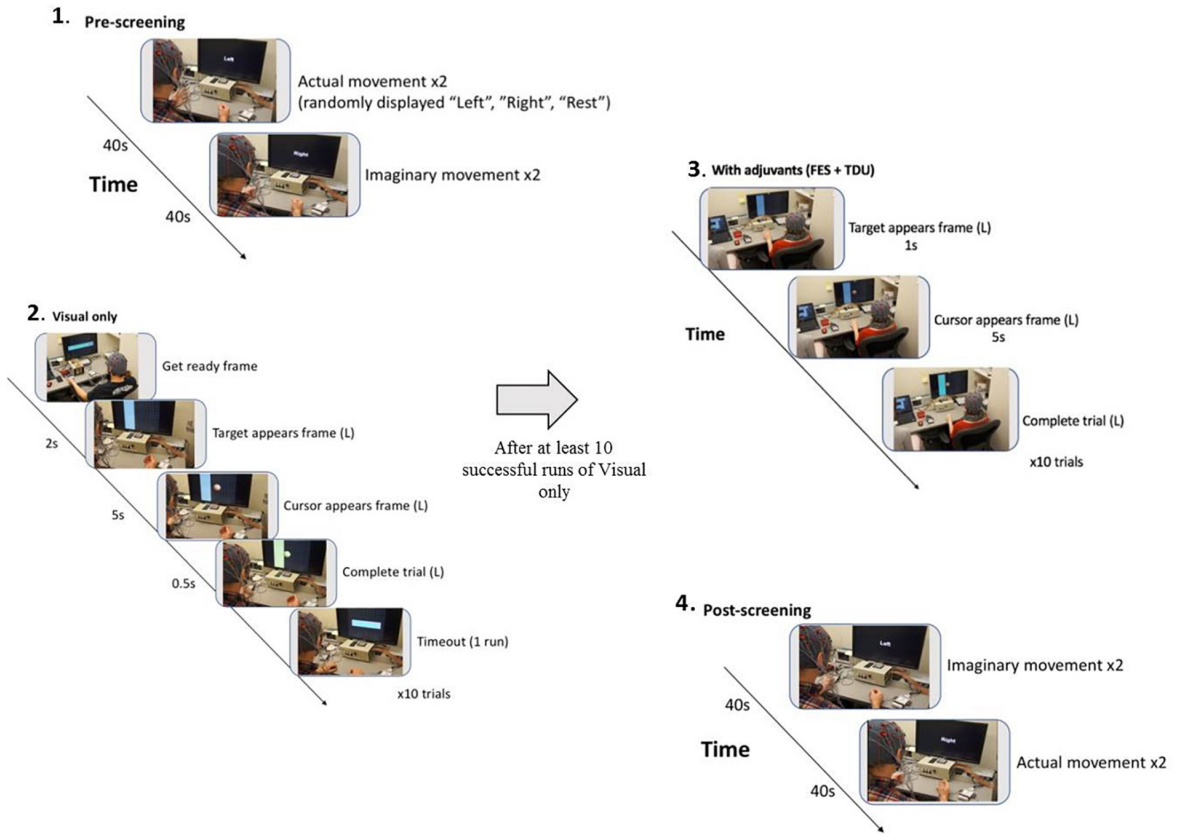

FIGURE 2 | BCI intervention block design: (1**)** A pre-session open-loop screening task of two attempted and then two imagined grasping tasks (left, right, rest) is used to set control features (BCI classifier) for the forthcoming intervention task (Cursor Task). (2) The closed-loop cursor and target (visual only) intervention condition consists of at least 10 runs of 10 trials of attempted grasping movements for the purpose of guiding a virtual cursor (Ball) either left, or right as cued by the target (Goal) presentation on the horizontal edge of the screen. (3) Following 10 successfully completed runs of the visual only condition, adjuvant stimuli are added to enrich the feedback environment and facilitate volitional movement of the affected extremity (grasping). Subsequent runs are attempted at the preferred pace of the participant, completing as many runs as time allows. (4) With 15 min remaining in the 2-h intervention session, the participant is switched into the post-session open-loop screening task of two imagined and then two attempted grasping tasks (left, right, rest).

Identifying Patients for BCI Intervention

These data suggest that particular participant characteristics may be associated with greater gains of functional capacity. The covariates of severity, concordance of strokes, age, gender, and chronicity, within this limited sample size, may not, at this sampling, significantly predict whether a participant will improve in ARAT primary outcome scores due to BCI intervention. However, increased $SIS_{mobility}$ and $SIS_{strength}$ scores do significantly help predict response outcome (**Table 4**). It is further possible that other outcome scores relatively close to significance ($p \leq 0.1$), such as SIS_{adl} and Hand Grip Strength (**Table 4**), may prove significant with an increase in sample size. Additionally, although gender, chronicity, severity, or concordance did not significantly predict if a participant would become a responder, 73% (8/11) of chronic and 100% (2/2) of mild participants who had room for ARAT improvement became responders. Responders to this intervention schedule were, like the larger cohort sample, a heterogeneous group and included survivors with severe motor impairment of non-dominant hand (**Table 5**) as measured post stroke. It may be possible to extrapolate upon these data, strengthened by systematic review of existing literature, to identify patients prepared to realize optimal recovery outcomes with BCI intervention.

DISCUSSION

Prescribing BCI as UE Therapy

Brain–computer interface intervention can impact functional motor capacities of the impaired UE (Remsik et al., 2016), and in this sample, primary outcome measurements of distal UE function did significantly improve from baseline to completion as well as baseline to follow-up (**Table 2**). Results also suggest the delayed therapy condition utilized in this cross-over controlled design did not adversely affect UE impairments in individuals randomized into the DTG. Participants in intervention showed greater rate of change compared to control (**Figure 3A**) as well as greater average gains by completion. However, these differences were not statistically significant. Insufficient power, especially following the removal of ceilings, as well as the duration of

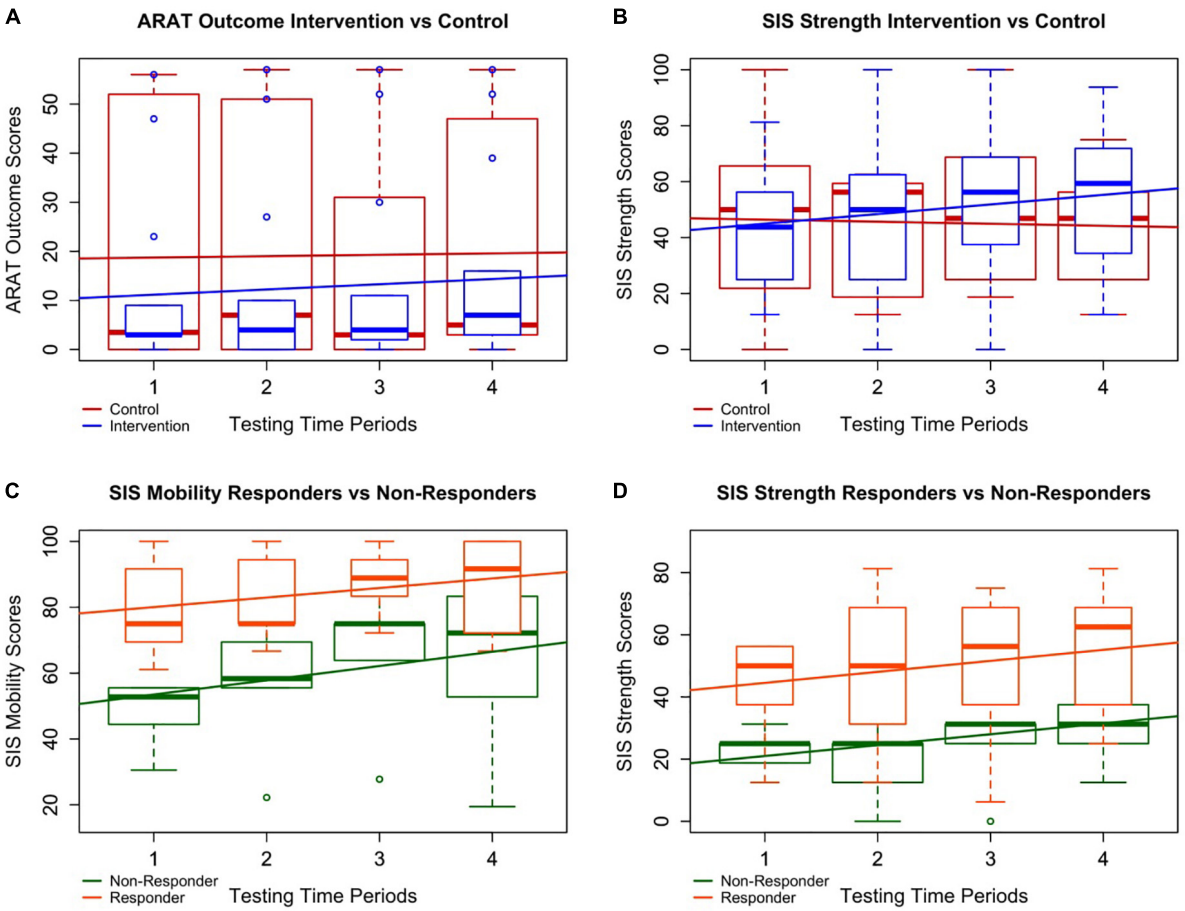

FIGURE 3 | Intervention vs. control and responder vs. non-responder plots. Four of the most notably significant relationships are plotted with boxplots of all patient data overlaid by simple linear best fit lines to depict general trends in the data. **A** and **B** specifically demonstrate differences in the data between all controls (in red) and all interventions (in blue) whereas **C** and **D** represent trends in the data between responders (in orange) and non-responders (in green). **(A)** Although the improvement rate in ARAT for subjects in intervention was not significantly higher than controls, participants in intervention did significantly improve over time, and the trend of the boxplot medians suggests a possible continuation of improvement through follow-up not present in the control period. **(B)** Participants in intervention significantly improved faster over time in $SIS_{strength}$ than those in the control period despite both groups starting at similar levels of ability. **(C, D)** Responders demonstrated significantly higher average $SIS_{mobility}$ and $SIS_{strength}$ scores than non-responders. This suggests patients with lower $SIS_{mobility}$ and $SIS_{strength}$ scores may not benefit from BCI intervention as well as those with higher scores.

specific neural plastic changes (weeks, months, or longer) (Jones, 2017), may contribute to this lack of significant differences.

Although BCI intervention appears to lead to functional reorganization of the central nervous system, or brain (Caria et al., 2011; Song et al., 2014, 2015; Zich et al., 2017; Cervera et al., 2018), it is not unreasonable to suggest that more time in therapy is needed for these CNS changes to manifest as measurable, clinically relevant changes in UE behavior. This possibility may explain the delay in primary outcome improvement between baseline and midpoint medians (2–3 weeks apart) compared to the differences between baseline and completion or even the middle time point and completion (**Figure 3A**). This assumption is supported by the continued improvement between midpoint and follow-up for those in intervention, a change which is not observed in the control group (**Figure 3A**). This delay of 2–3 weeks of the larger primary outcome score change is also consistent with a similar BCI therapy research design (Li et al., 2014). Further analysis about the rate of change at various time points is needed.

Mean projected FMA-UE changes from baseline to follow-up in this sample (5.4) are comparable to improvements in FMA-UE baseline to completion score changes (Cervera et al., 2018) in other published experimental BCI intervention studies. Subchronic patients generally experience greater therapeutic effects of BCI interventions than do chronic participants (Cervera et al., 2018), and a similar limiting relationship may exist between mild and severe UE impairment patients (Cramer and Nudo, 2010; Stinear and Byblow, 2014). Such trends may account for some differences between the presented projected FMA-UE score changes estimated from this sample (mean change of 2.2 and 5.4 at completion and 1-month post-completion, respectively) (**Table 1**), which are potentially labored by the heterogeneity of time since stroke and level of physical impairment post-stroke, and greater changes reported in similar studies (Li et al., 2014;

Kim et al., 2016) by other groups. For example, Li et al. (2014) (n = 7) demonstrated a 12.7 FMA-UE change, however with a sample of subjects that was much less chronic (all chronicity $\leq$ 6 months) than those participants examined herein (Li et al., 2014). Similarly, Kim et al. (2016) (n = 15) saw a 7.87 change in FMA-UE scores, however on average (baseline μ_{FMA-UE} = 26.8), those subjects had less severe strokes (Kim et al., 2016) than the participants in this sample. In general, most BCI intervention studies remain underpowered and inadequately constrained (Cervera et al., 2018), presenting threats to both internal and external validity.

The results of this study suggest that $SIS_{mobility}$ and $SIS_{strength}$ may be important factors to consider when designing or prescribing BCI regimes as higher scores were significantly indicative of increased likelihood for treatment success. While still unclear, other factors that may also play predictive roles in BCI interventional motor recovery include, but are not limited to, Hand Grip Strength and SIS_{adl} scores, as well as stroke chronicity and severity. While insignificant due to the small sample size, the large proportions of chronic and mild patients who became responders, 73% (8/11) and 100% (2/2), respectively, does follow previously reported trends (Caria et al., 2011; Ang and Guan, 2013; Young et al., 2014d; Ang et al., 2015; Remsik et al., 2016). The fact that BCI intervention appears to be able to specifically benefit chronic patients is especially interesting as many stroke patients reach a functional recovery plateau by completion of standard of care treatment (Wolf et al., 2006, 2010; Dromerick et al., 2009; Cramer and Nudo, 2010). The heterogeneity of these data and relatively small sample size may limit the external validity of all reported trends as well as limit the realization of other important predictors.

To date, the literature exploring the behavioral and rehabilitative implications of BCI treatments remains underpowered. Nonetheless, this body of research has shown rapid growth in the last decade and a half (Ang and Guan, 2013; Remsik et al., 2016; Bundy et al., 2017; Cervera et al., 2018). Research assessing which presenting stroke patients will profit most from BCI treatments remains mostly inconclusive. However, increased microstructural integrity of the ipsilesional posterior limb of the internal capsule (PLIC) has been correlated with greater motor recovery from BCI therapy (Song et al., 2014, 2015). Similarly, Young et al. (2016) demonstrated that changes to the integrity of the contralesional corticospinal tract (CST) during BCI therapy correlates to behavioral improvement scores for ARAT and 9-HPT. Thus far, most BCI treatment studies have observed participants in the chronic stage of stroke. As BCI is still a relatively new concept for treatment of UE paresis, it is possible that the majority of individuals participating in BCI research have exhausted standard clinical care. Thus, samples may be weighted disproportionately by participants with chronic persistent UE motor disability. It is also possible that the therapeutic impact of BCI intervention is dependent on several factors (i.e., residual motor capacity, lesion volume, and time since stroke) which should be considered before BCI treatment is prescribed (Stinear and Byblow, 2014). A forthcoming intent to treat analysis of this study should help address some of these unanswered questions in a more robust manner.

Motivational Influences of BCI Use

Changes in primary outcome scores (ARAT) during treatments suggested that this BCI design may deliver moderate objective positive UE motor changes, as seen in the 64% (9/14) of participant (out of those who had room for improvement) "Responders" who completed the BCI treatments protocol as designed. 43% (6/14) had changes in the ARAT who are considered to meet significant ARAT-specific thresholds [four of these participants had MDC of at least 3 (MDC_{90} = 3.0; Simpson and Eng, 2013) and two of these participants had MCID of at least 5.7 both at immediate completion and/or 1-month post-completion]. Additionally, the largest positive changes compared to baseline in ARAT were observed 1-month post treatment for a few participants. This might suggest that continuation of biological and behavioral recovery mechanisms induced by BCI systems may remain active in participants beyond their time in the lab setting.

Limitations

Suitability of Dichotomized Responder Analysis as a Sufficient Measure of Clinical Importance of Treatment Effects

A significant portion of this publication is dedicated to an analysis of participants according to *post hoc* dichotomized assignment by main effect in the primary outcome. Responder analyses are challenged by several inherent limitations (Snapinn and Jiang, 2007). First, the arbitrariness of a "responder" threshold value levies a substantial cost as dichotomization decreases efficiency and increases sample size requirements (limited power relative to analysis of the original selection). Further, the motivation for a responder analysis is to assess clinical relevance (to ensure clinical relevance of treatment effect), and as clinical relevance is ubiquitous with every clinical trial and setting, such logic may be seen as inherently circuitous. Beyond the inherent shortcomings of a *post hoc* responder analysis, this study was constrained by heterogeneity in many covariates including lesion location, level of impairment, age, gender, and time since stroke among the participants studied. Certainly, greater power is needed to adequately generalize results to a more adequate standard.

Nature of the Academic Research Environment

This is an ongoing study in its seventh year of data acquisition and enrollment. Multiple different project personnel have undergone and supervised the staffing, training, and data acquisition of this trial during its course. The authors work hard to best minimize differences in acquisition of study measures through extensive and repeated training of personnel.

CONCLUSION

Both primary (ARAT) and secondary ($SIS_{mobility}$, SIS_{adl}, $SIS_{strength}$, Hand Grip Strength, and $9HPT_{affected}$) outcome measures were significantly improved over the course of this

BCI interventional therapy. For $SIS_{strength}$ scores specifically, participants in intervention demonstrated significantly increased improvement rates through follow-up compared to controls while controlling for severity, chronicity, gender, and the independent effects of time and therapy type as measured through likelihood ratio tests of LME models. None of the analyses revealed any significant negative effect of delaying BCI treatments for participants. This particular result may be attributed to the chronicity of most of the recruited participants ($n = 16 \geq 1$ year, $n = 17 \geq 6$ months) since patients typically reach a functional plateau before the chronic phase of stroke and are not expected to realize a large degree of change, rehabilitative or otherwise, to their UE motor capacity. This particular study did not reveal significant differences between those who demonstrated improvement in ARAT outcome and those who did not in terms of age, gender, chronicity, severity, or concordance of stroke impairment suggesting that the BCI intervention design may be suitable for a large range of patients. However, 8/11 chronic, and both mild, participants with room for ARAT score improvement achieved "responder" designation, and the explicit capacity of BCI treatments to assist chronic (and mild) stroke patients, even after they have reached a functional plateau, is reported in other literature (Caria et al., 2011; Ang and Guan, 2013; Young et al., 2014d; Ang et al., 2015; Remsik et al., 2016). Despite statistical limitations of the heterogeneity of the relatively small sample size in this study, those who responded to the BCI intervention did have significantly higher self-reported $SIS_{mobility}$ and the $SIS_{strength}$ scores through follow-up. These findings may suggest that particular measures can assist in the prescription of a BCI intervention regimen necessary for an individual participant, as well as aid in the prediction and measurement of BCI interventional success as assessed by primary outcome measures of capacity and performance, like the ARAT.

Additional research is required to identify how BCI intervention dose–response relationships are influenced by the various potential classifications of stroke survivors. It is quite possible that prescribing BCI intervention as a one-size fits all treatment for UE motor impairment may not be an ideal approach for this rehabilitative technology. Rather, these data suggest that at least some outcome measures, along with stroke severity and chronicity, may prove valuable in determining if BCI treatments could be effective for a stroke survivor with persistent UE paresis. Therefore, patients receiving BCI treatments in future research or clinical contexts might benefit most from a treatment regimen tailored to the individual's presenting performance capacity as measured by the easily administered and scored SIS. Supplementary outcome measures (both objective and self-reported), impairment characteristics, and treatment goals should all be taken into account when designing a BCI intervention for a potential participant. Future studies should seek to more thoroughly examine the effects of patient characteristics on BCI effectiveness, and examine how to deliver targeted treatments based on individual impairments and treatment goals in a concerted effort to maximize rehabilitative effect with similar BCI intervention strategies.

AUTHOR CONTRIBUTIONS

AR and KD were involved in subject recruitment, data collection, data processing, analyses, as well as interpreting and writing of the manuscript. LW was involved in preprocessing data, writing, and editing the manuscript. KG and CR were involved in interpreting and writing of the manuscript. JT, TJ, JA, MMc, and MM were involved in data collection, analyses, and editing the manuscript. BY was involved in subject recruitment, data collection, and manuscript editing. ZN was involved in subject recruitment and data collection. MW, MM, MMc, SR, HA, RM, NT, LW, and JA were involved in data collection. VN contributed to data collection, manuscript editing and intellectual content. PvK contributed to manuscript editing and intellectual content. TK was involved in the recruitment of study participants. JS was involved in recruitment of study participants and intellectual content. JW, VP, and DFE are co-PIs and were involved in study conception, design, manuscript editing, and intellectual content.

FUNDING

This work was supported by NIH grants RC1MH090912-01, T32GM008692, UL1TR000427, K23NS086852, T32EB011434, R01EB000856-06, and R01EB009103-01 and by the DARPA RCI Program (MTO) N66001-12-C-4025 and HIST Program (MTO) N66001-11-1-4013. Additional funding was also provided through a Coulter Translational Research Award, the American Heart Association Grant 1T32EB011434-01A1, AHA Innovative Research Award – National (Marcus Foundation) 15IRG22760009, AHA Midwest Grant in Aid Award 15GRNT25780033, the Foundation of ASNR, UW Milwaukee–Madison Intercampus Grants, the UW Graduate School, and by Shapiro Foundation Grants.

ACKNOWLEDGMENTS

The authors would like to thank all the study participants and their families for their time and efforts participating in this study. The authors would also like to extend thanks to Drs. Justin Sattin and Kristin Caldera for referrals of stroke subjects and clinical documentation.

SUPPLEMENTARY MATERIAL

The Supplementary Material for this article can be found online at: https://www.frontiersin.org/articles/10.3389/fnins.2018.00752/full#supplementary-material

REFERENCES

An, K. N., Chao, E. Y., and Askew, L. J. (1980). Hand strength measurement instruments. *Arch. Phys. Med. Rehabil.* 61, 366–368.

Ang, K. K., Chua, K. S. G., Phua, K. S., Wang, C., Chin, Z. Y., Kuah, C. W. K., et al. (2015). A randomized controlled trial of EEG-based motor imagery brain-computer interface robotic rehabilitation for stroke. *Clin. EEG Neurosci.* 46, 310–320. doi: 10.1177/1550059414522229

Ang, K. K., and Guan, C. (2013). Brain-computer interface in stroke rehabilitation. *J. Comput. Sci. Eng.* 7, 139–146. doi: 10.5626/JCSE.2013.7.2.139

Beebe, J. A., and Lang, C. E. (2009). Relationships and responsiveness of six upper extremity function tests during the first 6 months of recovery after stroke. *J. Neurol. Phys. Ther.* 33, 96–103. doi: 10.1097/NPT.0b013e3181a33638

Benjamin, E. J., Blaha, M. J., Chiuve, S. E., Cushman, M., Das, S. R., Deo, R., et al. (2017). Heart disease and stroke statistics-2017 update: a report from the American Heart Association. *Circulation* 135, e146–e603. doi: 10.1161/cir.0000000000000485

Birbaumer, N., Weber, C., Neuper, C., Buch, E., Haapen, K., and Cohen, L. (2006). Physiological regulation of thinking: brain–computer interface (BCI) research. *Prog. Brain Res.* 159, 369–391. doi: 10.1016/S0079-6123(06)59024-7

Bundy, D. T., Souders, L., Baranyai, K., Leonard, L., Schalk, G., Coker, R., et al. (2017). Contralesional brain–computer interface control of a powered exoskeleton for motor recovery in chronic stroke survivors. *Stroke* 48, 1908–1915. doi: 10.1161/STROKEAHA.116.016304

Caria, A., Weber, C., Brötz, D., Ramos, A., Ticini, L. F., Gharabaghi, A., et al. (2011). Chronic stroke recovery after combined BCI training and physiotherapy: a case report. *Psychophysiology* 48, 578–582. doi: 10.1111/j.1469-8986.2010.01117.x

Cervera, M. A., Soekadar, S. R., Ushiba, J., Millán, J. D. R., Liu, M., Birbaumer, N., et al. (2018). Brain computer interfaces for post stroke motor rehabilitation: a meta analysis. *Ann. Clin. Transl. Neurol.* 5, 651–663. doi: 10.1002/acn3.544

Cramer, S. C., and Nudo, R. J. (eds) (2010). *Brain Repair After Stroke*. Cambridge: Cambridge University Press. doi: 10.1017/CBO9780511777547

Dodd, K. C., Nair, V. A., and Prabhakaran, V. (2017). Role of the contralesional vs. ipsilesional hemisphere in stroke recovery. *Front. Hum. Neurosci.* 11:469. doi: 10.3389/fnhum.2017.00469

Dombovy, M. L. (2009). Maximizing recovery from stroke: new advances in rehabilitation. *Curr. Neurol. Neurosci. Rep.* 9, 41–45. doi: 10.1007/s11910-009-0007-8

Dromerick, A. W., Lang, C. E., Birkenmeier, R. L., Wagner, J. M., Miller, J. P., Videen, T. O., et al. (2009). Very early constraint-induced movement during stroke rehabilitation (VECTORS) A single-center RCT. *Neurology* 73, 195–201. doi: 10.1212/WNL.0b013e3181ab2b27

Duncan, P. W., Wallace, D., Lai, S. M., Johnson, D., Embretson, S., and Laster, L. J. (1999). The stroke impact scale version 2.0: evaluation of reliability, validity, and sensitivity to change. *Stroke* 30, 2131–2140. doi: 10.1161/01.STR.30.10.2131

Hoonhorst, M. H., Nijland, R. H., van den Berg, J. S., Emmelot, C. H., Kollen, B. J., and Kwakkel, G. (2015). How do Fugl-Meyer arm motor scores relate to dexterity according to the action research arm test at 6 months poststroke? *Arch. Phys. Med. Rehabil.* 96, 1845–1849. doi: 10.1016/j.apmr.2015.06.009

Hsieh, C. L., Hsueh, I. P., Chiang, F. M., and Lin, P. H. (1998). Inter-rater reliability and validity of the action research arm test in stroke patients. *Age Ageing* 27, 107–113. doi: 10.1093/ageing/27.2.107

Irimia, D., Sabathiel, N., Ortner, R., Poboroniuc, M., Coon, W., Allison, B. Z., et al. (2016). "RecoveriX: a new BCI-based technology for persons with stroke," in *Proceedings of the 2016 IEEE 38th Annual International Conference of the Engineering in Medicine and Biology Society (EMBC)* (Piscataway, NJ: IEEE), 1504–1507.

Jones, T. A. (2017). Motor compensation and its effects on neural reorganization after stroke. *Nat. Rev. Neurosci.* 18, 267. doi: 10.1038/nrn.2017.26

Kaczmarek, K. A. (2011). The tongue display unit (TDU) for electrotactile spatiotemporal pattern presentation. *Sci. Iran.* 18, 1476–1485. doi: 10.1016/j.scient.2011.08.020

Kim, T., Kim, S., and Lee, B. (2016). Effects of action observational training plus brain–computer interface based functional electrical stimulation on paretic arm motor recovery in patient with stroke: a randomized controlled trial. *Occup. Ther. Int.* 23, 39–47. doi: 10.1002/oti.1403

Lang, C. E., Wagner, J. M., Dromerick, A. W., and Edwards, D. F. (2006). Measurement of upper-extremity function early after stroke: properties of the action research arm test. *Arch. Phys. Med. Rehabil.* 87, 1605–1610. doi: 10.1016/j.apmr.2006.09.003

Li, M., Liu, Y., Wu, Y., Liu, S., Jia, J., and Zhang, L. (2014). Neurophysiological substrates of stroke patients with motor imagery-based brain-computer interface training. *Int. J. Neurosci.* 124, 403–415. doi: 10.3109/00207454.2013.850082

Lin, K. C., Fu, T., Wu, C. Y., Wang, Y. H., Liu, J. S., Hsieh, C. J., et al. (2010). Minimal detectable change and clinically important difference of the stroke impact scale in stroke patients. *Neurorehabil. Neural Repair* 24, 486–492. doi: 10.1177/1545968309356295

Malhotra, R., Ang, S., Allen, J. C., Tan, N. C., Østbye, T., Saito, Y., et al. (2016). Normative values of hand grip strength for elderly singaporeans aged 60 to 89 years: a cross-sectional study. *J. Am. Med. Dir. Assoc.* 17, 864.e1–867.e1. doi: 10.1016/j.jamda.2016.06.013

Mathiowetz, V., Weber, K., Kashman, N., and Volland, G. (1985). Adult norms for the nine hole peg test of finger dexterity. *Occup. Ther. J. Res.* 5, 24–38. doi: 10.1177/153944928500500102

Mohanty, R., Sinha, A. M., Remsik, A. B., Dodd, K. C., Young, B. M., Jacobson, T., et al. (2018). Machine learning classification to identify the stage of brain-computer interface therapy for stroke rehabilitation using functional connectivity. *Front. Neurosci.* 12:353. doi: 10.3389/fnins.2018.00353

Mozaffarian, D., Benjamin, E. J., Go, A. S., Arnett, D. K., Blaha, M. J., Cushman, M., et al. (2015). Heart disease and stroke statistics—2015 update: a report from the American Heart Association. *Circulation* 131, e29–e322. doi: 10.1161/cir.0000000000000152

Muralidharan, A., Chae, J., and Taylor, D. (2011). Extracting attempted hand movements from EEGs in people with complete hand paralysis following stroke. *Front. Neurosci.* 5:39. doi: 10.3389/fnins.2001.00039

Nair, V. A., Young, B. M., La, C., Reiter, P., Nadkarni, T. N., Song, J., et al. (2015). Functional connectivity changes in the language network during stroke recovery. *Ann. Clin. Transl. Neurol.* 2, 185–195. doi: 10.1002/acn3.165

Oldfield, R. C. (1971). The assessment and analysis of handedness: the Edinburgh inventory. *Neuropsychologia* 9, 97–113. doi: 10.1016/0028-3932(71)90067-4

Pfurtscheller, G., Neuper, C., Andrew, C., and Edlinger, G. (1997). Foot and hand area mu rhythms. *Int. J. Psychophysiol.* 26, 121–135. doi: 10.1016/S0167-8760(97)00760-5

Power, J. D., Cohen, A. L., Nelson, S. M., Wig, G. S., Barnes, K. A., Church, J. A., et al. (2011). Functional network organization of the human brain. *Neuron* 72, 665–678. doi: 10.1016/j.neuron.2011.09.006

Remsik, A., Young, B., Vermilyea, R., Kiekhoefer, L., Abrams, J., Evander Elmore, S., et al. (2016). A review of the progression and future implications of brain-computer interface therapies for restoration of distal upper extremity motor function after stroke. *Expert Rev. Med. Dev.* 13, 445–454. doi: 10.1080/17434440.2016.1174572

Riehle, A., and Vaadia, E. (eds) (2004). *Motor Cortex(in)Voluntary Movements: a Distributed System for Distributed Functions*. Boca Raton, FL: CRC Press. doi: 10.1201/9780203503584

Schalk, G., McFarland, D. J., Hinterberger, T., Birbaumer, N., and Wolpaw, J. R. (2004). BCI2000: a general-purpose brain-computer interface (BCI) system. *IEEE Trans. Biomed. Eng.* 51, 1034–1043. doi: 10.1109/TBME.2004.827072

Simpson, L. A., and Eng, J. J. (2013). Functional recovery following stroke: capturing changes in upper-extremity function. *Neurorehabil. Neural Repair* 27, 240–250. doi: 10.1177/1545968312461719

Snapinn, S. M., and Jiang, Q. (2007). Responder analyses and the assessment of a clinically relevant treatment effect. *Trials* 8:31. doi: 10.1186/1745-6215-8-31

Song, J., Nair, V. A., Young, B. M., Walton, L. M., Nigogosyan, Z., Remsik, A., et al. (2015). DTI measures track and predict motor function outcomes in stroke rehabilitation utilizing BCI technology. *Front. Hum. Neurosci.* 9:195. doi: 10.3389/fnhum.2015.00195

Song, J., Young, B. M., Nigogosyan, Z., Walton, L. M., Nair, V. A., Grogan, S. W., et al. (2014). Characterizing relationships of DTI, fMRI, and motor recovery in stroke rehabilitation utilizing brain-computer interface technology. *Front. Neuroeng.* 7:31. doi: 10.3389/fneng.2014.00031

Stinear, C. M. (2016). Stroke rehabilitation research needs to be different to make a difference. *F1000Res.* 5:1467. doi: 10.12688/f1000research.8722.1

Stinear, C. M., and Byblow, W. D. (2014). Predicting and accelerating motor recovery after stroke. *Curr. Opin. Neurol.* 27, 624–630. doi: 10.1097/WCO.0000000000000153

Stinear, C. M., Byblow, W. D., Ackerley, S. J., Barber, P. A., and Smith, M. C. (2017). Predicting recovery potential for individual stroke patients increases rehabilitation efficiency. *Stroke* 48, 1011–1019. doi: 10.1161/STROKEAHA.116.015790

Vellone, E., Savini, S., Fida, R., Dickson, V. V., Melkus, G. D. E., Carod-Artal, F. J., et al. (2015). Psychometric evaluation of the stroke impact scale 3.0. *J. Cardiovasc. Nurs.* 30, 229–241. doi: 10.1097/JCN.0000000000000145

Waddell, K. J., Strube, M. J., Bailey, R. R., Klaesner, J. W., Birkenmeier, R. L., Dromerick, A. W., et al. (2017). Does task-specific training improve upper limb performance in daily life poststroke? *Neurorehabil. Neural Repair* 31, 290–300. doi: 10.1177/1545968316680493

Wilson, J. A., Walton, L. M., Tyler, M., and Williams, J. (2012). Lingual electrotactile stimulation as an alternative sensory feedback pathway for brain–computer interface applications. *J. Neural Eng.* 9:045007. doi: 10.1088/1741-2560/9/4/045007

Wolf, S. L., Thompson, P. A., Winstein, C. J., Miller, J. P., Blanton, S. R., Nichols-Larsen, D. S., et al. (2010). The EXCITE stroke trial: comparing early and delayed constraint-induced movement therapy. *Stroke* 41, 2309–2315. doi: 10.1161/strokeaha.110.588723

Wolf, S. L., Winstein, C. J., Miller, J. P., Taub, E., Uswatte, G., Morris, D., et al. (2006). Effect of constraint-induced movement therapy on upper extremity function 3 to 9 months after stroke: the EXCITE randomized clinical trial. *JAMA* 296, 2095–2104. doi: 10.1001/jama.296.17.2095

Young, B. M., Nigogosyan, Z., Nair, V. A., Walton, L. M., Song, J., Tyler, M. E., et al. (2014a). Case report: post-stroke interventional BCI rehabilitation in an individual with preexisting sensorineural disability. *Front. Neuroeng.* 7:18. doi: 10.3389/fneng.2014.00018

Young, B. M., Nigogosyan, Z., Remsik, A., Walton, L. M., Song, J., Nair, V. A., et al. (2014b). Changes in functional connectivity correlate with behavioral gains in stroke patients after therapy using a brain-computer interface device. *Front. Neuroeng.* 7:25. doi: 10.3389/fneng.2014.00025

Young, B. M., Nigogosyan, Z., Walton, L. M., Song, J., Nair, V. A., Grogan, S. W., et al. (2014c). Changes in functional brain organization and behavioral correlations after rehabilitative therapy using a brain-computer interface. *Front. Neuroeng.* 7:26. doi: 10.3389/fneng.2014.00026

Young, B. M., Williams, J., and Prabhakaran, V. (2014d). BCI-FES: could a new rehabilitation device hold fresh promise for stroke patients? *Expert Rev. Med. Dev.* 11, 537–539. doi: 10.1586/17434440.2014.941811

Young, B. M., Nigogosyan, Z., Walton, L. M., Remsik, A., Song, J., Nair, V. A., et al. (2015). Dose-response relationships using brain–computer interface technology impact stroke rehabilitation. *Front. Hum. Neurosci.* 9:361. doi: 10.3389/fnhum.2015.00361

Young, B. M., Stamm, J. M., Song, J., Remsik, A. B., Nair, V. A., Tyler, M. E., et al. (2016). Brain–computer interface training after stroke affects patterns of brain–behavior relationships in corticospinal motor fibers. *Front. Hum. Neurosci.* 10:457. doi: 10.3389/fnhum.2016.00457

Zich, C., Debener, S., Schweinitz, C., Sterr, A., Meekes, J., and Kranczioch, C. (2017). High-intensity chronic stroke motor imagery neurofeedback training at home: three case reports. *Clin. EEG Neurosci.* 48, 403–412. doi: 10.1177/1550059417717398

Conflict of Interest Statement: The authors declare that the research was conducted in the absence of any commercial or financial relationships that could be construed as a potential conflict of interest.

Copyright © 2018 Remsik, Dodd, Williams, Thoma, Jacobson, Allen, Advani, Mohanty, McMillan, Rajan, Walczak, Young, Nigogosyan, Rivera, Mazrooyisebdani, Tellapragada, Walton, Gjini, van Kan, Kang, Sattin, Nair, Edwards, Williams and Prabhakaran. This is an open-access article distributed under the terms of the Creative Commons Attribution License (CC BY). The use, distribution or reproduction in other forums is permitted, provided the original author(s) and the copyright owner(s) are credited and that the original publication in this journal is cited, in accordance with accepted academic practice. No use, distribution or reproduction is permitted which does not comply with these terms.

frontiers in Neuroscience

ORIGINAL RESEARCH
published: 27 November 2018
doi: 10.3389/fnins.2018.00861

Evaluation of Changes in the Motor Network Following BCI Therapy Based on Graph Theory Analysis

Mohsen Mazrooyisebdani[1,2*], *Veena A. Nair*[2], *Po-Ling Loh*[1,3], *Alexander B. Remsik*[2,4], *Brittany M. Young*[2,5,6], *Brittany S. Moreno*[4], *Keith C. Dodd*[7], *Theresa J. Kang*[2], *Justin C. William*[7,8] *and Vivek Prabhakaran*[2,5,6]

[1] Department of Electrical and Computer Engineering, University of Wisconsin–Madison, Madison, WI, United States, [2] Department of Radiology, University of Wisconsin–Madison, Madison, WI, United States, [3] Department of Statistics, University of Wisconsin–Madison, Madison, WI, United States, [4] Department of Kinesiology, University of Wisconsin–Madison, Madison, WI, United States, [5] Neuroscience Training Program, University of Wisconsin–Madison, Madison, WI, United States, [6] Medical Scientist Training Program, School of Medicine and Public Health, University of Wisconsin–Madison, Madison, WI, United States, [7] Department of Biomedical Engineering, University of Wisconsin–Madison, Madison, WI, United States, [8] Department of Neurological Surgery, University of Wisconsin–Madison, Madison, WI, United States

OPEN ACCESS

Edited by:
Mikhail Lebedev,
Duke University, United States

Reviewed by:
Ali Yadollahpour,
Ahvaz Jundishapur University of Medical Sciences, Iran
Waldemar Karwowski,
University of Central Florida, United States
Giuseppe D'Avenio,
Istituto Superiore di Sanità (ISS), Italy

***Correspondence:**
Mohsen Mazrooyisebdani
mazrooyisebd@wisc.edu

Specialty section:
This article was submitted to Neural Technology, a section of the journal Frontiers in Neuroscience

Received: *15 March 2018*
Accepted: *05 November 2018*
Published: *27 November 2018*

Citation:
Mazrooyisebdani M, Nair VA, Loh P-L, Remsik AB, Young BM, Moreno BS, Dodd KC, Kang TJ, William JC and Prabhakaran V (2018) Evaluation of Changes in the Motor Network Following BCI Therapy Based on Graph Theory Analysis. Front. Neurosci. 12:861. doi: 10.3389/fnins.2018.00861

Despite the established effectiveness of the brain-computer interface (BCI) therapy during stroke rehabilitation (Song et al., 2014a, 2015; Young et al., 2014a,b,c, 2015; Remsik et al., 2016), little is understood about the connections between motor network reorganization and functional motor improvements. The aim of this study was to investigate changes in the network reorganization of the motor cortex during BCI therapy. Graph theoretical approaches are used on resting-state functional magnetic resonance imaging (fMRI) data acquired from stroke patients to evaluate these changes. Correlations between changes in graph measurements and behavioral measurements were also examined. Right hemisphere chronic stroke patients (average time from stroke onset = 38.23 months, standard deviation (SD) = 46.27 months, $n = 13$, 6 males, 10 right-handed) with upper-extremity motor deficits received interventional rehabilitation therapy using a closed-loop neurofeedback BCI device. Eyes-closed resting-state fMRI (rs-fMRI) scans, along with T-1 weighted anatomical scans on 3.0T MRI scanners were collected from these patients at four test points. Immediate therapeutic effects were investigated by comparing pre and post-therapy results. Results displayed that th average clustering coefficient of the motor network increased significantly from pre to post-therapy. Furthermore, increased regional centrality of ipsilesional primary motor area ($p = 0.02$) and decreases in regional centrality of contralesional thalamus ($p = 0.05$), basal ganglia ($p = 0.05$ in betweenness centrality analysis and $p = 0.03$ for degree centrality), and dentate nucleus ($p = 0.03$) were observed (uncorrected). These findings suggest an overall trend toward significance in terms of involvement of these regions. Increased centrality of primary motor area may indicate increased efficiency within its interactive network as an effect of BCI therapy. Notably, changes in centrality of the bilateral cerebellum regions have strong correlations with both clinical variables [the Action Research Arm Test (ARAT), and the Nine-Hole Peg Test (9-HPT)]

Keywords: BCI therapy, brain-computer interface, stroke recovery, graph theory, motor functional recovery, motor network

INTRODUCTION

Eight lakhs Americans experience a stroke each year, a number that is predicted to rise by 22% by 2030 (Go et al., 2013). Recent medical advances have decreased stroke mortality rates (Go et al., 2013). However, the growing number of stroke survivors continue to struggle as their independence are notably diminished. These survivors often suffer from persistent functional deficits, resulting in billions of dollars of economic costs each year (Towfighi and Saver, 2011). Kelly-Hayes et al. (2003) shows that acquisition of a lasting motor impairment is one of the most prominent sources of such functional deficits, with up to 50% of survivors suffering from hemiparesis, and 26% requiring assistance with activities of daily living (ADLs) 6 months post-stroke. Consequently, this expanding population of stroke survivors increases the demand for effective stroke rehabilitation therapies and mechanistic break-down of stroke recovery.

The most critical time-frame for significant post-stroke recovery has been shown to occur within the first few months following stroke onset (Stinear and Byblow, 2014). During this period before plateauing around 6 months post-stroke (Wolf et al., 2006, 2010; Dromerick et al., 2009; Cramer and Nudo, 2010), spontaneous biological recovery (SBR) plays a major role in the complex process of motor recovery. spontaneous motor and cognitive recovery may no longer occur within the same manner as it is observed during SBR. Although patients in the chronic stages of stroke recovery retain the capability of neuroplasticity (Caria et al., 2011; Ang et al., 2015), traditional therapies have not been effective after 6 months post-stroke. As a result, chronic stroke survivors have fewer options for recovery.

In the absence of effective traditional rehabilitation therapy for chronic stroke survivors, novel therapeutic techniques show success in generating some functional motor recovery beyond traditional rehabilitation window (Cramer and Nudo, 2010; Ang et al., 2015; Irimia et al., 2016).

Brain-computer interface (BCI) therapy is being used in non-traditional therapies for stroke rehabilitation. An increasing number of studies indicate that with different neuro-rehabilitative BCI therapy strategies, both acute and chronic stroke patients can achieve significant changes in behavioral measures [such as the Action Research Arm Test (ARAT), and the Nine-Hole Peg Test (9-HPT)] of persistent upper extremity (UE) impairment (Young et al., 2014a,b; Irimia et al., 2016; Remsik et al., 2016). One such strategies that was applied in the ongoing clinical trial [(NCT02098265) interventional, non-invasive closed-loop electroencephalography (EEG) based BCI therapy for the restoration of distal UE motor function in stroke survivors Song et al., 2014a, 2015; Young et al., 2014a,b,c,d, 2015; Remsik et al., 2016] is to use electroencephalography (EEG) to detect neural activity. The signals from the EEG are translated into a video-game simulation which responses to user's neural patterns. The video game simulation provides real-time feedback which allows the user to observe and learn to modulate their brain activity. This method may stimulate neuroplastic changes and exploit any recovery potential that remains after a patient reaches a functional plateau with traditional therapies.

BCI therapies are designed to reward the consistent production of specific brain activity patterns relative to other patterns in the context of an intended task. While growing number of studies (Muralidharan et al., 2011; Song et al., 2014a, 2015; Young et al., 2014a,b,c,d, 2015; Irimia et al., 2016) have shown the effectiveness of BCI therapies in rehabilitating volitional movements in stroke survivors, little is known about the network reorganization patterns that occur in stroke patients by such therapies.

Overview of This Study

The aim of this study was to determine topological changes in the motor network of chronic stroke patients who participated in BCI therapy. Task-free (resting-state) fMRI was chosen to map brain network changes as it is easily acquired on all patients irrespective of the degree of impairment. In order to evaluate reorganization of the motor network, a pure data-driven methodology known as the graph theoretical analysis was applied. The graph theory has been recognized in recent years as a novel method to study functional networks of the brain (Bullmore and Sporns, 2009; Wang et al., 2010).

The fundamental basis of graph theory is to represent a network in terms of nodes (or vertices) and links (or edges) between pairs of nodes. This approach helps researchers to describe topologies of complex networks by quantifying properties of a network (Wang et al., 2010). When representing a large-scale brain networks in this way, nodes are usually defined as anatomical brain regions and links can be represented as functional connectivity (FC) between these nodes, in which FC is defined as the magnitude of temporal correlation of the activity of two brain regions (Boccaletti et al., 2006). Functional segregation and integration have been recognized as the two most important principles when considering networks in the human brain (Wang et al., 2010). Graph theoretical methods also enable researchers to evaluate hubs in a network (Wang et al., 2010). In a complex network, hubs have an essential importance in controlling over flowing information.

In this study, functional segregation and integration of the executive motor network was examined via clustering coefficient (measure of segregation) and shortest path lengths of the network (measures of the integration) (Bassett and Bullmore, 2006), and two measures of centralities (i.e., betweenness centrality and degree centrality) was used to evaluate alteration of hubs.

The main hypotheses in this study were:

I. Gradual improvement in the ipsilesional primary sensorimotor cortex during the stroke recovery–potentially as a result of SBR–has been observed in recent longitudinal studies (Carey et al., 2002; Wang et al., 2010). An increase in the regional centrality of the ipsilesional primary sensorimotor following the administration of BCI therapy was hypothesized.
II. Behavioral measurements (i.e., ARAT and 9-HPT) were predicted to be correlated with changes in the topology of the motor network. Specifically, it was hypothesized that changes in graph properties (regional centrality, etc.) will correlate with gains in motor function. Similar associations between

regional centralities of the motor network and improvement in some clinical outcomes have been reported in spontaneous stroke recovery during the acute stroke stage (Wang et al., 2010). Also the association with improvement in the pattern of activity in fMRI data and improvement in some clinical variable during chronic stage has been observed previously (Carey et al., 2002; Gauthier et al., 2008; Richards et al., 2008).

MATERIALS AND METHODS

Recruitment Methods, Exclusion Criteria, and Ethic Statement

Thirteen patients who suffer from persistent upper extremity motor impairment caused by ischemic or hemorrhagic stroke were enrolled for the BCI therapy. All of these subjects were recognized as proper for participation in this study by one or more physicians at the University of Wisconsin Hospital and Clinics. Patients with concurrent neurodegenerative disorders, such as dementia, or other neurological or psychiatric disorders, such as epilepsy, schizophrenia, or substance abuse, were excluded from this study. All subjects provided written informed consent. This study was approved by the Health Sciences Institutional Review Board of the University of Wisconsin–Madison. Participant characteristics are summarized in **Table 1**.

Randomization and Study Paradigm

All participants in this study were randomly assigned to one of two groups (BCI therapy group or crossover control group) using a permuted-block design accounting for gender, stroke chronicity, and severity of motor impairment. Those in the BCI therapy group immediately received interventional rehabilitation therapy using the BCI device with functional assessment and MRI scanning at four time points: before the start of BCI therapy (Pre therapy), at the midpoint of BCI therapy, upon completion of all BCI therapy (Post therapy), and 1 month following the last BCI therapy session. Those in the crossover control group completed three additional functional assessments and MRI scans during the control phase of the study and then crossed over to complete the same BCI therapy phase of the study as the first group. For more information about the study paradigm and details about interventions, please refer to Young et al. (2014a). Data analyzed in this paper is from the intervention phase for both groups and using only two time points: before therapy (or therapy baseline) and post-therapy. This is because several of our studies have shown the most significant gains following therapy at these time-points (Young et al., 2014b,d; Remsik et al., 2016).

Functional Assessments

Subjects' motor function of the impaired arm was assessed with behavioral objective measures. These measures included subjects' performance in the Action Research Arm Test (ARAT)–a standardized series of scored movements designed to evaluate upper extremity motor function in the domains of grip, grasp, strength, and gross movement (Carroll, 1965; Beebe and Lang, 2009; Young et al., 2014b), and the Nine-Hole Peg Test (9-HPT)–a timed task in which the subject attempts to first place the pegs in each of the 9 holes on a pegboard and then removes each peg using only one hand (Carroll, 1965; Young et al., 2014b). These scores were standardized as follows: scores for the ARAT were reported as the total points scored when using the impaired hand, and scores for 9-HPT were taken as an average of two timed trials using the impaired hand (Young et al., 2014b).

At each of the visits for behavioral evaluation, anatomical and functional MRI scans were also obtained for each subject.

Image Acquisition and Processing

MRI data were collected on 3 Tesla GE MR750 scanners equipped with high-speed gradients (Sigma GE Healthcare, Milwaukee, Wisconsin) using an 8-channel head coil. In order to minimize head movements, padding was used around each subject's head. Ten minutes resting-state (R-s) fMRI data were collected using a T2*-weighted gradient-echo planar imaging (EPI) pulse sequence sensitive to BOLD contrast. Technical parameters used to acquire these EPI scans were as follows: field of view 224 mm,

TABLE 1 | Clinical and demographic data.

ID	Infarcted hemisphere	Localization of infarct	ARAT affected hand Score		9-HPT Score	
1	Right	Temporal, Frontal	3	3	29.31	21.06
2	Right	Occipital	57	57	27.5	22.99
3	Right	Temporal, Frontal	9	10	37.12	32.52
4	Right	Frontal	3	16	20.93	20.6
5	Right	Putamen	–	–	24.61	23.62
6	Right	Pons	27	40	30.51	28.00
7	Right	Cerebellum	57	57	26.48	21.79
8	Right	PLIC putamen	23	40	26.69	20.71
9	Right	Prefrontal, Midfrontal, Temporal	–	–	37.84	34.97
10	Right	Internal capsule, Thalamus	56	57	20.05	18.22
11	Right	Frontal, Parietal	7	7	19.46	18.62
12	Right	Frontaltemporal, Occipital	3	4	20.29	18.58
13	Right	Anterior temporal, Frontoparietal	0	2	26.77	24.25

matrix 64 × 64, TR 2600 ms, TE 22 ms, flip angle 60°, and 40 axial plane slices of 3.5 mm thickness with 3.5 mm spacing between slices. A T1-weighted high-resolution anatomical image was also obtained for each subject using a BRAVO FSPGR pulse sequence. Technical parameters used to acquire these scans are as follows: field of view 256 mm, matrix 256 × 256, TR 8.16 ms, TE 3.18 ms, flip angle 12°, and 156 axial plane slices of 1 mm thickness with 1 mm spacing between slices.

R-s fMRI data were processed using the AFNI package (Cox, 1996). Images were despiked, slice time-corrected, motion-corrected, aligned with the anatomical scan, normalized to MNI space, re-sampled to 3.5 mm, and spatially smoothed with a 4 mm FWHM Gaussian kernel. Motion censoring (per TR motion > 1 mm or 1°), nuisance regression, and bandpass filtering (0.009–0.08 Hz) were performed simultaneously in one regression model. Nuisance signals that were regressed out included six motion estimates and their temporal derivatives, the voxel-wise locally averaged white matter signal, and the cerebrospinal fluid signal. Global signal regression was omitted due to the controversial position associated with it in the literature (Murphy and Fox, 2017).

Graph Construction

Figure 1 illustrates the standard procedure of graph theory analysis applied on f-MRI data that has been well-stablished and used in many studies (Humphries et al., 2006; Achard and Bullmore, 2007; He et al., 2008; Bullmore and Sporns, 2009, 2012; Meunier et al., 2009; Alexander-Bloch et al., 2010; Van Wijk et al., 2010; Wang et al., 2010; Bernhardt et al., 2011; De Vico Fallani et al., 2014; Song et al., 2014b). Reign of interest (ROI) from the network under investigation is first identified. These ROIs would be nodes in the graph. Then the correlation matrix (or functional connectivity (FC) matrix) between these ROIs is acquired using temporal correlations among all ROIs. Next, the proportional thresholding is applied to exclude weak or irrelevant FCs from the analysis of the graph. A threshold value in the context of

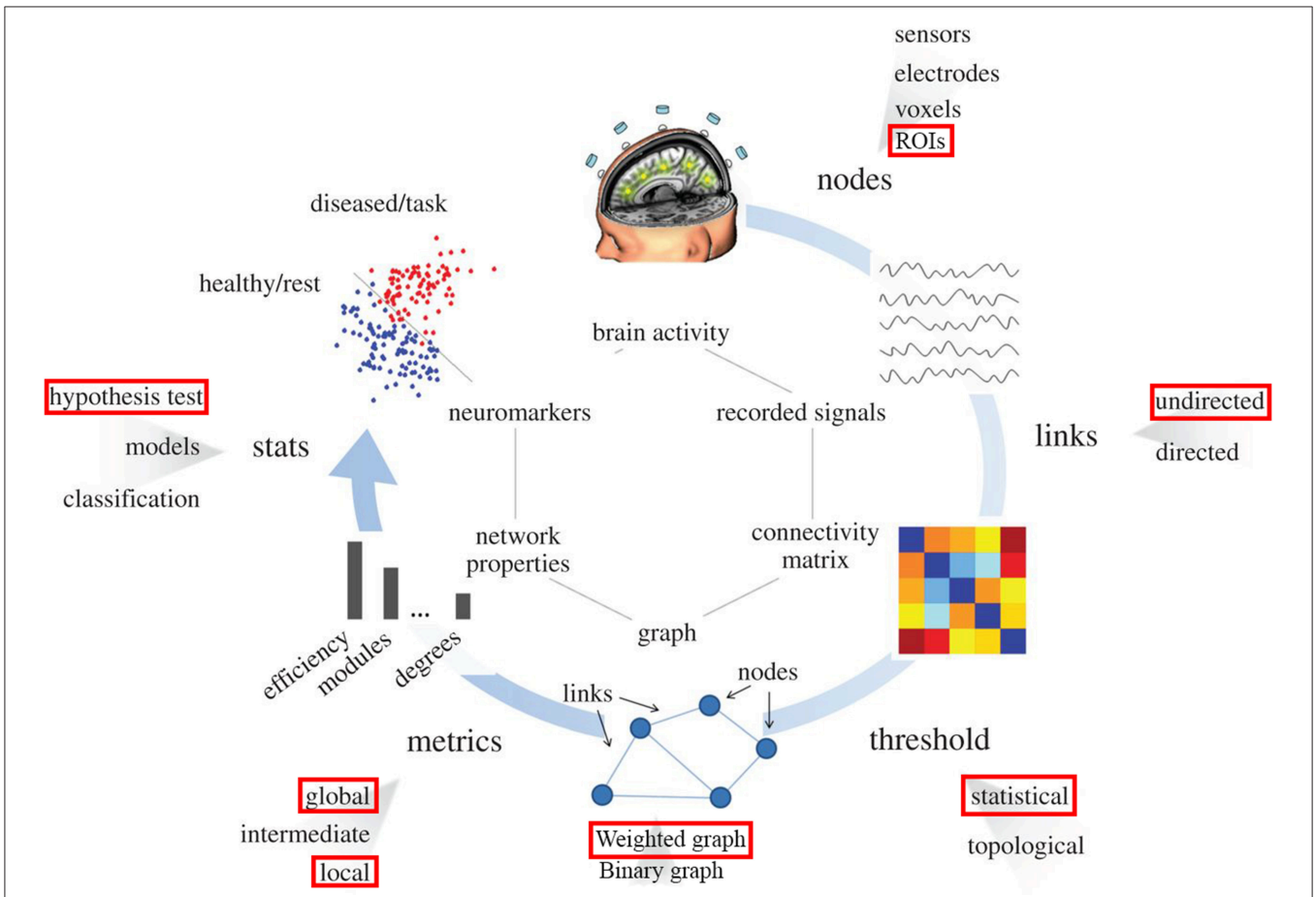

FIGURE 1 | Pipeline for the graph theory analysis applied on functional brain network. Red rectangulars specify the submethodology used in this study at each step. Nodes correspond to specific region in the brain (predifined ROI in our study). Links are estimated by measuring the FC between different regions in the brain (undirected links); connectivity matrix would be constructed using this information. By means of filtering procedures, based on thresholds, only the most important links constitute the brain graph. The topology of the brain graph is quantified by different graph metrics that can be represented as numbers. These graph indices can be input to statistical analysis in order to look for significant differences between populations/conditions (e.g., red points correspond to brain graph indices of diseased patients or tasks, blue points stand for healthy subjects).

proportional thresholding (known as network sparsity) is defined as the number of correlations that is considered as connections in the final graph divided by number of all possible correlations exist in the correlation matrix (Latora and Marchiori, 2001; Achard et al., 2012). After proportional thresholding and excluding weak FCs, each remaining FC is identified as a link (or edge) between its associated ROIs and the graph is constructed. From this graph, topological properties of the network under investigation can be evaluated.

Optimally thresholding correlation matrix to only include important FCs is critical in this methodology. Having too few FCs may obscure group differences, whereas too many FCs may lead to a random graph structure (Humphries et al., 2006). However, applying this method on a brain network model has a potential to move the graphical model away from the actual network that it represents. In the section Preserving graph connectedness and network thresholding, this limitation of the thresholding is explained and a technique (the Maximum Spanning Tree, MST) to circumvent this potential limitation is introduced.

In the following subsections, the criterion for choosing ROIs in our study is explained, and the proportional thresholding is discussed in more details.

Regions of Interest in Executive Motor Network

Twenty-one anatomical ROIs associated with the motor execution network were defined by creating 5 mm diameter spheres around coordinates for regions in the motor network previously defined by Wang et al. (2010) (**Table 2**). One ROI (located in the right ventrolateral premotor cortex) was excluded due to overlap with subject's stroke lesions. The 20 ROIs include the primary motor cortex, bilateral superior parietal lobule, bilateral basal ganglia, bilateral thalamus, anterior inferior cerebellum, postcentral gyrus, and dentate nucleus (Wang et al., 2010). These ROIs were used to derive Pearson's R correlation coefficient matrices from each subject's r-s fMRI, using AFNI's doROICorrMat command. Fisher z transform was then applied on R correlations across each patient and used z-score correlation matrices in further analysis (Since hypotheses about the significance of the population correlation wanted to be evaluated, Fisher z-score was more proper than r-correlation value). In this study, the alteration in the magnitude of the functional connections was tended to be evaluated; hence, absolute values of these matrices were used in all analyses.

TABLE 2 | Regions of interest for the motor network.

ID	Region	Abbreviation	Side	MNI coordinate		
				x	*y*	*z*
1	Superior cerebellum	SCb	R	16	−59	−21
2	Primary motor cortex	M1	L	−38	−22	56
3	Primary motor cortex	M1	R	38	−22	56
4	Thalamus	Th	L	−10	−20	11
5	Superior parietal lobule	SPL	L	−22	−62	54
6	Supplementary motor area	SMA	L	−5	−4	57
7	Supplementary motor area	SMA	R	5	−4	57
8	Dorsolateral premotor cortex	PMd	R	28	−10	54
9	Ventrolateral premotor cortex	PMv	L	−49	−1	38
10	Superior cerebellum	SCb	L	−25	−56	−21
11	Superior parietal lobule	SPL	R	16	−66	57
12	Dentate nucleus	DN	R	19	−55	−39
13	Anterior inferior cerebellum	AICb	L	−22	−45	−49
14	Anterior inferior cerebellum	AICb	R	16	−45	−49
15	Postcentral gyrus	PCG	R	37	−34	53
16	Dorsolateral premotor cortex	PMd	L	−22	−13	57
17	Basal ganglia	BG	R	22	−2	12
18	Basal ganglia	BG	L	−25	−14	8
19	Thalamus	Th	R	7	−20	11
20	Dentate nucleus	DN	L	−28	−55	−43

MNI, Montreal Neurological Institute; R, Right; L, Left.

Preserving Graph Connectedness and Network Thresholding

As it is described earlier in this section, applying thresholding without any consideration for the reality of the circulation of information in the network has some potential issues. Thresholding raises two critical issues; (1) It may lead the final graph to be disconnected–in which a region that is part of the brain network will be left without any connection to any other region in the graph, (2) In addition, there is no comprehensive agreement in the field on the cutoff value above which correlations should be considered as edges.

To address the first issue a growing number of studies have used the maximum spanning tree (MST) method (Alexander-Bloch et al., 2010; Achard et al., 2012; Song et al., 2014b; Iyer et al., 2018). An MST is a weighted spanning tree that would serve as a backbone for the main graph. In this method, to calculate the existing tree in the graph with the maximum weights, N-1 FCs is chosen by the prime algorithm to connect all N nodes of the network together.

As for the second issue, analysis of the graph in the whole-network level (such as evaluation of the shortest path length, clustering coefficient, small-worldness, etc.) has been done in various numbers of threshold values in almost all previous studies (Loui et al., 2012; Rutter et al., 2013; Vaessen et al., 2014; He et al., 2017). This was to capture a proper and complete understanding of the network topology.

For regional properties of the network (e.g., centrality, or local efficiency) however, there is still a debate about the proper threshold value. For instance, Bullmore and his colleagues (Bullmore and Sporns, 2012) believe that each node in a graph conforms to the profile of its realistic brain region only in small threshold values not more than 16% (same thresholding criteria has been used in Meunier et al., 2009). Another example is Iyer et al. (2018) in which the author used 6% as the threshold value. However, in the growing numbers of studies researchers have used all significant correlations to construct the brain graphical model (Alexander-Bloch et al., 2010; Wang et al., 2010; Achard et al., 2012; Song et al., 2014b).

In this study, all significant correlations were used to generate the graph of each patient's brain in order to analysis of regional

properties. From each patient's connectivity matrix, z-values > 1.96 (two-tailed significant value for z-score) were used as the threshold to identify percentage of correlations that are above this threshold, i.e., the ratio of significant connections to all the possible connections were calculated (**Supplementary Figure 1**). By this approach, it has been found that the minimum sparsity was more than 42%. Hence, the sparsity threshold of 42% was used to convert connectivity matrices into weighted networks.

In summary, after applying the MST and extracting the backbone, any other FCs identified as a connection in the thresholding step are added to this tree to get weighted undirected connection matrices that represent a sparse, connected, and biologically meaningful graph for each patient (Song et al., 2014b).

While most of brain network studies have investigated the brain's topology by analyzing binaries graph (in which every edge in the network has an equal weight of 1), here alteration in the executive motor network was evaluated by a weighted network analysis approach, in which every edge in the network has a weight equal to its equivalent FC in the connectivity matrix, and hence the network would contain more information about the actual brain circuity.

Graph Measurements

Weighted Clustering Coefficient and Weighted Shortest Path Length

The clustering coefficient (C) is a measure of the degree to which nodes in a graph tend to cluster together (Watts and Strogatz, 1998). For an undirected weighted graph, the clustering coefficient of a node i (ci) is defined as follows:

$$C_i = \frac{1}{S_i(K_i - 1)} \sum_{(j,k)} W_{ij} + W_{ik}$$

Here, S_i is the strength of the node i (defined as sum of the FC between node i and other regions), W_{ij} is the FC between node i and node j, and K_i is the number of edges connected to the node I. The sum over (j,k) carries out sum of weights for any two pairs of j and k connected to the node i (Wang et al., 2010; Bernhardt et al., 2011).The clustering coefficient over all nodes in a network is then defined as:

$$C = \frac{1}{N} \sum_{i=1}^{N} c_i$$

The characteristic path length (L) reflects the level of global integration in the network. A shortest path between two nodes A and B is the path between A and B with the smallest number of edges. The characteristic path length l_i of a node i is defined as Watts and Strogatz (1998):

$$l_i = \frac{1}{N-1} \sum_{i \neq j} \min \{I_{ij}\}$$

Where min $\{Iij\}$ is the shortest path length between the i^{th} and j^{th} nodes. The characteristic path length L of a network is then defined as the mean of characteristic path lengths over all nodes in the network:

$$L = \frac{1}{N} \sum_{i=1}^{N} l_i$$

Regional Centrality Measurements

In network analysis, indicators of centrality identify the most important nodes within a graph (Brandes, 2001). In the present study, each node's importance in the network was evaluated using degree centrality and betweenness centrality.

Degree centrality (DC) counts the number of neighbors of each node. In this context, a node with higher degree centrality, would have more FCs with other parts of the network and hence is more involved in the network communication.

Betweenness centrality (BC) captures the influence that one node has over the flow of information between all other nodes in the network. The betweenness centrality of a node v is calculated as follows (Brandes, 2001):

$$BC(v) = \sum_{S \neq v \neq t} \frac{\sigma_{st}(v)}{\sigma_{st}}$$

Where σ_{st} is the total number of shortest paths from node s to node t and $\sigma_{st}(v)$ is the number of shortest paths from node s to node t that passes through node v. A node with high centrality is considered to be a hub in the network. Since this summation scales with the number of pairs of nodes, the quantity is rescaled and normalized by the average of BC over all nodes (Wang et al., 2010).

In this work, all graph measurements were calculated by using the Brain Connectivity Toolbox (2016) in MATLAB R2015.

Statistical Analysis

All tests between two time-points were assessed using non-parametric Wilcoxon signed-rank test. For all statistical tests α was set to 0.05 and then for each family of tests (i.e., tests of betweenness centrality, degree centrality, and correlations), correction for multiple comparisons were performed separately using false discovery rate (FDR) (Benjamini and Hochberg, 1995). All p-values reported in this study are unadjusted p-values (i.e., p-values are not FDR adjusted p-values, also known as q-values) and after FDR correction, any significant test was reported and marked with asterisk in the figures and tables. Tests with p-values < 0.07 were also considered trend toward significance and marked with plus in figures and tables.

RESULTS

Participant Characteristics and Behavioral Outcomes

The average age of the 13 participants in this study was 64.92 years ($SD = 12.19$ years), and the average time from stroke onset was 38.23 months ($SD = 46.28$ months). Of the 13 patients, two patients were unable to perform the ARAT (**Table 1**). For the other participants, a Wilcoxon sign rank test was performed on each of the behavioral scores (i.e., 9-HPT, and ARAT) **(Figure 2)**.

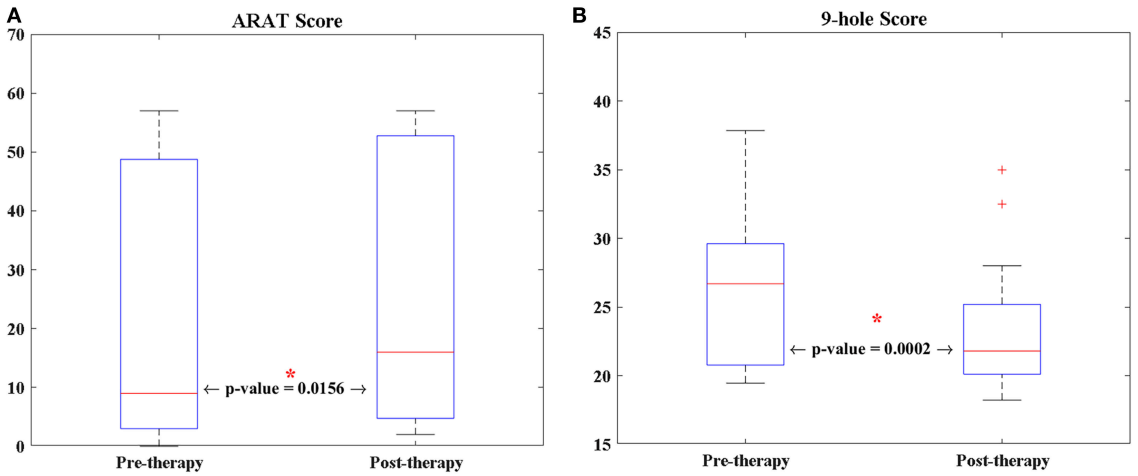

FIGURE 2 | The longitudinal changes of patients' performance in **(A)** ARAT, and **(B)** 9-HPT scores analyzed via Wilcoxon signed-rank test. 9-HPT, Nine-Hole Peg Test; ARAT, Action Research Arm Test. *Indicates that *p*-value is significant ($p < 0.05$).

Compared to pre-therapy, both the 9-HPT and ARAT scores demonstrated significant recovery ($p = 0.0156$ for ARAT and $p = 0.0002$ for 9-HPT).

Adjacency Matrices

Changes in group-level FCs between two scans were evaluated by median–a more robust measure of central tendency compared to mean–of each group's z-score connectivity matrices. As depicted in **Figure 3**, patients showed higher FCs among the contralesional subcortical regions (thalamus and basal ganglia) and other contralesional sensorimotor regions before therapy (**Figure 3B**). The median metric after therapy showed a decrease in the FCs of these regions while ipsilesional sensorimotor and subcortical regions of the motor network showed increased their FC with other parts of the network (this is clear from comparing the entries in the bottom right of the matrix in **Figure 3D** with same entries of the matrix in **Figure 3B**).

Global Network Parameters

Analysis of the shortest path length of the brain network showed no significant differences at any sparsity level over the study period (**Figure 4B**).

For the clustering coefficient (**Figure 4A**), mean clustering coefficient at post-therapy showed significant increase, comparted to pre-therapy, across several threshold values. Specifically, the network consisting of strongest FCs (sparsity lower than 12% in **Figure 4B**) showed no significant difference from pre to post. However, after including more mild edges (network sparsity between 12 and 36%), clustering coefficients in post-therapy gradually increased, and the gap between each time-point's distribution broadened as the sparsity increased.

Local Centrality Parameters

Betweenness centrality showed a trend toward significant increase from pre to post-therapy (**Figure 5A**) in the ipsilesional primary motor cortex ($p = 0.0201$). While the contralesional dentate nucleus, basal ganglia, and the thalamus in post-therapy showed a trend toward significant decrease in BC compared to pre-therapy ($p = 0.0324$, $p = 0.0502$, and $p = 0.0537$, respectively).

Changes in the degree centrality of the motor network over the study period were investigated (**Figure 5B**). Results indicate that compared to pre-therapy, the degree centrality of the contralesional dentate nucleus ($p = 0.0593$) and basal ganglia ($p = 0.0334$) decreased over the study period.

Behavioral Correlations With Changes in Network Parameters

To examine the behavioral implications of the changes in graph theoretical measures, the linear associations between changes in network parameters and actual recovery reflected in the behavioral assessments were examined. A summary of Pearson's correlations between changes in outcome measures (ARAT and 9-HPT scores) and changes in network parameters found to be significant or showing a trend toward significance after FDR correction is presented in **Table 3**. The majority of these relationships involved the bilateral cerebellum. Changes in centrality of the contralesional anterior inferior cerebellum were highly correlated with both objective measurements (ARAT and 9-HPT). **Figure 6** presents graphs of the relationships that were found to be significant.

DISCUSSION

Effectiveness of rs-fMRI in Evaluation of Recovery in Stroke

This study demonstrates the effectiveness of rs-fMRI using graph theoretical methods to capture brain changes during the stroke recovery following rehabilitative therapy. rs-fMRI requires about 10 min for image acquisition without any exogenous task demands on the subject. This method is particularly well-suited

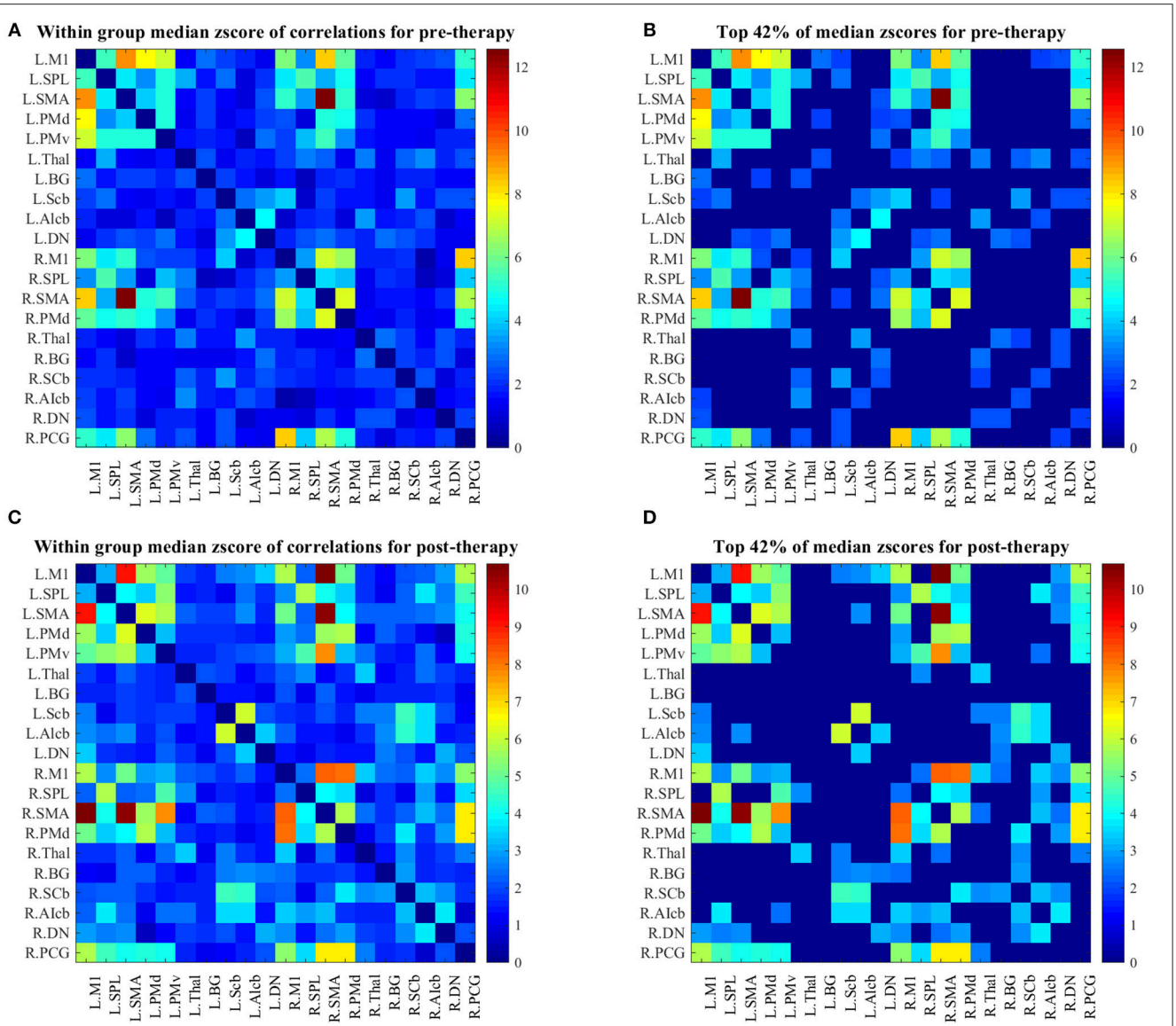

FIGURE 3 | (A) Median z-score of r-correlation matrices in pre-therapy. **(B)** Median z-score of r-correlation matrices for pre-therapy at threshold value = 42%. **(C)** Median z-score of r-correlation matrices in post-therapy. **(D)** Median z-score of r-correlation matrices for post-therapy at threshold value = 42%. R = Right, L = Left. See **Table 2** for the abbreviations of the regions. Note that the correlation matrices presented only serve as a visual representation, and are not corrected for multiple comparisons.

for stroke patients, who often suffer from motor impairment and hence may not be capable of doing specific tasks during MR scanning.

Impact of BCI-Based Stroke Rehabilitation on FC Among Regions of the Motor Network

This study shows that during the course of BCI therapy, the motor network strengthens its FC among different regions mostly in the ipsilesional part of the network. A similar study (Wang et al., 2010) in patients with subcortical infarcts in acute stage of recovery found significantly decreased FC involving the contralesional subcortical structures (such as the thalamus) during the recovery. Findings in the study highlights a similar pattern of decreasing median of FC in these regions (**Figure 3**, z-score connection matrices of left thalamus for pre-therapy **Figure 3A** compared to post-therapy **Figure 3C**). From this result, it seems that during the period of therapy, ipsilesional cortical and subcortical regions in the network have strengthened their FCs with other parts of the network.

Graph Theory as a Tool to Evaluate Stroke Recovery

Several studies have shown changes in the brain activation and functional connectivity following BCI therapy (Young et al.,

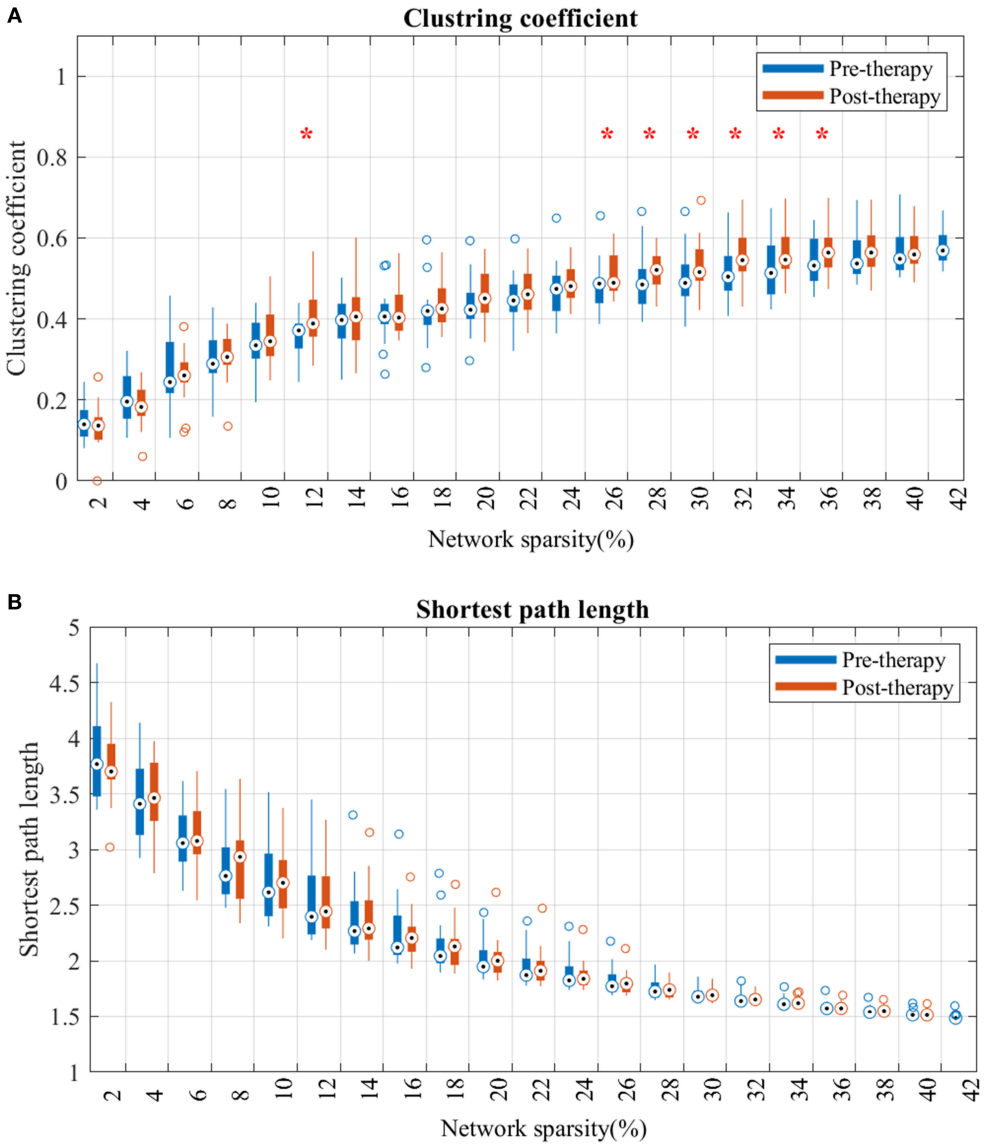

FIGURE 4 | Changes in clustering coefficient **(A)** and average shortest path length **(B)** from pre-therapy (Blue) to post-therapy (red) across range of networks' sparsity. Vertical lines denote the standard deviation of each group. Statistical analyses were carried out using Wilcoxon signed-rank test. *Indicates significant after correction for multiple comparison.

2014a,b). The focus in this study was on investigating brain reorganization using network analysis methods. Specifically, graph theoretical methods were used to capture topological properties associated with therapy over time. Previous study (Wang et al., 2010) have used this mathematical method to determine changes in patients who were in the acute stage of stroke, when abnormal changes are more observable. Here, this method has been used to identify abnormal changes in chronic stroke patients with average time since stroke onset of 38.23 months. Results of this study demonstrate the efficacy of this method in detecting brain network changes in stroke patients over time following rehabilitative therapy.

Effect of BCI-Based Therapy on the Large-Scale Motor Network

Changes in the topology of the motor network has been determined on a larger scale by evaluating the average clustering coefficients and the average shortest path lengths across all regions in the network. Results highlight that during the course of therapy, the clustering coefficient of the network increases significantly across different network sparsities (**Figure 4**). The higher clustering coefficient suggests that the brain follows principles of efficient network structures (Watts and Strogatz, 1998). Therefore, BCI therapy might help the motor network to facilitate more enhanced communication between communities

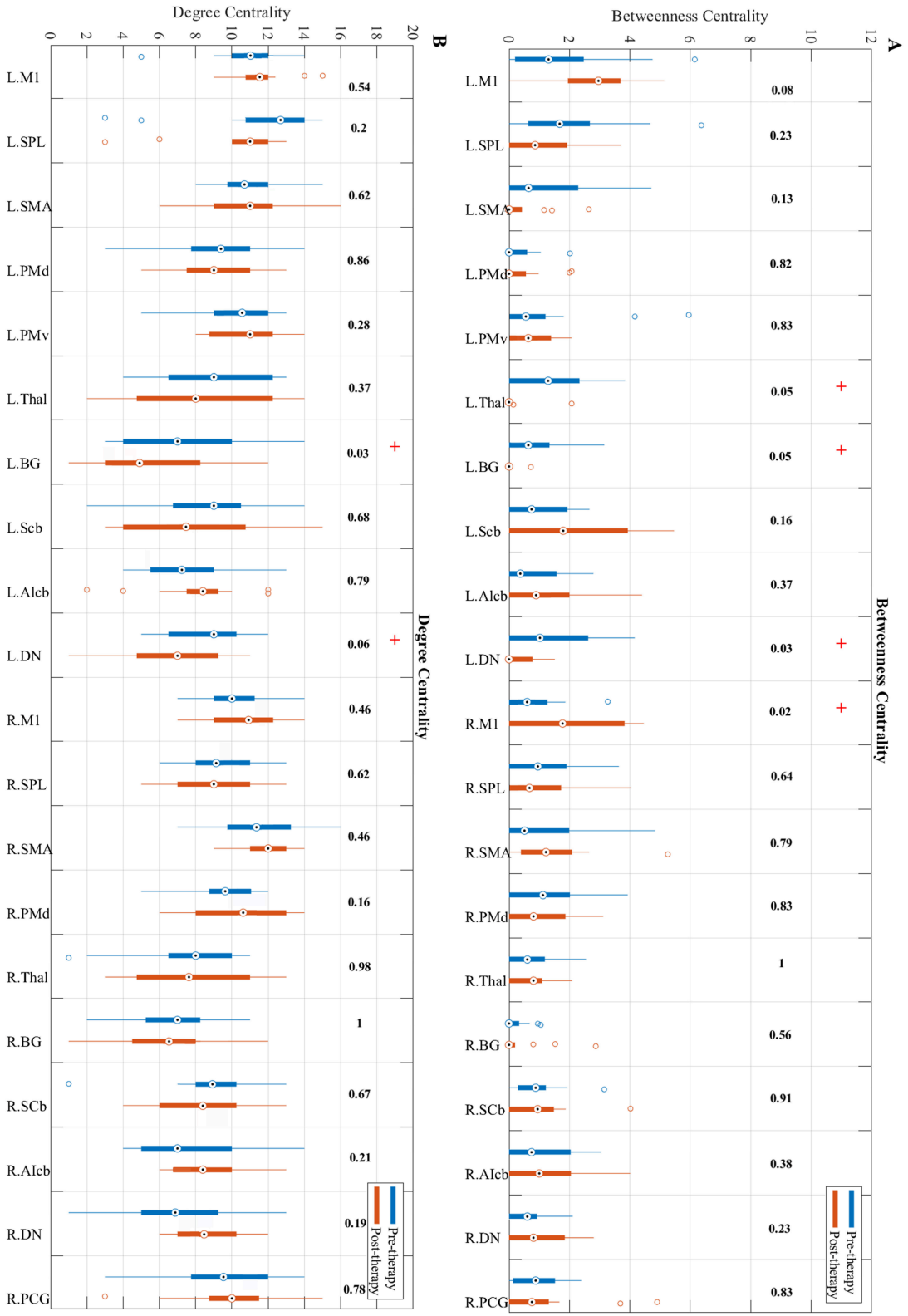

FIGURE 5 | Changes in betweenness centrality **(A)** and degree centrality **(B)** measures from pre-therapy (Blue) to post-therapy (Red) across all regions in the network calculated at a density level of 42% analyzed via Wilcoxon signed-rank test. R, Right, L, Left. See **Table 2** for the abbreviations of the regions. + trend toward significance (i.e., raw p-value < 0.07). P-values are round up with 2 integers in order to be shown in the figure.

TABLE 3 | Correlation analysis between centrality changes and behavioral changes from pre- to post-BCI therapy assessments.

Behavioral measure	Graph measure	Pearson *R*-value	*P*-value
ARAT	L.Alcb (BC)	0.8295	*0.0016
ARAT	R.Scb (BC)	−0.6832	+0.0205
ARAT	R.BG (BC)	0.6458	+0.0318
ARAT	L.Alcb (DC)	0.6022	+0.0499
9-HPT	R.BG (BC)	0.7400	*0.0038
9-HPT	R.DN (BC)	0.5720	+0.0411
9-HPT	L.Alcb (DC)	−0.5589	+0.0471
9-HPT	R.BG (DC)	0.6237	+0.0227

*ARAT, Action Research Arm Test; 9-HPT, 9-Hole Peg Test; R, Right; L, Left; * Significant p-value after correction for multiple comparison with FDR, + trend toward significant (i.e., $p < 0.07$). See **Table 2** for the abbreviations of the regions.*

of nodes (i.e., nodes sharing similar neighbors), resulting in faster transmission of information between brain regions.

Alteration in Regional Centrality

Alterations in the importance of different regions in the motor network have been investigated in our study. The word "importance" has different meaning in different contexts, leading to different definitions of centrality (Borgatti, 2005). The importance of regions in facilitating information transfer within the network were evaluated using two different forms of centralities. Degree centrality, in the group of radial centralities (Borgatti and Everett, 2006), computes the number of edges connected to each node. This definition of centrality is particularly attractive, since a change in degree centrality is associated with a decrease or increase in the number of significant FCs of that node. A trend toward significant Decrease in degree centrality of the contralesional basal ganglia ($p = 0.03$) were observed in our study, similar pattern was observed in Wang et al. (2010). Also, a trend toward significant decrease ($p = 0.06$) has been found in the degree centrality on contralesional dentate nucleus.

This study also investigated the hub properties of nodes from the viewpoint of betweenness centrality. Betweenness centrality is a measure of the functional importance of a node in terms of being a bridge for information processing. In this context, most of the information flowing in the network passes through a node with high BC. Results showed a trend toward significant increased BC in the ipsilesional primary motor cortex ($p = 0.02$), which is similar to other studies (Wang et al., 2010), (Dong et al., 2007). Also, a trend toward significant decrease has been found in BC of contralesional subcortical regions (e.g., thalamus and basal ganglia). The decrease of BC in the contralesional dentate nucleus ($p = 0.03$) seen in our study was not observed in Wang et al. (2010). This may be due to the differences in study samples, with chronicity and stroke location in the patients varying between the two studies.

These findings suggest an increase in the role of ipsilesional primary motor area as a hub during the period of therapy. The increased important of ipsilesional primary motor areas may instigate the gradual recovery of contralesional affected hand in terms of contralateral motor control. Also it suggests a decrease in the role of the contralesional subcortical and cerebellum regions following therapy. One possible explanation for these findings might be that the recovery of overall brain connectivity in the ipsilesional subcortical and cerebellum regions. In other words, the connections going through the ipsilesional subcortical and cerebellum regions become stronger as a result of the therapy. This recovery might lead to a decreased role for the contralesional subcortical and cerebellar regions in transferring information within the motor network.

Correlations Between Brain Network Changes and Behavioral Outcomes

Significant correlations between changes in centrality measures and changes in behavioral outcome measures are consistent with the view that the motor network changes with BCI therapy to facilitate information transfer between key regions in the motor network. Significant positive correlations between centrality of specific regions (e.g., anterior inferior cerebellum, and basal ganglia) and performance on the ARAT suggest that behavioral performance improves as the centrality of these regions increases. Similarly, significant negative correlations between centrality and 9HPT suggest that as centrality increases, processing time is reduced (i.e., time taken to perform the 9HPT is decreased). Interestingly, results showed similar correlations between centrality of the bilateral cerebellar regions and behavioral performance to that reported by Wang et al. (2010), in which the authors used the same ROIs. Also results from Dong et al. (2007) show reorganization of adaptive activity within the primary motor cortex and the cerebellum is in relation to relevant behavioral changes of patients with the upper extremity.

Cerebellar activity is solely associated with ipsilateral motor actions (Shibasaki et al., 1993; Allen et al., 1997). Addition studies have displayed that increased contralesional cerebellar activity is linked with the restoration of motor function (Chollet et al., 1991; Jaillard et al., 2005). Small et al. (2002) study further indicated that the larger the contralesional cerebellar activation, the better the recovery is Small et al. (2002). The results from this research study also mimic this trend.

However, it is common in individuals with upper-extremity motor impairments to overuse the unaffected arm more which may result in increases of centrality of the ipsilesional cerebellum. The negative correlation found between the centrality of ipsilesional superior cerebllum and ARAT performance—and ipsilesional basal ganglia with 9HPT performance—suggests that the recovery is enhanced by reducing over-recruitment of the contralateral extremity.

Overall these brain changes in subcortical structures (such as basal ganglia) and cerebellum and its interaction with cortical regions as well as the brain-behavioral correlations are consistent with these brain structures' involvements in movement related functions (i.e., basal ganglia has been implicated in functions including control of voluntary movements, procedural learning and the cerebellum contributes to functions such as coordination, precision, and timing of movements). However, given the small

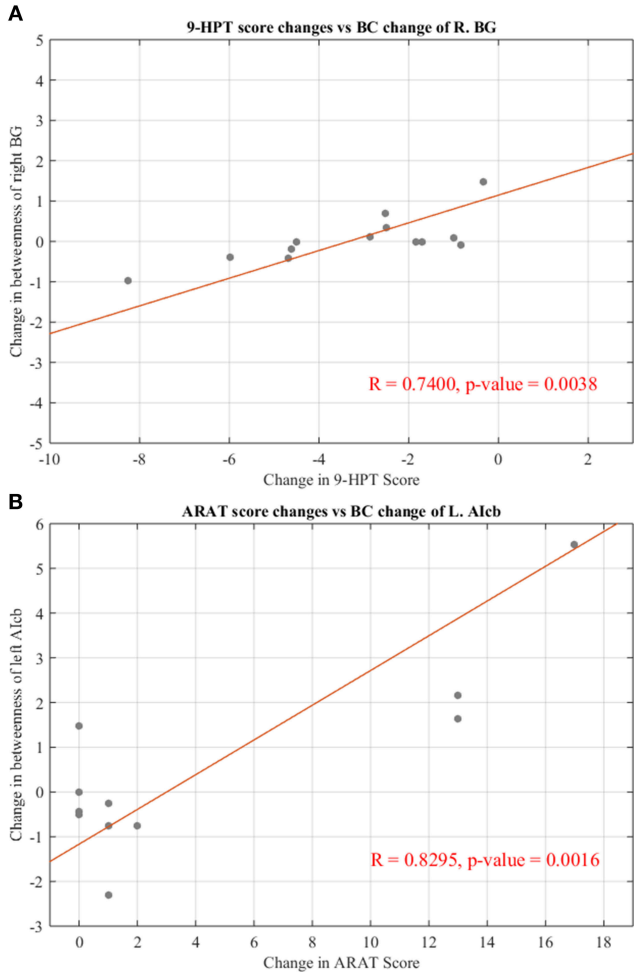

FIGURE 6 | Significant correlations between changes in regional centralities and changes in behavioral measures. **(A)** Relationship between changes in BC measure of right basal ganglia and individual changes in 9-HPT score. **(B)** Relationship between changes in BC measure of left anterior inferior cerebellum and individual changes in ARAT score. Red line representing the slope of correlation between measurements. 9-HPT, Nine-Hole Peg Test; ARAT, Action Research Arm Test; R, Right; L, Left. See **Table 2** for the abbreviations of the regions.

sample size and the fact that some of subjects were showing floor effects, these correlational results must be considered exploratory and interpreted carefully.

Limitations and Methodological Considerations

This study had a limited sample size, given that we chose to focus on a relatively homogenous group of stroke patients, with all patients having right-sided lesions and being in a chronic stage. We thus eliminated the confounding effect of lesion hemispheres by choosing only right hemisphere patients. However, the localization of the infarct in the sample size is still heterogeneous within the right hemisphere. Therefore, results of this study should be interpreted with cautious. Future studies should be done with larger sample size and more homogenous infarct.

The rsFCs within the motor regions were constructed using the seed regions reported in the work of Wang et al. (2010), which studied spontaneous recovery in stroke patients. A large number of studies report slightly varying coordinates for the motor network; however, given that the Wang et al. seed regions cover crucial regions of the motor network, it was decided to construct RSFC matrices using these regions. By focusing on a within-groups analysis, effects of other confounding variables such as age, gender, and stroke severity were mitigated. Also, attempts to reduce false positives in results were made by applying the FDR correction and reported only those results that survived the corrected p-value. However, given the small sample size and the rehabilitative focus of the study, we have also reported results showing a trend toward significance, since these results, although statistically not significant, may have practical implications.

The findings of this study showcase effective theoretical approaches that may be further optimized in designing neurofeedback devices and paradigms for stroke recovery. These methods are also particularly useful when used to discern brain activity patterns for training and conditioning purposes. A review performed by Dimyan and Cohen (2011), determined that increased ipsilesional lateralization may be more optimal for motor recovery by its association with spontaneous recovery (Dimyan and Cohen, 2011). The conclusions made by Dimyan and Cohen (2011) are consistent with the possibility that is a diversity in neuronal pattering/organization that facilitate more effective recoveries following stroke. Furthermore, these progressive patterns may be modulated with interventional therapeutic technologies in ways that are not evicted by spontaneous recovery.

CONCLUSIONS

This study provides a graph theoretical approach toward investigating brain changes following BCI therapy in chronic right hemisphere stroke patients with upper extremity motor impairments. Results showed that improvement in ipsilesional brain connectivity in the motor network can be observed concurrently with a period of training using a BCI device, and that these changes might be correlated with improved in behavioral outcomes. Due to small sample size and hetorogenous localization of the infarct in the sample size, these results should be interpreted with cautious and further studies will be needed with larger sample size to follow up on these findings. This study sheds light on the underlying mechanisms of recovery following BCI therapy, and may contribute toward developing more patient-specific BCI therapy protocols to facilitate recovery in chronic stroke patients.

AUTHOR CONTRIBUTIONS

MM was involved in data collection, data analysis, interpreting results, and writing of the manuscript. VN contributed to data

collection, manuscript writing, and intellectual content. P-LL contributed to editing the manuscript and intellectual content. AR, BM, and BY were involved in data collection and editing the manuscript. KD was involved in data collection. TK was involved in the recruitment of study participants. JW and VP are co-PIs and were involved in study conception, design, manuscript editing, intellectual content, and supervision for all aspects of the study.

FUNDING

This work was supported by NIH grants RC1MH090912-01, T32GM008692, UL1TR000427, K23NS086852, T32EB011434, R01EB000856-06, and R01EB009103-01 and by the DARPA RCI Program (MTO) N66001-12-C-4025 and HIST Program (MTO) N66001-11-1-4013. Additional funding was also provided through a Coulter Translational Research Award, the American Heart Association Grant 1T32EB011434-01A1, AHA Innovative Research Award–National(Marcus Foundation) 15IRG22760009, AHA Midwest Grant in Aid Award 15GRNT25780033, the Foundation of ASNR, UW Milwaukee-Madison Intercampus Grants, the UW Graduate School, and by Shapiro Foundation Grants.

ACKNOWLEDGMENTS

The authors would like to thank all the study subjects and their families for participating in the study, and all the MR technologists for their support in collection of the data. The authors would also like to extend thanks to Dr. Justin Sattin for referrals of stroke subjects and clinical documentation.

SUPPLEMENTARY MATERIAL

The Supplementary Material for this article can be found online at: https://www.frontiersin.org/articles/10.3389/fnins.2018.00861/full#supplementary-material

Supplementary Figure 1 | Percentage of significant FCs for each patient in each session. Percentage of significant is defined as the number of significant FCs divided by the number of all possible FCs in the network.

REFERENCES

Achard, S., and Bullmore, E. (2007). Efficiency and cost of economical brain functional networks. *PLoS Comput Biol.* 3:e17. doi: 10.1371/journal.pcbi.0030017

Achard, S., Delon-Martin, C., Vértes, P. E., Renard, F., Schenck, M., Schneider, F., et al. (2012). Hubs of brain functional networks are radically reorganized in comatose patients. *Proc. Natl. Acad. Sci. U.S.A.* 109, 20608–20613. doi: 10.1073/pnas.1208933109

Alexander-Bloch, A. F., Gogtay, N., Meunier, D., Birn, R., Clasen, L., Lalonde, F., et al. (2010). Disrupted modularity and local connectivity of brain functional networks in childhood-onset schizophrenia. *Front. Syst. Neurosci.* 4:147. doi: 10.3389/fnsys.2010.00147

Allen, G., Buxton, R. B., Wong, E. C., and Courchesne, E. (1997). Attentional activation of the cerebellum independent of motor involvement. *Science* 2751940–1943. doi: 10.1126/science.275.5308.1940

Ang, K. K., Chua, K. S., Phua, K. S., Wang, C., Chin, Z. Y., Kuah, C. W., et al. (2015). A randomized controlled trial of EEG-based motor imagery brain-computer interface robotic rehabilitation for stroke. *Clin. EEG Neurosci.* 46, 310–320. doi: 10.1177/1550059414522229

Bassett, D. S., and Bullmore, E. (2006). Small-world brain networks. *Neuroscientist* 12, 512–23. doi: 10.1177/1073858406293182

Beebe, J. A., and Lang, C. E. (2009). Relationships and responsiveness of six upper extremity function tests during the first six months of recovery after stroke. *J. Neurol. Phys. Ther.* 33, 96–103. doi: 10.1097/NPT.0b013e3181a33638

Benjamini, Y., and Hochberg, Y. (1995). Controlling the false discovery rate: a practical and powerful approach to multiple testing. *J. Royal Stat. Soc. Series B* 57, 289–300.

Bernhardt, B. C., Chen, Z., He, Y., Evans, A. C., and Bernasconi, N. (2011). Graph-theoretical analysis reveals disrupted small-world organization of cortical thickness correlation networks in temporal lobe epilepsy. *Cereb. Cortex* 21, 2147–2157. doi: 10.1093/cercor/bhq291

Boccaletti, S., Latora, V., Moreno, Y., Chavez, M., and Hwang, D. U. (2006). Complex networks: structure and dynamics. *Phys Rep.* 424, 175–308. doi: 10.1016/j.physrep.2005.10.009

Borgatti, S. P. (2005). Centrality and Network Flow. *Soc. Netw. Elsevier* 27, 55–71. doi: 10.1016/j.socnet.2004.11.008

Borgatti, S. P., Everett, M. G. (2006). A graph-theoretic perspective on centrality. *Soc. Netw. Elsevier.* 28, 466–484. doi: 10.1016/j.socnet.2005.11.005

Brandes, U. (2001). A faster algorithm for betweenness centrality (PDF). *J. Mathematical Sociol.* 25, 163–177. doi: 10.1080/0022250X.2001.9990249

Bullmore, E., and Sporns, O. (2009). Complex brain networks: graph theoretical analysis of structural and functional systems. *Nat Rev Neurosci.* 10, 186–98. doi: 10.1038/nrn2575

Bullmore, E., and Sporns, O. (2012). The economy of brain network organization. *Nat. Rev. Neurosci.* 13, 336–349. doi: 10.1038/nrn3214

Carey, J. R., Kimberley, T. J., Lewis, S. M., Auerbach, E. J., Dorsey, L., Rundquist, P., et al. (2002). Analysis of fMRI and finger tracking training in subjects with chronic stroke. *Brain* 125, 773–788. doi: 10.1093/brain/awf091

Caria, A., Weber, C., Brötz, D., Ramos, A., Ticini, L. F., Gharabaghi, A., et al. (2011). Chronic stroke recovery after combined BCI training and physiotherapy: a case report. *Psychophysiology* 48, 578–582. doi: 10.1111/j.1469-8986.2010.01117.x

Carroll, D. (1965). A quantitative test of upper extremity function. *J. Chronic Dis.* 18, 479–491. doi: 10.1016/0021-9681(65)90030-5

Chollet, F., DiPiero, V., Wise, R. J., Brooks, D. J., Dolan, R. J., and Frackowiak, R. S. (1991). The functional anatomy of motor recovery after stroke in humans: a study with positron emission tomography. *Ann. Neurol.* 29, 63–71. doi: 10.1002/ana.410290112

Cox, R. W. (1996). AFNI: software for analysis and visualization of functional magnetic resonance neuroimages. *Comput. Biomed. Res.* 29, 162–173. doi: 10.1006/cbmr.1996.0014

Cramer, S. C., and Nudo, R. J. (eds.). (2010). *Brain Repair After Stroke.* Cambridge, UK: Cambridge University Press.

De Vico Fallani, F., Richiardi, J., Chavez, M., and Achard, S. (2014). Graph analysis of functional brain networks: practical issues in translational neuroscience. *Phil. Trans. R. Soc. B.* 369:20130521. doi: 10.1098/rstb.2013.0521

Dimyan, M. A., and Cohen, L. G. (2011). Neuroplasticity in the context of motor rehabilitation after stroke. *Nat. Rev. Neurol.* 7, 76–85. doi: 10.1038/nrneurol.2010.200

Dong, Y., Winstein, C. J., Albistegui-DuBois, R., and Dobkin, B. H. (2007). Evolution of FMRI activation in the perilesional primary motor cortex and cerebellum with rehabilitation training-related motor gains after stroke: a pilot study. *Neurorehabil. Neural. Repair.* 21, 412–428. doi: 10.1177/1545968306298598

Dromerick, A. W., Lang, C. E., Birkenmeier, R. L., Wagner, J. M., Miller, J. P., Videen, T. O., et al. (2009). Very early constraint-induced movement during stroke rehabilitation (VECTORS) A single-center RCT. *Neurology* 73, 195–201. doi: 10.1212/WNL.0b013e3181ab2b27

Gauthier, L. V., Taub, E., Perkins, C., Ortmann, M., Mark, V. W., and Uswatte, G. (2008). Remodeling the brain: plastic structural brain changes produced by different. *Stroke* 39, 1520–1525.

Go, A. S., Mozaffarian, D., Roger, V. L., Benjamin, E. J., Berry, J. D., Borden, W. B., et al. (2013). Heart disease and stroke statistics—2013 update: a report from the American Heart Association. *Circulation* 127, e6–e245. doi: 10.1161/CIR.0b013e31828124ad

He, X., Doucet, G. E., Pustina, D., Sperling, M. R., Sharan, A. D., and Tracy, J. I. (2017). Presurgical thalamic "hubness" predicts surgical outcome in temporal lobe epilepsy. *Neurology* 88, 2285–2293. doi: 10.1212/WNL.0000000000004035

He, Y., Chen, Z., and Evans, A. (2008). Structural insights into aberrant topological patterns of large-scale cortical networks in Alzheimer's disease. *J Neurosci.* 28, 4756–4766. doi: 10.1523/JNEUROSCI.0141-08.2008

Humphries, M. D., Gurney, K., and Prescott, T. J. (2006). The brainstem reticular formation is a small-world, not scale-free, network. *Proc. Biol. Sci.* 273, 503–511. doi: 10.1098/rspb.2005.3354

Irimia, D., Sabathiel, N., Ortner, R., Poboroniuc, M., Coon, W., Allison, B. Z., et al. (2016). "Recoverix: a new BCI-based technology for persons with stroke," in *Engineering in Medicine and Biology Society (EMBC), 2016 IEEE 38th Annual International Conference of the IEEE* (Orlando, FL), 1504–1507. doi: 10.1109/EMBC.2016.7590995

Iyer, S., Jedidiah, M., Candida, U., Veena, N., Megan, R., Taylor, M., et al. (2018). *Altered Frontal Lobe Network Function in Temporal Lobe Epilepsy Revealed by Graph Theory Analysis (P1. 279).* P1-279. Available online at: http://n.neurology.org/content/90/15_Supplement/P1.279

Jaillard, A., Martin, C. D., Garambois, K., Lebas, J. F., and Hommel, M. (2005). Vicarious function within the human primary motor cortex? A longitudinal fMRI stroke study. *Brain* 128, 1122–1138. doi: 10.1093/brain/awh456

Kelly-Hayes, M., Beiser, A., Kase, C. S., Scaramucci, A., D'agostino, R. B., and Wolf, P. A. (2003). The influence of gender and age on disability following ischemic stroke: the framingham study. *J. Stroke Cerebrovasc. Dis.* 12, 119–126. doi: 10.1016/S1052-3057(03)00042-9

Latora, V., and Marchiori, M. (2001). Efficient behavior of small-world networks. *Phys. Rev. Lett.* 87:198701. doi: 10.1103/PhysRevLett.87.198701

Loui, P., Zamm, A., and Schlaug, G. (2012). Enhanced functional networks in absolute pitch. *Neuroimage* 63, 632–640. doi: 10.1016/j.neuroimage.2012.07.030

Meunier, D., Achard, S., Morcom, A., and Bullmore, E. (2009). Age-related changes in modular organization of human brain functional networks. *Neuroimage* 44, 715–723. doi: 10.1016/j.neuroimage.2008.09.062

Muralidharan, A., Chae, J., and Taylor, D. (2011). Extracting attempted hand movements from EEGs in people with complete hand paralysis following stroke. *Front. Neurosci.* 5:39. doi: 10.3389/fnins.2011.00039

Murphy, K., and Fox, M. D. (2017). Towards a consensus regarding global signal regression for resting state functional connectivity MRI. *Neuroimage* 154, 169–173. doi: 10.1016/j.neuroimage.2016.11.052

Remsik, A., Young, B., Vermilyea, R., Kiekhoefer, L., Abrams, J., Evander Elmore, S., et al. (2016). A review of the progression and future implications of brain-computer interface therapies for restoration of distal upper extremity motor function after stroke. *Exp. Rev. Med. Dev.* 13, 445–454. doi: 10.1080/17434440.2016.1174572

Richards, L. G., Stewart, K. C., Woodbury, M. L., Senesac, C., and Cauraugh, J. H. (2008). Movement-dependent stroke recovery: a systematic review and meta-analysis of TMS. *Neuropsychologia* 46, 3–11.

Rutter, L., Nadar, S. R., Holroyd, T., Carver, F. W., Apud, J., Weinberger, D. R., et al. (2013). Graph theoretical analysis of resting magnetoencephalographic functional connectivity networks. *Front. Comput. Neurosci.* 7:93. doi: 10.3389/fncom.2013.00093

Shibasaki, H., Sadato, N., Lyshkow, H., Yonekura, Y., Honda, M., Nagamine, T., et al. (1993). Both primary motor cortex and supplementary motor area play an important role in complex finger movement. *Brain* 116, 1387–1398. doi: 10.1093/brain/116.6.1387

Small, S. L., Hlustik, P., Noll, D. C., Genovese, C., and Solodkin, A. (2002). Cerebellar hemispheric activation ipsilateral to the paretic hand correlates with functional recovery after stroke. *Brain* 125, 1544–1557. doi: 10.1093/brain/awf148

Song, J., Birn, R. M., Boly, M., Meier, T. B., Nair, V. A., Meyerand, M. E., et al. (2014b). Age-related reorganizational changes in modularity and functional connectivity of human brain networks. *Brain Connectivity* 4, 662–676. doi: 10.1089/brain.2014.0286

Song, J., Nair, V. A., Young, B. M., Walton, L. M., Nigogosyan, Z., Remsik, A., et al. (2015). DTI measures track and predict motor function outcomes in stroke rehabilitation utilizing BCI technology. *Front. Human Neurosci.* 9:195. doi: 10.3389/fnhum.2015.00195

Song, J., Young, B. M., Nigogosyan, Z., Walton, L. M., Nair, V. A., Grogan, S. W., et al. (2014a). Characterizing relationships of DTI, fMRI, and motor recovery in stroke rehabilitation utilizing brain-computer interface technology. *Front. Neuroeng.* 7:31. doi: 10.3389/fneng.2014.00031

Stinear, C. M., and Byblow, W. D. (2014). Predicting and accelerating motor recovery after stroke. *Curr. Opin. Neurol.* 27, 624–630. doi: 10.1097/WCO.0000000000000153

Towfighi, A., and Saver, J. L. (2011). Stroke declines from third to fourth leading cause of death in the United States: historical perspective and challenges ahead. *Stroke* 42, 2351–2355. doi: 10.1161/STROKEAHA.111.621904

Vaessen, M. J., Jansen, J. F., Braakman, H. M., Hofman, P. A., De Louw, A., Aldenkamp, A. P., et al. (2014). Functional and structural network impairment in childhood frontal lobe epilepsy. *PLoS ONE* 9:e90068. doi: 10.1371/journal.pone.0090068

Van Wijk, B. C., Stam, C. J., and Daffertshofer, A. (2010). Comparing brain networks of different size and connectivity density using graph theory. *PLoS ONE* 5:e13701. doi: 10.1371/journal.pone.0013701

Wang, L., Yu, C., Chen, H., Qin, W., He, Y., Fan, F., et al. (2010). Dynamic functional reorganization of the motor execution network after stroke. *Brain* 133, 1224–1238. doi: 10.1093/brain/awq043

Watts, D. J., and Strogatz, S. H. (1998). Collective dynamics of 'small-world' networks. *Nature* 393, 440–442. doi: 10.1038/30918

Wolf, S. L., Thompson, P. A., Winstein, C. J., Miller, J. P., Blanton, S. R., Nichols-Larsen, D. S., et al. (2010). The EXCITE stroke trial: comparing early and delayed constraint-induced movement therapy. *Stroke* 41, 2309–2315. doi: 10.1161/STROKEAHA.110.588723

Wolf, S. L., Winstein, C. J., Miller, J. P., Taub, E., Uswatte, G., Morris, D., et al. (2006). Effect of constraint-induced movement therapy on upper extremity function 3 to 9 months after stroke: the EXCITE randomized clinical trial. *Jama* 296, 2095–2104. doi: 10.1001/jama.296.17.2095

Young, B. M., Nigogosyan, Z., Nair, V. A., Walton, L. M., Song, J., Tyler, M. E., et al. (2014c). Case report: post-stroke interventional BCI rehabilitation in an individual with preexisting sensorineural disability. *Front. Neuroeng.* 7:18. doi: 10.3389/fneng.2014.00018

Young, B. M., Nigogosyan, Z., Remsik, A., Walton, L. M., Song, J., Nair, V. A., et al. (2014a). Changes in functional connectivity correlate with behavioral gains in stroke patients after therapy using a brain-computer interface device. *Front. Neuroeng.* 7:25. doi: 10.3389/fneng.2014.00025

Young, B. M., Nigogosyan, Z., Walton, L. M., Remsik, A., Song, J., Nair, V. A., et al. (2015). Dose-response relationships using brain–computer interface technology impact stroke rehabilitation. *Front. Human Neurosci.* 9:361. doi: 10.3389/fnhum.2015.00361

Young, B. M., Nigogosyan, Z., Walton, L. M., Song, J., Nair, V. A., Grogan, S. W., et al. (2014b). Changes in functional brain organization and behavioral correlations after rehabilitative therapy using a brain-computer interface. *Front. Neuroeng.* 7:26. doi: 10.3389/fneng.2014.00026

Young, B. M., Williams, J., and Prabhakaran, V. (2014d). BCI-FES: could a new rehabilitation device hold fresh promise for stroke patients? *Exp. Rev. Med. Dev.* 11, 537–539. doi: 10.1586/17434440.2014.941811

Conflict of Interest Statement: The authors declare that the research was conducted in the absence of any commercial or financial relationships that could be construed as a potential conflict of interest.

Copyright © 2018 Mazrooyisebdani, Nair, Loh, Remsik, Young, Moreno, Dodd, Kang, William and Prabhakaran. This is an open-access article distributed under the terms of the Creative Commons Attribution License (CC BY). The use, distribution or reproduction in other forums is permitted, provided the original author(s) and the copyright owner(s) are credited and that the original publication in this journal is cited, in accordance with accepted academic practice. No use, distribution or reproduction is permitted which does not comply with these terms.

frontiers in Neuroscience

CLINICAL TRIAL
published: 06 March 2019
doi: 10.3389/fnins.2019.00053

Ipsilesional Mu Rhythm Desynchronization and Changes in Motor Behavior Following Post Stroke BCI Intervention for Motor Rehabilitation

Alexander B. Remsik[1,2,3†], Leroy Williams Jr.[1,4,5†], Klevest Gjini[1,6], Keith Dodd[1,7], Jaclyn Thoma[1,8], Tyler Jacobson[1,8], Matt Walczak[1], Matthew McMillan[1,7], Shruti Rajan[1,9], Brittany M. Young[1,3,8,10,11], Zack Nigogosyan[1], Hemali Advani[1], Rosaleena Mohanty[1,12], Neelima Tellapragada[1], Janerra Allen[13], Mohsen Mazrooyisebdani[1], Leo M. Walton[7,8], Peter L. E. van Kan[2], Theresa J. Kang[1,6], Justin A. Sattin[8], Veena A. Nair[1], Dorothy Farrar Edwards[2], Justin C. Williams[7,14] and Vivek Prabhakaran[1,6,8,9,11,15]*

[1] Department of Radiology, University of Wisconsin–Madison, Madison, WI, United States, [2] Department of Kinesiology, University of Wisconsin–Madison, Madison, WI, United States, [3] Institute for Clinical and Translational Research, University of Wisconsin–Madison, Madison, WI, United States, [4] Department of Educational Psychology, University of Wisconsin–Madison, Madison, WI, United States, [5] Center for Women's Health Research, University of Wisconsin–Madison, Madison, WI, United States, [6] Department of Neurology, University of Wisconsin–Madison, Madison, WI, United States, [7] Department of Biomedical Engineering, University of Wisconsin–Madison, Madison, WI, United States, [8] Neuroscience Training Program, University of Wisconsin School of Medicine and Public Health, Madison, WI, United States, [9] Department of Psychology, University of Wisconsin–Madison, Madison, WI, United States, [10] Clinical Neuroengineering Training Program, University of Wisconsin–Madison, Madison, WI, United States, [11] Medical Scientist Training Program, University of Wisconsin School of Medicine and Public Health, Madison, WI, United States, [12] Department of Electrical and Computer Engineering, University of Wisconsin–Madison, Madison, WI, United States, [13] Department of Materials Science and Engineering, University of Wisconsin–Madison, Madison, WI, United States, [14] Department of Neurological Surgery, University of Wisconsin–Madison, Madison, WI, United States, [15] Department of Psychiatry, University of Wisconsin–Madison, Madison, WI, United States

OPEN ACCESS

Edited by:
Ioan Opris,
University of Miami, United States

Reviewed by:
Ranganatha Sitaram,
Pontifical Catholic University of Chile, Chile
David Thomas Bundy,
University of Kansas Medical Center Research Institute, United States

***Correspondence:**
Alexander B. Remsik
alexbremsik@gmail.com

[†]Co-first authors

Specialty section:
This article was submitted to Neural Technology, a section of the journal Frontiers in Neuroscience

Received: 01 March 2018
Accepted: 21 January 2019
Published: 06 March 2019

Citation:
Remsik AB, Williams L Jr, Gjini K, Dodd K, Thoma J, Jacobson T, Walczak M, McMillan M, Rajan S, Young BM, Nigogosyan Z, Advani H, Mohanty R, Tellapragada N, Allen J, Mazrooyisebdani M, Walton LM, van Kan PLE, Kang TJ, Sattin JA, Nair VA, Edwards DF, Williams JC and Prabhakaran V (2019) Ipsilesional Mu Rhythm Desynchronization and Changes in Motor Behavior Following Post Stroke BCI Intervention for Motor Rehabilitation. Front. Neurosci. 13:53. doi: 10.3389/fnins.2019.00053

Loss of motor function is a common deficit following stroke insult and often manifests as persistent upper extremity (UE) disability which can affect a survivor's ability to participate in activities of daily living. Recent research suggests the use of brain–computer interface (BCI) devices might improve UE function in stroke survivors at various times since stroke. This randomized crossover-controlled trial examines whether intervention with this BCI device design attenuates the effects of hemiparesis, encourages reorganization of motor related brain signals (EEG measured sensorimotor rhythm desynchronization), and improves movement, as measured by the Action Research Arm Test (ARAT). A sample of 21 stroke survivors, presenting with varied times since stroke and levels of UE impairment, received a maximum of 18–30 h of intervention with a novel electroencephalogram-based BCI-driven functional electrical stimulator (EEG-BCI-FES) device. Driven by spectral power recordings from contralateral EEG electrodes during cued attempted grasping of the hand, the user's input to the EEG-BCI-FES device modulates horizontal movement of a virtual cursor and also facilitates concurrent stimulation of the impaired UE. Outcome measures of function and capacity were assessed at baseline, mid-therapy, and at completion of therapy while EEG was recorded only during intervention sessions. A significant increase in r-squared values [reflecting Mu rhythm (8–12 Hz) desynchronization as the result of attempted

movements of the impaired hand] presented post-therapy compared to baseline. These findings suggest that intervention corresponds with greater desynchronization of Mu rhythm in the ipsilesional hemisphere during attempted movements of the impaired hand and this change is related to changes in behavior as a result of the intervention. BCI intervention may be an effective way of addressing the recovery of a stroke impaired UE and studying neuromechanical coupling with motor outputs.

Clinical Trial Registration: ClinicalTrials.gov, identifier NCT02098265.

Keywords: brain–computer interface, hemiparesis, r-squared, coherence, chronic, acute, neuroplasticity, homunculus

INTRODUCTION

Stroke

Stroke is a leading cause of acquired adult long-term disability in the United States (Benjamin et al., 2017) and occurs when blood supply to the brain is compromised, leading to functional deficits that may affect activities of daily living (ADLs). Approximately 85% of patients who suffer and survive a new or recurrent stroke in the United States each year require rehabilitation (Yang et al., 2017). Six months post-stroke, nearly 50% of survivors have some residual motor deficits (Benjamin et al., 2017). By 2050, stroke burden on the United States economy will approach $2.2 trillion (Benjamin et al., 2017). Despite advances in acute stroke care, the estimated direct and indirect costs of stroke continue to escalate and are disproportionally associated with long-term care and rehabilitation (Benjamin et al., 2017). Current standard of care seems insufficiently developed to treat long-term motor deficits, potentially further burdening patients as untreated motor impairment can lead to deconditioning and underutilization of the affected upper extremity (UE), a consequence deemed, learned non-use (LNU) (Schaechter, 2004).

Customary Care and the Opportunities for Improvement

Several rehabilitation techniques are traditionally used for stroke recovery including conventional physical-occupational-speech therapies, provided in acute care settings as well as newer motor therapies such as constraint-induced movement therapy (CIMT), robot-aided therapy, transcranial direct current stimulation (tDCS), transcranial magnetic stimulation (TMS), and virtual reality (VR) (Kollen et al., 2006; Lindenberg et al., 2010; Fleet et al., 2014; Young et al., 2014a,b,c; Laver et al., 2015; Song et al., 2015; Babaiasl et al., 2016; Smith and Stinear, 2016). Importantly, a much different level of evidence exists for CIMT and traditional therapies than experimental therapies such as tDCS and VR-based approaches. Existing pharmacological treatments, Botox injections for example, and traditional physical therapy methods primarily serve to treat symptoms associated with stroke (Benjamin et al., 2017) and may not focus on bringing about basic changes to the underlying impaired brain function associated with relevant post-stroke pathologies. Patients with UE motor impairment traditionally receive rehabilitation regimens that involve passive, repetitive movement of the impaired limb without directly linking brain activity to these movements (Dromerick et al., 2009). Whereas passive movement repetition can be an effective rehabilitation strategy, recovery can be slow, and suboptimal. In contrast, linking brain activity to movement is important for motor skill learning (e.g., walking, running, throwing, writing, etc.) and the formation of central to peripheral connections. Leveraging this innate and robust motor learning circuitry, harnessing brain plasticity (Thakor, 2013), may be the next step toward improve patient outcomes.

Motor Recovery

Research suggests that motor recovery post-stroke, similar to motor learning, requires specific internal and external environmental conditions (Power et al., 2011; Wenger et al., 2017). For example, lesion load is a limiting factor as sufficient existing neural-architecture is needed for motor recovery to occur (Power et al., 2011). Recovery likely manifests either by the return of function to surviving neural architecture, or via neural reorganization and neural network remapping of proximal (i.e., near-by) neural architecture (Gazzaniga, 2005; Jones, 2017). Perhaps such processes may even be related. If neuroplasticity in the motor system, though likely attenuated by age, is continuous (Gazzaniga, 2005) over the life course (Power et al., 2011; Wenger et al., 2017), long-studied learning theories such as Hebbian plasticity and classical conditioning might be better integrated in treatment designs to aid recovery of stroke impaired UE motor capacities (Power et al., 2011; Remsik et al., 2016). The incorporation of neurorehabilitation techniques has yielded operational clinical therapies and devices (Pfurtscheller et al., 1997, 2005; Neuper and Pfurtscheller, 2001; Pineda, 2005; Felton et al., 2007; Schalk et al., 2008; Power et al., 2011; Kuiken et al., 2013; Young et al., 2014a; Wenger et al., 2017). As a number of existing approaches suffer from issues of high cost, passive movement repetition, large equipment, personnel and time constraints it is crucial efforts are made to pursue more expedient and efficacious means of rehabilitation, improve our quality of care, and better serve our survivors.

Sensorimotor Rhythms

Human brain rhythms associated with motor output, sensorimotor rhythms (SMRs), are recorded superficial to the motor and somatosensory cortical strip of the brain (electrode sites C3 and C4) and originate according to homuncular

organization (Pfurtscheller et al., 1997; Birbaumer et al., 2006). At the motor cortical strip (generally, Brodmann areas 3–6), each brain hemisphere desynchronizes with imagined, attempted, and also preparation of movement. This phenomenon is known as event-related desynchronization (ERD). Specific frequency bands have been associated with specific aspects of event-related motor behaviors (Pfurtscheller et al., 1997, 2005; Felton et al., 2007; Schalk et al., 2008; Song et al., 2014; Young et al., 2014b). In normal effortful movement, Mu rhythms of the contralateral cortex are desynchronized and attenuated (ERD) as movements are planned and executed (Pfurtscheller et al., 1997). This is followed by an increased presence of Beta rhythm ERD in the contralateral motor cortex which is associated with the later stages of motor command output and control (Pineda, 2005). After the completion, or at the cessation of movement, the SMRs in Mu and Beta frequency bands synchronize (ERS). ERD and ERS were key elements in the development and use of early BCIs for the rehabilitation of motor functions (Pfurtscheller et al., 1997, 2005; Nam et al., 2011). The early designs confirmed that ERD or ERS in specific spatial areas and neural networks (e.g., thalamocortical networks, frontoparietal networks) associated with a task or triggered events can be utilized to control a device or output command (Pfurtscheller et al., 1997; Neuper and Pfurtscheller, 2001).

Mu and Beta sensorimotor rhythms (SMRs) in human subjects are recorded exclusively over sensorimotor areas at frequencies of about 10–20 Hz (Pfurtscheller et al., 1997; Birbaumer et al., 2006). Two basic strategies in SMR-based control have been introduced for motor rehabilitation in stroke patients: motor imagery (Wolpaw et al., 1991; Ortner et al., 2012; Irimia et al., 2016) and attempted movement-based approaches (Wolpaw et al., 1991; Schalk et al., 2004; Young et al., 2014a,b,c). Either approach utilizes essentially overlapping neural architecture to provide input signals (electrophysiological recordings by the EEG cap) to the BCI. The authors of this study designed the protocol to utilize attempted hand movements during the intervention according to the logic that a motor therapy intended to restore volitional motor function of the affected UE should utilize voluntary attempted movements of that impaired hand in a continuous effort to improve the participant's UE capacity and performance.

Brain–Computer Interface (BCI) and Electroencephalography for Assistive Design

Noninvasive brain–computer interfaces (BCIs), which utilize ancillary adjuvant peripheral devices and electrical muscle stimulation, as well as invasive BCI approaches with electrodes implanted in the skull, have been introduced (Wolpaw et al., 1991; Leuthardt et al., 2004; Schalk et al., 2004, 2008; McFarland et al., 2006; Felton et al., 2007) as contemporary intervention and rehabilitation techniques following neural disease or trauma, such as stroke. Devices similar to what was utilized in this research are controlled by input signals generated by scalp electroencephalographic (EEG) recordings from electrodes superficial to the sensorimotor cortices. EEG signals associated with various components of voluntary movement are identified and translated into a device command or specified output (Pfurtscheller et al., 1997, 2005; Felton et al., 2007; Schalk et al., 2008; Wilson et al., 2012), like activation of an FES pad (Song et al., 2014; Young et al., 2014a,b). BCIs can monitoring volitional modulation of electrical brain rhythms and execute an augmentative, facilitative, or rehabilitative command in the presence or absence of such signals.

Adjuvants

In this study, EEG driven BCI was linked to tongue stimulation (TS) via a Tongue Display Unit (TDU) (Kaczmarek, 2011; Wilson et al., 2012) (designed as a visual supplementation for any participant with visual impairments) and FES, which can act not only as therapeutic adjuvants but, when tied to intent-to-move brain signals, also provide users with multi-modal feedback as a form of monitoring and reward for producing relevant brain activity patterns (SMR modulation) during tasks. Adjuvant stimulation may not only aid execution of the motor plan by causing the contraction of the impaired UE musculature but may also help the user learn new movement strategies for the impaired extremity. Adjuvant-induced proprioceptive and general afferent inputs to the motor system complete the BCI design's replication of the native neurobiological closed-loop motor system. Such adjuvant-aided volitional movement may not only make a movement possible but also contribute ancillary components for motor learning. Rewards of tactile, kinesthetic feedback to the system and the visual revelation of a previously impaired appendage now voluntarily animated may prove powerful (Moe and Post, 1962; Krafi et al., 1992; Popovic et al., 2009; Howlett et al., 2015) reinforces.

Evidence

Growing evidence from our lab (Young et al., 2014a,b,c; Song et al., 2015) and other groups (Hill et al., 2006; Daly and Wolpaw, 2008; Daly et al., 2009; Caria et al., 2011; Muralidharan et al., 2011; Ang and Guan, 2013; Varkuti et al., 2013; Bundy et al., 2017) suggest that noninvasive EEG-BCI-FES systems hold potential for facilitating recovery in the chronic phase after stroke by linking central nervous system (CNS) commands, or brain activity, with distal motor effectors (the manifestation of the motor plan via trained muscle synergies) of the peripheral nervous system (PNS). Integration of the aforementioned command with facilitated movements within strict reinforcement constraints (e.g., task accuracy: drop the cup, move the ball or not) might thereby better harness neuroplastic capacities leading to functional gains in recovery for individuals with stroke related hemiparesis. Previous studies suggest that change in the pattern of brain activity linked to attempted movements of the affected hand contributes to motor re-conditioning and induces brain plasticity or reorganization which, if properly directed and reinforced, should lead to improvement in a stereotyped motor function of interest (Daly et al., 2009; Caria et al., 2011; Muralidharan et al., 2011; Varkuti et al., 2013). This is of special importance for patients in the chronic phase (generally >6 months post stroke) of recovery who may have little to no residual function in the affected arm, in addition to learned compensatory motor strategies

(Muralidharan et al., 2011). Given that these participants have also likely exhausted other forms of intervention available to them through standard healthcare channels, it is imperative to explore novel intervention technologies that show promise in this population.

Overview of This Study

It was hypothesized that (1) the EEG-BCI-FES intervention sessions would result in increased hemispheric desynchronization levels of Mu (8–12 Hz) rhythm and, or Beta (18–26 Hz) band signals over the ipsilesional motor cortices, as reflected by increased r-squared values (i.e., lower power in the impaired hand movement trials compared to rest), and (2) changes in functional connectivity (coherence) are greatest in the affected contralateral (ipsilesional) motor cortex and, over time, are associated with beneficial behavior and quality of life improvements as measured by objective and subjective measures of upper extremity motor function and activities of daily living. This interim analysis, of the larger ongoing prospective randomized crossover-controlled clinical trial, seeks to determine whether greater desynchronization of motor related SMRs in the ipsilesional hemisphere during attempted movements of the impaired hand are related to changes in behavior as a result of intervention.

MATERIALS AND METHODS

Subjects and Design

Ethics Statement

Participants were recruited from the greater Madison, WI, United States area as part of an on-going prospective randomized, cross-over controlled design stroke rehabilitation study investigating interventional BCI targeting UE motor function. This study is approved by the University of Wisconsin Health Sciences Institutional Review Board (Study ID 2015-0469); all subjects provided written informed consent upon enrollment. A CONSORT flow diagram is made available in **Supplementary Figure S1**.

Recruitment and Enrollment

This on-going study, registered with ClinicalTrials.gov (study ID[1] NCT02098265), employs an open call for participants with a wide range of (1) UE hemiparesis resulting from stroke, (2) time-since-stroke, (3) stroke type, (4) lesion location, (5) number of previous strokes, (6) and stroke severity. Subsequent to informed, written consent, stroke survivors were randomized by permuted-block design accounting specifically for gender, stroke chronicity, as well as severity of motor impairment as measured by the Action Research Arm Test (ARAT) (Lang et al., 2008) (n = 21, mean age = 61.6 years ± 15.3 years, 12 female, 13 right lateralized lesion, mean chronicity = 1127 days ± 1326.5 days, median chronicity 588 days, 11 with severe UE motor deficit, mean baseline ARAT score of impaired side = 26.6 ± 26.1). Chronicity is measured as time since stroke, in days, to baseline measurement day. Participant characteristics are displayed in **Table 1**. This interim analysis of the larger ongoing study seeks to elucidate the electrophysiological consequences and associations of BCI participation and the authors focus specifically on the behavioral (primary outcome) associations in another manuscript published in tandem with this effort (Remsik et al., 2018).

Inclusion–Exclusion Criteria

Participants age 18 years or older with persistent UE motor impairment resulting from stroke and no other known neurologic (cognitive, expressive), psychiatric (affect), or developmental disabilities were included. Exclusion criteria were: allergy to electrode gel, surgical tape, metals, concurrent treatment for infectious disease, apparent lesions or inflammation of the oral cavity, pregnancy or intention to become pregnant during the course of the study, or any contraindication for magnetic resonance imaging (MRI). Subjects from the greater study cohort were excluded from the presented analyses if they (1) failed to complete at least 9 of 15, two-hour BCI intervention sessions occurring at least twice each week, (2) failed to complete all four MRI and behavioral testing sessions occurring in the intervention phase (**Figure 1**).

Randomization and Study Schema

Participants, when assigned to the intervention phase, have at least 9 and up to 15 EEG-BCI-FES intervention sessions (two-to-three sessions/week) wherein they receive EEG-BCI-FES intervention lasting up to 2 h for a potential total dosing of 30 h of EEG-BCI-FES intervention. Along with the EEG-BCI-FES intervention sessions, subjects also receive fMRI and behavioral testing at four time points: prior to the first EEG-BCI-FES intervention session (baseline), after the first few weeks of intervention (midpoint), following the final intervention session (endpoint), and again 1 month after the endpoint assessment (follow-up). Subjects assigned to the delayed intervention group (DTG) are encouraged to continue with their normal and customary care while in the delay period. While in the delay period, participant EEG data are not recorded and participants are instructed not to use a BCI device. During this time, there are three assessment visits consisting of MRI and behavioral testing which are matched in sequence and duration to those conducted in the BCI intervention period as demonstrated in **Figure 1**. After completion of the delay period, these participants cross over into the intervention phase and are assessed in accordance with previously described methods. All data and time points analyzed and presented herein were recorded during the BCI intervention period only, for all participants. EEG data were only collected during the intervention phase.

The BCI System

The BCI system and intervention sequence were consistent with those previously described (Wilson et al., 2012; Song et al., 2014, 2015; Young et al., 2014a,b,c) using BCI2000 software (Schalk et al., 2004) version 2 with in-house modifications for input from a 16-channel EEG cap and amplifier (Guger Technologies) and integration with the ball and target gaming visual display as

[1]https://clinicaltrials.gov/ct2/show/NCT02098265

TABLE 1 | Participant characteristic and ARAT score.

Participants	Age (years)	Chronicity (days)	Severity	Clinical cause Lesion location	Baseline ARAT	Completion ARAT	Follow-up ARAT	ARAT change
1	47–51	160	Severe	L-Lateral medulla	3	2	7	−1 (4)
2	49–53	490	Severe	R-MCA stroke	3	4	8	*1 (5)
3	76–80	658	Mild	Leg/periventricular white, MHR	57	57	57	0 (0)
4	67–51	2723	Severe	R-PLIC putamen	23	40	39	*17 (16)
5	81–85	580	Mild	Cerebellar vermis	47	52	52	*5 (5)
6	73–77	197	Severe	R-Prefrontal, midfrontal, temporal	0	0	3	0 (3)
7	62–66	101	Mild	R-White matter	56	57	57	*1 (1)
8	40–44	2645	Severe	R-Frontal parietal	7	7	7	0 (0)
9	55–59	588	Severe	R-MCA	3	4	0	*1 (−3)
10	45–49	452	Severe	L-Hemorrhagic stroke	0	2	0	*2 (0)
11	30–34	494	Mild	L-ICA	57	57	57	0 (0)
12	60–64	44	Mild	L-PCA	57	57	57	0 (0)
13	57–61	849	Mild	L-MCA	57	57	57	0 (0)
14	44–48	3017	Severe	R-MCA/R-FI	3	4	5	*1 (2)
15	69–73	790	Severe	R-MCA/R-TP	3	0	3	−3 (0)
16	78–82	631	Mild	R-Occipital	57	57	57	0 (0)
17	75–79	5125	Severe	R-MCA/ACA	9	11	10	*2 (1)
18	42–46	177	Mild	L-MCA	57	57	57	0 (0)
19	62–66	392	Severe	R-Frontal hematoma	3	5	16	*2 (13)
20	55–59	2767	Mild	R-VAOA, subarachnoid hemorrhage	57	57	57	0 (0)
21	69–73	783	Severe	R-MCA	0	0	0	0 (0)
(A) Mean	61.6	1127			26.6	27.9	28.9	1.3 (2.2)
Median	61.9	588			9	11	16	0 (0)
SD	15	1327			26.4	26.6	25.9	3.9 (4.5)
(B) Mean	61.1	1289			11.4	13.4	14.8	2 (3.4)
Median	64	584			3	4	7	1 (1.5)
SD	13.5	1497			18	20.2	19.6	4.7 (5.2)

ARAT, Action Research Arm Test; MCA, middle cerebral artery; ICA, internal carotid artery; PCA, posterior cerebral artery; FI, frontoparietal infarct; TP, temporal frontal-parietal; ACA, anterior cerebral artery; MHR, motor hand region; VAOA, vertebral artery origin aneurysm; L, left; R, right; ARAT change, completion-baseline (follow-up baseline). (A) Indicates descriptive statistics for all (n = 21) participants; (B) indicates descriptive statistics for (n = 14) participants able to achieve ARAT improvements (ceilings removed). Positive change in outcome measure at competition of BCI intervention denoted by ''.*

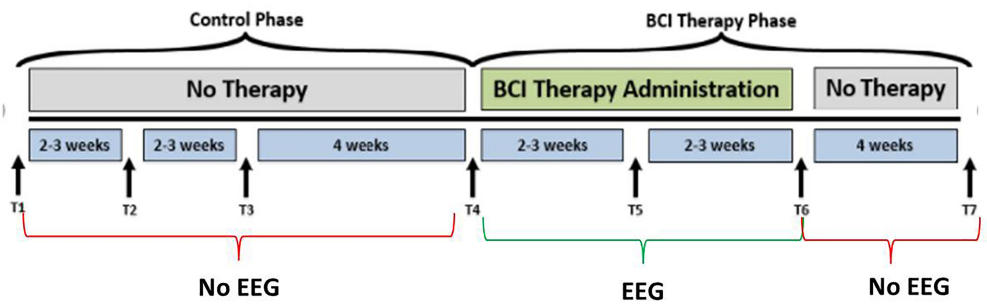

FIGURE 1 | Study design. The time-points at which neuroimaging data were collected are represented by, T1, control baseline; T2, control middle; T3, control completion; T4, intervention baseline; T5, mid-intervention; T6, completion of intervention; T7, 1-month post-intervention. While the crossover control group (DTG) completed visits T1 through T7, the immediate therapy (ITG) group completed only visits T4 through T7. EEG-BCI-FES intervention is only administered during the BCI Therapy Phase (green), from baseline (T4) to completion (T6), and EEG recordings are neither acquired between T1 and T4, nor between T6 and T7 during which only MRI and behavioral testing batteries are administered. EEG data were only collected during the intervention phase.

well as tongue stimulation (TDU 01.30 Wicab Inc.) (Kaczmarek, 2011) and functional electrical stimulation (FES) (LG-7500, LGMedSupply; Arduino 1.0.4). FES of the UE was delivered through a pair of 2" × 2" square electrodes, commercially available stimulus isolator units, which ensure clean, opto-electrical isolation, placed securely on the affected forearm using highly conductive Electrolyte Spray and produced by the LG-7500 Digital Muscle Stimulator LGMedSupply, Cherry Hill, NJ,

United States). The electrodes were placed to facilitate either a grasping motion (finger flexion), or finger extension according to participant preference. Specific placement sites were superficial to flexor digitorum superficialis to facilitate hand and finger flexion, or superficial to extensor digitorum communis to facilitate hand and finger extension. The natural absence of a flexor digitorum superficialis tendon to the fifth digit in some individuals was not considered in this study design. Stimulation was controlled through the PC using an Arduino Uno R3 (Adafruit Industries, New York, NY, United States) and a simple Reed-Relay circuit, with the amplitude set to elicit observable muscle activation (e.g., finger grasping) without pain. The pulse rate of the stimulation was set to 60 Hz in order to produce tetanic contraction of the muscle and the pulse width was set to 150 μs. The input signal, initially set to zero, was adjusted by steps of 0.5 mA, unless the stimulation became uncomfortable for the subject. The device was never set to deliver an output greater than 5 mA. In previous publications, the TDU (Kaczmarek, 2011) has been described and its use in a BCI paradigm detailed (Wilson et al., 2012). This BCI system uses the same TDU stimulation parameters as were reported previously (Wilson et al., 2012).

Brief Overview of the Procedure (EEG Tasks)

EEG-BCI-FES Intervention

Subjects went through intervention sessions on separate days. The number of EEG-BCI-FES intervention sessions varied across subjects with a mean of 13.8 ± 1.3. Each EEG-BCI-FES intervention session consisted of multiple runs of the 'Cursor Task' (mean of 31.3 ± 10.5 runs per session), about 1/3rd of which included only visual feedback, and roughly two thirds of which were comprised of BCI facilitated functional electric stimulation of the impaired hand and lingual electrotactile stimulation through a tongue display unit (TDU) (Kaczmarek, 2011; Wilson et al., 2012) (**Figure 2**). The EEG-BCI-FES device was driven by spectral power recordings from contralateral (to the hand active in the grasping task) EEG electrodes during cued attempted grasping movements of the hand which was designed to modulate the horizontal movement of a cursor (Schalk et al., 2008) in a computer display space as well as facilitate concurrent functional electrical stimulation of the participant's impaired UE (should the target appear on the side corresponding to their stroke-impaired hand). BCI classifier inputs were therefore at C3 and C4, respectively in Mu (8–12Hz) and Beta (18–26Hz) frequency bands in this design. Each EEG-BCI-FES (closed-loop) intervention session was preceded by an open-loop pre-therapy screening phase and followed by an open-loop post-therapy screening phase (**Figure 2**). The successive order of intervention procedure was as follows: visual only, visual + FES, visual + FES + tongue feedback. All intervention sessions included in this analysis contained a similar distribution of these conditions across all participants.

Familiarization With BCI Device and Procedures

The first BCI session was focused on assisting the participant to comprehend and engage the BCI device and protocol.

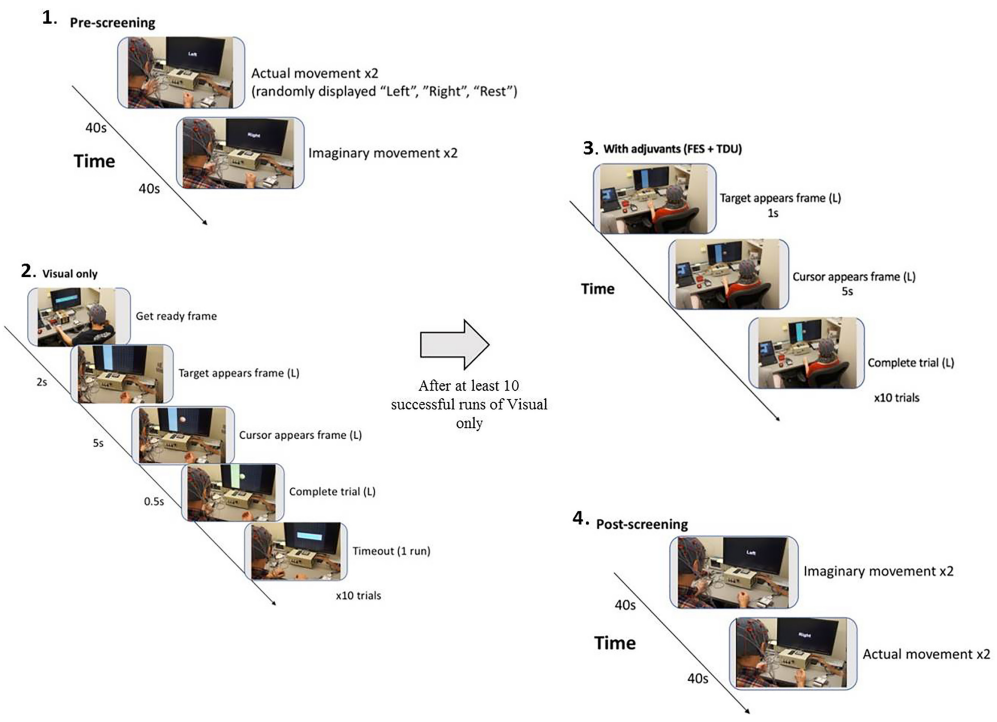

FIGURE 2 | BCI intervention block design. **(1)** Pre-screening (two actual movement trials, two imagined movement trials). **(2)** Cursor task (≥10 trials with visual-only feedback). **(3)** Cursor task with adjuvant stimuli (≥10 trials with adjuvant stimuli). **(4)** Post-screening (two imagined movement trials, two actual movement trials).

Stroke survivors often present with a myriad of cognitive, affective, and physical impairments (Nair et al., 2015) and out of respect for individual participant needs and abilities, the researchers intended to provide at outset an opportunity for a generous orientation rather than rigorous acquisition. During this preliminary session, the EEG cap (**Figure 3**), FES device, and TDU device were faithfully administered as described previously (Wilson et al., 2012). Participants were verbally instructed before each session, and as needed, to aim for successful completion of BCI tasks and for each attempted movement to be performed to the participant's autonomously elected level of comfort and ability. There were no participants in this study whom were unable to comprehend or participate successfully in the intervention protocol as a result of any associated cognitive or aphasic impairments associated with their stroke. The study design requires at least 10 runs for each closed-loop condition, per session; however, enforcement discretion was encouraged until a participant demonstrated task comprehension during the first BCI intervention session.

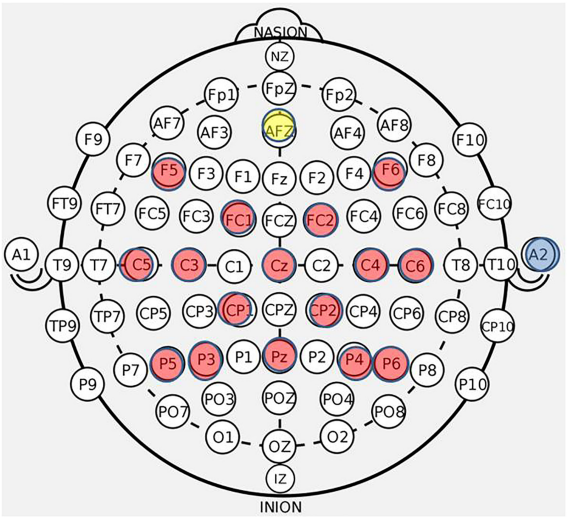

FIGURE 3 | BCI cap array. Electrode array and cap arrangement for all $n = 21$ participants. Control signals generated at C3 and C4 electrodes for right and left hand movement trials, respectively. Ear clip always placed on the right ear.

Description of the Raw EEG Data

EEG data were recorded using a 16-ch bioamplifier (g.USBamp; G.TEC Medical Engineering GmbH, Austria) from 16 active electrodes using a g.GAMMA cap (F5, C5, FC1, C3, P5, F6, C6, P6, Pz, P4, P3, FC2, Cz, CP2, C4, CP1) (**Figure 3**) according to 10-20 EEG electrode placement system with a right ear-lobe reference in a BCI2000 system environment (Schalk et al., 2004). The frequency bandwidth of the recorded signals was 0.1–100 Hz, with an additional notch-filter applied at 60 Hz. The sampling rate was 256 Hz. During each of the screening phases (pre- and post-therapy) EEG data were collected in four separate runs. Each screening EEG data file contained 15 trials for rest, left hand and right hand movements (i.e., five trials for each of the three conditions), separated by an interstimulus interval of 1.5–2 s. The order of trials in a run was random. Each of the trials had a duration of 4 s. The first two runs of the pre-therapy screening phase and the last two runs of the post-therapy screening phase incorporated cued "attempted" hand movements. The last two runs of the pre-therapy screening phase and the first two runs of the post-therapy screening phase incorporated cued "imaginary" hand movements.

Description of the EEG Data Analysis

The raw EEG data files were loaded into Fieldtrip (a MATLAB-based toolbox for advanced neurophysiological data analyses), and fully processed using tools incorporated in this toolbox (Oostenveld et al., 2011) and MATLAB environment[2]. The main processing steps for the EEG data collected during screening phases were as follows:

(1) Digital filtering with a high-pass filter cutoff of 4 Hz, and a low-pass filter cutoff of 30 Hz. (2) Extraction and grouping of trials according to condition (rest, left hand movement, right hand movement), movement type (attempted, imaginary), and the screening phase (pre, post). This resulted in 10 trials for each of condition/movement/screening phase combinations. (3) Identification (variance based: thresholds set to 10 and 250 μV^2 for low and high variance signals, respectively) and repair of bad (noisy) channels (spline interpolation), followed by the removal of three trials showing the highest variance (Thomson, 1982; Mitra and Pesaran, 1999). The channel was identified as bad (noisy, poor connection, etc.) if the variance was <10 or >250 μV^2 in more than three trials (Thomson, 1982; Mitra and Pesaran, 1999). The units of the variance were those of the data squared: as the EEG data units were in micro Volts, the variance units were squared micro Volts. If more than four channels were identified as bad, the data for that session were removed from further analysis (i.e., 20.4% of data were discarded by not meeting the defined criteria). At session level, this step resulted in 28 s of EEG data (7 trials $\times$ 4 s) for each condition/movement/screening phase combination set. (4) An average-reference montage was applied to the data (i.e., re-referencing from the original monopolar recordings). (5) Spectral analyses with Fourier transforms computed using a multi-taper method (Thomson, 1982; Mitra and Pesaran, 1999) at a 0.25 Hz resolution: this finally resulted in estimates of absolute spectral power sampled for every 1 Hz bin during the interval of 4–30 Hz, and cross-spectral density. The trial length was 4 s and the resolution of Fourier Transforms was 1/4 = 0.25 Hz. (6) Coherence estimation was calculated between all pairs of channels (120 pairs from 16 available scalp channels) at every 1 Hz frequency bin of the mentioned interval. Coherence was calculated as the absolute value of the ratio of the cross-spectrum to the square-root of the product of the two auto-spectra (as applied in Fieldtrip software). (7) Calculation of signed r-squared (r-squared: coefficient of determination) values from the absolute power estimates between left or right hand movements and rest trials, and between the two movement conditions (left vs. right). The r-squared values were signed in a such way that a large

[2]https://www.mathworks.com/

negative number (−) would mean larger "desynchronization" of the rhythm (Mu or Beta) (Pfurtscheller et al., 1997, 2005; Neuper and Pfurtscheller, 2001; Pineda, 2005). (8) Calculation of change (POST–PRE) in signed r-squared values: the following formula was used: −(POST–PRE), so one would obtain positive numbers for "increases" in desynchronization. This was done for easier interpretation of the associations of r-squared changes with behavior changes as the result of EEG-BCI-FES intervention. Here the "flipping" of values (in order to assess the "impaired hand," L or R) was applied to the impaired R-hand scores to put them together with scores from the impaired L-hand subjects. (9) Calculation of the laterality index (LI) for averaged coherence values (i.e., average coherence of each site with all others), used to evaluate shifts in coherence, as: (C3 − C4)/(C3 + C4). (10) Change (POST–PRE) in coherence LI values: LI as a number becomes more positive if there is a shift toward Left, and more negative if there is a shift toward Right (as the result of intervention). Therefore, for POST–PRE change in LI, the impaired L-hand values were multiplied with (−1) and the impaired R-hand values remained unchanged, as they were originally calculated. This way, the "expected change" is positive and the associations with behavioral changes can be more seasily interpreted.

Statistics

The independent variables were the signed r-squared values and the coherence estimates. At individual subject level, the data consisted of average estimates per each session for condition/movement/screening phase combination sets, and at group level the estimates consisted of grand averages over sessions of each individual subject data in the group (pre- and post-therapy scores averaged separately across sessions). Non-parametric statistical tests were run by calculating Monte-Carlo estimates of the significance probabilities and critical values from the permutation distribution (Maris and Oostenveld, 2007), followed by correction for multiple comparisons using false discovery rate (FDR) when no prior hypothesis was available. The *priori* hypotheses of expected changes in the r-squared values and coherence as the result of intervention time at C3 and C4 sites were tested using paired *t*-tests in MATLAB. Associations between the r-squared changes and the total number of intervention runs as well as behavioral changes (e.g., ARAT scores) were assessed using Pearson's and Spearman's correlation, respectively. Finally, the associations between the signed r-squared values with behavioral scores from several tests at baseline were assessed using Spearman's or Pearson's correlation coefficients, as appropriate. Thresholds for significance and trend toward significance were set *a priori* at $p \leq 0.05$ and $0.05 < p < 0.1$, respectively, for all statistical analyses.

Description of the Behavioral Outcome Measures

The primary outcome measure was the ARAT. The ARAT is a 57-point test designed to assess specific changes in upper limb function with sub-components for grasp, grip, pinch, and gross motor movement (Hsieh et al., 1998). The secondary measures include: The Stroke-Impact Scale (SIS), widely used to measure quality of life in stroke survivors that consists of 8 dimensions and a composite disability score (Vellone et al., 2015). The SIS is a 59-item patient-reported outcome measure, covering eight domains; strength (4 items), hand function (5 items), mobility (9 items), ADLs (10 items), memory (7 items), communication (7 items), emotion (9 items), and handicap (8 items); the domains are scored on a metric of 0–100, with higher scores indicating better self-reported health (Vellone et al., 2015). The National Institutes of Health Stroke Scale (NIHSS) is a tool used by healthcare providers to objectively quantify impairments caused by a stroke (Ortiz and Sacco, 2008). The NIHSS is composed of 11 items, each of which scores a specific ability between zero and four with higher scores indicating increased impairment (Ortiz and Sacco, 2008). The Barthel scale, or Barthel ADL index, is a scale used to measure performance in ADLs (Shah et al., 1989). It utilizes ten variables describing ADL and mobility. The ten variables addressed in the Barthel scale are: presence or absence of fecal incontinence, presence or absence of urinary incontinence, help needed with grooming, help needed with toilet use, help needed with feeding, help needed with transfers (e.g., from chair to bed), help needed with walking, help needed with dressing, help needed with climbing stairs, help needed with bathing. This scale yields a score of 0–100 with higher scores indicating improved performance (Shah et al., 1989). Gross grasp grip strength was measured using a dynamometer (Nam et al., 2011). The Nine-Hole Peg Test (9-HPT) is a brief, standardized, quantitative test of UE function (Mathiowetz et al., 1985). The score for the 9-HPT is an average of the two trials (Mathiowetz et al., 1985). Mini-Mental State Examination (MMSE) is scored out of 30 (Pangman et al., 2000). An MMSE score of 27–30 is generally associated with normal memory: a score 10–26 could indicate mild to moderate dementia, and a score less than 10 suggests severe dementia (Pangman et al., 2000). The Center for Epidemiologic Studies-Depression (CES-D) scale is one of the most frequently used self-report measures of depressive experiences (Shinar et al., 1986). The CES-D contains 20 items that are summed so that scores have a potential range from 0 to 60, with higher scores indicating greater frequency of depressive experiences (Shinar et al., 1986).

Analyses of Outcome Measures

Primary analysis was a paired-sample *t*-test to evaluate the statistical significance of ARAT and secondary outcome measure changes (i.e., SIS, NIHSS, Barthel scale, grip strength, 9-HPT, MMSE, and CES-D) between baseline, completion, and follow-up scores (**Table 2**).

RESULTS

Results of Outcome Measures

Of the 21 participants who completed the study and met the aforementioned criteria, 14 participants had room for improvement in the primary outcome measure, ARAT ($ARAT_{total}$), of which nine (64%) realized improved scores after intervention, both at immediate completion and 1 month

TABLE 2 | Summary of mean outcome measure scores for baseline, completion, and follow-up of the BCI training conditions.

Outcome measures	Baseline score	Completion score	Follow-up score	Change score	*p*-Value
Stroke Impact Scale (SIS) (Max = 100) $SIS_{Hand\ function}$	33.6(15) ± 38.1	39(25) ± 37.5	39.8(25) ± 39.7	5.4 (62)	0.482 *(0.050)
$SIS_{recovery}$	50.1(50) ± 23.7	53.4(60) ± 24.9	54.6(60) ± 21.8	3.3 (4.5)	0.509 (0.216)
NIH Stroke Scale/Score (NIHSS) (Max = 4)	3.8(3) ± 3.5	3.8(2.5) ± 3.1	3.7(2.5) ± 3.1	0 (−0.1)	1.0 (0.749)
Barthel Index-Total (Max = 100)	91.4(100) ± 14	92(97) ± 13.9	92.8(100) ± 14.8	0.6 (1.3)	0.431 (0.167)
Grip strength (lbs)	18.8(8.3) ± 21.5	22.6(14.3) ± 23.5	20.5(5) ± 24.6	3.8 (1.7)	*0.046 (0.246)
9-HPT (seconds)	17.7(0) ± 22.8	15(0) ± 19.1	14.4(0) ± 20.3	−2.5 (−3.2)	0.083 (0.054)
MMSE (Max = 30)	27.2(29) ± 3.8	27.8(29) ± 2.7	28.3(29) ± 2.7	0.6 (1)	0.467 (0.494)
CES-D (Max = 60)	7.6(7.5) ± 5.8	7.8(3) ± 9.9	5.6(3) ± 5.9	0.2 (−2)	0.802 (0.096)
Action Research Arm Test (ARAT) $ARAT_{Total}$ (Max = 57)	16.9(9) ± 23	18.3(11) ± 23.4	21.4(16) ± 23.4	1.3 (4.3)	*0.046 *(0.020)
$ARAT_{Grasp}$ (Max = 18)	22(3) ± 5.1	2.9(5) ± 5.3	3.6(6) ± 6.3	0.7 (01.5)	0.106 (0.163)
$ARAT_{Grip}$ (Max = 12)	2.9(2) ± 4.7	2.9(3) ± 4.8	3.8(4) ± 4.6	0.1 (0.9)	0.582 *(0.025)
$ARAT_{Pinch}$ (Max = 18)	4.5(1) ± 7.3	4.9.(0) ± 7.9	5.1(4) ± 7.7	0.4 (0.6)	0.289 (0.106)
$ARAT_{Gross}$ (Max = 9)	3.4(5) ± 2.7	3.4(6) ± 3	3.6(6) ± 3	0 (0.3)	1.000 (0.453)

*Measures are reported as mean (median) ± SD. Change score and p-value are reported as mean scores change between baseline and completion (mean scores change between baseline and follow-pp). ARAT scores are reported as mean scores change with ceilings removed. *$p < 0.05$, **$p < 0.01$, ***$p < 0.001$.*

after completion. Participant characteristics are summarized in **Table 1** and group outcome measures are further described in **Table 2**. All participant assessments at each time point were averaged to give a metric of cohort motor function change at the group level. Secondary measures were similarly group averaged to determine cohort measure changes as a result of time in intervention as well as at the 1 month follow-up (**Table 2**). The primary analysis showed significant change in baseline scores and completion scores (**Figure 1**: T4, T6) in the primary outcome measure (ARAT) ($p = 0.046$), and change at follow-up ($p = 0.020$) (**Figure 1**: T7), change in Grip Strength was found to be significant by completion of intervention ($p = 0.046$). This particular finding did not persist at the 1-month follow-up time point. Statistical significance was observed in the baseline to follow-up score analyses (**Figure 1**: T4 to T7) not only for the primary outcome measure but also in secondary outcome measures of hand function (i.e., SIS Hand Function $p = 0.05$) (**Table 2**). All statistically significant findings were observed in measures of hand function. Additionally, the secondary analyses presented no significant results.

EEG Measures

Results reported below in Section "R-Squared" echoed in the graph in **Figure 4**, compared the signed r-squared values for the impaired hand separately from the non-impaired hand. The signed r-squared values from the Right-hand impaired participants at C3 (i.e., the ipsilesional motor site) were "pooled together" with the signed r-squared values from the Left-hand impaired participants at C4 (i.e., the ipsilesional motor site) consistent with methods described previously. **Figures 4–8** display topoplots of group level averages of signed r-squared values and coherence values and do not use flipped-maps. Therefore, the maps for the left hand movements represent "an average" of these measures from impaired hand movements (as the majority of participants in this group were left-hand impaired) and non-impaired left hand movements (minority of subjects). In the same fashion, the maps for the right hand movements represent an average of these measures from impaired hand movements (minority of participants in this group were right-hand impaired) and non-impaired right hand movements (majority of subjects). In essence, the authors didn't flip the maps that are displayed in the figures.

EEG Results

R-Squared

The signed r-squared value (at the ipsilesional C4 or C3 sites) for the Mu (8–12 Hz) rhythm significantly decreased in the post-therapy stage compared to the pre-therapy stage [one-tailed paired *t*-test: $t(20) = 1.85$; $p = 0.039$; meanPRE = −0.142; meanPOST = −0.161], while the subject attempted movements of the impaired hand (**Figure 4**). This suggests that as the result of the intervention sessions, the "desynchronization" of the Mu rhythm signals significantly increases post-therapy at the ipsilesional motor site. The bar graph displays the significant difference in the group mean r-squared values. The signed r-squared values of the Mu band signals decreased also post-therapy at the contralesional motor site during attempted movements of the impaired hand, but these differences did not reach significance [one-tailed paired *t*-test: $t(20) = 1.24$; $p = 0.114$; meanPRE = −0.131; meanPOST = −0.145]. **Figure 5** shows topographies of group-level grand averaged r-squared values obtained from data of 21 participants. Topoplots for both Mu and Beta bands are shown. While the presented results only describe

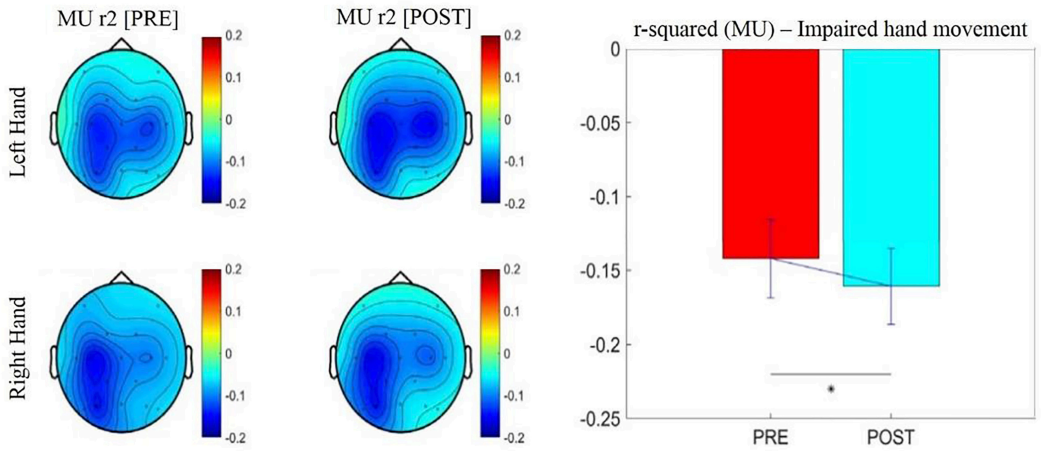

FIGURE 4 | Topographical plots (topoplots) of grand averages for Mu rhythm (8–12 Hz) signed r-squared values at group level (n = 21). The bar plot shows the group means for the Mu rhythm signed r-squared values from the impaired hand attempted movement trials (vs. rest) at ipsilesional electrode site. Asterisk denotes statistical significance from a one-tailed paired t-test ($p < 0.05$). Error bars denote standard error of the mean. The majority of participants were left hand impaired. Prescreening, open-looped training (PRE) and open-looped post screening BCI training (POST) runs (color bar: [–0.2 = blue – 0.2 = red]). The majority of participants had a right lateralized lesion.

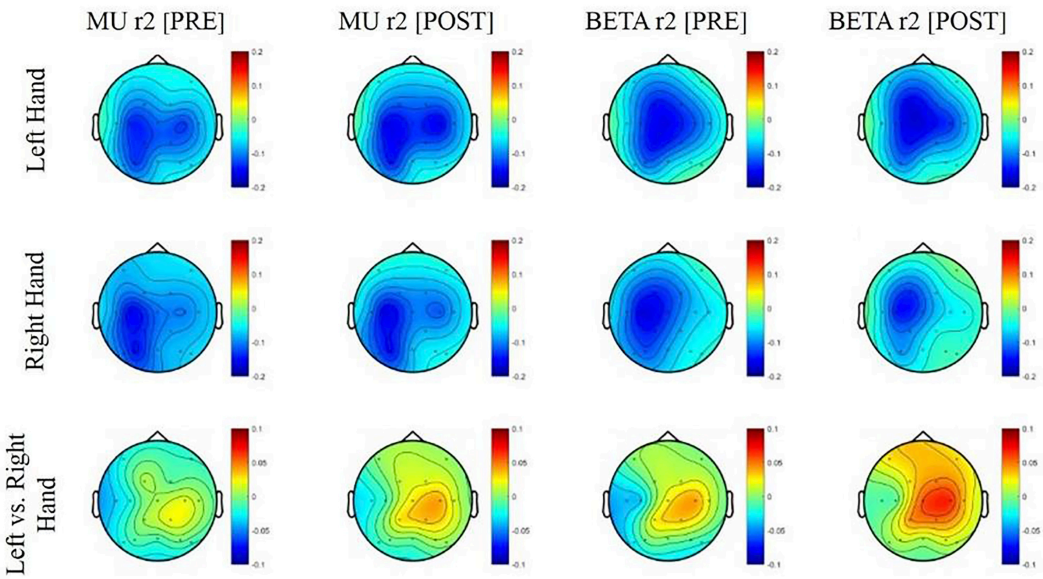

FIGURE 5 | Topoplots of grand averages for signed r-squared values at group level (n = 21) for attempted movements. In the top two rows of topoplots, a larger negative value (blue) denotes stronger desynchronization (rest vs. left or right hand actual movement); in the bottom row of topoplots a larger positive value (red) denotes desynchronization (left vs. right hand actual movements). The mentioned distinction reflects the way in which the signed r-squared values were calculated in a rest vs. left/or right comparison, and in a left vs. right comparison. Prescreening, open-looped training (PRE) and open-looped post screening BCI training (POST) runs (color bar: [–0.2 = blue – 0.2 = red]). The majority of participants had a right lateralized lesion.

changes in the Mu band, statistics from beta band did not reach significance. The Mu band and Beta band signals were both used for BCI control.

LI

Laterality index (LI) values, calculated from coherence estimates at C3 and C4 sites from Beta band (18–26 Hz) signals, decreased

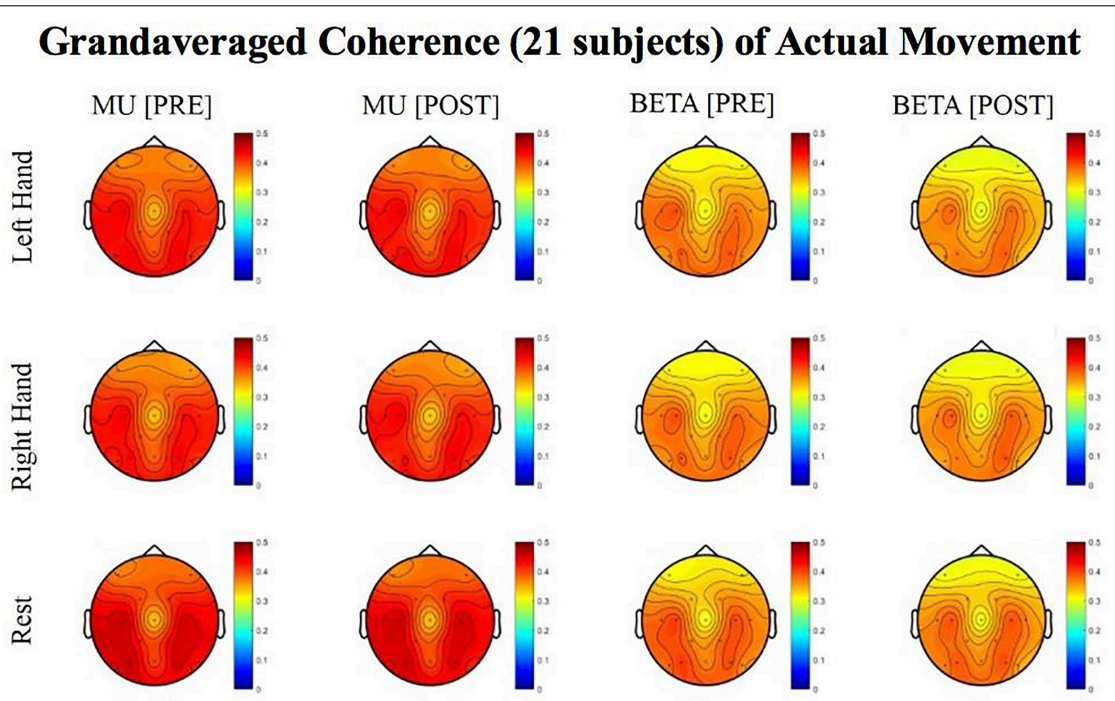

FIGURE 6 | Topoplots of grand averaged coherence values at group level (n = 21) for Mu (8–12 Hz) and Beta (18–26 Hz) bands during attempted movement trials. Prescreening, open-looped training (PRE) and open-looped post screening BCI training (POST) runs (color bar: [0 = blue – 0.5 = red]). The majority of participants had a right lateralized lesion.

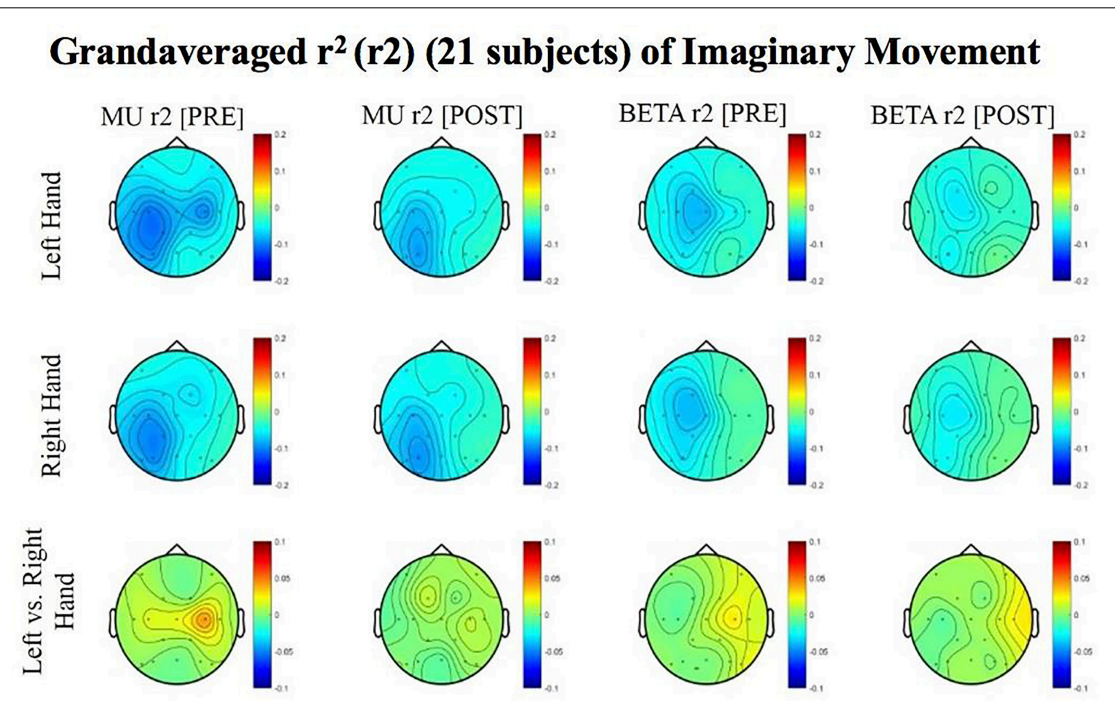

FIGURE 7 | Topoplots of grand averages for signed r-squared values at group level (n = 21) for imaginary movements. Prescreening, open-looped training (PRE) and open-looped post screening BCI training (POST) runs (color bar: [0 = blue – 0.5 = red]). The majority of participants had a right lateralized lesion.

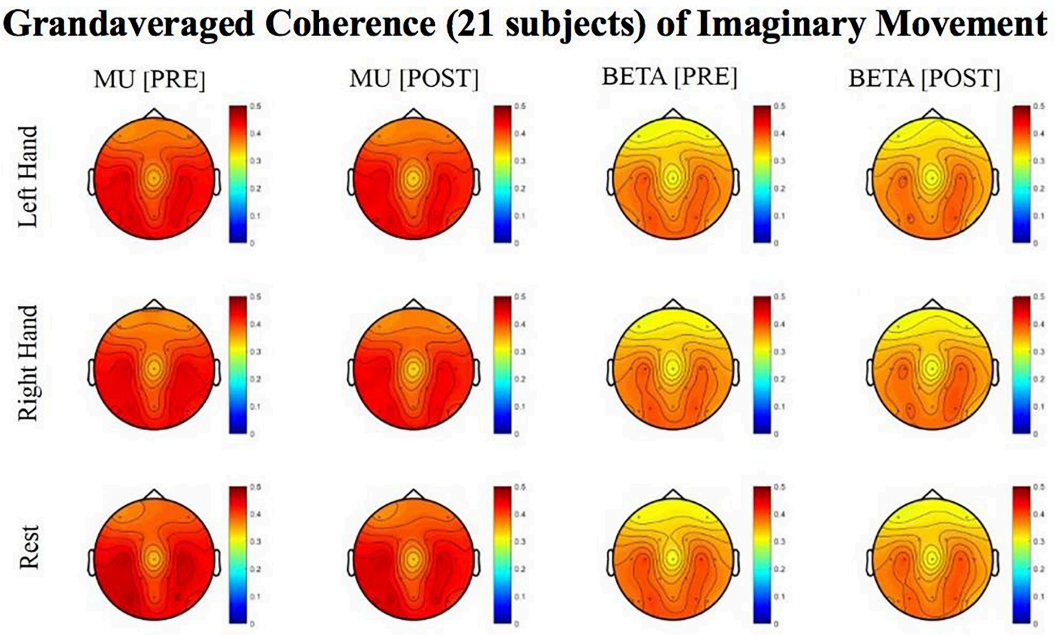

FIGURE 8 | Topoplots of grand averaged coherence values at group level (n = 21) for Mu (8–12 Hz) and Beta (18–26 Hz) bands during imaginary movement trials. Prescreening, open-looped training (PRE) and open-looped post screening BCI training (POST) runs (color bar: [0 = blue – 0.5 = red]). The majority of participants had a right lateralized lesion.

in post-therapy stage compared to the pre-therapy stage [one-tailed paired t-test: $t(20) = 0.983$, $p = 0.168$; meanPRE = 0.017; meanPOST = 0.009] while the subjects attempted movements of the impaired hand, although this change did not achieve statistical significance (**Figure 6**). This suggests that as a result of the intervention sessions, coherence in the affected motor site compared to the contralesional site showed a statistically insignificant increase at group level. **Figure 6** shows topographies of group-level grand averaged coherence values from data of 21 subjects. The value entered in each electrode site of the mentioned topographies represents the average coherence of that site with all others.

Imaginary Movement

Although no significant results were obtained from the analyses of data from imaginary movement trials, the topographical maps of r-squared and coherence values showed meaningful spatial distributions (**Figures 7**, **8**). **Figures 7**, **8** show topographical maps (topoplots) of grand averages for signed r-squared values at group level (n = 21) and topoplots of grand averaged coherence values at group level for Mu (8–12 Hz) rhythm and Beta (18–26 Hz) band during imaginary movement trials, respectively. As the protocol was designed to train and reward attempted movements, it is possible participants were not sufficiently able to master imagined movement related SMR modulation.

Amount of Intervention: Number of Runs

The change in r-squared values (Beta band) in the ipsilesional hemisphere motor site during impaired hand attempted movements, following the intervention, showed a significant correlation with the total number of cursor trials (i.e., amount of BCI practice) runs [$r(20) = 0.393$; $p = 0.043$] (**Figure 9**). Item number eight in Section "Description of the EEG Data Analysis" clarifies that for the calculation of change (POST–PRE) in signed r-squared values the following formula was used: −(POST–PRE), so one would again obtain positive numbers for "increases" in desynchronization. This

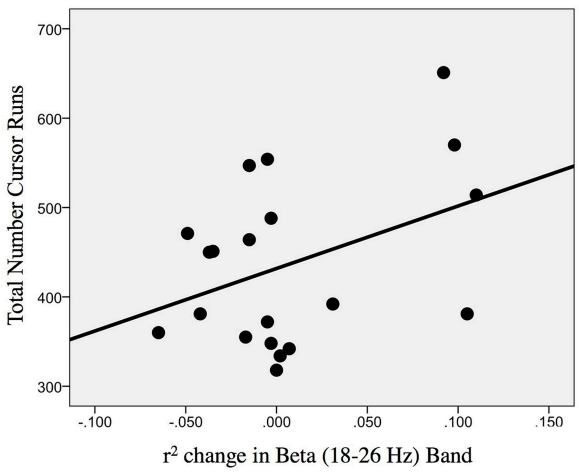

FIGURE 9 | Association between the change in r-squared values (Beta band, 18–26 Hz) as the result of BCI training with the total number of cursor trial (i.e., intervention) runs [$r(20) = 0.393$; $p = 0.043$].

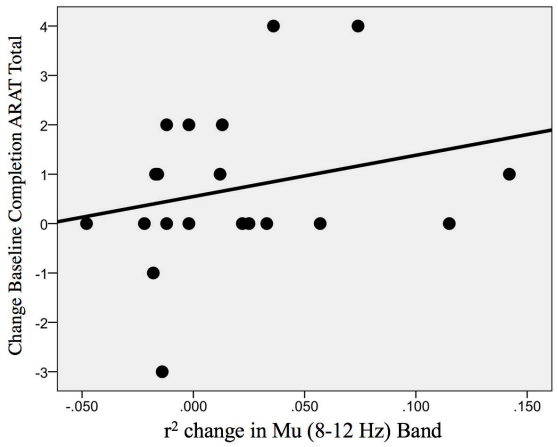

FIGURE 10 | Association between the change in r-squared values (Mu rhythm, 8–12 Hz) as the result of BCI training with the change in ARAT scores (obtained post-intervention in comparison to baseline) [$\rho(20) = 0.30$; $p = 0.098$].

was done for easier interpretation of the associations of r-squared changes with behavior changes as the result of EEG-BCI-FES intervention and in accord with the previously described methods. In essence, the positive correlation suggests that a greater amount of BCI practice relates to "greater" ERD.

Influences on Primary Outcome Measure

In addition, the change in r-squared values (Mu rhythm) in the ipsilesional hemisphere motor site during impaired hand attempted movements, as the result of EEG-BCI-FES intervention, showed a positive, non-statistically significant correlation with the change in ARAT scores (obtained post-therapy in comparison to baseline) [$\rho(20) = 0.30$; $p = 0.098$] (**Figure 10**).

Influences of Stroke and ERD on Baseline Behavioral Measures of Function and Capacity

Finally, to test some of the fundamental assumptions of the study design and BCI device (that diminished SMR desynchronization is related to the post-stroke impairment of simple motor outputs), signed Mu and Beta r-squared values for the impaired hand attempted at baseline (i.e., first intervention session) were compared to measures of behavior (SIS, ARAT, Grip Strength), and measures of stroke-related impairments to functional capacities (NIHSS, Barthel Index) at baseline (**Table 3**). A few measures of behavior (Grip Strength, SIS) and independence, capacity to perform ADLs (Barthel Index, NIHSS), correlated significantly in the anticipated direction (**Table 3**). Relevant statistical significance tests were chosen for normal and non-normal distributions, respectively. These results suggest that SMR desynchronization may represent a fundamental neuromechanical component of motor capacity as well as motor learning and, therefore, any subsequent motor recovery potential.

TABLE 3 | Summary Pearson's r and Spearman's ρ correlates of baseline outcome measures and EEG-based signed r-squared scores ($n = 21$).

Variables	Pre-screening MU	Pre-screening BETA
Baseline SIS hand function	$\rho = -0.449$, $p = 0.041$	$\rho = -0.408$, $p = 0.066$
Baseline SIS recovery	$\rho = -0.237$, $p = 0.301$	$\rho = -0.384$, $p = 0.085$
Baseline ARAT total	$\rho = -0.367$, $p = 0.102$	$\rho = -0.405$, $p = 0.068$
Baseline Barthel Index	$\rho = -0.292$, $p = 0.199$	$\rho = -0.573$, $p = 0.007$
Baseline grip strength	$r = -0.369$, $p = 0.10$	$r = -0.437$, $p = 0.047$
Baseline NIHSS	$\rho = 0.244$, $p = 0.28$	$\rho = 0.473$, $p = 0.03$

Pearson's r was used for grip strength and Spearman's ρ was used for all other variables (two-tailed tests).

Adverse Events

No adverse events were reported during or after participation in the research experiment.

DISCUSSION

EEG Measure and Behavior Measure Fidelity

The findings that motor cortex EEG measures during attempted movements of the impaired hand (more specifically, r-squared values reflecting desynchronization levels of Mu rhythm and Beta band signals at key motor cortical sites) are positively correlated with behavioral changes and seem to offer a measurable link between electrophysiology and behavior is in line with the hypotheses set forth in this analysis. More importantly, the significant group level changes in r-squared values post-therapy compared to pre-therapy suggest an effect of the applied EEG-BCI-FES intervention protocol which may be beneficial for motor recovery, though data are currently inconclusive. As stated in Section "Amount of Intervention: Number of Runs," the amount of BCI practice was positively correlated with Beta band ERD of the ipsilesional motor cortex. Thus, it may be possible to conceive that, following adequate amounts of training; electrophysiological measures of connectivity such as coherence may allow additional insights into the potentials and mechanisms of functional change to the neuromuscular and neuromechanical coupling of effortful motor movement.

EEG Utility in Stroke Rehabilitation

A strength of this design and analyses for evaluation of objective physiological or functional changes as the result of the EEG-BCI-FES intervention is that the EEG-based measures extracted and compared were obtained immediately before, and immediately following each BCI intervention session (e.g., EEG-BCI-FES based rehabilitative intervention), at the pre an post screening periods (**Figure 2**). By comparing the EEG-based measure (i.e., r-squared, coherence) changes at post- to pre-intervention session, this allowed a more controlled evaluation of the specific effects of EEG-BCI-FES intervention. In addition, because the EEG signals are continuously recorded as part of the procedure, EEG-based measures can be obtained with no additional cost at any desired time (restricted only by the short interval required to

extract reliable individual measure scores from spectral analyses of the signals). Furthermore, the study design allowed extraction and comparison of spectral estimates separately from attempted actual, as well as imaginary, hand movements. The current study did not, however, obtain statistically significant results when evaluating changes in EEG-based measures from imaginary hand movements at group level. This may be influenced by limited and insufficient time spent training participants to use imagination to properly control their SMR activity. Participants were explicitly and repeatedly instructed to attempt actual hand movements in an unblinded effort to regain or relearn volitional movement of their hands. None-the-less, reasonably distributed spatial maps of EEG activity in the SMR frequencies of interest from motor imagery attempts were observed (**Figure 8**). It is important, however, to note that motor imagery approaches are increasingly popular (Hatem et al., 2016; Irimia et al., 2016) and might be a relevant means of EEG-BCI translation, particularly in stroke patients with severely impaired motor function.

Limitations

These results suggest that EEG-BCI-FES has the potential to induce neuroplastic change and aid recovery of UE paresis. However, this analysis was constrained by sample size and heterogeneity in lesion location, level of impairment, and time since stroke. Greater power is needed to adequately generalize these results. Utilizing a larger and more homogeneous subject cohort could allow for more generalizable conclusions in future research. Further, 16 electrodes were used in EEG signal data acquisition and EEG were recorded only during the intervention phase and at no other time during the study. While there is no EEG data recorded in the control period to compare with the recordings during intervention, there are brain (EEG) – behavior correlations specifically in EEG measures associated with motor function originating specifically from electrodes (C3/C4) (**Figure 3**) overlying regions conventionally attributed to motor function. Scalp or surface level EEG recordings are understood to read the dipolar or regional sources assumed to represent the synchronous activity of hundreds of thousands of underlying neighboring neurons. It is therefore possible that even if stroke lesions damage traditional cortical areas associated with motor output (primary motor cortex), perilesional brain regions, as well as established functional areas (pre-motor area and supplementary motor areas) may contribute to ipsilesional signal recordings sufficient to drive successful classifier activation (i.e., brain signal oscillations 'discrete' enough for the BCI to interpret SMR change and execute the relevant device or output command – in this case, horizontal cursor movement and facilitated FES activation) of a BCI.

Spatial Coverage and Sampling

It is generally understood that using 16 electrodes is insufficient for source localization, especially given the limited spatial coverage and non-equidistant spacing of the electrodes in this cap array (**Figure 3**) and thus, the present analysis does not consider such undertakings. In future research, the directionality and polarity of EEG-BCI-FES associated changes may lead to better understanding of the nature and sequence of motor related neuroplasticity as well as the neuroplastic influences of BCI technologies. Source reconstruction will be done once the sample size increases to sufficiently examine this aspect in a subset of stroke participants with homogeneity in lesion location. Given the heterogeneity of lesion location in the existing sample set, source localization might be premature.

Statistical approach

Such heterogeneity and restricted sample size similarly dissuaded the authors from attempting further conservative controls, such as multiple comparisons corrections. The authors conceived that further conservative data manipulations may wash out any potential ('trending to') significant relationships the authors or other groups may want to follow-up with future research. This manuscript, part of a larger on-going clinical trial, is an interim analysis which sought to elucidate any significant trends in the data as the study progressed so as to inform our future questioning of the data and to be better prepared to identify and test potentially significant interactions and factors in the larger post-stroke population.

Nature of the academic research environment

This is an on-going study in its seventh year of data acquisition and participant enrollment. Various project personnel have undergone and supervised the staffing, training, and data acquisition of this trial during its course. The authors work hard to best minimize differences in acquisition of study measures through extensive and repeated training of personnel.

Future Scope

Despite the existing challenges to providing evidence-based treatment strategies in the stroke rehabilitation field, combined therapies may be used to achieve the maximal motor function recovery for participants (Oostenveld et al., 2011). Development of effective strategies for rehabilitation of impaired motor functions in stroke patients, as well as for monitoring and evaluation of changes during an applied intervention is yet needed.

CONCLUSION

EEG Conclusions

Non-invasive EEG-based measures of motor cortex function, such as r-squared (reflecting desynchronization levels of the relevant SMR rhythms), could provide an efficient means of tracking and even predicting functional changes in stroke patients during the course of the EEG-BCI-FES intervention. As ERD changes were reported at the group level, and given the heterogeneity in the sample, it may be argued that the reported changes not only suggest a change in function for the majority of participants (despite few changes attaining clinically significant differences) but also, given more selective sampling and independent variable control, an even more clinically relevant relationship between ERD and recovery may exist. Tracking SMR modulations may be a potential predictor of recovery or indicator of recovery potential in a patient.

BCI Conclusions

The observed effects to motor measures might also be a consequence of challenging and rewarding movements associated with (ADLs), which the participants previously may have thought to be impossible or too difficult to produce successfully. BCI intervention may help challenge a survivor's individual conception of their limitations by pushing a participant to use the affected hand and rewarding them (according to an anticipatable, clear, and consistent schedule) for doing so. This is to suggest that the minimal gains observed by most participants, in comparison to the significant gains obtained by some, and their absence in others, may be related to the encouragement of attempting previously ineffective motor behaviors. It is possible the statistically significant gains observed, supported by the higher incidence of significance in subjective measures than the number of lab-based objective measures, could be the result of the specific reward structure of the design in addition to, or more so than any reliable neuromechanical or electrophysiological contributions.

Biological Limitations and Contribution of Learning Theories

If normal muscle synergies (e.g., the same muscles act to abduct one's arm each time, in a healthy adult) are disrupted by an insult such as stroke, robbing the motor circuity of its primary output components (e.g., central nervous system efference to peripheral nervous system effectors), residual functional capacities are limited by the ability of the system to retrain or re-map (link) the CNS commands to PNS effectors (Power et al., 2011). Successful BCI intervention must connect the peripheral muscle activation with the muscle effectors necessary to execute a motor function according to the user's CNS command to do so. Unfortunately, retraining the processes of the descending motor system is not always an option as stroke often results in irreparable tissue damage or death to motor pathways and even their sensorimotor confederates. Post-stroke neuronal loss alters recruitment of downstream muscle synergies (Cheung et al., 2009), and alters a synergy's internal structure (Roh et al., 2013) depending on stroke severity (Roh et al., 2015). One biological mechanism left to these survivors is to adapt existing synergistic capacities toward a compensatory strategy (e.g., recruitment of novel synergistic families to accomplish a familiar movement). Thus, future BCI methodologies should rely on classical conditioning and Hebbian learning theories as well as predictive modeling for developmental guides to practice. Future BCI designs may also benefit from classification of distal muscle capacities and synergistic integrities so as to better measure, represent, facilitate, or compensate for the functional consequences of the stroke disturbed CNS and PNS circuitry.

From previously published findings (Young et al., 2014a,b,c; Song et al., 2015), we can comprehend that BCIs induce neuronal changes which, in turn, might help the participants challenge their paresis or perceived disabilities (Dromerick et al., 2009; Remsik et al., 2016), as they access or develop (i.e., train) new functional aptitudes, or reinvigorate old synergies and neural networks dampened by insult (Remsik et al., 2016). Participants may have the perception that their ability has improved or changed; however, when assessed by objective measures, those perceptions, at least here, are not always confirmed at equal magnitude. The authors posit that neural changes reported by other groups and in our previous publications may not always manifest as clinically significant objective changes in motor function (Wenger et al., 2017) because there is either, or both a threshold effect, or a missing component to this type of intervention (such as sufficient dosing parameters, subject selection, etc.). This opinion is potentially fortified by these results which suggest more time in intervention is related to greater electrophysiological change. Electrophysiological changes are understood to be possible biological precursors to function network change and eventually, functional behavioral change (Gazzaniga et al., 2009). Other than the simple explanation that objective lab-based measures might not reliably capture UE impairment well in stroke survivors, perhaps, as a result of engaging with this BCI intervention, this discrepancy might also arise because participants are beginning to engage their environment with the distal musculature of the impaired hand in ways they had been previously averse (unwilling) or unable to.

More Intervention

Losing strategies, more often than not, do not win (e.g., adaptive vs. maladaptive behaviors). Maladaptive associations may simply need more time to be pruned away and relevant adaptive associations strengthened by increased and more highly structured reinforcement (Gazzaniga et al., 2009; Wenger et al., 2017). If one assumes such a threshold effect, the neural-remodeling realized in these participants may suggest that more intervention trials were needed to translate to clinically significant, not just relevant, changes in objective measures of function. Results suggest a relationship between more trials and greater outcome measure change, paralleling a concept associated with training, or learning a new motor skill: practice makes permanent. It may be that amount of intervention, or inadequate 'dosage' in this case, explains the weak translation of observed brain level changes into behavioral gains for this cohort. Little evidence has thus far been offered to suggest an optimal BCI regimen. Perhaps there is even an upper limit, or even some consequence of fatigue. It is therefore suggested that future research address these questions and aim to better understand dose-response relationships and independent variable (lesion location, lesion volume, time since stroke, comorbid impairments, etc.) contributions to predict recovery potential and more efficaciously prescribe BCI intervention as therapy. All BCI research would benefit by a concerted effort to identify a therapeutic index for various BCI interventions (regimens) as well as attempt to target ideal patient profiles for prescription of BCI intervention as a therapy.

AUTHOR CONTRIBUTIONS

AR and LW contributed equally to the writing of this manuscript. AR was involved in subject recruitment, staff training, data

collection, data processing, data analysis, interpreting data, and writing of the manuscript. LW was involved in staff training, data collection, data processing, data analysis, interpreting data, and writing of the manuscript. KG was involved in analysis, interpreting and writing of the manuscript. KD, JT, TJ, were involved in data collection, analysis, and editing the manuscript. BY was involved in subject recruitment, staff training, data collection, data processing, data analysis, interpreting data, intellectual content, and manuscript editing. ZN was involved in subject recruitment and data collection. MW, MMc, MMa, SR, HA, RM, NT, JA, and LW were involved in data collection. VN contributed to subject recruitment, staff training, data collection, data processing, data analysis, interpreting data, manuscript editing, and intellectual content. PVK contributed to manuscript editing and intellectual content. JS was involved in recruitment of study participants, study design, and intellectual content. TK was involved in the recruitment of study participants, manuscript editing, and intellectual content. JCW, DE, and VP are co-PIs and were involved in study conception, design, staff training, manuscript editing, intellectual content, and supervised all aspects of the study.

FUNDING

This work was supported by NIH/NINDS grants 1R01NS105646-01A1, RC1MH090912-01, T32GM008692, UL1TR000427, K23NS086852, T32EB011434, R01EB000856-06, and R01EB009103-01 and by the DARPA RCI Program (MTO) N66001-12-C-4025 and HIST Program (MTO) N66001-11-1-4013. Additional funding was also provided through a Coulter Translational Research Award, the American Heart Association Grant 1T32EB011434-01A1, AHA Innovative Research Award – National (Marcus Foundation) 15IRG22760009, AHA Midwest Grant in Aid Award 15GRNT25780033, the Foundation of ASNR, UW Milwaukee-Madison Intercampus Grants, the UW Graduate School, and by Shapiro Foundation Grants.

ACKNOWLEDGMENTS

The authors would like to thank all the study subjects and their families for participating in the study and all the hospital staff for their support. The authors would also like to extend thanks to Dr. Justin Sattin for referrals of stroke subjects and clinical documentation. The authors would like to acknowledge that parts of this manuscript were presented in previously published manuscripts, which are listed in the present reference section.

SUPPLEMENTARY MATERIAL

The Supplementary Material for this article can be found online at: https://www.frontiersin.org/articles/10.3389/fnins.2019.00053/full#supplementary-material

FIGURE S1 | CONSORT flow diagram.

REFERENCES

Ang, K., and Guan, C. (2013). Brain-computer interface in stroke rehabilitation. *J. Comput. Sci. Eng.* 7, 139–146. doi: 10.5626/JCSE.2013.7.2.139

Babaiasl, M., Mahdioun, S. H., Jaryani, P., and Yazdani, M. (2016). A review of technological and clinical aspects of robot-aided rehabilitation of upper-extremity after stroke. *Disabil. Rehabil. Assist. Technol.* 11, 263–280. doi: 10.3109/17483107.2014.1002539

Benjamin, E. J., Blaha, M. J., Chiuve, S. E., Cushman, M., Das, S. R., Deo, R., et al. (2017). Heart disease and stroke statistics—2017 update: a report from the American Heart Association. *Circulation* 135, e229–e445. doi: 10.1161/CIR.0000000000000485

Birbaumer, N., Weber, C., Neuper, C., Buch, E., Haapen, K., and Cohen, L. (2006). Physiological regulation of thinking: brain-computer interface (BCI) research. *Prog. Brain Res.* 159, 369–391. doi: 10.1016/S0079-6123(06)59024-7

Bundy, D. T., Souders, L., Baranyai, K., Leonard, L., Schalk, G., Coker, R., et al. (2017). Contralesional brain-computer interface control of a powered exoskeleton for motor recovery in chronic stroke survivors. *Stroke* 48, 1908–1915. doi: 10.1161/STROKEAHA.116.016304

Caria, A., Weber, C., Brötz, D., Ramos, A., Ticini, L. F., Gharabaghi, A., et al. (2011). Chronic stroke recovery after combined BCI training and physiotherapy: a case report. *Psychophysiology* 48, 578–582. doi: 10.1111/j.1469-8986.2010.01117.x

Cheung, V. C., Piron, L., Agostini, M., Silvoni, S., Turolla, A., and Bizzi, E. (2009). Stability of muscle synergies for voluntary actions after cortical stroke in humans. *Proc. Natl. Acad. Sci. U.S.A.* 106, 19563–19568. doi: 10.1073/pnas.0910114106

Daly, J. J., Cheng, R., Rogers, J., Litinas, K., Hrovat, K., and Dohring, M. (2009). Feasibility of a new application of noninvasive Brain Computer Interface (BCI): a case study of training for recovery of volitional motor control after stroke. *J. Neurol. Phys. Ther.* 33, 203–211. doi: 10.1097/NPT.0b013e3181c1fc0b

Daly, J. J., and Wolpaw, J. R. (2008). Brain-computer interfaces in neurological rehabilitation. *Lancet Neurol.* 7, 1032–1043. doi: 10.1016/S1474-4422(08)70223-0

Dromerick, A. W., Lang, C. E., Birkenmeier, R. L., Wagner, J. M., Miller, J. P., Videen, T. O., et al. (2009). Very early constraint-induced movement during stroke rehabilitation (VECTORS): a single-center RCT. *Neurology* 73, 195–201. doi: 10.1212/WNL.0b013e3181ab2b27

Felton, E. A., Wilson, J. A., Williams, J. C., and Garell, P. C. (2007). Electrocorticographically controlled brain-computer interfaces using motor and sensory imagery in patients with temporary subdural electrode implants. Report of four cases. *J. Neurosurg.* 106, 495–500. doi: 10.3171/jns.2007.106.3.495

Fleet, A., Page, S. J., MacKay-Lyons, M., and Boe, S. G. (2014). Modified constraint-induced movement therapy for upper extremity recovery post stroke: what is the evidence? *Top. Stroke Rehabil.* 21, 319–331. doi: 10.1310/tsr2104-319

Gazzaniga, M. S. (2005). Forty-five years of split-brain research and still going strong. *Nat. Rev. Neurosci.* 6, 653–659. doi: 10.1038/nrn1723

Gazzaniga, M. S., Ivry, R. B., and Mangun, G. R. (2009). *Cognitive Neuroscience: The Biology of the Mind*, 3rd Edn. New York, NY: W W NORTON.

Hatem, S. M., Saussez, G., Della Faille, M., Prist, V., Zhang, X., Dispa, D., et al. (2016). Rehabilitation of motor function after stroke: a multiple systematic review focused on techniques to stimulate upper extremity recovery. *Front. Hum. Neurosci.* 10:442. doi: 10.3389/fnhum.2016.00442

Hill, N. J., Lal, T. N., Schröder, M., Hinterberger, T., Wilhelm, B., Nijboer, F., et al. (2006). Classifying EEG, and ECoG signals without subject training for fast BCI implementation: comparison of nonparalyzed, and completely paralyzed subjects. *IEEE Trans. Neural Syst. Rehabil. Eng.* 14, 183–186. doi: 10.1109/TNSRE.2006.875548

Howlett, O. A., Lannin, N. A., Ada, L., and McKinstry, C. (2015). Functional electrical stimulation improves activity after stroke: a systematic review with

meta-analysis. *Arch. Phys. Med. Rehabil.* 96, 934–943. doi: 10.1016/j.apmr.2015.01.013

Hsieh, C. L., Hsueh, I. P., Chiang, F. M., and Lin, P. H. (1998). Inter-rater reliability and validity of the action research arm test in stroke patients. *Age. Ageing* 27, 107–113. doi: 10.1093/ageing/27.2.107

Irimia, D., Sabathiel, N., Ortner, R., Poboroniuc, M., Coon, W., Allison, B. Z., et al. (2016). recoveriX: a new BCI-based technology for persons with stroke. *Conf. Proc. IEEE Eng. Med. Biol. Soc.* 2016, 1504–1507. doi: 10.1109/EMBC.2016.7590995

Jones, T. A. (2017). Motor compensation and its effects on neural reorganization after stroke. *Nat. Rev. Neurosci.* 18, 267–280. doi: 10.1038/nrn.2017.26

Kaczmarek, A. K. (2011). The tongue display unit (TDU) for electrotactile spatiotemporal pattern presentation. *Sci. Iran.* 18, 1476–1485. doi: 10.1016/j.scient.2011.08.020

Kollen, B., Kwakkel, G., and Lindeman, E. (2006). Functional recovery after stroke: a review of current developments in stroke rehabilitation research. *Rev. Recent. Clin. Trials* 1, 75–80. doi: 10.2174/157488706775246111

Krafi, G. H., Fitts, S. S., and Hammond, M. C. (1992). Techniques to improve function of the arm and hand in chronic hemiplegia. *Arch. Phys. Med. Rehabil.* 73, 220–227.

Kuiken, T. A., Schultz Feuser, A. E., and Barlow, A. K. (2013). *Targeted Muscle Reinnervation: A Neural Interface for Artificial Limbs*. Didcot: Taylor & Francis. doi: 10.1201/b15079

Lang, C. E., Edwards, D. F., Birkenmeier, R. L., and Dromerick, A. W. (2008). Estimating minimal clinically important differences of upper extremity measures early after stroke. *Arch. Phys. Med. Rehabil.* 89, 1693. doi: 10.1016/j.apmr.2008.02.022

Laver, K., George, S., Thomas, S., Deutsch, J. E., and Crotty, M. (2015). Virtual reality for stroke rehabilitation: an abridged version of a Cochrane review. *Eur. J. Phys. Rehabil. Med.* 51, 497–506.

Leuthardt, E. C., Schalk, G., Wolpaw, J. R., Ojemann, J. G., and Moran, D. W. (2004). A brain-computer interface using electrocorticographic signals in humans. *J. Neural Eng.* 1, 63–71. doi: 10.1088/1741-2560/1/2/001

Lindenberg, R., Renga, V., Zhu, L. L., Nair, D., and Schlaug, G. (2010). Bihemispheric brain stimulation facilitates motor recovery in chronic stroke patients. *Neurology* 75, 2176–2184. doi: 10.1212/WNL.0b013e318202013a

Maris, E., and Oostenveld, R. (2007). Nonparametric statistical testing of EEG- and MEG-data. *J. Neurosci. Methods* 164, 177–190. doi: 10.1016/j.jneumeth.2007.03.024

Mathiowetz, V., Weber, K., Kashman, N., and Volland, G. (1985). Adult norms for the nine-hole peg test of finger dexterity. *Occup. Ther. J. Res.* 5, 24–38. doi: 10.1177/153944928500500102

McFarland, D. J., Krusienski, D. J., and Wolpaw, J. R. (2006). Brain-computer interface signal processing at the Wadsworth Center: mu and sensorimotor beta rhythms. *Prog. Brain Res.* 159, 411–419. doi: 10.1016/S0079-6123(06)59026-0

Mitra, P. P., and Pesaran, B. (1999). Analysis of dynamic brain imaging data. *Biophys. J.* 76, 691–708. doi: 10.1016/S0006-3495(99)77236-X

Moe, J. H., and Post, H. W. (1962). Functional electrical stimulation for ambulation in hemiplegia. *J. Lancet* 82, 285–288.

Muralidharan, A., Chae, J., and Taylor, D. M. (2011). Extracting attempted hand movements from EEGs in people with complete hand paralysis following stroke. *Front. Neurosci.* 5:39. doi: 10.3389/fnins.2001.00039

Nair, V. A., Young, B. M., La, C., Reiter, P., Nadkarni, T. N., Song, J., et al. (2015). Functional connectivity changes in the language network during stroke recovery. *Ann. Clin. Transl. Neurol.* 2, 185–195. doi: 10.1002/acn3.165

Nam, C. S., Jeon, Y., Kim, Y. J., Lee, I., and Park, K. (2011). Movement imagery-related lateralization of event-related (de)synchronization (ERD/ERS): motor-imagery duration effects. *Clin. Neurophysiol.* 122, 567–577. doi: 10.1016/j.clinph.2010.08.002

Neuper, C., and Pfurtscheller, G. (2001). Event-related dynamics of cortical rhythms: frequency-specific features and functional correlates. *Int. J. Psychophysiol.* 43, 41–58. doi: 10.1016/S0167-8760(01)00178-7

Oostenveld, R., Fries, P., Maris, E., and Schoffelen, J. M. (2011). FieldTrip: open source software for advanced analysis of MEG, EEG, and invasive electrophysiological data. *Comput. Intell. Neurosci.* 2011:156869. doi: 10.1155/2011/156869

Ortiz, G. A., and Sacco, R. L. (2008). *National Institutes of Health Stroke Scale (NIHSS)*. Hoboken, NJ: Wiley Encyclopedia of Clinical Trials. doi: 10.1002/9780471462422.eoct400

Ortner, R., Irimia, D. C., Scharinger, J., and Guger, C. (2012). A motor imagery based brain-computer interface for stroke rehabilitation. *Stud. Health Technol. Inform.* 181, 319–323.

Pangman, V. C., Sloan, J., and Guse, L. (2000). An examination of psychometric properties of the mini-mental state examination and the standardized mini-mental state examination: implications for clinical practice. *Appl. Nurs. Res.* 13, 209–213. doi: 10.1053/apnr.2000.9231

Pfurtscheller, G., Neuper, C., Andrew, C., and Edlinger, G. (1997). Foot and hand area mu rhythms. *Int. J. Psychophysiol.* 26, 121–135. doi: 10.1016/S0167-8760(97)00760-5

Pfurtscheller, G., Neuper, C., and Birbaumer, N. (2005). "Human brain-computer interface (BCI)," *Motor Cortex in Voluntary Movements. A Distributed System for Distributed Functions,* eds A. Riehle, E. Vaadia (Boca Raton, FL: CRC Press), 367–401.

Pineda, J. A. (2005). The functional significance of mu rhythms: translating "seeing" and "hearing" into "doing" *Brain Res. Rev.* 50, 57–68. doi: 10.1016/j.brainresrev.2005.04.005

Popovic, D. B., Sinkaer, T., and Popovic, M. B. (2009). Electrical stimulation as a means for achieving recoveryof function in stroke patients. *NeuroRehabilitation* 25, 45–58.

Power, J. D., Cohen, A. L., Nelson, S. M., Wig, G. S., Barnes, K. A., Church, J. A., et al. (2011). Functional network organization of the human brain. *Neuron* 72, 665–678. doi: 10.1016/j.neuron.2011.09.006

Remsik, A. B., Dodd, K., Williams, L. Jr., Thoma, J., Jacobson, T., Allen, J. D., et al. (2018). Behavioral outcomes following brain–computer interface intervention for upper extremity rehabilitation in stroke: a randomized controlled trial. *Front. Neurosci.* 12:752. doi: 10.3389/fnins.2018.00752

Remsik, A., Young, B., Vermilyea, R., Kiekhoefer, L., Abrams, J., Evander Elmore, S., et al. (2016). A review of the progression and future implications of brain-computer interface therapies for restoration of distal upper extremity motor function after stroke. *Expert Rev. Med. Devices* 13, 445–454. doi: 10.1080/17434440.2016.1174572

Roh, J., Rymer, W. Z., and Beer, R. F. (2015). Evidence for altered upper extremity muscle synergies in chronic stroke survivors with mild and moderate impairment. *Front. Hum. Neurosci.* 9:6. doi: 10.3389/fnhum.2015.00006

Roh, J., Rymer, W. Z., Perreault, E. J., Yoo, S. B., and Beer, R. F. (2013). Alterations in upper limb muscle synergy structure in chronic stroke survivors. *J. Neurophysiol.* 109, 768–781. doi: 10.1152/jn.00670.2012

Schaechter, J. D. (2004). Motor rehabilitation and brain plasticity after hemiparetic stroke. *Prog. Neurobiol.* 73, 61–72. doi: 10.1016/j.pneurobio.2004.04.001

Schalk, G., McFarland, D. J., Hinterberger, T., Birbaumer, N., and Wolpaw, J. R. (2004). BCI2000: a general-purpose brain-computer interface (BCI) system. *IEEE Trans. Biomed. Eng.* 51, 1034–1043. doi: 10.1109/TBME.2004.827072

Schalk, G., Miller, K. J., Anderson, N. R., Wilson, J. A., Smyth, M. D., Ojemann, J. G., et al. (2008). Two-dimensional movement control using electrocorticographic signals in humans. *J. Neural Eng.* 5, 75–84. doi: 10.1088/1741-2560/5/1/008

Shah, S., Vanclay, F., and Cooper, B. (1989). Improving the sensitivity of the Barthel Index for stroke rehabilitation. *J. Clin. Epidemiol.* 42, 703–709. doi: 10.1016/0895-4356(89)90065-6

Shinar, D., Gross, C. R., Price, T. R., Banko, M., Bolduc, P. L., and Robinson, R. G. (1986). Screening for depression in stroke patients: the reliability and validity of the Center for Epidemiologic Studies Depression Scale. *Stroke* 17, 241–245. doi: 10.1161/01.STR.17.2.241

Smith, M. C., and Stinear, C. M. (2016). Transcranial magnetic stimulation (TMS) in stroke: ready for clinical practice? *J. Clin. Neurosci.* 31, 10–14. doi: 10.1016/j.jocn.2016.01.034

Song, J., Nair, V. A., Young, B. M., Walton, L. M., Nigogosyan, Z., Remsik, A., et al. (2015). DTI measures track and predict motor function outcomes in stroke rehabilitation utilizing BCI technology. *Front. Hum. Neurosci.* 9:195. doi: 10.3389/fnhum.2015.00195

Song, J., Young, B. M., Nigogosyan, Z., Walton, L. M., Nair, V. A., Grogan, S. W., et al. (2014). Characterizing relationships of DTI, fMRI, and motor recovery in stroke rehabilitation utilizing brain-computer interface technology. *Front. Neuroeng.* 7:31. doi: 10.3389/fneng.2014.00031

Thakor, N. V. (2013). Translating the brain-machine interface. *Sci. Transl. Med.* 5:210s17.

Thomson, D. J. (1982). Spectrum estimation and harmonic analysis. *Proc. IEEE* 70, 1055–1096. doi: 10.1109/PROC.1982.12433

Varkuti, B., Guan, C., Pan, Y., Phua, K. S., Ang, K. K., Kuah, C. W., et al. (2013). Resting state changes in functional connectivity correlate with movement recovery for BCI and robot-assisted upper-extremity training after stroke. *Neurorehabil. Neural Repair* 27, 53–62. doi: 10.1177/1545968312445910

Vellone, E., Savini, S., Fida, R., Dickson, V. V., Melkus, G. D. E., Carod-Artal, F. J., et al. (2015). Psychometric evaluation of the stroke impact scale 3.0. *J. Cardiovasc. Nurs.* 30, 229–241. doi: 10.1097/JCN.0000000000000145

Wenger, E., Brozzoli, C., Lindenberger, U., and Lövdén, M. (2017). Expansion and renormalization of human brain structure during skill acquisition. *Trends Cogn. Sci.* 21, 930–939. doi: 10.1016/j.tics.2017.09.008

Wilson, J. A., Walton, L. M., Tyler, M., and Williams, J. (2012). Lingual electrotactile stimulation as an alternative sensory feedback pathway for brain-computer interface applications. *J. Neural Eng.* 9:045007. doi: 10.1088/1741-2560/9/4/045007

Wolpaw, J. R., McFarland, D. J., Neat, G. W., and Forneris, C. A. (1991). An EEG-based brain-computer interface for cursor control. *Electroencephalogr. Clin. Neurophysiol.* 78, 252–259. doi: 10.1016/0013-4694(91)90040-B

Yang, Q., Tong, X., Schieb, L., Vaughan, A. S., Gillespie, C. D., Wiltz, J. L., et al. (2017). Vital signs: recent trends in stroke death rates – United States, 2000-2015. *MMWR* 2017, 933–939. doi: 10.15585/mmwr.mm6635e1

Young, B. M., Nigogosyan, Z., Nair, V. A., Walton, L. M., Song, J., Tyler, M. E., et al. (2014a). Case report: post-stroke interventional BCI rehabilitation in an individual with preexisting sensorineural disability. *Front. Neuroeng.* 7:18. doi: 10.3389/fneng.2014.00018

Young, B. M., Nigogosyan, Z., Walton, L. M., Song, J., Nair, V. A., Grogan, S. W., et al. (2014b). Changes in functional brain organization and behavioral correlations after rehabilitative therapy using a brain-computer interface. *Front. Neuroeng.* 7:26. doi: 10.3389/fneng.2014.00026

Young, B. M., Williams, J., and Prabhakaran, V. (2014c). BCI-FES: could a new rehabilitation device hold fresh promise for stroke patients? *Expert Rev. Med. Devices* 11, 537–539. doi: 10.1586/17434440.2014.941811

Conflict of Interest Statement: The authors declare that the research was conducted in the absence of any commercial or financial relationships that could be construed as a potential conflict of interest.

Copyright © 2019 Remsik, Williams, Gjini, Dodd, Thoma, Jacobson, Walczak, McMillan, Rajan, Young, Nigogosyan, Advani, Mohanty, Tellapragada, Allen, Mazrooyisebdani, Walton, van Kan, Kang, Sattin, Nair, Edwards, Williams and Prabhakaran. This is an open-access article distributed under the terms of the Creative Commons Attribution License (CC BY). The use, distribution or reproduction in other forums is permitted, provided the original author(s) and the copyright owner(s) are credited and that the original publication in this journal is cited, in accordance with accepted academic practice. No use, distribution or reproduction is permitted which does not comply with these terms.

frontiers in Neuroscience

TECHNOLOGY REPORT
published: 27 March 2019
doi: 10.3389/fnins.2019.00191

Brain–Computer Interface (BCI) Applications in Mapping of Epileptic Brain Networks Based on Intracranial-EEG: An Update

Rafeed Alkawadri[1,2,3]*

[1] Human Brain Mapping Laboratory, Department of Neurology, University of Pittsburgh, Pittsburgh, PA, United States, [2] Yale Human Brain Mapping Program, Yale University, New Haven, CT, United States, [3] The Department of Neurology, School of Medicine, Yale University, New Haven, CT, United States

The main applications of the Brain–Computer Interface (BCI) have been in the domain of rehabilitation, control of prosthetics, and in neuro-feedback. Only a few clinical applications presently exist for the management of drug-resistant epilepsy. Epilepsy surgery can be a life-changing procedure in the subset of millions of patients who are medically intractable. Recording of seizures and localization of the Seizure Onset Zone (SOZ) in the subgroup of "surgical" patients, who require intracranial-EEG (icEEG) evaluations, remain to date the best available surrogate marker of the epileptogenic tissue. icEEG presents certain risks and challenges making it a frontier that will benefit from optimization. Despite the presentation of several novel biomarkers for the localization of epileptic brain regions (HFOs-spikes vs. Spikes for instance), integration of most in practices is not at the prime time as it requires a degree of knowledge about signal and computation. The clinical care remains inspired by the original practices of recording the seizures and expert visual analysis of rhythms at onset. It is becoming increasingly evident, however, that there is more to infer from the large amount of EEG data sampled at rates in the order of less than 1 ms and collected over several days of invasive EEG recordings than commonly done in practice. This opens the door for interesting areas at the intersection of neuroscience, computation, engineering and clinical care. Brain–Computer interface (BCI) has the potential of enabling the processing of a large amount of data in a short period of time and providing insights that are not possible otherwise by human expert readers. Our practices suggest that implementation of BCI and Real-Time processing of EEG data is possible and suitable for most standard clinical applications, in fact, often the performance is comparable to a highly qualified human readers with the advantage of producing the results in real-time reliably and tirelessly. This is of utmost importance in specific environments such as in the operating room (OR) among other applications. In this review, we will present the readers with potential targets for BCI in caring for patients with surgical epilepsy.

Keywords: high frequency oscillations, high frequency brain stimulation, single pulse electrical stimulation, BCI, epilepsy surgery, coherence analysis, epileptogenicity index, connectivity index

Technology alone is not enough–it's technology married with liberal arts, married with the humanities, that yields the results that make our heart sing.

Steve Jobs

OPEN ACCESS

Edited by:
Christoph Guger, g.tec Medical Engineering GmbH, Austria

Reviewed by:
Adam Olding Hebb, Colorado Neurological Institute (CNI), United States
Bachir Estephan, Mayo Clinic Arizona, United States
Vassiliy Tsytsarev, University of Maryland, College Park, United States

***Correspondence:**
Rafeed Alkawadri
drraf81@gmail.com

Specialty section:
This article was submitted to Neural Technology, a section of the journal Frontiers in Neuroscience

Received: *26 March 2018*
Accepted: *18 February 2019*
Published: *27 March 2019*

Citation:
Alkawadri R (2019) Brain–Computer Interface (BCI) Applications in Mapping of Epileptic Brain Networks Based on Intracranial-EEG: An Update. Front. Neurosci. 13:191. doi: 10.3389/fnins.2019.00191

CURRENT STANDARDS AND RECENT ADVANCES IN SEIZURE LOCALIZATION AND INTRACRANIAL EEG

Intracranial-EEG (icEEG) indicated in the subset of patients with drug-resistant epilepsy (i.e., patients who failed two anti-seizure medications, as mono-therapy or in a combination, composing approximately a one-third of all patients with epilepsy), may present a few challenges:

(i) icEEG is invasive and may present complications, which increase in rate as a function of duration of recording (Fong et al., 2012) (ii) The chances of sustained seizure freedom after epilepsy surgery falls between 30 and 80% (Jehi et al., 2009; Simasathien et al., 2013) depending on the lobe involved suggesting that the current methods of localization are not optimal and approaching epileptogenicity implying zones, while practical, falls short of "ideal" (ii) recording of seizures remain to date the best surrogate marker of the epileptogenic zone which may not be always feasible even after a few weeks of EEG recording (Asano et al., 2009). There are only a few exceptions where the interictal profile, may be adequate for localization of the epileptic tissue in the operating room (OR) such as in focal cortical dysplasia (FCD) (Tripathi et al., 2010).

A standard single electrode (**Figure 1**) provides an estimate of the field potential of the summation of excitatory and inhibitory post-synaptic evoked potentials roughly from 100 million to 1 billion of neurons. Electrocorticography (ECOG) has the advantage of proximity to the source of electrical activity only separated by highly conductive media and low impedances. Using simultaneous scalp and intracranial recording, cortical spike sources having an area of 10 cm^2 or more commonly resulted in scalp-recordable EEG spikes (Tao et al., 2007). ECOG is less susceptible to artifact and provides higher signal-to-noise ratio. Additionally, depth electrodes allow exploring mesial brain structures and deeply seated foci not accessible otherwise.

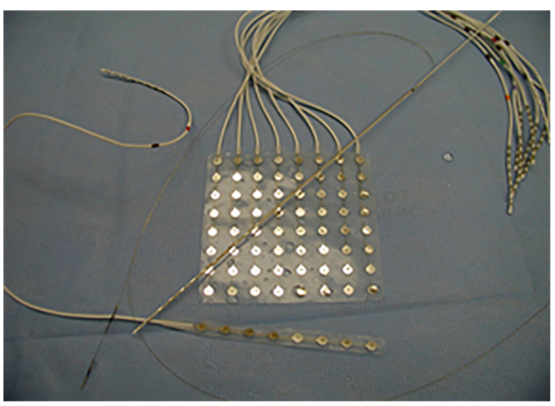

FIGURE 1 | Different type of electrodes currently employed in practices. The depth electrodes and stereo-EEG commonly employed in Europe especially in France, and more recently in the United States. Whereas subdural electrodes constituted the mainstay of evaluations in the United States until the last few years.

TABLE 1 | Summary of Cortical Zones and their assessment with clinical tools.

Cortical zone	Methods of assessment
Ictal onset zone	EEG, ictal SPECT
Irritative zone	EEG, Magnetoencephalography, functional MRI triggered by EEG
Symptomatogenic zone	History and semiology
Epileptogenic lesion	MRI
Eloquent cortex	Cortical stimulation, functional MRI, evoked potentials, Magnetoencephalography
Functional deficit zone	Physical examination, neuropsychiatric testing, EEG, PET, SPECT, MRS
Epileptogenic zone	None (theoretical construct)

Indication: The traditional goal of epilepsy surgery is to disconnect the epileptogenic zone which is the area of the cortex indispensable for seizure generation, and which resection leads to seizure freedom (**Table 1**). The decision about implantation is discussed during a multi-disciplinary surgical conference attended by neurosurgeons, neurologists, neuropsychologists, radiologists, trainees, and nurses among others. The typical indications include:

- Discordant non-invasive pre-surgical work-up
- MRI-negative neocortical epilepsy and select cases of mesial temporal epilepsy
- MRI-lesional cases if:
    - Adjacent to eloquent cortex
    - Detailed language or functional mapping needed
    - Plan to maximally define the epileptic zone for completeness of resection such as in focal cortical dysplasia (FCD)
    - Dual pathology or multi-focality (i.e., tuberous sclerosis)
    - If discordance with EEG data (i.e., scalp EEG is non-localizable).

The standard approach is to record seizures in the epilepsy monitoring unit.

Intra-Operative ECOG

There is somewhat conflicting evidence to support precision of pre- and post-resection ECOG for localization of the epileptic focus, owing to the heterogeneity and the retrospective non-randomized or non-controlled designs in the available studies and the multiple clinical variables to control. That is, some studies correlated resection of spikes with seizure freedom (Palmini et al., 1995; Bautista et al., 1999; Sugano et al., 2007; Stefan et al., 2008; Tripathi et al., 2010) but not others (Cascino et al., 1995; Kanazawa et al., 1996; Tran et al., 1997). Several studies have suggested that residual spikes in the final post-ECoG predict poor surgical outcome (Wennberg et al., 1998; Oliveira et al., 2006), but this is again contradicted by others. Recording in the intra-operative settings may be adequate in

- Select-cases in children especially younger ones

- Lesions with concordant non-invasive evaluations in focal cortical dysplasia
- As an adjunct in multiple-subpial-transections (MSTs)
- Adjunct during intra-operative monitoring and mapping of eloquent cortex
- As an adjunct in placement of Responsive Neuro-Stimulation (RNS) electrodes.

Limitations of intra-operative ECOG: Seizure onset almost always not recorded in the operating room. Chemical induction fell out of trend. There is a tunnel-vision related to the limited spatial sampling. Thus, successful localization must be guided by a strong clinical hypothesis. Anesthesia may limit the analysis of epileptic activity. The ideal agents for intra-operative recording are those with minimal effect on baseline spike frequency. Inhaled agents tend to suppress background EEG activity, with reports of enflurane (Flemming et al., 1980) and sevoflurane (Dahaba et al., 2013) exhibiting activating effect. Synthetic opiates such as remifentanil and alfentanil may increase the yield of recording epileptiform activity (McGuire et al., 2003). The latter may induce non-habitual seizures from healthy brain regions. A few studies have shown that dexmedetomidine has no or little activating effect on epileptiform activity (Chaitanya et al., 2015). Propofol, barbiturates, and benzodiazepines increase EEG background beta-sigma frequency-power and may obscure epileptiform discharges (Dahaba et al., 2013; Nishida et al., 2016; Bayram et al., 2018a).

Surgical Outcomes and Safety

Over the past decade, there has been a plethora of literature reporting on long-term outcomes following epilepsy surgery with chances of long-term and sustained seizure freedom ranging from 30% in frontal lobe epilepsy and up to 80% in lesional mesial temporal lobe epilepsy. This outcome compares favorably to a 5%-per-year chance of seizure freedom using anti-seizure medications alone in medically intractable cases (Callaghan et al., 2011). Duration of implantation correlates with the histopathological changes such as micro-hemorrhages and inflammatory response (Herman et al., 2017). Commonly, electrodes are removed within 3 weeks following implantation. There has been a steady decrease in risk of complications with advances in surgical techniques (Yuan et al., 2012; Arya et al., 2013; Herman et al., 2017).

For the aforementioned, any future electrophysiological markers ideally would emphasize both efficiency and reliability in classification of brain tissue. Studies of markers that are more specific of localization of the epileptogenic brain regions in the interictal phase are always welcome and still badly needed preferably as part of large, multi-center consortia.

RECENT ADVANCES IN BRAIN–COMPUTER INTERFACE (BCI)

The brain–computer interface (BCI) (**Figure 2**) is a device that reads voluntary changes in brain activity then translates these signals into a message or computational command in real-time. It is a method to communicate with the brain, that does not depend on the brain's normal output pathways. Current BCI's record electrophysiological signals using non-invasive or invasive methods. These BCIs can provide a much more detailed picture of the brain activity, which can facilitate prosthetic applications or surgery for epilepsy and tumor removal. The emphasis in this article is to describe possible applications to enhance care for patients affected by drug-resistant epilepsy via invasive sensors and electrophysiology. For other applications and for BCI engineering aspects please refer to other sections.

The applications of BCI are more relevant nowadays given recent advances in the sampling of icEEG and in computational power. The amount of information encoded within the icEEG that is untapped into on a regular basis is enormous. It appears that interacting with live-streaming electrophysiological data, sampled at high-frequency, and processed in real-time will be the future, by natural, or artificial for this matter, evolution.

In general, the critical components of BCI are:

1. Sensors: In this case is an intracranial icEEG electrode placed at the surface of the brain.

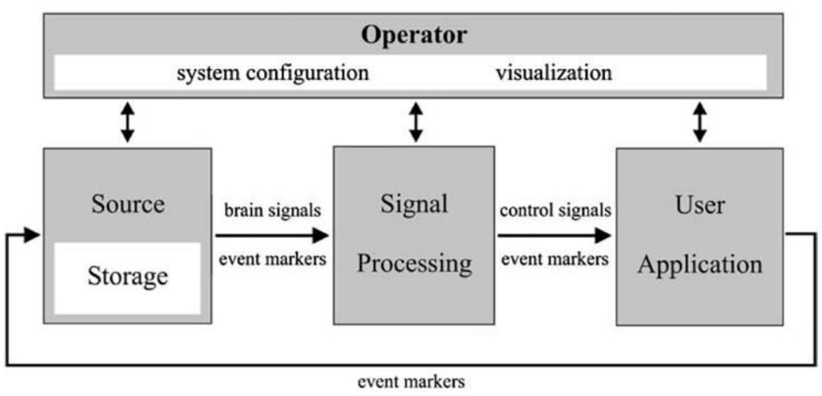

FIGURE 2 | A schematic showing a universal design for BCI systems. Adapted from BCI2000 IEEE TRANSACTIONS ON BIOMEDICAL ENGINEERING, VOL. 51, NO. 6, JUNE 2004.

2. Translation for communication: Programming language and commands.
3. Real-time acquisition and processing of EEG signal. This includes EEG amplifiers enabling access to data as they are recorded.

Different methods of interfacing are available:

1. Many of the commercially available EEG amplifiers may provide Software Development Kits (SDKs) to enable an interface with EEG signal as it is acquired. Skills in programming and software development are required.
2. EEG amplifiers designed for interfacing with widely used languages in signal and image processing such as MATLAB®, Simulink®, and python®. This approach is commonly employed for development, in academia, and for research.
3. One or multi-purpose integrated end-to-end hardware and software. The best consumer experience (patient and practitioner in this case), as learned from industry, come from the "whole widgets" kind of products with the software carefully tailored to the hardware and vice versa. Commercializing the BCI applications in the field of epilepsy surgery will likely follow this path.

A remarkable amount of funds has been raised to support research in BCI and its applications in the private sector over the past few years. It is only logical if parallel strides are taking place in the epilepsy world, so that the community and researchers with a specific interest in management of drug-resistant epilepsy, could tap into and benefit from the growing popular interest.

CURRENT BCI APPLICATIONS IN DRUG-RESISTANT EPILEPSY

This is an area at the intersection of multiple disciplines of science and has yet to be integrated in clinical practices in the broader sense. Ongoing parallel research is in progress. Developing algorithms tailored for clinical use, beyond abstract research-statistics, and validated by surgical outcomes continue to be needed; one challenge is that parametric statistics are often not clinically compelling, hence, expert-driven non-parametric evaluation of results will most likely benefit the clinical applications (Maris and Oostenveld, 2007). Multi-center efforts are required in order to increase the number of cases and hence the statistical power of the findings. Among other methods, the iEEG.org portal provides a potential seed for collaboration and data sharing.

Some of the known BCI applications in caring for patients with drug-resistant epilepsy include:

* Real-time localization of the language centers especially in patients in whom current gold standards are not applicable. The most practical use at the present point is to make mapping by electrical cortical stimulation (ECS) more efficient, by supplementing the planning process. It is our experience, however, (**Figure 3**) to encounter false-detections in the clinical-sense in the 1. Occipital and junctional regions 2. Frontal attention network and 3. The epileptic brain regions. In fact, the issue of spatial sampling is a pertinent one in any research involving icEEG, as generally speaking there is a consistent bias toward sampling from epileptic brain regions, and this fact should be incorporated into the interpretation of available literature reporting on predictive values of markers of function or epilepsy.
  It is an active area of research to optimize detections within functional brain regions that are most important for the surgical decision and to exclude less relevant ones (i.e., increase the clinical specificity). This will require employing more steps than simple parametric and energy-based detection of gamma activity (Alkawadri and Gaspard, 2018). Elaborating on current non-parametric methods and expert validated outcomes will likely benefit practices. For instance, we have been able to optimize methods to localize the hand motor area (Alkawadri, 2017; Alkawadri et al., 2015), and the entire sensorimotor strip successfully during sleep (**Figure 4**).

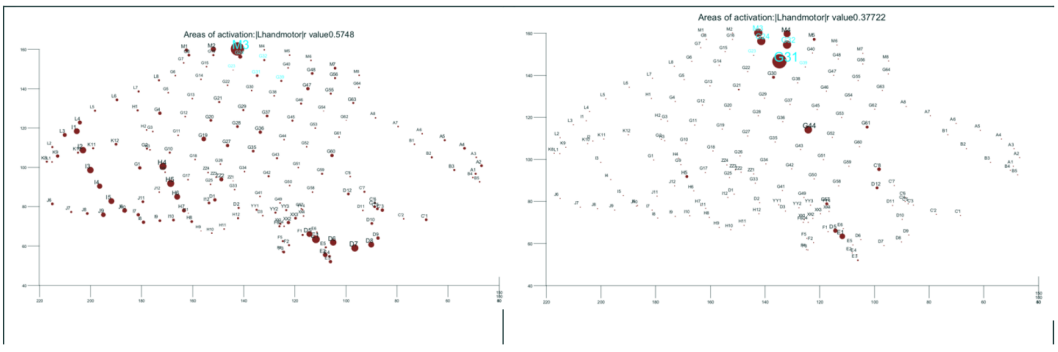

FIGURE 3 | Function: **(Left)** hand motor according to commonly employed parametric methods of analysis of task-related gamma activation. **(Right)** Improving on the results by custom made algorithm. The results of direct electrical cortical stimulation are highlighted in cyan both figures for references. All shown in the electrode space. The size of the dot is proportional with the strength of task-related activation.

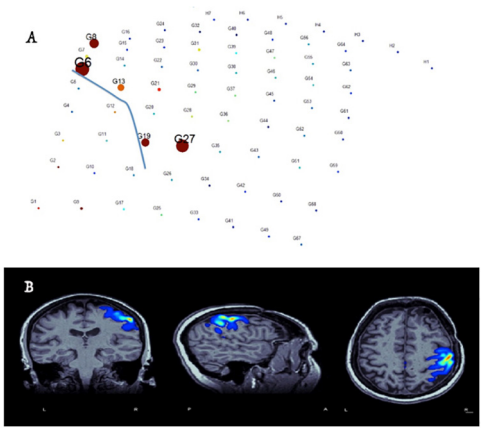

FIGURE 4 | Identification of hand-motor area and the central sulcus (blue-line in electrode plain) and co-registration of the results with brain MRI in real-time based on free-running ECOG and custom-made software (Alkawadri et al., 2015). **(A)** Size of circles corresponds to the value M specific to the anterior lip of the central sulcus – whereas the color represents local field normalized power in the electrode space. **(B)** Co-registration of M values in the MRI space and proper thresholding to demonstrate the localization of the hand area.

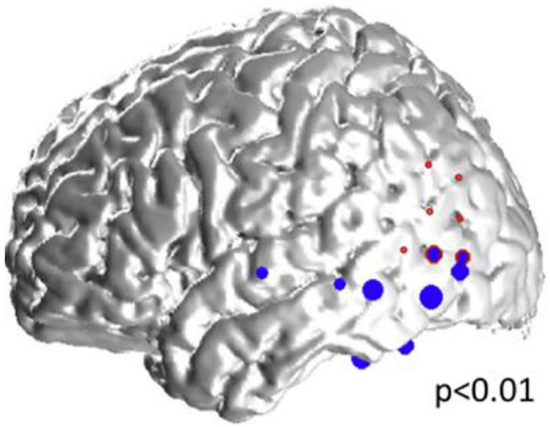

FIGURE 5 | Representative case: 34-year old woman with left neocortical temporo-parietal epilepsy. The size of the blue dots represents the "spikiness" of the automatic-detected spikes which are located in the left inferior and lateral temporal lobes, as well as in the left inferior parietal lobe, and overlap partly with, and within the vicinity of the seizure onset zone (red circles).

- Responsive Neuro-Stimulation (RNS) for seizure detection and electrical stimulation for modulation and management of drug-resistant epilepsy.
- Near-Instantaneous classification of perceptual states from cortical surface recordings.
- Real-time seizure detection.

In the next few sections, we will present areas and markers in surgical epilepsy with BCI potential.

Epileptiform Discharges

Interictal EEG spikes are known to be categorically correlated with the presence of epilepsy. However, interictal discharges can be seen also in areas other than SOZ and tissues distant from the epileptic tissue (Jasper et al., 1961). Jasper's early work had led to the conclusion that not all spikes are equal and that there are ones that are more localizing of the epileptic region than others.

The agreement between the seizure zone and the irritative zone, however, is estimated at approximately 56% based on a surgical series and more so in focal cortical dysplasia FCD ∼75% (Bartolomei et al., 2016). The prominent spikes tend to arise mostly from contacts located in the close vicinity of the seizure onset area rather than from within it. We found that the most sharply looking ones are those in the vicinity of the seizure onset zone rather than precisely within it (Gaspard et al., 2017) (**Figure 5**). More recently, there has been a suggestion that high-frequency oscillations co-occurring with spikes are highly specific for the seizure-onset zone (Wang et al., 2013). In fact, co-occurrence increases the specificity for both (Ren et al., 2015). Due to Gibbs phenomenon, fine-tuning of reliable detectors of spike-HFOs, especially those that are based on non-sine methods, such as wavelet spectral analysis or Hilbert transformation and power ratios in different bands, appear more efficient than standard energy-based ones (Birot et al., 2013).

Intraoperative Spike Monitoring

Extra-operative video-EEG monitoring and recording of the seizure onset remain to date the best surrogate marker of the epileptogenic zone. Until a reliable interictal biomarker is available for the clinical decision making, there remain situations where the intra-operative monitoring is desired. "Spike chasing" and "tailored resections" may not lead to desired outcomes if not supported by a valid hypothesis. Randomized controlled trials are still needed as there is a somewhat a lack of strong evidence on the best use of it. Some studies have suggested that residual spikes in the final post-ECOG predict poor surgical outcomes, but this was contraindicated by other studies. A primary concern is that surgical manipulation of the cortex may agitate the tissue, evoking spikes in the resection margin, which are not correlated with the seizure outcome. Spike-HFOs may present somewhat a more reliable and specific interictal biomarker for the epileptogenic brain region in that settings.

Until these studies are completed, the concept of intraoperative localization of the epileptic focus will remain an active area for fine-tuning. The clinical implementation of HFOs will be hampered by the existing gaps of knowledge such as the need to discriminate between physiological and pathological HFOs and the requisite for reliable computational detection methods that address existing concerns. The first randomized, controlled, clinical trial (The HFO Trial) to evaluate our hypothesis that use of HFOs intraoperatively can improve outcome is underway. Furthermore, it is important to fill a critical gap of the effect of anesthesia and the ideal anesthetic regimen for intraoperative ECOG monitoring. There is no consensus in regard to the ideal anesthesia regimen for intraoperative monitoring. Existing studies often do not employ common gold standard for localization, and the concept of pharmacological spike activation is challengeable.

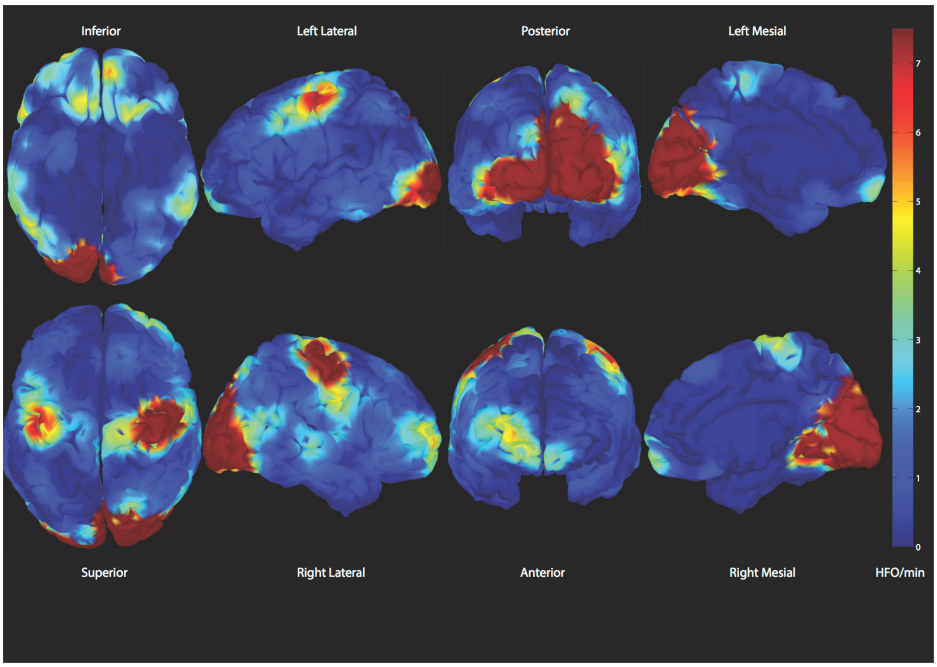

FIGURE 6 | Demonstration of spatial distribution of physiologic high frequency oscillations. A reliable classifier to distinguish those from epileptic ones is desired (Alkawadri et al., 2014).

In our review of literature, of the five studies only provided specifics on site of resection and correlation with surgical outcomes out of 23 stduies reporting on spike activation of a total altogether 54 studies that met inclusion criteria (Bayram et al., 2018b).

High-Frequency Oscillations (HFOs) and Very High-Frequency Oscillations (VHFOs) – See Also the Previous Section

There has been a growing interest in the utility of interictal high-frequency oscillations HFOs (80–500 Hz, classically) for localization of the epileptic focus (Bragin et al., 1999; Jacobs et al., 2008, 2009a,b). Several challenges arose as similar oscillations have been associated with specific tasks or occur naturally during sleep (**Figure 6**), and no known signal parameter can reliably distinguish between physiologic and epileptic subtypes in a given individual (Alkawadri et al., 2014) (**Figure 7**). Hence, interictal HFOs, although useful, are not highly specific and do not replace current standards. Ironically, it appears that to-date, the most effective factor that increases the specificity of HFOs for detection of epileptogenicity is their co-occurrence with other markers, i.e., spikes. One common denominator among studies reporting on HFOs is that the analysis often performed at the group level and case-wise results are not always presented. The latter perhaps is more relevant for the decision-making in clinical practice. Furthermore, the approach of assessing surgical resections and relatively short-term seizure-free outcomes while commonly employed, has inherent limitations. This holds true especially in the face of the concept of ongoing epileptogenesis even after seemingly successful resections (Najm et al., 2013; Simasathien et al., 2013).

Very-high-frequency oscillations (VHFOs), i.e., Oscillations 500–2000 Hz or above may be more specific for localization of the epileptogenic region (Usui et al., 2015; Brazdil et al., 2017). The frequency exceeds the firing-rate of individual single neurons and likely represent a rhythm generated by in- and out- of phase action potentials of neuron clusters.

Some of the variable results with HFOs and VHFOs in the existing literature stem from; the extent of spatial sampling (**Figure 8**); methods undertaken to exclude detections with filtering artifact; the review montage; methods implemented in detection and analysis and effort made to exclude filter-related false detections; areas sampled; size of contacts; time of study and relation to tasks/meds/seizures. Some have employed a battery-powered amplifier system to eliminate the noise of alternating current cycles. Others have subtracted the averaged signal in the white matter from all signals, providing thus additional noise reduction and an optimal reference in theory. It is important to investigate the occurrence of VHFOs outside the epileptic regions, to avoid bias and inflation of positive predictive values resulting from the natural inclination toward sampling epileptic brain regions. The extent of spatial sampling at Yale, has led to detection of ripples and fast ripples consistently at a significantly higher rate outside the epileptic network.

In summary, the ability to sample EEG at high frequencies is perhaps the most suitable tool, in theory, to tap into neuronal communications. Current data seems to suggest, that shorter HFOs bursts, higher-peak-frequencies, and higher entropy in HFOs bands are more suggestive of pathology. No single feature,

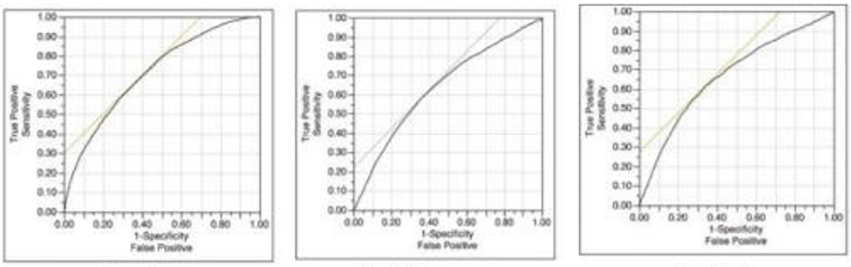

Duration Peak Frequency Amplitude

Receiver operating curves and corresponding odds ratios for epileptic vs. nonepileptic at the effective cutoff per HFO event				
	Effective cutoff	AUC	Sen/spec/acc	Odds ratio (p<0.01)
Duration (ms)	<168	.71	.66/.64/.69	3.40 (3.16-3.68)
Amplitude (uV)	<59	.65	.62/.65/.65	3.09(2.87-3.33)
Frequency (HZ)	>100	.64	.58/.64/.63	2.43 (2.26-2.62)

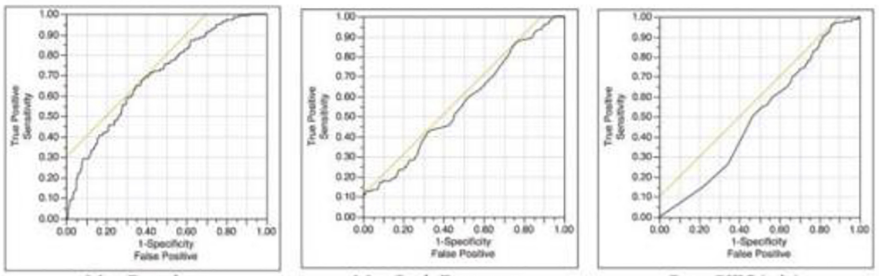

Max Duration Max Peak Frequency Rate (HFO/min)

Receiver operating characteristics and corresponding odds ratios for epileptic vs. non-epileptic at the effective cutoff per channel (max value per channel)				
	Effective cutoff	AUC	Sen/spec/acc	Odds ratio (p<0.01)
Duration (ms)	<242	.70	.65/.65/.65	1.78 (1.49-2.13)
Frequency (Hz)	>185	.56	**.13**/.97/.77	10.00 (3.91-25.92)
Rate (HFO/min)	<4.3	.50	.96/.14/.35	4.22 (1.65 – 10.75)
Amplitude (uV)	Not statistically significant			

$$d = \sqrt{(1 - sensitvity)^2 + (1 - specificity)^2}.$$

FIGURE 7 | To-date no single EEG feature can reliably distinguish epileptic from non-epileptic HFOs.

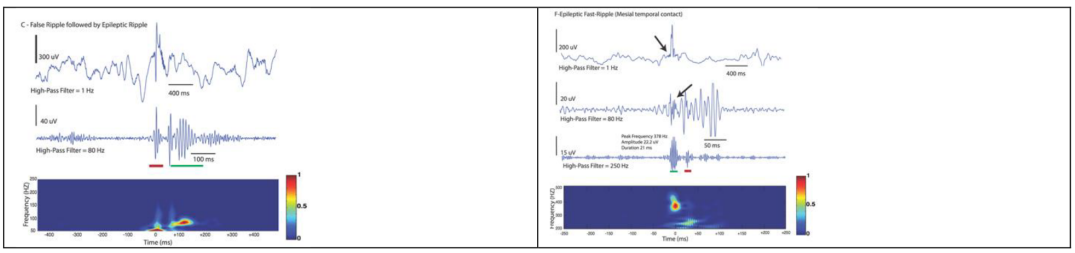

FIGURE 8 | Examples demonstrating a false detection in red (not discerned on raw data and does not occupy a blob in the Morley-Wavelet based spectral window), and true ripple marked by a green line. The spectral analysis is even more important in analysis of fast ripples (lower).

however, can reliably classify the groups other than perhaps co-occurrence with epileptiform spikes. Presently employing a real-time detection of spike-HFOs and addressing the issue of false detections are of interest. Until then, it appears we are arriving at the time of integrating real-time detection of HFOs/spike-HFOs in clinical practice. Clinician-friendly and commercially available automatic real-time detection algorithms (highly specific) are needed as we continue to advance knowledge on that end.

Brain Connectivity

Functional connectivity is defined as the study of temporal correlations between spatially distinct neurophysiological events. There are several conceptual distinctions between the different functional connectivity measures: They either reveal directed or undirected, linear or non-linear connections in the time or frequency domains. The calculation is either amplitude or phase-based, and the measure can be bivariate or multivariate. Standard coherence is the equivalent of correlation within a specific band. The temporal resolution of EEG presents a unique modality for analysis of different connectivity and association indices beyond the uni-dimensional correlation coefficient, which is the practical choice in slow fluctuating signals such as those encountered in functional imaging.

The connectivity measures could be conceptually subdivided into four subgroups (van Mierlo et al., 2014):

1. Correlation and coherence: Pearson correlation coefficient, and loosely its equivalent when applied on specific frequency bands. A variant of this measure is the cross-correlation that investigates the correlation between two time-series that are shifted in time concerning each other. The phase of the coherence can be used to infer the directionality. The temporal resolution of EEG presents a unique modality for analysis of different connectivity and association measures beyond the uni-dimensional correlation coefficient, which is the practical choice in a slow fluctuating signal such as the one encountered in functional imaging.
2. Instead of investigating the relationship between the amplitudes of the signals, one could also examine how the phases of the considered signals are coupled, the so-called phase synchronization measures. The most commonly used measures are the phase-locking value and phase-lag index.
3. Information-theory-based, with the most frequently employed is mutual-information and the transfer-entropy which enable investigating non-linear relations.
4. The fourth category of functional connectivity measures is based on the concept of Granger causality for which Clive Granger received a Nobel-prize when invented to be applied in Economics. One time-series is said to Granger-cause the second one if the inclusion of the past values of the first into the modeling of the second significantly reduces the variance of the modeling error. Most of the Granger causality measures are constructed based on an autoregressive (AR) model, in which the present samples of the signals are predicted using a linear combination of the past samples. From the coefficients of the AR model many measures can be derived: The Granger-causality index the directed coherence, the directed transfer function and the partial directed coherence.

None of these methods are perfect, and one should employ depending on the questions, for instance, whether directionality or non-linearity are of interest. Studies have suggested that there is an increase in synchronization in the inter-ictal phase within the resection bed (Avoli, 2014). Recently, it has been shown that high-frequency Granger causality before the actual seizure onset and higher values correlated highly with contacts at seizure onset (Rummel et al., 2015; Park and Madsen, 2018). Also, interictal connectivity within temporal lobe showed more loose patterns as a function of the duration of epilepsy before the surgical evaluation (Englot et al., 2015). Most EEG-based connectivity techniques are research-based, but many will be potentially useful for evaluation of cerebral abnormalities. Further studies to correlate connectivity findings with seizure localization and functional mapping results are still desired and in concept will be a suitable application for BCI.

Some technical issues that should be paid attention to:

1. The quality of recording and montage of review are of particular significance in the setting. For instance, a slightly contaminated reference may result in a false inflation of direct correlation or coherence-based values (Arunkumar et al., 2012).
2. Studies are lacking to correlate spontaneous ECOG-based connectivity measures and other measures of functional connectivity such as fMRI or anatomical connectivity such as Diffusion Tensor Imaging (DTI). We did not find a meaningful correlation between coherence in different frequency bands and cortico-cortical evoked potentials (unpublished work). We hypothesize that this is because stimulation activates complex poly-synaptic networks at a distance, whereas spontaneous connectivity measures identify local networks.

The Connectivity Index (CI) as New Measure to Grade Epileptogenicity Based on Single-Pulse Electrical Stimulation (SPES)

Victor Horsley used faradic electrical stimulation to confirm the localization of the epileptic focus in one of John Hughlings Jackson's patients who underwent resection of an epileptic focus in 1886 (Vilensky and Gilman, 2002). Harvey Cushing used this technique in 1909 to define the sensorimotor cortex surrounding a tumor and to confirm the localization of epileptic seizures that manifested with sensory auras (Feindel et al., 2009). Following the advances in EEG acquisition after 1929 and the standardization of the use of electrical stimulation in brain mapping by Wilder Penfield, induction of seizures through electrical stimulation fell out of favor in North America (Isitan et al., 2018). In Europe, and particularly in France, electrical stimulation continued to be used for seizure induction with variable reports of reliability and specificity for localization of epileptic brain regions (Kovac et al., 2016). Controlled studies on stimulation parameters, efficacy, and specificity of seizure induction are methodologically challenging due to the difficulty in controlling for several covariates. However, our experience aligns with previous reports that suggest seizures produced by 50-Hz stimulation are not specific for localization of the epileptic focus though perhaps more sensitive than 1-Hz stimulation. There is a school that suggests seizures induced by high-frequency stimulation if similar to habitual seizures, i.e.,

electro-clinical syndrome may be more specific. Our experience in extra-temporal epilepsy aligns well with the limited reports emphasizing the specificity of seizures and auras induced by low-frequency single pulse stimulation in temporal lobe epilepsy.

Recently, we have shown that a new metric we labeled the connectivity index (Alkawadri et al., 2013) which is based on the normalized number of averaged evoked responses to single pulse electrical stimulation weighted by the normalized distance at which the responses recorded at.

$$CI = \frac{n.\bar{d}}{N.\bar{D}}$$

C*i* Connectivity index, n, number of contacts with evoked responses, N total number of contacts, d, D average Euclidian distance of contacts with evoked responses and all contacts from site of stimulation, respectively. This measure accentuates responses recorded at different sites. Also, it may bypass some limitations related to the sampling bias (i.e., epileptic areas are more sampled than non-epileptic brain regions).

We analyzed responses in thirty-nine stimulation sessions in 19 patients. Stimulation of the epileptic contacts generated reproducible responses at significantly higher rates than the control sites (medians of normalized number of contacts 0.74 vs. 0.32, $p = 0.0007$). These differences were even stronger when normalized to average distance of recorded responses from the stimulation site (medians of normalized values 0.71 vs. 0.15 $p = 0.0003$) (**Figure 9**). The evoked responses after stimulation of the epileptic contacts were seen at further distance from the site of stimulation (medians of normalized distances 0.93 vs. 0.58, $p = 0.0004$, median absolute values: 58 mm vs. 44 mm). It was 2.2 times more likely to record an evoked response from the seizure onset zone than other contacts after stimulation of a remote-control site. Habitual partial seizures or auras were triggered in 26% of the patients and 33% of the seizure onset contacts (median stimulation intensity 3.5 mA), but in none of the control or within network contacts. Stimulation of control sites in multifocal or poor surgical outcome cases tended to exhibit higher number of evoked responses at distant sites compared to the localizable onsets or good surgical outcome (median number of contacts normalized to total number of contacts and average distance 0.5 vs. 0.12, $p = 0.06$). Stimulation of epileptic contact generated responses with longer latencies (medians 48 vs. 38 ms, $p < 0.0001$), and longer duration (medians 73 vs. 62 ms, $p < 0.0001$). There was a correlation between the current intensity and normalized number of evoked responses ($r = +0.50$, $p < 0.01$) but not with distance ($r = +0.1$, $p < 0.64$), suggesting perhaps that stimulation at lower currents may possibly help in identifying distant nodes within the epileptic network and help differentiating between epileptic and non-epileptic sites. Furthermore, we demonstrated that it is possible to co-register volumes based on abnormal responses to single-pulse stimulation with patient's MRI for reliable visualization.

The Epileptogenicity Index (EI), and Other Seizure-Related Metrics

Quantitative seizure analysis is of interest in clinical practice. An expert review remains to-date the mainstay of analysis. Low-frequency high-amplitude repetitive spiking (LFRS) is the most frequently reported pattern in mesial temporal lobe epilepsy and seems to correlate with degree of volume loss. In neocortical epilepsy, focal low voltage fast activity is the most localizing rhythms and it appears that the slower and the more wide-spread the rhythms are, the more likely that site of onset is not sampled, or alternatively this may be viewed as a sign of a complex epileptic networks (Singh et al., 2015). Some authors employed non-parametric and parametric methods for seizure localization and incorporated time to involvement (Bartolomei et al., 2008; David et al., 2011). In our practice, in the majority of the seizures that are poorly localized by conventional clinical analysis, the quantitative EEG analysis identified strongly overlapping networks.

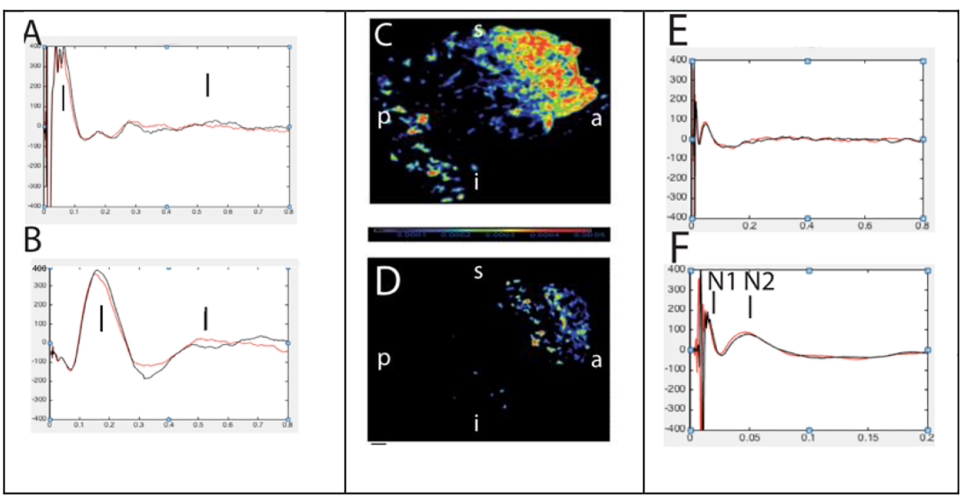

FIGURE 9 | Abnormal (left, **A,B**) and normal evoked responses (right, **E,F**) to single pulse electrical stimulation. Panels **(C,D)** represents source localization of late and slow responses after stimulation of epileptic and non-epileptic orbitofrontal brain regions in two patients, respectively (Alkawadri et al., 2015).

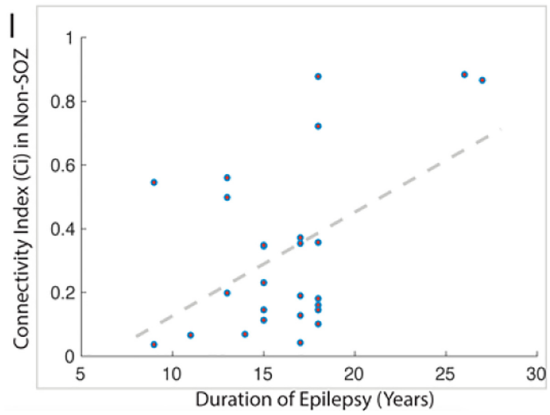

FIGURE 10 | This figure demonstrates the strong correlation between the duration of epilepsy and the degree of epileptogenicity from non-SOZ tissue as graded by the connectivity index.

Other benefits of quantification of seizure onset:

1. Evidence showing a correlation between duration of epilepsy and non-SOZ contacts (Bartolomei et al., 2008) compilable with other reports and our observations (**Figure 10**).
2. Limited evidence suggesting that resection of ictal high-frequency oscillations phsae-locked to lower frequencies/spikes correlate with better surgical outcomes (Weiss et al., 2013).
3. Interestingly, our practice has led us that in difficult to localize cases and even those seizures that are classified of seizure analysis, quantitative analysis of ictal rhythms tends to show somewhat more stable networks (**Figure 11**).

Provoked Seizures and Seizure Detection

As presented above, the implementation of electrical stimulation in awake craniotomies predate the discovery of EEG in 1929. As recently reviewed by Kovac et al. (2016), there has been several studies published on the subject and almost all agree that seizures induced by 50-Hz stimulation are not specific for the localization – though more sensitive for induction than 1 Hz. On the other hand, there is a suggestion that seizures recorded with 1-Hz stimulation may be specific for the SOZ, but the technique is less powerful for seizure induction especially outside the medial temporal lobe structures. Seizures can be induced by ECS but there is controversy regarding the utility of ECS induced seizures in defining the epileptogenic zone and hence practice varies considerably between centers. We reviewed the Yale experience with seizures included by electrical cortical stimulation in 24 patients undergoing intracranial EEG evaluation Seizures Provoked by Low Frequency Stimulation. Habitual partial seizures or auras were triggered in 27% of the patients and 35% of all seizure onset contacts that were stimulated with 1 Hz stimulation (median stimulation intensity 4 mA, range 0–59 s from onset of electrical stimulation), but in none of the control or IZ contacts. Only habitual seizures and auras were recorded. None of the evoked auras led to generalized seizures. All but one was focal with retained awareness. There are no non-habitual seizures recorded by 1-Hz stimulation. In relation to BCI, the issue of auto-seizure detection and prediction in real-time becomes of interest. Seizure detection is of interest and has different clinical applications whether based on intracranial EEG, scalp EEG, or other markers. Different seizure detection algorithms exist, most of which achieve sensitivities in the order of 60%-> 90% and false detection rate of <1 seizure – many seizures per hour. It appears that methods based on trained support-vector-machine-learning and artificial neural networks are the ones that achieve the highest performance. As a general rule, the more sensitive a method is the more computationally simple (Ramgopal et al., 2014).

FUTURE RESEARCH AND DIRECTIONS

A quick look at a recent submission to the annual BCI society award and research trends available from the BCI community annual conference shows:

1. There is a steady increasing trend in BCI research with emphasis on epilepsy and movement disorders.
2. This constituted, however, only 3.8% of the projects submitted. These numbers eclipsed by other uses.

There is a responsibility that most probably falls on the shoulder of subspecialized funding agencies and supporting communities to augment research in this area which will continue to benefit patients with drug-resistant epilepsy, in the

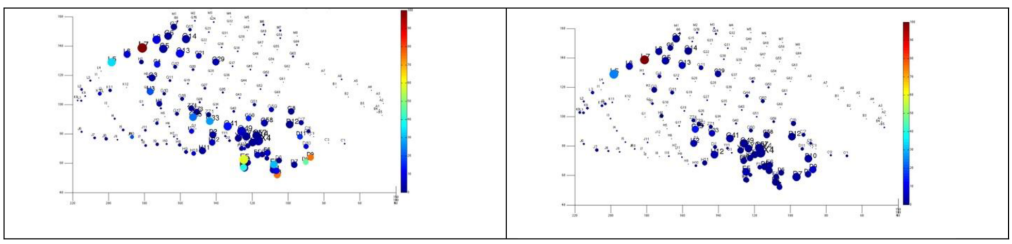

FIGURE 11 | Quantitative analysis based on cumulative ictal high frequency oscillations in two difficult-to-localize seizures. The size represents the length of electrode's involvement in ictal HFOs, and the color represents normalized cumulative power up to 20 s after seizure onset. Note the strong spatial overlap and that these seizures were interpreted differently by the clinical team as temporal (above), and fronto-parietal (below).

foreseen future, until, researchers identify less invasive, and more preemptive and efficient methods to treat epilepsy in the future.

In summary, icEEG data is an ideal medium for applications of artificial intelligence and machine learning in real-time. The applications within the domain of epilepsy surgery and seizure localization have lagged behind, however, the transformation is inevitable. Investment from funding agencies is needed to help revamping of care in this sub-group of general population.

Invasive electrophysiology presents some caveats though it remains the standard of care in subset of cases with drug-resistant epilepsy; firstly, the spatial resolution is at the level of local field potential, i.e., in the order of hundreds of millions of neurons and is inherently influenced by the clinical hypothesis and expertise, secondly analysis often performed group-wise not patient-wise and render networks not always outcome-validated clinically meaningful data. That is in addition to the risks presented above. In the long term, and besides advances on this front, it would be desired to continue to investigate new mechanisms of action for pharmacological control of seizures, as well as investigating interventions that prevent epilepsy altogether. Reliable identification of pathologic brain regions is also of interest, functional imaging on the other hand presents unique advantages especially in regard to the spatial resolution, non-invasiveness and safety profile. However, as a general rule non-of the available techniques is a match to the superiority of EEG excellent temporal resolution and are all, to our knowledge, with the exception of MRI imaging – considered complimentary in the presurgical evaluation and do not replace icEEG when the latter is indicated on a clinical basis. Direct cortical brain cooling may prove beneficial in studying the effect of isolating brain regions. Optogenetic approaches present excellent potential for localization of function and dysfunction in epilepsy and modulation of epileptic networks via open- or close-loop circuits if optimized for use in humans – as it enables highly specific and high-resolution activation or deactivation of brain regions/cluster of cells that is induced by light of specific wavelength via light-sensitive genetically modified neuronal receptors and channels (opsins) (Zhao et al., 2015). Genetically encoded voltage gated channels if successfully translated into humans may further improve our ability to map seizure events. These approaches have been successfully applied experimentally in rodents. Several important challenges presently exist: significant progress is still needed in the technical scalability of the approach, safe and effective opsin gene delivery, reliable light delivery in clinical settings, and specific cluster activation *in vivo*. In summary, and while promising, much remains to be understood before application of optogenetics in humans.

AUTHOR CONTRIBUTIONS

The author confirms being the sole contributor of this work and has approved it for publication.

FUNDING

I wish to acknowledge research support by the American Epilepsy Society (award #412064) and CTSA Grant Number KL2TR000140 from the National Center for Advancing Translational Science (NCATS), a component of the National Institute of Health (NIH), the C.G. Swebilius Trust, and TUBITAK Grant Number 1059B191700801. Note, the contents of the manuscript is solely the responsibility of the author and do not necessarily represent the official view of the NIH.

ACKNOWLEDGMENTS

The author wishes to thank Rebecca Khozein DOM, MS, REEG/EPT, RPSGT, RNCST, and Tamara Wing REEGT for assistance in EEG data acquisition.

REFERENCES

Alkawadri, R. (2017). 2293: Passive intracranial EEG-based localization of the central sulcus during sleep. *J. Clin. Trans. Sci.* 1, 14–15. doi: 10.1017/cts.2017.67

Alkawadri, R., and Gaspard, N. (2018). Averaging in time-frequency domain reveals the temporal and spatial extent of seizures recorded by scalp EEG. *Epileptic Disord.* 20:132–138. doi: 10.1684/epd.2018.0962

Alkawadri, R., Gaspard, N., Goncharova, I. I., Spencer, D. D., Gerrard, J. L., Zaveri, H., et al. (2014). The spatial and signal characteristics of physiologic high frequency oscillations. *Epilepsia* 55, 1986–1995. doi: 10.1111/epi.12851

Alkawadri, R., Zaveri, H., Duckrow, R. B., Spencer, D. D., Gerrard, J. L., and Hirsch, L. J. (2013). *(Dys)Functional Connectivity of the Seizure Onset Zone: Low Frequency Stimulation and Cortico-cortical Evoked Responses Study*. Seattle, WA: Wiley.

Alkawadri, R., Zaveri, H., Gerrard, J. L., Hirsch, L. J., and Spencer, D. D. (2015). Passive intracranial EEG based localization of the central sulcus during sleep. *Am. Clin. Neurophysiol.* 32, 382–399.

Alkawadri, R., Zaveri, H. P., Gaspard, N., Yan, Q., Hirsch, L. J., and Spencer, D. D. (2015). The connectivity index: a novel metric to grade epileptogenicity. *Clin. Neurophysiol.* 129:e42. doi: 10.1016/j.clinph.2018.04.104

Arunkumar, A., Panday, A., Joshi, B., Ravindran, A., and Zaveri, H. P. (2012). Estimating correlation for a real-time measure of connectivity. *Conf. Proc. IEEE Eng. Med. Biol. Soc.* 2012, 5190–5193. doi: 10.1109/EMBC.2012.6347163

Arya, R., Mangano, F. T., Horn, P. S., Holland, K. D., Rose, D. F., and Glauser, T. A. (2013). Adverse events related to extraoperative invasive EEG monitoring with subdural grid electrodes: a systematic review and meta-analysis. *Epilepsia* 54, 828–839. doi: 10.1111/epi.12073

Asano, E., Juhasz, C., Shah, A., Sood, S., and Chugani, H. T. (2009). Role of subdural electrocorticography in prediction of long-term seizure outcome in epilepsy surgery. *Brain* 132(Pt 4), 1038–1047. doi: 10.1093/brain/awp025

Avoli, M. (2014). Mechanisms of epileptiform synchronization in cortical neuronal networks. *Curr. Med. Chem.* 21, 653–662. doi: 10.2174/09298673206613119151136

Bartolomei, F., Chauvel, P., and Wendling, F. (2008). Epileptogenicity of brain structures in human temporal lobe epilepsy: a quantified study from intracerebral EEG. *Brain* 131(Pt 7), 1818–1830. doi: 10.1093/brain/awn111

Bartolomei, F., Trebuchon, A., Bonini, F., Lambert, I., Gavaret, M., Woodman, M., et al. (2016). What is the concordance between the seizure onset zone and the irritative zone? A SEEG quantified study. *Clin. Neurophysiol.* 127, 1157–1162. doi: 10.1016/j.clinph.2015.10.029

Bautista, R. E., Cobbs, M. A., Spencer, D. D., and Spencer, S. S. (1999). Prediction of surgical outcome by interictal epileptiform abnormalities during intracranial EEG monitoring in patients with extrahippocampal seizures. *Epilepsia* 40, 880–890. doi: 10.1111/j.1528-1157.1999.tb00794.x

Bayram, A., Rao, S., Spencer, D. D., and Alkawadri, R. (2018a). T143. Effect of anesthesia on electrocorticography for localization of epileptic focus: Literature review and future directions. *Clin. Neurophys.* 129, e57–e58. doi: 10.1016/j.clinph.2018.04.144

Bayram, A., Rao, S., Spencer, D., and Alkawadri, R. (2018b). Effect of anesthesia on electrocorticography for localization of epileptic focus: literature review and future directions (P2. 271). *Neurology* 90, 271.

Birot, G., Kachenoura, A., Albera, L., Benar, C., and Wendling, F. (2013). Automatic detection of fast ripples. *J. Neurosci. Methods* 213, 236–249. doi: 10.1016/j.jneumeth.2012.12.013

Bragin, A., Engel, J. Jr., Wilson, C. L., Fried, I., and Mathern, G. W. (1999). Hippocampal and entorhinal cortex high-frequency oscillations (100–500 Hz) in human epileptic brain and in kainic acid–treated rats with chronic seizures. *Epilepsia* 40, 127–137. doi: 10.1111/j.1528-1157.1999.tb02065.x

Brazdil, M., Pail, M., Halamek, J., Plesinger, F., Cimbalnik, J., Roman, R., et al. (2017). Very high-frequency oscillations: novel biomarkers of the epileptogenic zone. *Ann. Neurol.* 82, 299–310. doi: 10.1002/ana.25006

Callaghan, B., Schlesinger, M., Rodemer, W., Pollard, J., Hesdorffer, D., Allen Hauser, W., et al. (2011). Remission and relapse in a drug-resistant epilepsy population followed prospectively. *Epilepsia* 52, 619–626. doi: 10.1111/j.1528-1167.2010.02929.x

Cascino, G. D., Trenerry, M. R., Jack, C. R. Jr., Dodick, D., Sharbrough, F. W., So, E. L., et al. (1995). Electrocorticography and temporal lobe epilepsy: relationship to quantitative MRI and operative outcome. *Epilepsia* 36, 692–696. doi: 10.1111/j.1528-1157.1995.tb01048.x

Chaitanya, G., Arivazhagan, A., Sinha, S., Reddy, K. R., Thennarasu, K., Bharath, R. D., et al. (2015). Dexmedetomidine anesthesia enhances spike generation during intra-operative electrocorticography: a promising adjunct for epilepsy surgery. *Epilepsy Res.* 109, 65–71. doi: 10.1016/j.eplepsyres.2014.10.006

Dahaba, A. A., Yin, J., Xiao, Z., Su, J., Bornemann, H., Dong, H., et al. (2013). Different propofol-remifentanil or sevoflurane-remifentanil bispectral index levels for electrocorticographic spike identification during epilepsy surgery. *Anesthesiology* 119, 582–592. doi: 10.1097/ALN.0b013e3182976036

David, O., Blauwblomme, T., Job, A. S., Chabardes, S., Hoffmann, D., Minotti, L., et al. (2011). Imaging the seizure onset zone with stereo-electroencephalography. *Brain* 134(Pt 10), 2898–2911. doi: 10.1093/brain/awr238

Englot, D. J., Hinkley, L. B., Kort, N. S., Imber, B. S., Mizuiri, D., Honma, S. M., et al. (2015). Global and regional functional connectivity maps of neural oscillations in focal epilepsy. *Brain* 138(Pt 8), 2249–2262. doi: 10.1093/brain/awv130

Feindel, W., Leblanc, R., and de Almeida, A. N. (2009). Epilepsy surgery: historical highlights 1909-2009. *Epilepsia* 50(Suppl. 3), 131–151. doi: 10.1111/j.1528-1167.2009.02043.x

Flemming, D. C., Fitzpatrick, J., Fariello, R. G., Duff, T., Hellman, D., Hoff, B. H., et al. (1980). Diagnostic activation of epileptogenic foci by enflurane. *Anesthesiology* 52, 431–433. doi: 10.1097/00000542-198005000-00010

Fong, J. S., Alexopoulos, A. V., Bingaman, W. E., Gonzalez-Martinez, J., and Prayson, R. A. (2012). Pathologic findings associated with invasive EEG monitoring for medically intractable epilepsy. *Am. J. Clin. Pathol.* 138, 506–510. doi: 10.1309/AJCPGSNL9VDVNJMX

Gaspard, N., Alkawadri, R., Farooque, P., Goncharova, I. I., and Zaveri, H. P. (2014). Automatic detection of prominent interictal spikes in intracranial EEG: validation of an algorithm and relationsip to the seizure onset zone. *Clin Neurophysiol.* 125, 1095–1103. doi: 10.1016/j.clinph.2013.10.021

Herman, W. X., Smith, R. E., Kronemer, S. I., Watsky, R. E., Chen, W. C., Gober, L. M., et al. (2017). A switch and wave of neuronal activity in the cerebral cortex during the first second of conscious perception. *Cereb. Cortex* 29, 461–474. doi: 10.1093/cercor/bhx327

Hill, N. J., Gupta, D., Brunner, P., Gunduz, A., Adamo, M. A., Ritaccio, A., et al. (2012). Recording human electrocorticographic (ECoG) signals for neuroscientific research and real-time functional cortical mapping. *J. Vis. Exp.* 64:3993. doi: 10.3791/3993

Isitan, C., Benjamin, C. F., Quraishi, I. H., Spencer, D. D., and Alkawadri, R. (2018). Brief history of electrical cortical stimulation: a journey in time from volta to penfield (P5. 299). *Neurology* 90:299.

Jacobs, J., LeVan, P., Chander, R., Hall, J., Dubeau, F., and Gotman, J. (2008). Interictal high-frequency oscillations (80-500 Hz) are an indicator of seizure onset areas independent of spikes in the human epileptic brain. *Epilepsia* 49, 1893–1907. doi: 10.1111/j.1528-1167.2008.01656.x

Jacobs, J., Levan, P., Chatillon, C. E., Olivier, A., Dubeau, F., and Gotman, J. (2009a). High frequency oscillations in intracranial EEGs mark epileptogenicity rather than lesion type. *Brain* 132(Pt 4), 1022–1037. doi: 10.1093/brain/awn351

Jacobs, J., Zelmann, R., Jirsch, J., Chander, R., Dubeau, C. E., and Gotman, J. (2009b). High frequency oscillations (80-500 Hz) in the preictal period in patients with focal seizures. *Epilepsia* 50, 1780–1792. doi: 10.1111/j.1528-1167.2009.02067.x

Jasper, H. H., Arfel-Capdeville, G., and Rasmussen, T. (1961). Evaluation of EEG and cortical electrographic studies for prognosis of seizures following surgical excision of epileptogenic lesions. *Epilepsia* 2, 130–137.

Jehi, L. E., O'Dwyer, R., Najm, I., Alexopoulos, A., and Bingaman, W. (2009). A longitudinal study of surgical outcome and its determinants following posterior cortex epilepsy surgery. *Epilepsia* 50, 2040–2052. doi: 10.1111/j.1528-1167.2009.02070.x

Kanazawa, O., Blume, W. T., and Girvin, J. P. (1996). Significance of spikes at temporal lobe electrocorticography. *Epilepsia* 37, 50–55. doi: 10.1111/j.1528-1157.1996.tb00511.x

Kovac, S., Kahane, P., and Diehl, B. (2016). Seizures induced by direct electrical cortical stimulation–mechanisms and clinical considerations. *Clin. Neurophysiol.* 127, 31–39. doi: 10.1016/j.clinph.2014.12.009

Maris, E., and Oostenveld, R. (2007). Nonparametric statistical testing of EEG- and MEG-data. *J. Neurosci. Methods* 164, 177–190. doi: 10.1016/j.jneumeth.2007.03.024

McGuire, G., El-Beheiry, H., Manninen, P., Lozano, A., and Wennberg, R. (2003). Activation of electrocorticographic activity with remifentanil and alfentanil during neurosurgical excision of epileptogenic focus. *Br. J. Anaesth.* 91, 651–655. doi: 10.1093/bja/aeg241

Najm, I., Jehi, L., Palmini, A., Gonzalez-Martinez, J., Paglioli, E., and Bingaman, W. (2013). Temporal patterns and mechanisms of epilepsy surgery failure. *Epilepsia* 54, 772–782. doi: 10.1111/epi.12152

Nishida, M., Zestos, M. M., and Asano, E. (2016). Spatial-temporal patterns of electrocorticographic spectral changes during midazolam sedation. *Clin. Neurophysiol.* 127, 1223–1232. doi: 10.1016/j.clinph.2015.10.044

Oliveira, P. A., Garzon, E., Caboclo, L. O., Sousa, P. S., Carrete, H. Jr., Centeno, R. S., et al. (2006). Can intraoperative electrocorticography patterns predict surgical outcome in patients with temporal lobe epilepsy secondary to unilateral mesial temporal sclerosis? *Seizure* 15, 541–551.

Palmini, A., Gambardella, A., Andermann, F., Dubeau, F., da Costa, J., Olivier, C. A., et al. (1995). Intrinsic epileptogenicity of human dysplastic cortex as suggested by corticography and surgical results. *Ann. Neurol.* 37, 476–487. doi: 10.1002/ana.410370410

Park, E. H., and Madsen, J. R. (2018). Granger causality analysis of interictal iEEG predicts seizure focus and ultimate resection. *Neurosurgery* 82, 99–109. doi: 10.1093/neuros/nyx195

Ramgopal, S., Thome-Souza, S., Jackson, M., Kadish, N. E., Sanchez Fernandez, I., Klehm, J., et al. (2014). Seizure detection, seizure prediction, and closed-loop warning systems in epilepsy. *Epilepsy Behav.* 37, 291–307. doi: 10.1016/j.yebeh.2014.06.023

Ren, L., Kucewicz, M. T., Cimbalnik, J., Matsumoto, J. Y., Brinkmann, B. H., Hu, W., et al. (2015). Gamma oscillations precede interictal epileptiform spikes in the seizure onset zone. *Neurology.* 84:602–608. doi: 10.1212/WNL.0000000000001234

Rummel, C., Abela, E., Andrzejak, R. G., Hauf, M., Pollo, C., Muller, M., et al. (2015). Resected brain tissue, seizure onset zone and quantitative eeg measures: towards prediction of post-surgical seizure control. *PLoS One* 10:e0141023. doi: 10.1371/journal.pone.0141023

Simasathien, T., Vadera, S., Najm, I., Gupta, A., Bingaman, W., and Jehi, L. (2013). Improved outcomes with earlier surgery for intractable frontal lobe epilepsy. *Ann. Neurol.* 73, 646–654. doi: 10.1002/ana.23862

Singh, S., Sandy, S., and Wiebe, S. (2015). Ictal onset on intracranial EEG: do we know it when we see it? State of the evidence. *Epilepsia* 56, 1629–1638. doi: 10.1111/epi.13120

Stefan, H., Hopfengartner, R., Kreiselmeyer, G., Weigel, D., Rampp, S., Kerling, F., et al. (2008). Interictal triple ECoG characteristics of temporal lobe epilepsies: an intraoperative ECoG analysis correlated with surgical outcome. *Clin. Neurophysiol.* 119, 642–652. doi: 10.1016/j.clinph.2007.11.046

Sugano, H., Shimizu, H., and Sunaga, S. (2007). Efficacy of intraoperative electrocorticography for assessing seizure outcomes in intractable epilepsy patients with temporal-lobe-mass lesions. *Seizure* 16, 120–127. doi: 10.1016/j.seizure.2006.10.010

Tao, J. X., Baldwin, M., Hawes-Ebersole, S., and Ebersole, J. S. (2007). Cortical substrates of scalp EEG epileptiform discharges. *J. Clin. Neurophysiol.* 24, 96–100. doi: 10.1097/WNP.0b013e31803ecdaf

Tran, T. A., Spencer, S. S., Javidan, M., Pacia, S., Marks, D., and Spencer, D. D. (1997). Significance of spikes recorded on intraoperative electrocorticography in patients with brain tumor and epilepsy. *Epilepsia* 38, 1132–1139. doi: 10.1111/j.1528-1157.1997.tb01203.x

Tripathi, M., Garg, A., Gaikwad, S., Bal, C. S., Chitra, S., Prasad, K., et al. (2010). Intra-operative electrocorticography in lesional epilepsy. *Epilepsy Res.* 89, 133–141. doi: 10.1016/j.eplepsyres.2009.12.007

Usui, N., Terada, K., Baba, K., Matsuda, K., Usui, K., Tottori, T., et al. (2015). Significance of very-high-frequency oscillations (Over 1,000Hz) in epilepsy. *Ann. Neurol.* 78, 295–302. doi: 10.1002/ana.24440

van Mierlo, P., Papadopoulou, M., Carrette, E., Boon, P., Vandenberghe, S., Vonck, K., et al. (2014). Functional brain connectivity from EEG in epilepsy: seizure prediction and epileptogenic focus localization. *Prog. Neurobiol.* 121, 19–35. doi: 10.1016/j.pneurobio.2014.06.004

Vilensky, J. A., and Gilman, S. (2002). Horsley was the first to use electrical stimulation of the human cerebral cortex intraoperatively. *Surg. Neurol.* 58, 425–426. doi: 10.1016/S0090-3019(02)00920-5

Wang, S., Wang, I. Z., Bulacio, J. C., Mosher, J. C., Gonzalez-Martinez, J., Alexopoulos, A. V., et al. (2013). Ripple classification helps to localize the seizure-onset zone in neocortical epilepsy. *Epilepsia* 54, 370–376. doi: 10.1111/j.1528-1167.2012.03721.x

Weiss, S. A., Banks, G. P., McKhann, G. M. Jr., Goodman, R. R., Emerson, R. G., Trevelyan, A. J., et al. (2013). Ictal high frequency oscillations distinguish two types of seizure territories in humans. *Brain* 136(Pt 12), 3796–3808. doi: 10.1093/brain/awt276

Wennberg, R., Quesney, F., Olivier, A., and Rasmussen, T. (1998). Electrocorticography and outcome in frontal lobe epilepsy. *Electroencephalogr. Clin. Neurophysiol.* 106, 357–368. doi: 10.1016/S0013-4694(97)00148-X

Yuan, J., Chen, Y., and Hirsch, E. (2012). Intracranial electrodes in the presurgical evaluation of epilepsy. *Neurol. Sci.* 33, 723–729. doi: 10.1007/s10072-012-1020-2

Zhao, M., Alleva, R., Ma, H., Daniel, A. G., and Schwartz, T. H. (2015). Optogenetic tools for modulating and probing the epileptic network. *Epilepsy Res.* 116, 15–26. doi: 10.1016/j.eplepsyres.2015.06.010

Conflict of Interest Statement: The author declares that the research was conducted in the absence of any commercial or financial relationships that could be construed as a potential conflict of interest.

Copyright © 2019 Alkawadri. This is an open-access article distributed under the terms of the Creative Commons Attribution License (CC BY). The use, distribution or reproduction in other forums is permitted, provided the original author(s) and the copyright owner(s) are credited and that the original publication in this journal is cited, in accordance with accepted academic practice. No use, distribution or reproduction is permitted which does not comply with these terms.

frontiers in Neuroscience

ORIGINAL RESEARCH
published: 19 June 2019
doi: 10.3389/fnins.2019.00622

Median Nerve Stimulation Based BCI: A New Approach to Detect Intraoperative Awareness During General Anesthesia

Sébastien Rimbert[1]*, *Pierre Riff*[1], *Nathalie Gayraud*[2], *Denis Schmartz*[3] and *Laurent Bougrain*[1]

[1] Université de Lorraine, CNRS, Inria, LORIA, Nancy, France, [2] Université Côte d'Azur, Inria, Sophia-Antipolis Méditerrannée, Athena Team, Nice, France, [3] Le Centre Hospitalier Universitaire (CHU) Brugmann, Université Libre de Bruxelles, Brussels, Belgium

Hundreds of millions of general anesthesia are performed each year on patients all over the world. Among these patients, 0.1–0.2% are victims of Accidental Awareness during General Anesthesia (AAGA), i.e., an unexpected awakening during a surgical procedure under general anesthesia. Although anesthesiologists try to closely monitor patients using various techniques to prevent this terrifying phenomenon, there is currently no efficient solution to accurately detect its occurrence. We propose the conception of an innovative passive brain-computer interface (BCI) based on an intention of movement to prevent AAGA. Indeed, patients typically try to move to alert the medical staff during an AAGA, only to discover that they are unable to. First, we examine the challenges of such a BCI, i.e., the lack of a trigger to facilitate when to look for an intention to move, as well as the necessity for a high classification accuracy. Then, we present a solution that incorporates Median Nerve Stimulation (MNS). We investigate the specific modulations that MNS causes in the motor cortex and confirm that they can be altered by an intention of movement. Finally, we perform experiments on 16 healthy participants to assess whether an MI-based BCI using MNS is able to generate high classification accuracies. Our results show that MNS may provide a foundation for an innovative BCI that would allow the detection of AAGA.

Keywords: brain-computer interface, median nerve stimulation, motor imagery, anesthesia, intraoperative awareness

OPEN ACCESS

Edited by:
Christoph Guger,
g.tec Medical Engineering GmbH,
Austria

Reviewed by:
Xiaoli Li,
Beijing Normal University, China
Damien Coyle,
Ulster University, United Kingdom

***Correspondence:**
Sébastien Rimbert
sebastien.rimbert@inria.fr

Specialty section:
This article was submitted to Neural Technology, a section of the journal Frontiers in Neuroscience

Received: *13 December 2018*
Accepted: *29 May 2019*
Published: *19 June 2019*

Citation:
Rimbert S, Riff P, Gayraud N, Schmartz D and Bougrain L (2019) Median Nerve Stimulation Based BCI: A New Approach to Detect Intraoperative Awareness During General Anesthesia. Front. Neurosci. 13:622. doi: 10.3389/fnins.2019.00622

1. INTRODUCTION

Waking up during a surgery is a haunting experience, both for patients, who consider it as the worst in their lives (Pomfrett, 1999), and for healthcare personnel, who fear this situation (Tasbighou et al., 2018). This phenomenon, called "accidental awareness during general anesthesia" (AAGA), can be defined as an unexpected awakening of the patient during a surgical procedure under general anesthesia (Pandit et al., 2014; Almeida, 2015). This situation occurs when the depth of anesthesia induced by anesthetic concentration is not enough to compensate for surgical and environmental stimuli and prevent awakening (Myles et al., 2004; MacGregor, 2013). Although the statistics are still under debate, the estimated number of AAGA in high-risk practices is up to 1% (Sebel et al., 2004; Avidan et al., 2008; Xu et al., 2009). The percentage of patients affected by AAGA may appear

low, but considering the hundreds of millions of general anesthesia performed each year around the world (Weiser et al., 2016), the occurrence of this phenomenon is in fact high. Therefore, new solutions are required to better prevent it (Sebel et al., 2004; Monk and Weldon, 2011).

The main problem for patients experiencing AAGA is the explicit or implicit memory of this distressing experience which can cause severe trauma, termed post-traumatic stress disorder (PTSD) (Osterman et al., 2001). The PTSD following AAGA should not be underestimated: it can last several years and have a severe impact on the victim's life (Avidan and Mashour, 2013; MacGregor, 2013; Almeida, 2015). After experiencing AAGA, more than 70% of patients are reported to be suffering from PTSD (Leslie et al., 2010). They are frequently associated with an increased risk of suicide (Hendin, 1991) and often lead to anxiety, insomnia, flashbacks, chronic fear, avoidance tendencies, loneliness, irritability, concentration difficulty, and lack of confidence in the medical staff (Schwender et al., 1995; Lau et al., 2006; Bischoff and Rundshagen, 2011; MacGregor, 2013; Pandit et al., 2014; Almeida, 2015). AAGA also generates a high anxiety level in anesthesiologists (Xu et al., 2009), and is in the top 3 causes of legal action taken against hospitals (Pandit et al., 2014) which can be expensive if the claim is successful (Mihai et al., 2009).

There are currently two ways to monitor the depth of anesthesia: observing clinical features (e.g., heart rate, blood pressure, movement, sweating; Schafer and Stanski, 2008); or using electroencephalographic (EEG) analysis, mainly of the frontal cortex activity. Unfortunately, an anesthesiologist's observation of clinical signs is not enough to prevent AAGA during surgery (Punjasawadwong et al., 2014). Indeed, observing clinical signs is but an indirect way of monitoring the patients' cerebral state. Hence, it does not always permit the prediction of AAGA before it occurs. New indexes using part of the EEG signal at the frontal level have been employed to prevent AAGA, such as the Bispectral Index (BIS), the Patient State Index (PSI) or the Entropy (Li et al., 2008; Kent and Domino, 2009). Although these devices are already in use (Punjasawadwong et al., 2014; Liang et al., 2015), some studies have failed to demonstrate a superiority of these monitors compared to clinical surveillance or end-tidal anesthetic gas (ETAG) (Avidan et al., 2008; Mashour and Avidan, 2015). Moreover, a number of studies have shown the unreliability of these techniques (Schneider et al., 2004; Schuller et al., 2015). The concentration measurement of anesthetic gases can also be an interesting way to quantify the depth of anesthesia, since it is a measurement and not an estimation, the latter being the case for monitoring anesthesia depth under intravenous products like propofol (Avidan et al., 2008). However, anesthetic gases are much less widespread in Europe (Absalom et al., 2016). In addition, current practices aim to reduce the concentration of anesthetic agents as much as possible in order to reduce post-operative cognitive dysfunction and morbidity (Pandit and Cook, 2013). In fact, most monitoring techniques are less reliable when the concentration of anaesthetic is increased (Mashour et al., 2011) which is why no technique is currently satisfactory and sufficient to evaluate the depth of general anesthesia and detect intraoperative awareness.

Intraoperative awareness leads to this kind of testimony: "*I couldn't breathe,* ***couldn't move*** *or open my eyes, or tell the doctor that I wasn't asleep*." Such testimonies show that, during AAGA, the first reaction from a patient is usually to move to alert the medical staff of this terrifying situation (Ghoneim et al., 2009; Pandit et al., 2014). However, in the majority of surgeries, the patient is curarized, which causes a neuromuscular blockage and inhibits any movement (Tasbighou et al., 2018). Presently, a real movement (RM) or a Motor Imagery (MI) can be detected by analyzing the EEG signal, such as in Brain-Computer Interfaces (BCI, Jonathan Wolpaw, 2012). Detecting RM or MI using EEG is feasible because both the preparation phase and the motor execution phase present power variations in the mu and the beta frequency bands (Pfurtscheller and Lopes da Silva, 1999). These sensorimotor rhythms are characterized, before and during an imagined movement, by a gradual decrease of power in the mu-alpha (7–13 Hz) and beta (15–30 Hz) bands; and after the end of the motor imagery, by an increase of power–mainly–in the beta band. These modulations are respectively known as Event-Related Desynchronization (ERD) and Event-Related Synchronization (ERS) or post-movement beta rebound (Pfurtscheller, 2003; Hashimoto and Ushiba, 2013; Kilavik et al., 2013; Clerc et al., 2016) (**Figure 1A**).

According to these observations, it would be possible to discover AAGA by detecting an intention of movement from the patient. In 2016, Blockland et al., studied the effect of propofol, a commonly used anesthetic, on the EEG signals of the motor cortex. They verified the relevance of this approach for improving monitoring of AAGA (Blokland et al., 2016). In this study, patients were not completely anesthetized and were asked to perform movements according to sound beeps while an increasing dosage of anesthetic was administered to them. This first approach shows that the BCI domain could contribute to the issue of AAGA. However, the study conducted by Blockland et al. was based on synchronous active communication, i.e., the voluntary subject was explicitly asked to perform a movement during the experiment after a visual and audible signal, which does not realistically reflect the conditions during intraoperative awareness. Therefore, a strategy must be found to design a passive BCI whose task would be to detect the intention of movement of an AAGA victim. In particular, this new BCI should not be based on motor actions previously planned over time by the experimenter and performed by the patient according to specific auditory or visual markers, but rather on the accidental reaction of a patient experiencing AAGA.

The design of such a BCI presents us with two challenges. The first challenge is to be able to detect the intention of movement of a person who is a victim of AAGA without any time markers. This is equivalent to continuously analyzing the EEG signal with few indications regarding the time phases to be studied. While there exist some BCIs that do not use time markers or triggers (known as asynchronous BCIs), the literature clearly shows that their classification rate is lower than that of a synchronous BCI with triggers (Nicolas-Alonso and Gomez-Gil, 2012). The second challenge is therefore to obtain a high level of accuracy, which would guarantee the reliability of the BCI device so that it can be used with patients. The accuracy obtained for a MI vs.

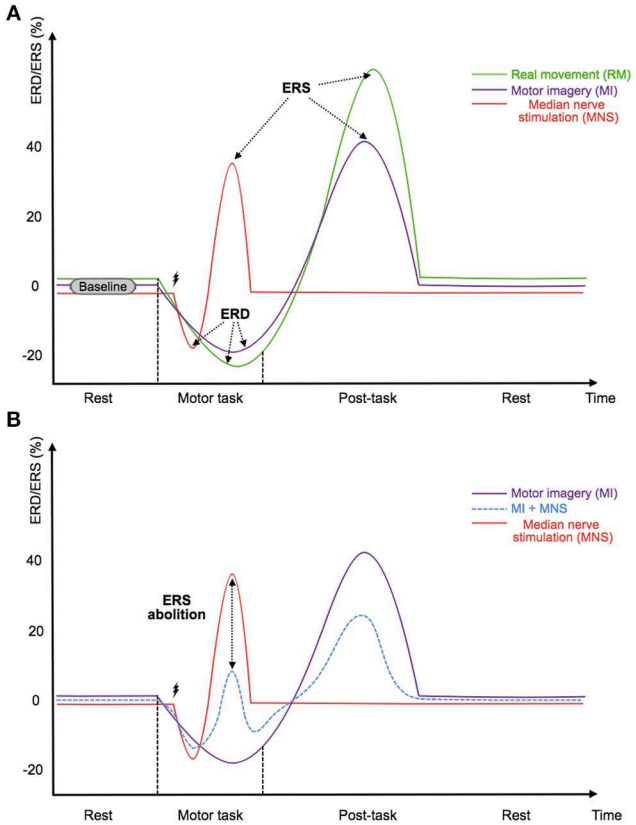

FIGURE 1 | (A) Illustration of the timings and amplitudes of the desynchronization and the followed synchronization induced by a real movement, a motor imagery, and a median nerve stimulation according to Salenius et al. (1997),Schnitzler et al. (1997), and Neuper and Pfurtscheller (2001) in the mu and beta frequency bands. **(B)** Illustration of the expected timing and amplitudes of the desynchronization and the followed synchronization induced by a median nerve stimulation during a motor imagery according to Salenius et al. (1997),Schnitzler et al. (1997),Neuper and Pfurtscheller (2001), and Kilavik et al. (2013) in the mu and beta frequency bands. The time scale is not precisely detailed.

Rest classification in the BCI field in general remain low and should be improved to create a reliable device which can be used in hospitals.

To satisfy these two requirements, we propose the use of median nerve stimulation (MNS) and show that it is a very promising approach. Indeed, previous studies have shown that a painless stimulation of the median nerve induces an ERD during the stimulation while an ERS appears after the stimulation (Salenius et al., 1997; Schnitzler et al., 1997; Neuper and Pfurtscheller, 2001) (**Figure 1A**). More interestingly, a very long motor task performed during a MNS abolishes the patterns previously generated by this stimulation. The gating hypothesis suggests that patterns are contracting (Kilavik et al., 2013) (**Figure 1B**). If this hypothesis is verified it could make the detection of AAGA with a passive BCI possible. Indeed, we can imagine a routine system where the patient would be stimulated at the median nerve, and the analysis of ERD and ERS modulations of the motor cortex would be used to find out if the patient has an intention to move. Unfortunately, very few studies exist on this topic, and the effect of a MNS during a MI needs to be investigated further, especially for a shorter MI. In addition, no study has shown that a MI + MNS vs. MNS classification results in better accuracies than a MI vs. Rest classification, suggesting that MNS could be used as a trigger.

The objective of this study is to analyze the EEG activity over the motor cortex and (i) verify that median nerve stimulation generates desynchronizations (ERD) and synchronizations (ERS); (ii) confirm that they are modulated by an intention of movement; and (iii) demonstrate that a classification based on this phenomenon would be more effective than conventional classification based on modulations generated by an intention of movement vs. resting state. In order to achieve the above, we recorded 128 EEG signals from 16 voluntary healthy subjects who had performed 3 motor tasks (a real movement, a motor imagery, a MNS during a MI) and reacted to a MNS. To show the influence of a MI on the ERD and ERS generated by a MNS, we computed time-frequency and topographic maps and a classification based on MNS+MI and MNS only. Our results indicate that a MI significantly modulates the ERDs and ERSs generated by a MNS and also that classification based on MNS is more efficient than conventional classification based on MI vs. rest. These results are promising for creating a BCI that detects AAGA.

2. MATERIALS AND METHODS

2.1. Participants

Sixteen right-handed healthy volunteers (8 females; 19 to 57 years-old; 28.56 $\pm$ 13.3 years old) were recruited for this study. All voluntary subjects satisfied the inclusion criteria (right-handed, between 18 and 60 years-old, without medical history which could have influenced the task, such as diabetes, antidepressant treatment, or neurological disorders). This experiment followed the statements of the WMA declaration of Helsinki on ethical principles for medical research involving human subjects (World Medical Association, 2002). In addition, participants signed an informed consent which was approved by the ethical committee of Inria (COERLE, approval number: 2016-011/01) as it satisfied the ethical rules and principles of the institute.

2.2. Experimental Tasks

The aim of this research is to investigate the occurrence of motor patterns under 4 different conditions : real movement (RM), motor imagery (MI), median nerve stimulation during a motor imagery (MI + MNS), and median nerve stimulation during rest (MNS) (**Figure 2**). The first two conditions were designed to assess the reliability of our experimental setup and data processing by comparing these results to the literature. The last two conditions were the core of our study and aim at showing that a MNS can be used and is more helpful as a trigger to improve the detection of intraoperative awareness.

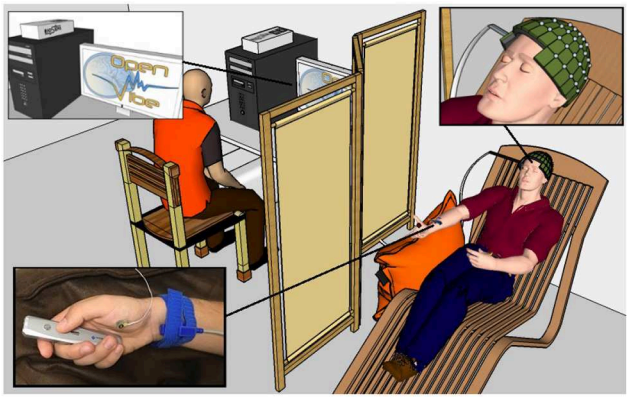

FIGURE 2 | A healthy voluntary subject is lying on a comfortable chair with his eyes closed. His legs rest on a footrest and his right forearm rests on a cushion to prevent movement. The OpenViBE software records 128 EEG electrodes and delivers starting and stopping beeps and stimulations of the median nerve when necessary according to the experimental conditions. The subject physically or mentally presses and releases a remote button. The operator displays the EEG signals during the experiment.

2.2.1. Condition 1: Real Movement

The RM condition (C1) consisted of an isometric grasp between the thumb and the index finger on a pointer button (**Figure 2**). A low frequency beep indicated when the subject had to start the movement. The grasping task was maintained during 2 s. Then a second beep indicated when the subject had to stop pressing the pointer button and the task's end (**Figure 3**). The states of the pointer button were recorded as triggers and allowed us to know exactly when the participant executed and stopped the RM. This simple movement, easy to understand and execute, generates enough brain activity changes which can be observed in EEG (Shibasaki et al., 1993).

2.2.2. Condition 2: Motor Imagery

For the MI condition (C2), subjects had to imagine the previous movement, i.e., they had to try to feel a maximum of sensations caused by the real movement, but without any movement. Similarly to condition 1, a low frequency beep indicated when the subject had to start the motor imagery, the grasping MI was maintained during 2 s, then a second beep indicated the end of the imagined task (**Figure 3**).

Condition 3: Motor Imagery With a Median Nerve Stimulation

During the MI + MNS condition (C3), subjects had to perform a motor imagination while their median nerve was stimulated 750 ms after the start of the motor imaginary task (**Figure 3**). Uniformly to the previous conditions, a low frequency beep indicated when the subject had to start the motor imagery and a high frequency beep indicated when to stop it. We chose the 750 ms of delay according to the reaction time of the average person, in order to stimulate during the ERD corresponding to the imagination's start. The duration of the stimulation was 100 ms and stimulation intensity was adapted for each subject and varied between 8 and 15 mA.

2.2.3. Condition 4: Median Nerve Stimulation Only

The MNS only condition (C4) consisted of a series of stimulation of the median nerve during rest. We placed the two electrodes of stimulation on the wrist according to the standards (Schnitzler et al., 1997; Kumbhare et al., 2016). We considered as an inclusion criterion for our population of subjects the fact that the stimulation was not felt as painful and that it caused a slight movement between the thumb and the index finger of the voluntary subject. The stimulation intensity was adapted for each subject and varied between 8 and 15 mA.

2.3. Experimental Design

Each participant took part in one session of 120 min divided in 4 phases: (1) installation of the EEG cap (40 min); (2) selection of the intensity of median nerve stimulation needed to produce a micro movement between the thumb and index finger (10 min); (3) execution of RM, MI, MI + MNS, and MNS in runs during which participants had to perform the different motor tasks (60 min); (4) uninstallation and debriefing (10 min).

The study contained 4 conditions: real movement (RM), motor imagery (MI), median nerve stimulation during motor imagery (MI + MNS), and stimulation only (MNS). These conditions were completed on the same day and divided into two runs of 26 trials each, representing 52 trials for each condition. The duration of one trial was 8 ± 1 s (**Figure 3**). The runs were randomized for each subject in order to avoid fatigue, gel drying, or other confounding factors that might have caused possible biases in the results. At the beginning of each run, the subject remained relaxed for 15 s. Breaks of a few minutes were taken between runs to prevent fatigue of the subject.

For the entirety of the experiment, the subject were seated in a comfy chair including a leg rest, with their right arm resting on a pillow, a presentation remote placed in their right hand. The subject didn't actively hold the remote, it was simply resting in their hand with the button placed under their thumb. Subjects were asked to keep their eyes closed (**Figure 2**).

2.4. Data Acquisition

EEG signals were acquired using the *OpenViBE* platform (Renard et al., 2010) with a *Biosemi Active* Two 128-channel EEG system, arranged in the *Biosemi*'s ABC system covering the entire scalp at 2,048 Hz. Among all registered sites, some of the electrodes were localized around the primary motor cortex, the motor cortex, the somatosensory cortex, and the occipital cortex, which allowed us to observe the physiological changes due to the real movement, the kinesthetic motor imagery, and the median nerve stimulation (Salenius et al., 1997; Schnitzler et al., 1997; Guillot et al., 2009; Filgueiras et al., 2017). In the Biosemi^{TM} system the ground electrodes used were two separate electrodes: Common Mode Sense (CMS) active electrode and Driven Right Leg (DRL) passive electrode located over the parietal lobe. Impedance was kept below 10 kΩ for all electrodes to ensure that the background noise in the acquired signal was low. An external electromyogram (EMG) electrode was added in order to verify that there was no movement during the MI task.

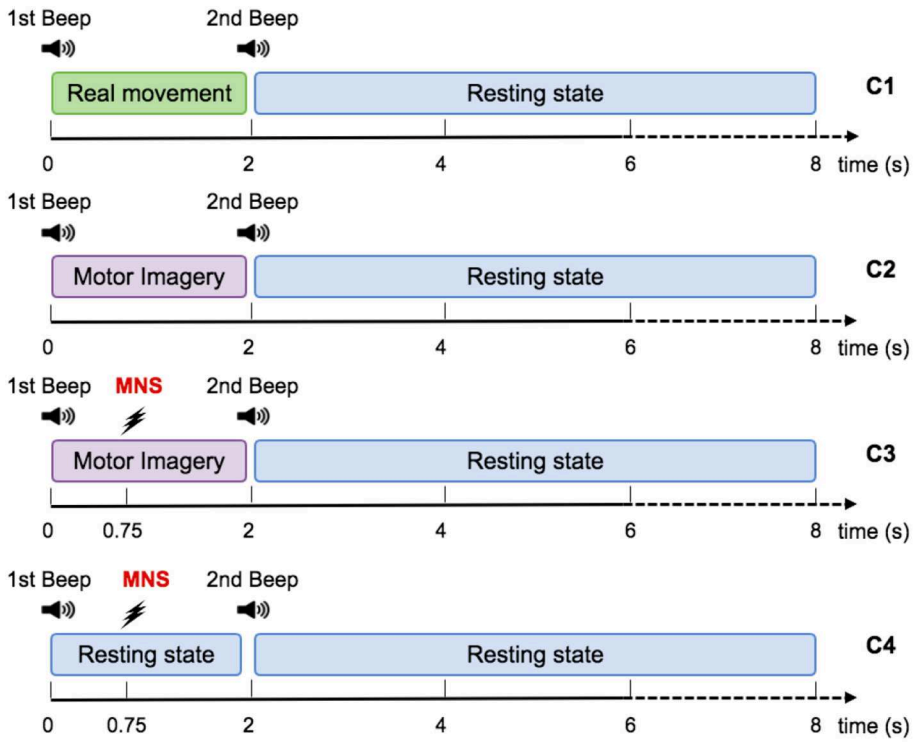

FIGURE 3 | Representation scheme for one trial. Timing schemes of a trial for C1, C2, C3, and C4. For all motor tasks, one low frequency beep indicates when to start the task. For the MNS+MI condition, the MNS occurs at 750 ms after the first beep. The end of the MI is announced by a high frequency beep and followed by a rest period of 6 s.

2.5. Data Pre-Processing

All offline analyses were performed using the EEGLAB toolbox (Delorme and Makeig, 2004) and Matlab2015b (The MathWorks Inc. Natick, MA, USA). The data was processed in General Data Format (GDF). Considering the large number of electrodes used in this study (e.g., =128) and the purpose of this research (motor patterns over the motor cortex) we chose to use a common average referencing (CAR) performed using EEGLAB (Dien, 1998; Lei and Liao, 2017). The results were also visualized by applying a Laplacian filter and a Mastoidal re-referencing and confirmed those described below (Perrin et al., 1989). Then, EEG signals were resampled at 128 Hz and divided into 9 s epochs corresponding to 2 s before and 7 s after the motor task for each run. Finally, we removed the trials containing muscle artifacts that may have affected ERD/ERS modulations. For this purpose, we used the EMG electrode present throughout the experiment. We also eliminated trials which included ERDs and ERS outlayers (i.e., ERDs and ERSs that significantly exceeded the confidence interval for the same run). The number of trials deleted are described in the corresponding result section (see section 3.1).

2.6. Time-Frequency Analysis

To analyze the differences between all four conditions, we performed an event-related spectral perturbation (ERSP) analysis between 8 and 35 Hz using EEGLAB. We used a 256 point sliding fast Fourier transform (FFT) window with a padratio of 4 and computed the mean ERSP 2s before the task to 7 s after the task. ERSP allows to visualize event-related changes in the average power spectrum relative to a baseline of 1.5 s taken 2 s before the auditory cue for C1 and C2, and 2 s before stimulation for C3 and C4 (Brunner et al., 2013). A surrogate permutation test ($p < 0.05$; 2,000 permutations) from the EEGLAB toolbox was used to validate differences in terms of time-frequency of this ERSPs.

2.7. Topographies

Brain topography allowed us to display the possible changes over different electrodes on the scalp in order to localize which part of the brain was involved when the subject performed the requested task. In particular, it allowed us to understand how MI + MNS and MNS conditions can be discriminated and which time parameters we can choose to guide the classification. We have decided to compute ERSPs in a merged band (mu+beta, 8–30 Hz) for MI + MNS and MNS conditions (**Figure 5**). A surrogate permutation test ($p < 0.05$; 2,000 permutations) from the EEGLAB toolbox was used to validate differences in terms of localization of this ERSPs. In addition to this analysis, we applied a false discovery rate (FDR) correction test in order to clarify how the false discovery rate was controlled for multiple comparisons. This test consists of repetitively shuffling values between conditions and recomputing the measure of interest using the shuffled data. It was performed by drawing data samples without replacement and is considered suitable to

show the difference between MI + MNS and MNS conditions (Manly, 2006).

2.8. ERD/ERS Quantification

We compute the ERD/ERS% using the "band power method" (Pfurtscheller and Lopes da Silva, 1999).

$$ERD/ERS\% = \frac{\overline{x^2} - \overline{BL^2}}{\overline{BL^2}} \times 100, \quad (1)$$

where $\overline{x^2}$ is the average of the squared signal smoothed using a 250 ms sliding window with a 100 ms shifting step, $\overline{BL^2}$ is the mean of a baseline segment (1.5 s) taken 2 s before the auditory cue of the corresponding trial, and ERD/ERS% is the percentage of the oscillatory power estimated for each step of the sliding window. A positive ERD/ERS% indicates a synchronization whereas a negative ERD/ERS% indicates a desynchronization. This percentage was computed separately for all EEG channels. The EEG signal was filtered in the mu rhythm (7–13 Hz), in the beta band (15–30 Hz), and in the mu+beta band (8–30 Hz) for all subjects using a 4th-order Butterworth band-pass filter.

ERD and ERS are difficult to observe from the raw EEG signal. Indeed, an EEG signal expresses the combination of activities from many neuronal sources. We used the averaging technique to represent the modulation of power of the mu and beta rhythms during MI, MNS + MI, and MNS conditions (**Figure 6**) since it is considered one of the most effective and accurate techniques used to extract events (Pfurtscheller, 2003; Quiroga and Garcia, 2003).

2.9. Classification

The classification was performed for the following classes: RM vs. Rest, MI vs. Rest, and MI + MNS vs. MNS. For RM and MI conditions, each trial was segmented into a motor task time for classification during the RM or the MI task and a rest time for classification during the resting state, both lasting 2.5 s. The time-window of motor task started 0.5 s after the go signal for the MI activity (1st beep), and the rest time windows started 3 s before the go signal. For MI + MNS and MNS conditions, we selected a time window of 3 s starting 0.5 s before the median nerve stimulation for all trials of both conditions. The recorded EEG signals were bandpassed using a 5th-order Butterworth filter between 8 and 30 Hz. For each classes, we collected a total of 52 trials.

We computed the performance of four different classification methods in a 4-fold cross-validation scheme. The first one uses a Linear Discriminant Analysis classifier (LDA) trained and evaluated using Common Spatial Pattern (CSP) features generated from the first and last 4 CSP filters (Blankertz et al., 2008) (referred to as CSP+LDA). The CSP method is widely used in the field of MI-base BCI, as it provides a feature projection onto a lower dimensional space that minimizes the variance of one class while maximizing the variance of the other. The other three classifiers are Riemannian Geometry based classification methods. Riemannian geometry based methods work with the covariance matrices of each trial, which live on the Riemannian manifold of symmetric positive definite matrices. These features have therefore the advantage of being immune to linear transformations (Barachant et al., 2010) First, we used the covariance matrix of each trial and applied the Minimum Distance to Riemannian Mean algorithm (MDM) to classify them, as in Barachant et al. (2010). Since this method produces a high-dimensional feature space, we trained a second instance of the MDM algorithm using a spatially filtered signal. The signal was, once more, generated using the first and the last 4 CSP filters. Finally, we computed the Riemannian barycenter of all covariance matrices in the dataset, and projected them onto the tangent space at that point. Then, since the tangent space is a Euclidean space, we trained and used a Linear Regression classifier (TS+LR). We chose to apply a paired t-test (two-sided) to show the significant difference about accuracy obtained for MI vs. Rest and MI + MNS vs. Rest with the TS + LR classifier (**Figure 8**, p-value < 0.01).

2.10. Software

Signal recording (EEG and EMG), synchronization/control of the median nerve stimulator and sound beep generation was designed with OpenViBE software (Renard et al., 2010). Data processing and analysis of ERD/ERS modulations were performed using MATLAB 2015b (MathWorks, Inc., Natick, MA, United States). All the classification algorithms were performed using the same computer and same software, making use of the Scikit Learn Python 2.7 machine learning package (Pedregosa et al., 2011).

3. RESULT

3.1. Behavioral result

Behavioral result includes two reaction times for the real movement between the auditory cues (first and second beep) and the subsequent motor task (pressing or releasing the button). It also includes the number of trial rejected because of acquisition artifacts.

3.1.1. Reaction Time

For the Real Movement condition, the reaction time between the first beep and the movement start was 0.5948 s $\pm$ 0.1929. The reaction time between the second beep and the movement stop was 0.5038 s $\pm$ 0.1174. These two reaction times can be considered as normal in the light of the literature on this domain (Jain et al., 2015).

3.1.2. Removing Trials

For each condition, 832 trials were acquired (52 for each subject). Due to the presence of artifacts acquired during the experiment, we used an artifact rejection script to remove the most important ones. We removed 125 (15%) trials for the RM condition, 119 trials (14,3%) for the MI condition, 114 trials (13,7%) for the MNS condition, 138 trials (16,6%) for the MI+MNS condition. The removed artifacts are homogeneously distributed among the subjects.

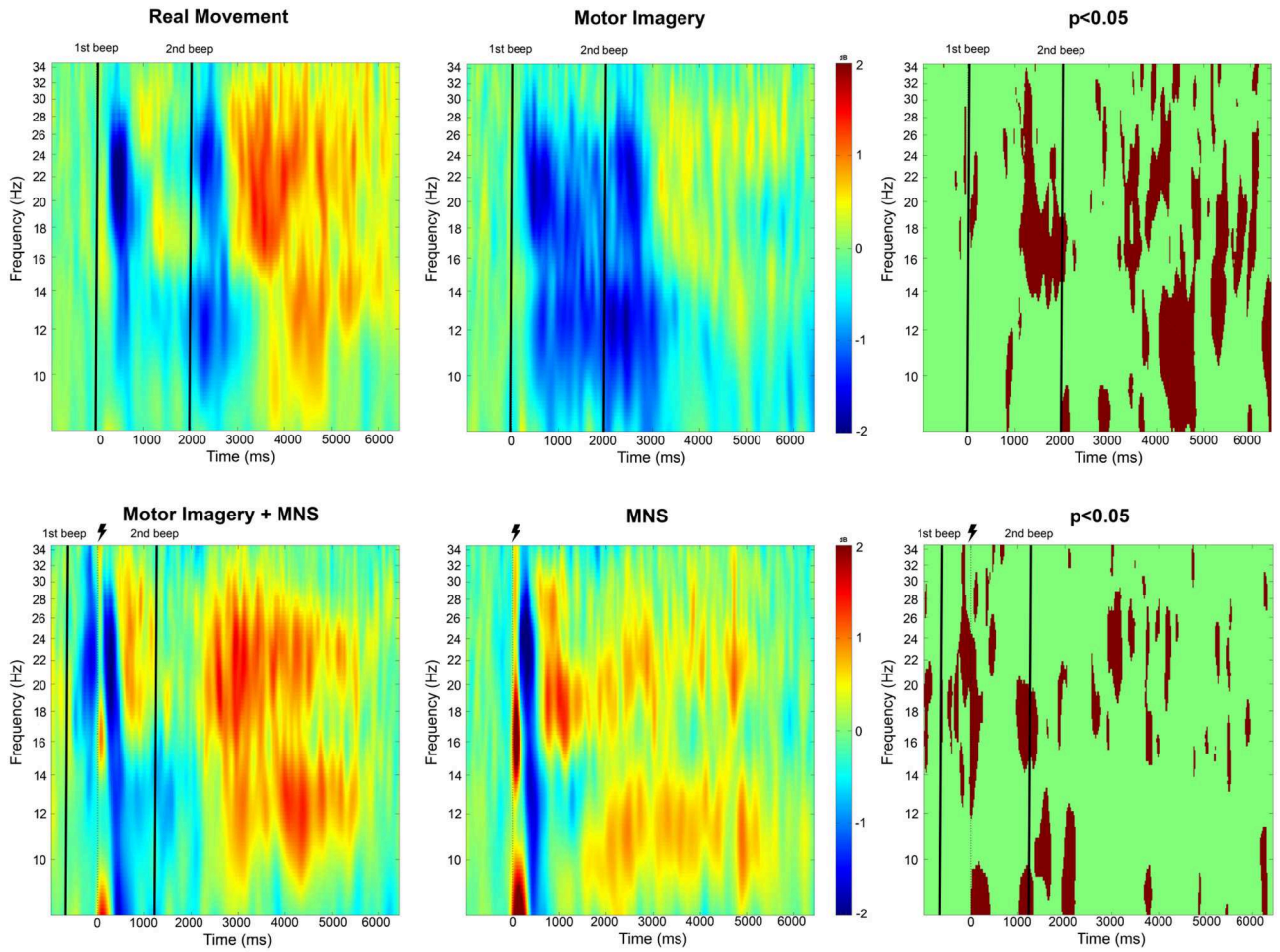

FIGURE 4 | Time-frequency grand average analysis (ERSP) for Real movement, Motor Imagery, Motor Imagery + MNS, and MNS conditions for electrode C_3. A black line indicates when the motor task started and finished. A flash picture indicates when the median nerve stimulation started. A red color corresponds to a strong ERS and a blue one to a strong ERD. Significant difference ($p < 0.05$) are shown in the final part of the figure.

3.2. Time frequency

The time-frequency maps display the signal's power evolution and are useful to establish the frequency and time windows in which ERSP appears (**Figure 4**).

3.2.1. Real Movement and Motor Imagery

For the Real Movement condition (C1), we can observe two separate ERDs during the motor task in both mu (7–13Hz) and beta (15–30Hz) band (**Figure 4**). In the beta band, the first ERD starts 300 ms after the auditory cue and switches to an ERS 1 s later. The second ERD appears after the end-of-task beep and disappears 750 ms later. In the mu frequency band, instead of an ERS there is only a slight decrease of the desynchronization. A post-movement beta rebound (PMBR) arises in the beta band and shortly after in the mu band.

Throughout the Motor Imagination condition (C2), a continuous ERD occurs in both mu and beta band (**Figure 4**). It starts 300 ms after the auditory cue and lasts 1,200 ms after the end-of-task beep. The statistical comparison ($p < 0.05$) shows a significant difference between the MI constant ERD and the RM interrupting ERS. Additionally after the motor task in C1, there is an ERS in the mu band which doesn't exist for C2. Finally, PMBR for MI seems weaker than the rebound for RM.

3.2.2. Median Nerve Stimulation During Motor Imagery

In the case of median nerve stimulation (MNS) during rest state (C3), a powerful and robust ERS appears immediately (0–250 ms) after the stimulation in low mu (7–10 Hz) and low beta (15–22 Hz) (**Figure 4**). For the rest of this article, this very first ERS will be named post-stimulation rebound (PSR). Then, the MNS generates an ERD (first in high beta) lasting 500 ms followed by a second rebound in both bands. MI + MNS is characterized by the presence of an pre-stimulation ERD. Interestingly, the PSR is almost nonexistent in this condition ($p < 0.05$) but the ERD (250–500 ms after the MNS) is very similar. The MNS-generated beta rebound appears less powerful than the one from C3 and, instead of a return to baseline, a continuous mu ERD last until

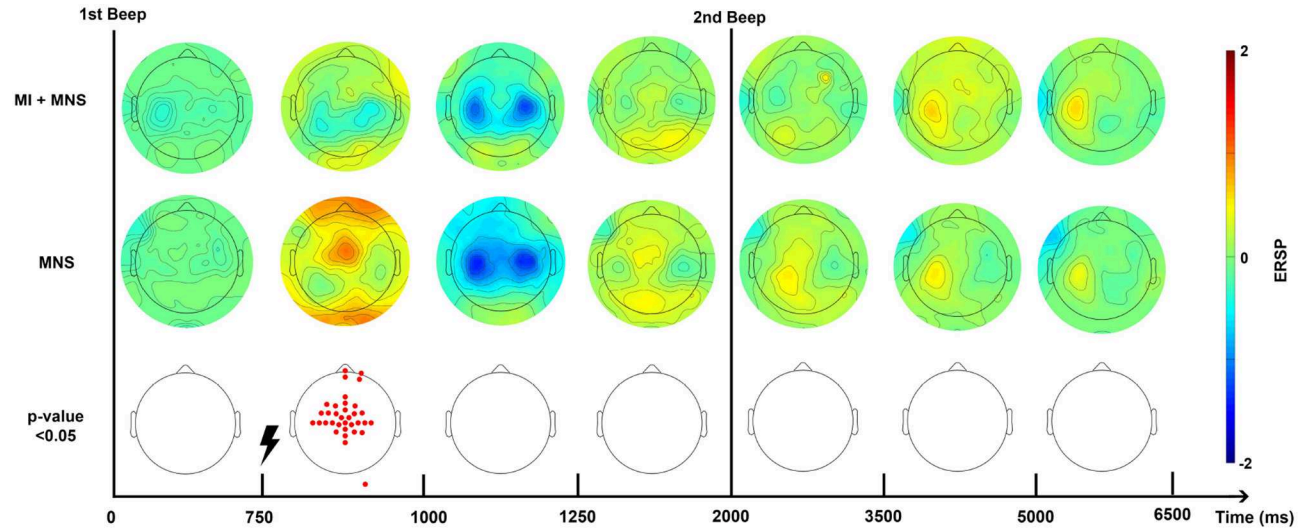

FIGURE 5 | Topographic map of ERD/ERS% (grand average, $n = 16$) in the alpha/mu+beta band during two conditions: MI + MNS and MNS only. A red color corresponds to a strong ERS and a blue one to a strong ERD. A black line indicates when the motor imagery started or finished for the MI + MNS condition. Red electrodes indicate a significant difference between the two conditions ($p < 0.05$).

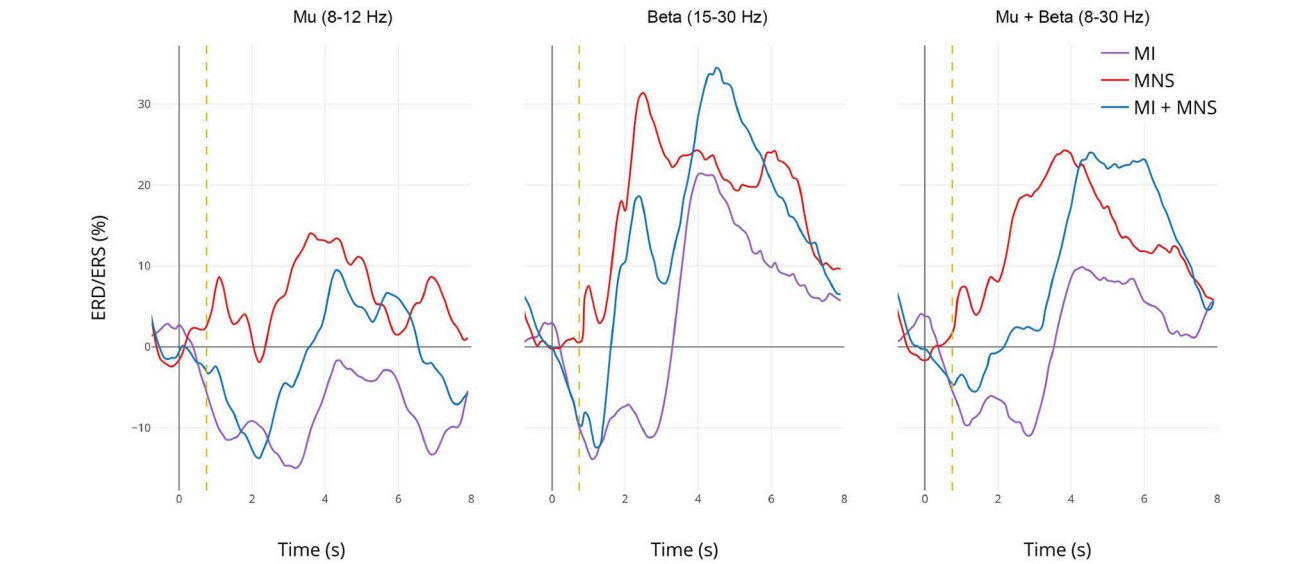

FIGURE 6 | Grand average ($n = 16$) ERD/ERS% curves in the mu (7–13 Hz), the beta (15–30 Hz), and the mu+beta (8–30 Hz) bands for MI (in violet), MI + MNS (in blue), and MNS (in red) conditions for electrode C_3. The yellow bar at 750 ms corresponds to the median nerve stimulation performed. For the MI and MI + MNS conditions, the MI starts at 0 s and ends at 2 s.

the end of the motor task. Finally a third rebound appears in both frequency bands 1,200 ms after the motor task.

3.3. Topographic Map

Analysis of these time-frequencies maps showed that both mu (7–13 Hz) and beta (15–30 Hz) bands were impacted in term of synchronization/desynchronization in all four conditions. Since the previous results for C1 and C2 are consistent with the literature and the purpose of this study is to discriminate C3 and C4, we will only look into the last two conditions. Consequently, a larger frequency band (8–30Hz) was chosen to analyse the ERD and ERS localization. **Figure 5** shows that the MNS doesn't have the same impact depending of the subject being in a rest or MI state. Indeed, 250 ms after the MNS there is a significant difference on several electrodes in term of PSR (mostly on motor, pre-motor, and sensorimotor areas both central and bilateral). A bilateral ERD appears for both condition 500 ms after the MNS followed by a beta rebound slightly diminished for the MI + MNS condition than for MNS only.

According to this **Figure 5**, and in the views of discriminating these two conditions, we distinguished a promising time window which should start just before the MNS and stop after the end-of-task beep. For the MI + MNS condition, this time window includes the (i) pre-stimulation MI-generated ERD, (ii) the abolished PSR, and (iii) the diminished MNS-generated beta rebound.

3.4. ERD and ERS modulation

In accordance with the results obtained from the time-frequency and topographic analyses, the ERD and ERS modulations have been computed for three frequency bands, mu: 8–12 Hz, beta: 15–30 Hz and mu+beta band: 8–30 Hz for all subjects. The **Figure 6** represents the grand average of all subjects for the C3 electrode.

3.4.1. Mu band

In the mu frequency band, a desynchronization appears and reaches –15% during both MI task (C2 in purple and C4 in blue during 0–2,000 ms). This observation confirms that the ERD created by the MI task isn't impacted by the following MNS (besides the slight PSR in C4) in the mu band. Logically, this desynchronization doesn't exist for the MNS condition. After the motor task, a slight rebound appears for MNS and MI + MNS condition.

3.4.2. Beta Band

The ERD in the beta frequency band behaves similarly to the ERD in the mu band, only C2 and C4 display this desynchronization. However, during MI + MNS, the ERD is shorter (1,700 ms) than the one in MI only. Logically, during C3 no ERD appears. As seen on the topography and time-frequency figures, an ERS appears for all conditions 3 and 4 after the stimulation. This ERS is partially diminished for MI + MNS but is followed by a stronger post-motor task rebound (33% at 4,500 ms), also present for C2.

3.4.3. Mu+Beta Band

If we merge the two frequency bands, the behavior of ERD and ERS is particularly interesting since the difference between condition 3 and 4 is strong on a 0–3,000 ms time window. On the same note, after 3,000 ms, the condition 3 ERS starts to disappear but the MI + MNS ERS keeps a level of 24%. Those results highlight the interest of the 8-30Hz frequency band if we seek to discriminate C3 and C4.

3.5. Classification

In order to verify that a MNS is useful as a trigger to detect a movement intention, we decided to compare the classification score obtained for the traditional MI vs Rest class and our MI + MNS vs. MNS class.

We pre processed our data in the following manner: (a) the frequency band is restricted to 8–30Hz; (b) we consider only the premotor frontocentral, primary motor cortex, and somatosensorial central and occipital electrodes; and (c) the classification time window is [–0.5 to 2.5 s] for MI+MNS vs. MNS, [0.5–3 s] for MI vs. Rest. These values are based on the existing literature for MI-based BCI. The average classification accuracies between a MI and a rest period, and between MI + MNS and MNS were computed for 4 different classifiers (MDRM, CSP+LDA, FgMDRM, TS+LR, see **Figure 7**). TS+LR gave the best results for both classifications, which was not an unexpected result. Indeed, this classification method combines the invariance properties of Riemannian Geometry-based methods and the well-established linear regression method. For the rest of the results, we only use the output of the TS+LR classification method.

Figure 8 shows that a MI + MNS vs. MNS classification allows better accuracies than a MI vs. Rest classification, and proves that a MNS can be used as a trigger and improves MI detection.

Individual classification shows a greater classification performance with MNS for 14 subjects (**Figure 9**). Only subject 3 and subject 13 shows better performance for a MI vs. Rest classification, but the results don't exceed 60%.

DISCUSSION

This work confirmed that median nerve stimulation indeed generates ERD and ERS in the motor cortex. When the median nerve is stimulated during an intention of movement, those ERD and ERS are significantly impacted. Based on these differences, we confirmed that a classifier is able to discriminate a stimulation during a rest state from a stimulation during an intention of movement. Our results show that the TS+LR classifier performs better for the two conditions involving a MNS, in comparison to the typical discrimination task between rest state and MI state. This confirms the feasibility of implementing a MNS-based BCI to detect intraoperative awareness. In this section we discuss the consistency of the ERD and ERS modulation for all our conditions, including the MNS impact on MI, the benefits of our classifier and how our work could be used in the intraoperative awareness situation.

ERD/ERS Modulations During a Real Movement and a Motor Imagery

According to Erbil's work (Erbil and Ungan, 2007), maintaining a real movement creates an ERS. This would explain the results obtained in **Figure 4**, showing two distinct ERDs separated by an ERS during the real movement task. During the MI task, a continuous ERD is observed (**Figures 4**, **6**) which suggests that the subjects applied the instruction of maintaining the MI during 2 s. The continuous ERD and the weaker post-MI ERS, in comparison with the post-RM ERS, are consistent with the findings of several articles (Pfurtscheller and Neuper, 1997, 2001; Neuper and Pfurtscheller, 2001; Filgueiras et al., 2017). In addition, a previous study showed that a closed-eyed condition generated a stronger ERD in the mu band (Rimbert et al., 2018).

ERD/ERS Modulations During a Median Nerve Stimulation

Our results showed that MNS modulates the ERD and ERS in the EEG signal from the motor cortex. More precisely, MNS produces a first PSR (**Figure 4**) which is visible in all subjects (not presented in this article). This PSR was not mentioned in the very few articles that discussed this topic (Salenius et al., 1997; Neuper and Pfurtscheller, 2001) and could be interpreted as an

	RM vs Rest	MI vs Rest	MI + MNS vs MNS
MDM	74.4	69.1	76.6
CSP+LDA	74.2	68	74
CSP+MDM	73.9	70.8	77.2
TS+LR	**76.7**	**70.5**	**82.03**

FIGURE 7 | Grand average accuracies obtained by 4 differents classifiers (MDM, CSP + LDA, CSP + MDM, TS + LR) for the 3 conditions (RM, MI and MI + MNS) in the mu + beta band (8–30 Hz).

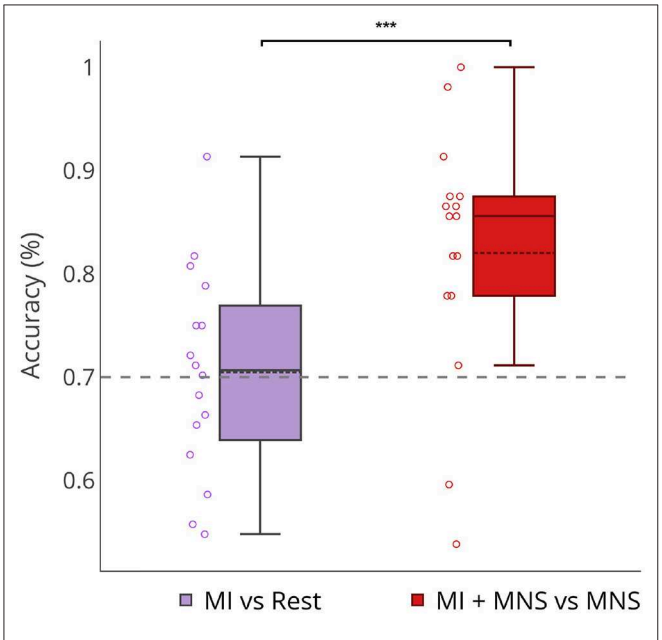

FIGURE 8 | Boxplots showing the distribution of average classification accuracies (n = 16) for MI vs Rest and MI + MNS vs. MNS class. ***p-value < 0.001.

attention marker (Saleh et al., 2010). Five hundred milliseconds after the MNS, a strong ERD appears in the mu and beta band and had already been mentioned by Salenius in the beta band for MEG (Salenius et al., 1997) and by Neuper in both bands for EEG (Neuper and Pfurtscheller, 2001).

Impact of a Median Nerve Stimulation During a MI

Several articles have already shown that performing a MI during median nerve stimulation has an impact on motor patterns previously generated by MNS (Salenius et al., 1997; Schnitzler et al., 1997; Neuper and Pfurtscheller, 2001). Our results confirm that the intention to move tends to modify the ERD/ERS normally present during a single MNS. Indeed, the PSR is almost abolished during the MI (**Figure 4**). In contrast, the post-stimulation ERD is unchanged while the second ERS tends to be decreased as already shown in the literature (Neuper and Pfurtscheller, 2001). Interestingly, our results indicate that the mu band (500–1,400 ms) is unaffected by the MNS effect, which suggests a functional difference between the two frequency bands. Finally, the post MI rebound is stronger than in MI condition alone, which implies a rebound additive phenomenon.

Median Nerve Stimulation As an Innovative Trigger for Intraoperative Awareness Detection

Intraoperative awareness is an uncertain phenomenon. There is no absolute way to predict when it will occur (Pandit et al., 2014). However, several studies have shown that moving is a patient's first reflex to warn about his awakening (Ghoneim et al., 2009). Theoretically, if a BCI could detect a patient's intention of movement during his awakening, it would need to use classification without any trigger, since it's impossible to know the moment when the patient tries to move. While there exist some BCIs that do not use time markers or triggers (known as asynchronous BCIs), the literature clearly shows that their classification rate is lower than that of a synchronous BCI with triggers (Nicolas-Alonso and Gomez-Gil, 2012).

Our results show a performance of 70% for MI vs Rest classification with a trigger. In the absence of this trigger these results would be weaker (**Figure 8**). On the other hand, our MI+MNS vs. MNS classification displays accuracy results of 80%. This method brings about the possibility of a more efficient way to detect intraoperative awareness.

According to our results, we can imagine a routine system where the patient would be stimulated at the median nerve (e.g., every 5 s), while a passive BCI device would analyze the ERD and ERS modulations of the motor cortex to see if the patient intends to move or not. In case of such BCI could detect a modulation suggesting an intention of movement, the anesthesiologist could therefore adjust the doses of anesthetics.

Perspectives

Getting Closer to the Anesthetized State

Our study was conducted on non-anesthetized subjects, and as shown by Blokland et al., we can expect some difference in the cerebral activity behavior once propofol is used (Blokland et al., 2016). Our results will be confirmed during a clinical protocol where the same conditions will be used on voluntary anesthetized subject. If we can find similar results on anesthetized subject, we also plan to repeat the experimentation on subjects with induced neuromusclar blockade in order to study real movement intention instead of motor imagination. A final experiment we could combine both condition with paralyzed and anesthetized patient in order to investigate if the combination could change the results.

Getting Closer to the Implementation

Another perspective we are interested in is to create a new way to classify our data online. We need to have an easy-to-implement classification pipeline in order to make this hypothetical device as practical to use as possible. One of the most important parts of a BCI pipeline is the calibration of the pre-processing and

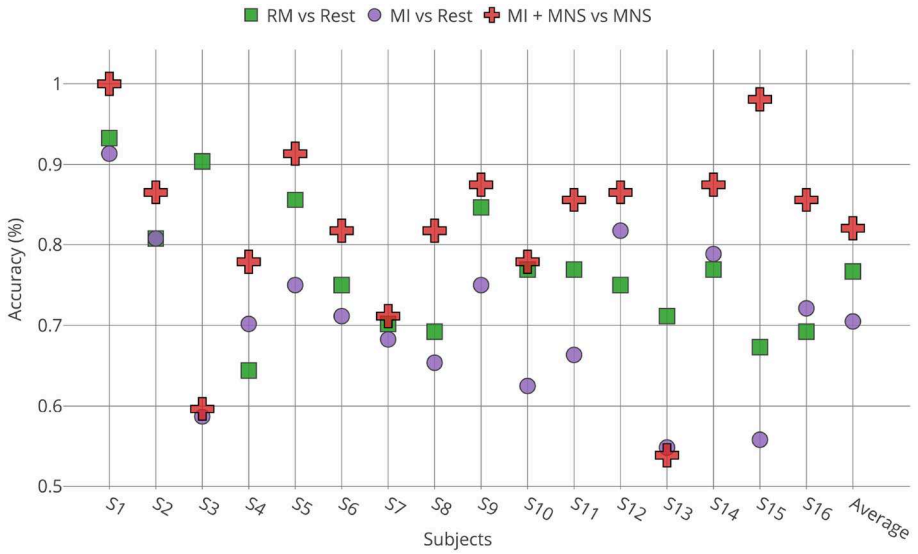

FIGURE 9 | Accuracies obtained for all subjects (n = 16) by TS + LR analyses in the 8–30 Hz for the 3 conditions (RM, MI and MI + MNS).

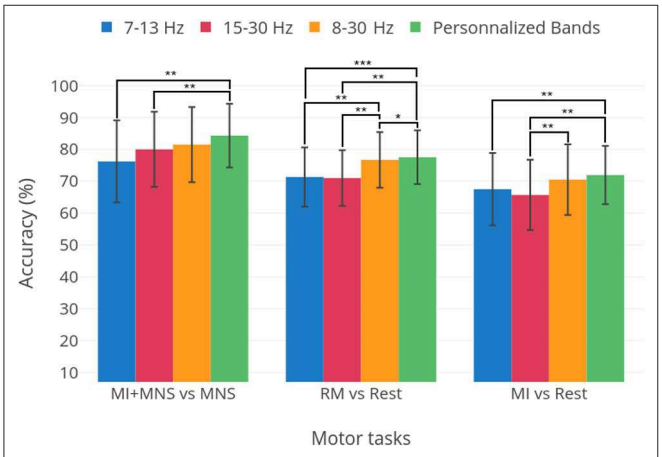

FIGURE 10 | Average performances and standard deviation for thee classification tasks: MI+MNS vs. MNS, RM vs. Rest, and MI vs. Rest. The three first bars show the results obtained for the 7–130, 15–30, and 8–30 Hz frequency bands. The fourth bar labeled "Personalized bands" is the average and standard deviation of results when the best frequency band for each subject is chosen, i.e., the frequency band yielding the highest performance. Statistical significances are displayed as well, obtained in a student's t-test. The classifier is the TS+LR, described in section 2.9. *p-value < 0.05, **p-value < 0.01, ***p-value < 0.001.

classification parameters. It is clear that in this application, calibration data from the same user can be difficult to obtain. A thorough analysis of existing datasets, such as leave-one-subject-out analyses could enable us to determine pre-processing parameters, including the optimal frequency bands or the number of electrodes required to obtain good results.

A preliminary analysis, presented in **Figure 10** shows the optimal results for each patient for three frequency bands: μ, β and 8–30 Hz. These results are compared to selecting a single frequency band for all subjects. We see that, although for a fixed frequency band selection, the 8–30 Hz range is the apparent best choice, it is clear that personalizing the choice of a frequency band yields better results. This warrants the use of methods that improve classification accuracy by adapting the classification pipeline to each subject (Ang et al., 2012; Duprès et al., 2016). Nevertheless, our results indicate that the difference is not significant for the MI vs Rest and MI+MNS vs MNS classifications ($p < 0.05$). Moreover, the implementation of methods that depend on data coming from the same BCI session might be hard to implement in clinical settings.

In future works, we intend to address such issue by using transfer learning approaches such as Riemannian geometry based methods (Rodrigues et al., 2018) or optimal transport based methods (Gayraud et al., 2017). Indeed, transfer learning has proven to be very effective in designing BCIs with little or no calibration for a new user (Lotte, 2015).

Finally, one last thing we wish to study is the impact of MNS at various times during a MI task. In this study we stimulated our subjects at the same time for the entire experimentation (750 ms after the MI task start), but in a real surgery, the MNS would intervene at different times and the cerebral activity could be modulated differently.

CONCLUSION

In this study, we verified that median nerve stimulation modulates the motor cortex by first generating an ERD during stimulation and then an ERS post-stimulation. In addition, we discovered a new Post-Stimulation Rebound ERS which appears 250 ms after the stimulation in the mu and low beta band. Median nerve stimulation combined with the intention to move, i.e., the MI, has a significant impact on the ERD

and ERS generated by the MNS. Indeed, despite the fact that the ERD was unaltered, the PSR is almost abolished and the rebound in the beta band is diminished. Those differences have resulted into a high accuracy classification. With these findings, we show that a BCI based on MNS is more effective than a BCI based on a MI state vs. rest. This innovative approach may improve the detection of intraoperative awareness during general anesthesia.

ETHICS STATEMENT

This study was carried out in accordance with the recommendations of COERLE ethic committee of INRIA with written informed consent from all subjects. All subjects gave written informed consent in accordance with the Declaration of Helsinki. The protocol was approved by the COERLE ethic committee.

AUTHOR CONTRIBUTIONS

SR and PR conceived, designed, and performed the experiments. SR, PR, NG, DS, and LB analyzed the data, contributed reagents, materials, analysis tools, prepared figures and/or tables, authored or reviewed drafts of the paper, approved the final draft.

FUNDING

This research was supported by the Inria Project Lab BCI Lift.

ACKNOWLEDGMENTS

The authors thank Johann Benerradi, Charles-Antoine Robert and Guy-Junior Richard for help during the experiments. We also wish to give our thanks to all the participants.

REFERENCES

Absalom, A., Gien, J., Zwart, G., Schnider, T., and Struys, M. (2016). Target-controlled infusion: a mature technology. *Anesth. Analg.* 122, 70–78. doi: 10.1213/ANE.0000000000001009

Almeida, D. (2015). Awake and unable to move: what can perioperative practitioners do to avoid accidental awareness under general anesthesia? *J. Perioper. Pract.* 25, 257–261. doi: 10.1177/175045891502501202

Ang, K. K., Chin, Z. Y., Wang, C., Guan, C., and Zhang, H. (2012). Filter bank common spatial pattern algorithm on bci competition iv datasets 2a and 2b. *Front. Neurosci.* 6:39. doi: 10.3389/fnins.2012.00039

Avidan, M. S., and Mashour, G. A. (2013). II. The incidence of intraoperative awareness in the uk: under the rate or under the radar? *Br. J. Anaesth.* 110, 494–497. doi: 10.1093/bja/aet012

Avidan, M. S., Zhang, L., Burnside, B. A., Finkel, K. J., Searleman, A. C., Selvidge, J. A., et al. (2008). Anesthesia awareness and the bispectral index. *New Engl. J. Med.* 358, 1097–1108. doi: 10.1056/NEJMoa0707361

Barachant, A., Bonnet, S., Congedo, M., and Jutten, C. (2010). "Riemannian geometry applied to bci classification," in *International Conference on Latent Variable Analysis and Signal Separation* (Saint-Malo: Springer), 629–636.

Bischoff, P., and Rundshagen, I. (2011). Awareness under general anesthesia. *Dtsch. Arztebl. Int.* 108, 1–7. doi: 10.3238/arztebl.2011.0001

Blankertz, B., Tomioka, R., Lemm, S., Kawanaba, M., and Müller, K. (2008). Optimizing spatial filters for robust EEG single-trial analysis. *IEEE Signal Process. Mag.* 25, 41–56. doi: 10.1109/MSP.2008.4408441

Blokland, Y., Farquhar, J., Lerou, J., Mourisse, J., Scheffer, G. J., van Geffen, G.-J., et al. (2016). Decoding motor responses from the EEG during altered states of consciousness induced by propofol. *J. Neural Eng.* 13:026014. doi: 10.1088/1741-2560/13/2/026014

Brunner, C., Delorme, A., and Makeig, S. (2013). EEGLAB - an open source matlab toolbox for electrophysiological research. *Biomed. Tech.* 58, 9–21. doi: 10.1515/bmt-2013-4182

Clerc, M., Bougrain, L., and Lotte, F. (2016). "EEG feature extraction," in *Brain-Computer Interfaces, Vol. 1, Foundations and Methods* (Hoboken, NJ: John Wiley & Sons), 130–131.

Delorme, A., and Makeig, S. (2004). EEGLAB: an open source toolbox for analysis of single-trial EEG dynamics including independent component analysis. *J. Neurosci. Methods* 134, 9–21. doi: 10.1016/j.jneumeth.2003.10.009

Dien, J. (1998). Issues in the application of the average reference: review, critiques, and recommendations. *Behav. Res. Methods* 30, 34–43.

Duprès, A., Cabestaing, F., and Rouillard, J. (2016). "Human expert supervised selection of time-frequency intervals in EEG signals for brain-computer interfacing," in *2016 24th European Signal Processing Conference (EUSIPCO)* (Budapest: IEEE), 1733–1737.

Erbil, N., and Ungan, P. (2007). Changes in the alpha and beta amplitudes of the central EEG during the onset, continuation, and offset of long-duration repetitive hand movements. *Brain Res.* 1169, 44–56. doi: 10.1016/j.brainres.2007.07.014

Filgueiras, A., Quintas Conde, E., and Hall, C. (2017). The neural basis of kinesthetic and visual imagery in sports: an ale meta-analysis. *Brain Imaging Behav.* 12, 1513–1523. doi: 10.1007/s11682-017-9813-9

Gayraud, N. T., Rakotomamonjy, A., and Clerc, M. (2017). "Optimal transport applied to transfer learning for p300 detection," in *BCI 2017-7th Graz Brain-Computer Interface Conference* (Graz), 6.

Ghoneim, M. M., Block, R. I., Haffarnan, M., and Mathews, M. J. (2009). Awareness during anesthesia: risk factors, causes and sequelae: a review of reported cases in the literature. *Anesth Analg.* 108, 527–535. doi: 10.1213/ane.0b013e318193c634

Guillot, A., Collet, C., Nguyen, V. A., Malouin, F., Richards, C., and Doyon, J. (2009). Brain activity during visual versus kinesthetic imagery: an fMRI study. *Hum. Brain Mapp.* 30, 2157–2172. doi: 10.1002/hbm.20658

Hashimoto, Y., and Ushiba, J. (2013). EEG-based classification of imaginary left and right foot movements using beta rebound. *Clin. Neurophysiol.* 124, 2153–2160. doi: 10.1016/j.clinph.2013.05.006

Hendin, H. (1991). Suicide and guilt as manifestations of ptsd in vietnam combat veterans. *Am. J. Psychiatry* 148, 586–591. doi: 10.1176/ajp.148.5.586

Jain, A., Bansai, R., Kumar, A., and Singh, K. (2015). A comparative study of visual and auditory reaction times on the basis of gender and physical activity levels of medical first year students. *Int. J. Appl. Basic Med. Res.* 5, 124–127. doi: 10.4103/2229-516X.157168

Jonathan Wolpaw, E. W. W. (ed.). (2012). *Brain-Computer Interfaces: Principles and Practice*. Oxford; New York, NY: Oxford University Press.

Kent, C., and Domino, K. (2009). Depth of anesthesia. *Curr. Opin. Anaesthesiol.* 22, 782–787. doi: 10.1097/ACO.0b013e3283326986

Kilavik, B. E., Zaepffel, M., Brovelli, A., MacKay, W. A., and Riehle, A. (2013). The ups and downs of beta oscillations in sensorimotor cortex. *Exp. Neurol.* 245, 15–26. doi: 10.1016/j.expneurol.2012.09.014

Kumbhare, D., Robinson, L., and Buschbacher, R. (2016). "Mediane nerve to the abductor pellicis brevis," in *Buschbacher's Manual of Nerve Conduction Studies, 3rd Edn* (New York, NY: Demos Medical Publishing), 10.

Lau, K., Matta, B., Menon, D., and Absalom, A. (2006). Attitudes of anaesthetists to awareness and depth of anaesthesia monitoring in the UK. *Eur. J. Anaesthesiol.* 23, 921–930. doi: 10.1017/S0265021506000743

Lei, X., and Liao, K. (2017). Understanding the influences of eeg reference: a large-scale brain network perspective. *Front. Neurosci.* 11:205. doi: 10.3389/fnins.2017.00205

Leslie, K., Chan, M., Myles, P., Forbes, A., and McCulloch, T. (2010). Posttraumatic stress disorder in aware patients from the b-aware trial. *Anesth. Analg.* 110, 823–828. doi: 10.1213/ANE.0b013e3181b8b6ca

Li, X., Cui, S., and Voss, L. (2008). Using permutation entropy to measure the electroencephalographic effects of sevoflurane. *Anesthesiology* 109, 448–456. doi: 10.1097/ALN.0b013e318182a91b

Liang, Z., Wang, Y., Sun, X., Li, D., Voss, L. J., Sleigh, J. W., et al. (2015). Eeg entropy measures in anesthesia. *Front. Comput. Neurosci.* 9:16. doi: 10.3389/fncom.2015.00016

Lotte, F. (2015). Signal processing approaches to minimize or suppress calibration time in oscillatory activity-based brain–computer interfaces. *Proc. IEEE* 103, 871–890. doi: 10.1109/JPROC.2015.2404941

MacGregor, K. (2013). A waking nightmare: how can we avoid accidental awareness during general anaesthesia? *J. Perioper. Pract.* 23, 185–190. doi: 10.1177/175045891302300902

Manly, B. (2006). "The generation of random permutations," in *Randomization, Bootstrap and Monte Carlo Methods in Biology* (Boca Raton, FL: Chapman & Hall/CRC).

Mashour, G., and Avidan, M. (2015). Intraoperative awareness: controversies and non-controversies. *Br. J. Anaesth.* 115, 20–26. doi: 10.1093/bja/aev034

Mashour, G., Orser, B., and Avidan, M. (2011). Intraoperative awareness: from neurobiology to clinical practice. *Anesthesiology* 114, 1218–1233. doi: 10.1097/ALN.0b013e31820fc9b6

Mihai, R., Scott, S., and Cook, T. (2009). Litigation related to inadequate anaesthesia: an analysis of claims against the NHS in england 1995-2007. *Anaesthesia* 64, 829–835. doi: 10.1111/j.1365-2044.2009.05912.x

Monk, T., and Weldon, B. (2011). Does depth of anesthesia monitoring improve postoperative outcomes? *Curr. Opin. Anesthesiol.* 24, 665–669. doi: 10.1097/ACO.0b013e32834c7acf

Myles, P., Leslie, K., McNeil, J., Forbes, A., and Chan, M. (2004). Bispectral index monitoring to prevent awareness during anaesthesia: the b-aware randomised controlled trial. *Lancet* 363, 1757 – 1763. doi: 10.1016/S0140-6736(04)16300-9

Neuper, C., and Pfurtscheller, G. (2001). Event-related dynamics of cortical thythms: frequency-specific features and functional correlates. *Int. J. Psychophysiol.* 43, 41–58. doi: 10.1016/S0167-8760(01)00178-7

Nicolas-Alonso, L., and Gomez-Gil, J. (2012). Brain computer interfaces, a review. *Sensors* 12, 1211–1279. doi: 10.3390/s120201211

Osterman, J. E., Hopper, J., Heran, W. J., Keane, T. M., and van der Kolk, B. A. (2001). Awareness under anesthesia and the development of posttraumatic stress disorder. *Gen. Hosp. Psychiatry* 23, 198–204. doi: 10.1016/S0163-8343(01)00142-6

Pandit, J., and Cook, T. (2013). National institute for clinical excellence guidance on measuring depth of anaesthesia: limitations of eeg-based technology. *Br. J. Anaesth.* 110, 325–328. doi: 10.1093/bja/aet006

Pandit, J. J., Andrade, J., Bogod, D. G., Hitchman, J. M., Jonker, W. R., Lucas, N., et al. (2014). 5th national audit project (NAP5) on accidental awareness during general anaesthesia: summary of main findings and risk factors. *Br. J. Anaesth.* 113, 549–559. doi: 10.1111/anae.12826

Pedregosa, F., Varoquaux, G., Gramfort, A., Michel, V., Thirion, B., Grisel, O., et al. (2011). Scikit-learn: machine learning in Python. *J. Mach. Learn. Res.* 12, 2825–2830.

Perrin, F., Pernier, J., Betrand, O., and Echallier, J. (1989). Spherical splines for scalp potential and current density mapping. *Electroencephalogr. Clin. Neurophysiol.* 72, 184–187. doi: 10.1016/0013-4694(89)90180-6

Pfurtscheller, G. (2003). Induced oscillations in the alpha band: functional meaning. *Epilepsia* 44, 2–8. doi: 10.1111/j.0013-9580.2003.12001.x

Pfurtscheller, G., and Lopes da Silva, F. H. (1999). Event-related EEG/MEG synchronization and desynchronization: basic principles. *Clin. Neurophysiol.* 110, 1842–1857. doi: 10.1016/S1388-2457(99)00141-8

Pfurtscheller, G., and Neuper, C. (1997). Motor imagery activates primary sensorimotor area in humans. *Neurosci. Lett.* 239, 65–68. doi: 10.1016/S0304-3940(97)00889-6

Pfurtscheller, G., and Neuper, C. (2001). Motor imagery and direct brain-computer communication. *Proc. IEEE* 89, 1123–1134. doi: 10.1109/5.939829

Pomfrett, C. (1999). Heart rate variability, BIS and 'depth of anaesthesia'. *Br. J. Anaesth.* 82, 659–662. doi: 10.1093/bja/82.5.659

Punjasawadwong, Y., Phongchiewboon, A., and Bunchungmongkol, N. (2014). Bispectral index for improving anaesthetic delivery and postoperative recovery. *Cochrane Database Syst. Rev.* 17:CD003843. doi: 10.1002/14651858.CD003843.pub3

Quiroga, R., and Garcia, H. (2003). Single-trial event-related potentials with wavelet denoising. *Clin. Neurophysiol.* 114, 376–390. doi: 10.1016/S1388-2457(02)00365-6

Renard, Y., Lotte, F., Gibert, G., Congedo, M., Maby, E., Delannoy, V., et al. (2010). Openvibe: an open-source software platform to design, test and use brain-computer interfaces in real and virtual environments. *Presence* 10, 35–53. doi: 10.1162/pres.19.1.35

Rimbert, S., Al-Chwa, R., Zaepffel, M., and Bougrain, L. (2018). Electroencephalographic modulations during an open- or closed-eyes motor task. *PeerJ* 6:e4492.doi: 10.7717/peerj.4492

Rodrigues, P. L. C., Jutten, C., and Congedo, M. (2018). Riemannian procrustes analysis: Transfer learning for brain-computer interfaces. *IEEE Trans. Biomed. Eng.* doi: 10.1109/TBME.2018.2889705. [Epub ahead of print]

Saleh, M., Reimer, J., Penn, R., Ojakangas, C., and Hatsopoulos, N. (2010). Fast and slow oscillations in human primary motor cortex predict oncoming behaviorally relevant cues. *Neuron* 65, 461–471. doi: 10.1016/j.neuron.2010.02.001

Salenius, S., Schnitzler, A., Salmelin, R., Jousmäki, V., and Hari, R. (1997). Modulation of human cortical rolandic rhythms during natural sensorimotor tasks. *Neuroimage* 5, 221–228. doi: 10.1006/nimg.1997.0261

Schafer, S. L., and Stanski, D. R. (2008). Defining depth of anesthesia. *Handb. Exp. Pharmacol.* 409–423. doi: 10.1007/978-3-540-74806-9_19

Schneider, G., Mappes, A., Neissendorfer, T., Schabacker, M., Kuppe, H., and Kochs, E. (2004). Eeg-based indices of anaesthesia: correlation between bispectral index and patient state index? *Eur. J. Anaesthesiol.* 21, 6–12. doi: 10.1097/00003643-200401000-00002

Schnitzler, A., Salenius, S., Salmelin, R., Jousmaki, V., and Hari, R. (1997). Involvement of primary motor cortex in motor imagery: a neuromagnetic study. *Neuroimage* 6, 201–208. doi: 10.1006/nimg.1997.0286

Schuller, P., Newell, S., Strickland, P., and Barry, J. (2015). Response of bispectral index to neuromuscular block in awake volunteers. *Br. J. Anaesth.* 115, 95–103. doi: 10.1093/bja/aev072

Schwender, D., Klasing, S., Daunderer, M., Madler, C., Poppel, E., and Peter, K. (1995). Awareness during general anesthesia. definition, incidence, clinical relevance, causes, avoidance and medicolegal aspects. *Anaesthesist* 44, 743–754. doi: 10.1007/s001010050209

Sebel, P., Bowdle, T., Ghoneim, M., Rampil, I., Padilla, R., Gan, T., et al. (2004). The incidence of awareness during anesthesia: a multicenter united states study. *Anesth. Analg.* 99, 833–839. doi: 10.1213/01.ANE.0000130261.90896.6C

Shibasaki, H., Sadato, N., Lyshkow, H., Yonekurg, y., Hiroshi, M., Manabu, H., et al. (1993). Both primary motor cortex and supplementary motor area play an important role in complex finger movements. *Brain* 116, 1387–1398. doi: 10.1093/brain/116.6.1387

Tasbighou, S., Vogels, M., and Absalom, A. (2018). Accidental awareness during general anaesthesia - a narrative review. *Anaesthesia* 73, 112–122. doi: 10.1111/anae.14124

Weiser, T., Haynes, A., Molina, G., Lipsitz, S., Esquivel, M., Uribe Leitz, T., et al. (2016). Size and distribution of the global volume of surgery in 2012. *Bull. World Health Organ.* 94, 201–209. doi: 10.2471/BLT.15.159293

Xu, L., Wu, A.-S., and Yue, Y. (2009). The incidence of intra-operative awareness during general anesthesia in china: a multi-center observational study. *Acta Anaesthesiol. Scand.* 53, 873–882. doi: 10.1111/j.1399-6576.2009.02016.x

Conflict of Interest Statement: The authors declare that the research was conducted in the absence of any commercial or financial relationships that could be construed as a potential conflict of interest.

Copyright © 2019 Rimbert, Riff, Gayraud, Schmartz and Bougrain. This is an open-access article distributed under the terms of the Creative Commons Attribution License (CC BY). The use, distribution or reproduction in other forums is permitted, provided the original author(s) and the copyright owner(s) are credited and that the original publication in this journal is cited, in accordance with accepted academic practice. No use, distribution or reproduction is permitted which does not comply with these terms.

Advantages of publishing in Frontiers

OPEN ACCESS
Articles are free to read for greatest visibility and readership

FAST PUBLICATION
Around 90 days from submission to decision

HIGH QUALITY PEER-REVIEW
Rigorous, collaborative, and constructive peer-review

TRANSPARENT PEER-REVIEW
Editors and reviewers acknowledged by name on published articles

Frontiers
Avenue du Tribunal-Fédéral 34
1005 Lausanne | Switzerland

Visit us: www.frontiersin.org
Contact us: frontiersin.org/about/contact

REPRODUCIBILITY OF RESEARCH
Support open data and methods to enhance research reproducibility

DIGITAL PUBLISHING
Articles designed for optimal readership across devices

FOLLOW US
@frontiersin

IMPACT METRICS
Advanced article metrics track visibility across digital media

EXTENSIVE PROMOTION
Marketing and promotion of impactful research

LOOP RESEARCH NETWORK
Our network increases your article's readership